SPATIAL ORIENTATION OF GALAXIES IN THE SDSS DR7 SUPERCLUSTERS

A THESIS SUBMITTED TO THE

CENTRAL DEPARTMENT OF PHYSICS

INSTITUTE OF SCIENCE AND TECHNOLOGY

TRIBHUVAN UNIVERSITY

NEPAL

FOR THE AWARD OF

DOCTOR OF PHILOSOPHY

IN PHYSICS

BY

JANAK RATNA MALLA

SEPTEMBER, 2022

DECLARATION

Thesis entitled **“Spatial Orientation of Galaxies in The SDSS DR7 Superclusters"** which is being submitted to the Central Department of Physics, Institute of Science and Technology (IoST), Tribhuvan University, Nepal for the award of the degree of Doctor of Philosophy (Ph.D.), is a research work carried out by me under the supervision of Prof. Dr. Binil Aryal of Central Department of Physics Tribhuvan University, Nepal and co-supervised by Prof. Dr. Walter Saurer of Institute of Astro-particle Physics, Innsbruck University, Austria.

This research is original and has not been submitted earlier in part or full in this or any other form to any university or institute, here or elsewhere, for the award of any degree.

....
Janak Ratna Malla

RECOMMENDATION

This is to recommended that **Mr. Janak Ratna Malla** has carried out research entitled **"Spatial Orientation of Galaxies in The SDSS DR7 Superclusters"** for the award of Doctor of Philosophy (Ph.D.) in **Physics** under our supervision. To our knowledge, this work has not submitted for any other degree.

He has fulfilled all the requirements laid down by the Institute of Science and Technology (IoST), Tribhuvan University, Kirtipur for the submission of the thesis for the award of Ph.D. degree.

. . . .

Prof. Dr. Binil Aryal
Supervisor
Central Department Of Physics
Tribhuvan University
Kirtipur, Kathmandu, Nepal

. . . .

Prof. Dr. Walter Saurer
Co-Supervisor
Institute of Astro-particle Physics
Innsbruck University
Innsbruck, Austria

June 11, 2022

LETTER OF APPROVAL

September 7, 2022

On the recommendation of Prof. Dr. Binil Aryal and Prof. Dr. Walter Saurer, this Ph. D. thesis submitted by “**Janak Ratna Malla**", entitled **“Spatial Orientation of Galaxies in The SDSS DR7 Superclusters"** is forwarded by Central Department Research Committee (CDRC) to the Dean, IoST, T.U.

. . . .

Dr. Om Prakash Niraula
Professor
Head
Central Department of Physics
Tribhuvan University
Kirtipur, Kathmandu
Nepal

ACKNOWLEDGMENTS

I became able to know the fundamentals of research in physics and see the research world with a third eye; this is only due to my supervisors. So, first I would like to express my sincere gratitude to my supervisor Prof. Dr. Binil Aryal, Dean, IoST, TU, Kirtipur for the continuous scientific guidance, supports, and parent-ship throughout my research work. I acknowledge my co-supervisor Prof. Dr. Walter Saurer, Innsbruck University, Austria for his critical suggestion particularly in the interpretation of the results. His contribution during the manuscript preparation is highly acknowledged. I remember his visit to Kathmandu during his holidays.

My sincere thank goes to Sloan Digitized Sky Survey (SDSS), Polar Sky Survey (POSS) team for providing data through our collaboration. I am thankful to Dr. Wolfgang Kausch of Innsbruck University, Austria for providing his masters thesis, and Mr. Rajesh Kumar Bachchan of Lund Observatory, Sweden for their help during the process of data access and processing.

My special thanks go to Associate Prof. Dr. Shiv Narayan Yadav, Associate Prof. Ajay Kumar Jha, Associate Prof. Bhanu Bhakta Sapkota for the company. We learned a lot from each other.

Also, I am thankful to Assistant Prof. Devendra Raj Upadhyay and Mr. Saroj Raj Shahi, Observatory Manager, B.P. Koirala Memorial Planetarium, Observatory, and Science Museum Development Board.

I would like to express my gratitude to Prof. Dr. Om Prakash Neraula, Prof. Dr. Raju Khanal, Prof. Dr. Narayan Adhikari, Associate Prof. Dr. Balram Ghimire, Associate Prof. Dr. Gopi Chandra Kafle, Assistant Prof. Dr. Sanju Shrestha, and other faculty members of CDP for their constant support encouragement during the research work.

I would like to thank the organizers of International Astronomical Union symposium 353, Galactic Dynamics in the Era of Large Surveys (2019) Shanghai, China for allowing me to present my results in the poster form.

I am thankful to the Institute of Science and Technology, T.U., Kirtipur for providing me study leave and the Central Department of Physics to carry out my research work.

It is my great pleasure to thanks Nepal science and technology for providing Ph.D. fellowship. I also thank Amrit Campus, T.U., Thamel, for permitting me to carry out the Ph.D. research.

I would like to thank my parents and family members for their constant support, patience, and encouragement. I am thankful to my younger brother Janardan, sister Jyotshana, sister-in-law Raju, my daughter Yashashvi and son Sushant who always makes me fresh and dynamic. Lastly, my Special thank goes to my wife Nisha Malla for her support and encouragement in every step during my research work.

Janak Ratna Malla
June 2022

ABSTRACT

The evolution of galaxies in the substructures of Supercluster is extremely important to understand the formation process of the largest structures of the Universe. Superclusters are the largest aggregates of the gravitationally bound system of galaxies containing voids, filaments, and substructures. The distribution of angular momentum vectors of galaxies in the clusters and Superclusters reveal how galaxies form and how they obtain angular momentum for rotation. We present spatial orientation of angular momentum vectors of 8 973 galaxies in the six SDSS 7DR (Sloan Dizited Sky Survey 7 Data Release) Superclusters and their eighteen substructures having redshift (z) in the range 0.024 to 0.114. These Superclusters are S[195+027+0022], S[173+003+0077], S[247+040+0029], S[227+006+0078], S[231+030+0117], S[184+003+0077]. Present work can be divided into two sections namely search for substructures in the Superclusters and study the preferred alignments of angular momentum vectors of galaxies in those substructures. In order to identify substructures, we studied number density and redshift maps of all six Superclusters to identify substructures on the basis of their richness and compactness. In addition, the r and u-magnitude maps of galaxies and their distributions are studied in all six Superclusters. The selection criteria for the substructures are as follows: (a) richness (R) should be greater than Abell richness class 2, and (b) redshift dispersion should not exceed by 0.01 from the mean redshift of the Superclusters. In the second section of result and discussion chapter, we studied distributions of angular momentum vectors of galaxies. For this we adopted three steps: first, two dimensional observed parameters that we have compiled from SDSS 7DR (positions, position angles, and inclination angles of galaxies) are converted into three-dimensional angular momentum vectors of the galaxy using Godlowskian transformation. As a second step, we worked on an observed database of Superclusters and their substructures to find out selection effects. These selection effects are actually the noise in the database. We observed systematic noises in the inclination angle distribution of galaxies. In order to remove those systematic noise, we perform numerical simulation separately for all six Superclusters and their nineteen substructures. The basis of our simulation is the cosmological principle, i.e., isotropy for directional parameters (e.g., polar or inclination angle of galaxy rotation axes) and homogeneous for spatial parameters (e.g., azimuthal angle or positions of galaxies). For this, we virtually generated 10^7 galaxies to each noise responsible for anisotropy or inhomogeneity in the Supercluster. In this way, we obtained expected isotropic distribution curves for both angular momentum vectors and their projections in all six Superclusters and their substructures. As a final step, a

comparison between observed distribution and expected distribution is made using chi-square, autocorrelation, and the Fourier tests. We intend to find out non-random effects in the expected isotropic distributions in both polar and azimuthal angles of galaxy rotation axes of Supercluster and substructure galaxies. In general, we found no preferred alignments of galaxies in all six Superclusters. In the substructures, we noticed bimodal effects. It is therefore a plot between the number of galaxies in the substructures and their mean redshift are plotted and found a linear relationship with decreasing slope. In addition, the color-magnitude diagram of galaxies in the Superclusters showed a similar trend.

LIST OF ACRONYMS AND ABBREVIATIONS

A&A	Astronomy and Astrophysics Journal
ACO	Abell Catalogue
AJ	Astronomical Journal
ApJ	Astrophysical Journal
ApJS	Astrophysical Journal Suppliment
Ap&SS	Astrophysics and Space Science
APO	Apache Point Observatory
APOGEE	The Apache Point Observatory Galactic Evolution Experiment
ASJ	Astronomical Society Japan
BM	Bautz Morgan system
CCDs	Charge Coupled Devices
CDM	Cold Dark Matter
CMB	Cosmic Microwave Background
CMBR	Cosmic Microwave Background Radiation
DEC	Declination
DR	Data Released
eBoss	Extended Baryonic Oscillation Spectroscopic Survey
ECS	Equatorial Coordinate System
ESA	European Space Agency
ESO	European Space Observatory
FIRAS	Far Infrared Astronomical Satellite
HDM	Hot Dark Matter
HFI	High Frequency Instrument
HST	Hubble Space Telescope
LCRS	Las Companas Red Shift Survey
LFI	Low Frequency Instrument
LRG	Luminous Red Galaxy
LSC	Local Super Cluster
LSS	Large Scale Structure
MaNGA	Mapping Nearby Galaxies at Apache Point Observatory
MGC	Millennium Galaxy Catalogue
MNRAS	Monthly Notice of Royal Astronomical Society
NASA	National Aeronautical Space Administration
NED	NASA Extragalactic Database
OAJ	The Open Astronomy Journal

PA	Position Angle
PANBG	Photometric Atlas of Northern Bright Galaxies
PASJ	Journal of Asia Pacific Society
PhRvD	Physical Review D (Particles and Fields)
POSS	Palomar Observatory Sky Survey
PSF	Point Spread Function
QSOs	QUAsi-StellAR-object= Quasars
RA	Right Ascension
RAA	Research in Astronomy and Astrophysics
SDSS	Sloan Digital Sky Survey
SVs	Spin Vectors
VCC	Virgo Cluster Center
WMAP	Wilkinson Microwave Anisotripy Probe
2dFGRS	2degree Field Galaxy Redshift Survey

LIST OF TABLES

LIST OF FIGURES

Page No.

TABLE OF CONTENTS

CHAPTER 1

1. INTRODUCTION

1.1 Superclusters of Galaxies

A large group of smaller galaxy clusters or galaxy groups or aggregations of substructures of galaxies is named a Supercluster. Superclusters are considered the largest structures of the Universe known to us till date. Obviously the galaxies in the Superclusters are gravitationally bound with each other. In addition, there is a significant role of void (the space between the groups or substructures) for the structure formation and evolution. According to Einstein's general theory of relativity, large-scale structures are formed because of the manifold geometry of space-time (Hawking & Ellis, 1973). Our universe is the biggest laboratory available for astrophysicists. The knowledge known to us (on Earth) has already been challenged by cosmological observations of the formation of galaxies, their evolution and the expansion of the Universe.

The study of the large-scale structure of the universe is also undergoing tremendous growth. In the early 1980's, there were less than 5,000 galaxy redshifts known. However, we now have over 500,000 and will soon have more than 1,000,000. Several new surveys such as 2-Degree Field (2dF) Survey and Sloan Digital Sky Survey (SDSS) have recently been completed. Within a few years, the 3-dimensional distribution of galaxies in our local universe will be mapped. Furthermore, those structures can be matched to the early time snapshot of density perturbation. Since any model of structure formation must explain both the temperature fluctuations in CMBR and the large-scale structures we observe today in the universe, the combination of these two probes is especially powerful. The Milky Way is part of the Local Group galaxy group (which contains more than 54 galaxies), which in turn is part of the Virgo Supercluster, which is part of the Laniakea Supercluster (Gibney, 2014). In other words, galaxies tend to huddle in groups called clusters; regions where these clusters are densely packed are known as Superclusters. But the definition of these massive cosmic structures is vague.

The large size and low density of Superclusters mean that they, unlike clusters, expand with the Hubble expansion. The number of Superclusters in the observable universe is estimated to be 10 million. Cosmological observations suggest modifying our standard cosmological picture based upon known materials and fundamental laws on Earth, but current observations do not provide enough information to explain the abnormality at cosmological scales. The information of underlying science about the universe is given by looking at structure formation at large-scales. While current observations revealed the breakdown of our knowledge of physical science at cosmological scales, the future observation of large scale structure formation will provide us with a clue as to which part of our physical science should be modified - matter or gravity.

The Laniakea Supercluster is the Supercluster that contains the Virgo Cluster, Local Group, and by extension on the latter, our galaxy; the Milky Way. It is 153 Mpc in diameter (1 pc km) (Tully, 2014). Virgo Supercluster is another well-studied large scale structure. It contains the Local Group with our galaxy, the Milky Way. It also contains the Virgo Cluster near its centre and is sometimes called the Local Supercluster. It is thought to contain over 47,000 galaxies, having a diameter of 33 Mpc. In 2014, the newly announced Laniakea Supercluster subsumed the Virgo Supercluster, which became a component of the new Supercluster (Tully, 2014). Hydra-Centaurus Supercluster is composed of two lobes, namely Hydra Supercluster and Centaurus Supercluster. Pavo-Indus Supercluster. Saraswati Supercluster is one of the distant Superclusters which is at 1.2 Gpc, It is one of the largest structures found in the universe, with a major axis in diameter of about 200 Mpc (652 million light-years), It consists of 43 massive galaxy clusters such as Abell 2361 and has a mass of about 2 x 10^{16} $M_\odot$ and is seen in the Pisces constellation (Cucciati et al., 2018).

A rich Supercluster with several galaxy clusters was discovered around an unusual concentration of 23 QSOs at z=1.1 in 2001, named as SCL@1338+27 (Tanaka, 2004). The size of the complex of clusters may indicate a wall of galaxies exists there, instead of a single Supercluster. At the time of the discovery, it was the largest and most distant Supercluster beyond z=0.5. The Supercluster named MS 0302+17 has three extended lobes in three directions: the eastern cluster CL 0303+1706, southern cluster MS 0302+1659, and northern cluster MS 0302+1717 (Kaiser, 2009).

There are many other noticeable Superclusters that have redshift less than 0.1. These are Pisces-Cetus Supercluster, Coma Supercluster, Shapley Supercluster, Bootes Supercluster, Horologium-Reticulum Supercluster, Corona Borealis Supercluster, Columba Supercluster, Aquarius Supercluster, Aquarius B Supercluster, Aquarius-Capricornus Supercluster, Aquarius-Cetus Supercluster, Bootes A Supercluster, Caelum Supercluster, Draco Supercluster, Draco-Ursa Major Supercluster, Fornax-Eridanus Supercluster, Grus Supercluster, Leo A Supercluster, Leo-Sextans Supercluster, Leo-Virgo Supercluster, Microscopium Supercluster, Pegasus-Pisces Supercluster, Perseus-Pisces Supercluster, Pisces-Aries Supercluster, Ursa Majoris Supercluster and Virgo-Coma Supercluster

(Hasegawa et al. (2000), Nakata et al. (2004), Cucciati et al. (2018)).

1.1.1 SDSS Supercluster

The Sloan Digital Sky Survey (SDSS) is the most important galaxy redshift survey which provides three-dimensional maps of the Universe ever made, with deep multi-color images of one-third of the sky, and spectra for more than three million astronomical objects. The SDSS began regular survey operations in the year 2000, after a decade of design and construction of the telescope. It has progressed through several phases, SDSS-I (2000-2005), SDSS-II (2005-2008), SDSS-III (2008-2014), and SDSS-IV (2014-2020). Each of these phases has involved multiple surveys with interlocking science goals. Till date, SDSS has released 16th sets of huge databases. The final Data Release of SDSS-IV is scheduled for July 2021 and will include all APOGEE-2, eBOSS, and MaNGA spectra observed during SDSS-IV, as well as all final data products and catalogs. In addition to the final eBOSS clustering samples, DR17 will include new single-fiber, optical spectra associated with a completed reverberation mapping program and a pilot program of X-ray counterparts. SDSS-V will start observations in summer 2020, with its first data release expected two years later. Surveys in SDSS-V include Milky Way Mapper, Local Volume Mapper and Black Hole Mapper (Blanton et al. (2017), Eisenstein et al. (2011), York et al. (2000), https://www.sdss.org/).

We are interested in the SDSS Supercluster because it is the first such database that contains both photometric and spectroscopic databases of all galaxies up to a very high precision level. The photometric database includes the magnitudes in all pass-bands. SDSS uses five photometry covering ultra violet (UV), optical, and infrared with the help of five filters. We will describe these filters in the literature review section.

Einasto et al. (2011) studied the morphology of a set of Superclusters drawn from the SDSS data release 7 (SDSS (2008), Abazajian et al. (2009)). The selection criteria includes the apparent r magnitudes $12.5 \leq r \leq 17.77$. Their first step is to determine groups and clusters of galaxies with the friends-of-friends algorithm, where a galaxy belongs to a group of galaxies if this galaxy has at least one group member galaxy closer than the selected linking length. The linking length along with the distance was increased, to take into account selection effects, when constructing a group catalogue for a flux-limited s ample. As a result, the maximum sizes and velocity dispersions of groups are similar at all distances. For details and for the group catalogue we refer the reader to T101. To determine the luminosities of groups and to calculate the luminosity density field we also have to correct for the luminosities of galaxies that lie outside of the survey magnitude range. They calculated the smoothed luminosity density field of galaxies and determined extended systems of galaxies (Superclusters) using this density field. To determine Superclusters, they created a set of density contours by choosing a series of density thresholds. Then, they define connected volumes above a certain density threshold as Superclusters. Different threshold densities correspond to different Supercluster catalogues. In order to choose proper density levels to determine individual Superclusters, they analysed the density field Superclusters at a series of density levels. Finally, they calculated the luminosity density field to determine Superclusters from a flux-limited sample of galaxies from SDSS DR7 and select Superclusters with 300 and more galaxies for the study. Einasto et al. (2011) found that the large-scale distribution of the Superclusters is very inhomogeneous. Rich Superclusters in the sample form three chains, the Sloan Great Wall is the richest of them. Almost all Superclusters are elongated and have filamentarities that are larger than their planarities. More elongated Superclusters are also more luminous, have larger diameters, and contain a larger number of rich clusters.

Liivamägi et al. (2012) used the Millennium galaxy sample to evaluate the Supercluster-finding procedure as applied to an ideal volume-limited sample. As a consequence, there are no distance-related effects. A separate further study will look more closely at the differences in object selection and their properties using several simulated flux and volume-limited samples. The distributions of Superclusters are strikingly similar, with the main sample containing almost the same amount of Superclusters. The shape of the Millennium distributions at the density level D = 5.0, indicates the presence of large Sloan Great Wall-like structures (see Figure 1).

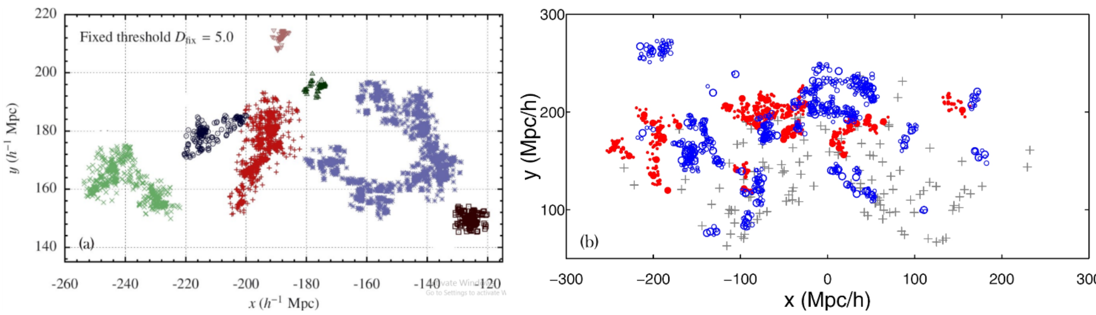

Figure 1: (a) The Supercluster SCl 1 and the surrounding Superclusters found with different methods for assigning the limiting threshold D. In the upper panel all Superclusters have the same threshold D_{fix} = 5.0 (Liivamägi et al., 2012). (b) Distribution of galaxy groups with at least four member galaxies in Superclusters in x, y, and z coordinates. Red filled circles correspond to groups in filament-type Superclusters. Blue empty circles represent groups in spider-type superclusters. Grey crosses denote groups with at least 30 member galaxies from the field (Einasto et al., 2014).

Einasto et al. (2014) compared the galaxy populations in Superclusters of different morphology in the nearby Universe (180 h^{-1} Mpc $\leq d \leq$ 270 h^{-1} Mpc). To check whether the inner structure and overall morphology of Superclusters are important in shaping galaxy properties in Superclusters. This study is extremely important to understand the formation, evolution and present-day properties of the cosmic web and objects forming it is an important task in cosmology. They used the main sample of the 8th data release of the Sloan Digital Sky Survey (Aihara et al., 2011) with the apparent Galactic extinction corrected r magnitudes $r \leq 17.77$, and the redshifts $0.009 \leq z \leq 0.200$, in total 576 493 galaxies. They have corrected the redshifts of galaxies for the motion relative to the CMB and computed the co-moving distances (Martinez & Saar, 2002) of galaxies. Figure 1b presents the distribution of rich galaxy clusters in Superclusters of filament and spider morphology, as well as from the field in cartesian coordinates defined as in Park et al. (2007) and Liivamägi et al. (2012). At the distance interval of about 180 h^{-1} Mpc $\leq d \leq 270$ h^{-1} Mpc the survey crosses several rich Superclusters, including the Sloan Great Wall. Einasto et al. (2014) found Supercluster morphology and analyze the probability density distributions of colours, morphological types, stellar masses, star formation rate (SFR) of galaxies, and the peculiar velocities of the main galaxy in groups in Superclusters of filament and spider types, and in the fi eld. Therefore, their work is extremely important to give a functional identification to the S uperclusters. The database of these Superclusters should be studied and compared with the nearby Supercluster, e.g., Local Supercluster and Coma Supercluster in the galaxy orientation aspect.

1.1.2 Organization of Ph.D. Thesis

1. In Chapter 2, we give theoretical consideration regarding the morphology of galaxies, redshift, and angular momentum of the galaxy in the clusters and Superclusters. After this, the galaxies evolution model will be presented and discussed. Finally, an extensive literature review will be presented in the tabular form followed by interpretations regarding origin of the angular momentum vectors of galaxies and their preferred distributions.

2. In Chapter 3, we present our methodology and the database of selected SDSS Superclusters. The methodology includes two parts: first, the data processing and finally the calculation of angular momentum vectors and their projections of galaxies will be explained and secondly, the numerical simulation process will be explained in order to satisfy the cosmological principle. Statistical methods that we have used, will also be discussed. After this, we introduce our selection criteria and hence give all-sky and axial-ratio distributions of our six SDSS Superclusters. At the end, two flow charts will be given to show the all processes.

3. In Chapter 4, we give our results and discussion of all six Supercluster galaxies one-by-one. In these subchapters, at first, we present number density maps and followed by identification of substructures on the basis of redshift and r and u-magnitude maps. After this, we present our results regarding the orientations of galaxies in the Superclusters and their substructures. This will be repeated in the

Chapters from 4.1 to 4.6 for six Superclusters. Finally in Chapter 4.7. there will be a general discussion and comparison with published works.

4. In Chapter 5, we present our conclusion based on our results, and interpretation with other published works. In the end, future prospectus will be recommended.

At the end, there will be a list of references, appendices and published papers in the national and international Journals.

CHAPTER 2

2. LITERATURE REVIEW

2.1 Superclusters

Superclusters are large groups smaller galaxy clusters or galaxy groups and are among the largest known structures of the cosmos. The milky way is in the Local Group of galaxies, which is true is in the Laniakea Supercluster. This supercluster spans over 500 million light-years, while the Local group spans over 10 million light-years. The number of Superclusters in the observable universe is estimated to be 10 million. Galaxies are grouped into clusters instead of being dispersed randomly. The cluster of galaxies is grouped together to form Supercluster. Superclusters are the tracer of dark and baryonic matter in the universe. These Superclusters are found to be arranged in filament or sheet-like structures, between which there are gigantic voids of empty space. Galaxy Superclusters usually consist of chains of around a dozen of galaxy clusters, each with a mass of about 10^{13}-10^{14} $M_{\odot}$ (NASA, 2020b). Typically, Superclusters contain dozens of individual clusters throughout an area of space about 150 million light-years across. Superclusters are not bound together by gravity. They are all shifting away from each other due to the Hubble flow.

The existence of Superclusters indicates out that the galaxies present in our Universe are not uniformly or well distributed. They are so large that they are not gravitationally bound. Their mutual gravity binds them together into long filaments(thin, string like-structures). Our Local Superclusters is located on Virgo (Figure 1) and with Coma, are up to 100 Mpc in extent. The system of Superclusters makes a network expanding throughout space, on which about 90 percent of galaxies are located.

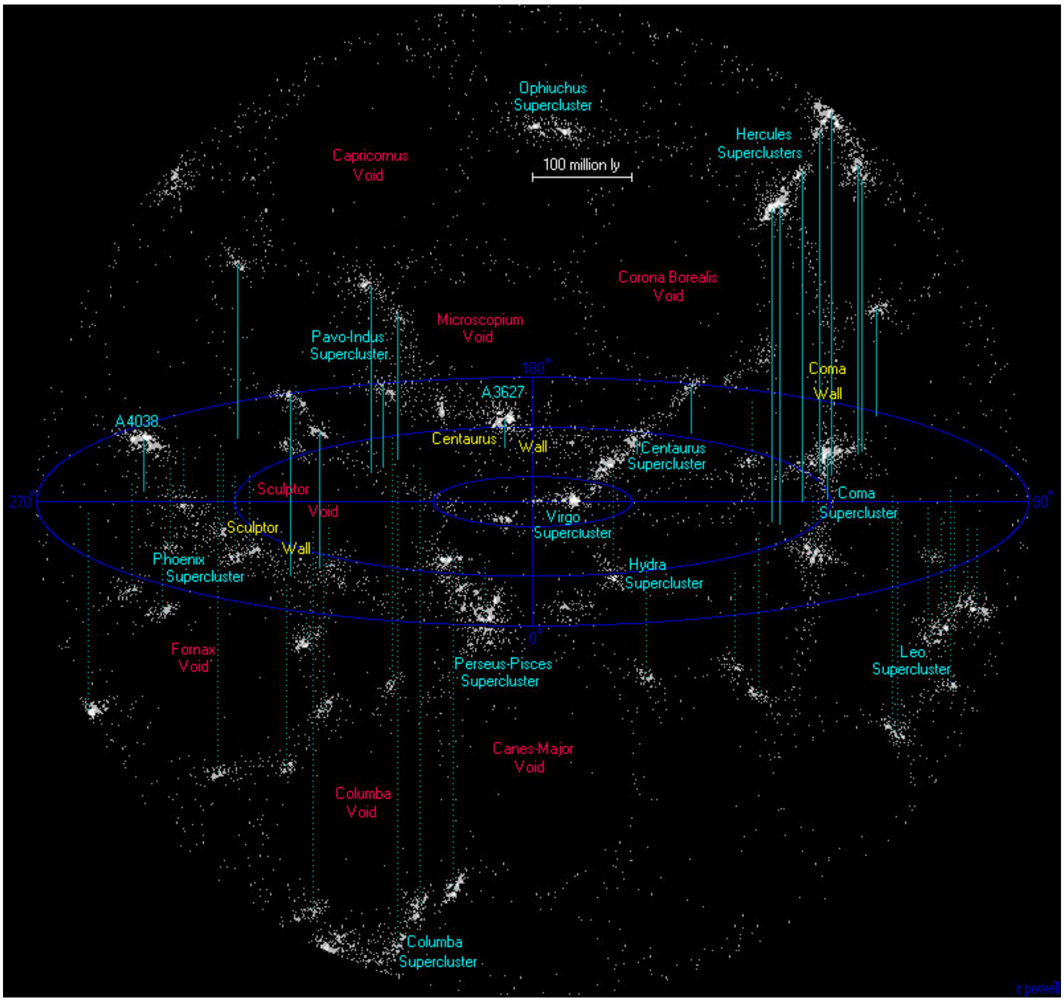

Figure 2: Image of Virgo Supercluster of galaxies. The bright object represents galaxy (NASA, 2020b).

2.1.1 Substructure

Multiple concentrations of the same object, growing and held together within the large structure are called substructures. In Supercluster, its constituent is not distributed uniformly results in the substructure. Local group and Virgo cluster are the substructures of our Local Supercluster. The term "Substructure" refers to clumping within the cluster. Some clusters are spherically symmetric with high density in the center and smoothly diminishing densities with radius. Other clusters have two or more density peaks or show other evidence of merging sub-systems of galaxies. Substructure and, more generally, evidence for mergers can be observed in many ways: 1) the spatial distribution of galaxies, 2) the velocity distributions of the galaxy, 3) spatial-velocity correlations, 4) the surface brightness distribution of x-ray emitting gas (intra- cluster medium or ICM), 5) the temperature distribution of the ICM, and 6) weak and strong gravitational lensing.

2.1.2 Clusters of Galaxies

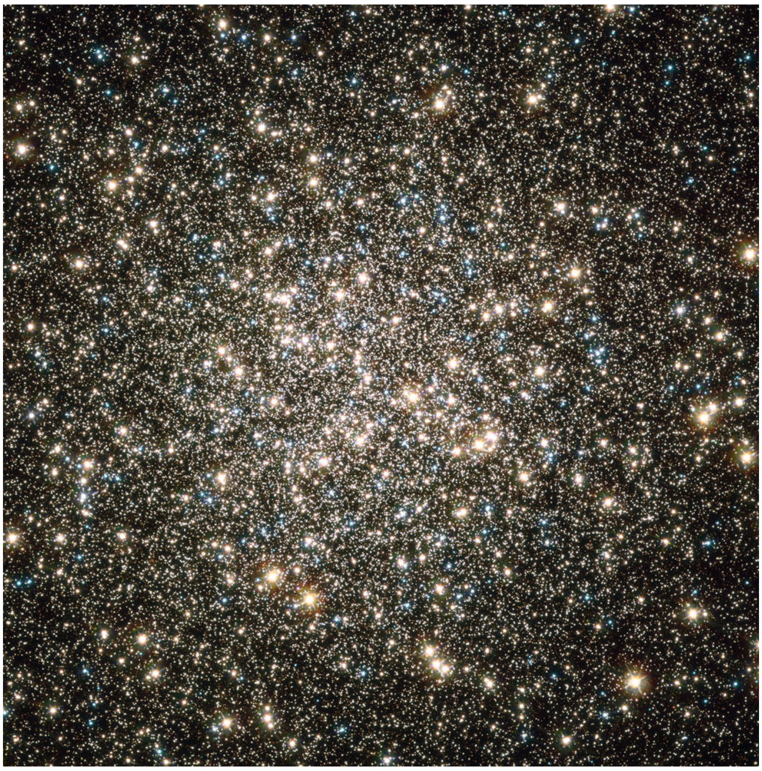

Figure 3: Image of cluster of Galaxies: Hercules cluster (NASA, 2020a).

A galaxy cluster, or cluster of galaxies, is a structure that consists of anywhere from hundreds to thousands of galaxies that are bound together by gravity with typical masses ranging from 10^{13}-10^{14} $M_\odot$ (NASA, 2020b). They are the largest known gravitationally bound structures in the universe and were believed to be the largest known structures in the universe until the 1980s when Superclusters were discovered. One of the key features of clusters is the intracluster medium (ICM). The ICM consists of heated gas between the galaxies and has a peak temperature between 2-15 keV that is dependent on the total mass of the cluster. Galaxy clusters should not be confused with star clusters, such as open clusters, which are structures of stars within galaxies, or with globular clusters, which typically orbit galaxies. Small aggregates of galaxies are referred to as galaxy groups rather than clusters of galaxies. The galaxy groups and clusters can themselves cluster together to form Superclusters.

Notable galaxy clusters in the relatively nearby Universe include the Virgo Cluster, Fornax Cluster, Hercules Cluster (shown in Figure3), and the Coma Cluster. A very large aggregation of galaxies known as the Great Attractor, dominated by the Norma Cluster, is massive enough to affect the local expansion of the Universe. Notable galaxy clusters in the distant, high-redshift Universe include SPT-CL J0546-5345 and SPT-CL J2106-5844, the most massive galaxy clusters found in the early Universe. In the last few decades, they are also found to be relevant sites of particle acceleration, a feature that has been discovered by observing non-thermal diffuse radio emissions, such as radio halos and radio relics. Using the Chandra X-ray Observatory, structures such as cold fronts and shock waves have also been found in many galaxy clusters. Our galaxy falls within the Local Group, which is a poor and irregular cluster of galaxies. Poor clusters may contain only a few dozen galaxies as compared to rich clusters that can contain hundreds or even thousands. The Local Group is near the Local Supercluster (also known as Virgo Supercluster) which has a diameter of 100 million light-years. The Local Supercluster contains a total of about10^{15} times the mass of the Sun.

2.1.3 Galaxy Group

Figure 4: Image of the Galaxy Cluster Abell 2537 Local Group.Our Milky Way galaxy is a part of this group.(NASA, 2017b).

A galaxy is a gravitationally bound system of stars, stellar remnants, interstellar gas, dust, and dark matter. Galaxies range in size from dwarfs with just a few hundred million stars to giants with one hundred trillion stars, each orbiting its galaxy's center of mass. Galaxies are categorized according to their visual morphology as elliptical, spiral, or irregular. Many galaxies are thought to have super-massive black holes at their centers. The Milky Way's central black hole, known as Sagittarius A*, has a mass four million times greater than the Sun.

Nature has provided an immensely varied array of galaxies, ranging from faint, diffuse dwarf objects to brilliant spiral-shaped giants. Virtually all galaxies appear to have been formed soon after the universe began, and they pervade space, even into the depths of the farthest reaches penetrated by powerful modern telescopes. Galaxies usually exist in clusters, some of which in turn are grouped into larger clusters that measure hundreds of millions of light-years across.

The space between galaxies is filled with a tenuous gas (the intergalactic medium) having an average density of less than one atom per cubic meter. The majority of galaxies are gravitationally organized into groups, clusters, and Superclusters. The Milky Way is part of the Local Group (Figure 5), which is dominated by it and the Andromeda Galaxy and is part of the Virgo Supercluster. At the largest scale, these associations are generally arranged into sheets and filaments surrounded by immense voids. Both the Local Group and the Virgo Supercluster are contained in a much larger cosmic structure named Laniakea,that the galaxies rotate may provide a clue to the physical conditions under which these systems formed. A Spiral galaxy is supported by rotation. It possesses angular momentum. The direction of angular momentum is orbitrary. The distribution of angular momentum vector refers to spatial orientation.

These so-called Superclusters are separated by nearly empty voids, and this causes the gross structure of the universe to look somewhat like a network of sheets and chains of galaxies.

Figure 5: Image of the Spiral galaxy NGC 1232 (NASA, 2017a).

2.2 Redshift

Apparent shifting of wavelength of photon emitted by heavenly body toward lower energy limit i.e. longer wavelength limit is called redshift. The redshift of any astronomical object can be written as:

$$z_{total} = z_d + z_c + z_g \tag{2.1}$$

There are three types of redshift,

(i) Doppler redshift (z_d): The redshift resulting from the relative motion of the light emitting object and the observer is attributed to the Doppler redshift. If the source of light is moving away from the observer then the wavelength of the light is stretched out, i.e., the light is shifted towards the red.

(ii) Cosmological redshift (z_c): The redshift may also be caused by the expansion of the space. The wavelength of light increases as it traverses the expanding universe between its point of emission and its point of detection. Such a process is termed as the cosmological redshift.

(iii) Gravitational redshift (z_g): The frequency of a photon may shift to lower energy as it climbs out of a gravitational field. This process by which electromagnetic radiation originating from a source that is in the gravitational field is reduced in frequency, or redshifted, when observed in a region of a weaker gravitational field is the gravitational redshift.

A brief description of these redshift are given below.

2.2.1 Relativistic Doppler Redshift

The relativistic Doppler redshift is the change in frequency (and wavelength) of light, caused by the relative motion of the source and the observer, when taking into account effects described by the special theory of relativity (Padmanabhan, 2006).

Let the observer and the source are moving away from each other with a relative velocity v in the reference frame of the source (Karttunen et al., 2006),

$$t = \frac{\lambda}{c - \mathrm{v}} \tag{2.2}$$

Let λ= c/ν_s where ν_s is frequency of source. Here λ is the wavelength, and c is the speed of light. Since the wavefront moves with velocity c and the observer escapes with velocity v, the time (measured in the reference frame of the source) between crest arrivals at the observer is given by,

$$t = \frac{c}{(c - \mathrm{v})\nu_{\mathrm{s}}} \tag{2.3}$$

$$t = \frac{c}{c(1 - \frac{\mathrm{v}}{c})\nu_s} \tag{2.4}$$

$$t = \frac{1}{(1 - \frac{\mathrm{v}}{c})\nu_s} \tag{2.5}$$

$$t = \frac{1}{(1 - \beta)\nu_s} \tag{2.6}$$

where $\beta = \mathrm{v}/c$. The observer will measure this time to be

$$t_\circ = t/\gamma \tag{2.7}$$

Where $\gamma = 1/(1 - \beta^2)^{1/2}$ is the Lorentz factor. Therefore, the observed frequency becomes

$$\nu_\circ = \frac{1}{t_\circ} = \gamma\,(1 - \beta)\,\nu_s = \left(\frac{1 - \beta}{1 + \beta}\right)^{1/2} \nu_s \tag{2.8}$$

The ratio

$$\frac{\nu_s}{\nu_\circ} = \left(\frac{1 + \beta}{1 - \beta}\right)^{1/2} \tag{2.9}$$

is called the Doppler factor of the source relative to the observer. The corresponding wavelengths are related by

$$\frac{\lambda_\circ}{\lambda_s} = \frac{\nu_s}{\nu_\circ} = \left(\frac{1 + \beta}{1 - \beta}\right)^{1/2} \tag{2.10}$$

and the resulting redshift

$$z = \frac{\lambda_\circ - \lambda_s}{\lambda_s} = \frac{\nu_s - \nu_\circ}{\nu_\circ} \tag{2.11}$$

can be written as

$$z + 1 = \left(\frac{1+\beta}{1-\beta}\right)^{1/2} \tag{2.12}$$

In the non-relativistic limit (when $v \lll c$) this redshift can be approximated by

$$z \simeq \beta = \frac{\mathrm{v}}{c} \tag{2.13}$$

corresponding to the classical Doppler effect.

When the light approaches at right angles to the direction of relative motion in the observer's frame, the relativistic redshift is known as the transverse redshift, given by,

$$z + 1 = [1 - \mathrm{v}^2/\mathrm{c}^2]^{-1/2}. \tag{2.14}$$

This redshift can be measured even if the source is moving towards the observer.

2.2.2 Cosmological Redshift

The cosmological redshift is due to the expansion of space, and sufficiently distant light sources show redshift corresponding to the rate of increase of their distance from earth (Padmanabhan, 2006). The metric expansion of space is the increase of distance with time between distant parts of the universe. Metric expansion is a key feature of Big Bang cosmology and is modeled mathematically with the Friedmann − Robertson − Walker (FLRW) metric (Weinberg, 1972). The FLRW describes a homogeneous, isotropic, expanding, or contracting universe. The cosmological redshift is caused by photons propagating through expanding space being extended and thereby increasing their wavelength as a result of the metric expansion of space. The redshift is related with the scale factor of now ($a_\circ$) and then (a_t) is given by (Padmanabhan, 2006),

$$z + 1 = \frac{a_\circ}{a_t} \tag{2.15}$$

In an expanding universe, the scale factor is monotonically increasing as time passes, therefore, z is positive and distant galaxies appear redshifted according to the above relation.

Redshift, z, is defined in wavelength as

$$z = \frac{\lambda_\circ - \lambda_e}{\lambda_e} = \frac{\lambda_\circ}{\lambda_e} - 1 \tag{2.16}$$

Where the subscripts o and e refer to observed (now) and emitted (then).

In the frequency domain, redshift, z, is defined as

$$z = \frac{f_e - f_\circ}{f_\circ} = \frac{f_e}{f_\circ} - 1 \tag{2.17}$$

2.2.3 Gravitational Redshift

The gravitational redshift is the change in the frequency of photons to lower energy as it climbs out of the gravitational field. This is one of the outcomes of Gravitational time dilation, in which the frequency of electromagnetic radiation is reduced in the area of the lower gravitational potential. There is a corresponding reduction in energy when electromagnetic radiation is redshifted, as given by Planck's relation. There also exists a corresponding blueshift when electromagnetic radiation propagates from a region of a weaker gravitational field to the stronger gravitational field.

The gravitational redshift of a photon can be calculated in the framework of general relativity using the Schwarzschild metric as (Padmanabhan, 2006),

$$Z + 1 = [1 - \frac{r_s}{R^*}]^{-1/2} = 1 + \frac{1}{2}\frac{r_s}{R^*} + ... = 1 + \frac{1}{2}\frac{r_s}{R^*} \tag{2.18}$$

with the Schwarzschild radius

$$r_s = \frac{2GM}{c^2} \tag{2.19}$$

Where G denotes Newton's gravitational constant, M be the mass of the gravitating body, c be the speed of light, and R^* be the distance between the centre of mass of the gravitating body and the point at which the photon is emitted.

In the Newtonian limit, the redshift becomes

$$Z + 1 = 1 + \frac{1}{2}\frac{2GM}{c^2 R^*} \tag{2.20}$$

$$Z + 1 = 1 + \frac{GM}{c^2 R^*} \tag{2.21}$$

$$Z \simeq \frac{GM}{c^2 R^*} = \frac{r_s}{2R^*} \tag{2.22}$$

Therefore, the value of gravitational redshift depends upon the ratio of mass and radius of the gravitating body.

2.3 Angular Momentum of Galaxies

The observed rotation of the galaxies is very important in order to understand the origin of the angular momentum of galaxies regarding the origin of the large scale structures Von Weizsäcker (1951) and Gamow (1952). They made it clear that the rotation of galaxies is important to test for the origin of galaxies. Rotation of the galaxy is very important for the study of the evolution of the universe.

The galaxy acquired rotation from gravitational coupling with the surrounding matter Hoyle (1949).

Let us consider the formation of galaxies in rotating and expanding universe. At some early epoch there is density fluctuation in a region then the expansion around the region began to increasily decelerated.

Let us assume the density fluctuation be spherically symmetric. The region containing the proto-galaxy or matter which will turn galaxy in future is sphere (approximately due to the spherically symmetric density fluctuation).

Let at that epoch angular momentum relative to the gyroscopic frame be Padmanabhan (2006),

$$J_i = \frac{2}{5} M r_i^2 \omega_i \tag{2.23}$$

Where M is the mass of the proto galaxies, r_i is the radius of the proto-galaxy, and ω_i is the angular velocity of the universe.

Again, we can also define a local frame called the galactic frame axis which correlates with the global rotation of universe, and its origin is fixed at the galactic center. This is the frame with which the measurement is taken later.

After the formation of the galaxy, it rotates relative to the galactic frames which are caused by the corollis force or conservation of the angular momentum. At any epoch, after the galaxy has formed, its angular momentum relative to the gyroscopic frame is given by

$$J_f = J + \beta M r_f^2 \omega_f \tag{2.24}$$

Where ω_f is the angular velocity of the universe at present, β is the parameter that depends on the distribution of mass in galaxy, r_f radius of the galaxy at present, and J is the angular momentum of the galaxy relative to the galactic frame.

Also we know that,

$$\omega_i = \omega_\circ(1 + z_i)^2 \tag{2.25}$$
$$\rho_d = \rho_{d_\circ}(1 + z_i)^3$$
$$M = \frac{4}{3}\pi\rho_{d_i} r_i^3$$

From (2.23), (2.24), (2.25) and using law of conservation of angular momentum we get,

$$\begin{aligned} J_i &= J_f \\ \frac{2}{5}Mr_i^2\omega_i &= J + \beta M r_f^2 \omega_f \end{aligned}$$

Finally ,

$$J = \frac{2}{5}\left(\frac{3}{4\pi\rho d_\circ}\right)^{2/3} \omega_\circ M^{\frac{5}{3}} - \beta r_f^2(1 + z_f)\omega_\circ M \tag{2.26}$$

For z_f not too large than 1, second term in (2.26) is sufficiently small compared to first term so

$$J \simeq kM^{5/3}$$
$$\text{where} \quad k = \frac{2}{5}\left(\frac{3}{4\pi\rho_{d_\circ}}\right)^{2/3} \omega_\circ$$

and this explains the observed empirical relation $J \propto M^{5/3}$.

Minimizing (2.26) with respect to M we get,

$$\begin{aligned} \left.\frac{dJ}{dM}\right|_{M_{min}} &= 0 \\ &= \left.\frac{d}{dM}\left(kM^{5/3} - lM\right)\right|_{M_{min}} \quad \text{where } l = \beta r_f^2(1 + z_f)^2\omega_\circ \\ &= k\frac{5}{3}M_{min}^{2/3} - l \end{aligned}$$

$$M_{min} = \left(\frac{3l}{5k}\right)^{3/2} = 1.95 r_f^3(1 + z_f)^3\rho_{d_\circ} \tag{2.27}$$

Hence the minimum angular momentum of a galaxy corresponds to the value of mass 1.95 r_f^3 $(1+z_f)^3$ $\rho_{d_\circ}$

From (2.26) we get,

J=0

$$kM^{5/3} = lM$$

$$\therefore \quad M = \left(\frac{l}{k}\right)^{3/2}$$

Hence, the mass corresponding to the zero angular momentum of the galaxy is $M_0 \simeq 2.15M_{min}$. It is easy to observe that for less and more massive structure predicts $\mid J \mid \neq 0$.

So that, here it was concluded that the galaxy obtained its angular momentum due to the global rotation of the universe. So, one may expect that the spin of galaxies should not distribute in the sky randomly, there should be a dipole anisotropy and such kind of anisotropy in the distribution of the spin of galaxies have been found at different levels. Here spherical symmetry is considered but the distribution of galaxy is quite complicated and the moment of inertia is complex so the angular momentum is different from the direction of angular velocity.

When proto-galaxy rotates and expands together with universe the angular velocity is equal to the global rotation of the universe in both magnitude and direction. The rotation of the universe makes the angular momentum of the proto-galaxy which is not aligned with the angular velocity with a fixed direction to process about the axis of rotation. The magnitude of angular momentum is constant during precision. When the proto-galaxies become separated from the global rotation and expansion of the universe and begin to collapse to form galaxies and the interaction with the surrounding should become more and more weak eventually negligible. Its angular momentum is constant in both magnitude and direction. It should be determined by the shape of the proto-galaxy and the time when proto-galaxy becomes an isolated system. Its distribution can be expected almost random instead of strong dipole distribution. As the galaxy evolves the dissipation process inside it causes the components of angular velocity perpendicular to the angular momentum to vanish gradually, eventually the galaxy rotates about the direction of angular momentum.

2.4 Photometry of Galaxies

Photometry is a technique used in astronomy that is concerned with measuring the flux or intensity of light radiated by astronomical objects (Johnston, 2015). This light is measured through a telescope using a photometer, often made using electronic devices such as a CCD photometer or a photoelectric photometer that converts light into an electric current by the photoelectric effect. When calibrated against standard stars (or other light sources) of known intensity and colour, photometers can measure the brightness or apparent magnitude of celestial objects. The methods used to perform photometry depend on the wavelength regime under study. At its most basic, photometry is conducted by gathering light and passing it through specialized photometric optical bandpass filters, and then capturing and recording the light energy with a photosensitive instrument. Standard sets of passbands (called a photometric system) are defined to allow accurate comparison of observations. A more advanced technique is spectrophotometry that measured with a spectrophotometer and observes both, the amount of radiation and its detailed spectral distribution.

2.4.1 SDSS Photometry

The first known standardized photometric system is the Johnson-Morgan (or UVB) photometric system (Johnson & Morgan, 1953). At present, there are more than 200 photometric systems. Photometric systems are usually characterized according to the widths of their passband (Rufener & Nicolet, 1988):

- broadband (passbands wider than 30 nm, of which the most widely used is Johnson-Morgan UBV system (Johnson & Morgan, 1953)),
- intermediate band (passbands between 10 and 30 nm wide) and
- narrow band (passbands less than 10 nm wide).

The photometry methods used vary depending on the wavelength regime being studied. Photometry is done by collecting radiation in a telescope, passing it through specialized optical filters if necessary, and then capturing and recording the light energy with a photosensitive instrument. A photometric device is a set of passbands (filters).

Photometry in the near infrared by long-wavelength ultra-violet used to be performed with a photoelectric photometer, which was an instrument that measured the light intensity of a single object by directing its light on to a photosensitive cell. While photoelectric photometers are still used in special situations, such as when high time resolution is needed, they have largely been replaced by CCD (charge-coupled device) cameras that can simultaneously image multiple objects. One of the most ambitious and influential surveys in the history of astronomy is the Sloan Digital Sky Survey (SDSS) (Adelman-McCarthy et al., 2006).

SDSS-I (2000-2005) obtained five-band CCD imaging over 8 000 square degrees of the high galactic latitude, northern sky, detecting 217 million celestial objects during its first five years of operation. It obtained spectra of 675 000 galaxies, 90 000 quasars, and 215 000 stars, selected from 5 700 square degrees of this imaging (Abazajian et al., 2009). The data, fully calibrated and reduced, carefully checked for quality, and accessible through efficient databases have been publicly released in cumulative form, beginning with an early release of commissioning data and continuing with a series of annual data releases.

Magnitude is a number that measures the brightness of a star or galaxy. It is because of the traditional convention, the brighter the object appears, the lower the value of its magnitudes; the very brightest objects have negative magnitudes. The apparent magnitudes do not tell us about the true brightness of stars, as the distance differs. A quantity measuring the intrinsic brightness of a star is the absolute magnitude. The absolute magnitude is equivalent to the apparent magnitude an object would have if it were at a standard luminosity distance of 10pc away from the observer, in the absence of astronomical extinction. The distance, magnitude, and extinction relation is given Karttunen et al. (2006) by,

$$m - m_{\circ} = 5\log r - 5 + (2.5\mathrm{loge})\alpha r \tag{2.28}$$

Here m, $m_{\circ}$, r and α represent apparent magnitude, absolute magnitude, distance and opacity of the medium. There are five different photometry (filters) in the SDSS telescope. There are u, g, r, z and i-filters. Here, u refers to ultravoilet (UV), g is for green, r for red, i near infrared and z for far infrared wavelengths. For SDSS u-filter,

$$u - m_u = 5\log r - 5 + (2.5\mathrm{loge})\alpha_u r \tag{2.29}$$

Here, α_u represents opacity of UV light light emitted from the galaxy. Thus, the extinction is different for different filters. For r and g filters,

$$r - m_r = 5\log r - 5 + (2.5\mathrm{loge})\alpha_r r \tag{2.30}$$

$$g - m_g = 5\log r - 5 + (2.5\mathrm{loge})\alpha_g r \tag{2.31}$$

subtracting equation (2.31) from (2.30), we get,

$$r = \frac{(r-g) - (m_r - m_g)}{(2.5\mathrm{loge})(\alpha_r - \alpha_g)} \tag{2.32}$$

This means that opacity data is important for determining the distance to the galaxy. If we know the database of extinction for given filters, we can measure the distance to the galaxy. The SDSS database contains extinction and redshift data for almost all galaxies.

SDSS has a dedicated 2.5-meter wide-angle optical telescope that was used to observe in both imaging and spectroscopic modes from 2000 to 2009. The transmission curves of SDSS filters u, g, r, i and z are shown in Figure 6.As shown figure (Abazajian et al., 2009), The pick wavelengths of these filters are 3551Å, 4686Å, 6165Å, 7481Å and

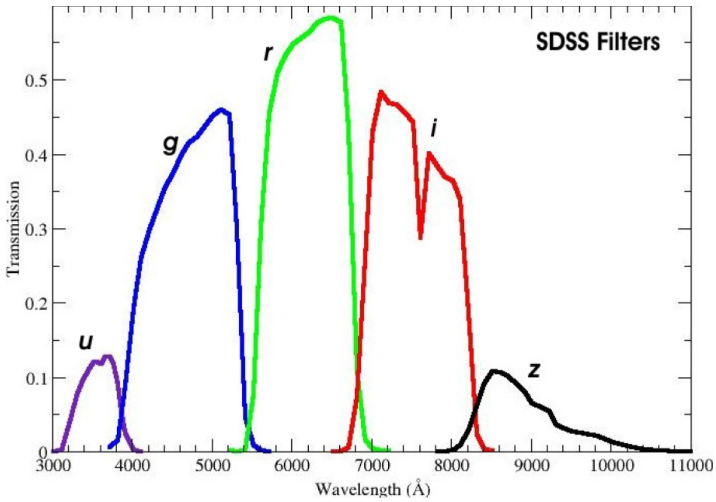

Figure 6: Standard photometric filter curves used by SDSS III telescope. (source: https://www.sdss3.org/instruments/camera.php)

8931Å, with 95% completeness in typical seeing to magnitudes of 22.0, 22.2, 22.2, 21.3 and 20.5 (D. SDSS, 2019). The r filter has the highest response, while the z filter has the lowest. The filter response was investigated by (Graves et al., 2010), who discovered that the u band has shifted over time and now tends to differ from the curve estimated previously.

2.5 Holmberg Equation

Erik Holmberg (1946) established a simple galaxy model which we have been used in the study of spin vector alignment. This model is used to find the inclination angle of the galaxy. Holmberg equation is the relation between the axial ratio, b/a and the inclination angle i, the angle between the line-of-sight and normal to the galactic plane. Figure 7 shows the oblate spheroid aside. Holmberg (1946) assumes oblate spheroid which has light curve $\sim kr^{-3}$ and is seen from a distance, where the perspective distortion is negligible. The two major axes in the main plane are of equal size a, the polar axis is the smallest one representing the relative thickness of the ellipsoid. It has length $q^* a$, q^* being the so-called flatness factor, a number $\in$ [0, 1] corresponding to the relative thickness of real spiral galaxies. Holmberg (1946) suggested a value of q^*=0.2 for oblate spheroid and q^*=0.33 for ellipticals. The celestial plane is perpendicular to the paper plane, intersection line is denoted by $\bar{g}$.

Figure 7 shows the line of sight to the observer, the inclination i is measured between this line and the Y-axis. This angle can be found between $\bar{g}$ and the X-direction.

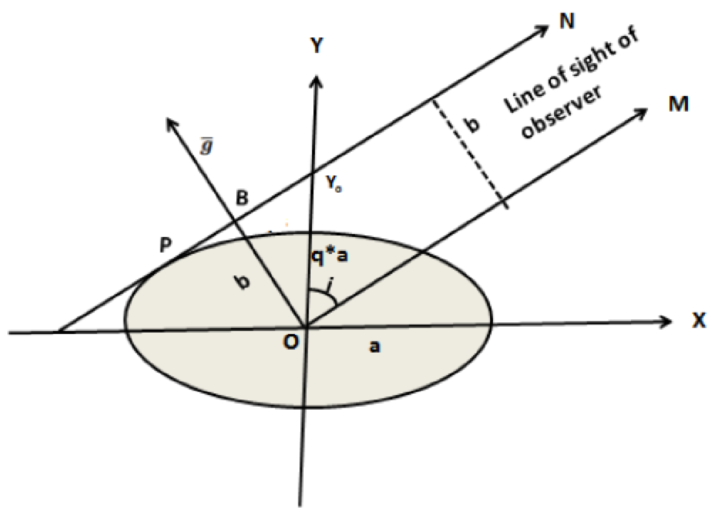

Figure 7: Illustration of Holmberg equation (Kausch et al., 2004). In the represent of semi major, semi minor, and intrinsic flatness of the projection of galaxy in the celestial sphere.

The equation of the ellipse is (Kausch et al., 2004)

$$\begin{aligned} &\frac{x^2}{a^2} + \frac{y^2}{a^2 q*^2} = 1 \\ &q*^2\, x^2 + y^2 = a^2 q*^2 \end{aligned} \tag{2.33}$$

from the observer's point of view, the oblate spheroid seems to be projected onto the celestial plane as an ellipse. The length b (connecting line OB) is the semi-minor axis of this ellipse. The semi-major axis a is independent of the projection because it is the same as the one of the oblate spheroids.

The equation of the tangent at point P is given by,

$$y = kx + c \tag{2.34}$$

where $k = \tan(90 - i) = \cot i$ is the slope of the tangent and c the intersection along Y-axis. The condition for contact to the ellipse in Fig 7 can be determined by applying the condition that (2.33) and (2.34) touches each other, i.e.,

$$a^2 k^2 + a^2 q*^2 = c^2 \tag{2.35}$$

On substituting $k = \cot i$, we get,

$$c^2 = a^2 \cot^2 i + a^2 (q*)^2 \tag{2.36}$$

From the figure, we have $b = c \sin i$. Substituting this in (2.36) we get,

$$\sin^2 i = \frac{b^2/a^2 - 1}{(q*)^2 - 1} \tag{2.37}$$

which leads to

$$\cos^2 i = \frac{b^2/a^2 - (q*)^2}{1 - (q*)^2} \tag{2.38}$$

The equation (2.38) is called ‘Holmberg Formula’.

Figure 8 shows a plot between the inclination angle (i) and the axial ratio (b/a). A strong nonlinearity can be seen at large diameter ratios. Therefore small errors in the measurement of semi-minor axes produce large deviations in the resulting inclination angle.

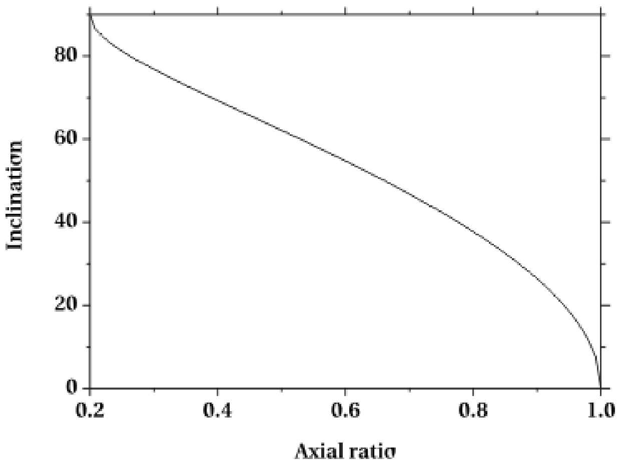

Figure 8: Axial ratio versus inclination angle. A strong nonlinearity at the lower and the upper end of the diameter ratio can be seen. Here flatness factor ($q*$) is assumed to be 0.2 (Holmberg, 1946)
.

2.6 Spatial Orientations of Galaxies

Jaaniste & Saar (1978) (JS hereafter), develop a method to convert two-dimensional position angle of a galaxy to the three-dimensional spin vector or rotation axis of that galaxy. JS (Jaaniste & Saar, 1978) realised the importance of inclination angle and proposed the PA-inclination method. They analysed not only the distributions of galaxy PA, but also considered another importance parameter- the galaxy’s inclination with respect to the observer’s line of sight, i.e., the inclination angle, as described by Holmberg (1946). These two angles allowed to find orientations of the two possible vectors normal to the galactic plane, one of them being assumed to be the galactic rotation axis or spin vector of galaxy. Later, Flin & Godlowski (1986) studied the JS’s (Jaaniste & Saar, 1978) approach and corrected a few inconsistencies and then proposed a model, called ’position angle - inclination angle’ method which we describe below.

2.6.1 Flin-Godlowski Transformation

The 'position angle-inclination' method is used to obtain three-dimensional information of the angular momentum vector of galaxies with respect to an arbitrary coordinate system. This method was established by Flin & Godlowski (1986). It is necessary to define a reference frame with respect to the plane of cluster to investigate the possible alignment.

We derive the expressions for angular momentum vectors of the galaxies and its projections assuming their distribution in the equatorial co-ordinate system (E, hereafter). An observer is situated at the origin of the E system. The X-Y plane represents the plane of the E system (i.e., equatorial plane) and the coordinates α and δ represent the equatorial longitude and latitude, respectively. The X-axis (EX) is directed towards the center of the equatorial plane ($\alpha = 0$, $\delta = 0$). The Y and Z-axis (EY and EZ) are directed towards the point $\alpha = \pi/2$, $\delta = 0$ and north equatorial pole ($\alpha = \pi/2$, $\delta = \pi/2$), respectively.

Let us assume another coordinate system. The origin of the this system is at the galaxy center. In this system, U and V-axes are perpendicular to each other and tangent to the celestial sphere, as shown in Figure 9. The U-axis is parallel to the equatorial latitude. The W-axis is perpendicular to both U and V-axes and is the extension of the connecting line between the centers of the cluster to the center of galaxy. This axis points out of the sphere. These can be seen in Figure 9. Figure 10a shows the detailed view of the galaxy showing the vectors described above. The angle q is an angle between the U-axis and the projection of galaxy major axis a on the celestial sphere. The minor axis is denoted by b. The angle q is related to the equatorial position angle p, measured in the equatorial coordinate system is given by the expression: $q = p - \pi/2$ and is measured from $-\pi/2$ to $+\pi/2$.

Let us extend the normal to the galaxy plane passing through the origin of equatorial system. For an inclination angle, i, there will be two possible normals N_1 and N_2, and hence two possible positions of the galaxy rotation axis. The angular momentum vector is situated along one of these two normals. Let us consider N_1 and N_2 as the galaxy angular momentum vectors. It is seen from the Figure 10a that there are other two spin vectors N_3 and N_4 oriented just opposite to N_1 and N_2. N_1 and N_3 can be identified as one rotation axis whereas N_2 and N_4 as second rotation axis. So the ambiguity of four solutions for the spin vectors can be reduced to an ambiguity of two solutions. Therefore, just N_1 and N_2 are used for the statistical investigation.

The vectors N_1 and N_2 in the E system are

$$\begin{aligned} N_1 &= -W \cos i + \sin i (V \cos q + U \sin q) \\ N_2 &= -W \cos i - \sin i (V \cos q + U \sin q) \end{aligned} \tag{2.39}$$

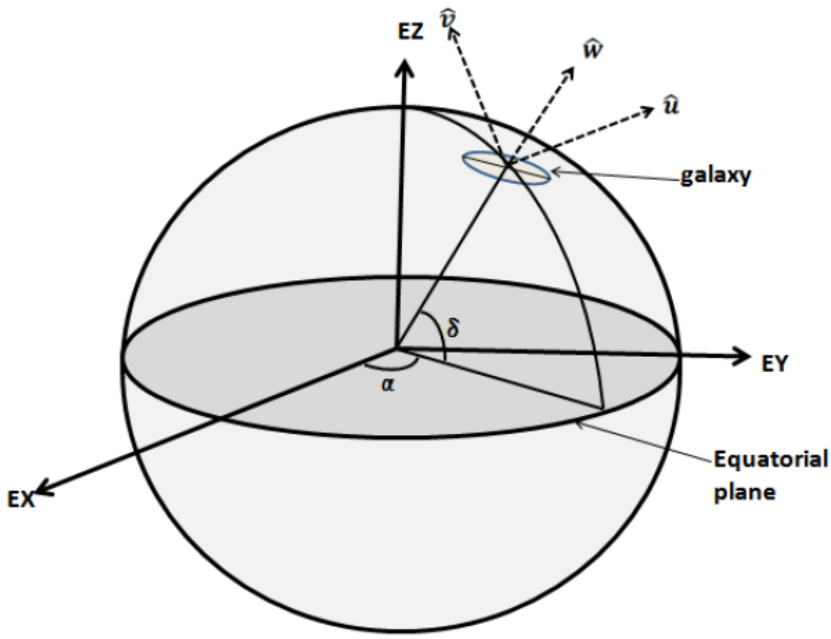

Figure 9: The coordinate system used for the derivation of the angular momentum vectors of the galaxy and its projection. Here α and δ represent right ascension and declination of the galaxy. (Kausch et al., 2004)

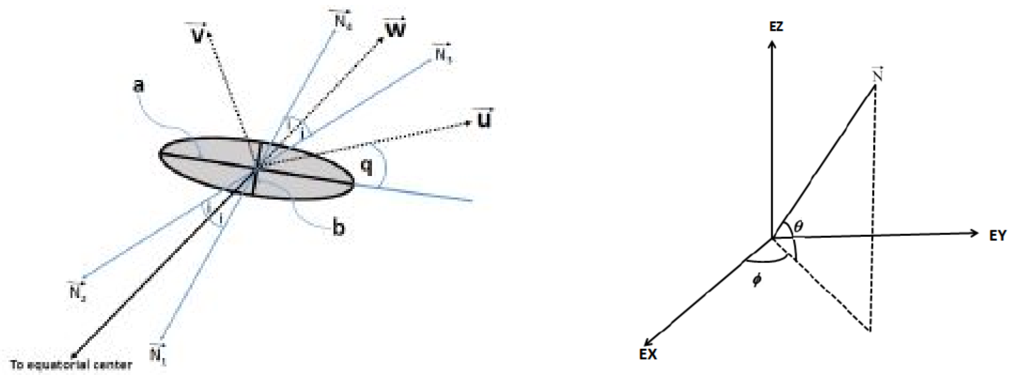

Figure 10: (a) Axial ratios and rotation axes of the galaxy: a and b are the major and the minor axes, $q = p - \pi/2$, N_1 and N_2 corresponds to the two possible rotation axes. (b) The polar and azimuthal angles (θ and ϕ) with respect to the equatorial coordinate system. (Kausch et al., 2004)

Where, $\cos i$ is given by Holmberg (1946) with the flatness factor $q*$ and is

$$\cos^2 i = \frac{[(b/a)^2 - (q*)^2]}{1 - (q*)^2} \tag{2.40}$$

and $(V \cos q + U \sin q)$ is the projection of the normals to the U-V plane. Now we apply the method of coordinate translation here. The galaxy related reference frame is translated to the center of the E system. This translation allows us to express the coordinates U, V and W in the E system. In the E system, these coordinates are the functions of right ascension (α) and declination (δ) only and they can be written as follows:

$$
\begin{aligned}
U &= (-\sin\alpha\ \cos\alpha, 0) \\
V &= (-\sin\delta\cos\alpha, \cos\delta\sin\alpha, \cos\delta) \\
W &= (\cos\delta\cos\alpha, \cos\delta\sin\alpha, \sin\delta)
\end{aligned}
\tag{2.41}
$$

here, $-\sin\alpha$, $\cos\alpha$ and 0 are the functions of the vector U along X, Y and Z axes, respectively. Similarly, $-\sin\delta\cos\alpha$, $-\sin\delta\sin\alpha$, $\cos\delta$ and $\cos\delta\cos\alpha$, $\cos\delta\sin\alpha$, $\sin\delta$ are the functions of the vectors V and W along X, Y and Z directions, respectively.

Substituting the values of U, V and W from equation (2.41) in (2.39) we get,

$$
\begin{aligned}
N_{ix} &= -\cos i\cos\delta\cos\alpha + \sin i(\mp\cos q\sin\delta\cos\alpha \mp \sin q\sin\alpha); \\
N_{iy} &= -\cos i\cos\delta\sin\alpha + \sin i(\mp\cos q\sin\delta\sin\alpha \pm \sin q\cos\alpha); \\
N_{iz} &= -\cos i\cos\delta \pm \sin i\cos q\cos\delta;
\end{aligned}
\tag{2.42}
$$

where the upper and lower signs are for $i = 1$ and 2, respectively. Now we introduce two angles: polar (θ) and azimuthal angle (ϕ) of galaxy rotation axis. The polar angle (θ), is the angle between the N_i vector and the galactic plane. The angle between the X-axis and the projection of the N_i vector on the galactic plane is termed as the azimuthal angle (ϕ). It should be noted that the reversal of the vectors N_1 and N_2 transforms the θ and ϕ values into $-\theta$ and $\phi + \pi$, respectively. From Figure 10b, we can write,

$$
\begin{aligned}
N_{ix} &= \cos\theta\cos\phi; \\
N_{iy} &= \cos\theta\sin\phi; \\
N_{iz} &= \sin\theta.
\end{aligned}
\tag{2.43}
$$

Comparing the equations (2.42) and (2.43) gives,

$$
\begin{aligned}
\sin\theta &= -\cos i\sin\delta \pm \sin i\cos q\cos\delta; \\
\sin\phi &= \frac{-\cos i\cos\delta\sin\alpha + \sin i(\mp\cos q\sin\delta\sin\alpha \pm \sin q\cos\alpha)}{\cos\theta}; \\
\cos\phi &= \frac{-\cos i\cos b\cos\alpha + \sin i(\mp\cos q\sin\delta\cos\alpha \mp \sin q\sin\alpha)}{\cos\theta}.
\end{aligned}
\tag{2.44}
$$

Substituting $q = p - \pi/2$ in equation (2.44),

$$
\begin{aligned}
\sin\theta &= -\cos i\sin\delta \pm \sin i\sin p\cos\delta; \\
\sin\phi &= \frac{-\cos i\cos\delta\sin\alpha + \sin i(\mp\sin p\sin\delta\sin\alpha \mp \cos p\cos\alpha)}{\cos\theta}; \\
\cos\phi &= \frac{-\cos i\cos\delta\cos\alpha + \sin i(\mp\sin p\sin\delta\cos\alpha \pm \cos p\sin\alpha)}{\cos\theta}.
\end{aligned}
\tag{2.45}
$$

Using equation (2.44), the spin vector orientation of a galaxy can be derived. These equations (2.42) and (2.43) derived above are called ‘Godlowski-Transformation’ or ‘Godlowskian Model’(Flin & Godlowski, 1986). In the equation (2.44) the position parameters are equatorial system parameters. Expressions (2.44) and (2.45) give two solutions for both θ and ϕ for a given value of i. Hence, 4 solutions are obtained for the angular momentum vector of the galaxy. However, for a large sample of galaxies it is hardly possible to determine - for each galaxy - which one is the physical correct one. We count each of these possibilities independently for statistical analysis. The expressions (2.44) and (2.45) give single solution for both θ and ϕ when a galaxy is seen exactly face-on ($i = 0°$). When seen edge-on ($i = 90°$), the two solutions for both and differ just in sign. In the case of θ, both solutions converge when approaching the equatorial pole or for galaxies with equatorial PA = 0°. In the case of ϕ, both solutions just differ in sign for $\alpha = 0°$. More interestingly, the characteristics of the solutions for and are also strongly influenced by the used coordinate system. This was already noted by Flin & Godlowski (1986). These authors suggested an analytical method to remove these selection effects due to positions.

2.7 Galaxy Evolution Models

Galaxy evolution process concerned with the formation of the heterogeneous Universe from the homogeneous beginning. Galaxy formation and evolution is the process that have generated variety of structures over time. It is driven by the dynamical process including mergers, tidal interactions and instability. To study these effects cluster environment may be the useful laboratory. Galactic clusters are gravitationally bounded large-scale structure of the multiple galaxies.

The evolution of these aggregates is determined by time and manner of formation and the process of how their structures and constituents have been changing with time. Gamow (1952) and Von Weizsäcker (1951) made it clear that the observed rotations of galaxies are important for cosmology. According to them, galaxy rotation might be a clue of physical conditions. Thus, the distribution of spatial orientations of the angular momentum vectors of galaxies to be very important.It could allow us to know the origin of angular momenta of galaxies.

The theoretical models explaining galaxy evolution are the ‘hierarchy’, the ‘primordial vorticity’,and ‘pancake’,. These three existing theories are contradictory as to their predictions are completely different from each other. A brief description of these theories are given in the next section.

2.7.1 Hierarchy Model

This model was established by Peebles in 1969 (Peebles, 1969). This model is thought of as a 'bottom-up' scenario. According to this model, the directions of angular momentum vectors of galaxies are distributed randomly. In this model, galaxies were first formed and they obtained their angular momenta by tidal force while they were gathering gravitationally to form a cluster. In the hierarchy scenario, galaxies form and grow by subsequent merging of proto-galactic condensations or even by merging of already fully formed galaxies. In this scheme, one could imagine that the large irregularities like galaxies grew under the influence of gravities from small imperfection in the early Universe. The angular momentum is transferred to a developing proto-galaxy by the gravitational interaction of the quadrupole moment of the system with the help of tidal field of matter. Peebles (1969) assumed that the torque experienced by a young galaxy is the product of its quadrupole moment and the tidal field due to other galaxies.

To find quadrupole moment of a young galaxy, a homogeneous ellipsoid of revolution model is taken into consideration. The quadrupole moment is given by Peebles (1969),

$$Q = \int \rho(3z^2 - r^2)d^3r \tag{2.46}$$

Where, ρ represent volume charge density, z and r position of field point and position of source point, respectively.

Let us consider another neighbor galaxy having M, is at a distance r away in a direction θ relative to the z-axis. The magnitude of the torque exerted by the tidal field of this galaxy is given by,

$$\tau = \frac{3}{4}\frac{GMQ}{r^3}\sin 2\theta \tag{2.47}$$

Now ensemble average value is determined by considering point masses and two-point distribution function. The expression for the mean square torque takes this form,

$$\langle\tau^2\rangle = \left(\frac{3}{4}GMQ\right)^2 \int P(r)d^3r\frac{\sin^2 2\theta}{r^6} \tag{2.48}$$

Here, $P(r)$ is the two-point distribution function which gives the probability that a galaxy is at $r_0 + r$, given that a galaxy is at r_0 is position of reference point. Peebles (1969), approximate P as zero inside an excluded separation distance D and constant separation outside. The radius of the volume belonging to each galaxy is found to be,

$$D \sim \left(\frac{3M}{4\pi\rho}\right)^{1/3} \tag{2.49}$$

Therefore, the ensemble average of torque is given by,

$$\langle \tau^2 \rangle^{1/2} = \left(\frac{2\pi}{5}\right)^{1/2} \frac{GMQ}{D^{3/2}} \left(\frac{\rho}{M}\right)^{1/2} = \frac{1}{3}\left(\frac{2}{15}\right)^{1/2} \frac{Q}{t^2} \tag{2.50}$$

where, $t^2 = 2R^3/(9GM)$, A few globular clusters can be disrupted because of tidal interactions between merging fragments. In the hierarchical merger model, the disrupted systems would have led to the present distribution of halo stars throughout the spheroid. It can be expected that there is no net rotation of object in the halo because of many random mergers. In addition, this model predicts that a few proto-galactic fragments should still be out there. A significant number of small galaxies orbiting the Milky way and near by Andromeda are possibly the examples.

2.7.2 Primordial Vorticity Theory

The primordial vorticity theory was proposed by Ozernoy (1974), Ozernoy (1978) and Stein (1974). This theory predicts that the angular momentum vectors of galaxies are distributed primarily perpendicular to the cluster plane. This model is called 'top-down' scenario and also called turbulence model. In this model, first flattened rotating proto-clusters formed due to cosmic vorticity in the early universe. Subsequent density and pressure fluctuations caused galaxies to form. The idea that galaxy formation is initiated by primordial turbulence has a long history Von Weizsäcker (1951);Gamow (1952).

Ozernoy (1978) proposes that galaxies form from high-density regions behind the shocks produced by turbulence. This theory predicts that the presence of large chaotic velocities generates turbulence, which, in turn, produces density and pressure fluctuations.

According to Stein (1974), Density fluctuations on the scale of clusters of galaxies could be gravitationally bound, but galactic mass fluctuations are always unbound. Galaxies form when unbound galactic mass eddies, expanding faster than their bound cluster background. So forming galaxies collide with each other as clusters start to recollapse. These collisions produce shocks and high-density proto-galaxies at the eddy interfaces. As clusters recollapse, the system of galaxies undergoes a violent collective relaxation.

2.7.3 Pancake Model

The pancake model of the galaxy evolution was first introduced by Zel'Dovich (1970) later extended by Doroshkevich (1973) and Doroshkevich & Shandarin (1978), which predicts that the angular momentum vectors of galaxies tend to lie within the cluster plane. This model is also called a 'top down' scenario. In this scenario, the formation of clusters took place first and it was followed by their fragmentation into galaxies due to adiabatic fluctuations. The non-linear gravitational instability theory Zel'Dovich (1970); Doroshkevich et al. (1974);Doroshkevich et al. (1976);Zeldovich & Novikov (1983), explain that the growth of small inhomogeneities in the early Universe causes the formation of thin, dense, and gaseous condensations that are called 'pancakes'. These condensations then compressed down and heated to high temperatures by shock waves causing them to quickly fragment into gas clouds and continuous clumping of these clouds lead to the formation of galaxies and their clusters.

Thermal, hydrodynamic, and gravitational instabilities arise during the course of evolution. It leads to the fragmentation of gaseous proto-clusters and, subsequently, clustering of galaxies takes place. The pancake scheme follows three simultaneous processes: first, gas cools and new clouds of cold gas form; secondly, these clouds cluster to form galaxies; and thirdly, the forming galaxies and, to an extent, single clouds cluster together to form a cluster of galaxies.

2.8 Spatial Orientation of Galaxies: Literature Review

A method for studying the galaxy orientation was proposed by Hawley & Peebles (1975). In their method, the observed position angles (hereafter PAs) and axial ratio distributions are analyzed independently. They also introduced the Fourier method of analyzing PA histograms. Jaaniste & Saar (1978) was proposed second approach in which another important parameter, the galactic plane inclination to the observer's line-of-sight, was also taken into the consideration.

Later, Flin & Godlowski (1986) corrected the inconsistencies in the Jaaniste & Saar (1978) approach in the name of position angle - inclination method. In this method two dimensional information is used to generate the full three dimensional information about the galaxy orientation. Aryal et al. (2001) developed a method to minimize the selection effect using numerical simulation. These days study of galaxy orientation is based on position angle−inclination method along with numerical simulation.

2.8.1 Two Dimensional Study: Between 1975 - 1985

The summary of the results that were published from 1975-1985 is presented in tabular form (Table 1) in which the two-dimensional study of the orientation of galaxies was carried out. The database is listed in the first column. The general results are explained in the second column and the last column, followed by references.

The pancake theory rose in popularity during the 1970s. Authors were expecting to observe strong alignments in the clusters.

(i) Hawley & Peebles (1975) observed position angles and axial ratio distributions are analysed independently. They also presented position angle distributions in 5 559 galaxies within the direction of Coma and Virgo cluster. No significant alignment effects were noticed.

(ii) Thompson's (Thompson, 1976) research into the galaxy orientations in eight Abell clusters was published. In the PA distribution, he found preferred alignment in the only cluster (Abell 2199). He also noticed a tendency for galaxies in Coma to point towards the cluster center. This result contradicts the result of Hawley & Peebles (Hawley & Peebles, 1975).

(iii) Macgillivary (MacGillivray et al. (1982); (MacGillivray & Dodd, 1985)) investigated several groups and clusters and found a weak tendency of galaxies to be aligned with, or perpendicular to, their radius vectors to the cluster or group centre. Their result for the Coma cluster was the same as the Thompson's result.

(iv) Djorgovski (1983) analysed their data and observed very prominent alignment effects. He found that galaxies tend to align in the east-west direction with a high degree of significance.

(v) Strom & Strom (1978) studied the Perseus-Pisces Supercluster and noticed a distinct preference of the ellipticals to align with the main cluster chain.

(vi) Gregory et al. (1981) noticed alignments and perpendicularity at a larger scale in the Perseus-Pisces Supercluster. During this time, database come from the transparent plates collected from ground based optical telescopes. The techniques of interferometry and photometry were widely used.The resolution was up to 20 mag/arcmin. This resolution was not sufficient to resolve dwarf galaxies as well as late type spirals. The error in the photometric measurement was up to 30% (Strom & Strom, 1978). Therefore, the database was dominated by either normal spirals and bright elliptical. As we know that spirals are supported by rotation where as elliptical are supported by random velocity dispersion. In any case, the net angular momentum of an isolated system (groups, clusters and Superclusters of galaxies) should vanish according to cosmological principle. These galaxies are formed because of merging and collision processes. These processes lead anisotropic in the distribution of angular momentum vectors (Peebles, 1969). Therefore most of authors have found anisotropic (non-vanishing angular momentum) result in the clusters. The database of Supercluster (LSC) galaxies was rich because of their low redshift (z<0.01). The position angle and axial ratio distribution were studied for spirals, ellipticals and irregulars. They (Helou, 1984); (Dekel, 1985) found inconsistent result in spirals and ellipticals.

Table 1: A brief description of the two-dimensional study in the field of spatial orientation of galaxies published before 1986.

Sample/Database	Result & Conclusion	Reference
Local Supercluster (LSC)	• spin vectors (SV) of local Supercluster galaxies tend to lie perpendicular to local Supercluster plane.	(Reinhardt & Roberts, 1972)
Several Clusters	• Couldn't find anything interesting	(Hawley & Peebles, 1975)
Eight Abell Clusters	• tendency for galaxies in Coma cluster to point toward the cluster center.	(Thompson, 1976)
Perseus-Pisces Supercluster	• noticed a distinct perference of the elliptical to align with the main cluster chain.	(Strom & Strom, 1978)
Several groups & Clusters	• weak tendency of galaxies to be aligned with, or perpendicular to, their radius vectors cluster.	(MacGillivray & Dodd, 1979), (MacGillivray & Dodd, 1985)
Perseus-Pisces Supercluster	• noticed alignments and perpendiculary at a large scale.	(Gregory et al., 1981)
Local Supercluster (LSC)	• tendency for galaxies to be parallel to Local Supercluster (LSC) plane with some secondary dependence on the Supergalactic latitude.	(MacGillivray et al., 1982)
6727 galaxies	• very prominent alignment effect.	(Djorgovski, 1983)
Spiral pairs in Spiral	• mutual orientations of the spin vectors in spiral pairs. • the spin vectors be antiparallel, effect was stronger for the pairs with the lower mass	(Helou, 1984)
Local Supercluster Spirals	• systematic effect in alignment and winding direction of local Supercluster spiral, the effect be strongest for intermediate types.	(MacGillivray & Dodd, 1985)

2.8.2 Three Dimensional Study: Between 1986-2003

The result of the works in which a three-dimensional analysis of galaxy orientation has been published during the period of 1986-2003 are summarized in Table 2. The nature of the database is given in the first column of the table. In the next column, the selection criteria based on the database are explained. General results and references are given in the last two columns. The spectrometric techniques and the application of charge couple device (CCD) has been extensively used in the ground based optical telescope, after 1985. Therefore, the error in the magnitude and the redshift has been significantly decreased. However, resolution was not significantly increased. It means the quality of photometric database (axial ratio, position angle, etc.) was moderately improved. For the high redshift galaxies, the information regarding morphology and magnitude was rather poor. However, the population of galaxies has been significantly increased. It can be seen in the Table 2 that the most of the results suggest anisotropy in the distribution of angular momentum vectors in the cluster. In other words, it is found that the net angular momentum of galaxies in the groups and clusters is non-vanishing, supporting either Pancake (Doroshkevich, 1973) or primordial vorticity theory (Ozernoy, 1978); (Stein, 1974). For the local Supercluter galaxies, most of the author (see Table 2) found to support pancake model. Because of this result, pancake model was becoming popular even in cosmology. The major achievement of this period is the realization of a three-dimensional parameter, called inclination angle, the angle between line-of-sight and the normal to the galaxy. The technique for calculating inclination angle was investigated using landmark experimental work of Holmberg (1946) . This method has been improved for different type of galaxies Godłowski et al. (2003).

Table 2: A brief description of published studies 1986-2003.

Database	Selection criteria	Result & conclusion	Reference
1275 LSC galaxies (UGC)	• Radial Velocity (hereafter RV) <2600 km s^{-1}	• anisotropic distribution. • SVs of galaxies tend to lie parallel to the LSC plane. • anisotropy increases as axial ratio increases. • supports pancake model.	(Flin & Godlowski, 1986)

Database	Selection criteria	Result & conclusion	Reference
618 LSC galaxies (PANBG)	• RV<3000 km s^{-1} • $-3 \leq$ • $-3 \leq$ T (morphological type index) ≤ 10	• isotropy in most cases. • noticed bimodal near LSC plane SVs distribution parallel, • Virgo cluster show anisotropic and spin vectors tend to towards Virgo cluster center • supports pancake model.	(Kashikawa & Okamura, 1992)
2227 LSC galaxies (UGC, ESO, RCGR & TNGC)	• RV < 2600 km s^{-1}	• anisotropic distribution. • SVs of galaxies tend to lie parallel to the LSC plane. • projections of SVs tend to point towards Virgo center. • supports pancake model.	(Godłowski, 1993)
2227 LSC galaxies (UGC, ESO, (UGC, ESO, RCGR & TNGC)	• RV < 2600 km s^{-1}	• anisotropic distribution. • azimuthal angle distribution strongly depends on supergalactic coordinates (L,B) and RV. • supports pancake model.	(Godłowski, 1994)
310 Virgo cluster galaxies (VCC, FGCP, UGC)	• RV<2700 km s^{-1}	• anisotropic distribution. • SVs projections of galaxies towards the Virgo center • morphological dependence. • SVs tend to perpendicular	(Hu et al., 1995)
302 Field galaxies (PANBG)	• RV < 3000 km s^{-1} • $-3 \leq T \leq 10$ • $R \geq 6^0$	• anisotropy in the azimuthal angle • projections of SVs point $\pm 30^0$ to Virgo center.	(Yuan et al., 1997)

Sample	Selection criteria	Result & conclusion	Reference
491 galaxies in field of the Abell 0754 (CUSSC)	• $b/a < 0.30$ (a & b: major and minor diameters,	• galaxy major planes be perpendicular to direction of PA of the cluster. • SVs parallel	(Godlowski et al., 1998)
18 subclusters of the LSC	• RV < 2800 km s^{-1}	• a strong systematic effect,	(Godlowski & Ostrowski, 1999)
557 galaxies of Coma Supercluster (CGCG,UGC, RC3, NED)	• 6000 ≤ RV ≤ 8000 km s^{-1} • $11^h.5 < \alpha < 13^h.5$, $18^0 < \delta < 32^0$	• anisotropic distribution. • SVs lie in plane of Supercluster. • projection of SVs towards the Supercluster	(Flin, 2001)
Cluster II Abell 14	Southern Sky Object Catalogue, 947 galaxies	evidence for non-random alignment in Abell and confirm subclustering	(Baier et al., 2003)
Coma cluster	6724 galaxies within region of about 2.6° x 2.6°	• a deviation from random orientation is noticed because of merging mutual interaction of merging galaxies	(Kitzbichler & Saurer, 2003)

2.8.3 Three Dimensional Study: Between 2004-2020

This period begins with the work of Godlowski (Flin et al., 2004) and Aryal & Saurer (2004). Their work is different from previous work because of two following aspects: (1) They identified in completeness of the database and used numerical simulations to minimize such effects. (2) They used various statistical methods including Fourier tests in which the orientation has used as third parameter which is obviously a dependent variable.

Table 3: A brief description of the study which was published during 2004 to till date.

Sample/Database	Result & Conclusion	Reference
8 Abell clusters of BM type I	• supports pancake model by 4 clusters where as Hierarchy by the rest 4 Abell clusters	(Aryal & Saurer, 2004)
Shapley Supercluster	• low radial velocity galaxies showed anisotropy	(Aryal & Saurer, 2005a)
Tully's galaxy groups	• found limiting case for vanishing and non-vanishing angular momentum of galaxies	(Godłowski et al., 2005)
7 Abell clusters of BM type II	• systematic change in the galaxy alignments from BM type I to type III is found	(Aryal et al., 2007)
10,562 galaxies in the local supercluster	• preferred alignments are noticed for two subsamples having 1500-2000 Km s^{-1} 3000-3500 Km s^{-1} radial velocities	Aryal et.al. 2010
247 optically selected rich Abell cluster having ≥100 galaxies	• dependence of alignments with respect to cluster richness is noticed	(Godłowski et al., 2010)
Galaxy groups in local Supercluster	• a random orientation of galaxies in the group is noticed	Godlowski & Flin 2010
18 Tully groups of galaxies	• orientation of galaxies in all 18 Tully groups of galaxies are found to be random	(Godlowski, 2011)
Three merging binary cluster	• A relation between stages of merging and the non-random alignments of galaxies in the Superclusters are noyiced	(Aryal et al., 2012)
1056 galaxy structures with known morphology	• significant alignment was found for elongated BM type I clusters	(Panko et al., 2013)
Six rotating cluster of galaxies	• No preferred alignment of galaxies is noticed	(Aryal et al., 2013)
377 Rich ACO galaxy Cluster with redshift< 0.2	• strong alignment is noticed for B-M type I clusters with ellipticities e>0.2	(Biernacka et al., 2015)
Six dynamically unstable Abell clusters	• Random orientation of galaxies in these cluster is noticed	(Yadav et al., 2017)
Supercluster S [202-001+0084]	• no preferred alignments of galaxies in the cluster is noticed	(Malla et al., 2019).
247 Abell rich galaxy cluster	• found preferred alignments of galaxies in the cluster • noticed morphological independence	(Pajowska et al., 2019)

2.9 Research Gap in Galaxy Orientation Study

After an extensive literature review, we noticed following research gaps in the study of preferred alignments of angular momentum of galaxies in the Superclusters and their substructures:

1. According to the cosmological principle, the directional parameters or dynamical variables (e.g., angular momentum vectors of galaxies) should be distributed isotropically at the large scale structure. Therefore, the total angular momentum vectors galaxies in the clusters or Superclusters should be zero (or vanishing angular momenta). Though, a large number of studies showed that the clusters of galaxies advocate non-vanishing angular momentum. In the case of Supercluster, only a few studies have been carried out. Therefore a study of distribution of angular momentum vectors of galaxies is important to validate the cosmological principle at the large scale structure. For a rotationally supported system (e.g., galaxies, stars, clouds, etc), the distribution of the angular momentum vectors can be an indicator of the initial conditions when these structures formed, provided the angular momentum of have not significantly changed since their formation ((Von Weizsäcker, 1951), (Gamow, 1952)). Thus, a thorough study of the spatial orientations of angular momentum vectors of galaxies in the large scale structure is needed. Sloan Dizited Sky Survey (SDSS) data provides a very accurate spectroscopic and photometric data of a large number of galaxies in the clusters and Superclusters. A systematic analysis of angular momentum of galaxies in the Superclusters would be important to understand evolution of galaxies in the large scale structure of the Universe.

2. Peebles (2019 Noble prize winner) pioneer work (1969) on angular momentum of galaxies was published in 1969 (Peebles, 1969). Since then, many researchers began working on this issue. For the last 45 years, more than 150 works on angular orientation have been published. Here we summarize a few leading works. Doroshkevich (1973) and Shandarin (1974) suggested the 'pancake model' in which they predicted that the angular momentum vectors of galaxies tend to lie within the cluster plane. Another important model, named 'primordial vorticity' (Ozernoy, 1978) advocates that the angular momentum vectors of galaxies tend to be oriented perpendicular to the cluster plane. According to the 'hierarchy model' (Peebles, 1969) the directions of the angular momentum vectors should be distributed randomly. Authors have drawn different conclusions regarding these three scenarios: (1) no preferred alignment supporting hierarchy model ((Helou & Salpeter, 1982), (Bukhari & Cram, 2003), (Aryal & Saurer, 2005a), (Aryal, Paudel, & Saurer, 2008), (Aryal et al., 2012), (Aryal et al., 2013), (Godlowski

et al., 1998) (Yadav et al., 2017), (Malla et al., 2019)), (2) tend to orient parallel ((Jaaniste & Saar, 1978), (Flin & Godlowski, 1986), (Godłowski, 1993), (Godłowski, 1994), (Godlowski et al., 1998), (Wu et al., 1998), (Flin, 2001)) or perpendicular ((Reinhardt & Roberts, 1972), (Gregory et al., 1981),(MacGillivray et al., 1982), (Baier et al., 2003)) with respect to the cluster (or LSC) plane, (3) bimodal tendency (Kashikawa & Okamura, 1992) (4) local anisotropy ((Flin, 1995), (Djorgovski, 1983),(Aryal & Saurer, 2004), (Aryal & Saurer, 2005b), (Aryal & Saurer, 2006), (Aryal & Saurer, 2006), (Aryal et al., 2013)), (5) global anisotropy (Parnovsky et al., 1994), etc. (Godlowski & Ostrowski, 1999) noticed a strong systematic effect, generated by the process of de-projection of a galactic axis from its optical image. These results suggest different alignments of galaxies in clusters and Superclusters. However, SDSS database was not available at that time and all of the above works have used photometric databases (e.g., ESO, POSS, IC, MGC, etc). It is essential to reveal the reason behind these differences. These differences might be correct or need revision. We plan to work on an SDSS database using both photometric and spectroscopic parameters of Supercluster galaxies.

3. The Local Supercluster (LSC hereafter) is the nearby Supercluster of galaxies that have mean radial velocity less than 3000 km/s galaxies. Godłowski (1993) analysed the orientations of 2227 LSC galaxies and concluded anisotropic distributions. (Godłowski, 1994) studied the dependence of galaxy alignment on radial velocity (RV) of 2227 galaxies in the Local Supercluster (LSC) and found anisotropy for the galaxies that have RVs 1000 km sto 1500 km/s. He concluded the dominance of Virgo cluster galaxies in this bin. (Aryal et al., 2010) studied preferred alignments of 10,562 galaxies in the LSC. This is the largest analysed database till date. They concluded that the galaxies having low radial velocities (less than 800 km/s) showed a preference in the alignments. In the present work, we intend to go deep in the sky (higher redshift than LSC galaxies) to study the preferred alignments of galaxies in the distant Superclusters and compare it with the LSC galaxies. Fortunately the SDSS database provides such a rare opportunity these days.

4. Aryal & Saurer ((Aryal & Saurer, 2004),(Aryal & Saurer, 2005a), (Aryal & Saurer, 2006)) and (Aryal et al., 2007) analysed the spatial orientations of galaxies in 32 Abell clusters of BM type I, II, II-III and III (Bautz & Morgan, 1970) using Palomar Sky Survey database. BM classification is actually morphological classification of galaxy clusters: BM type I refers to regular clusters with dominating central galaxy, BM type II are those clusters which have more or less similar photometric galaxies with any to-be-regular shape, BM type II corresponds to those aggregates of galaxies which are irregularly shaped having more late-type

spirals, can be L-type or even more complex. They noticed a systematic change in the galaxy alignments from early-type (BM I) to late-type (BM III) clusters. This result suggests that the spiral-rich (late-type) clusters (BM II-III and BM III) show a preferred alignment than that of elliptical-rich (early-type) clusters. Supercluster contain various substructures. These substructures are similar to clusters of galaxies in many respects. We are interested to study preferred alignments in those substructures of Superclusters and compare it with the alignments of Abell clusters of galaxies.

5. Liivamägi et al. (2012) compiled a set of Supercluster catalogues for the galaxies using SDSS survey main and luminous red galaxy (LRG) flux-limited samples. They calculated luminosity density fields using the B3-spline kernel of the radius of 8 Mpc/h for the main sample and 16 Mpc/h for the LRG sample and define regions with densities over a selected threshold as Superclusters. They created two types of catalogues, one with an adaptive local threshold and a set of catalogues with different global thresholds. They described the Supercluster catalogues and their general properties. Using smoothed bootstrap, they found uncertainty estimates for the density field and used these to attribute confidence levels to the catalogue objects. They have also created a test catalogue for the galaxies from the Millennium simulation to compare the simulated and observed Superclusters and to clarify the methods we use. Finally they find that the Superclusters are well-defined systems, and the properties of the Superclusters of the main and LRG samples are similar. We also show that with adaptive local thresholds we get a sample of Superclusters, the properties of which do not depend on their distance from the observer. We are very much interested in compiling a database of at least six Superclusters and finding substructures within those aggregates.

6. Einasto et al. (2011) studies the morphology of a set of Superclusters drawn from the SDSS DR7. We calculate the luminosity density field to determine Superclusters from a flux-limited sample of galaxies from SDSS DR7, and select Superclusters with 300 and more galaxies for our study. The morphology of Superclusters is described with the fourth Minkowski functional V3, the morphological signature (the curve in the shapender's K1-K2 plane) and the shape parameter (the ratio of the shapenders K1/K2). We investigate the Supercluster sample using multidimensional normal mixture modelling, and use Abell clusters to identify our superclusters with known Superclusters and to study the large-scale distribution of Superclusters. The superclusters in our sample form three chains of Superclusters; one of them is the Sloan Great Wall. Most Superclusters have lament-like overall shapes. Superclusters can be divided into two sets; more elongated Superclusters are more luminous, richer, have larger diameters, and a

more complex structure than less elongated Superclusters. Superclusters can be divided into four main morphological types: spiders, multispiders, laments, and multibranching laments. They presented the 2D and 3D distribution of galaxies and rich groups, the fourth Minkowski functional, and the morphological signature for all Superclusters. Widely different morphologies of Superclusters show that their evolution has been dissimilar. It is therefore we hypothesize that the preferred alignments of angular momentum of galaxies in isolated and connected Superclusters might be different if their evolution is dissimilar. Therefore it is essential to carry out study on all four morphological type Superclusters. We plan to do this in the present work.

7. A complete photometric data gives valuable information regarding galaxy information. The SDSS survey uses ultraviolet to far-infrared CCD filters in almost all redshift limits. A strong emission through ultraviolet filter suggests the star formation rate might be halted or slowed down in these galaxies because of the collision within the groups, subclusters, clusters or Superclusters. Similarly, a strong emission through infrared filter suggests a rapid star formation rate in these galaxies. It is believed that the slow star formation rate indicates the possibility of anisotropy (preferred orienting angle might be distorted due to collision or merging) and the rapid star formation rate slows down the angular momentum of the system, leading to a non-vanishing angular momentum. We intend to use a huge database of both low (< 0.1) and high (> 0.5) redshifted galaxies in both the ultraviolet and infrared filters in order to study the above mentioned effects.

8. In every database there are limitations, called selection effects. Selection effects may play an important role when galaxies are distant. The SDSS database has this effect because it is a ground based telescope located in the northern hemisphere (New Mexico, USA) of our planet. These effects can lead to artificial structures (Aryal et al., 2001). In most of the published works in galaxy orientation studies, selections of various kinds can be seen. These are mainly due to the face-on galaxies and inhomogeneity in positions. Only a few authors have made an attempt to minimize these effects (Hu et al., 2002), (Godłowski & Flin, 2009)). It is essential to remove such effects to avoid misinterpretations in the results. We intend to work on the removal of such effects by performing numerical simulation in all sorts of databases.

9. Godlowski et al. (2011) studied orientations of galaxies in 18 Tully's group of galaxies. These groups are gravitationally bound. Therefore it has been assumed that these groups might be responsible for the formation of clusters of galaxies. Godlowski et al. (Godlowski et al., 2011) found that these groups show vanishing angular momenta. Panko (Panko, 2013) studied spatial orientation of galaxies

in 247 Abell clusters of galaxies. They noticed preferred alignments, opposite results than that of the (Godlowski et al., 2011). We think that the evolution of Tully's group of galaxies and Abell clusters might be different. We intend to find out the reason behind these two contradictory results by studying preferred alignments of galaxies in Superclusters and their substructures.

10. Pajowska et al. (2019) found preferred alignments of galaxies in clusters when studying rich clusters of galaxies. In addition, they noticed morphological independence. In this paper, the crucial problem during analysis of the angles giving spatial orientation of galaxies is that if for any reason we exclude from analysis any type of galaxies (for example face-on galaxies), then the theoretical distribution of analyzed angles will be modified, even in the case when the distribution of galaxy planes is random and isotropic. In this case, a random distribution of analyzed angles which is the base of comparison with the real one must be, in practice, obtained from numerical simulations (Aryal & Saurer, 2000). In this work, we want to remove such problems by performing numerical simulation for each and every case of Superclusters and their substructures.

2.10 Objectives

The general and specific objectives of this study are given below.

2.10.1 General Objective

We aim to study preferred alignments of angular momentum of galaxies in the Supercluster and their substructures by calculating rotation axes and simulating it to satisfy cosmological principle regarding large scale structure evolution.

2.10.2 Specific Objectives

Our specific objectives are as follows:

(1) We have planned to work on SDSS (Sloan Digital Sky Survey) database of six Supercluster galaxies of which angular momentum vectors and its projections are calculated to identify preferred alignments of galaxies in the Superclusters and substructures.

(2) We aim to identify substructures in the Supercluster region using redshifts of each individual galaxies and develop empirical relations between mean redshift and number density of galaxies.

(3) We are interested to study u-magnitude and r-magnitude distributions and hence to find empirical relations between color-magnitude for all six Superclusters using SDSS database of photometry.

CHAPTER 3

3. MATERIALS AND METHODS

3.1 Selection Effect in the Database

Aryal & Saurer (2000) studied the database used by previous authors (Flin & Godlowski, 1986); (Kashikawa & Okamura, 1992); (Hu, 1999); (Yuan et al., 1997); (Ensslin et al., 1997) in their studies. They found a systematic effect in the database and realized that these effects should be removed from the database in order to avoid misinterpretations in the expected or theoretical distribution for polar and azimuthal angles of galaxies.

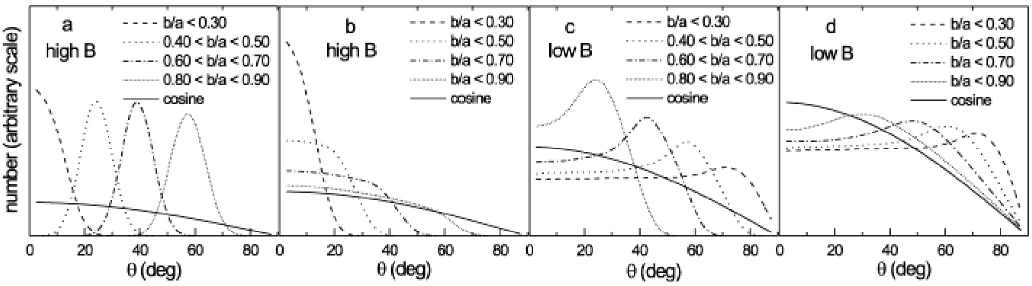

Figure 11: The expected isotropic distribution curves of the polar angle (here Θ) for different selections on supergalactic latitude (B) and axial ratios (b/a) (Aryal & Saurer, 2000).

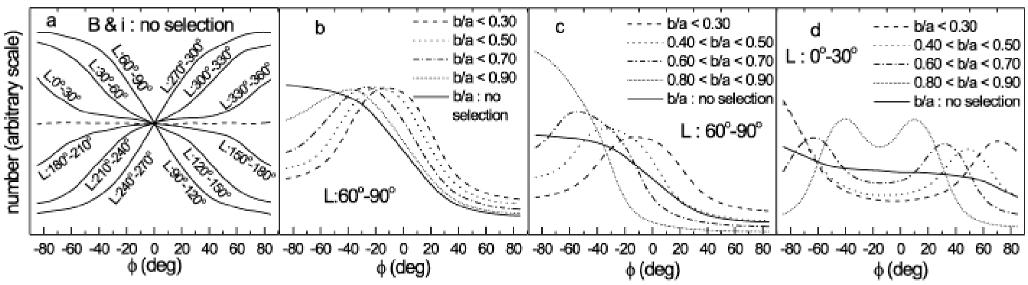

Figure 12: The expected isotropic distribution of azimuthal angle (here ϕ) for different selections on supergalactic longitudes (L) and axial ratios (b/a) (Aryal & Saurer, 2000).

Aryal & Saurer (2000) found that selection effects concerning position and inclination angles of galaxies result a prominent change in the shape of the distributions of polar and azimuthal angles of galaxies in a cluster. The role of selection effects of this kind may be more significant when galaxies are taken from an incomplete dataset (e.g., from a limited region of sky). Due to these effects, artificial structures of the distributions are obtained which in turn lead to misinterpretation of results based upon them. In this paper Aryal & Saurer (2000) discuss various possible effects due to the selection in the database. They have shown that nature of the expected isotropic curve changes severely when selection criteria are imposed on the dataset. They found that the isotropic distribution curve remains *cosine* for polar angle and a straight line for azimuthal angle(as previously adopted) only when there is no selection on L, B, P and i. The analytical method of Flin & Godlowski (1986) can be used only, when there is no selection in i. In the following points Aryal & Saurer (2000) summarize how selection effects change the shape of the isotropic distributions:

- The isotropic polar angle distribution is independent of L but changes with B when making selection on i.
- The isotropic distribution for polar angle is independent of B and L only when the range of i is full (i.e. no selections made); this distribution is independent of i, if there are no selection on positions.
- The azimuthal angle distribution is independent of the range of B, provided the range of i is full. It changes with L even when range of B and i is full.
- The isotropic polar angle distribution is different for edge on and face- on galaxies when making selection on B. However, the isotropic azimuthal angle distribution remains unchanged for face-on and edge-on galaxies when the range of L is full.

Here a list publications (Table 4) in which author's have used the method proposed by Aryal & Saurer (2000) is shown.

Table 4: Authors used numerical simulation method. The first column gives list of published papers in which authors have used the method proposed by Aryal & Saurer (2000). The second column gives the number of virtual galaxies created in the simulation. Third column represents selection effect that was noticed in their database.

S.N.	Authors	No. of virtual galaxies	selection effect
1	(Baier et al., 2003)	10^5	inclination
2	(Aryal & Saurer, 2004)	10^5	inclination
3	(Aryal & Saurer, 2005a)	10^5	inclination & positions
4	(Hu et al., 2006)	10^6	position angle
5	(Aryal & Saurer, 2006)	10^5	inclination & positions
6	(Aryal, Paudel, & Saurer, 2008)	10^6	inclination & positions
7	(Aryal et al., 2012)	10^6	inclination
8	(Godlowski et al., 2013)	N/A	inclination
9	(Aryal et al., 2013)	10^6	inclination

S.N.	Authors	No. of virtual galaxies	selection effect
10	(Yadav et al., 2016)	10^7	inclination & positions
11	(Yadav et al., 2017)	10^7	inclination & positions
12	(Malla et al., 2019)	10^7	inclination & positions
14	(Malla et al., 2020)	10^7	inclination & positions
15	(Godlowski et al., 2018)	10^7	inclination
16	(Yadav et al., 2017)	10^7	inclination & positions

In the present work, we have extensively used the numerical simulation method to find the expected isotropic distributions for both polar and azimuthal angles.

3.2 Numerical Simulation

In the selection of position and inclination angles generated by SDSS survey, there may cause various error in the results, so as to minimize these selection effects we have to use the numerical simulation. Theoretically, the isotropic distribution curve for the polar angle is *cosine* and that for azimuthal angle is the *average* distribution curve, with the restriction that the database is free from selection effect. Any selections imposed on the database, according to Aryal & Saurer (2000), may cause severe changes in the shapes of the expected isotropic distribution curves. In their method, a true spatial distributions of the galaxy rotation axis is supposed to be isotropic. Then, due to the projection effects, i can be distributed $\propto$ sin i, δ can be distributed $\propto$ cos δ, the variables α and p can be distributed randomly, and the equation (2.45) can be used to calculate the corresponding values of polar angle (θ) and azimuthal angle (ϕ). We run simulations to determine expected isotropic distribution curves for both the θ- and ϕ-distributions. The isotropic distribution curves are based on simulations generating 10^7 virtual galaxies.

The procedure for removing selection effects to obtain the isotropic distributions for both θ and ϕ as given by Aryal & Saurer (2000) is described here. We present the process of numerical simulation for the sample $S[195 + 027 + 0022]$ (a sample described in the chapter 4.1.4).

At first, we studied the of right ascension (α), declination (δ), position angle (P) and inclination angle (i) distributions for the galaxies in the sample $[195 + 027 + 0022]$. The distributions of α, δ, P and i for the galaxies in the sample $S[195 + 027 + 0022]$ are shown in Fig. 13. The histograms represent the number of observed galaxies.

Table 5 shows right ascension (α) and declination (δ) of galaxies in the sample S [195+027+0022]. The value of α and the observed number of galaxies are shown in the first two columns, respectively. The last column shows the corresponding number of virtual galaxies created for the simulation. The total number of virtual galaxy is 10^7 in

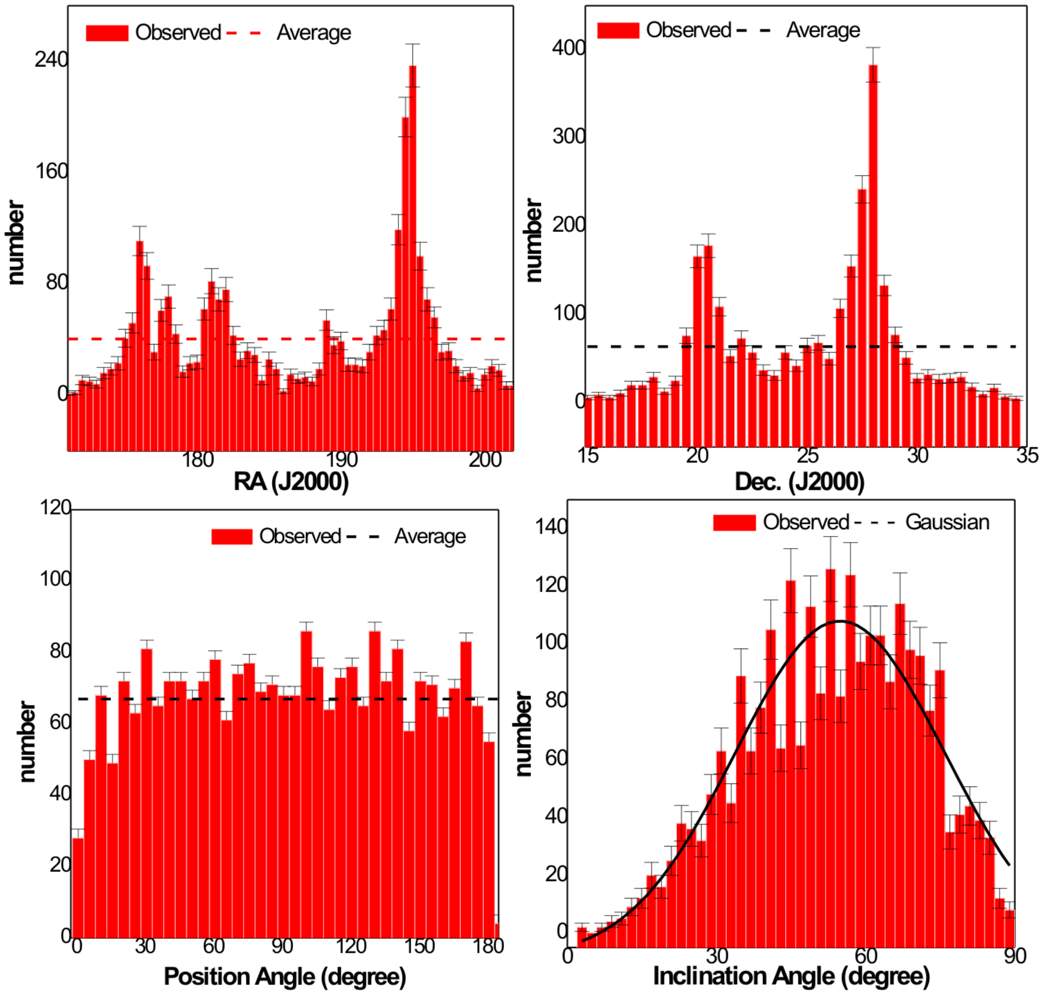

Figure 13: The distributions of right ascension (α), declination (δ), position angle (P) and inclination angle (i) of the galaxies in the Supercluster S[195+027+0022] (described in the chapter 4.1.4). The Y-axes of histograms represent the number of observed galaxies.

the simulation. These numbers are used to make input file for the simulation.

Similarly, Table 6 shows the distributions of position angle (P) and inclination angle (i) for the galaxies in the sample S [195+027+0022], respectively.

Table 5: Distributions of right ascension (α/step size = 1.0°) and the declination (δ/step size = 0.5°) of galaxies in Supercluster $S[195 + 027 + 0022]$ (a Supercluster described in the chapter 4.1.4). The distributions of right ascension and declination of galaxies are shown in Figure 13a and 13b. There distributions are found to be inhomogeneous. Here N and N' represent the observed (real) number and the corresponding virtual (generated) numbers of galaxies in the Supercluster. The total number of virtual galaxy is 10^7 in the simulation.

α	N	N'	δ	N	N'
171.5	31	238095	7.25	57	438461
172.5	138	1059908	7.75	86	661538
173.5	202	1551459	8.25	52	400000
174.5	154	1182796	8.75	20	153846
175.5	286	2196620	9.25	13	100000
176.5	151	1159754	9.75	16	123077
177.5	203	1559140	10.25	20	153846
178.5	93	714286	10.75	49	376923
179.5	33	253456	11.25	82	630769
180.5	11	84485	11.75	79	607692
			12.25	103	792308
			12.75	173	1330769
			13.25	103	792308
			13.75	112	861538
			14.25	110	846154
			14.75	73	561538
			15.25	44	338461
			15.75	29	223077
			16.25	29	223077
			16.75	32	246154
1760	1302	10^7	240	1280	10^7

Table 6: Distributions of the position angle (P/step size = 10°) and the inclination angle (i/step size = 5°) of galaxies in Supercluster $S[195 + 027 + 0022]$ (a Supercluster described in the chapter 4.1.4). The distributions of position angles and inclination angle of galaxies are shown in the Figure 13c and 13d. These distributions are found to be deviated from the expected distribution (homogeneous and cosine) Here N and N' represent the observed (real) number and the corresponding virtual (created) numbers of galaxies in the Supercluster. The total number of virtual galaxy is 10^7 in the simulation.

P	N	N'	i	N	N'
5	70	543478	2.5	7	54517
15	66	512422	7.5	3	23364
25	70	543478	12.5	11	85670
35	63	489130	17.5	23	179128
45	70	543478	22.5	49	381620
55	66	512422	27.5	65	506230
65	67	520186	32.5	86	669790
75	79	613354	37.5	113	880062
85	92	714286	42.5	115	895639
95	91	706522	47.5	141	1098131
105	94	729814	52.5	122	950156
115	80	621118	57.5	135	1051402
125	96	745343	62.5	142	1105919
135	75	582298	67.5	87	677570
145	52	403727	72.5	94	732087
155	54	419255	77.5	61	475078
165	59	458074	82.5	23	179128
175	44	3416140	87.5	7	54517
1620	1288	10^7	810	1284	10^7

The right ascension is randomly distributed between 0° to 360° in 10 bins keeping the bin size 1°. The number of bin size has been fixed by using minimum standard error propagation method (Table 6). The declination δ is randomly distributed in the range 7.25° to 17.25° in 21 bins of size 0.5° (Fig.13b). The distribution of the position angle P in the range 0° to 180° in 18 bins of bin size 10° (Fig.13c) is quite homogeneous. There is a inhomogeneous distribution of the inclination angle i in the range 0° to 90° (Table 6), therefore distributed in 18 bins of size 5°.

3.2.1 Program and Input Files for Galaxy orientation Study

Matlab 7.0.1 is used to write programme and input files for the simulation. As an example, we give program and input file for the galaxies of sample S [195+027+0022] (a sample described in the chapter 4.1.4). The program and input files is in Appendix D.

3.3 Number Density Map

Figure 14 shows number density map of galaxies in the Supercluster S[195+027+0022]. In the Figure, number density map for the nearest neighbour galaxies at the distance (or radius) r=1.0° is shown. In other words, we have find out the number of galaxies from each individual galaxies within a radius of 1.0° from that galaxy. For we have written a program in MATLAB 7.0.1 named 'galaxy counting code' (given in Appendix D).

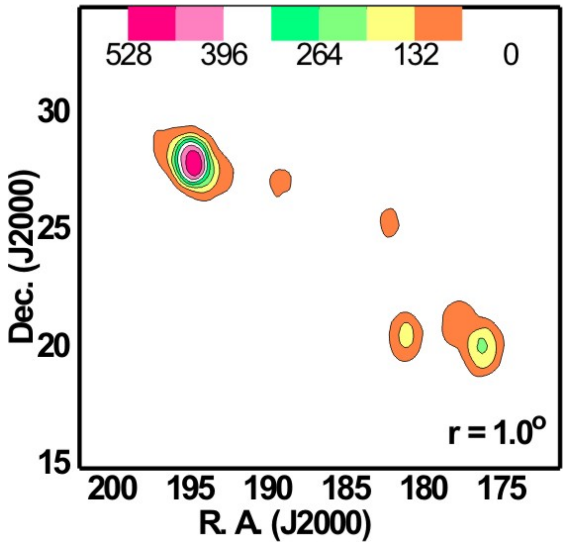

Figure 14: Number density map of galaxies in the Supercluster S[195+027+0022] having nearest neighbour distance r=1.0°. Here color bars are shown.

The contour levels are shown in the color bars. Here the pink color indicates high density of galaxies where as orange color shows low density of galaxies. In Figure 14, one dense substructure at ~193° RA (J2000) can be seen. In addition, there is another substructure can be seen at ~176° RA (J2000). We varied radius from 0.1° to 1.5° to observe the varing nature of substructures in the result and discussion chapter.

3.4 Redshift Map

Figure 15 shows redshift map of galaxies in the Supercluster that have mean redshift 0.023. The color map shows that the velocity dispersion is minimum in the region where number density of galaxy is minimum.

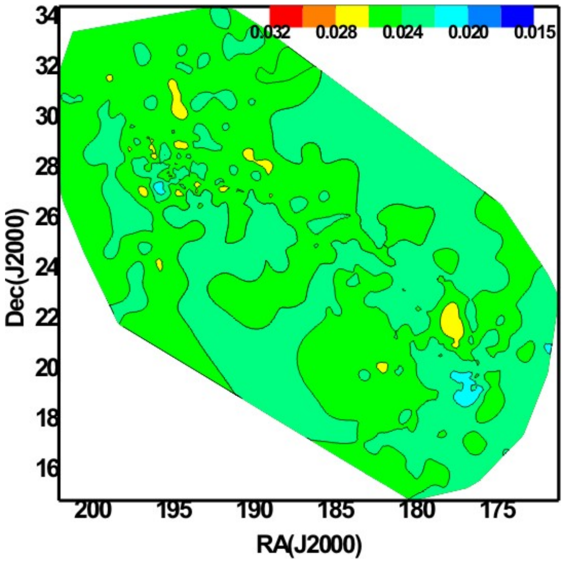

Figure 15: Redshift map of shown for the galaxies in the Supercluster S[195+027+0022]. The color bars for redshift is shown. The yellow region is the region of high redshifted galaxies sky blue region consists low redsifted galaxies in this Supercluster.

Figure 15 shows that the galaxies with high redshift is not centrally located. They are located along the major diameter of the Supercluster. We will study redshift distribution of galaxies in the substructures of each Supercluster in the result and discussion chapter.

3.5 Magnitude Map

Figure 16 shows magnitude map of galaxies in the Supercluster S[195+027+0022]. The SDSS r-magnitude refers to the peak wavelength 6165 Å with the bandwidth 1380 Å, where as the u-magnitude corresponds to the wavelength of 3551Å with the bandwidth 81.673Å. In the result and discussion section, we discuss the magnitude distributions in

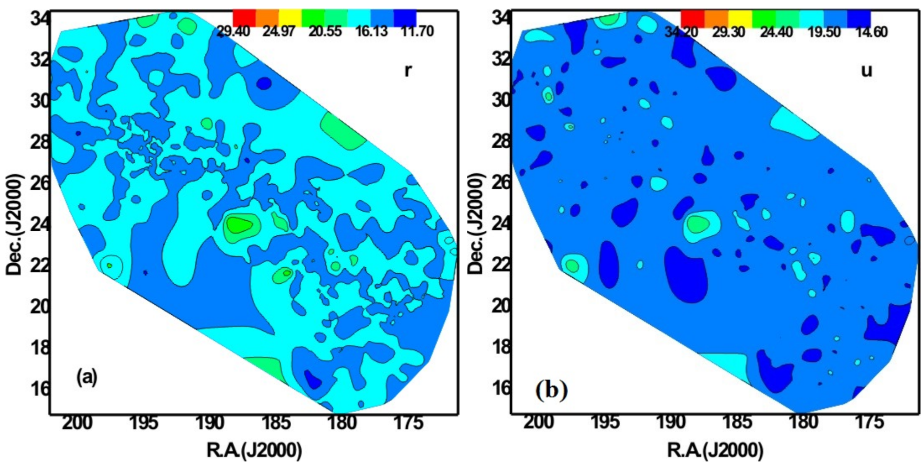

Figure 16: Magnitude maps of galaxies in the Supercluster S[195+027+0022]: (a) r-magnitude, (b) u-magnitude. The colors bar are shown.

the context of spatial orientation of galaxies.

3.6 Statistical Tests

When looking at pictures of galaxy clusters, there is no obvious alignment. Therefore, to check preferred alignments, statistical analysis is needed. In this work, we used the Fourier tests, auto-correlation and the chi-square. The investigation of galaxies alignments is carried out using statistical tests of the θ and ϕ-distributions resulting from the Godlowskian transformation. The computer program used in these statistical computations were MICROSOFT EXCEL 2007, ORIGIN5.0 and ORIGINE8.0.

3.6.1 Fourier Test

The infinite series of *sines* and *cosines* which describe periodic functions whether it is continuous or not, is known as Fourier series. In our case, we intend to study distributions of spatial orientations of galaxies in the supercluster. We expect a periodic function regarding orientation as suggested by physical cosmology. According to cosmological principle, distribution of vector quantities at the large scale should be isotropic and homogeneous. The Fourier test can be applied if the deviation from isotropy is only varying with angles (in our case: θ and ϕ).

N denote the total number of solutions for galaxies in the sample, Here we assume that the symbol and N_k the number of solutions in the k^{th} bin, N_0 the mean number of solutions per bin, and N_{0k} the expected number of solutions in the k^{th} bin. Then, the Fourier series is given by,

$$N_k = N_{ok}(1 + \Delta_{11} \cos 2\theta_k + \Delta_{21} \sin 2\theta_k + \Delta_{12} \cos 4\theta_k + \Delta_{22} \sin 4\theta_k) \tag{3.1}$$

Here, Δ_{ij} coefficients represent parameters of the distribution and the angle θ_k is the polar angle of k^{th} bin. In the year 1975, Hawley & Peebles (1975) used the Fourier Test in the galaxy orientation studies . Flin & Godlowski (1986) used it again and later Godlowski ((Godłowski, 1993), (Godłowski, 1994)) improved the method. If we take into account only the the first or second Fourier mode separately, then we obtain the following expressions for the Fourier coefficients Godłowski (1994),

$$\Delta_{11} = \sum_{k=1}^{n}(N_k - N_{0k}) \cos 2\theta_k / \sum_{k=1}^{n} N_{0k} \cos^2 2\theta_k \tag{3.2}$$

$$\Delta_{21} = \sum_{k=1}^{n}(N_k - N_{0k}) \sin 2\theta_k / \sum_{k=1}^{n} N_{0k} \sin^2 2\theta_k \tag{3.3}$$

where n is the number of bins. We can obtain standard deviations ($\sigma(\Delta_{11})$ and $\sigma(\Delta_{21})$)

using expressions,

$$\sigma(\Delta_{11}) = \left(\sum_{k=1}^{n} N_{0k} \cos^2 2\theta_k \right)^{-1/2} \tag{3.4}$$

$$\sigma(\Delta_{21}) = \left(\sum_{k=1}^{n} N_{0k} \sin^2 2\theta_k \right)^{-1/2} \tag{3.5}$$

The amplitude of first order coefficients is

$$\Delta_1 = (\Delta_{11}^2 + \Delta_{21}^2)^{1/2} \tag{3.6}$$

of which the Fourier probability is given by,

$$P(> \Delta_1) = \exp(-nN_0\Delta_1^2/4) \tag{3.7}$$

with the standard deviation

$$\sigma(\Delta_1) = (2/nN_0)^{1/2} \tag{3.8}$$

This test was improved by Godlowski (1994) for the case when higher Fourier modes is taken into account:

$$N_k = N_{0k} \, (1 + \Delta_{11} \cos 2\theta_k + \Delta_{21} \sin 2\theta_k + \Delta_{12} \cos 4\theta_k + \Delta_{22} \sin 4\theta_k + \ldots\ldots) \tag{3.9}$$

This is applicable for the data (galaxies) of very large scale structure. So, the Δ_{ij} coefficients are:

$$\Delta_{1j} = \sum_{k=1}^{n} (N_k - N_{0k}) \cos 2\,j\theta_k \Big/ \sum_{k=1}^{n} \cos^2 2\,j\theta_k \tag{3.10}$$

$$\Delta_{2j} = \sum_{k=1}^{n} (N_k - N_{0k}) \sin 2\,j\theta_k \Big/ \sum_{k=1}^{n} \sin^2 2\,j\theta_k \tag{3.11}$$

where n is the number of bins. The standard deviation is given by,

$$\sigma(\Delta_{1j}) = \left(\sum_{k=1}^{n} N_{0k} \cos^2 2\,j\theta_k \right)^{-1/2} \tag{3.12}$$

$$\sigma(\Delta_{2j}) = \left(\sum_{k=1}^{n} N_{0k} \sin^2 2\,j\theta_k \right)^{-1/2} \tag{3.13}$$

If we analyze Fourier modes separately, the amplitude will be

$$\Delta_j = \left(\Delta_{1j}^2 + \Delta_{2j}^2\right)^{\frac{1}{2}} \tag{3.14}$$

Which is greater than a certain chosen value of probability, given by,

$$P(>\Delta_j) = exp\left(-\frac{n}{4}N_0\Delta_j^2\right) \tag{3.15}$$

where N_0 is the numbers per bin, with standard deviation

$$\sigma(\Delta_J) = (2/nN_0)^{1/2} \tag{3.16}$$

However, in this approximation, the theoretical probability function p_k is still symmetric with respect to the value θ that corresponds to the value $\delta = 0$. The expressions becomes,

$$\Delta_{11} = \frac{CK - UM}{AC - U^2}, \tag{3.17}$$

$$\Delta_{21} = \frac{DL - WN}{BD - W^2}, \tag{3.18}$$

$$\Delta_{12} = \frac{-UK + AM}{AC - U^2}, \tag{3.19}$$

$$\Delta_{22} = \frac{-WL + BN}{BD - W^2}, \tag{3.20}$$

where we have denoted following symbols as follows:

$$A = \sum N_{ok}\cos^2 2\theta_k\,, \qquad B = \sum N_{ok}\sin^2 2\theta_k\,, \tag{3.21}$$

$$C = \sum N_{ok}\cos^2 4\theta_k\,, \qquad D = \sum N_{ok}\sin^2 4\theta_k\,, \tag{3.22}$$

$$U = \sum N_{ok}\cos^2 2\theta\cos 4\theta_k\,, \qquad W = \sum N_{ok}\sin^2 2\theta\sin 4\theta_k, \tag{3.23}$$

$$K = \sum(N_k - N_{ok})\cos 2\theta_k\,, \qquad L = \sum(N_k - N_{ok})\sin 2\theta_k\,, \tag{3.24}$$

$$M = \sum(N_k - N_{ok})\cos 4\theta_k\,, \qquad N = \sum(N_k - N_{ok})\sin 4\theta_k\,, \tag{3.25}$$

The covariance matrix Cov = G^{-1} is

$$G^{-1} = \begin{pmatrix} C/(AC-U^2) & 0 & -U/(AC-U^2) & 0 \\ 0 & D/(BD-W^2) & 0 & -W/(BD-W^2) \\ -U/(AC-U^2) & 0 & A/(AC-U^2) & 0 \\ 0 & -W/(BD-W^2) & 0 & B/(BD-W^2) \end{pmatrix}$$

$$\Delta_{11} = \frac{\sum N_{ok}\cos^2 4\theta_k \sum(N_k - N_{ok})\cos 2\theta_k - \sum N_{ok}\cos^2 2\theta \cos 4\theta_k \sum(N_k - N_{ok})\cos 4\theta_k}{\sum N_{ok}\cos^2 2\theta_k \sum N_{ok}\cos^2 4\theta_k - (\sum N_{ok}\cos^2 2\theta|\cos 4\theta_k)^2} \tag{3.26}$$

$$\begin{aligned}\sigma^2(\Delta_{11}) = &\left[\sum N_{ok}\cos^2 2\theta_k \sum N_{ok}\cos^2 4\theta_k - \left(\sum N_{ok}\cos^2 2\theta \cos 4\theta_k\right)^2\right]^{-1} \\ &\times \left(\sum N_{ok}\cos^2 4\theta_k\right)\end{aligned} \tag{3.27}$$

$$\Delta_{22} = \frac{-\sum N_{ok}\sin^2 2\theta \sin 4\theta_k \sum(N_k - N_{ok})\sin 2\theta_k - \sum N_{ok}\sin^2 2\theta_k \sum(N_k - N_{ok})\sin 4\theta_k}{\sum N_{ok}\sin^2 2\theta_k \sum N_{ok}\sin^2 4\theta_k - (\sum N_{ok}\sin^2 2\theta \sin 4\theta_k)^2} \tag{3.28}$$

$$\begin{aligned}\sigma^2(\Delta_{22}) = &\sum N_{ok}\sin^2 2\theta_k \sum N_{ok}\sin^2 4\theta_k - \left(\sum N_{ok}\sin^2 2\theta \sin 4\theta_k)^2\right) \\ &\times \left(\sum(N_k - N_{ok}\right)\sin 2\theta_k\end{aligned} \tag{3.29}$$

It is important to understand whether the analysed distribution in the same as the theoretical one. We need the expression for the probability that the amplitude Δ(obtained from all Δ_{ij}) is greater than a certain chosen value. The formulae are given below.

$$\boldsymbol{I} = \begin{pmatrix} \Delta_{11} \\ \Delta_{21} \\ \Delta_{12} \\ \Delta_{22} \end{pmatrix}$$

Then the formula for probability is $P(\Delta) = (1+J/2)^2 \exp(-J/2)$, where, $J = \sum\sum G_{ij} I_i I_j$. It should note that in the case when all probabilities p_k are equal (as an example, in the case of angle η) the expressions (3.26) and (3.27) reduce to (3.10) and (3.12), respectively.

3.6.2 Chi-square Test

Chi-square test is commonly used to compare observed data we would expect to obtain according to a specific hypothesis. This test can be applicable even if we have independent variables. In general, it is better to have dependent variable so that degrees of freedom can be reduced. This test can be used to decide whether the discrepancy between theory and experiment is significant or not. The chi-square test is always testing the null hypothesis, which states that there is no significant difference between the observed (i.e. experimental) values and the corresponding expected (or theoretical) values. Mathematically, it is defined by,

$$\chi_v^2 = \frac{\chi^2}{v} \tag{3.30}$$

$$\chi^2 = \sum \frac{(N_{oi} - N_{ei})^2}{N_{ei}} \tag{3.31}$$

Where the summation is taken from one to n. Here n represents the number of bins (categories), N_{oi} and N_{ei} represent the observed and expected isotropic distributions.

The χ^2-distribution is a continuous probability distribution. The quantity χ_v^2 defined in equation (3.30) has the probability distribution given by

$$f(\chi^2) = \frac{1}{2^{v/2}\Gamma(v/2)}(\chi^2)^{v/2}e^{-\chi^2/2} \tag{3.32}$$

where $\Gamma(z)$ is the gamma function defined by

$$\Gamma(z) = \int_0^\infty u^{z-1}e^{-u}du; \quad z > 0 \tag{3.33}$$

The equation (3.31) is known as the χ^2 distribution with v degrees of freedom and is a positive integer.

In an isotropic distribution, the χ_v^2 value is expected to be nearly zero. The probability $P(> \chi_v^2)$ gives the observed χ_v^2 value is realized by the isotropic distribution. When $P(> \chi_v^2)$ is larger. The observed distribution is more consistent with the expected isotropic distributions. We set $P(> \chi_v^2) = 0.050$ as the critical value to discriminate isotropy from anisotropy, it corresponds to the deviation from the isotropy at 2σ level. To examine the test is applied to all samples the deviations of the observed θ and ϕ-distributions from the expected isotropic distribution.

3.6.3 Auto-correlation Test

The auto-correlation is defined as correlation between member of series of observation ordered in time or space. In our case, our observations are ordered in space for all kinds of variables, whether it is spatial orientation or redshift or magnitudes. Auto-correlation test is a mathematical tool for finding repeating patterns and measures the degree to which there is a linear relationship between two variables. In general, our variables are 'dependent' variables. But we expect to find a week or almost no dependence as well. If the function is well defined, its value must lie in the range $[-1,1]$, with 1 indicating perfect (increasing) correlation and -1 indicating perfect anti-correlation (decreasing correlation). The correlation coefficient is,

$$C = \sum \frac{(N_k - N_{ok})(N_{k+1} - N_{ok+1})}{(N_{ok}N_{ok+1})^{1/2}} \tag{3.34}$$

with the standard deviation

$$\sigma(C) = (n)^{1/2} \tag{3.35}$$

In an isotropic distribution, correlation vanishes, so we expect to have $C \to 0$ for there systems which obeys cosmological principle. The correlation function is important for theoretical models of physical cosmology because it provides a means of testing models which assume different things about the contents of the universe.

3.6.4 Linear, Polynomial & Gaussian Fittings

In addition to above mentioned statistical tests, we also perform linear and non-linear fittings as well. If the tested variables are dependent, or obey cosmological principle, we apply linear fits. If the regression coefficients of linear fit is too low. we apply higher order polynomial to measure the deviation. Gaussian fits are applied in many cases where we expect homogeneous distributions.

3.6.5 Summary

In the present work, the conditions for anisotropy are as follows:

- the chi-square probability $P(>\chi^2) < 0.050$
- the correlation coefficient $C/\sigma(C) > 1$
- the first order Fourier coefficient $\Delta_{11}/\sigma(\Delta_{11}) > 1.5$ and
- the first order Fourier probability $P(<\Delta_1) < 0.150$
- regression coefficient for linear/polynomial fits R^2<0.10

These tests are used by many authors in galaxy orientation studies, as follows: Godłowski (1993), Godłowski (1994), Aryal & Saurer (2004),Aryal & Saurer (2006) Aryal et al. (2007),Yadav et al. (2016) and Malla et al. (2020).

3.7 Database of Supercluster of Galaxies

In the present study, we have used database of six Superclusters namely S[195+027+0022], S[173+014+0082], S[247+040+0029], S[227+006+0078], S[231+030+0117], S[184+003+0077]. The database are obtained from SDSS DR7 (Percival et al., 2010). The complete database is obtained from our collaboration with the Institutes of Astrophysics, Innsbruck University, Austria.

We received 28 spectroscopic and photometric parameters of individual galaxies through our collaborations. All together, there was 560,000 data of about 18,000 galaxies of Superclusters. In the Appendix C, we have listed the parameters that we have used for this study.

Below we give all sky distributions of galaxies in the six selected Superclusters. In addition, axial ratio distributions of galaxies in their Superclusters are also given. Our selection criteria was as follows:

(1) Database should be complete up to the axial ratio $b/a = 0.75$.

(2) The distributions of galaxies should not be homogeneous.

(3) Redshift of Supercluster should not exceed 0.2.

(4) SDSS database of all galaxies should be available.

3.7.1 S[195+027+0022]

Figure 17a shows all sky distribution of galaxies in the Supercluster S[195+027+0022]. A marker galaxy is the galaxy of which luminosity profile is maximum. Total number of galaxies in this Supercluster is 2590. Axial ratio distribution of galaxies in this Supercluster is shown in the figure 17b. Both edge-on ($b/a < 0.20$) and face-on ($b/a < 0.90$) are found to be less in the SDSS database. It is therefore, a selection effect is noticed. We will remove selection effect by performing numerical simulation technique.

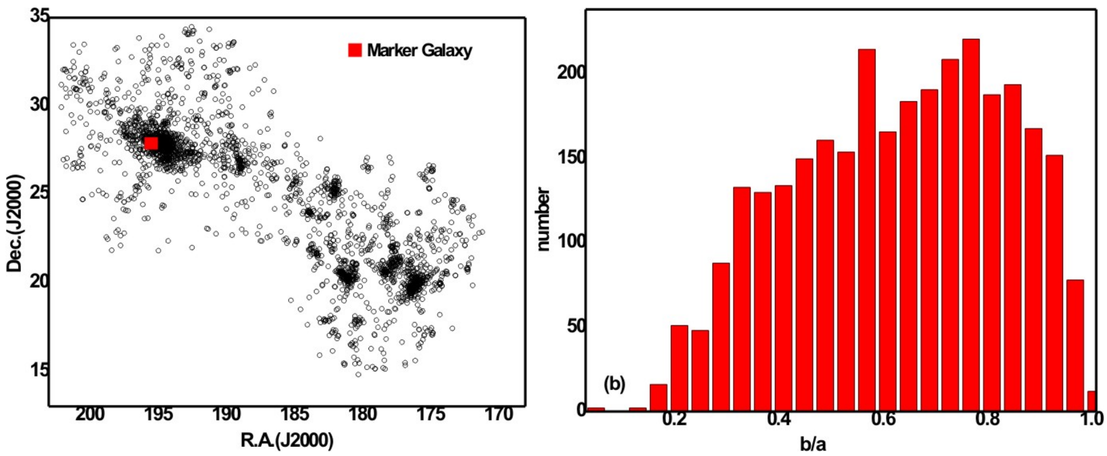

Figure 17: (a) All sky distribution of total galaxies of Supercluster S[195+027+0022] in the equatorial co-ordinate system. R.A. and Dec. represent the right ascension and declination in degree. Each hollow circle represents a galaxy. A marker galaxy (shown by red square) is the bright galaxy. There are 2590 galaxies in this Supercluster. Inhomogeneous distribution of galaxies can be seen. (b) Axial ratio (b/a) distribution of galaxies. The Y-axis represents the number of observed galaxies in the Supercluster S[195+027+0022].

3.7.2 S[173+014+0082]

Distribution of galaxies in the Supercluster S173+014+0082] is shown in Figure 18a. A marker galaxy (brightest galaxy) is found to be off centrally located. Similar to the Supercluster S[195+027+0022], selection effect against edge-on and face-on galaxies can be seen in the axial ratio distribution (Figure 18b).

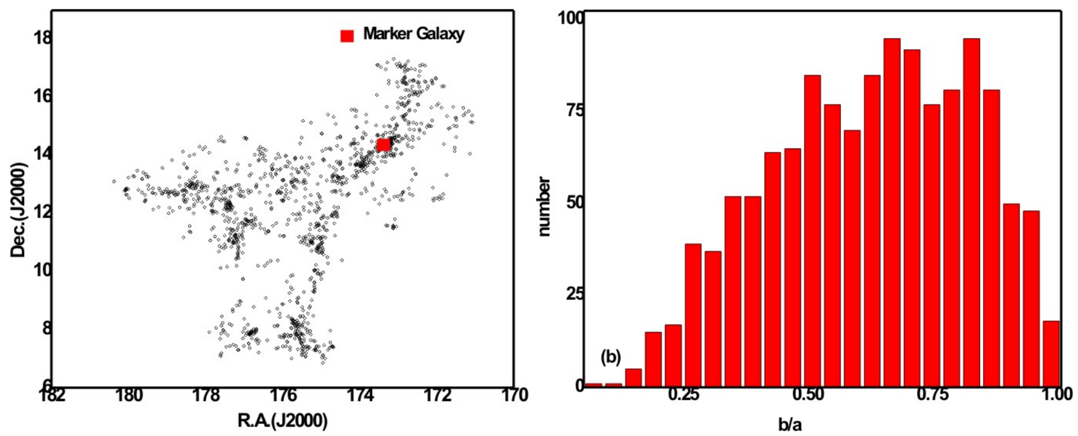

Figure 18: (a) All sky distribution of SDSS Supercluster S[173 + 014 + 0082] of total galaxies in equatorial coordinate system. The right ascension (R.A.) and declination (Dec.) represent in degree. Each hollow circle represents a galaxy. A marker galaxy (shown by red square) near the highest density peak in the Supercluster volume. There are 1302 galaxies in this Supercluster. Inhomogeneous distribution of galaxies can be seen.(b) Axial ratio (b/a) distribution of galaxies. The Y-axis represents the number of observed galaxies in the Supercluster S[173+014+0082].

3.7.3 S[247+040+0029]

The all sky distribution of galaxies of our database in Supercluster S[247+040+0029] is shown in Figure 19a, which indicates the inhomogeneous distribution of galaxies. From the figure, we can see more galaxies were found to be concentrated at the central region of Supercluster. Figure 19b shows the axial ratio (*b*/*a*) distribution, less number of solutions in the last four bins (nearly face-on galaxies) can be seen. Similarly, less number of solution in the first two bins (nearly edge-on galaxies) can be noticed.

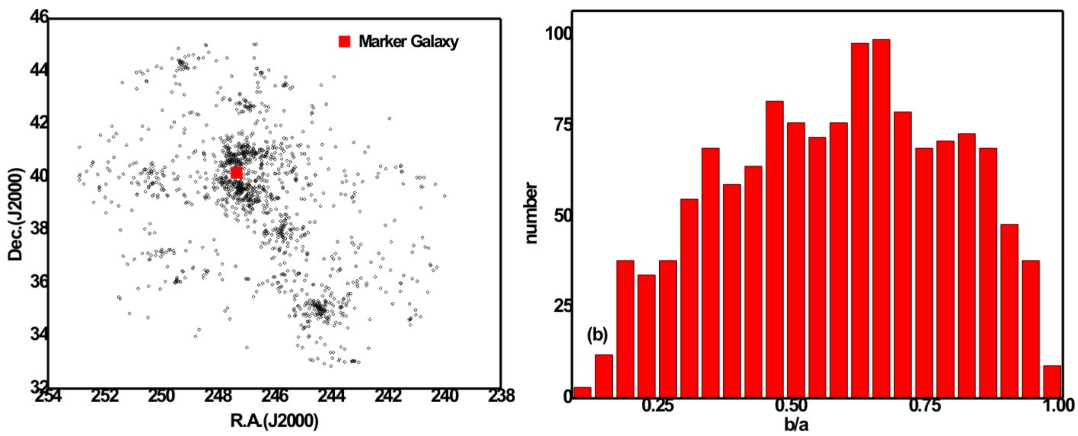

Figure 19: (a) All sky distribution of total galaxies of Supercluster S[247+040+0029] in the equatorial co-ordinate system. Each hollow circle represents a galaxy. A marker galaxy (shown by red square) are denoted by solid square. This Supercluster have 1331 galaxies. A Marker galaxies are denoted by solid red square. Inhomogeneous distribution of galaxies can be seen.(b) Axial ratio (*b*/*a*) distribution of galaxies. The Y-axis represents the number of observed galaxies in the Supercluster S[247+040+0029].

3.7.4 S[227+006+0078]

Figure 20a shows the all sky distribution of total number of galaxies in Supercluster S[227+006+0078]. This distribution clearly reveals that the galaxies are not equally distributed through out the whole region: a heterogeneous distribution. The morphology of this Supercluster can be defined as a spider type. The histogram advocates the deficiency of face-on galaxies in this Supercluster, giving the dominant of edge-on galaxies (Figure 20b).

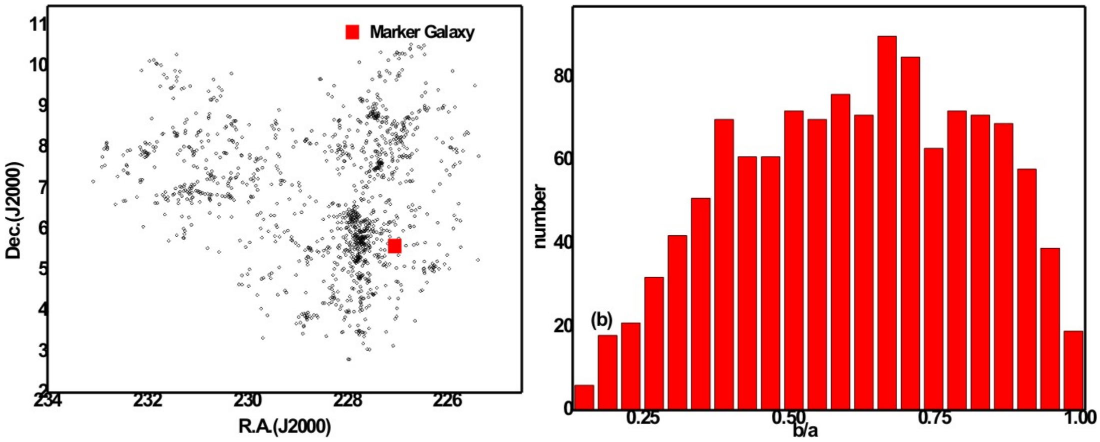

Figure 20: (a) All-sky diagram of Supercluster S[227+006+0078] showing Abell clusters. Each hollow circle represents a galaxy. A Marker galaxy shown by red square in the Supercluster. This Supercluster contains 1213 galaxies. Inhomogeneous distribution of galaxies can be seen.(b) Axial ratio (b/a) distribution of galaxies. The Y-axis represents the number of observed galaxies in the Supercluster S[227+006+0078].

3.7.5 S[231+030+0117]

The all sky distribution of 1172 galaxies of our database in the Supercluster S[231+030+0117] is shown in Figure 21a. We expect homogeneous distribution of galaxies according to cosmological principle. But the inhomogeneous can be observed in the figure. The histograms of the observed axial ratio (b/a) distribution of galaxies is shown in Figure 21b. In the middle of the histogram, distribution of solutions are more.

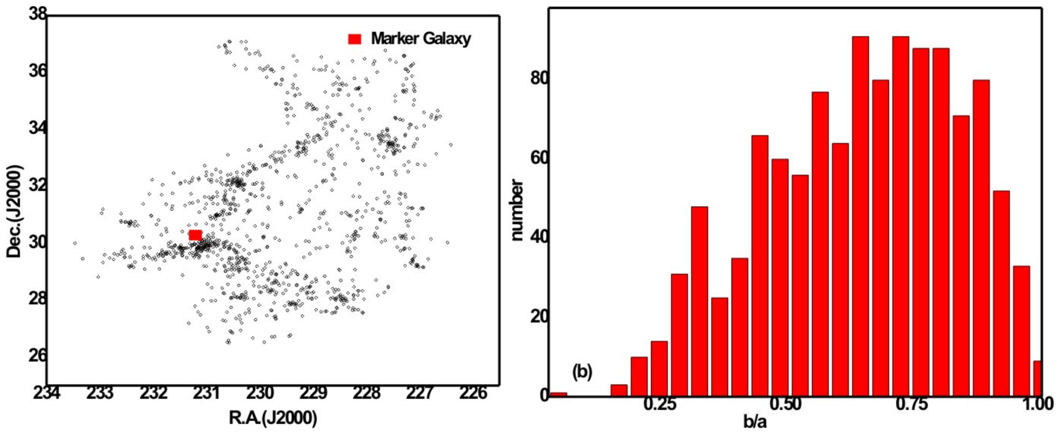

Figure 21: (a) All sky distribution of galaxies in the Supercluster S[231+030+0117]. Each hollow circle represents a galaxy. A marker galaxy (shown by red square) in the Supercluster is the bright galaxy. This Supercluster have 1172 galaxies. Inhomogeneous distribution of galaxies can be seen.(b) Axial ratio (b/a) distribution of galaxies. The Y-axis represents the number of observed galaxies in the Supercluster S[231+030+0117].

3.7.6 S[184+003+0077]

As we observe the all sky plot of Supercluster S[184+003+0077] is shown in Figure 22a, various galaxy rich regions can be noticed. Which indicates the inhomogeneous distribution of galaxies. We can see that, almost all the galaxies were found to be grouped in the different region of space of Supercluster. We noticed that observed number of galaxies in lower angle region is very less but in case of higher angle region of last few bins the observed number of galaxies is slightly greater (Figure 22b).

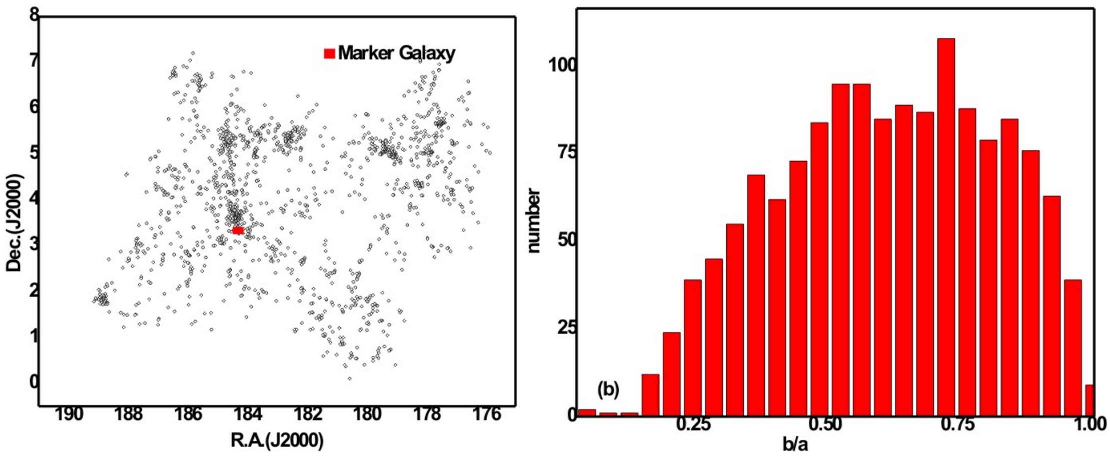

Figure 22: (a) All sky distribution of galaxies in the Supercluster S[184+003+0077]. Each hollow circle represents a galaxy. A marker galaxy shown by red square in the Supercluster. There are 1365 galaxies in this Supercluster. Inhomogeneous distribution of galaxies can be seen. (b) Axial ratio (b/a) distribution of galaxies. The Y-axis represents the number of observed galaxies in the Supercluster S[184+003+0077].

3.8 Flow chart of the process

Figure 23 shows flow chart of the whole methodology. Top left corner box represents the database of SDSS Supercluster. At first, substructure classification has been made by performing number density map of the galaxies. For this, redshift and magnitude distributions are studied. As a next step, SDSS axial ratio is converted into photometric axial ratio to make it comparable it with other Superclusters. After this, inclination angle is calculated using Holmberg's method (Holmberg, 1946). This inclination angle of galaxies has been used to convert two-dimensional database to three dimension along with positions angles. Later, polar and azimuthal angle distributions of galaxy rotation axis are determined and studied using three different statistical tests mentioned above. This is actually our observed distributions.

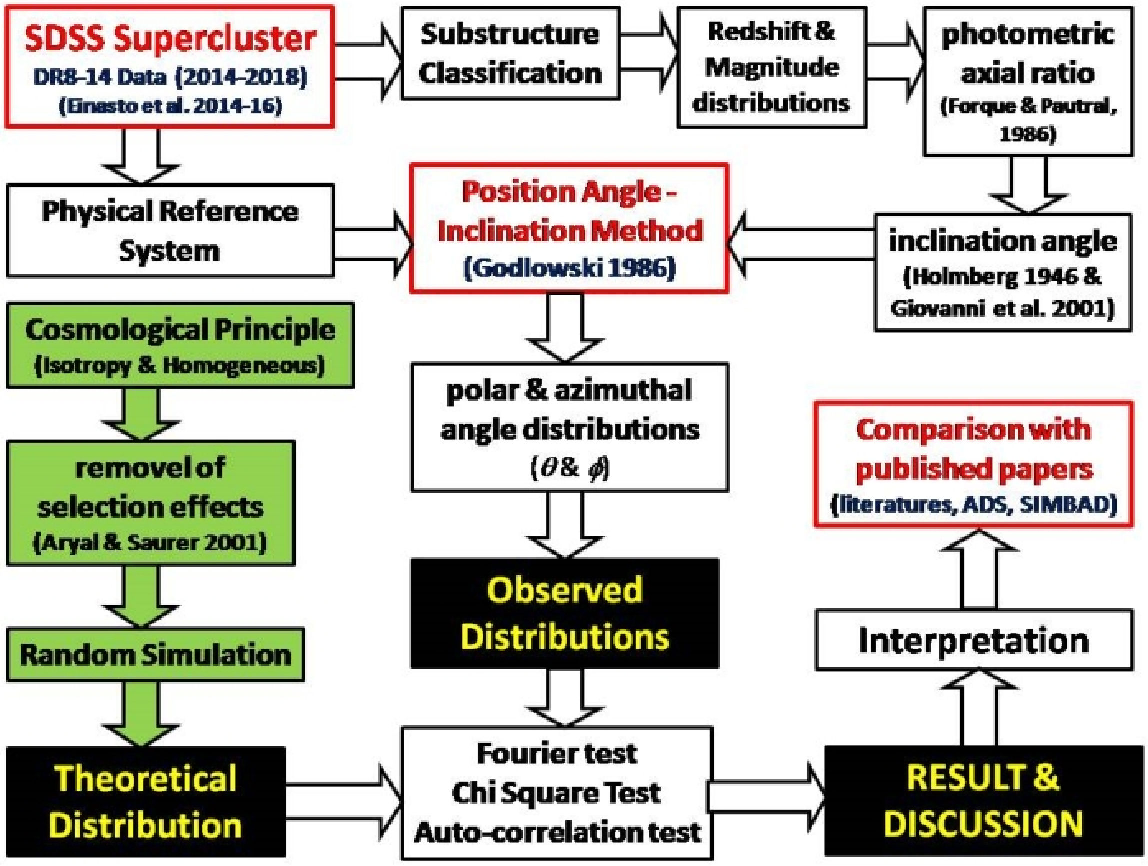

Figure 23: Flowchart showing data reduction and calculation of polar and azimuthal angle of galaxies in the SDSS Supercluster.

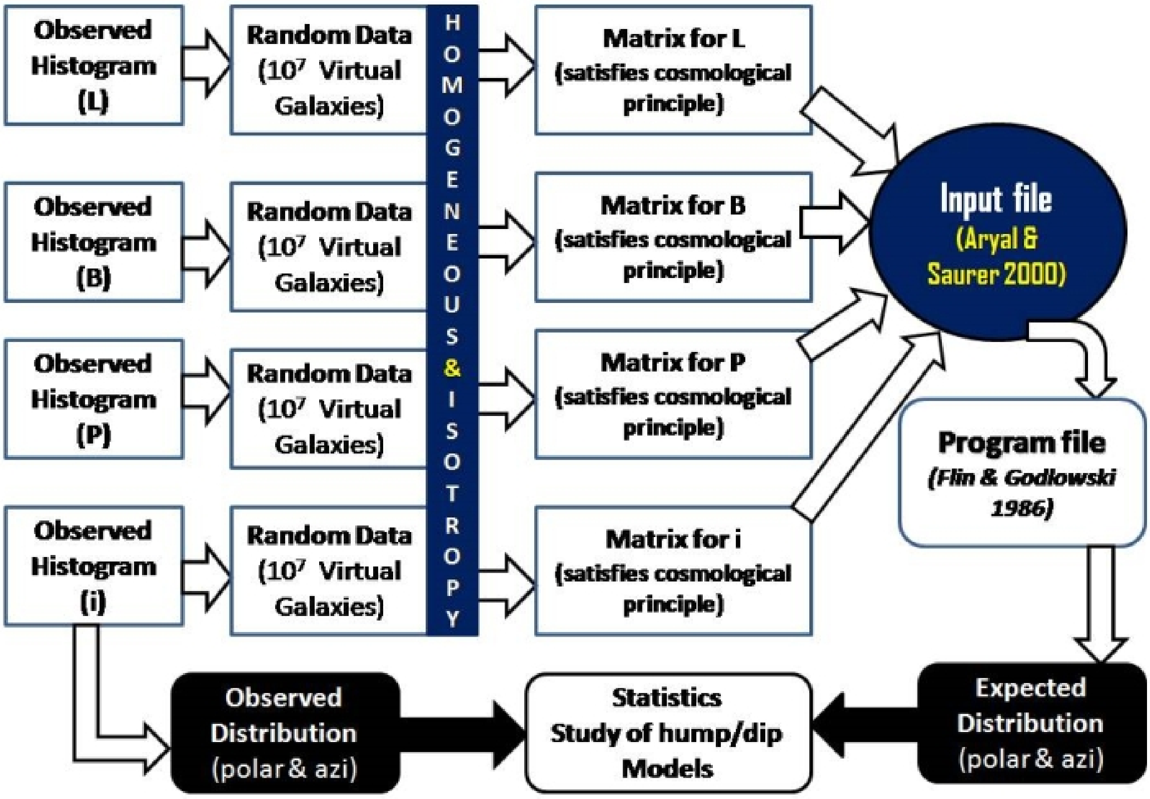

Figure 24: Flowchart showing random simulation method with input and program file. We have virtually generated 10^7 galaxies having the similar selection effects as found in the SDSS Superclusters.

Figure 24 shows a flow chart of random simulation as suggested by Aryal & Saurer (2000), to find expected isotropic distribution curves for both polar and azimuthal angle of galaxy rotation axis. At first observed distributions of positions (both RA & Dec.), position angles (P) and inclination angles (i) of galaxies of Supercluster has been studied. In general, we noticed that there is inhomogeneous distributions of positions of galaxies contradicting cosmological principle in all six Superclusters. So, we generated virtual galaxies and put it in each bins of the observed distribution to make it homogeneous. Similarly, distributions of position angles and noticed a mild deviation from expected distribution in there parameters, suggesting a deviation from isotropy. Finally a input program file is written for all Superclustere and their substructures. All together, we perform 22 separate simulations to find expected isotropic distribution curves, namely, polar and azimuthal angle distributions of galaxy rotation axes. These distributions are compared with observed distributions.

CHAPTER 4

4. RESULTS AND DISCUSSION

In this chapter, we present our results regarding the spatial orientation of galaxies in six Superclusters and their substructures. For this, the number density map, redshift map, and magnitude map will be presented. On the basis of these studies, we classify substructures in the Superclusters. Finally, we perform random simulations to find expected isotropic distribution curves for both polar and azimuthal angles of galaxy rotation axes for the Superclusters and their substructures. In this way, we discuss all six Superclusters and finally, the comparison will be made with previously published works.

4.1 Supercluster S[195+027+0022]

In this section, we study Supercluster S[195+027+0022] which is located in the northern hemisphere with respect to the equatorial coordinate system. The mean redshift of this Supercluster is 0.023 (radial velocity 6,900 km s^{-1}), and it has 2590 galaxies. The distance of this Supercluster is 100 h^{-1}Mpc (Einasto et al., 2011). At first, we studied the number density map by varying distances from each galaxy. After this, we discuss the redshift map of this Supercluster. On the basis of these two studies, we classify substructure regions in the Supercluster. As a next step, we validate substructures using r- and u-magnitude distributions. The red (r) magnitude refers to the Hα emission from the galaxies in the Supercluster, and the ultraviolet (u) magnitude refers to the abundance of young stellar objects. Finally, preferred alignments of galaxies in the Superclusters and their substructures will be studied. For the preferred alignments, angular momentum vectors are calculated for each galaxy. These vectors are resolved as polar and azimuthal angles of galaxies. To sum up, a general discussion will be made at the end.

4.1.1 Number Density Map

Figure 25 shows the number density map of galaxies in the Supercluster S[195+027+0022]. We have determined number density around each galaxy using an algorithm named ′galaxy counting code′ (Appendix D). Here, In Fig. 25a, the number density map for the nearest neighbour galaxies at the distance (or radius r) 0.50° is shown. At 28° declination, the number density of galaxy is found to be maximum. The color levels are shown. Now, the nearest neighbor distance is increased to 0.75°, 1.0° and 1.25° from each galaxies (Figures 25b-e). The size of the largest substructure at 28° declination continuously increased. One additional substructure appeared at 20° declination. When the radius increased to 1.5°, the lower substructure gets merged. it is therefore, we set nearest neighbour radius r = 1.5° for the substructure classification.

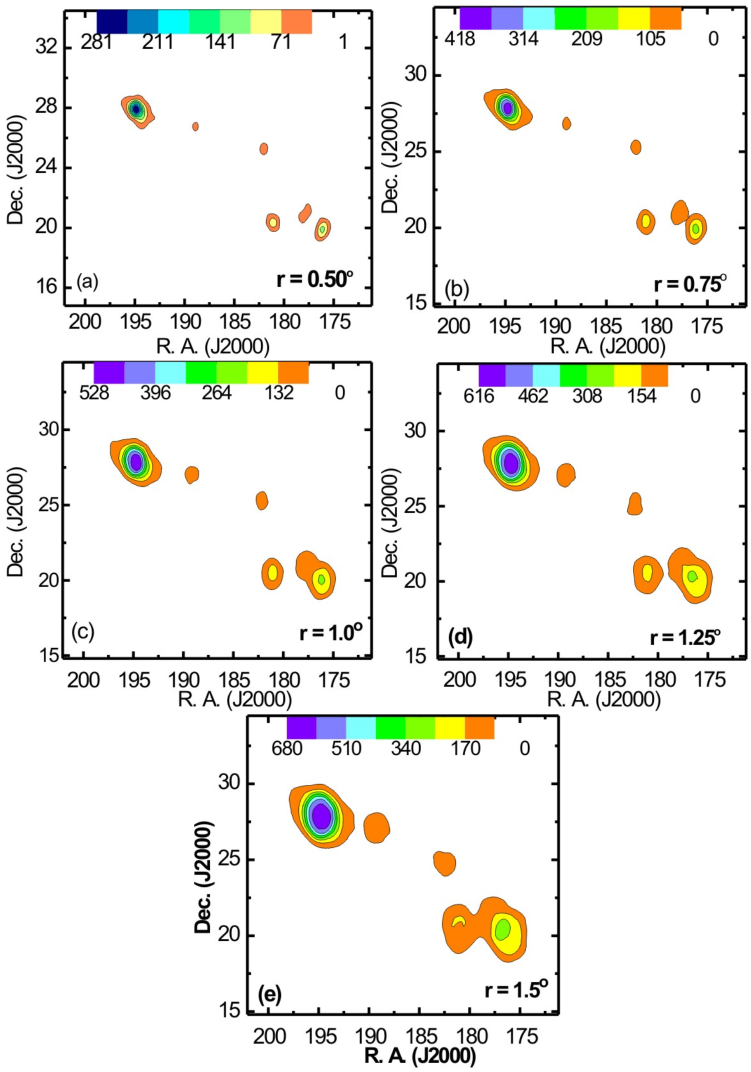

Figure 25: Number density map of galaxies in the Supercluster S[195+027+0022] having nearest neighbour distance of each individual galaxies at (a) r=0.5°, (b) r=0.75°,(c) r=1.0°, (d) r=1.25° and (e) r=1.5°. The color bars are shown. As the radius increases, the subclustering becomes prominent.

4.1.2 Redshift Map

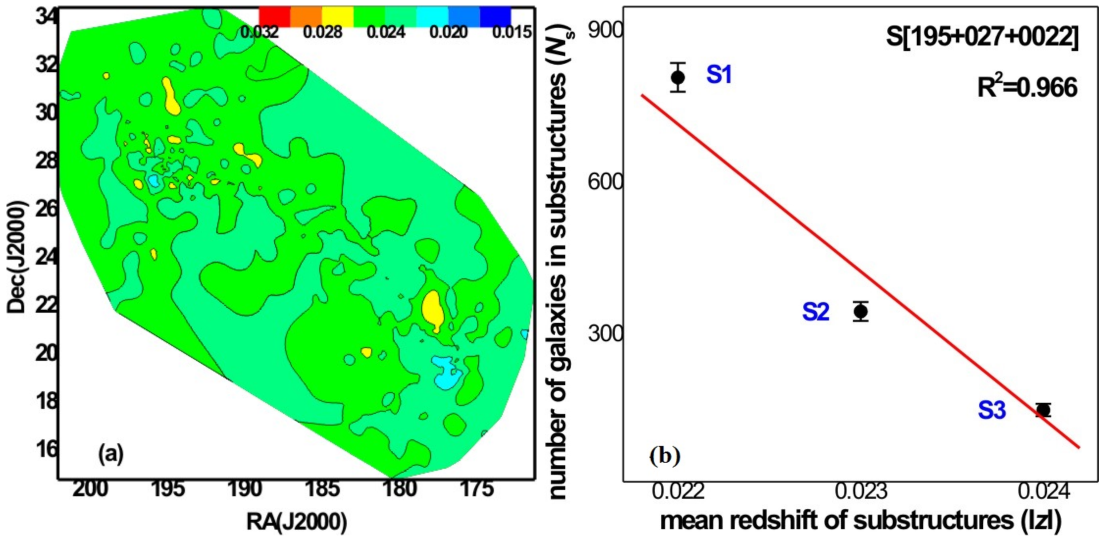

Figure 26: Redshift map is shown for galaxies in the Supercluster S[195+027+0022]. The mean redshift of Supercluster is 0.023. The contour levels are at the redshift 0.015, 0.020, 0.024, 0.028, 0.032. In the substructure region, galaxies hardly have identical redshifts. (b) Number of galaxies in substructures versus mean redshift plot in the Supercluster. The statistical $\pm 1\sigma$ error bars are shown. Here S1, S2, S3 represent substructures in the Supercluster. Coefficients of regression is shown.

Figure 26 shows a redshift map of galaxies in the Supercluster that have a mean redshift of 0.023. The color map shows that the velocity dispersion is minimum in the region where the number density of galaxy is minimum. In the substructure region at 28° declination, the mean redshift is found to be |z|= 0.023, whereas the lower and upper substructure show |z|= 0.022 and 0.024, respectively. It seems that there is a linear relationship between redshift dispersion and the number density of galaxies in the substructures,

$$N_s(1) = -2.91 \times 10^5 |z| + 7130.20 \tag{4.1}$$

We varied the nearest neighbour radius to 1.0° and 1.25° and calculated the slope of a linearly fitted line as above and found exactly the same. Therefore, we propose empirical relation (equation 4.1) between number density and redshift dispersion of galaxies in Supercluster S[195+027+0022].

The redshift dispersion (Δz) of galaxies in the Coma Superclusters are 1000 km s^{-1} (Struble & Rood, 1999). Its value is 68 km s^{-1} for the local group (Struble & Rood, 1999). These are nearby Superclusters and groups, of which peculiar velocity is relatively higher than that of the distant Superclusters.

4.1.3 Magnitude Map

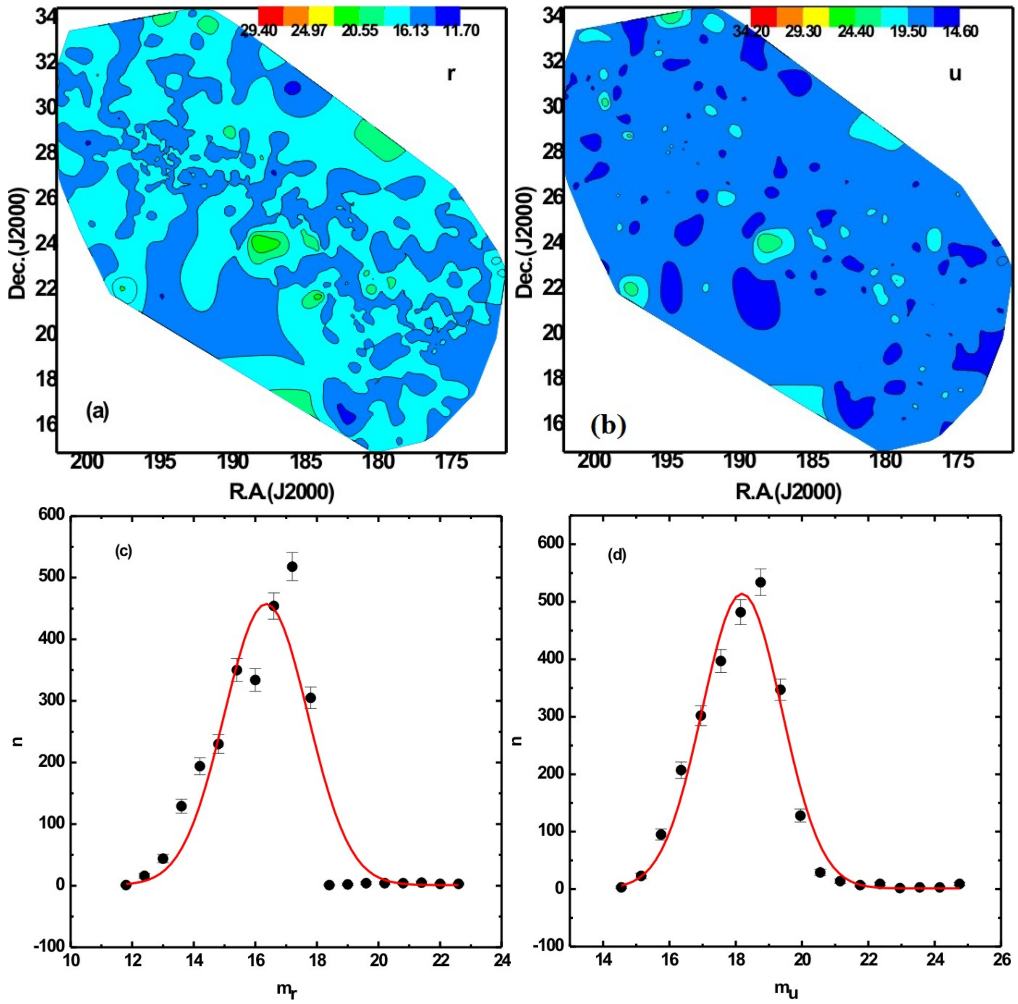

Figure 27: Magnitude map of galaxies in the Supercluster S[195+027+0022] (a) r-magnitude, (b) u-magnitude. The color bar is shown. The contour levels are at 11.70, 16.13,20.55, 24.97, 29.40 for r-filter and 14.60, 19.50, 24.40, 29.30, 34.20 for u- filter, respectively. The distribution of r and u-magnitude with Gaussian fit. Statistical $\pm 1\sigma$ errors bars are shown.

Figure 27ab shows r and u magnitude maps of galaxies in the Supercluster S[195+027+0022]. The SDSS r-magnitude refers to the peak wavelength 6165 Å with the bandwidth 141.7 Å. This wavelength range covers Hα, ionized Oxygen and ionized Nitrogen lines, as well as their continuum. In the substructure region, the mean magnitude is found to be identical in both filters. In the$u$-filter, the substructure located in the northern region is found to have a higher magnitude. As we know, the higher the magnitude, the lower the brightness. Therefore substructure regions are UV inactive regions, suggesting a lower abundance of newly formed stellar objects.

The magnitude distribution of galaxies in the Supercluster S[195+027+0022] can be seen in figure 27cd. The solid curve represents Gaussian fits. The Gaussian centre is found to be at 15.619 for r- and 18.073 for u-filters. The Gaussian functions for r- and

u-magnitude distributions are given by

$$n_r = -0.62 + 230.06 \exp\left(\frac{-2(m_r - 16.543)^2}{9.74}\right) \tag{4.2}$$

$$n_u = 1.19 + 514.30 \exp\left(\frac{-2(m_u - 18.191)^2}{5.77}\right) \tag{4.3}$$

The negative intercept indicates the strong skewness factor, observed in the case of r-magnitude. Other parameters are found to be comparable. Therefore, magnitude distributions shows Gaussian-like nature. This suggest that the Supercluster is stable and gravitationally bounded (Martinez & Saar, 2002).

4.1.4 Preferred Alignments in the Supercluster

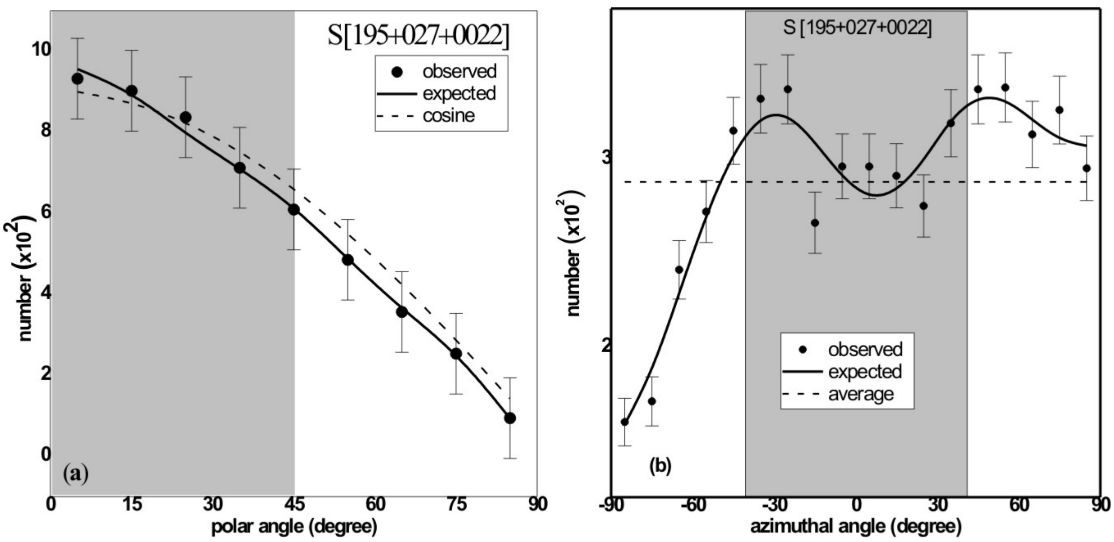

Figure 28: Polar (a) and azimuthal (b) angle distributions of galaxies in the Supercluster S[195+027+0022]. The solid circles with statistical error bars ($\pm 1\sigma$) represent observed distribution. The solid curves are obtained from random simulation assuming isotropic distributions. The grey shaded region shows predominance of Pancake model (Doroshkevich, 1973), (Doroshkevich et al., 1978) if observed solution is found to be more than that of expected.

Table 7 shows statistical parameters P($>\chi^2$), $\Delta_{11}/\ \sigma(\Delta_{11})$, P($>\ \Delta_1$) and C/$C(\sigma)$ for the total sample (Supercluster) and subsample (substructures). In the polar angle (θ) distribution chi-square probability (P($>\chi^2$)) is found to be 93.2% (much more then 5% significance level), suggesting isotropy. Similar to this Fourier coefficients ($\Delta_{11}/\ \sigma(\Delta_{11})$) are 0.2 (less than 1.5σ), advocating isotropy. The Fourier probability (P($>\ \Delta_1$)) and auto-correlation (C/$C(\sigma)$) are found to be 94.1% (more than 15% significance level) and 0.1 (less than 1σ), supporting isotropy. It is therefore all statistical tests suggest isotropic. It means, there is no preferred alignment of galaxies in the Supercluster S[195 + 027 + 0022]. However all three statistical tests suggest isotropy.

In the azimuthal angle (ϕ) distribution (Table 7), chi-square probability ((P(>χ^2))) and Fourier probabilities (P(> Δ_1)) are found to be 66.0% (more than15% significant level) and 94.3% (more than 5% significance level), suggesting isotropy. Similar to the polar angle distribution,Fourier coefficients to be found 0.6, and auto-Correlation is −0.8 are well within +1σ level, supporting isotropy.

In addition to the statistical tests, we also study the 'humps' (bins with more solutions than the expected) and 'dips' (bins with less solutions than the expected) in the polar (θ) and azimuthal (ϕ) angle distributions.

The polar angle (θ) distribution in the Supercluster as shown in Fig. 28a, There are no significant hump and dip are observed. Thus, a very good agreement between observed and expected distribution is found.

Fig 28b shows the azimuthal angle (ϕ) distribution, there are no significant hump and dip are seen in the region between −45°<ϕ>+45°. For the region −45°<ϕ<+45°, two dips (at −15° and +25°) are found in the grey-shaded region (Fig. 28b). It is a local effect. It suggests that the projection of spin vectors of galaxies tend to orient parallel with respect to the equatorial co-ordinate system.

Table 7: Statistical parameters in the polar and azimuthal angles of galaxies in the Supercluster S [195+027+0022] and its substructures (first column). The chi-square probability (P> χ^2) is given in the second column. The third and fourth columns list the values of first order Fourier coefficient ($\Delta_{11}/\sigma(\Delta_{11})$ and Fourier probability. The last column shows the values of auto co-relation coefficient.

Sample	P(> $\chi)^2$	$\Delta_{11}/\sigma(\Delta_{11})$	P(> Δ_1)	C/$C(\sigma)$
Polar Angle				
S[195+027+0022]	0.932	0.2	0.941	0.1
S1[195+028+0022]	0.924	0.6	0.848	−0.3
S2[176+020+0023]	0.533	0.1	0.916	−0.3
S3[181+020+0024]	0.976	−0.4	0.923	−0.1
Azimuthal Angle				
S[195+027+0022]	0.660	−0.1	0.943	−0.8
S1[195+028+0022]	0.415	−0.3	0.937	−1.1
S2[176+020+0023]	0.273	−0.5	0.878	−0.2
S3181+020+0024]	0.980	−2.6	0.021	−0.3

4.1.5 Substructure Classification

We noticed three substructure regions on the basis of number density and redshift maps as discussed in the previous subsections. Table 8 shows position, mean redshift, magnitude, etc of substructures in the Supercluster S[195 + 027 + 0022].

Table 8: Substructures of the Supercluster S[195+027+0022]. Second and third columns show positions of substructures. The next two columns represent mean redshift and number of galaxies in the substructures. The last two columns list mean u-magnitude and r-magnitude of substructures, respectively.

Substructure	R.A.(J2000)	Dec.(J2000)	$\|Z\|$	N_g	$\|u\|$	$\|r\|$
S1[195+028+0022]	194.730°	27.812°	0.022	810	16.3	18.1
S2[176+020+0023]	176.799°	20.330°	0.023	347	16.4	18.0
S3[181+020+0024]	181.118°	20.419°	0.024	152	16.3	18.1

Last two substructures seem to be connected, probably in the process of clustering. The first substructure is isolated and have morphology of BM type I (regular cluster) clusters.

4.1.6 Preferred Alignment in Substructures

Figs. 29 a,c,e represent polar angle distributions of galaxies in the substructures S1[195+028 + 0022], S2[176 + 020 + 0023] and S3[181 + 020 + 0024], respectively. The substructure S1[195+028+0022] consists of 810 galaxies. The statistics for the polar angle (θ) distribution is shown in Table 16. The chi-square probability (P> χ^2) test, all these substructures show isotropy because the probabilities are found to be 92.4%, 53.3%, and 97.6% (more than 5% significance level), respectively. The first order Fourier coefficients $\Delta_{11}/\ \sigma(\Delta_{11})$, are found to be 0.6, 0.1 and −0.4 which is less than the limit 1.5σ. Similar to this, Fourier probabilities (P(> Δ_1), are 84.8%, 91.6% and 92.3% (greater than 15%), suggesting isotropy in the polar angle distributions. The auto-correlation are −0.3, −0.3 and −0.1 (less than limit 1σ), suggesting no preference in the alignments of galaxies. Therefore, similar to the Supercluster, all substructures show isotropy, supporting Hierarchy model (Peebles, 1969) of galaxy formation as supported by Peebles (Peebles, 1969).

Fig. 29b,d,f show azimuthal angle distributions in the substructures S1[195+028+0022], S2[176 + 020 + 0023] and S3[181 + 020 + 0024], respectively. The statistics for the azimuthal angle (ϕ) distribution is shown in Table 16. For these substructures, the chi-square probability P(>χ^2) are found to be 41.5%, 27.3% and 98.0%, respectively (which are greater than 5%) indicating isotropy. The first order Fourier coefficients $\Delta_{11}/\ \sigma(\Delta_{11})$, are found to be −0.3, −0.5 and −2.6 are less than the limit 1.5σ. The Fourier probability (P(> Δ_1)), for two substructures S1[195 + 027 + 0022] and S2[176 + 020 + 0023] are 93.7%, 87.8%, respectively, more than significant level 15%, these substructures shows isotropy. But, Fourier probability (P(> Δ_1)), for S3[181 + 020 + 0024] is found to be 2.1% (less than 15% significance level) suggesting anisotropy. The auto-correlation are −1.1, −0.2 and −0.3 (which are less than limit 1σ, suggesting isotropy.

The substructures S1[195+028+0022] have 810 galaxies with a mean redshift of 0.023. It is the most populated substructure that contains the marker galaxy of the Supercluster.

Isotropy is noticed in the statistical tests, as well as in the polar angle (θ) distributions of galaxies, there are no significant hump and dip are observed (Table 7, Fig. 29a).

The substructure S2[176+020+0023] contains 347 galaxies. The observed distribution is found to be consistent with the expected distribution in the polar angle (θ) distribution. All four statistical parameters advocate isotropic. No significant hump or dip is found. Therefore, spin vectors of galaxies in the substructure S2[176 + 020 + 0023] should random distribution (Fig. 29c).

The substructure S3[181+020+0024] consists of 152 galaxies. A very good agreement between observed and expected distributions are found in the polar angle (θ) distribution (Fig 29e). Therefore, no preferred alignment of spin vectors of galaxies is noticed in the θ-distribution. Statistical parameters also support this result (see table 7).

In the substructure S1[195+028+0022], the azimuthal angle (ϕ) distribution, in contrast to the substructure S2[176 + 020 + 0023] and S3[181 + 020 + 0024], a good agreement between observed and expected distribution is noticed (Fig 29b). However, statistical tests suggest a marginal deviation from isotropy (see Table 7).

The azimuthal angle (ϕ) distribution in the substructure S2[176+020+0023], no agreement between the observed and expected distribution is noticed. Many humps (solutions more than the expected) and dips (solutions less than the expected) can be seen (Fig. 29d). It is, therefore, first order Fourier probability is found to be 0.878 and the auto-correlation coefficient is -0.169, suggesting isotropy. Therefore, Spin Vector projections of galaxies in the substructure S2[176 + 020 + 0023] tend to point towards the centre of the equatorial co-ordinate system.

The azimuthal angle (ϕ) distribution in the substructure S3[181+020+0024] is shown in Fig. 29f, several humps ($-25°$, $+35°$, $+45°$) and dips ($-45°$, $+5°$, $25°$) are seen. Statistical parameters suggest isotropy expect first order Fourier coefficient (Table 7). The value of $(\Delta_{11}/\sigma(\Delta_{11}))$ is found to be negative at $< 1.5\sigma$ levels, suggesting that the projections of spin vectors of galaxies in this substructure tend to be oriented parallel with respect to equatorial co-ordinate system. Similar to the substructure S2[176+020+0023], projections of spin vectors of galaxies in the substructure S3[181 + 020 + 0024] tend to point towards the centre of the equatorial co-ordinate.

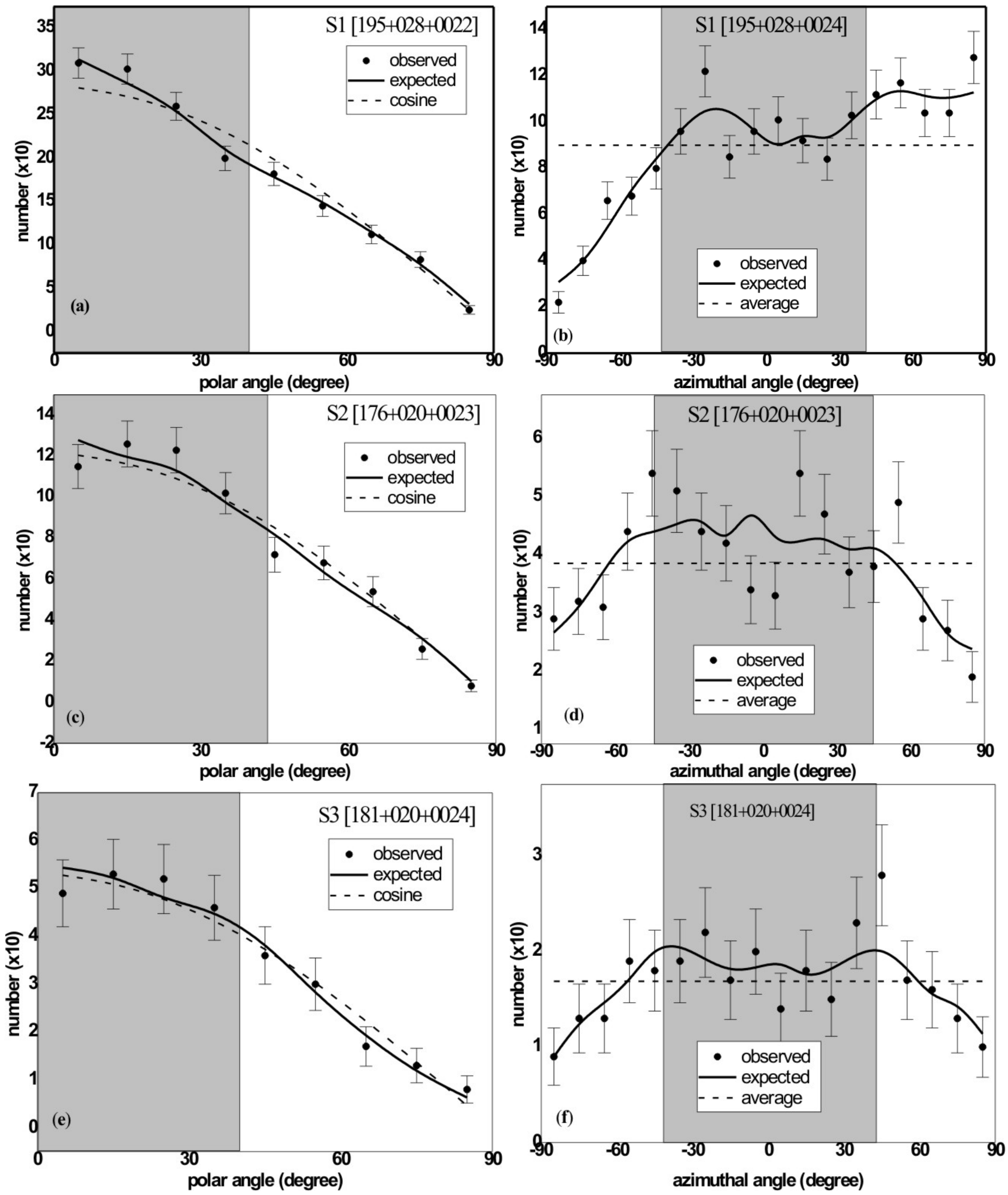

Figure 29: Polar (a, c, e) and azimuthal angle (b, d, f) distributions of galaxies in the substructures of Supercluster S[195+027+0022]. Solid circles with statistical error bars ($\pm 1\sigma$) represent observed distributions. The expected distributions are represented by solid curves. These solid curves are obtained by preforming random simulation. The grey-shaded region supports pancake model (Doroshkevich, 1973),(Doroshkevich et al., 1978) if there is excess solution than the expected.

4.1.7 General Discussion

We know that many celestial objects are receding from us (i.e redshifted) and few are approaching us (i.e blueshifted) with different speeds. Since a common radial velocity for a group of galaxies allows us to identify the group as a cluster of genetically related galaxies, this information may be extremely useful in studying structure evolution on a large scale. As shown in Fig. 30, we've studied velocity contour map for our database based on redshift values.

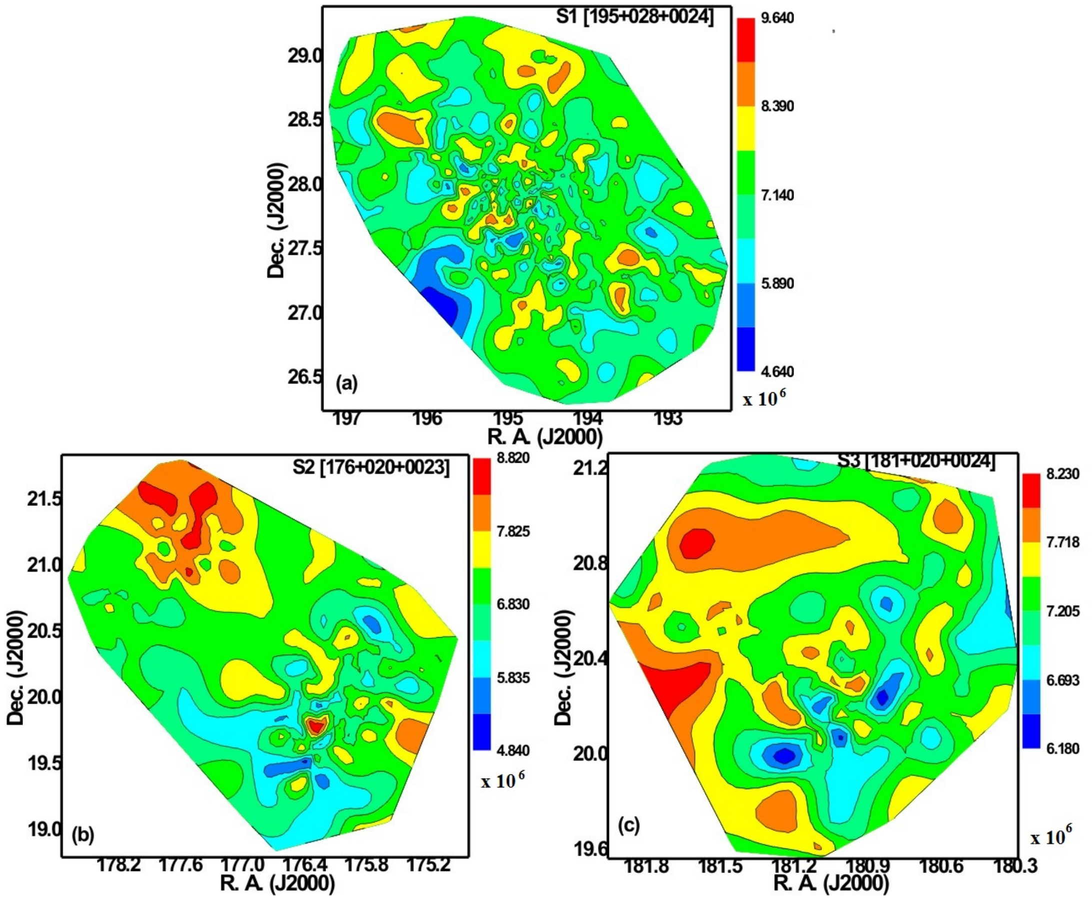

Figure 30: Radial velocity contour maps of galaxies in the substructures. X-axis and Y-axis represent right ascension and declination respectively and vertical line on right side represent radial velocity in $\times 10^6$ meter per second.

Already from the three statistical tests and from nature of polar and azimuthal angle distribution of our database, we found isotropy that suggests random orientation of spin vectors of galaxies in the Supercluster and substructure i.e hierarchical model (Peebles, 1969) of galaxy evolution.

Hierarchy model (Peebles, 1969) predicts that the radial velocity distribution should not be unipolar. The redshift contour maps shows that the velocity dispersion at the central region of the substructures are very small, suggesting cluster-like morphology. It is therefore, we conclude that the Supercluster [195+027+0022] contains three clusters like aggregations in which a random orientation of angular momentum vectors of galaxies are noticed.

4.2 Supercluster S[173+014+0082]

In this section, we study Supercluster S[173+014+0082] which is located in the northern hemisphere of the equatorial coordinate system. The mean redshift of this Supercluster is 0.083 (radial velocity 2.49×10^{7} m s^{-1}), and it has 1302 galaxies. The distance of this Supercluster is 242 h^{-1}Mpc and diameter (the maximum distance between galaxies in the Supercluster) is 50 h^{-1}Mpc (Einasto et al., 2011). This Supercluster is separated from the Sloan Great Wall (SGW) by a void and is connected to it by a filament of galaxies. The morphology of this Supercluster resembles a multi-branching filament or an elongated multispider (Einasto et al., 2011).

4.2.1 Number Density Map

Figure 31 shows the number density map of galaxies in the Supercluster S[173+014+0082]. Fig. 31a represents the number density map of galaxies when the distance (or radius) is fixed at 0.25° from each galaxy. In this diagram, we notice that there are some distinct substructures but the number of nearest galaxies for each is less than 75. Thus, this radius does not full-fill the imposed constraint. Then, we increased the radius to 0.50° whose number density map is shown in Fig. 31b. However, the plot shows a clear picture of substructure, it contains only one such structure whose neighbouring galaxy. Further, we vary the radius of a circle to find out any other substructures. For the radius 0.75°, we observed more substructures than for radius 0.50°. Hence, this radius is to identify substructures in the Supercluster. Similarly, an appropriate number density map for a radius equal to 1.0° is shown in Fig.31d.

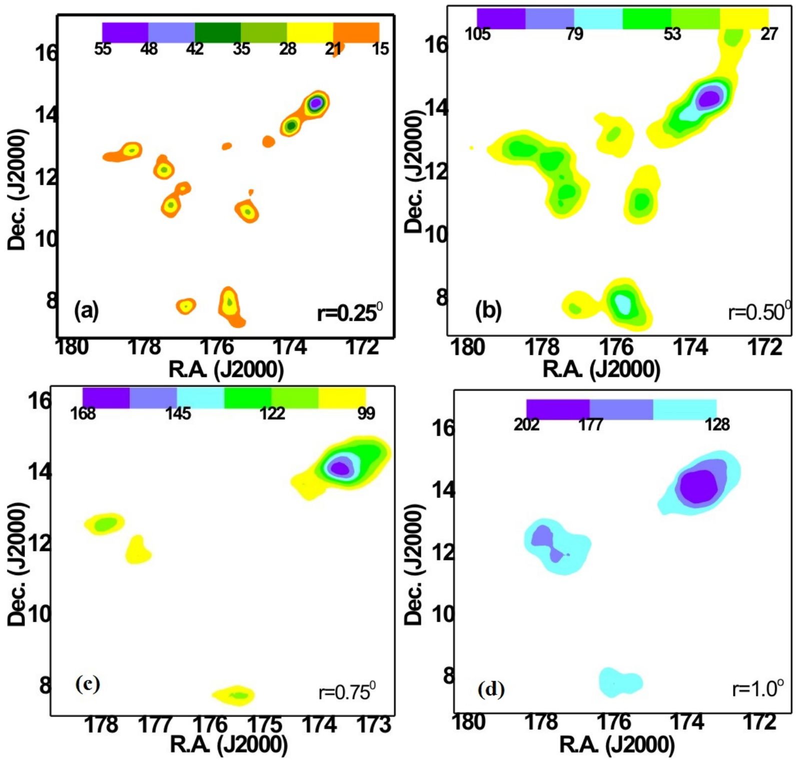

Figure 31: Number density map of galaxies in the Supercluster S[173+014+0082] having nearest neighbour distance of each galaxies at (a) r=0.25°, (b) r=0.5°,(c) r=0.75°, (d) r=1.0°. The color bar is shown. As the radius increases, the subclustering becomes prominent.

4.2.2 Redshift Map

The redshift map of galaxies in the Supercluster with a mean redshift of 0.083 is shown in Figure 32. The color map shows that the velocity dispersion is maximum in the region where the number density of galaxy is maximum. In the substructure region at 13° declination, the redshift dispersion is found to be |z|= 0.085, whereas the lower and upper substructure show |z|= 0.082 and 0.090, respectively. It seems that there is the linear relationship between redshift dispersion and the number density of galaxies in the substructures,

$$N_s(2) = -1.7 \times 10^4 |z| + 1660.32 \tag{4.4}$$

We change the nearest neighbour radius to 0.5° and 0.75° and calculated the slope of a linearly fitted line as described above, and the results were identical. As a result, we suggest an empirical relation (equation 4.4) between number density and mean redshift of galaxies in the Supercluster S[173+014+0082].

Galaxies in the Virgo-Coma Superclusters have redshift dispersion (Δz) of 600 km s^{-1} (Struble & Rood, 1999). For the local group, it has a value of 68 km s^{-1} (Struble &

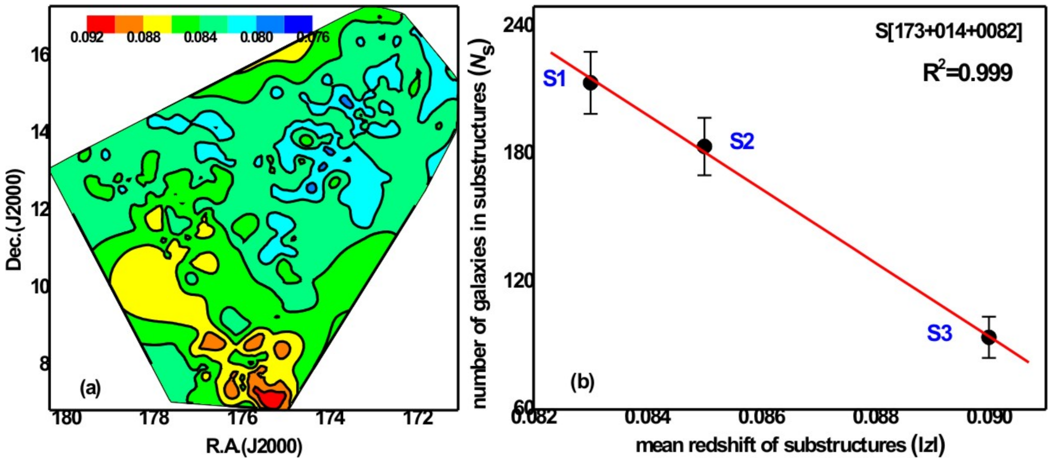

Figure 32: Redshift map is shown for galaxies in the Supercluster S[173+014+0082]. The mean redshift of Supercluster is 0.083. The contour levels are at the redshift 0.076, 0.080, 0.084, 0.088, 0.092. In the substructure region, galaxies hardly have identical redshifts. (b) Number of galaxies in three substructures versus redshift dispersion plot. The statistical $\pm 1\sigma$ error bars are shown.

Rood, 1999).

4.2.3 Magnitude Map

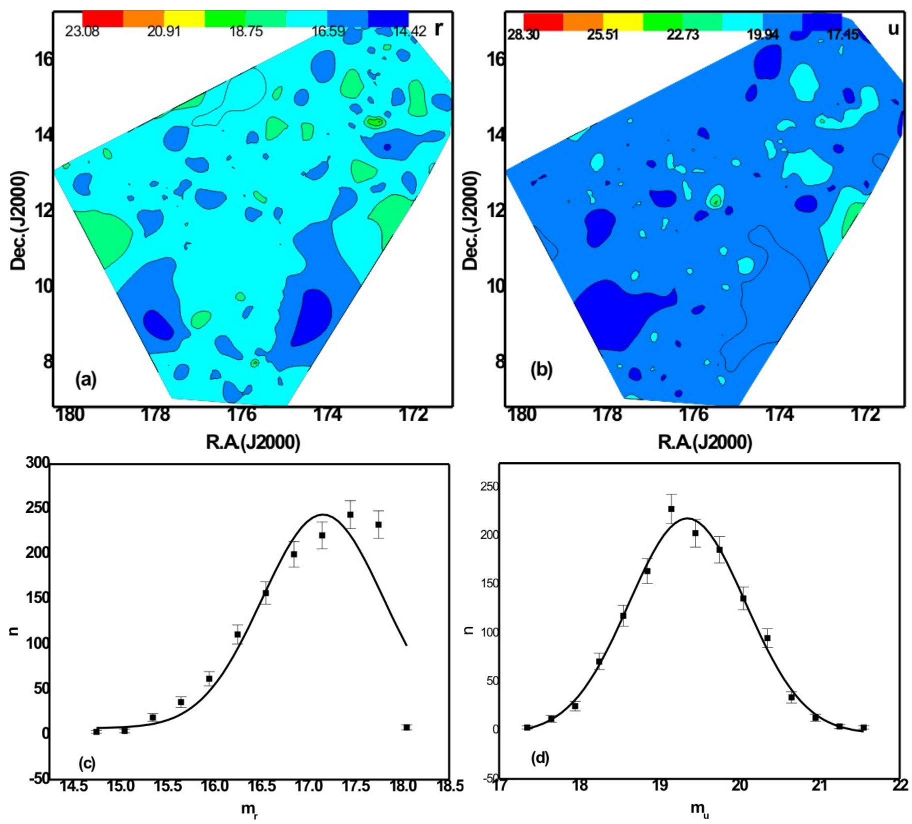

Figure 33: Magnitude map of galaxies in the Supercluster S[173+014+0082] (a) r-magnitude, (b) u-magnitude. The color bar is shown. The contour levels are at 14.42, 16.59, 18.75, 20.91, 23.08 for r-filter and 17.15, 19.94, 22.73, 25.51, 28.30 for u- filter, respectively. The distribution of r and u-magnitude shows Gaussian like distribution.

Magnitude maps of galaxies in the Supercluster S[173+014+0082] are shown in Fig. 33ab. The peak wavelength 6165 Å with the bandwidth 511.7 Å is the SDSS r-magnitude. In the u-filter, the substructure located in the northern region is found to have a higher magnitude. As know, The higher the magnitude, the lower the brightness.

Figure 33cd shows the magnitude distribution of galaxies in the Supercluster S[173+014 +0082]. Gaussian fits are shown by the solid curve. For r- and u-filters, the Gaussian center is found to be at 17.158 for and 19.350, respectively. The Gaussian functions for r- and u-magnitude distributions are given by

$$n_r = 7.18 + 237.65 \exp\left(\frac{-2(m_r - 17.158)^2}{1.66}\right) \tag{4.5}$$

$$n_u = -3.40 + 222.32 \exp\left(\frac{-2(m_u - 19.350)^2}{2.12}\right) \tag{4.6}$$

4.2.4 Substructure Classification

Table 9: Substructures of the Supercluster S[173+014+0082]. Second and third columns show positions of Superclusters. The next two column represent mean redshift and number of galaxies in the substructures. The last two columns list mean u-magnitude and r-magnitude of substructures, respectively.

Substructure	R.A.(J2000)	Dec.(J2000)	$\|Z\|$	N_g	$\|u\|$	$\|r\|$
S1[173+014+0082]	173.216°	14.461°	0.083	214	16.3	18.3
S2[173+014+0082]	178.335°	13.000°	0.085	184	16.2	18.1
S3[173+014+0082]	175.508°	08.227°	0.090	94	16.3	18.2

Based on number density maps, redshift magnitude distributions, we noticed three substructures in the Supercluster S[173+014+0082]. These substructures are found to be located at different latitudes. The mean redshift of galaxies in these substructures is similar to that of the Supercluster itself.

4.2.5 Preferred Alignments in the Supercluster

The Supercluster S[173+014+0082] has 1302 galaxies. We used three different statistical tests to identify the preferred alignment of the spin vector of galaxies. Table 10 shows the statistics for the polar angle (θ) distribution in the Supercluster S[173+014+0082], the chi-square probability (P(>χ^2)) is found to be 0.653 more than the critical value of 0.050 i.e., (5%), the first order Fourier coefficient (Δ_{11})/σ(Δ_{11}) is 0.9 which is less than 1.5σ, Fourier probability (P(>Δ_{11})) is to be found 0.643 more than 0.150 significant

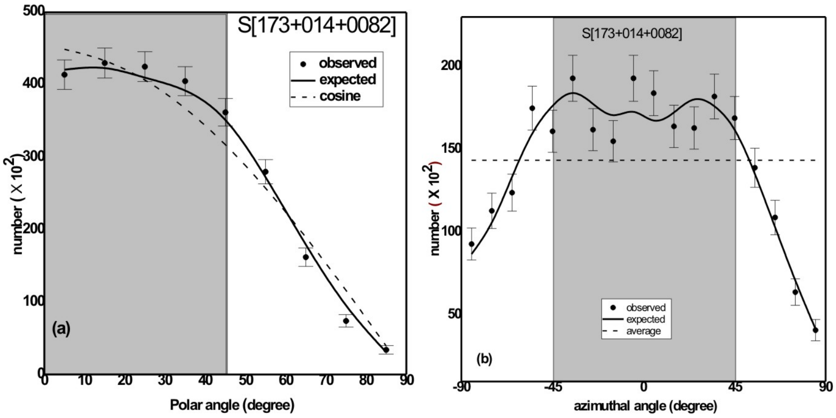

Figure 34: Polar (a) and azimuthal (b) angle distributions of galaxies in the Supercluster S[173+014+0082]. The solid circles with statistical error bars ($\pm 1\sigma$) represent observed distribution. The solid curves are obtained from random simulation assuming isotropic distributions.

level and the auto-correlation coefficient (C/C(σ)) to be 0.4 less than the critical value (1σ). These results support the isotropic distribution. As a result, all three statistical tests show strong isotropic distribution, indicating the random orientation of the spin vector of galaxies. From this result, we can conclude that the galaxy formation model supports the Hierarchy model (Peebles, 1969).

The statistics test in azimuthal angle (ϕ) distribution (Table 10), the chi-square probability (P(>χ^2)) is 61.0% (more than 5%), the value of first order Fourier coefficient ($\Delta_{11}/\sigma(\Delta_{11})$) is -0.4 (less than 1.5σ), Fourier probability (P(>Δ_{11})) is found to be 88.3% which is greater than 15%) and auto-correlation coefficient (C/C(σ)) to be -0.5 (less than 1σ). These results are strong evidences to advocate Hierarchy model (Peebles, 1969) of galaxy evolution in our Supercluster.

Fig. 34a shows the polar angle (θ)-distribution of galaxies in the Supercluster S[173+014 +0082]. In the small-angle (θ<45°) angle region, i.e., in the shaded region no significant hump and dip are observed. While in larger angle (θ>45°), a significant dip, is observed at 75° with 1σ error limit. It may happen due to the gravitational tidal effect.

Fig. 34b represents the distribution of the azimuthal angle of galaxies in the Supercluster. For outside the shaded region, no significant humps and dips are observed in the distribution curve. In this region, two clear humps are observed, at $-5°$, 5°, and dip is observed, at $-15°$ within 1σ error limit.

4.2.6 Preferred Alignment in Substructures

Substructure S1[173+014+0082] consisting 214 galaxies. Table 10 shows the statistics for the polar angle (θ) distribution in the substructure S1[173+014+0082]. The value of chi-square probability (P>(χ^2)) is found to be 57.8% greater than the 5% significant

Table 10: Statistical parameters in the polar and azimuthal angles of galaxies in the Supercluster S[173 + 014 + 0082] and its substructures (first column). The chi-square probability (P> χ^2) is given in the second column. The third and fourth columns show first order Fourier coefficient ($\Delta_{11}/\sigma(\Delta_{11})$ and fourier probability. the last column tests the auto co-relation coefficient.

Sample	P(> χ^2)	$\Delta_{11}/\sigma(\Delta_{11})$	P(> Δ_1)	C/$C(\sigma)$
Polar Angle				
S[173+014+0082]	0.653	0.9	0.643	0.4
S1[173+014+0082]	0.578	0.4	0.917	−0.7
S2[173+014+0082]	0.670	1.1	0.503	0.5
S3[173+014+0082]	0.000	−6.9	0.000	38.7
Azimuthal Angle				
S[173+014+0082]	0.610	−0.4	0.883	−0.5
S1[173+014+0082]	0.923	−0.1	0.992	−0.6
S2[173+014+0082]	0.435	−0.6	0.832	0.0
S3[173+014+0082]	0.530	0.5	0.851	−2.1

level, the first order Fourier coefficient $\Delta_{11}/\sigma(\Delta_{11})$ to be 0.4 less than the limit 1.5σ, the first order Fourier probability P(>Δ_1) is 0.917 i.e., 91.7% more than 0.150 i.e., 15% level; whereas the auto-correlation coefficient C/C(σ) to be found -0.7, is less than the limit 1σ. All these statistical tests suggest isotropic distribution of polar angle, suggesting random orientation of spin vector of galaxies.

The statistical tests for the azimuthal angle (ϕ) distribution are shown in Table 10. The value of chi-square probability (P>(χ^2)) is found to be 0.923 i.e., 92.3% which is more than 0.050 i.e., 5% significant level, the value of first order Fourier coefficient $\Delta_{11}/\sigma(\Delta_{11})$ is found to be -0.1, which is also less than 1.5σ limit, the first order Fourier probability (P(>Δ_1)) to be 99.2% greater than 15% and the auto-correlation coefficient C/C(σ) is −0.6 which is less than 1σ limit. All these statistical tests support the isotropic distribution azimuthal angle (ϕ) of galaxies in this substructure.

The polar angle (θ) distribution in the substructure S1[173+014+0082] is shown in Fig 35a. In the shaded region (θ<45°), at the small-angle region no significant hump and dip is observed. It may be due to binning effect. But in the larger angle region (θ>45°), a dip are seen clearly at 75° with a 1.5σ error limit.

The azimuthal angle (ϕ) distribution in the substructure S1[173+014+0082] is shown in Fig 35b. In small-angle region (−90°<ϕ<−45°), the hump and dip in the distributions show that the observed number of solutions at this small angle region is more and less than the expected shows hump and dip respectively. Thus, hump at an angle −75° and dip at −65° both with 1σ error limit. For the shaded (bimodal) region −45°<ϕ<45°, there are two clear humps and dips are seen. Here, humps are at −45° and 35° similarly, two dips, are −35° and at 25°, all these are within the error limit of 1.5σ. Although, the observed solution is more than that expected value in a larger angle region (45°<ϕ<90°).

The distribution curve does not show any significant hump in this region. Thus, it is due to the binning effect.

The substructure S2[173+014+0082] has 184 galaxies. The statistics for the polar angle (θ) distribution in the substructure S2[173+014+0082] shows (Table 10) the value of chi-square probability (P>(χ^2)) is 67% (greater than 5%), first order Fourier coefficient $\Delta_{11}/\sigma(\Delta_{11})$ is 1.1 (less than 1.5σ) and Fourier probability (P(>Δ_1)) is 50.3% which is greater than reference value 15% and the value of auto-correlation coefficient is 0.5 (smaller than 1σ). These statistics follow strong isotropy.

The statistics for the azimuthal angle (ϕ) distribution in table 10, shows the chi-square probability (P>(χ^2)) is to be found 43.5% greater than 5%, the value of first order Fourier coefficient $\Delta_{11}/\sigma(\Delta_{11})$ to be -0.6 less than 1.5σ and Fourier probability (P(>Δ_1)) is 83.2% greater than significant level (15%) and auto-correlation coefficient to be found 0.0 smaller than 1σ. Similar to the polar angle distribution, azimuthal angle distribution shows strong isotropy.

The polar angle (θ) distribution in the substructure S2[173+014+0082] is shown in Fig 35c, In the small-angle region θ<45°, the number of observed solutions (209) to be very few bins (7) more than the expected solution (214). Thus, a hump is seen at 35° in this region. But, there is no significant dip is observed. For large angle region θ>45°, two dips seen at 65° with 1.5σ error limit and 75° with 1σ error limit. Also, a hump is seen at 55° within error limit 1σ.

The distribution of azimuthal angle (ϕ) is shown in Fig. 35d. In the small-angle region $-90°<\phi<-45°$, one hump at $-75°$ and one dip at $-65°$ within 1.5σ limit are observed. In the range between $-45°<\phi<45°$, there are three significant dips at $-25°$, 25° and 35° and one hump at 5° with error limit 1.5σ. At a higher angle ϕ>45°, one clear hump at 65° is noticed. No dip is seen at the larger angle region. The existence of dip at the shaded region and hump at the outer region indicates that spin vector projection of galaxies tends to lie tangentially towards the center of the reference plane.

The substructure S3[173+014+0082] contains 94 galaxies. The statistical tests of polar angle (θ) distribution are given in Table 10. The value of chi-square probability (P>(χ^2)) and Fourier probability (P(>Δ_1)) are found to be zero, which is less than their significant level, i.e., 5% and 15% respectively and the value of first order Fourier coefficient ($\Delta_{11}/\sigma(\Delta_{11})$) is -6.9 less than 1.5σ similarly, the result of auto-correlation coefficient C/C(σ) is found to be 38.7 greater than the limit 1σ. These results show the anisotropic distribution. As a result, we may conclude that this substructure is deviated from the Hierarchy model (Peebles, 1969) of galaxy formation, suggesting that the angular momentum vector of galaxy rotation axes showed preferred alignment-either parallel or perpendicular to the reference plane. To identify such orientation we further analyze the hump and dip in each bin.

The statistics for the azimuthal angle (ϕ) distribution in Table 10, the statistical results are found to be; the value of chi-square probability (P>(χ^2)) is 53.0% greater than 5%, the value of first order Fourier coefficient $\Delta_{11}/\sigma(\Delta_{11})$ is 0.5 which is less than error limit 1.5σ, the value of Fourier probability (P(>Δ_1)) is 85.1% which is more than 15% and the result of auto-correlation coefficient C/C(σ) is −2.1 less than 1σ limit. As a result, all statistics support the isotropic distribution.

The distribution of polar angle (θ) is given in Fig. 35e. In the small-angle region θ<45°, the observed number of solutions is less than the expected number of solutions. This strongly suggests that there should be a hump in this region. On the other hand, at a larger angle region θ>45°, the expected number of solutions is more than the observed number of solutions indicating the presence of hump in this region: in contrast, a small angle (θ<45°), a significant hump at 25° (>1σ) and larger angle (θ>45°) two clear dips at 75° with 2σ error limit and at 85° with 5σ error limit. The hump at a small angle (<45°) and dips at a larger angle (> 45°) cause negative Δ_{11} in Fourier test, indicating that the angular momentum vectors of galaxies in S3[173+014+0082] tend to lie parallel to the reference plane. The value of Δ_{11} is found to be 7σ. This result is in favor of Pancake model ((Doroshkevich, 1973), (Doroshkevich et al., 1978)) of galaxy formation. In this model, it is assumed that the formation of cluster took place first then after fragmentation of cluster leads to the formation of the galaxy with the help of adiabatic fluctuation.

The azimuthal angle (ϕ) distribution of galaxies in S3[173+014+0082] is shown in Fig. 35f. From this distribution curve it is seen that there is a hump at −85° within 2σ error limit and dip at −65° (> 1σ) in (−90°<ϕ<−45°). Similarly, two humps at 65° and 85° and a dip at 55° with an error limit of 1.5σ of each are observed in (45°<ϕ<90°) region. In the shaded region, a hump with an error limit of 1σ has appeared at −35° and two dips are seen at 15° with 1σ error limit and 35° with an error limit of 1.5σ.

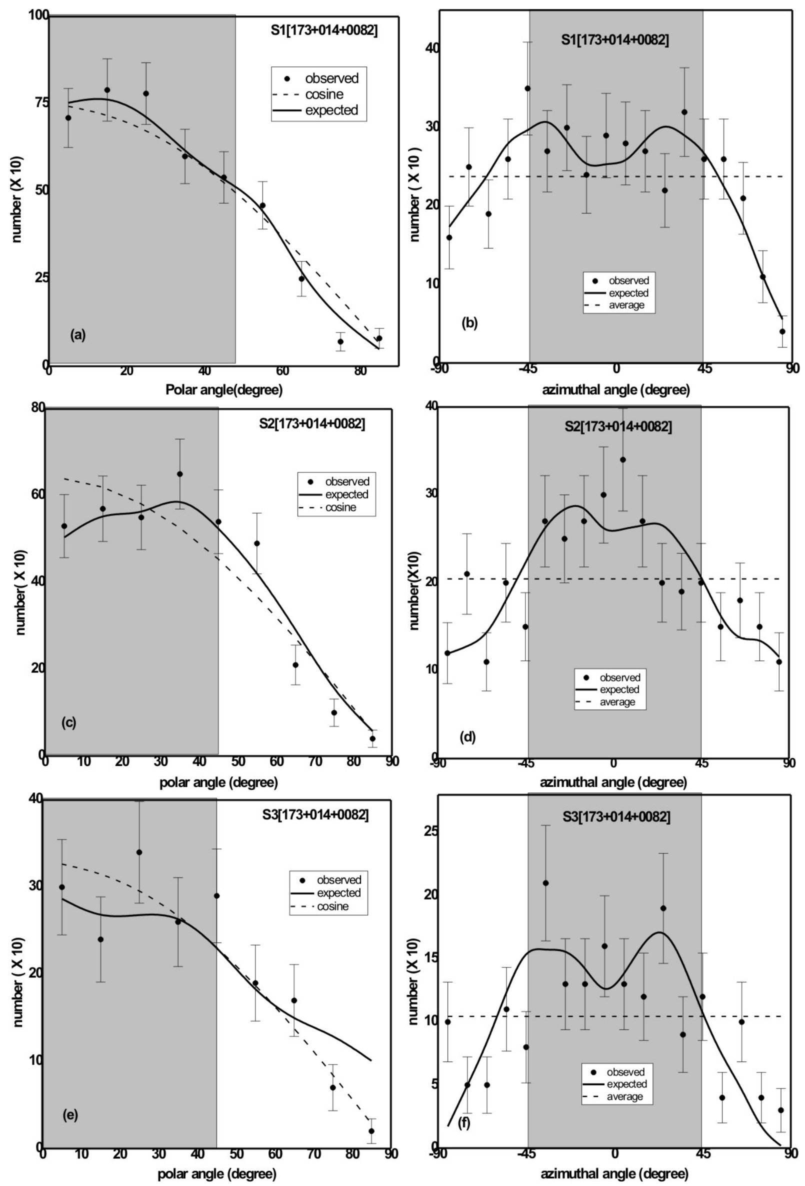

Figure 35: Polar (a, c, e) and azimuthal angle (b, d, f) distributions of galaxies in the substructures of Supercluster S[173+014+0082]. Solid circles with statistical error bars ($\pm 1\sigma$) represent observed distributions. The expected distributions are represented by solid curves. These solid curves are obtained by preforming numerical simulation. The grey-shaded region supports pancake model (Doroshkevich, 1973),(Doroshkevich et al., 1978) if there is excess solution than the expected.

4.2.7 General Discussion

In the polar angle distribution, Isotropy is observed in all samples except in the substructure S3[173+014+0082], indicating that there are no preferred alignments, while consistency is observed in the azimuthal angle distribution. The radial velocity distribution should not be unipolar, according to the hierarchy model (Peebles, 1969). Thus, to test whether the obtained statistical results are in accordance with hierarchy model (Peebles, 1969), we need to study the radial velocity distribution of each sample. For this, we plotted the radial velocity distribution map which is shown in Fig. 36.

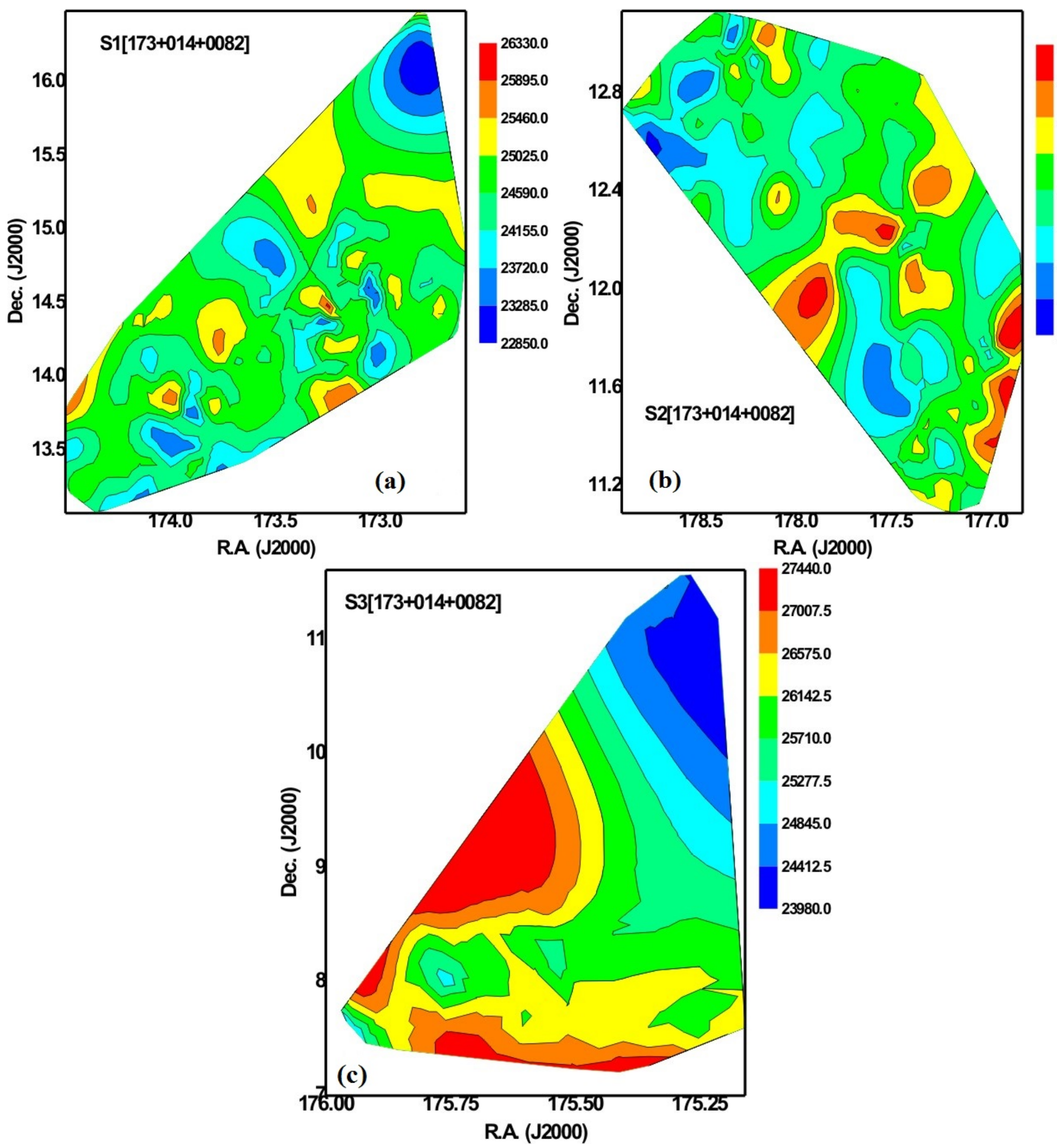

Figure 36: The radial velocity distribution of galaxies in three substructures : (a) S1[173+014+0082] (b) S2[2173+014+0082] and (c) S3[S2173+014+0082] R.A. and Dec. represent the right ascension and declination in degree respectively. Color scale represents the radial velocity.

As the database contains the redshift value of an individual galaxy, this value can be use to find the radial velocity of galaxies using the following relation :

$$z = v/c \tag{4.7}$$

Where z is redshift, v is radial velocity, and c is the speed of light in km/s. From Fig. 36 we observed that two substructures (S1[173+014+0082] and S2[173+014+0082]) have different kinds of radial velocity distribution than for S3[173+014+0082]. In the case of substructure S3[173+014+0082], we noticed a systematic pattern in the velocity distribution from the inner region to the outer. In the inner part of the contour map, galaxies have the maximum velocity to be located. As we go outward the velocity decreases. That means the particular number of galaxies are localized in a particular region of the substructure. This result advocates the Hierarchy model (Peebles, 1969) of galaxy evolution in this substructure suggesting that galaxies have a particular orientation. But, in the case of a remaining sample, we observed that there is no such systematic localization, indicating galaxies are distributed randomly. This result showed isotropic distribution in the Supercluster as well as in this substructure S1[173+014+0082] and S2[173+014+0082].

To sum up, the statistical analysis and radial velocity distribution maps suggest a random orientation of spin vector of galaxies in all samples except in the substructure S3[173+014+0082]. This result strongly advocates the Hierarchy model (Peebles, 1969) of galaxy evolution in this Supercluster.

4.3 Supercluster S[247+040+0029]

In this section, we study Supercluster S[247+040+0029] which is located in the northern hemisphere of the equatorial coordinate system. The mean redshift of this Supercluster is 0.031 (radial velocity 9,100 km s^{-1}), and it has 1331 galaxies. The distance of this Supercluster is 92 h^{-1}Mpc and diameter is 21 h^{-1}Mpc and contain clusters that are exceptionally rich (Einasto et al., 2011). The morphology of this Supercluster resembles a spider (Einasto et al., 2011).

4.3.1 Number Density Map

The Number density map of Supercluster S[247+040+0029] is shown in Fig. 37. First, we try to find the number of galaxies around each galaxy within the different radius values such as 0.2°, 0.3°, 0.35°, 0.4°, 0.5°,0.75°, 1.0°, and 1.25°. By analyzing the distribution of galaxy in the contour map in various radius values, we choose the particular value of radius for which a clear substructure is observed. As a result, we have chosen 0.3° and 1.0° as two values of radius for our work. For radius value 0.3°, three substructures, namely S1[247+0040+0029], S2[247+0040+0029] and S3[244+0035+0029] have been found. Similarly, for radius value 1.0°, one substructure, namely S4[247+0041+0029] has been found. The number density map for different radius values is shown in Fig. 37.

Based on the number density map (Fig. 37), four different substructures are separated by using the threshold number of galaxies belonging to the four substructures based on their peak values and standard deviation of galaxies density. Four different substructures based on the above number density map are S1[247+0040+0029], S2[247+0040+0029], S3[244+0035+0029], and S4[247+0041+0029].

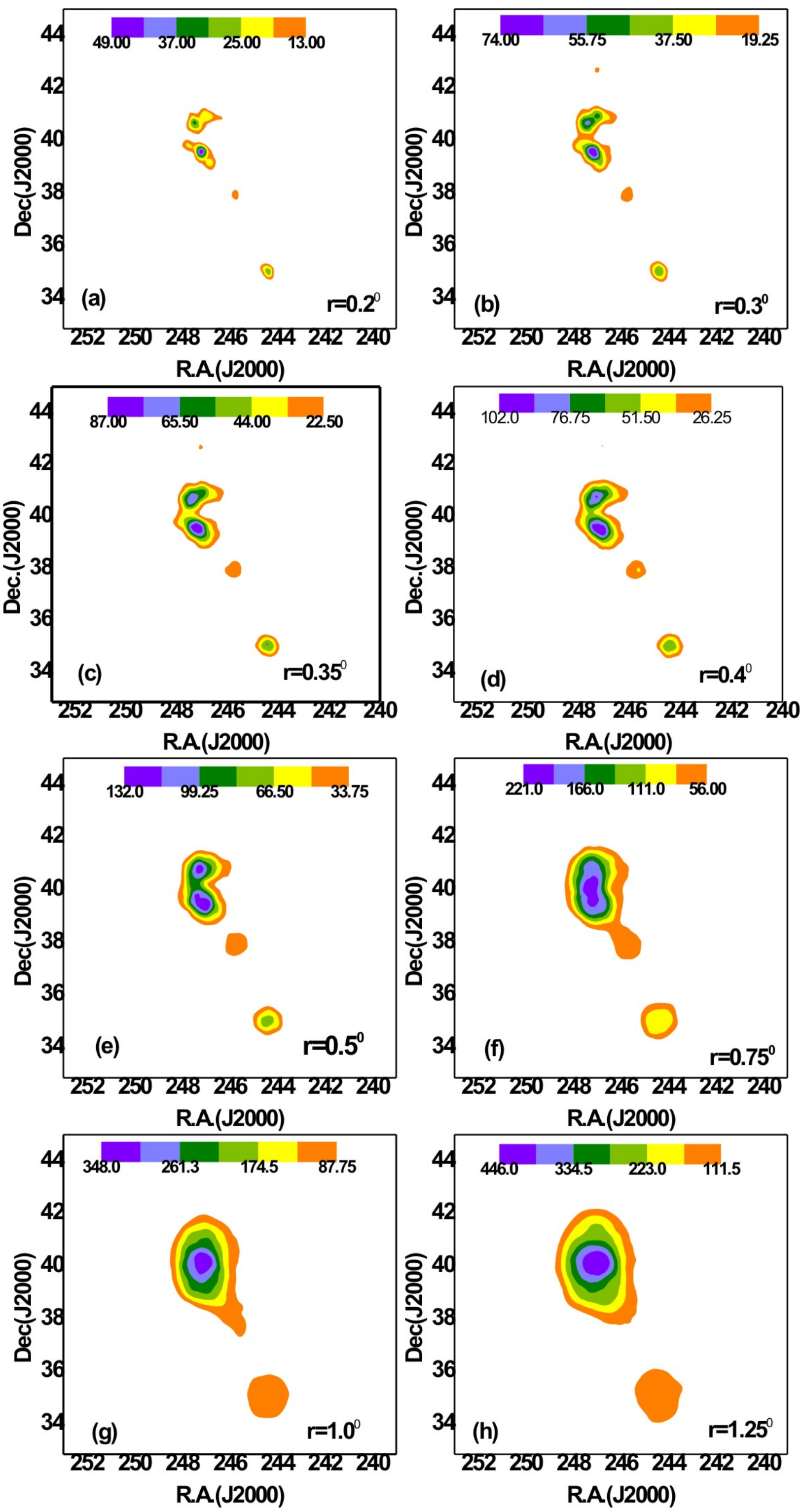

Figure 37: Number density map of galaxies in the Supercluster S[247+040+0029] having nearest neighbour distance of each galaxies at (a) r=0.2°, (b) r=0.3°, (c) r=0.35°, (d) r=0.4°(e) r=0.5°, (f) r=0.75°,(g) r=1.0°, (h) r=1.25° and the color bar is shown. As the radius increases, the subclustering becomes prominent.

4.3.2 Redshift Map

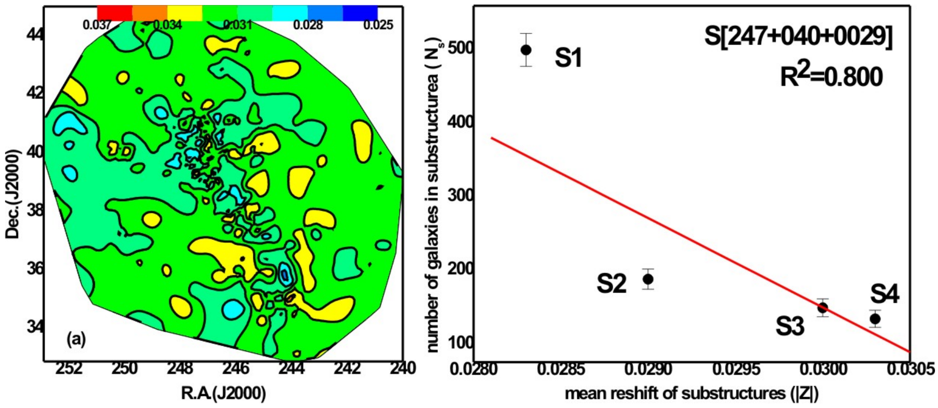

Figure 38: Redshift map is shown for galaxies in the Supercluster S[247+040+0029]. The mean redshift of Supercluster is 0.031. The contour levels are at the redshift 0.025, 0.028, 0.031, 0.034, 0.037. In the substructure region, galaxies hardly have identical redshifts.(b) Number of galaxies in five substructures versus redshift dispersion plot. The statistical $\pm 1\sigma$ error bars are shown.

Figure 38 shows a redshift map of galaxies in the Supercluster that have a mean redshift of 0.031. The color map shows that the velocity dispersion is minimum in the region where the number density of galaxy is minimum. In the substructure region at 35.0° declination, the redshift dispersion is found to be |z|= 0.030, whereas the lower and upper substructure show |z|= 0.028 and 0.031, respectively. It seems that there is a linear relationship between redshift dispersion and the number density of galaxies in the substructures,

$$N_s(3) = -9.5 \times 10^4 |z| + 3035.52 \tag{4.8}$$

We varied the nearest neighbour radius to 0.3° and 1.00° and calculated the slope of a linearly fitted line as above and found the same. Therefore, we propose empirical relation (equation 4.8) between number density and redshift dispersion of galaxies in the Supercluster S[247+040+0029].

The galaxies inside the Hercules Superclusters have a redshift dispersion (Δz) of 593 km s^{-1} (Struble & Rood, 1999). For the local group, it has a value of 68 km s^{-1} (Struble & Rood, 1999). This is a set of local Superclusters with a peculiar velocity that is higher than that of distant Superclusters.

4.3.3 Magnitude Map

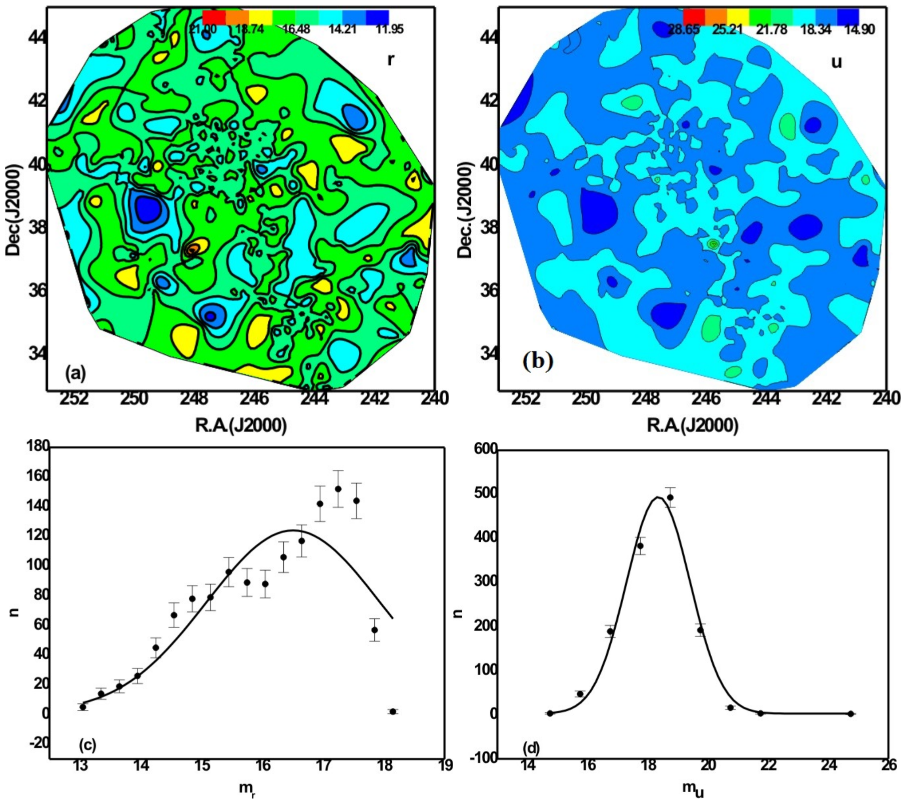

Figure 39: Magnitude map of galaxies in the Supercluster S[247+040+0029]: (a) r-magnitude, (b) u-magnitude. The color bar is shown. The contour levels are at 11.95, 14.21, 16.48, 18.74, 21.00 for r-filter and 14.90, 18.34, 21.78, 25.21, 28.65 for u- filter, respectively. The distribution of r and u-magnitude.

Magnitude maps of galaxies in the Supercluster S[247+040+0029] are shown in Fig. 39ab. The SDSS r-magnitude refers to the peak wavelength 6165 Å with the bandwidth 191.1 Å. In the u-filter, the substructure located in the northern region is found to have a higher magnitude. As we know, the higher the magnitude, the lower the brightness.

The magnitude distribution of galaxies in the Supercluster S[247+040+0029] can be seen in figure 39cd. The solid curve represents Gaussian fits. The Gaussian centre is found to be at 16.448 for r- and 18.351 for u-filters. The Gaussian functions for r- and u-magnitude distributions are given by

$$n_r = 0.20 + 167.55 \exp\left(\frac{-2(m_r - 16.448)^2}{7.34}\right) \tag{4.9}$$

$$n_u = 2.59 + 492.84 \exp\left(\frac{-2(m_u - 18.351)^2}{6.71}\right) \tag{4.10}$$

4.3.4 Substructure Classification

Table 11: Substructures of the Supercluster S[247+040+0029]. Second and third columns show positions of Superclusters. The next two columns represent the mean redshift and number of galaxies in the substructures. The last two columns list mean u-magnitude and r-magnitude of substructures, respectively.

Substructure	R.A.(J2000)	Dec.(J2000)	$\|Z\|$	N_g	$\|u\|$	$\|r\|$
S1[247+040+0029]	247.998°	39.712°	0.028	500	18.0	17.3
S2[247+040+0029]	246.956°	41.038°	0.029	188	17.8	16.9
S3[244+035+0029]	244.359°	35.016°	0.030	149	18.1	17.6
S4[247+0041+0029]	250.163°	39.941°	0.0303	134	18.0	17.8

On the basis of the number density maps, five different substructures are separated by using the threshold number of galaxies belonging to the five substructures based on their peak values and standard deviation of galaxies density.

4.3.5 Preferred Alignments in the Supercluster

The Supercluster S[247+040+0029] consists of 1331 galaxies. To identify the preferred alignment of the spin vector of galaxies, we have performed three different statistical tests (Table 12). Thus, In the polar angle (θ) distribution (Table 12), the values of chi-square probability P(> χ^2) is 51.1% which is greater than 5%, first order Fourier coefficient $\Delta_{11}/\sigma(\Delta_{11})$ is -0.2 which is less than 1.5σ, first order Fourier probability (P(>Δ_1)) is 95.4% which is more than critical value 15% and auto-correlation coefficient (C/C(σ)) to be found -0.7 which is less than 1σ. Thus, all statistics show the isotropic distribution of angular momentum vectors of galaxies in the Supercluster S[247+040+0029].

In the azimuthal angle (ϕ) distribution (Table 12), the value obtained for the chi-square probability P(> χ^2), is found to be 95% more than significant level 5%, first order Fourier coefficient $\Delta_{11}/\sigma(\Delta_{11})$ to be 0.4 less than 1.5σ, first order Fourier probability (P(>Δ_1)) to be found 63.3%, auto-correlation coefficient (C/C(σ)) is -2.2 which is less than 1σ. Thus, all statistical test shows the strong isotropic distribution of spin vectors.

Fig. 40a shows the plot of θ-distribution, there are no significant humps and dips are in the small-angle region θ<45°. But, in large angle regions θ>45°, a hump is seen at 55°. This hump is due to observed solutions more than the expected solution. It is due to the local effects. So, there is no preferred alignment of spin-vectors of galaxies.

Fig. 40b shows the plot of ϕ-distribution. In the small-angle region ϕ>45°, there is a small dip at -75°. In large-angle region ϕ>45°, there is a small dip, at 55° both within limit 1.5σ . So, we can conclude that there is no preferred alignment of spin-vectors of galaxies.

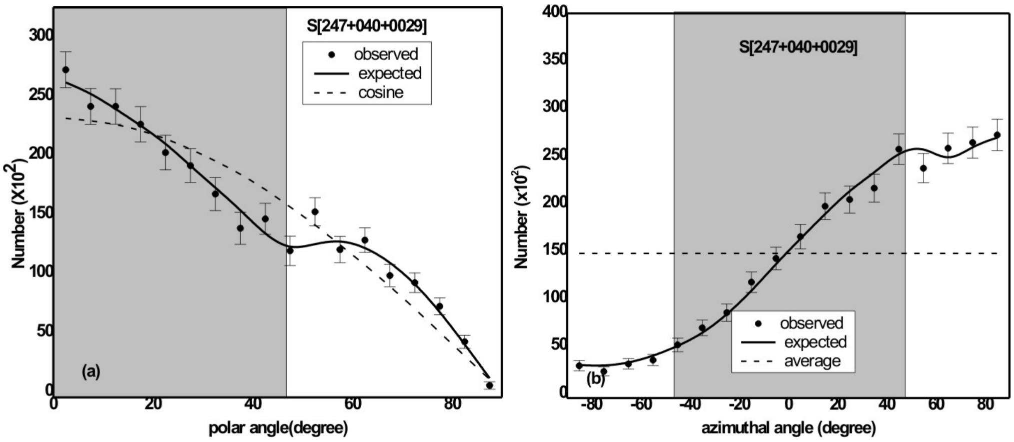

Figure 40: Polar (a) and azimuthal (b) angle distributions of galaxies in the Supercluster S[247+040+0029]. The solid circles with statistical error bars ($\pm 1\sigma$) represent observed distribution. The solid curves are obtained from random simulation assuming isotropic distributions.

Table 12: Statistical parameters in the polar and azimuthal angles of galaxies in the Supercluster S[247 + 040 + 0029] and its substructures is in the first column. The chi-square probability (P> χ^2) is given in the second column. The third and fourth columns show first order Fourier coefficient ($\Delta_{11}/\sigma(\Delta_{11})$ and Fourier probability. the last column tests the auto co-relation coefficient.

Sample	P(> χ^2)	$\Delta_{11}/\sigma(\Delta_{11})$	P(> Δ_1)	C/$C(\sigma)$
Polar Angle				
S[247+040+0029]	0.511	− 0.2	0.954	−0.7
S1[247+0040+0029]	0.943	−0.3	0.952	−1.2
S2[247+0040+0029]	0.909	−0.1	0.984	−0.9
S3[244+0035+0029]	0.893	0.2	0.982	−0.6
S4[247+0041+0029]	0.996	−0.3	0.871	−0.1
Azimuthal Angle				
S[247+040+0029]	0.950	0.4	0.633	−2.2
S1[247+040+0029]	0.570	−0.3	0.855	−1.0
S2[247+040+0029]	0.911	0.7	0.964	−0.1
S3[247+040+0029]	0.969	−0.1	0.966	−0.0
S4[247+0041+0029]	0.838	−0.5	0.804	−0.9

4.3.6 Preferred Alignment in Substructures

The substructure S1[247+0040+0029] has 500 galaxies. Table 12 shows the statistics for the polar angle (θ) distribution in the substructure S1[247+0040+0029]. The values of chi-square probability P(> χ^2) is 94.3% which is greater than 5%, first order Fourier coefficient $\Delta_{11}/\sigma(\Delta_{11})$ is −0.3 which is less than 1.5σ and first order Fourier probability (P(>Δ_1)) is 95.2%, auto-correlation coefficient (C/C(σ)) is −1.2 less than 1σ. Here, all statistics show the distribution of spin vectors is strong isotropic distribution.

The statistics for the azimuthal angle (ϕ)-distribution are shown in Table 12. The statistics value obtained for the chi-square probability P(> χ^2) is 57.0% which is more than 5%, first order Fourier coefficient $\Delta_{11}/\sigma(\Delta_{11})$ is −0.3 less than 1.5σ, first order Fourier probability (P(>Δ_1)) is 85.5% more than 15% , auto-correlation coefficient (C/C(σ)) is -1.1 less than 1σ. These all statistics shows the strong isotropic distribution.

In Fig. 41a, at small angle region θ<45°, the number of observed solutions (699) are slightly less than expected (670) solutions (the difference between observed and expected solution in that range is 1). At this region, there is one dip at 22°. For the large angles(θ>45°), the number of expected solutions is less than that of observed (observed solutions are more than one that of expected). These are both within limit 1σ. Again there is one hump at 47°. This hump is due to the local effect. Thus, we conclude no preferred alignment of spin vectors of galaxies.

In the azimuthal angle distribution as shown in Fig 41b. For the range −45°<ϕ<+45°, there is a significant dip at 38°. For small angle region ϕ<−45°, observed solutions are less than that of expected solutions. Thus, there is a dip at −55°. For the region of the large angles (ϕ>45°), there are no significant hump and dip in this range. So we can conclude that there is no preferred alignment among spin-vectors of galaxies.

The substructure S2[247+0040+0029] contains 188 galaxies. The statistics for the polar angle (θ)-distribution in the substructure S2[247+0040+0029] is shown in Table 12. The value of chi-square probability P(> χ^2) is 90.9% greater than 5%, first order Fourier coefficient $\Delta_{11}/\sigma(\Delta_{11})$is -0.1 smaller than 1.5σ, first order Fourier probability (P(>Δ_1)) is 98.4% more than 15% , auto-correlation coefficient (C/C(σ))is -0.9 less than 1σ. Here, all statistics shows the strong isotropic distribution of spin vectors of galaxies.

Table 12 shows the statistics for the azimuthal angle (ϕ)-distribution, the statistic value obtained for the chi-square probability P(> χ^2) is 91.1% larger than 5%,first order Fourier coefficient $\Delta_{11}/\sigma(\Delta_{11})$ is 0.2 smaller than 1.5σ, first order Fourier probability (P(>Δ_1)) is 96.4% greater than 15%, auto-correlation coefficient (C/C(σ)) is -0.1 less than 1σ.

The polar angle (θ)-distribution is shown in Fig 41c, for the small-angle (θ<45°) region, there is one dip at 18° and one significant hump at 26° both within limit 1.5σ. For the large angles (θ>45°), there is one significant dip at 67°. This dip may be due to local effects. Thus, we conclude that there is no preferred alignment of spin vectors of galaxies.

In the azimuthal angle (ϕ)-distribution as shown in Fig 41d, in the small-angle region (ϕ<45°), a small dip is seen at −65°. In the bimodal region (−45°<ϕ<+45°) two humps at −15° and 15°, also two dips, are seen at 5° and 35°, these all are seen due to local effect. In the large-angle region (ϕ<45°), there is one significant dip at 65°. It is also due to the local effect. Thus, we conclude that there is no preferred alignment among spin-vectors of galaxies.

This substructure S3[244+0035+0029] contains 149 galaxies. Table 12 shows the statistics for the polar angle (θ)-distribution in the substructure S3[244+0035+0029]. The values of chi-square probability P(> χ^2) to be 0.893 i.e., 89.3% (greater than the significant level 0.050 i.e.,5%), first order Fourier coefficient $\Delta_{11}/\sigma(\Delta_{11})$ is found to be 0.2 (smaller than the limit 1.5σ), first order Fourier probability (P(>Δ_1)) is 0.982 i.e., 98.2% (greater than 15% limit), auto-correlation coefficient (C/C(σ)) is −0.6 (smaller than 1σ). Thus in all statistics suggest strong isotropic.

The statistics for the azimuthal angle ϕ-distribution (Table 12), the statistics value obtained for the chi-square probability P(> χ^2) to be 96.9% (much more greater than significant level 5%), first order Fourier coefficient $\Delta_{11}/\sigma(\Delta_{11})$ is −0.1 (less than the limit 1.5σ), first order Fourier probability (P(>Δ_1)) is found to be 96.6% (greater than 15% limit), auto-correlation coefficient (C/C(σ)) is −0.0 (less than the limit 1σ). Thus, all the statistical tests suggest strong isotropy.

In Fig 42e, at a small-angle region (θ<45°), the number of observed solutions is found to be very slightly smaller than expected solutions (Difference in that range 2). At this region, there is one dip at 13°. For the large angles region (θ>45°), the number of expected solutions is less than that of the observed solution (Difference in that range 2). There is one significant hump at 48° in that range which cancels the dip observed at lower angles. Thus, we conclude no preferred alignment of spin vectors of galaxies.

In the azimuthal angle (ϕ) distribution as shown in Fig 42f, at ϕ<−45°, there are no dips is seen. But there is one hump is seen at an angle −65° within limit 1.5σ. For range −45°<ϕ<+45°, there is one significant hump at an angle 4° within probable error 1σ. For the large angles (ϕ>45°), There is one significant dip at 65° which cancels the significant hump at −65°. But there is no more hump and dip in other range so we can conclude that there is no preferred alignment among spin-vectors of galaxies.

This substructure S4[247+0041+0029] consists of 134 galaxies. The statistics for the polar angle (θ)-distribution in the substructure S4[247+0041+0029] is shown in Table 12. By statistics, the values of chi-square probability P(> χ^2) is 99.6% (greater than the significant level 0.050 i.e., 5%), first order Fourier coefficient $\Delta_{11}/\sigma(\Delta_{11})$ to be −0.3 (less than limit 1.5σ), first order Fourier probability (P(>Δ_1)) is found to be 87.1% (more than significant level 0.150 i.e., 15%) and auto-correlation coefficient (C/C(σ)) to be −0.1 (less than the limit 1σ). Thus, all statistics test shows the isotropic distribution of spin vectors.

Table 12 shows the statistics for the azimuthal angle (ϕ)-distribution, the statistics value obtained for the chi-square probability P(> χ^2) to be 83.8% (which is greater than significant level 0.050 i.e., 5%), first order Fourier coefficient $\Delta_{11}/\sigma(\Delta_{11})$ is −0.5 smaller than limit 1.5σ, first order Fourier probability (P(>Δ_1)) to be found 80.4% more than 15%, auto-correlation coefficient (C/C(σ)) is −0.9 less than limit 1σ.

Fig 42g shows the polar angle (θ)- distribution, in the small-angle (θ<45°) region, there are two significant dips at 20° and 32° both within the limit 1.5σ respectively. Similarly, two significant humps at28° and 26° both within error limit 1.5σ. For the large angles (θ>45°), there is again one small dip at 57°(difference in range 1) within limit 1σ. Thus, we conclude that there is no preferred alignment of spin vectors of galaxies.

In the azimuthal angle (ϕ)-distribution as shown in Fig 42h, the observed solutions for the range −45°<ϕ<+45° are found to be 143, whereas the expected solutions are 142. This shows that observed solutions exceeded the expected solution by 1. For ϕ<−45°, observed and expected solutions both are 11. For the large angles (ϕ>45°), the observed 114 solutions are 1 less than what was expected. There is a significant humps at −45°. It is due to the local effect but there are no other significant humps and dips. We again conclude that there is no preferred alignment among spin-vectors of galaxies.

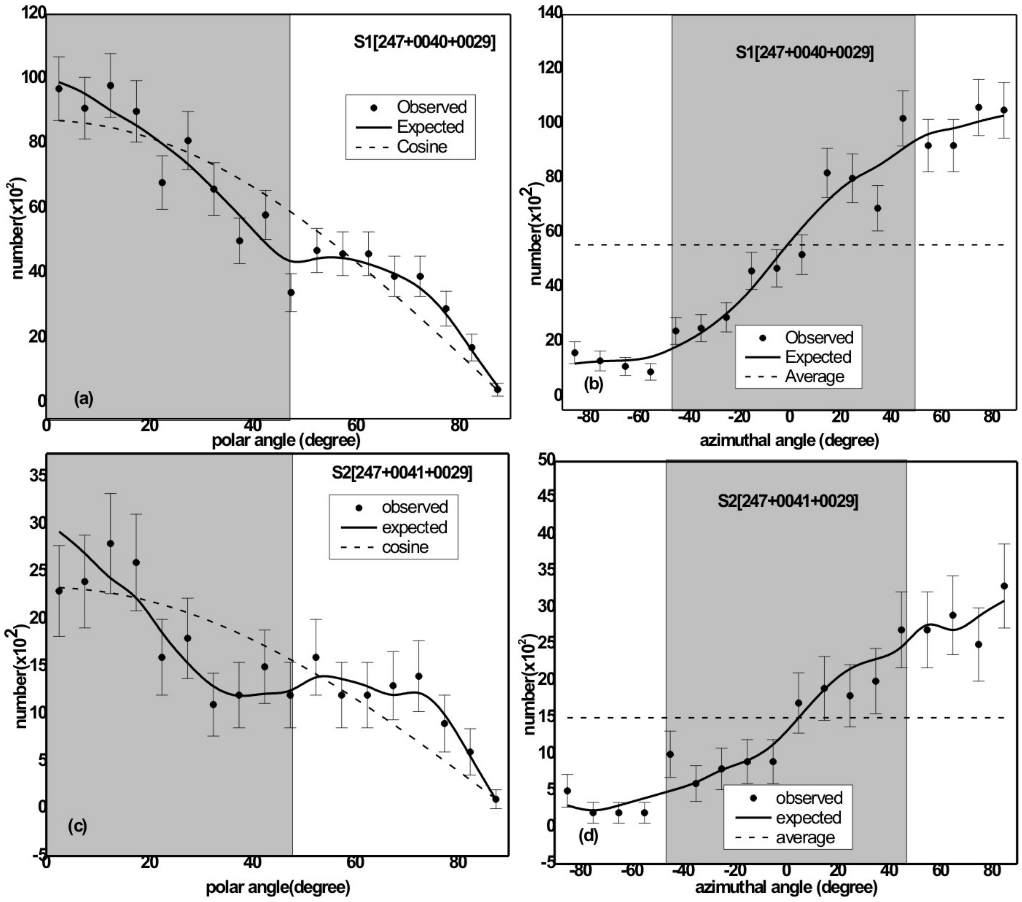

Figure 41: Polar (a, c) and azimuthal angle (b, d) distributions of galaxies in the substructures of Supercluster S[247+040+0029]. Solid circles with statistical error bars (±1σ) represent observed distributions. The expected distributions are represented by solid curves. These solid curves are obtained by preforming random simulation. The grey-shaded region supports pancake model if there is excess solution than the expected.

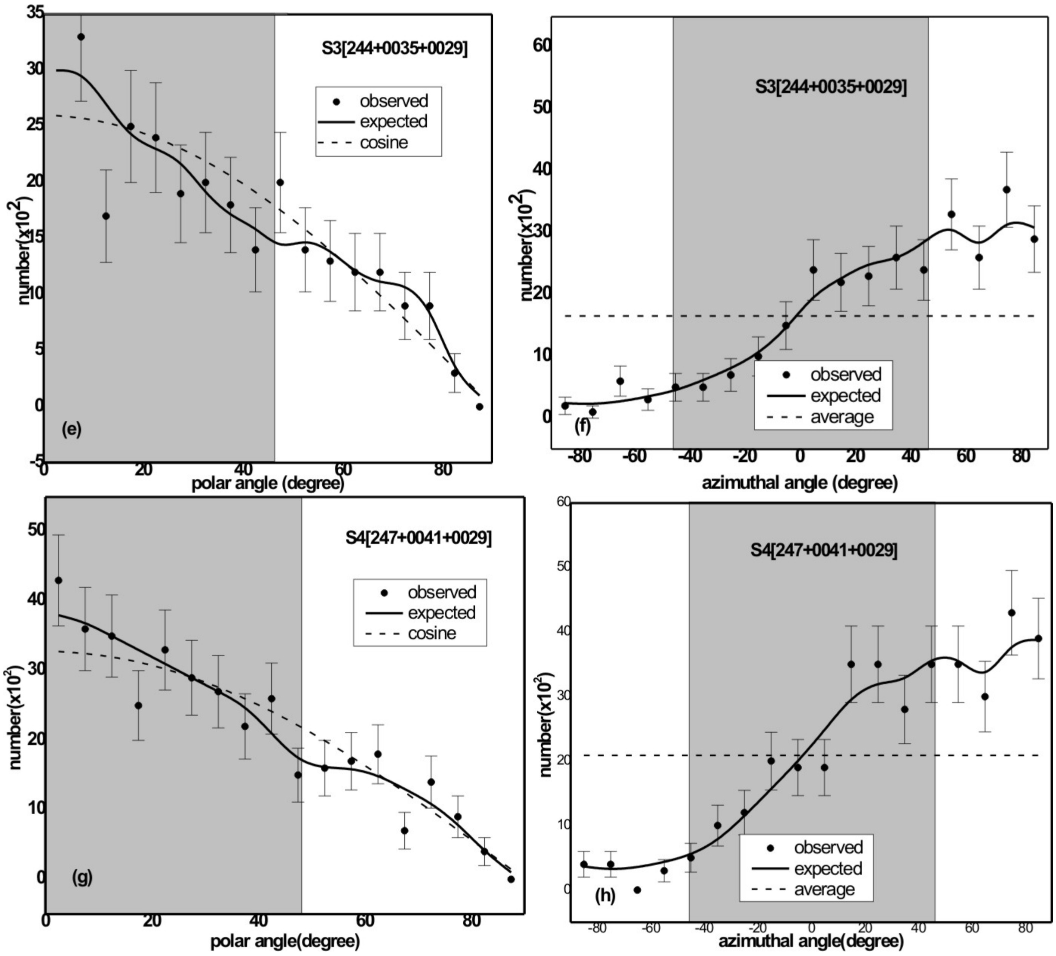

Figure 42: Polar (e, g) and azimuthal angle (f, h) distributions of galaxies in the substructures of Supercluster S[247+040+0029]. Solid circles with statistical error bars ($\pm 1\sigma$) represent observed distributions. The expected distributions are represented by solid curves. These solid curves are obtained by performing random simulations. The grey-shaded region supports the pancake model if there is excess solution than the expected.

4.3.7 General Discussion

We studied the spatial orientation of galaxies in the four substructures of the Supercluster S[247+040+0029]. We found a random orientation of galaxies suggesting vanishing angular momentum in the substructures.

4.4 Supercluster S[227+006+0078]

In this section, we study Supercluster S[227+006+0078] located in the northern hemisphere of the equatorial coordinate system. The mean redshift of this Supercluster is 0.078 (radial velocity 2.24×10^7 m s^{-1}), and it has 1213 galaxies. The distance of this Supercluster is 233 h^{-1}Mpc, and this Supercluster contains two Abell clusters, A2040 and A2028 (Einasto et al., 2011). The morphology of this Supercluster resembles a sparse multispider or multi-branching filament with a uniform density (Einasto et al., 2011).

4.4.1 Number Density Map

It is seen from the number density map Fig. 43a, three different substructures that can be visualized for counting bin of radius 0.25°. Out of that two substructures are not relevant to consider this as the substructure. Because they (Declination angle between 7.5° and 9°) have contains a small number of galaxies. But there are possible to seem substructure in between Dec. 5.699° and R.A. 227.641°. This substructure contains a large number of galaxies which has at least 65 neighbour galaxies. From Fig. 43b, the radius of 0.5° gives one clear distinct substructure. The two groups that lie on the same contour tend to separate. Approximately this radius gives three different substructures. A similar kind of picture seen in the Fig. 43c, for the radius 0.75°, give two group lies within the same contour suggesting the same distribution of number density of neighbour galaxies. Again taking the radius as 1.0°, there is no lucid picture of the substructure, which is shown in Fig. 43d.

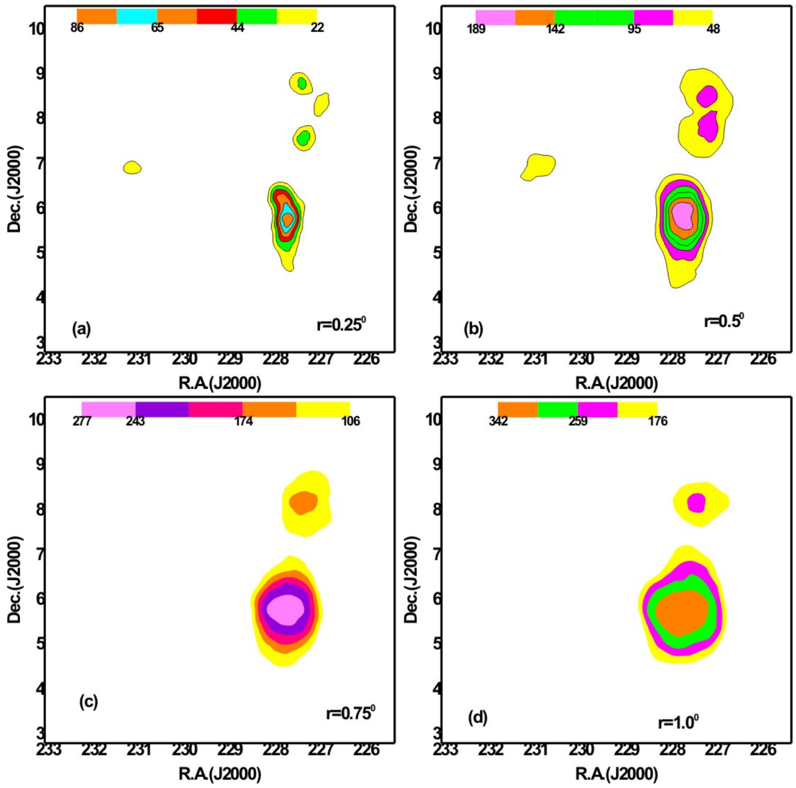

Figure 43: Number density map of galaxies in the Supercluster S[227+006+0078] having nearest neighbour distance of each galaxies at (a) r=0.25°, (b) r=0.5°,(c) r=0.75°, (d) r=1.0°. The color bar is shown. As the radius increases, the subclustering becomes prominent.

4.4.2 Redshift Map

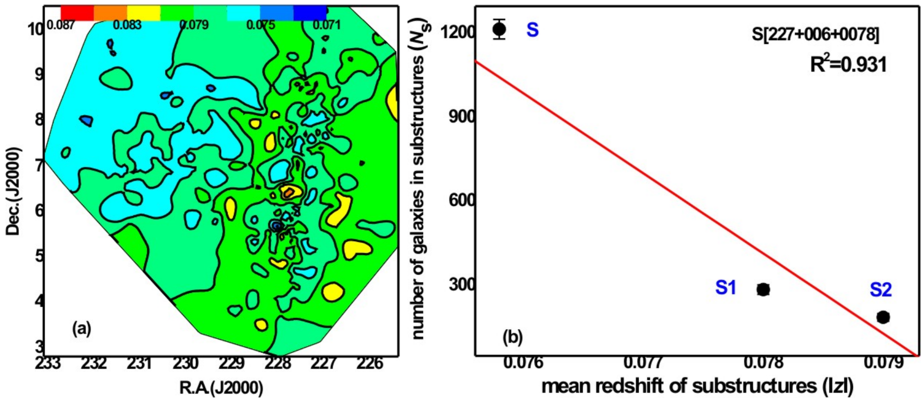

Figure 44: Redshift map is shown for galaxies in the Supercluster S[227+006+0078]. The mean redshift of Supercluster is 0.078. The contour levels are at the redshift 0.071, 0.075, 0.079, 0.083, 0.087. In the substructure region, galaxies hardly have identical redshifts. (b) The Number of galaxies in two substructures and Supercluster it self versus redshift dispersion plot. The statistical $\pm1\sigma$ error are shown.

Figure 44 shows a redshift map of galaxies in the Supercluster that have a mean redshift of 0.078. The color map shows that the velocity dispersion is minimum in the region where the number density of galaxy is minimum. In the substructure region at 5°

declination, the redshift dispersion, is found to be |z|= 0.078, whereas the lower and upper substructure show |z| = 0.076 and 0.079, respectively. It seems that there is a linear relationship between redshift dispersion and the number density of galaxies in the substructures,

$$N_s(4) = -2.8 \times 10^5 |z| + 22762.62 \tag{4.11}$$

We varied the nearest neighbour radius to 0.75° and 1.0° and calculated the slope of a linearly fitted line as above and found exactly the same. Therefore, we propose empirical relation (equation 4.11) between number density and redshift dispersion of galaxies in the Supercluster S[227+006+0078].

The redshift dispersion (Δz) of galaxies in the Bootes A Superclusters are 673 km s^{-1} (Struble & Rood, 1999). Its value is 68 km s^{-1} for the local group (Struble & Rood, 1999). These are nearby Superclusters and groups have peculiar velocity is relatively higher than that of distant Superclusters.

4.4.3 Magnitude Map

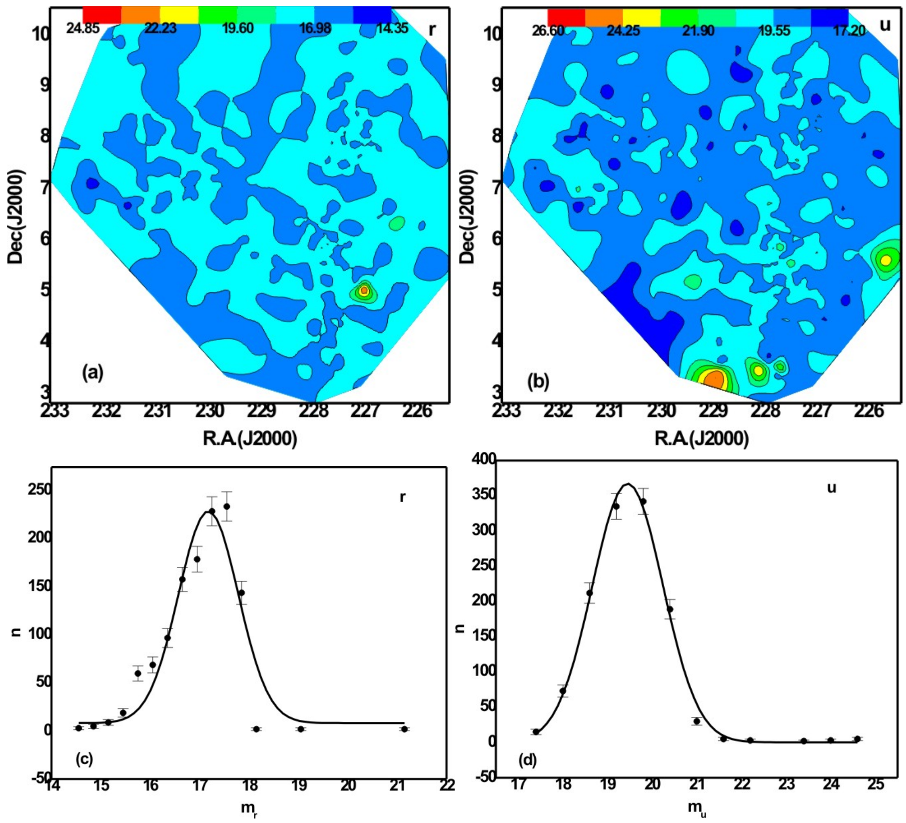

Figure 45: Magnitude map of galaxies in the Supercluster S[227+006+0078](a) r-magnitude, (b) u-magnitude.The color bar is shown. The contour levels are at 14.35, 16.98, 19.60, 22.23, 24.85 for r-filter and 17.20, 19.55, 21.90, 24.25, 26.60 for u- filter, respectively. The distribution of r and u-magnitude with Gaussian fit can be seen.

Fig. 45ab shows magnitude maps of galaxies in the Supercluster S[227+006+0078]. The SDSS r-magnitude refers to the peak wavelength 6165 Å with the bandwidth 480.9Å. In the u-filter, the substructure located in the northern region is found to have a higher magnitude. As we know, the higher the magnitude, the lower the brightness.

The magnitude distribution of galaxies in the Supercluster S[227+006+0078] can be seen in figure 45cd. The solid curve represents Gaussian fits. The Gaussian center is found to be at 17.178 for r- and 19.453 for u-filters. The Gaussian functions for r- and u-magnitude distributions are given by

$$n_r = 8.38 + 221.37 \exp\left(\frac{-2(m_r - 17.178)^2}{1.47}\right) \tag{4.12}$$

$$n_u = 0.21 + 368.03 \exp\left(\frac{-2(m_u - 19.453)^2}{2.50}\right) \tag{4.13}$$

4.4.4 Substructure Classification

Table 13: Substructures of the Supercluster S[227+006+0078]. Second and third columns show positions of Superclusters. The next two columns represent the mean redshift and number of galaxies in the substructures. The last two columns list mean u-magnitude and r-magnitude of substructures, respectively.

Substructure	R.A.(J2000)	Dec.(J2000)	$\lvert Z\rvert$	N_g	$\lvert u\rvert$	$\lvert r\rvert$
S1[228+006+0079]	227.641°	5.699°	0.078	287	19.4	17.5
S2[227+008+0078]	226.935°	8.321°	0.079	94	19.6	17.7

Based on the number density maps, two different substructures are separated by using a mean redshift of galaxies and the number of galaxies.

4.4.5 Preferred Alignments in the Supercluster

Supercluster S[227+006+0078] has 1213 galaxies. The statistics tests for polar angle (θ) distribution of galaxies in the Supercluster S[227+006+0078], is shown in Table 14. the value of chi-square probability P(>χ^2) to be 0.848 i.e., 84.8% more than the significant level 0.05,i.e., 5%, the first order Fourier coefficient $\Delta_{11}/\sigma(\Delta_{11})$ is -0.2 which is less than limit 1.5σ, the value of the first order Fourier probability (P(>Δ_1)) to be found 0.970 i.e., 97.0% greater than significant level 15% and the value of auto-correlation coefficient (C/C(σ)) is -0.3 which is less than limit 1σ. Thus, all statistics advocate strong isotropy.

Similarly, the statistical tests for the azimuthal angle (ϕ) distribution of galaxies are shown in Table 14, the value of chi-square probability P(> χ^2) to be found 0.763 i.e., 76.3% greater than 0.050 i.e., 5%, the first order Fourier coefficient $\Delta_{11}/\sigma(\Delta_{11})$ is 0.1 less than 1.5σ limit, the first order Fourier probability (P(>Δ_1)) to be 78.9 i.e., 78.9% which is more than 0.150 i.e., (15%) and the value of auto-correlation coefficient (C/C(σ)) is 0.2 less than 1σ level. Thus, all statistics advocate strong isotropy.

The plot of polar angle (θ)-distribution is shown in Fig. 46a, in the small-angle region θ<45°, there is one hump at an angle 35° within 1σ level. At this angle, the observed (410) number of galaxies is more than expected (384) by 26. This hump signifies that the spin vector orientation of galaxies tends to orient parallel to the equatorial coordinate system. Similarly, at this region, one dip at an angle 15° within 1σ level is seen. The large-angle θ>45°, does not give any significant hump and dip (maybe binning effect) suggests strong isotropy in polar angle distribution. These results suggest that galaxy evolution in the Supercluster S[227+006+0078] supports Hierarchy model (Peebles, 1969). This model predicts that galaxies were formed from clustering.

The plot of azimuthal angle ϕ-distribution is shown in Fig. 46b, in the small-angle region θ<−45°, small dips at −50° within limit 1σ level. For the range between −45°<ϕ<+45°, small dips are at −40° and 30° within limit 1σ level. There is no significant hump and dip up to region 80°. One dip is seen at angle 90° with 1σ level. At this angle, the number of observed solutions (143) is 19 number of solutions less than the expected solution (162). The dip observed in this distribution is due to the local effect. Thus, the result is strong isotropy in ϕ-distribution also insinuates the evolution of galaxy supports Hierarchy model (Peebles, 1969) in this Supercluster S[227+006+0078].

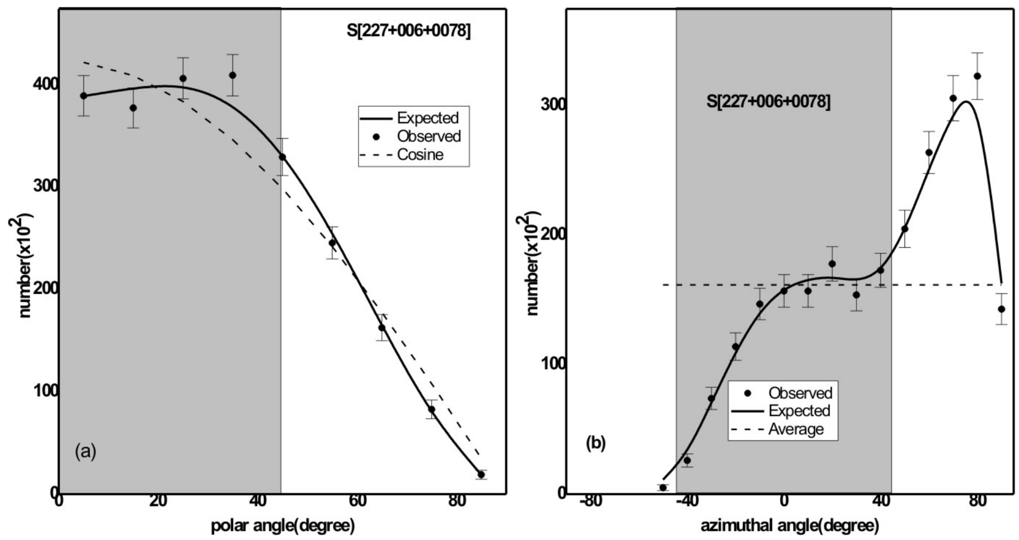

Figure 46: Polar (a) and azimuthal (b) angle distributions of galaxies in the Supercluster S[227+006+0078]. The solid circles with statistical error bars (±1σ) represent observed distribution. The solid curves are obtained from random simulation assuming isotropic distributions.

Table 14: Statistical parameters in the polar and azimuthal angles of galaxies in the Supercluster S[227 + 006 + 0078] and its substructures (first column). The chi-square probability (P> χ^2) is given in the second column. The third and fourth columns show first order Fourier coefficient ($\Delta_{11}/\sigma(\Delta_{11})$ and Fourier probability. The last column tests the auto co-relation coefficient.

Sample	P(> χ^2)	$\Delta_{11}/\sigma(\Delta_{11})$	P(> Δ_1)	C/$C(\sigma)$
Polar Angle				
S[227+006+0078]	0.848	−0.2	0.970	−0.3
S1[228+006+0079]	0.521	−0.8	0.650	−0.4
S2[227+008+0078]	0.772	−0.3	0.793	− 0.3
Azimuthal Angle				
S[227+006+0078]	0.763	0.1	0.789	0.2
S1[228+006+0079]	0.127	0.1	0.791	0.0
S2[227+008+0078]	0.724	0.3	0.100	−0.6

4.4.6 Preferred Alignment in Substructures

The substructure S1[228+006+0079] consists of 287 galaxies. The statistics used for polar angle distribution are shown in Table 14, the value of chi-square probability (P> χ^2) to be found 0.521 i.e., 52.1% more than the significant level 0.050 i.e., 5%, the first order Fourier coefficient $\Delta_{11}/\sigma(\Delta_{11})$ is −0.8 which is less than 1.5σ limit, the first order Fourier probability (P(>Δ_1)) is 65.0% greater than (15%) and the value of auto-correlation coefficient (C/C(σ)) is −0.4 less than 1σ level. Thus, the statistics suggest the result as strong isotropy.

Table 14 shows the statistics tests for azimuthal angle (ϕ) distribution of galaxies, the value of chi-square probability P(> χ^2) is 12.7% greater than 5%, the first order Fourier coefficient $\Delta_{11}/\sigma(\Delta_{11})$ is 0.1 less than 1.5σ limit, the first order Fourier probability (P(>Δ_1)) is 79.1% which is greater than 15% and the value of auto-correlation coefficient (C/C(σ)) is 0.0 less than 1σ level. Thus, all statistics advocate strong isotropy.

The plot of polar angle θ-distribution is shown in Fig. 47a, in the small-angle region θ<45°, a significant hump seen at 25°. The hump at an angle less than 45° suggests that the spin vector of galaxies tends to orient parallel with respect to the equatorial coordinate system. There are small dips are noticed at 15° and 35° within limit 1σ level. For the larger angle region θ>45°, one hump is seen at 75° giving a significant hump with ~ 2σ error limit. This significant hump at angle 75° suggests the spin vector of galaxies tends to orient perpendicular with respect to the equatorial coordinate system. Thus, the result of strong isotropy.

For the azimuthal angle distribution of galaxies, as shown in Fig. 47b There are three humps and one dip is noticed. One dip is seen at angle of 87.5° with 1.5σ error limit is very significant. Three humps are noticed at angles −32°, at −22°, and at an angle, 77.5°, these three humps lie within 1σ error limit. Here, the result advocates strong isotropy.

This substructure S2[227+008+0078] has 94 galaxies. The statistics for the polar angle (θ)-distribution of S2[227+008+0078] is shown in Table 14, the value of chi-square probability (P> χ^2) to be 0.772 i.e., 77.2% greater than the significant level 0.050 i.e., 5%, The first order Fourier coefficient $\Delta_{11}/\sigma(\Delta_{11})$ is -0.3 less than the 1.5σ limit, the first order Fourier probability is 0.793 i.e., 79.3% which is greater than 0.150 i.e., 15% limit and the auto-correlation coefficient found to be 0.3 less than the limit 1σ. Thus, all the statistics suggest isotropy.

Table 14 shows the statistical tests for the azimuthal angle (ϕ) distribution of galaxies. The value of chi-square probability P(> χ^2) found to be 72.4% greater than 5%, the first order Fourier coefficient $\Delta_{11}/\sigma(\Delta_{11})$ is 0.3 less than 1.5σ limit, the first order Fourier probability (P(>Δ_1)) is 10.0% which is less than 15% (which suggest for anisotropy) and the value of auto-correlation coefficient (C/C(σ)) is$-$ 0.6 less than 1σ level. Thus, all statistics advocate strong isotropy except first order probability. This is due to the local effect.

The plot of polar angle θ-distribution is shown in Fig. 47c. There are no significant dips, these small dips are observed in the plot within error limit 1σ level. In the small-angle region θ<45°, there are no significant humps are observed. But at the bimodal region, θ~45°, a small hump is seen within limit 1σ (the observed solution is greater than expected solutions by one only). In the larger angle region θ>45°, a small hump is noticed at 55° within error 1σ limit (observed solutions exceed by two than expected solutions) and the observed distribution follows the same path as that of the expected distribution giving isotropy in the result which in turn supports the fact that this substructure formed through the process of clustering.

The distribution of azimuthal angle (ϕ) in Fig. 47d shows there are no humps and dips in the small-angle region ϕ<45°. For the range between $-45°<\phi<+45°$, there are observed two small dips at $-25°$ and at 15° both with 1.5σ error limit. For the larger angle region ϕ>45°, a dip is seen at 85°. This is due to the local effect. Similarly, for the range between $-45°<\phi<+45°$, three small humps are seen at $-15°$, 5° and 25° all are with 1.5σ error limit. For the larger angle region ϕ>45°, there are two significant humps are observed at 55° and 75°. These are due to local effects. Thus, the result advocates strong isotropy.

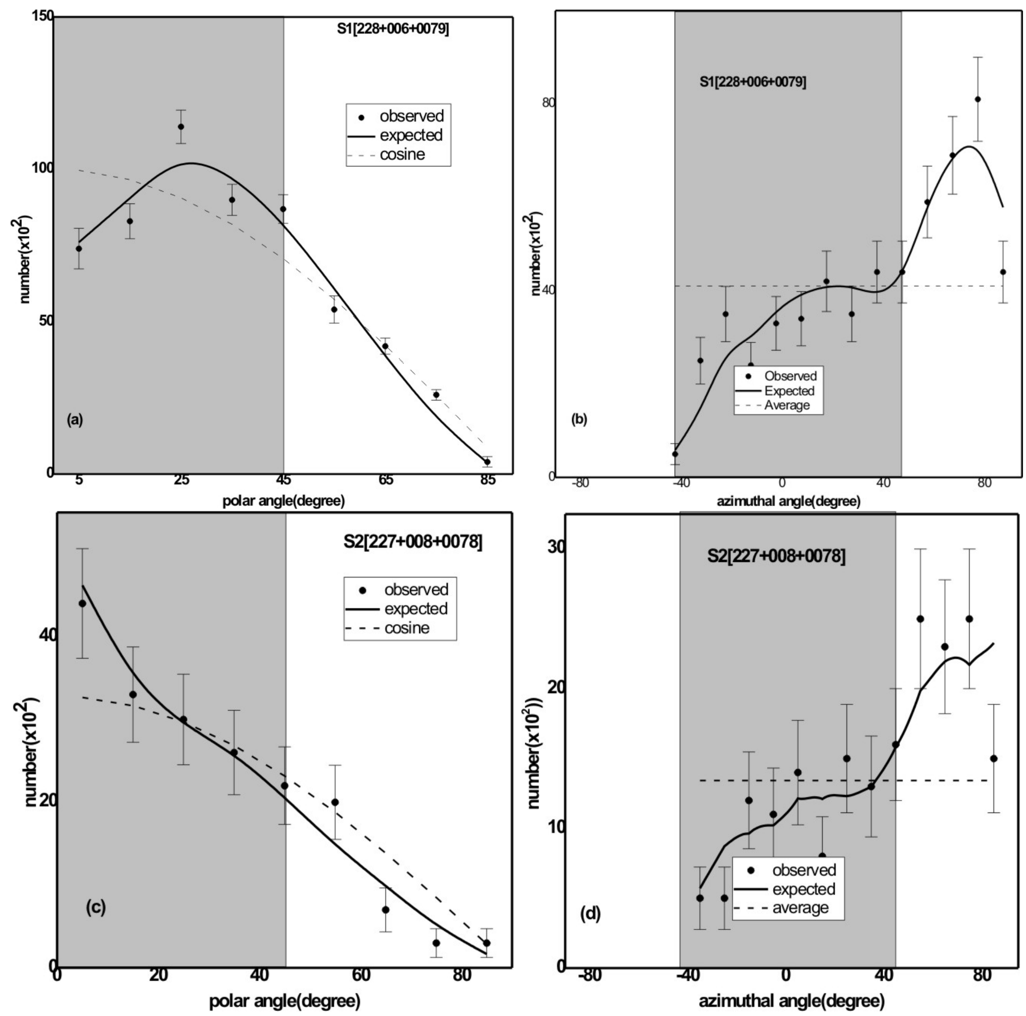

Figure 47: Polar (a, c) and azimuthal angle (b, d) distributions of galaxies in the substructures of Supercluster S[227+006+0078]. Solid circles with statistical error bars ($\pm 1\sigma$)represent observed distributions. The expected distributions are represented by solid curves. These solid curves are obtained by performing the random simulations.

4.4.7 General Discussion

We convert two-dimensional given parameters (R.A., Dec. and equatorial PA) into three-dimensional (spin vectors of polar/azimuthal angles) parameters using axial ratios and intrinsic flatness of galaxies. For this, we adopt the method described by Flin & Godowski (Flin & Godlowski, 1986) and calculate the polar (θ) and azimuthal (ϕ) angles of galaxies. In their method, the three-dimensional orientation of the angular momentum vector of galaxies is characterized by polar and azimuthal angles. We study the spatial orientation of the angular momentum vector of galaxies with respect to the equatorial coordinate system. The formulae given by Flin & Godlowski (1986) provide four solutions of the angular momentum vector of galaxies orientation for a galaxy. We count all four possibilities independently in our analysis. Three kinds of selection effect are removed and the expected isotropic distribution curves (θ and ϕ) are determined using the numerical simulation method as proposed by Aryal & Saurer (2000). The isotropic distribution curves are based on simulations including 10^7 virtual galaxies.

We study the spatial orientation of the spin vector of 1213 galaxies of Supercluster S[227+006+0078]. We have three equally acceptable possible scenarios (pancake (Doroshkevich et al., 1978), primordial vorticity (Ozernoy, 1978), and hierarchy model (Peebles, 1969)). To check for anisotropy or isotropy we have carried out three statistical tests: chi−square, auto−correlation, and Fourier. When we studied the preferred alignments of angular momentum of galaxies in our Supercluster, it ruled out the possibility of a model described by the pancake and primordial vorticity. The isotropy result found in the Supercluster S[227+006+0078] gave the random orientation of the angular momentum vector of galaxies with the equatorial plane. Statistical tests mentioned in Table 14 support carrying out the result for isotropy. In addition to Supercluster S[227+006+0078], we found the same result for two subclusters: S1[228+006+0079], containing 287 number galaxies; and S2[227+008+0078], containing 94 galaxies. The random orientation of the angular momentum vector of galaxies in these two substructures implies the formation of substructure takes place due to clustering of galaxies rather than due to fragmentation of large structures. Therefore, the Supercluster S[227+006+0078] along with two substructures S1[228+006+0079] and S2[227+008+0078] supports Hierarchy model (Peebles, 1969) in which galaxies were believed to be first formed and then they obtained their angular momenta by tidal forces while they were gathering gravitationally to form a cluster.

4.5 Supercluster S[231+030+0117]

In this section, we study Supercluster S[231+030+0117] located in the northern hemisphere of the equatorial coordinate system. The mean redshift of this Supercluster is 0.114 (radial velocity 3.42×10^7 m s^{-1}), and it has 1172 galaxies (Einasto et al., 2011).

4.5.1 Number Density Map

From the all-sky distribution of galaxies in a large-scale structure, we can see the distribution of galaxies in this Supercluster S[227+006+0078] is not uniform. We found some regions with high-density contrast, so we study about such density contrast regions to understand how the overall structure and contrast region affect the evolution and formation of galaxies in that region. We have classified our database of total samples into substructures based on the number density distribution of galaxies. In order to identify substructure within the Supercluster S[231+030+0117], we try to find the number of neighbouring galaxies within a certain range of radius. Fig 48 shows the counter map within the different radii of the circle. In Fig 48a and Fig 48b, we can see that for counting bin of radius 0.5° and 0.6° three substructures may be seen but out of that observed one clear high-density contrast region that may be substructure. In Fig 49d, at radius 0.8° the substructures start to overlap, and two substructure forms. In Fig 49e, at 0.9° and Fig 49f, at 1.0° only one substructure forms throughout the whole region.

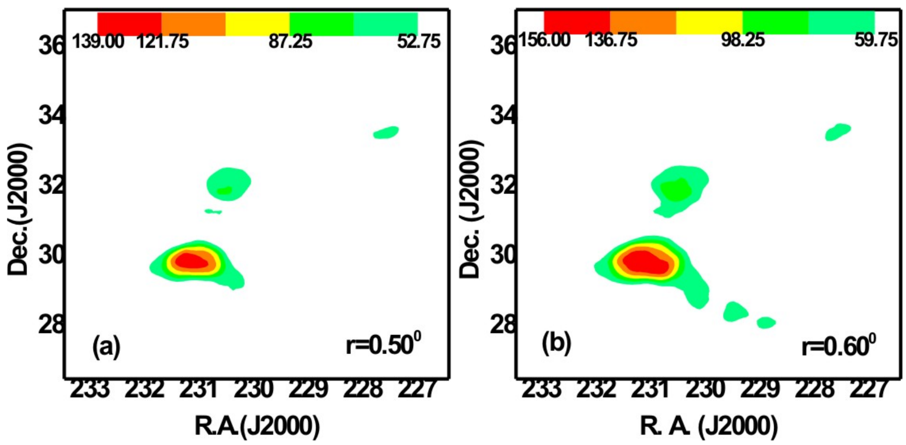

Figure 48: Number density map of galaxies in the Supercluster S[231+030+0117] having nearest neighbour distance of each galaxies at (a) r=0.50°, (b) r=0.60°. The color bar is shown. As the radius increases, the subclustering becomes prominent.

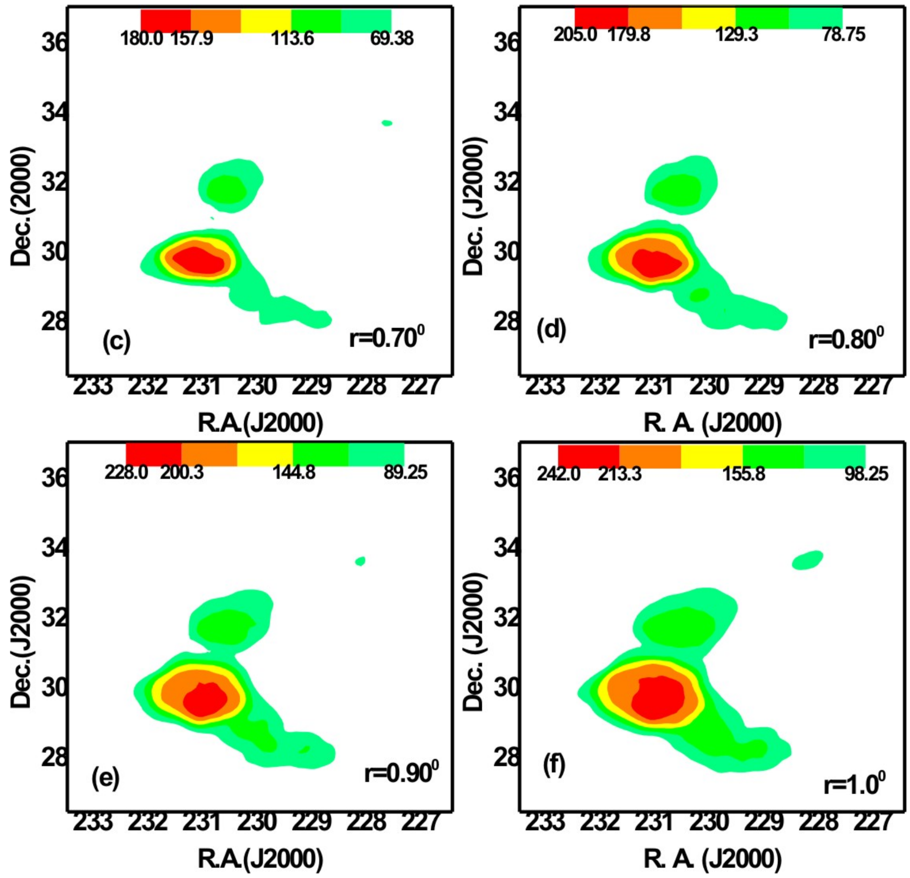

Figure 49: Number density map of galaxies in the Supercluster S[231+030+0117] having nearest neighbour distance of each galaxies at (c) r=0.70°, (d) r=0.80°, (e) r=0.90°, (f) r=1.0°. The color bar is shown. As the radius increases, the subclustering becomes prominent.

4.5.2 Redshift Map

Figure 50 shows a redshift map of galaxies in the Supercluster that have a mean redshift of 0.114. The color map shows that the velocity dispersion is minimum in the region where the number density of galaxy is minimum. In the substructure region at 30° declination, the redshift dispersion, is found to be |z|= 0.115, whereas the lower and upper substructure show |z|= 0.114 and 0.116, respectively. It seems that there is a linear relationship between redshift dispersion and the number density of galaxies in the substructures,

$$N_s(5) = -3.2 \times 10^5 |z| + 38114.11 \tag{4.14}$$

We varied the nearest neighbour radius to 0.05° and 1.00° and calculated the slope of a linearly fitted line as above and found the same. Therefore, we propose empirical relation (equation 4.14) between number density and redshift dispersion of galaxies in the Supercluster S[231+030+0117].

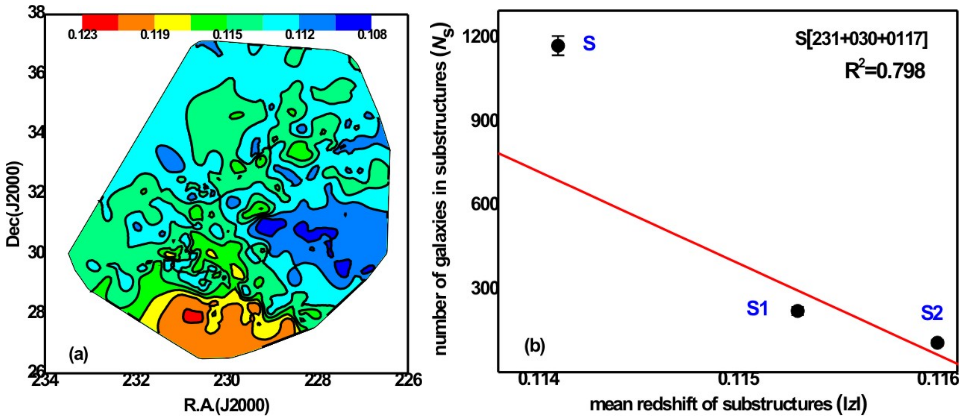

Figure 50: Redshift map is shown for galaxies in the Supercluster S[231+030+0117]. The mean redshift of Supercluster is 0.114. The contour levels are at the redshift 0.108, 0.112, 0.115, 0.119, 0.123. In the substructure region, galaxies hardly have identical redshifts. (b) Number of galaxies in two substructures versus redshift dispersion plot. The statistical $\pm1\sigma$ error bars are shown.

The redshift dispersion (Δz) of galaxies in the Bootes A Superclusters are 831 km s^{-1} (Struble & Rood, 1999). Its value is 68 km s^{-1} for the local group (Struble & Rood, 1999). These are nearby Superclusters and a group of which peculiar velocity is relatively higher than that of the distant Superclusters.

4.5.3 Magnitude Map

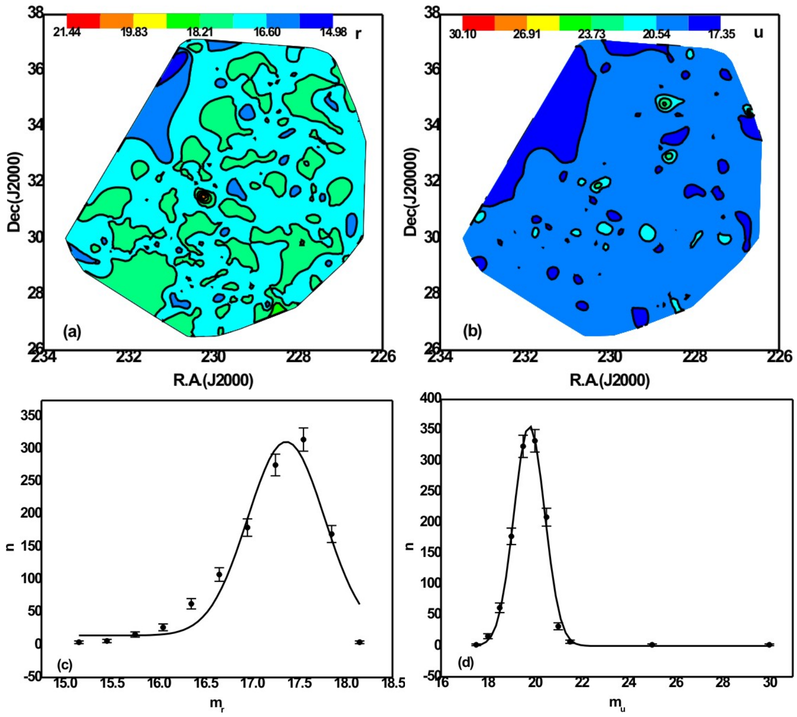

Figure 51: Magnitude map of galaxies in the Supercluster S[231+030+0117] (a) r-magnitude, (b) u-magnitude. The color bar is shown. The contour levels are at 14.98, 16.00, 18.21, 19.83, 21.44 for r-filter and 17.35, 20.54, 23.73, 26.91, 30.10 for u-filter, respectively. The distribution of r and u-magnitude.

Fig. 51ab shows magnitude maps of galaxies in the Supercluster S[231+030+0117]. The

SDSS r-magnitude refers to the peak wavelength 6165 Å with the bandwidth 702.81 Å. In the u-filter, the substructure located in the northern region has a higher magnitude. As we know, the higher the magnitude, the lower the brightness.

The magnitude distribution of galaxies in the Supercluster S[231+030+0117] can be seen in figure 52cd. The solid curve represents Gaussian fits. The Gaussian center is found to be at 17.364 for r- and 19.769 for u-filters. The Gaussian functions for r- and u-magnitude distributions are given by

$$n_r = 14.47 + 298.13 \exp\left(\frac{-2(m_r - 17.364)^2}{0.67}\right) \tag{4.15}$$

$$n_u = 0.13 + 358.41 \exp\left(\frac{-2(m_u - 19.769)^2}{1.69}\right) \tag{4.16}$$

4.5.4 Substructure Classification

Table 15: Substructures of the Supercluster S[231+030+0117]. Second and third columns show positions of Superclusters. The next two columns represent mean redshift and number of galaxies in the substructures. The last two columns list mean u-magnitude and r-magnitude of substructures, respectively.

Substructure	R.A.(J2000)	Dec.(J2000)	$\|Z\|$	N_g	$\|u\|$	$\|r\|$
S1[231+030+0117]	231.053°	29.910°	0.115	224	19.8	17.3
S2[231+030+0117]	230.420°	32.090°	0.116	110	19.9	17.5

On the basis of number density maps, two substructure is identified within the Supercluster S[231+030+0117]. The magnitude distributions of these substructures are seemed to be connected, probably in the process of clustering.

4.5.5 Preferred Alignments in the Supercluster

The Supercluster S[231+030+0117] contains a group of 1172 galaxies. Table 16 shows the statistics for the polar angle (θ) distribution in the Supercluster S[231+030+0117]. The value of chi-square probability P(> χ^2), the first order Fourier coefficient $\Delta_{11}/\sigma(\Delta_{11})$, the first order Fourier probability (P(>Δ_1)) and the auto-correlation coefficient (C/C(σ)) obtained for the the polar angle (θ) distribution are 0.884 greater than the significant level 0.050, 0.0 less than the error limit 1.5σ, 0.999 more than significant level 0.150 and −0.6 less than 1σ level respectively. Thus, all these statistics advocate very strong isotropy.

The statistics for azimuthal angle (ϕ) distribution is shown in Table 16, the value of chi-square probability (P> χ^2), the first order Fourier coefficient $\Delta_{11}/\sigma(\Delta_{11})$, the first order

Fourier probability (P(>Δ_1)) and the auto-correlation coefficient (C/C(σ)) obtained for the azimuthal angle (ϕ) distribution are 0.779 more than the significant level 0.050, 0.2 less than the error limit 1.5σ, 0.905 more than significant level 0.150 and −0.1 less than 1σ level respectively. Here, all these statistics advocate very strong isotropy.

In Fig. 52a, in the small-angle region θ<45°, there are two dips at 22.5°, 42.5° and one hump at 32.5° all these are within error limit 1σ. For large angles region (θ>45°), one significant hump at 52.5° with 1.5σ error limit. The hump and dip observed in this distribution are due to the local effect. Thus, we conclude that no preferred alignment of spin vectors of galaxies found in polar angle distribution.

In Fig. 52b, in the small-angle region (ϕ<−45°) and for the range between −45°<ϕ>+45°, there are no significant humps, and dips, are seen. In the large-angle region (ϕ>45°), one hump is observed at an angle 85° within 2σ error limit, which is due to the local effect. Thus, there is no preferred alignment is noticed in azimuthal angle distribution.

Thus, in the study of both statistics and graphs of polar and azimuthal angles. We conclude isotropy in the spin-vector orientation of galaxies in the Supercluster and lack of preferred alignment. This supports the Hierarchy model (Peebles, 1969) of galaxy evolution.

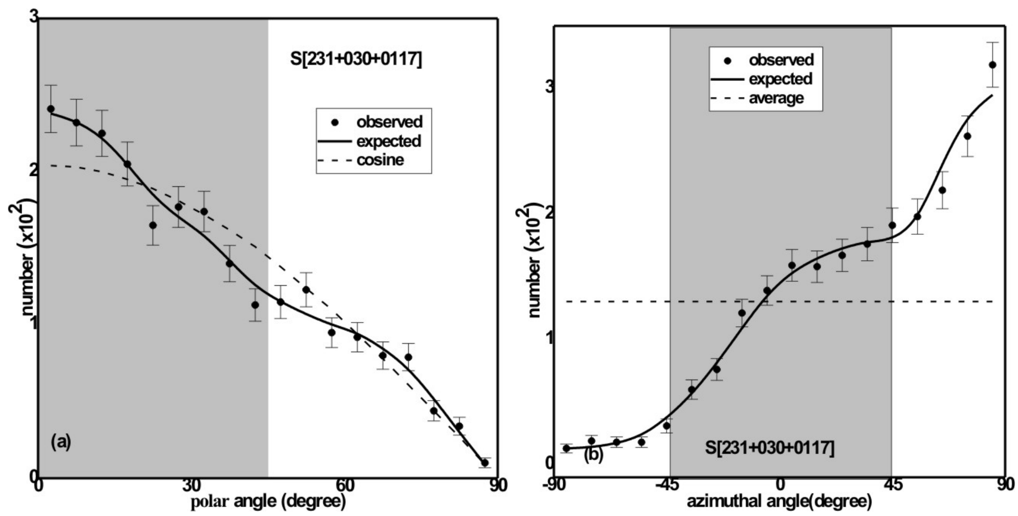

Figure 52: Polar (a) and azimuthal (b) angle distributions of galaxies in the Supercluster S[231+030+0117]. The solid circles with statistical error bars (±1σ) represent observed distribution. The solid curves are obtained from random simulation assuming isotropic distributions.

Table 16: Statistical parameters in the polar and azimuthal angles of galaxies in the Supercluster S[231 + 030 + 0117]and its sub- structures (first column). The chi-square probability(P> χ^2) is given in the second column. The third and fourth columns show first order fourier coefficient ($\Delta_{11}/\sigma(\Delta_{11})$ and fourier probability. The last column tests the auto co-relation coefficient.

Sample	P(> χ^2)	$\Delta_{11}/\sigma(\Delta_{11})$	P(> Δ_1)	C/$C(\sigma)$
Polar Angle				
S[231+030+0117]	0.884	0.1	0.999	−0.6
S1[231+030+0117]	0.227	0.1	0.994	−0.2
S2[231+030+0117]	0.664	0.4	0.812	− 0.3
Azimuthal Angle				
S[231+030+0117]	0.779	0.2	0.905	−0.1
S1[231+030+0117]	0.873	−0.1	0.898	−0.5
S2[231+030+0117]	0.504	−0.1	0.919	−0.9

4.5.6 Preferred Alignment in Substructures

The substructure S1[231+030+0117] consists of 224 galaxies. The statistics for the polar angle (θ) distribution is shown in Table 16, the value of chi-square probability (P> χ^2), the first order Fourier coefficient $\Delta_{11}/\sigma(\Delta_{11})$, the first order Fourier probability (P(>Δ_1)) and the value of auto-correlation coefficient (C/C(σ)) obtains for polar angle (θ) are 0.227 more than the significant level 0.050, 0.1 less than the error limit 1.5σ, 0.994 more than significant level 0.150 and −0.2 less than 1σ level, respectively. Thus, all these statistics suggest strong isotropy.

The statistics for azimuthal angle (ϕ) distribution is shown in Table 16, the value of chi-square probability (P> χ^2), the first order Fourier coefficient $\Delta_{11}/\sigma(\Delta_{11})$, the first order Fourier probability (P(>Δ_1)) and the value of auto-correlation coefficient (C/C(σ)) obtains for polar angle (ϕ) are 0.873 more than the significant level 0.050,−0.1 less than the error limit 1.5σ, 0.898 more than significant level 0.150 and −0.5 less than 1σ level, respectively. Thus, all these statistical tests suggest strong isotropy.

In Fig. 53a, for small angles region (θ<45°), there is one hump at 32.5° with error limit 1.5σ and two dips at 12.5° and 22.5° with 1σ and 1.5σ error limit are seen. For large angles region (θ>45°), there is one significant hump observed at an angle of 52.5° with an error limit of 2σ. Also, there are three effective dips at an angles 57.5°, 62.5° and 72.5° with 2σ, 1.5 $\sigma$and 2σ error limit. These humps and dips observed in the polar angle distribution are due to the local effect.

In Fig. 53b, there are no significant humps and dips are observed in the small-angle region ϕ<−45°, for the range between −45°<ϕ<+45°, there are two humps at an angles −5° and 25° within error limit 1σ and one dip at an angle 35° within error limit 1.5σ are seen. For large angles region (ϕ>45°), one hump at an angle 85° and one dip at an angle 65° within 1.5σ, error limit are observed due to some local effects. Overall, there is no preferred alignment of the spin vectors of galaxies is noticed in azimuthal angle distribution.

Hence, with the help of the statistics and plots of polar and azimuthal angles, we obtain the conclusion of isotropy in the spin-vector orientation of galaxies in the substructure S1[231+030+0117] and lack of preferred alignment. This is in favor of the hierarchy model of galaxy evolution.

This substructure S2[231+030+0117] has 110 galaxies. The value of chi-square probability (P> χ^2), the first order Fourier coefficient $\Delta_{11}/\sigma(\Delta_{11})$, the first order Fourier probability (P(>Δ_1)) and the value of auto-correlation coefficient (C/C(σ)) obtains for polar angle (θ) are 0.664 more than the significant level 0.050, 0.4 less than the error limit 1.5σ, 0.812 greater than significant level 0.150 and −0.3 less than 1σ level, respectively. Thus, all these statistics advocate strong isotropy.

The statistics for azimuthal angle (ϕ) distribution is shown in Table 16, the value of chi-square probability (P> χ^2), the first order Fourier coefficient $\Delta_{11}/\sigma(\Delta_{11})$, the first order Fourier probability (P(>Δ_1)) and the value of auto-correlation coefficient (C/C(σ)) obtains for polar angle (θ) are 0.504 greater than the significant level 0.050, −0.1 less than the error limit 1.5σ, 0.919 more than significant level 0.150 and −0.9 less than 1σ level, respectively. Here, all these statistics suggest strong isotropy in the ϕ-distribution.

In Fig. 53c, for the region of small-angles (θ<45°), there is one significant hump at an angle 12.5° with 1.5σ error limit and two dips at an angle 22.5° and 22.5° with 2σ error limit, are observed. At the bimodal region, i.e.,θ∼45°, no humps and dips are seen. For the large angles region (θ>45°), no significant humps and dips, are observed. Due to the difference between observed (48) and expected (46) solution is 2. In this region, small humps, and dips, are seen due to the local effect. Thus, no preferred alignment of the spin vectors of galaxies is found in polar angle distribution.

In Fig. 53d, no significant humps, and dips, are seen in the small-angle region (ϕ<−45°). For the range between −45°<ϕ<+45°, two humps at an angle −25° with 1σ error limit and at −5° with 1.5σ error limit, are observed. Further, three dips at an angles −35°, 5° and 15° with 1σ, 1.5σ and 1.5σ, error limits, are observed in this region. In the bimodal region ϕ∼45°, one significant hump with an error limit of 1.5σ is seen. For the larger angle region (ϕ>45°), no significant dips are observed but one significant hump is observed at 85°. This is due to local effects. Thus, no preferred alignment is noticed in the azimuthal angle distribution.

Hence, after the study of the statistics and plots of polar and azimuthal angles, we concluded that there is strong isotropy in the spin-vector orientation of galaxies in the substructure S2[231+030+0117] and lack of preferred alignment. This supports the Hierarchy model (Peebles, 1969) of galaxy evolution.

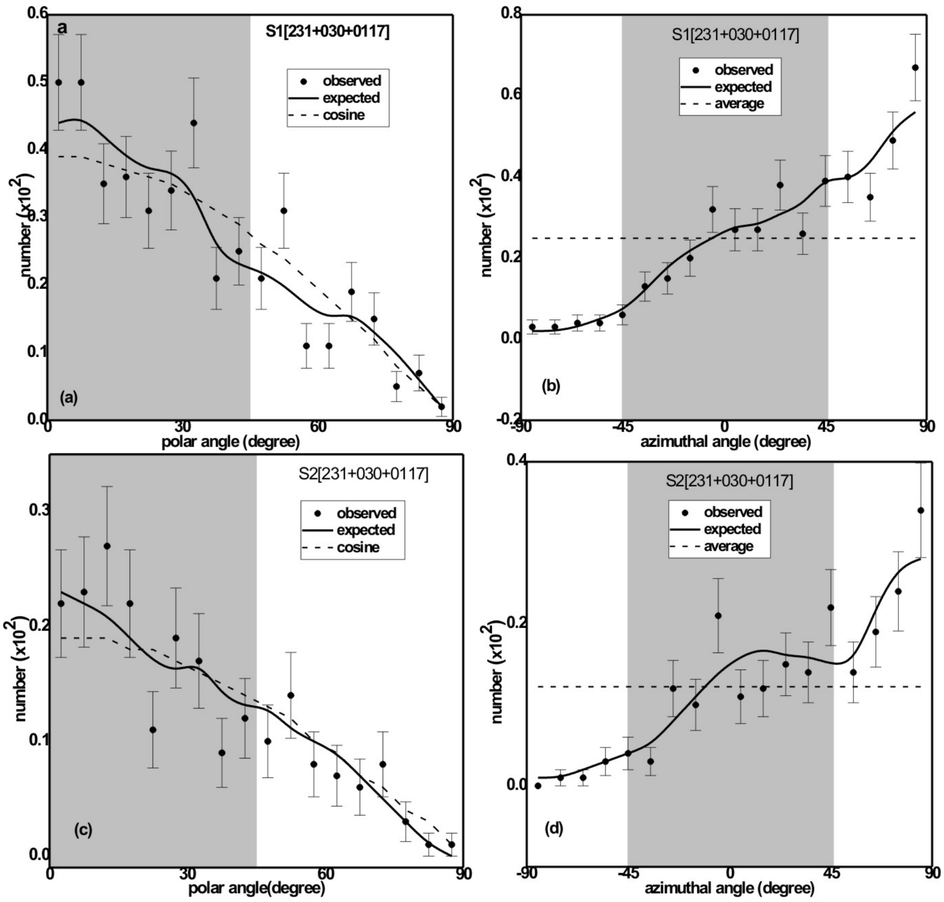

Figure 53: Polar (a, c) and azimuthal angle (b, d) distributions of galaxies in the substructures of Supercluster S[231+030+0117]. Solid circles with statistical error bars ($\pm 1\sigma$) represent observed distributions. The expected distributions are represented by solid curves. These solid curves are obtained by preforming random simulation.

4.5.7 General Discussion

We convert two-dimensional given parameters (R.A., Dec., and equatorial PA) into three-dimensional (spin vectors or polar/azimuthal angles) parameters using axial ratios (b/a) and intrinsic flatness (q*) of galaxies. For this, we adopt the method described by Flin & Godlowski (1986) and calculate the polar (θ) and azimuthal (ϕ) angles of galaxies. The selection effects are removed and the expected isotropic distribution curves are determined using the numerical simulation by creating 10^7 virtual galaxies and adopting the method as proposed by Aryal & Saurer ((Aryal & Saurer, 2000) (Aryal & Saurer, 2004)).

We study the spatial orientation of the spin vector of galaxies in Supercluster S[231+030+0117] and its two substructures S1[231+030+0117] and S2 [231+030+0117]. We have carried out three statistical tests: chi- square, Auto-correlation, and Fourier test to check for isotropy or anisotropy distribution. We found that the galaxy spin orientation is random and isotropic in both Supercluster and substructures. This may indicate that the substructures within the Supercluster are relatively younger and evolve due to the clustering of galaxies rather than due to the fragmentation of large structures. Therefore, the Supercluster along with its substructures supports the hierarchy model (Peebles, 1969).

In addition, we carry out research to check whether or not there is a dependence of magnitude with polar angle and azimuthal angle. The apparent magnitudes depend on the instrument used to measure them. The different instrumental detects different wavelength ranges. Thus, the flux measured by the instrument is not the total flux produced by the source but only a fraction of it. The sensitivity of the detector is different at different wavelengths. Photographic plates are most sensitive to blue and violet wavelength. As we know that the higher the value of magnitude, the fainter the star is. So that the galaxy has a higher magnitude consists of the stars with low brightness.

4.6 Supercluster S[184+003+0077]

In this section, we study Supercluster S[184+003+0077] located in the northern hemisphere of the equatorial coordinate system. The mean redshift of this Supercluster is 0.077 (radial velocity 2.21×10^7 m s^{-1}), and it has 1365 galaxies. This Supercluster at a distance of 230 h^{-1}Mpc and volume 10040 (h^{-1}Mpc)^3 is the second richest member of the Sloan Great Wall (SGW) (Einasto et al., 2011).

4.6.1 Number Density Map

The study of substructure plays a crucial role to understand the details about large-scale structure (Supercluster). From the all-sky distribution of galaxies in a large-scale structure, we can see the distribution of galaxies is not uniform. We found some regions are high-density contrast, so we must study such density contrast to understand how overall structure and contrast region affect the evolution and formation of galaxies in that region.

To identify substructure within the Supercluster S[184+003+00077], First, we try to find the number of galaxies around each galaxy within the different radius values such as 0.50°, 0.75°,1.0°, 1.25°. By analyzing the distribution of galaxy in the contour map in various radius values, we choose the particular value of radius for which a clear substructure is seen. In Fig. 54a, we can see four clear high-density contrast regions at different regions in the equatorial coordinate system. If we look at Fig. 54b, even though we see different substructures, there is no prominent structure because the density contrast region begins to overlap. Due to this region, it is very difficult to separate different substructures to study precisely. Similarly, in Fig. 54c and 54d, we only see two different substructures, however, we are searching for as many as different strong density regions. Further, the reason for not accepting this as an appropriate bin size is the substructure is largely overlapped and does not form a small high-density region. So, we choose finally the suitable counting bin size values as 0.50° to find the substructure because four different clear strong regions are noticed.

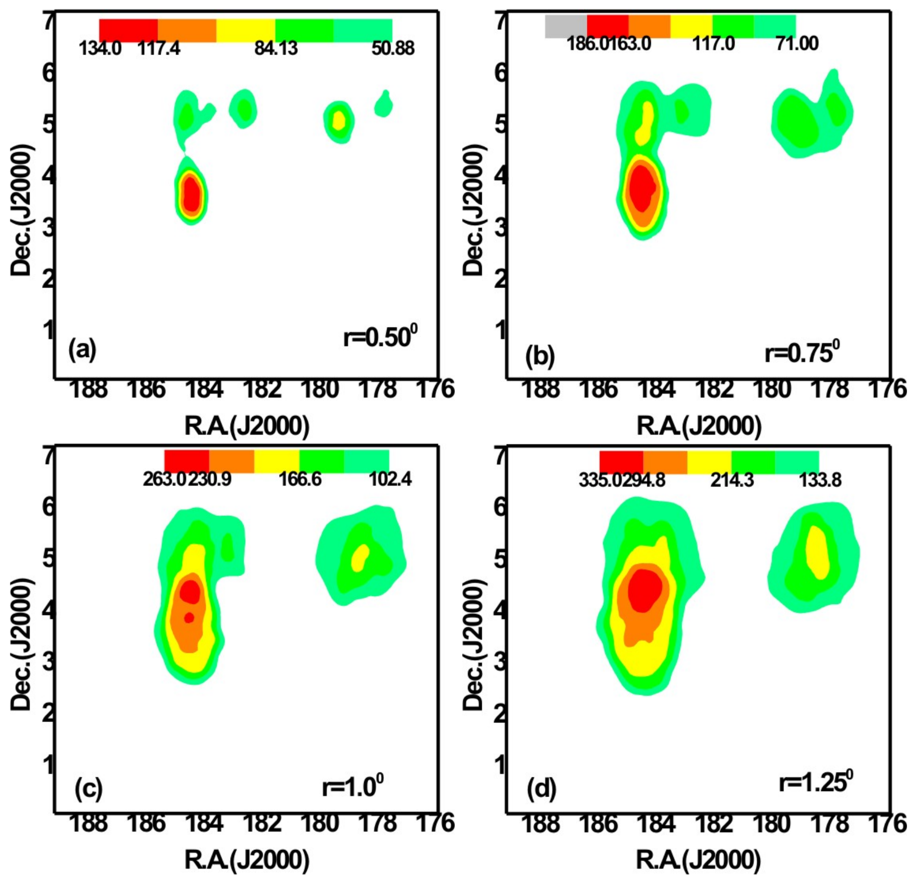

Figure 54: Number density map of galaxies in the Supercluster S[184+003+0077] having nearest neighbour distance of each galaxies at (a) r=0.50°, (b) r=0.75°, (c) r=1.0°, (d) r=1.25°. The color bar is shown. As the radius increases, the subclustering becomes prominent.

4.6.2 Redshift Map

Figure 55 shows a redshift map of galaxies in the Supercluster that have a mean redshift of 0.077. The color map shows that the velocity dispersion is minimum in the region where the number density of galaxy is minimum. In the substructure region at 5° declination, the redshift dispersion is found to be |z|= 0.079, whereas the lower and upper substructure show |z|= 0.077 and 0.081, respectively. It seems that there is a linear relationship between redshift dispersion and the number density of galaxies in the substructures,

$$N_s(6) = -2.8 \times 10^4 |z| + 2353.25 \tag{4.17}$$

We varied the nearest neighbour radius to 0.50° and 1.00°, and calculated the slope of a linearly fitted line as above, and found the same. Therefore, we propose empirical relation (equation 4.17) between number density and redshift dispersion of galaxies in the Supercluster S[184+003+0077].

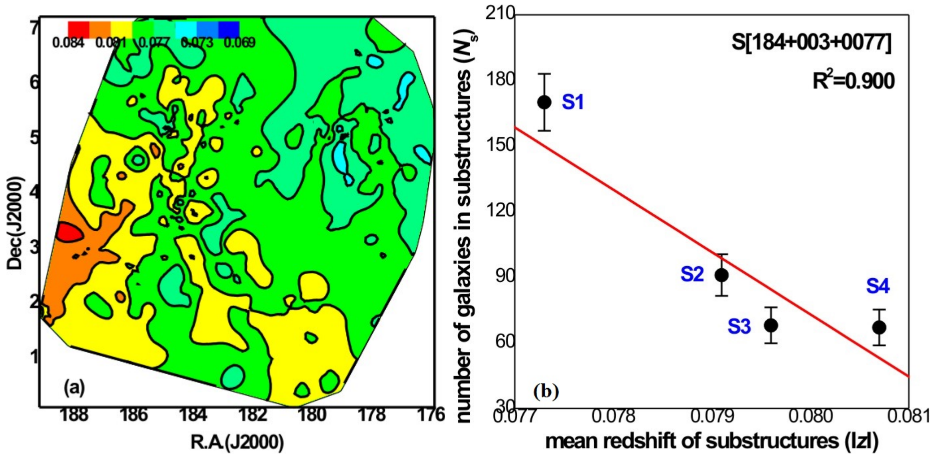

Figure 55: Redshift map is shown for galaxies in the Supercluster S[184+003+0077]. The mean redshift of Supercluster is 0.077. The contour levels are at the redshift 0.069, 0.073, 0.077, 0.081, 0.084. In the substructure region, galaxies hardly have identical redshifts. (b) Number of galaxies in three substructures versus redshift dispersion plot. The statistical $\pm 1\sigma$ error bars are shown.

The redshift dispersion (Δz) of galaxies in the Virgo-Coma Superclusters are 1057 km s^{-1} (Struble & Rood, 1999). Its value is 68 km s^{-1} for the local group (Struble & Rood, 1999). These are nearby Superclusters and groups of which peculiar velocity is relatively higher than that of the distant Superclusters.

4.6.3 Magnitude Map

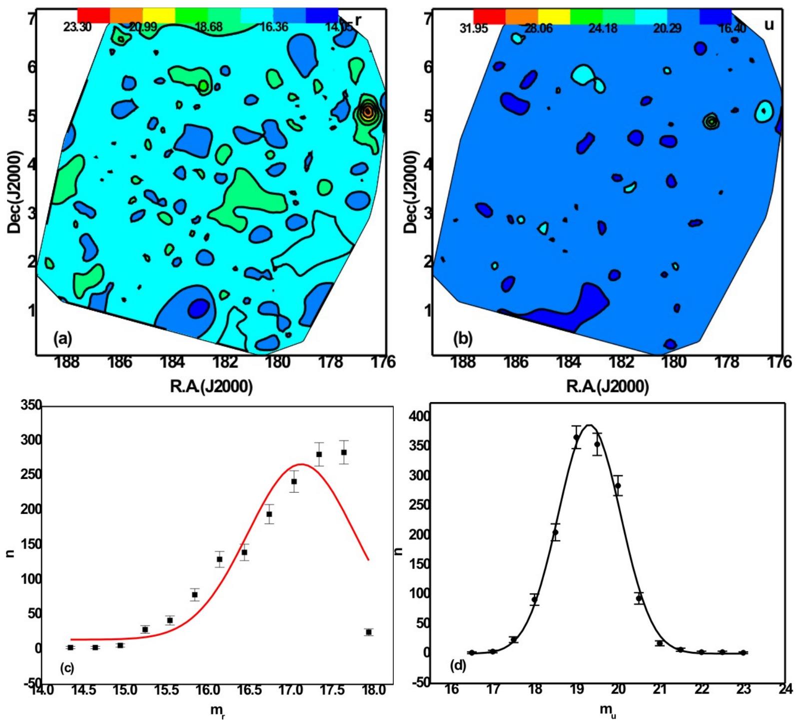

Figure 56: Magnitude map of galaxies in the Supercluster S[184+003+0077] (a) r-magnitude, (b) u-magnitude. The color bar is shown. The contour levels are at 14.05, 16.36, 18.68, 20.98, 23.30 for r-filter and 16.40, 20.29, 24.18, 28.06, 31.95 for u- filter, respectively. The distribution of r and u-magnitude.

Fig. 56ab shows magnitude maps of galaxies in the Supercluster S[184+003+0077]. The SDSS r-magnitude refers to the peak wavelength 6165 Å with the bandwidth 474.7 Å. In the u-filter, the substructure located in the northern region has a higher magnitude. As we know, the higher the magnitude, the lower the brightness.

The magnitude distribution of galaxies in the Supercluster S[184+003+0077] can be seen in Figure 56cd. The solid curve represents Gaussian fits. The Gaussian centre is found to be at 17.136 for r- and 19.314 for u-filters. The Gaussian functions for r- and u-magnitude distributions are given by

$$n_r = 14.42 + 253.21 \exp\left(\frac{-2(m_r - 17.136)^2}{1.66}\right) \tag{4.18}$$

$$n_u = 0.43 + 389.02 \exp\left(\frac{-2(m_u - 19.314)^2}{2.24}\right) \tag{4.19}$$

4.6.4 Substructure Classification

Table 17: First column shows Substructures of the Supercluster S[184+003+0077]. Second and third columns show positions of Superclusters. The next two columns represent mean redshift and number of galaxies in the substructures. The last two columns list mean$u$-magnitude and r-magnitude of substructures, respectively.

Substructure	R.A.(J2000)	Dec.(J2000)	$\lvert Z\rvert$	N_g	$\lvert u\rvert$	$\lvert r\rvert$
S1[185+0035+0077]	184.378°	3.601°	0.0773	170	18.7	17.8
S2[180+0050+0077]	179.205°	5.038°	0.0791	91	18.9	17.9
S3[185+0050+0077]	182.597°	5.350°	0.0796	68	18.9	17.9
S4[183+0050+0077]	177.450°	5.639°	0.0807	67	19.1	18.0

Based on the number density maps, four different substructures, are separated by using the threshold number of galaxies belonging to the four substructures based on their peak values and standard deviation of galaxies density.

4.6.5 Preferred Alignments in the Supercluster

The Supercluster S[184 + 003 + 0077] consists of 1365 galaxies. The statistics for the polar angle (θ) distribution in the Supercluster S[184 + 003 + 0077] is shown in Table 18, the values of chi-square probability (P> χ^2) to found 0.084 which is greater than the significant level 0.050, the first order Fourier coefficient $\Delta_{11}/\sigma(\Delta_{11})$ found to be 0.6 less than the error limit 1.5σ, the first order Fourier probability (P(>Δ_1)) is 0.790 that is greater than 0.15; whereas the value of auto-correlation coefficient (C/C(σ)) to be 1.2 which is greater than 1σ level. This result shows anisotropic. Thus, all statistical tests except auto-correlation coefficient (C/C(σ)) show the distribution of spin vectors in the Supercluster is strong isotropic.

Table 18 shows the statistics for azimuthal angle (ϕ) distribution, the value of chi-square probability (P> χ^2) is 0.580 is more than the significant level 0.050, the first order Fourier coefficient $\Delta_{11}/\sigma(\Delta_{11})$, is to be found 0.7, that is less than the 1.5σ limit, the first order Fourier probability (P(>Δ_1)) is 0.490 more than 0.15, and the value of auto-correlation coefficient (C/C(σ)) to be 0.3 which is less than 1.5σ level. Here, all statistical tests show the distribution of spin vectors in the Supercluster is strong isotropic.

In Fig. 57a, the number of observed solutions that have θ<45° is found to be 2156, and expected solutions are found to be 2133, i.e., observed solution exceeds expected solutions by 23 which is consistent with the observed hump at 27.5° with ±2σ. For the large angles (θ> 45°), the number of observed solutions are less by 78 than that of expected and there is no significant hump and dips are seen in the large angles region θ>45°. In these regions, small humps and dips were noticed due to the local effect. Thus, we conclude no preferred alignment of spin vectors of galaxies.

In Fig. 57b, the observed solutions for the range −45°<ϕ<+45° are found to be 1923, whereas the expected solutions are only 1919. This shows that observed solutions exceeded the expected solution by 4. There is a significant hump at an angle 5° within the standard error of 1.5σ. There are no significant humps and dips in the region outside the shaded regions. In the bimodal region, there is one significant dip at an angle −45° within standard error limit 1.5σ. Owing to the statistics we conclude that the spin vector projection of galaxies shows the random orientation of spin vectors with respect to equatorial coordinate system.

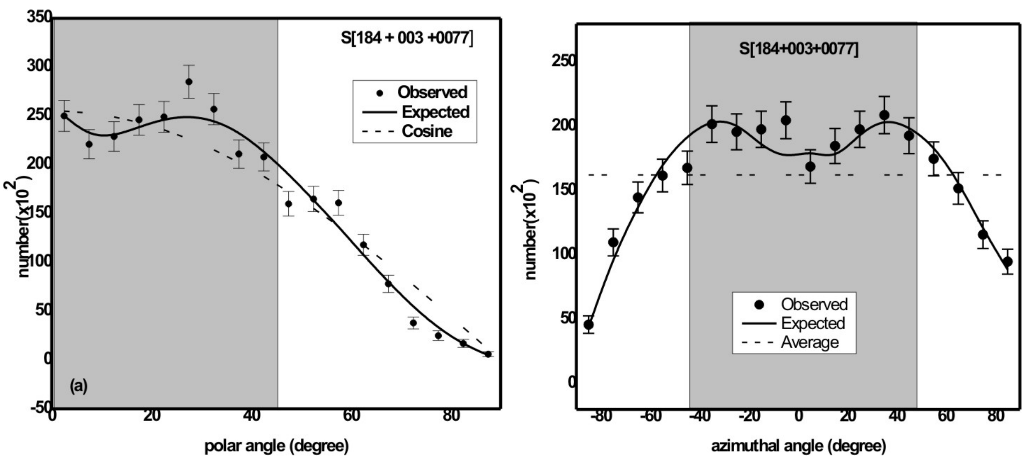

Figure 57: Polar (a) and azimuthal (b) angle distributions of galaxies in the Supercluster S[184+003+0077]. The solid circles with statistical error bars (±1σ) represent observed distribution. The solid curves are obtained from random simulation assuming isotropic distributions.

Table 18: Statistical parameters in the polar and azimuthal angles of galaxies in the Supercluster S[184 + 003 + 0077] and its substructures (first column). The chi-square probability (P> χ^2) is given in the second column. The third and fourth columns show first order Fourier coefficient ($\Delta_{11}/\sigma(\Delta_{11})$ and Fourier probability. The last column tests the auto co-relation coefficient.

Sample	P(> χ^2)	$\Delta_{11}/\sigma(\Delta_{11})$	P(> Δ_1)	C/$C(\sigma)$
Polar Angle				
S[184+003+0077]	0.084	0.6	0.790	1.2
S1[185+0035+0077]	0.648	0.9	0.623	0.9
S2[180+0050+0077]	0.888	−0.2	0.973	0.2
S3[185+0050+0077]	0.912	0.3	0.904	0.1
S4[183+0050+0077]	0.815	−0.5	0.846	− 0.4
Azimuthal Angle				
S[184+003+0077]	0.580	0.7	0.490	0.3
S1[185+0035+0077]	0.129	0.5	0.860	−1.1
S2[180+0050+0077]	0.960	−0.3	0.909	−0.1
S3[185+0050+0077]	0.339	−0.7	0.712	−1.1
S4[183+0050+0077]	0.822	0.5	0.855	−0.1

4.6.6 Preferred Alignment in Substructures

The substructure S1[185+0035+0077] consists of 170 galaxies. By statistics (Table 18), the polar angle (θ) distribution shows the value of chi-square probability (P> χ^2) is to be found 0.648 which is more than the significant level 0.050, the first order Fourier coefficient $\Delta_{11}/\sigma(\Delta_{11})$ is 0.9 that is less than the 1.5σ limit, the first order Fourier probability (P(>Δ_1)) to be 0.623 greater than 0.15 and the value of auto-correlation coefficient (C/C(σ)) is 0.9 less than 1σ level. Thus, all statistics show the distribution of spin vectors in large Supercluster is strong isotropic distribution.

The statistics for azimuthal angle distribution shows (Table 18), the value of chi-square probability (P> χ^2) is 0.129 that is greater than the significant level 0.050, the first order Fourier coefficient $\Delta_{11}/\sigma(\Delta_{11})$ to be 0.5 which is less than the 1.5σ limit, the first order Fourier probability (P(>Δ_1)) to be found 0.860 more than 0.150 and the value of auto-correlation coefficient (C/C(σ)) is to be found −1.1 which is less than 1σ level. Here, all these statistics suggest strong isotropy.

In the polar angle (θ) distribution as shown in Fig. 58a, in the small angles region θ<45°, there are two humps at 30° and 35°, and one significant dip at 55° within 1.5σ limit. In this region, there are no significant humps observed. Thus, we conclude no preferred alignment of angular momentum vectors of galaxies.

In the azimuthal angle (ϕ) distribution as shown in Fig. 58b, in the small-angles region ϕ<−45°, one hump at an angle −60° within 1.5σ limit, is observed, but there are no dips, are seen. For range between −45°<ϕ<+45°, there are two significant humps at an angle

-10° and 20° and two dips at an angle -40° and at 35° within significant limit 1.5σ. In the large angles region ϕ>45°, one dip at 50° can be seen. Due to the local effect, there are no other significant humps and dips outside this range. Thus, we conclude that there is no preferred alignment among spin-vectors of galaxies.

The substructure S2[180+0050+0077] has 91 galaxies. The statistics for polar angle (θ) distribution for galaxies of the substructure S2[180+0050+0077], which are shown in Table 18. The chi-square probability (P> χ^2) to be 0.888 i.e., 88.8% which is greater than the significant level5%), the first order Fourier coefficient $\Delta_{11}/\sigma(\Delta_{11})$ is -0.2 less than 1.5σ limit, the first order Fourier probability (P(>Δ_1)) to be found 0.973 i.e., 97.3% more than 0.15 i.e., 15% and the value of auto-correlation coefficient (C/C(σ)) is found to be 0.2 less than 1σ level. Thus, all statistics show the distribution of spin vectors in large Supercluster is strong isotropic distribution.

Table 18 shows statistics of the azimuthal angle ϕ-distribution for galaxies of the substructure S2[180+0050+0077], the value of chi-square probability (P> χ^2), is to be found 0.960, which is more than the significant level 0.050, the first order Fourier coefficient $\Delta_{11}/\sigma(\Delta_{11})$ to be -0.3 that is less than the 1.5σ limit, the first order Fourier probability (P(>Δ_1)) is 0.909 greater than 0.15, and the value of auto-correlation coefficient (C/C(σ)), is found to be -0.1 less than 1σ level. Here, all these statistics advocate strong isotropy in the ϕ-distribution.

In the polar angle (θ) distribution as shown in Fig. 58c, for the small-angle region θ<45°, there is one significant dip at an angle 35° with 1.5σ limit is seen. In the large angles region (θ>45°), there is one significant hump at 55° in that range which cancels the dip observed at lower angles. Thus, we conclude no preferred alignment of spin vectors of galaxies.

In the azimuthal angle (ϕ) distribution as shown in Fig. 58d, there is one significant dip at an angle -30° in the range between $-45^\circ<\phi<+45^\circ$, but there is no hump and dip outside this range, so we can conclude that there is no preferred alignment among spin-vectors of galaxies.

The substructure S3[185+0050+0077] contains 68 galaxies. The statistics for polar angle (θ) distribution for galaxies of the substructure S3[185+0050+0077], is shown in Table 18, the chi-square probability (P> χ^2), is to be found 0.912, which is more than the significant level 0.050, the first order Fourier coefficient $\Delta_{11}/\sigma(\Delta_{11})$ to be 0.3 that is less than 1.5σ limit, the first order Fourier probability (P(>Δ_1)) is 0.904 more than 0.15 and the value of auto-correlation coefficient (C/C(σ)), is to be 0.1 which is less than 1σ level. Thus, all statistics show the distribution of spin vectors in large Supercluster is strong isotropic distribution.

Table 18 shows the azimuthal angle (ϕ)-distribution for galaxies of the substructure S3[185+0050+0077], the value of chi-square probability (P> χ^2) is to be found 0.339 which is more than the significant level 0.050, the first order Fourier coefficient $\Delta_{11}/\sigma(\Delta_{11})$ to be -0.7 less than the 1.5σ limit, the first order Fourier probability (P(>Δ_1)) is 0.712 more than 0.15; whereas the value of auto-correlation coefficient (C/C(σ)) is found to be -1.1 which is less than 1σ level. Thus, all these statistics suggest strong isotropy in the ϕ-distribution.

In the polar angle (θ) distribution, as shown Fig. 59e, in the small-angle region θ<45°, the difference between observed (98) and expected (96) solution in that range is 2. Thus, in this region, there is no hump, and dip, are observed. For this large angle region (θ>45°), there is one significant dip at 75° it may be due to local effects. Thus, we conclude that no preferred alignment of spin vectors of galaxies.

In the azimuthal angle distribution as shown in Fig. 59f, in the small angles region (ϕ<45°), one significant hump at -55°, is seen. For large angles region (ϕ>45°), there is one hump at 65° and a dip at 35°. At small and large angles regions, these humps, and dips, are observed due to the local effect. There is no significant hump and dip in the range between $-45°<\phi<+45°$. Thus, We again conclude that there is no preferred alignment among spin-vectors of galaxies.

The substructure S4[183+0050+0077] consists of 67 galaxies. The statistics for polar angle distribution for galaxies of the substructure S4[183+0050+0077], is shown in Table 18, the chi-square probability (P> χ^2), is to be found 0.815, which is greater than the significant level 0.050, the first order Fourier coefficient $\Delta_{11}/\sigma(\Delta_{11})$ is -0.5 less than 1.5σ limit, the first order Fourier probability (P(>Δ_1)) to be 0.846 more than 0.15, i.e., and the value of auto-correlation coefficient (C/C(σ)) is found to be -0.4, which is less than 1σ level. Thus, all statistics show the distribution of spin vectors in large Supercluster is strong isotropic distribution.

Table 18 shows the statistics of azimuthal angle (ϕ)-distribution for galaxies of the substructure S4[183+0050+0077], the value of chi-square probability (P> χ^2) is to be found 0.822, more than the significant level 0.050, the first order Fourier coefficient $\Delta_{11}/\sigma(\Delta_{11})$ to be 0.5 which is less than the 1.5σ limit, the first order Fourier probability (P(>Δ_1)) is 0.855 greater than 0.15 and the value of auto-correlation coefficient (C/C(σ)), to be found -0.1 less than 1σ level. Here, all these statistics advocate strong isotropy in the ϕ-distribution.

In the polar angle (θ)-distribution as shown Fig. 59g, for the small-angle region θ<45°, There are two humps at 12.5° and 32.5° and also two dips at 7.5° and 22.5° are observed due to the local effect. In the large angles region (θ>45°), one hump at an angle 57.5° can be seen within the error limit 1.5σ and no significant dip seen in that range. Thus, we conclude no preferred alignment of spin vectors of galaxies.

In the azimuthal angle (ϕ)-distribution as shown in Fig. 59h, in the small-angle region ϕ<−45°, one significant hump at an angle −85° and dip at −65° due to local effect, can be seen. At bimodal region (ϕ~45°), one hump is observed within error limit 2σ. For the range between −45°<ϕ>+45°, there are four significant hump at −35°, −25°, −5°, 25° and one dip at 15° are observed within error limit 2σ. In the large-angle region (ϕ>45°), two significant dips at 55°) and 75° due to local effect. Thus, we again conclude that there is no preferred alignment among spin-vectors of galaxies.

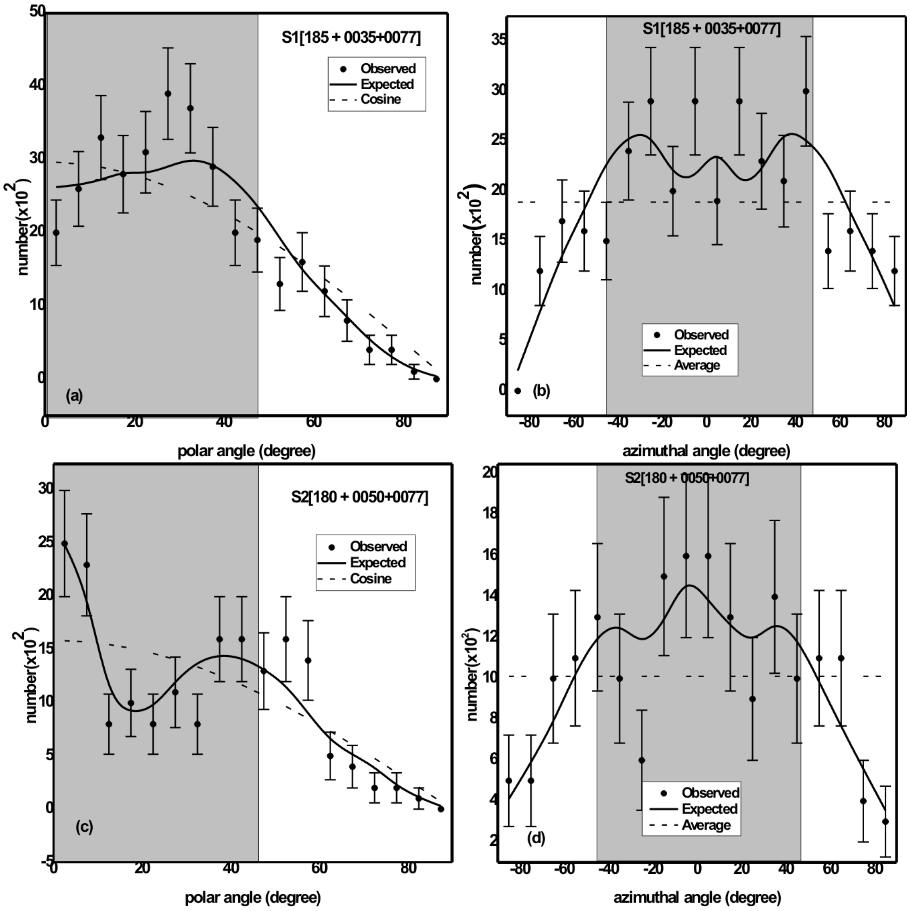

Figure 58: Polar (a, c) and azimuthal angle (b, d) distributions of galaxies in the substructures of Supercluster S[184+003+0077]. Solid circles with statistical error bars ($\pm 1\sigma$) represent observed distributions. The expected distribution are represented by solid curves. These solid curves are obtained by preforming random simulation.

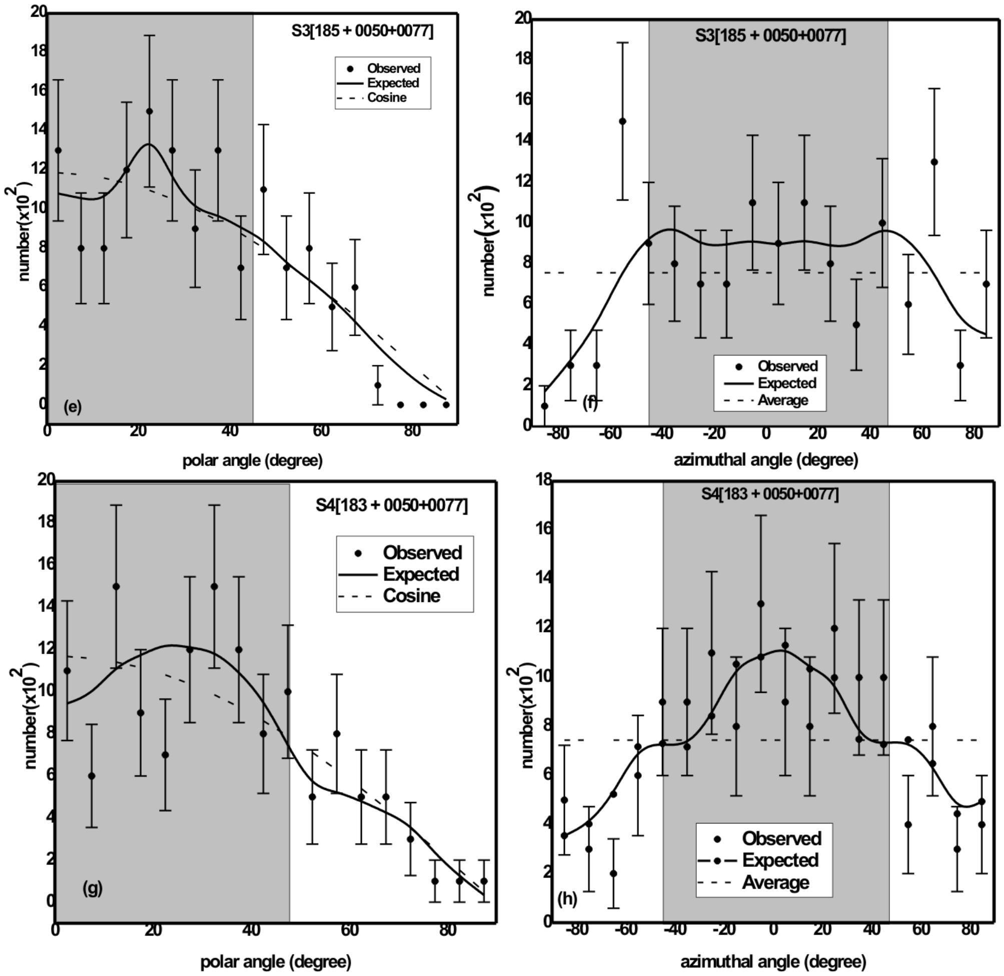

Figure 59: Polar (e, g) and azimuthal angle (f, i) distributions of galaxies in the substructures of Supercluster S[184+003+0077]. Solid circles with statistical error bars ($\pm 1\sigma$) represent observed distributions. The expected distributions are represented by solid curves. These solid curves are obtained by performing a random simulation.

4.6.7 General Discussion

As Peebles (1969) intimated that the transfer angular momentum calculated by computation effect agrees with the prediction value produced by the gravitational effects. To understand how the angular momentum of galaxies precisely measures the evolution and formation of structure in the universe. We adopt the method to analyze spin vectors orientation of galaxies in selected SDSS Supercluster S [184 + 003 + 0077]. By using this method given by Flin & Godlowski (1986), we obtained three-dimensional data of galaxies using the axial ratios and intrinsic flatness which is described by polar angle (θ) and azimuthal angle (ϕ). We found there is no preferred alignment of spin vectors orientation favoring cosmological principle− isotropic distribution of galaxies for this, we used three statistical tests: chi−square, auto−correlation, and Fourier tests.

Selection effects are removed and the expected isotropic distribution curves are determined using the numerical simulation by creating 10^7 virtual galaxies and adopting the method as proposed by Aryal & Saurer (2000).

Some humps and dips in the angular momentum distribution are observed in different substructure due to local effect suggesting a local tidal connection between the rotation axes of galaxies or due to merging process so angular momentum of galaxies get affected.

In addition, we researched whether or not there is a dependence of magnitude with polar angle and azimuthal angle. The flux measured by using our instrument is not a hundred percent total of the flux produced by source objects because the sensitivity of the detector is not equal for different wavelengths. The apparent magnitude depends on the instrument we use to measure it. The sensitivity of the detector is different at different wavelengths. Photographic plates are most sensitive to blue and violet wavelength. As we know, that the higher the value of magnitude, the fainter the star is so that the galaxy having higher magnitude consists of the stars with low brightness.

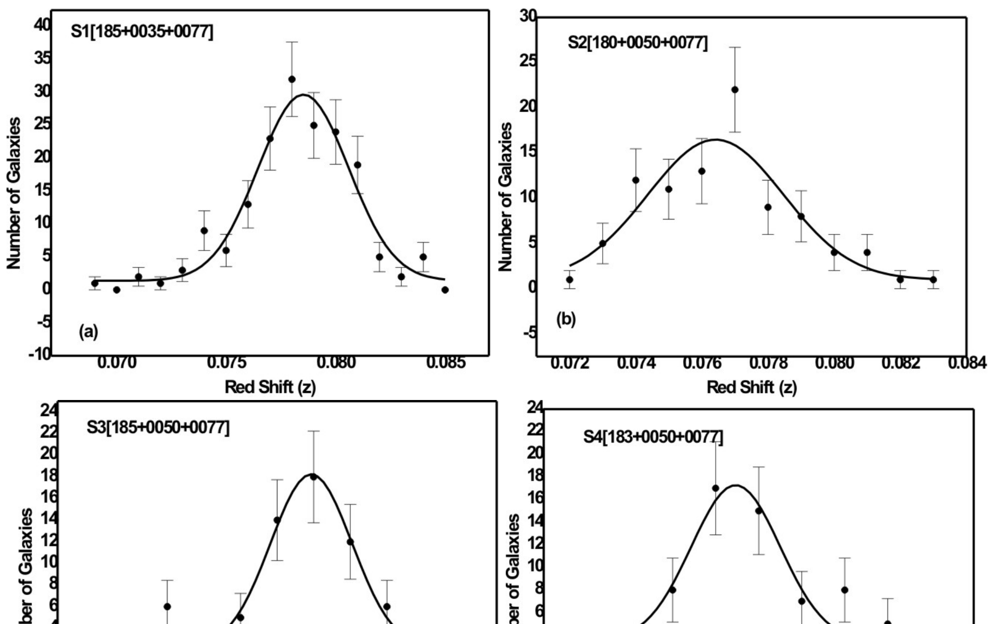

Figure 60: The red shift distribution of galaxies in the substructure S1[185 + 0035+0077] (a), S2[180 + 0050+0077] (b), S3[185 + 0050+0077] (c) and S4[183 + 0050+0077] (d). The solid circles with $\pm 1\sigma$ error bars represent the observed distribution. The solid line represent the Gaussian fit.

4.7 Comparison with Previous Works

Figure 61(a) shows 85° × 85° field of all sky distribution of all 6 Superclusters S[195 +027+0022], S[173+003+0077], S[247+040+0029], S[227+006+0078], S[231+ 030 +0117] and S[184+003+0077]. Three Superclusters are in the field whereas the other three are connected and a part of Sloan Great Wall (Einasto et al., 2003). All six Superclusters are located in the northern hemisphere. No trend is seen in the color-magnitude plot (Figure 61b). When plotted redshift (z) versus apparent magnitude (m_r), we noticed three groups. First group of Superclusters (S[247+040+0029] and S[195+027 +0022]) that have low redshift (z < 0.04) showed a wide range of apparent magnitude (12.5-18.0)(Figure 61c). There are three Superclusters having relatively narrow range of apparent magnitudes (14.4-18.0) have redshift in the range 0.07-0.09. These Superclusters are S[173+014+0082], S[227+006+0078] and S[184+003+0077]. The only high redshift (z > 0.11) Supercluster in our database is S[231+030+0117] have 1172 galaxies. The magnitude dispersion is found to decrease with the increase of redshift. As expected, a similar pattern of distribution of galaxies in 6 Superclusters are found when plotted redshift against color (Figure 61d).

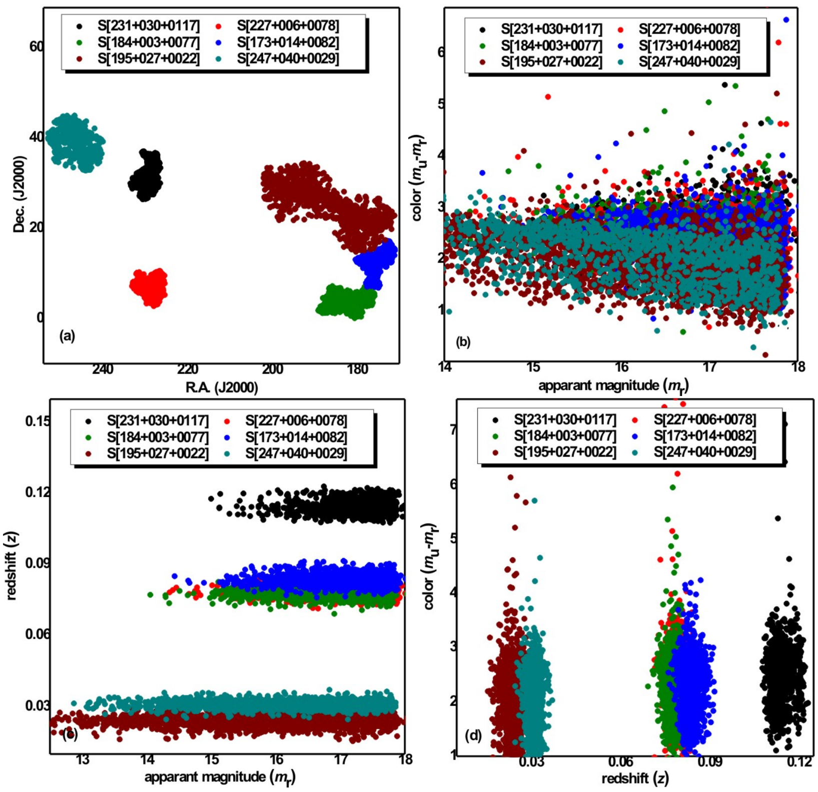

Figure 61: (a) All sky distribution of six Superclusters in 85° × 85° field. (b) color (m_u-m_r))-magnitude (m_r) scatter plot of all galaxies in 6 Superclusters. A spread of galaxies towards the higher magnitudes can be seen. (c) Redshift (z) versus apparent magnitude (m_r) plot of all galaxies in 6 Superclusters. A spread of apparent magnitude is found to decrease with the increase of redshift. (d) Color versus redshift distributions of galaxies in 6 Superclusters. Color dispersion is found to be similar in all 6 Superclusters.

.

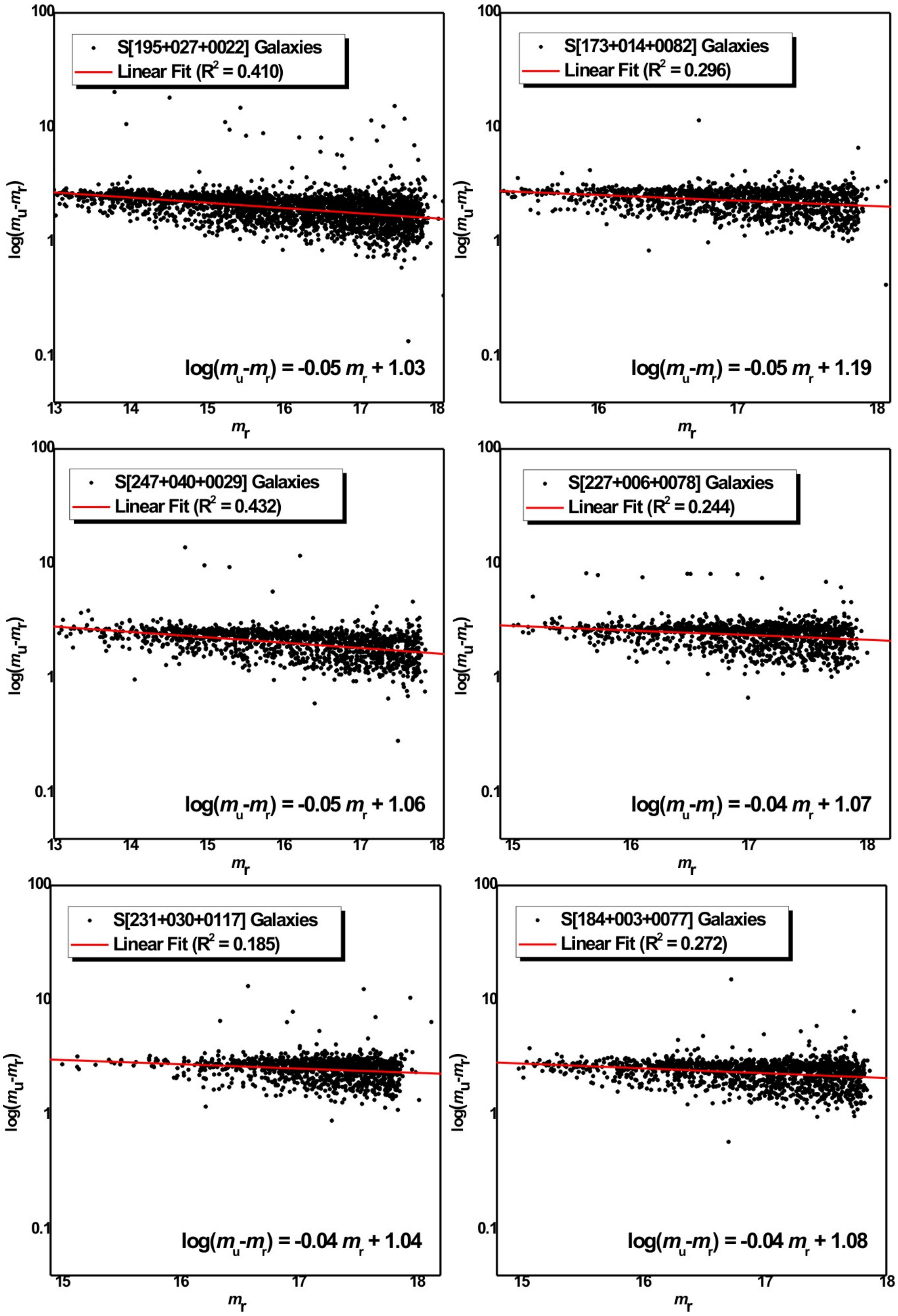

Figure 62: Color ($\log(m_u$-m_r))-magnitude(m_r) diagram of galaxies in the Superclusters: (a) S[195+027+0022], (b) S[173+014+0082], (c) S[247+040+0029], (d) S[227+006+0078], (e) S[231+030+0117], (F) S[184+003+0077]. Each black dots represents a galaxy. The best fit lines and equation are shown. Fitted lines and equations are shown.

Figure 62 shows a color-magnitude diagram of galaxies in six Superclusters. We have compiled the database of apparent magnitude in u- and r-filters using SDSS. Figure 62a showed logarithm of m_u-m_r versus r-magnitude of the galaxies in the Supercluster S[195+0027+0022]. When fitted, we found a relation in which slope is found to be negative but very small (-0.04) (the equation is given in the Figure 62a).

The slope is found to decrease very slowly with the increase of apparent magnitude. This suggests a very precise velocity dispersion of galaxies in the Supercluster. As expected, galaxies are found to be aggregated towards the upper limit of r-magnitude. For the Superclusters S[173+003+0077], S[247+040+0029], S[227+006+0078], S[231+030+0117] and S[184+003+0077], color-magnitude relations are found to be similar (equations are given in the field of the figures) In these relations, slopes and intercepts are found to be similar. This indicates a common behavior of SDSS Superclusters. Though, the values of R^2 are not very high. It is because of the dispersion in the color. This suggests that the star formation rate in these Superclusters differ.

Figure 63 shows orientation parameter versus redshift plots for all 6 Superclusters for both polar (angular momentum vector) and azimuthal (its projection) angles. The grey-shaded region is the region of isotropy. All Superclusters preferred isotropy in both polar and azimuthal angle distributions, suggesting no preferred alignments. In addition, redshift is found to be independent of orientation. This is an interesting result in the sense of cosmological principle. According to the cosmological principle, the universe is not only isotropic but also homogeneous at a large scale. Our results support this.

We have studied orientation parameters versus richness (population of galaxies) of substructures (Figure 63b). Low richness substructures are found to show a preference in both polar and azimuthal angle distributions. This results suggest a non-vanishing angular momenta for small groups or substructures of galaxies, as suggested by Godłowski (2012). Rich substructures showed a random orientation of galaxies in all 6 Superclusters. Therefore, the formation of small groups might be enhanced by some local inhomogeneities probably due to the gravitational shearing effect caused due to the relative motion of large substructures. Through the trend lines in both figures (Figure 63a,b) are unreliable because of very low values of R^2. It is therefore we have not discussed the fitted lines here.

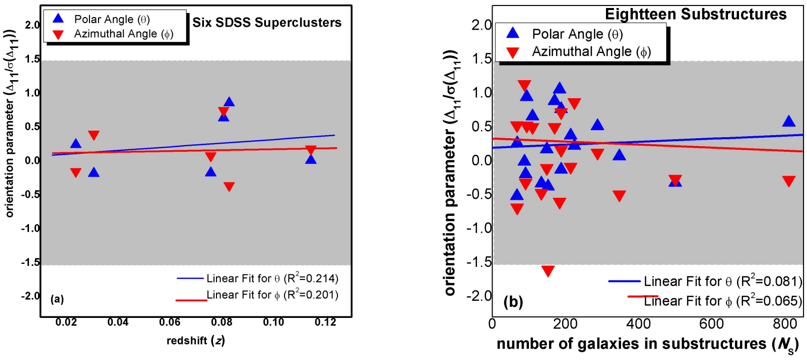

Figure 63: (a) Distribution of first order Fourier coefficient ($\Delta_{11}/\sigma(\Delta_{11})$ for both polar (θ) and azimuthal (ϕ) angles of all six Supercluster galaxies with their redshift(Z). Symbols and lines are described. First order Fourier coefficient is the orientation parameter to measure deviation from expected isotropic distribution. (b) Distribution of first order Fourier coefficient ($\Delta_{11}/\sigma(\Delta_{11})$ for both polar (θ) and azimuthal (ϕ) angles of 18 substructures(that we have identified in 6 Superclusters) with the number of galaxies in these substructures. Symbols and lines are described. The grey shaded region represents the region in which hierarchy model (Peebles, 1969) is preferred. The region above and below represents the region for pancake (Doroshkevich, 1973); (Doroshkevich et al., 1978) and primordial vorticity (Ozernoy, 1978); (Stein, 1974) models.

Figure 64 shows a comparison between the preferred alignments of galaxies in our work and previous published works. The grey-shaded region shows region of isotropy. A deviation from isotropy is noticed by Kashikawa & Okamura when studying Local Supercluster galaxies (Kashikawa & Okamura, 1992). They noticed a preferred alignments of angular momentum vectors of galaxies at the core region (Virgo cluster). Godłowski et al. (2010) noticed a similar result but the direction of orientation is found to be opposite in the rich Abell clusters. Aryal et al. (2007) studied core of the Shapley Superclusters and found no preferred alignments. In the irregular Abell cluster,Aryal & Saurer (2006) noticed preferred alignments. Similar results are noticed by Yadav et al. (2017), Pajowska et al. (2019) and Malla et al. (2019).

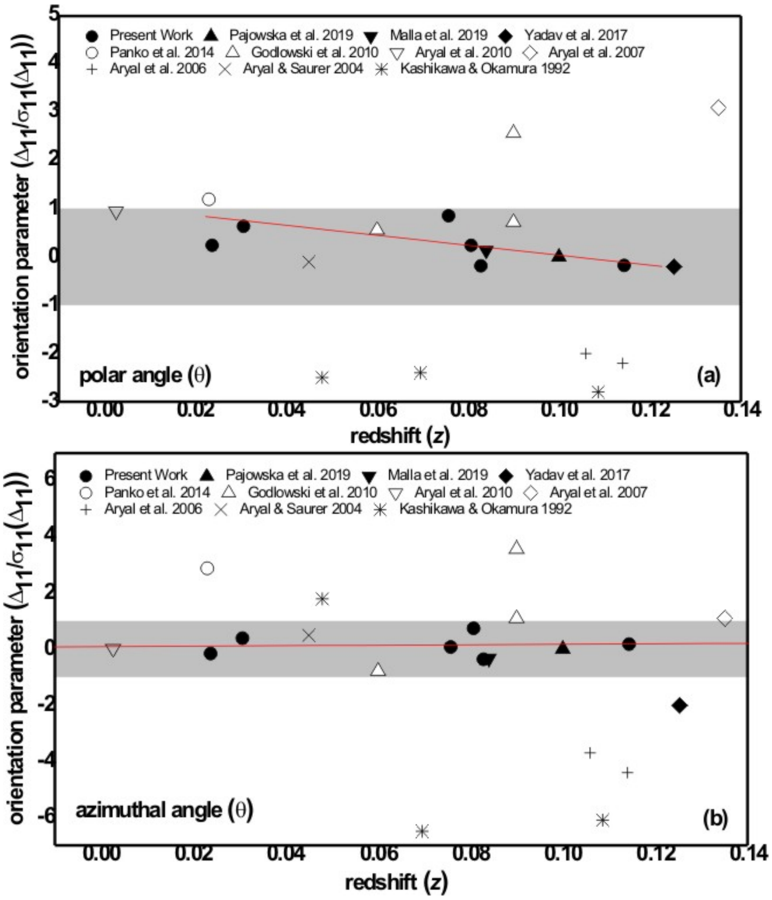

Figure 64: Comparison with published works: (a) orientation parameter versus redshift for polar angle distribution (b) orientation parameter versus redshift for azimuthal angle distribution. First order Fourier coefficients (($\Delta_{11}/\sigma(\Delta_{11})$) represent the orientation parameters for both polar and azimuthal angle distributions. We have compared our results for six SDSS Superclusters (solid circles) with ten similar published works on various clusters and Superclusters as follows: (Pajowska et al., 2019), (Malla et al., 2019), (Yadav et al., 2017), (E. Panko et al., 2014), (Godłowski et al., 2010), (Aryal et al., 2010), (Aryal et al., 2007), Aryal & Saurer (2006), (Aryal & Saurer, 2004) and (Kashikawa & Okamura, 1992). Symbols are given. Solid line represents the best fit of our six Superclusters only. Orientation parameters (Y-axis) are divided by respective errors. So, no need to show error bars in the data.

Melkonian & Nikogosian (1998) studied substructure of the core of the Perseus Supercluster of galaxies. They noticed hierarchical substructures in which radial segregation of galaxies is found. However, position angle distribution of galaxies is found to be uniform. Godlowski et al. (1998) studied rich cluster of galaxies Abell 754 and found evidence for non-random alignment of the galaxies and confirm the presence of subclustering.

Baier et al. (2003) Studied galaxy cluster Abell 14 and confirm the presence of subclustering. They noticed a preferred alignments of angular momentum vectors of galaxies in the cluster Abell 14. Noreña Blandón et al. (2018) proposed an idea that substructures could be formed due to the tidal stream produced in galactic mergers. Panko et al. (2018) investigated 2D distribution of galaxies in 254 rich open galaxy clusters. They noticed that about 25% of clusters showed four kinds of regular substructures namely crossing and divaricating filaments (or X and Y-type peculiarities) and curved strips with short dense chains. Malla et al. (2019) studied preferred alignments of galaxies in the SDSS Supercluster S[202-001+0084]. They noticed a random orientation of angular momentum of galaxies in this Supercluster. We also noticed a similar result in the Supercluster S[184+003+0077].

CHAPTER 5

5. CONCUSION AND RECOMMENDATIONS

5.1 Conclusion

We have studied number density, redshift and magnitude maps and angular momentum vectors of 8 973 galaxies in the six SDSS 7DR (Sloan Dizited Sky Survey 7 Data Release) Superclusters and their nineteen substructures having redshift (z) in the range 0.024 to 0.114. These Superclusters are S [195+027+0022], S [184+003+0077], S[247+040+0029], S [173+014+0082], S [227+006+0078] and S [231+030+0117]. The substructures in these Superclusters are identified using number density and redshift maps. The r and u magnitude maps and distributions are also studied in all six Superclusters. A color-magnitude diagram has been made for each Superclusters. Similarly, a plot between the number of galaxies in the substructures and their mean redshift are plotted and found a linear relationship with decreasing slope.

Astronomical data are affected by several selection effects depending on the nature of the techniques used in the telescope as well as the selection criteria. These selection effects can be treated as noise in the database. These noises show a systematic pattern and can be propagated in a way. In the case of galaxies, even though all control parameters (independent variables, e.g., positions and inclination) remain constant, the resultant outcomes (dependent variables, e.g., position and polar angles) vary. The selections effects should be removed from the database and the expected isotropic distribution curves are determined by performing numerical simulations. We used the method proposed by Flin & Godlowski (1986) in order to compute two-dimensional data to three dimensional galaxy rotation axes (polar&azimuthal angles). We have carried out random simulation by creating 10^7 virtual galaxies and adopting the method proposed by Aryal & Saurer (2000) in order to find a theoretical distribution of galaxy rotation axes. We have compared the differences between theoretical distributions and observed distributions using three statistics, namely chi-square, auto-correlation and the Fourier. We have presented our results in six sections as follows:

1. On the basis of the number density map, all together eighteen substructures are

identified having richness (R) greater than Abell richness class 2. It is found that the number of galaxies in the substructures decreases linearly with the increase of redshift. This suggests that the high redshift galaxies form a group whereas low redshift galaxies might form clusters of galaxies in the Supercluster.

2. Color-magnitude diagram of the galaxies in all Superclusters show a similar trend with negative slopes, suggesting a domination of the blue cloud. The blue clouds are mostly spiral galaxies. Therefore we conclude that the substructures include most blue galaxies. This is validated by the u-magnitude maps of Superclusters.

3. Four substructures are found in the Superclusters S[247+040+0029] and S[184+003 +0077]. Superclusters S[195+027+0022] and S[173+003+0077] showed 3 substructures whereas the Superclusters S[227+006+0078] and S[231+030+0117] have 2 substructures only.

4. In the Supercluster S[195+027+0022], a random orientation of angular momentum vectors of galaxies is found, suggesting hierarchy model. Among the three substructures, the smallest one (Abell richness 1) S3[181+020+0024] showed a preference in the distribution of projections of angular momentum vectors. Similar to the Supercluster S[195+027+0022], low richness substructure of this Supercluster S3[181+020+0024] showed a preferred alignments in both angular momentum vectors and its projections. Therefore, smaller the aggregates, the preferred the alignments, suggesting non-vanishing angular momenta of galaxies.

5. In the Supercluster S[184+003+0077], no preferred alignments of angular momentum vectors and its projections of galaxies are noticed. Angular momentum vectors of galaxies is found to lie along the direction of equatorial plane. This suggest vanishing angular momentum as suggested by Peebles (1969) and Godłowski et al. (2010). This Supercluster constitutes three substructures.

6. In the Supercluster S[247+040+0029], we noticed vanishing angular momentum vectors of galaxies and their projections, supporting hierarchy model. This Supercluster showed 4 substructures. No preferred alignment is noticed in the substructures as well.

7. In the Supercluster S[173+014+0082], random orientation of angular momentum vectors of galaxies is found. Out of three substructures, the smallest one of Abell richness class 1, showed a preference in the galaxy alignments. However, no preferred alignments angular momentum vectors of galaxies in other two substructures are noticed.

8. In the Supercluster S[227+006+0078], only two substructures are found. Both the substructures and the Supercluster showed random orientation of angular

momentum vectors and its projections. Both substructures are rich in galaxy numbers, of richness class 2.

9. In the Supercluster S[231+030+0117], two substructures of Abell richness class 2 and 1 are noticed. Both the substructures and the Superclusters showed random orientation of angular momentum of galaxies and their projections, supporting hierarchy model, as suggested by Peebles (1969).

5.2 Recommendations

Study of large scale structure and their evolution is extremely important to understand the Universe. Till date, we do not know exactly how galaxies form and how they evolve in the clusters or Superclusters. For the last 40 years, researchers have been studying the nearby Universe by analysing databases of only Coma and Virgo Superclusters. It is because of the SDSS telescope, now we are able to get a systematic database of many many distant Superclusters. These are actually the natural laboratories in which we can understand the evolution of galaxies in the large scale structure and hence many unanswered questions will be addressed. Following are our recommendations:

1. Sloan Digitized Sky Survey (SDSS) provides a huge database at all redshifts with a very high precision level. In addition, it provides a photometric database as well. We intend to study the preferred alignments of the angular momentum vectors of high redshift ($z \geq 0.2$) galaxies in the clusters and Superclusters. In addition, distribution of angular momentum of galaxies in the merging binary clusters, rotating clusters, irregular clusters provide information regarding origin of angular momentum in the large scale structure.

2. We have studied the galaxy orientation with respect to the equatorial coordinate system. We wish to define a physical reference system within the galaxies and study the preferred alignments of galaxies with respect to it. Though, the importance of galactic and Supergalactic coordinate systems cannot be denied.

3. The result of the statistical analysis has been noticed to have a strong dependence on the sample/subsample classification criteria. Finding out a straight mathematical computation method instead of a statistical method is essential and interesting in the future.

CHAPTER 6

6. SUMMARY

Galaxies are gravitationally bounded system and is supported by rotation. It possesses rotation axis and hence a winding sense with a differential rotation of stars and clouds around it. Spiral galaxies showed a preferred angular momentum vector whereas elliptical showed a changing angular momentum. According to the cosmological principle, the directional parameters or dynamical variables (e.g., angular momentum vectors of galaxies) should be isotropically distributed. Therefore, the total angular momentum vectors galaxies in the clusters or Superclusters should be vanishing. Though, a large number of studies showed that the clusters or groups of galaxies preferred non-vanishing angular momentum as well. In the case of Supercluster, only a few studies have been carried out. Therefore, a study of distribution of angular momentum vectors of galaxies is important to validate the cosmological principle. For a rotationally supported system (e.g., galaxies, stars, clouds, etc), the distribution of the angular momentum vectors can be an indicator of the initial conditions when these structures formed, provided the angular momentum of have not significantly changed since their formation ((Von Weizsäcker, 1951), (Gamow, 1952)). Thus, a thorough study of the spatial orientations of angular momentum vectors of galaxies in the large-scale structure is needed. Sloan Dizited Sky Survey (SDSS) data provides a very accurate spectroscopic and photometric data of a large number of galaxies in the clusters and Superclusters. A systematic analysis of angular momentum of galaxies in the Superclusters would be important to understand evolution of galaxies in the large-scale structure of the Universe.

Peebles (2019 Noble prize winner) pioneer work (1969) on angular momentum of galaxies was published in 1969 (Peebles, 1969). Since then, many researchers began working on this issue. For the last 45 years, more than 150 works on angular orientation have been published. Here we summarize a few leading works. Doroshkevich (1973) and Shandarin (1974) suggested the 'pancake model' in which they predicted that the angular momentum vectors of galaxies tend to lie within the cluster plane. Another important model, named 'primordial vorticity' (Ozernoy, 1978) advocates that the angular momentum vectors of galaxies tend to be oriented perpendicular to the cluster plane. According to the 'hierarchy model' (Peebles, 1969) the directions of the angular momentum vectors should be distributed randomly. Authors have drawn different conclusions regarding these three scenarios: (1) no preferred alignment supporting hierarchy model ((Helou & Salpeter, 1982), (Bukhari & Cram, 2003), (Aryal & Saurer, 2005a), (Aryal, Neupane, & Saurer, 2008), (Aryal et al., 2012), (Aryal et al., 2013), (Godlowski et al., 1998) (Yadav et al., 2017), (Malla et al., 2019)), (2) tend to orient parallel ((Jaaniste & Saar, 1978), (Flin & Godlowski, 1986), (Godłowski, 1993), (Godłowski, 1994), (Godlowski et al., 1998), (Wu et al., 1998), (Flin, 2001)) or perpendicular ((Reinhardt & Roberts, 1972), (Gregory et al., 1981), (MacGillivray et al., 1982), (Baier et al., 2003)) with respect to the cluster (or LSC) plane, (3) bimodal tendency ((Kashikawa & Okamura, 1992)) (4) local anisotropy ((Flin, 1995), (Djorgovski, 1983), (Aryal & Saurer, 2004), (Aryal & Saurer, 2005b), (Aryal & Saurer, 2006), (Aryal & Saurer, 2006), (Aryal et al., 2013)), (5) global anisotropy ((Parnovsky et al., 1994)), (Godlowski & Ostrowski, 1999) etc. noticed a strong systematic effect, generated by the process of de-projection of a galactic axis from its optical image. These results suggest different alignments of galaxies in clusters and Superclusters. However, SDSS database was not available at that time and all of the above works have used photometric databases (e.g., ESO, POSS, IC, MGC, etc). It is essential to reveal the reason behind these differences. These differences might be correct or need revision. We plan to work on an SDSS database using both photometric and spectroscopic parameters of Supercluster galaxies.

Aryal & Saurer ((Aryal & Saurer, 2004), (Aryal & Saurer, 2005a), (Aryal & Saurer, 2006)) and (Aryal et al., 2007)) analysed the spatial orientations of galaxies in 32 Abell clusters of BMtype I, II, II-III and III (Bautz & Morgan, 1970) using Palomar Sky Survey database. BM classification is actually morphological classification of galaxy clusters: BM type I refer to regular clusters with dominating central galaxy, BM type II are those clusters which have more or less similar photometric galaxies with any to-be-regular shape, BM type II corresponds to those aggregates of galaxies which are irregularly shaped having more late-type spirals, can be L-type or even more complex. They noticed a systematic change in the galaxy alignments from early-type (BM I) to late-type (BM III) clusters. This result suggests that the spiral-rich (late-type) clusters (BM II-III and BM III) show a preferred alignment than that of elliptical-rich (early-type) clusters. Supercluster contains various substructures. These substructures are similar to clusters of galaxies in many respects. Therefore, we study preferred alignments in those substructures of Superclusters and compare it with the alignments of Abell clusters of galaxies.

Supercluster is the largest observed structure in the Universe. It constitutes several clusters and groups of galaxies which are gravitationally bounded system. A large database of Superclusters is available because of Sloan Digital Sky Survey Data Release

7 (SDSS DR7 hereafter) and the pioneer work by Einasto et al. (Einasto et al., 2003), (Einasto et al., 2011), (Einasto et al., 2014), (Einasto et al., 2016)). Einasto et al. (Einasto et al., 2003) investigated Superclusters of galaxies in the SDSS and found that the clusters located at high-density environment showed luminosity a factor of 5-10 times higher than in low-density environment of the field. Further Einasto et al. (Einasto et al., 2011) classified morphology of a set of Superclusters using SDSS DR7 database and calculated luminosity to determine Superclusters from a flux-limited sample of galaxies and finally selected Superclusters with 300 and more galaxies. A widely different morphology of Superclusters is found. Liivamagi et al. Liivamägi et al. (2012) compiled a set of Supercluster catalogues for the galaxies using SDSS survey main and luminous red galaxy (LRG) flux limited samples. They have also created a test catalogue for the galaxies from the Millennium simulation to compare the simulated and observed Superclusters and to clarify the methods we use. Finally, they find that the Superclusters are well-defined systems, and the properties of the Superclusters of the main and LRG samples are similar. We also show that with adaptive local thresholds we get a sample of Superclusters, the properties of which do not depend on their distance from the observer. We are very much interested in compiling a database of at least six Superclusters and finding substructures within those aggregates. Einasto et al. (2011) studies the morphology of a set of Superclusters drawn from the SDSS DR7. They calculated the luminosity density field to determine Superclusters from a flux-limited sample of galaxies from SDSS DR7, and select Superclusters with 300 and more galaxies for our study.

It is believed that the slow star formation rate indicates the possibility of anisotropy (preferred orienting angle might be distorted due to collision or merging) and the rapid star formation rate slows down the angular momentum of the system, leading to a non-vanishing angular momentum. We intend to use a huge database of both low (< 0.1) and high (> 0.5) redshifted galaxies in both the ultraviolet and infrared filters in order to study the above-mentioned effects. In every database there are limitations, called selection effects. Selection effects may play an important role when galaxies are distant. The SDSS database has this effect because it is a ground-based telescope located in the northern hemisphere (New Mexico, USA) of our planet. These effects can lead to artificial structures (Aryal et al., 2001). In most of the published works in galaxy orientation studies, selections of various kinds can be seen. These are mainly due to the face-on galaxies and inhomogeneity in positions. Only a few authors have made an attempt to minimize these effects (Hu et al., 2002), (Godłowski & Flin, 2009)). It is essential to remove such effects to avoid misinterpretations in the results. We intend to work on the removal of such effects by performing numerical simulation in all sorts of databases.

We plan to study preferred alignments of angular momentum of galaxies in the Supercluster and their substructures by calculating rotation axes and simulating it to satisfy cosmological principle regarding large scale structure evolution. Our specific objectives is to work on SDSS (Sloan Digital Sky Survey) database of six Supercluster galaxies of which angular momentum vectors and its projections are calculated to identify preferred alignments of galaxies in the Superclusters and substructures. In addition, we are interested to identify substructures in the Supercluster region using redshifts of each individual galaxy and develop empirical relations between mean redshift and number density of galaxies.

We have studied number density, redshift, magnitudes and angular momentum vectors of 8,973 galaxies in the six SDSS DR7 (Sloan Dizited Sky Survey 7 Data Release) Superclusters and their nineteen substructures having redshift (z) in the range 0.024 to 0.114. These Superclusters are S[195+027+0022], S[184+003+0077], S[247+040+0029], S[173+014+0082], S[227+006+0078] and S[231+030+0117]. The substructures in these Superclusters are identified using number density and redshift maps. The r and u magnitude maps and distributions are also studied in all six Superclusters. A color-magnitude diagram has been made for each Superclusters. Similarly, a plot between the number of galaxies in the substructures and their mean redshift are plotted and found a linear relationship with decreasing slope. The selections effects should be removed from the database and the expected isotropic distribution curves are determined by performing numerical simulations. We used the method proposed by Flin & Godlowski (1986) in order to compute two-dimensional data to three-dimensional galaxy rotation axes (polar & azimuthal angles). We have carried out random simulation by creating 107 virtual galaxies and adopting the method proposed by Aryal & Saurer (2000) in order to find a theoretical distribution of galaxy rotation axes. We have compared the differences between theoretical distributions and observed distribution using three statistics, namely chi-square, auto-correlation and the Fourier. We have studied number density maps of all six Superclusters and found nineteen substructures of Abell richness class 2. It is found that the number of galaxies in the substructures decreases linearly with the increase of redshift. This suggests that the high redshift galaxies form a group whereas low redshift galaxies might form clusters of galaxies in the Supercluster. Color-magnitude diagram of the galaxies in all Superclusters show a similar trend with negative slopes, suggesting a domination of the blue cloud. The blue clouds are mostly spiral galaxies. Therefore, we conclude that the substructures include most blue galaxies. This is validated by the u-magnitude maps of Superclusters.

Four substructures are found in the Superclusters S[247+040+0029] and S[184+003+0077]. Superclusters S[195+027+0022] and S[173+003+0077] showed 3 substructures whereas the Superclusters S[227+006+0078] and S[231+030+0117] have 2 substructures only.

In the Supercluster S[195+027+0022], a random orientation of angular momentum vectors of galaxies is found, suggesting hierarchy model. Among the three substructures, the smallest one (Abell richness 1) S3[181+020+0024] showed a preference in the distribution of projections of angular momentum vectors. Similar to the Supercluster S[195+027+0022], low richness substructure of this Supercluster S3[173+014+0082] showed a preferred alignments in both angular momentum vectors and its projections. Therefore, smaller the aggregates, prefers the alignments, suggesting non-vanishing angular momenta of galaxies.

In the Supercluster S[184+003+0077], no preferred alignments of angular momentum vectors and its projections of galaxies are noticed. Angular momentum vectors of galaxies are found to lie along the direction of equatorial plane. This suggests vanishing angular momentum as suggested by Peebles (1969) and Godłowski et al. (2010). This Supercluster constitutes three substructures. In the Supercluster S[247+040+0029], we noticed vanishing angular momentum vectors of galaxies and their projections, supporting hierarchy model. This Supercluster showed 4 substructures. No preferred alignment is noticed in the substructures as well. In the Supercluster S[173+014+0082], random orientation of angular momentum vectors of galaxies is found. Out of three substructures, the smallest one of Abell richness class 1, showed a preference in the galaxy alignments. However, no preferred alignments angular momentum vectors of galaxies in other two substructures are noticed. In the Supercluster S[227+006+0078], only two substructures are found. Both the substructures and the Supercluster showed random orientation of angular momentum vectors and its projections. Both substructures are rich in galaxy numbers, of richness class 2. In the Supercluster S[231+030+0117], two substructures of Abell richness class 2 and 1 are noticed. Both the substructures and the Superclusters showed random orientation of angular momentum of galaxies and their projections, supporting hierarchy model, as suggested by Peebles (1969).

REFERENCES

Abazajian, K. N., Adelman-McCarthy, J. K., Agüeros, M. A., Allam, S. S., Prieto, C. A., An, D., . . . others (2009). The seventh data release of the sloan digital sky survey. *The Astrophysical Journal Supplement Series*, *182*(2), 543.

Adelman-McCarthy, J. K., Agüeros, M. A., Allam, S. S., Anderson, K. S., Anderson, S. F., Annis, J., . . . others (2006). The fourth data release of the sloan digital sky survey. *The Astrophysical Journal Supplement Series*, *162*(1), 38.

Aihara, H., Prieto, C. A., An, D., Anderson, S. F., Aubourg, É., Balbinot, E., . . . others (2011). Erratum:âĂIJthe eighth data release of the sloan digital sky survey: first data from sdss-iiiâĂİ(2011, apjs, 193, 29). *The Astrophysical Journal Supplement Series*, *195*(2), 26.

Aryal, B., Bachchan, R., & Saurer, W. (2010). Optical search limit and preferred position angles of galaxies in 35 clusters. *Bull. Astr. Soc. India*, *38*, 165–184.

Aryal, B., Bhattarai, H., Dhakal, S., Rajbahak, C., & Saurer, W. (2013). Spatial orientation of angular momentum vectors of galaxies in six rotating clusters. *Monthly Notices of the Royal Astronomical Society*, *434*(3), 1939–1945.

Aryal, B., Neupane, D., & Saurer, W. (2008). Morphological dependence in the spatial orientations of galaxies around the local supercluster. *Astrophysics and Space Science*, *314*(1-3), 177–191.

Aryal, B., Paudel, R., & Saurer, W. (2012). Spatial orientation of angular momentum vector of galaxies in three merging binary clusters. *Astrophysics and Space Science*, *337*(1), 313–319.

Aryal, B., Paudel, S., & Saurer, W. (2007). Spatial orientations of galaxies in seven abell clusters of bm type ii. *Monthly Notices of the Royal Astronomical Society*, *379*(3), 1011–1021.

Aryal, B., Paudel, S., & Saurer, W. (2008). Coexistence of chiral symmetry restoration and random orientation of galaxies. *Astronomy & Astrophysics*, *479*(2), 397–407.

Aryal, B., & Saurer, W. (2000). Comments on the expected isotropic distribution curves in galaxy orientation studies. *Astronomy and Astrophysics*, *364*, L97–L100.

Aryal, B., & Saurer, W. (2004). Spin vector orientations of galaxies in eight abell clusters of bm type i. *Astronomy & Astrophysics*, *425*(3), 871–879.

Aryal, B., & Saurer, W. (2005a). Morphological dependence in the spatial orientations of local supercluster galaxies. *Astronomy & Astrophysics*, *432*(2), 431–442.

Aryal, B., & Saurer, W. (2005b). Spin vector orientations of galaxies in seven abell clusters of bm type iii. *Astronomy & Astrophysics*, *432*(3), 841–849.

Aryal, B., & Saurer, W. (2006). Spatial orientations of galaxies in 10 abell clusters of bm type ii–iii. *Monthly Notices of the Royal Astronomical Society*, *366*(2), 438–448.

Aryal, B., Saurer, W., Funes, J., & Corsini, E. (2001). *Galaxy disc and disc galaxies.* Astron. Soc. Pac., San Francisco.

Baier, F., Godłowski, W., & MacGillivray, H. (2003). Substructures and galaxy orientations in clusters ii. cluster abell 14. *Astronomy & Astrophysics*, *403*(3), 847–856.

Bautz, L., & Morgan, W. (1970). On the classification of the forms of clusters of galaxies. *The Astrophysical Journal*, *162*, L149.

Biernacka, M., Panko, E., Bajan, K., Godłowski, W., & Flin, P. (2015). The alignment of galaxy structures. *The Astrophysical Journal*, *813*(1), 20.

Blanton, M. R., Bershady, M. A., Abolfathi, B., Albareti, F. D., Prieto, C. A., Almeida, A., ... others (2017). Sloan digital sky survey iv: Mapping the milky way, nearby galaxies, and the distant universe. *The Astronomical Journal*, *154*(1), 28.

Bukhari, F. A., & Cram, L. E. (2003). Orientation of galaxies in clusters. *Astrophysics and space science*, *283*(2), 173–223.

Cucciati, O., Lemaux, B., Zamorani, G., Le Fèvre, O., Tasca, L., Hathi, N., ... others (2018). The progeny of a cosmic titan: a massive multi-component proto-supercluster in formation at z= 2.45 in vuds. *Astronomy & Astrophysics*, *619*, A49.

Dekel, A. (1985). A search for galaxy-pancake alignments. *The Astrophysical Journal*, *298*, 461–473.

Djorgovski, S. (1983). Alignment of galaxies in the coma cluster. *The Astrophysical Journal*, *274*, L7–L11.

Doroshkevich, A. (1973). The origin of rotation of galaxies. *ASTROPHYS. LETTERS*, *14*(1), 11-13.

Doroshkevich, A., & Shandarin, S. (1978). A statistical approach to the theory of galaxy formation. *Soviet Astronomy*, *22*, 653–660.

Doroshkevich, A., Shandarin, S., & Saar, E. (1978). Spatial structure of protoclusters and the formation of galaxies. *Monthly Notices of the Royal Astronomical Society*, *184*(3), 643–660.

Doroshkevich, A., Sunyaev, R., Zeldovich, Y. B., & Longair, M. (1974). Confrontation of cosmological theories with observational data. *Dordercht, Holland/Boston, USA*.

Doroshkevich, A., Zeldovich, Y. B., & Sunyaev, R. (1976). Formation and evolution of galaxies and stars. *M., Nauka*.

Einasto, J., Hütsi, G., Einasto, M., Saar, E., Tucker, D., Müller, V., ... Allam, S. (2003). Clusters and superclusters in the sloan digital sky survey. *Astronomy & Astrophysics*, *405*(2), 425–443.

Einasto, M., Lietzen, H., Gramann, M., Tempel, E., Saar, E., Liivamägi, L. J., ... Einasto, J. (2016). Sloan great wall as a complex of superclusters with collapsing cores. *Astronomy & Astrophysics*, *595*, A70.

Einasto, M., Lietzen, H., Tempel, E., Gramann, M., Liivamägi, L., & Einasto, J. (2014). Sdss superclusters: morphology and galaxy content. *Astronomy & Astrophysics*, *562*, A87.

Einasto, M., Liivamägi, L., Saar, E., Einasto, J., Tempel, E., Tago, E., & Martínez, V. (2011). Sdss dr7 superclusters-principal component analysis. *Astronomy & Astrophysics*, *535*, A36.

Eisenstein, D. J., Weinberg, D. H., Agol, E., Aihara, H., Prieto, C. A., Anderson, S. F., ... others (2011). Sdss-iii: Massive spectroscopic surveys of the distant universe, the milky way, and extra-solar planetary systems. *The Astronomical Journal*, *142*(3), 72.

Ensslin, T. A., Biermann, P. L., Kronberg, P. P., & Wu, X.-P. (1997). Cosmic-ray protons and magnetic fields in clusters of galaxies and their cosmological consequences. *The Astrophysical Journal*, *477*(2), 560.

Flin, P. (1995). Global or local anisotropy in galaxy orientation? *Comments on Astrophysics*, *18*, 81–86.

Flin, P. (2001). The anisotropy of galaxy orientation in the coma/a1367 supercluster. *Monthly Notices of the Royal Astronomical Society*, *325*(1), 49–54.

Flin, P., & Godlowski, W. (1986). The orientation of galaxies in the local supercluster. *Monthly Notices of the Royal Astronomical Society*, *222*(3), 525–541.

Flin, P., Godlowski, W., & Szydlowski, M. (2004). On the angular momenta of galaxy structures. In *Dark matter in galaxies* (Vol. 220, p. 479).

Gamow, G. (1952). The role of turbulence in the evolution of the universe. *Physical Review*, *86*(2), 251.

Gibney, E. (2014). Earth's new address:'solar system, milky way, laniakea'. *Nature News*.

Godłowski, W. (1993). Galactic orientation within the local supercluster. *Monthly Notices of the Royal Astronomical Society*, *265*(4), 874–880.

Godłowski, W. (1994). Some aspects of the galactic orientation within the local supercluster. *Monthly Notices of the Royal Astronomical Society*, *271*(1), 19–30.

Godlowski, W. (2011). Some observational aspects of the orientation of galaxies. *arXiv preprint arXiv:1111.1777*.

Godłowski, W. (2012). Remarks on the methods of investigations of alignment of galaxies. *The Astrophysical Journal*, *747*(1), 7.

Godlowski, W., Baier, F., & MacGillivray, H. (1998). Substructures and galaxy orientations in clusters. i. the cluster abell 754. *Astronomy and Astrophysics*, *339*, 709–718.

Godłowski, W., & Flin, P. (2009). The orientations of galaxy groups and formation of the local supercluster. *The Astrophysical Journal*, *708*(2), 920.

Godlowski, W., & Ostrowski, M. (1999). Investigation of galactic alignment in local supercluster galaxy clusters. *Monthly Notices of the Royal Astronomical Society*, *303*(1), 50–64.

Godlowski, W., Panko, E., & Flin, P. (2011). The environmental effects in the origin of angular momenta of galaxies; pacs numbers: 98.52.-b, 98.65.-r.

Godlowski, W., Panko, E., Pajowska, P., & Flin, P. (2013). The investigations of anisotropy in orientations of galaxies. *arXiv preprint arXiv:1301.5477*.

Godłowski, W., Piwowarska, P., Panko, E., & Flin, P. (2010). The orientation of galaxies in galaxy clusters. *The Astrophysical Journal*, *723*(2), 985.

Godlowski, W., Popiela, J., Biernacka, M., Bajan, K., Panko, O. O., Pajowska, P., & Flin, P. (2018). The investigation of the luminosity function for sample 6168 galaxy clusters.

Godłowski, W., Szydłowski, M., & Flin, P. (2005). Some remarks on the angular momenta of galaxies, their clusters and superclusters. *General Relativity and Gravitation*, *37*(3), 615–625.

Godłowski, W., Szydłowski, M., Flin, P., & Biernacka, M. (2003). Rotation of the universe and the angular momenta of celestial bodies. *General Relativity and Gravitation*, *35*(5), 907–913.

Graves, G. J., Faber, S., & Schiavon, R. P. (2010). Dissecting the red sequence. iv. the role of truncation in the two-dimensional family of early-type galaxy star formation histories. *The Astrophysical Journal*, *721*(1), 278.

Gregory, S. A., Thompson, L. A., & Tifft, W. G. (1981). The perseus supercluster. *The Astrophysical Journal*, *243*, 411–426.

Hasegawa, T., Wakamatsu, K.-i., Malkan, M., Sekiguchi, K., Menzies, J. W., Parker, Q. A., . . . Okamura, S. (2000). Large-scale structure of galaxies in the ophiuchus region. *Monthly Notices of the Royal Astronomical Society*, *316*(2), 326–344.

Hawking, S., & Ellis, G. (1973). The large scale structure ofspace-time. *Cambridge University*.

Hawley, D., & Peebles, P. (1975). Distribution of observed orientations of galaxies. *The Astronomical Journal*, *80*, 477–491.

Helou, G. (1984). Spin statistics in binary galaxies-implications for formation and evolution. *The Astrophysical Journal*, *284*, 471–478.

Helou, G., & Salpeter, E. (1982). Galaxy spins in the virgo cluster. *The Astrophysical Journal*, *252*, 75–80.

Holmberg, E. (1946). On the apparent diameters and the orientation in space of extragalactic nebulae. *MeLuS*, *117*, 3–82.

Hoyle, F. (1949). On the cosmological problem. *Monthly Notices of the Royal Astronomical Society*, *109*(3), 365–371.

Hu, E. M., Cowie, L. L., McMahon, R. G., Capak, P., Iwamuro, F., Kneib, J.-P., . . . Motohara, K. (2002). A redshift z= 6.56 galaxy behind the cluster abell 370. *The Astrophysical Journal Letters*, *568*(2), L75.

Hu, F., Wu, G., Song, G., Yuan, Q., & Okamura, S. (2006). Orientation of galaxies in the local supercluster: a review. *Astrophysics and Space Science*, *302*(1), 43–59.

Hu, F., Wu, G., Su, H., & Liu, Y. (1995). Morphological dependence of the orientation of the spin vectors of disk galaxies in the virgo cluster. *Astronomy and Astrophysics*, *302*, 45.

Hu, W. (1999). Power spectrum tomography with weak lensing. *The Astrophysical Journal Letters*, *522*(1), L21.

Jaaniste, J., & Saar, E. (1978). in the large scale structure of the universe, ed. longair ms, einasto j.(dordrecht: Reidel). In *Proc. iau symp.* (Vol. 79, p. 448).

Johnson, H. L., & Morgan, W. (1953). Fundamental stellar photometry for standards of spectral type on the revised system of the yerkes spectral atlas. *The Astrophysical Journal*, *117*, 313.

Johnston, S. F. (2015). *A history of light and colour measurement: science in the shadows*. CRC Press.

Kaiser, C. (2009). Evolution of radio galaxies. *Astronomische Nachrichten: Astronomical Notes*, *330*(2-3), 270–274.

Karttunen, H., Kröger, P., Oja, H., Poutanen, M., & Donner, K. J. (2006). *Fundamental astronomy*. Springer.

Kashikawa, N., & Okamura, S. (1992). Spatial orientation of spin vectors of galaxies in the local supercluster. *Publications of the Astronomical Society of Japan*, *44*, 493–507.

Kausch, W., Schindler, S., Erben, T., Schwope, A., & Wambsganss, J. (2004). Arc statistics with a sample of the most x-ray luminous galaxy clusters. In *Baryons in dark matter halos* (Vol. 14, p. 009).

Kitzbichler, M., & Saurer, W. (2003). Investigation of galaxy orientations in the coma cluster. *ANS*, *324*(2), 94.

Liivamägi, L. J., Tempel, E., & Saar, E. (2012). Sdss dr7 superclusters-the catalogues. *Astronomy & Astrophysics*, *539*, A80.

MacGillivray, H., & Dodd, R. (1979). Properties of faint galaxies in two fields near the south galactic pole. *Monthly Notices of the Royal Astronomical Society*, *186*(1), 69–84.

MacGillivray, H., & Dodd, R. (1985). The anisotropy of the spatial orientations of galaxies in the local supercluster. *Astronomy and Astrophysics*, *145*, 269–274.

MacGillivray, H., Dodd, R., McNally, B., & Corwin, H. (1982). Orientations of galaxies in the local supercluster. *Monthly Notices of the Royal Astronomical Society*, *198*(2), 605–615.

Malla, J., Aryal, B., & Saurer, W. (2019). No preferred alignments of angular momentum vectors of galaxies in the sdss supercluster s [202-001+ 0084]. *International Astronomical Union. Proceedings of the International Astronomical Union*, *14*(S353), 259–261.

Malla, J., Saurer, W., & Aryal, B. (2020). Spatial orientation of galaxies in supercluster s [227+ 006+ 0078]. *BIBECHANA*, *17*, 117–122.

Martinez, V., & Saar, E. (2002). Clustering statistics in cosmology. In *Astronomical data analysis ii* (Vol. 4847, pp. 86–100).

Melkonian, A., & Nikogosian, E. (1998). Substructure of the core of the perseus supercluster of galaxies. *Astrophysics*, *41*(1), 41–46.

Nakata, F., Kajisawa, M., Yamada, T., Kodama, T., Shimasaku, K., Tanaka, I., . . . others (2004). Probing distant clusters of galaxies at z> 1. In *Studies of galaxies in the young universe with new generation telescope* (pp. 57–60).

NASA. (2017a, November). *Grand spiral galaxy ngc 1232.* `https://science.nasa.gov/grand-spiral-galaxy-ngc-1232`.

NASA. (2017b, November). *Hubble sees galaxy cluster warping space and time.* `https://www.nasa.gov/image-feature/goddard/2017/hubble-sees-galaxy-cluster-warping-space-and-time`.

NASA. (2020a, November). *Messier 13 (the hercules cluster).* `https://www.nasa.gov/feature/goddard/2017/messier-13-the-hercules-cluster`.

NASA. (2020b, November). *The nearest superclusters.* `https://imagine.gsfc.nasa.gov/features/cosmic/nearest_superclusters_info.html`.

Noreña Blandón, D. A., Muñoz Cuartas, J. C., Libeskind, N., & Quiroga, L. (2018). Substructures in minor mergersâĂŹ tidal streams.

Ozernoy, L. (1974). Whirl theory of the origin of galaxies and clusters of galaxies. In *Symposium-international astronomical union* (Vol. 63, pp. 227–240).

Ozernoy, L. (1978). The whirl theory of the origin of structure in the universe. In *Symposium-international astronomical union* (Vol. 79, pp. 427–438).

Padmanabhan, T. (2006). *An invitation to astrophysics* (Vol. 8). World Scientific.

Pajowska, P., Godłowski, W., Zhu, Z.-H., Popiela, J., Panko, E., & Flin, P. (2019). Investigation of the orientation of galaxies in clusters: the importance, methods and results of research. *Journal of Cosmology and Astroparticle Physics*, *2019*(02), 005.

Panko, E. (2013). The criteria for morphological classification of pf galaxy clusters. *Odessa Astronomical Publications*, *26*(1), 90–93.

Panko, E., Andrievsky, S., & Gotsulyak, A. (2014). Morphological types of 254 rich pf galaxy clusters. *Odessa Astronomical Publications*, *27*(1), 30–31.

Panko, E., Piwowarska, P., Godłowska, J., Godłowski, W., & Flin, P. (2013). Orientation of galaxies in structures. *Astrophysics*, *56*(3), 322–331.

Panko, O. O., Sirginava, A., & Stepaniuk, A. (2018). Detailed morphology of the rich concentrated galaxy clusters.

Park, C., Choi, Y.-Y., Vogeley, M. S., Gott III, J. R., Blanton, M. R., Collaboration, S., et al. (2007). Environmental dependence of properties of galaxies in the sloan digital sky survey. *The Astrophysical Journal*, *658*(2), 898.

Parnovsky, S., Karachentsev, I., & Karachentseva, V. (1994). Global anisotropy in galaxy orientations. *Monthly Notices of the Royal Astronomical Society*, *268*(3), 665–680.

Peebles, P. (1969). Origin of the angular momentum of galaxies. *The Astrophysical Journal*, *155*, 393.

Percival, W. J., Reid, B. A., Eisenstein, D. J., Bahcall, N. A., Budavari, T., Frieman, J. A., ... others (2010). Baryon acoustic oscillations in the sloan digital sky survey data release 7 galaxy sample. *Monthly Notices of the Royal Astronomical Society*, *401*(4), 2148–2168.

Reinhardt, M., & Roberts, M. (1972). Orientation of galaxies and the local supercluster. *Astrophysical Letters*, *12*, 201–206.

Rufener, F., & Nicolet, B. (1988). A new determination of the geneva photometric passbands and their absolute calibration. *Astronomy and Astrophysics*, *206*, 357–374.

SDSS, D. (2019, October). *Sdss data release 7*. `http://classic.sdss.org/dr7/`.

SDSS, J. (2008). Adelman-mccarthy et al. *Astrophys. J. Suppl*, *175*(297), 0707–3413.

Shandarin, S. (1974). Orientation of angular momenta of galaxies. *Soviet Astronomy*, *18*, 392.

Stein, R. (1974). Galaxy formation from primordial turbulence. *Astronomy and Astrophysics*, *35*, 17–29.

Strom, K., & Strom, S. (1978). Surface brightness and color distributions of elliptical and s0 galaxies. i-the coma cluster elliptical galaxies. *The Astronomical Journal*, *83*, 73–134.

Struble, M. F., & Rood, H. J. (1999). A compilation of redshifts and velocity dispersions for aco clusters. *The Astrophysical Journal Supplement Series*, *125*(1), 35.

Tanaka, I. (2004). Subaru observation of a supercluster of galaxies and qsos at z= 1.1. In *Studies of galaxies in the young universe with new generation telescope* (pp. 61–64).

Thompson, L. A. (1976). The angular momentum properties of galaxies in rich clusters. *The Astrophysical Journal*, *209*, 22–34.

Tully, C. H. H. Y. P. D., B. (2014). The laniakea supercluster of galaxies. *Nature*, *513*, 71-73.

Von Weizsäcker, C. (1951). The evolution of galaxies and stars. *The Astrophysical Journal*, *114*, 165.

Weinberg, S. (1972). Gravitation and cosmology: principles and applications of the general theory of relativity.

Wu, H., Zou, Z., Xia, X., & Deng, Z. (1998). A statistical study of the spectra of very luminous iras galaxies-ii. spectral and environmental analysis. *Astronomy and Astrophysics Supplement Series*, *132*(2), 181–193.

Yadav, S., Aryal, B., & Saurer, W. (2016). Spatial orientation of spin vectors of blue-shifted galaxies. *arXiv preprint arXiv:1606.02881*.

Yadav, S., Aryal, B., & Saurer, W. (2017). Preferred alignments of angular momentum vectors of galaxies in six dynamically unstable abell clusters. *Research in Astronomy and Astrophysics*, *17*(7), 064.

York, D. G., Adelman, J., Anderson Jr, J. E., Anderson, S. F., Annis, J., Bahcall, N. A., ... others (2000). The sloan digital sky survey: Technical summary. *The Astronomical Journal*, *120*(3), 1579.

Yuan, Q., Hu, F., Su, H., & Huang, K. (1997). Orientation of the field galaxies in the local supercluster. *The Astronomical Journal*, *114*, 1308.

Zeldovich, I. B., & Novikov, I. (1983). Relativistic astrophysics. vol. 2: The structure and evolution of the universe. *Chicago: University of Chicago Press*.

Zel'Dovich, Y. B. (1970). Gravitational instability: An approximate theory for large density perturbations. *Astronomy and astrophysics*, *5*, 84–89.

Appendix A

Publications

(A) **International Journals with SJR**

(1) Malla, J. R., Saurer, W., & Aryal, B. (2019). No preferred alignments of angular momentum vectors of galaxies in the SDSS supercluster S [202-001+ 0084]. International Astronomical Union. *Proceedings of the International Astronomical Union*, 14(S353), 259-261.

(2) Malla, J. R., Saurer, W., & Aryal, B. (2022). Spatial Orientation of Galaxies in the Substructures of SDSS Supercluster S [184+003+0077]. *Bulgarian Astronomical Journal*, 37,97-107.

(B) **International Journals**

(1) Malla, J. R., Saurer, W., & Aryal, B. (2021). Identification of substructures in the Supercluster S [195+027+0022] having redshift 0.022. *Researchline international Journal*. (Vol XXXXVI 8-12).

(C) **National Journals**

(1) Malla, J. R., Saurer, W.,& Aryal, B. (2020). Spatial orientation of galaxies in supercluster S [227+ 006+ 0078]. *BIBECHANA*, 17, 117-122.

(2) Malla, J. R., Saurer, W., & Aryal, B. (2021) Spatial orientations of angular momentum vectors of galaxies in Supercluster S [173+ 014+ 0082]. *BIBECHANA*, 18(1), 26-32.

(3) Malla, J. R., Saurer, W., & Aryal, B. (2020). Preferred Alignments of Angular Momentum Vector of Galaxies in the SDSS Supercluster S [231+ 030+ 0117]. *Journal of Institute of Science and Technology*, 25(2), 72-79.

(4) Malla, J. R., Aryal, B., & Saurer, W. (2021). Spatial Orientation of angular momentum vectors of Galaxies in Supercluster S [247+ 040+ 0029]. *Journal of Nepal Physical Society*, 7(1), 39-48.

(5) Malla, J. R., Aryal, B., & Saurer, W. (2021). Spatial Orientation of angular momentum vectors of Galaxies in Supercluster S [195+ 027+ 0022] and Substructure . *Journal of Nepal Physical Society*, 7(2), 81-88.

(6) Malla, J. R., Aryal, B., & Saurer, W. (2022). Study of substructure analysis of Supercluster S [227+006+ 0078]. *Scientific World*, 15(15), 167-171.

Appendix B

Participation in conferences

(A) **International**

(1) IAU Symposium 353: Galactic Dynamics in the Era of Large Surveys, 1-5 July, 2019. Shanghai, China. Poster Presentation entitled “ Preferred Alignments of Angular Momentum Vectors of Galaxies in the SDSSS Supercluster S[202-001+0084]".

(2) Association of Nepali Physicist in America Conference-2020, USA, 17-19 July, 2020, Oral Presentation entitled “ Spatial orientations of angular momentum vectors of galaxies in Supercluster S [247+040+0029] and substructures".

(3) The 6^{th} East African Astronomical Society Workshop(EAASW), 20-22 May, 2021. Tanzania. Oral Presentation entitled “ Spatial Orientations of Angular Momentum Vectors of Galaxies in Supercluster S[227+006+0078] and Substructures".

(B) **National**

(1) International conference on Physics of Space And Materials, St.Xavier’s college, Kathmandu, 2-3 September, 2017, Poster presentation entitled “ Spatial Orientation of Galaxies in the SDSS DR7 Superclusters. " .

(2) International Conference on Nano-Metarials and Computational Physics, Central Department of Physics, T.U., 27-28 December, 2017, Poster presentation entitled “ Orientation of Galaxies in Supercluster " .

(3) International Conference on Explorations in Physics, Department of Physics, Amrit Campus, T. U., 29-31 May, 2018, Oral Presentation entitled “Spatial Orientation of Galaxies in the SDSS DR7 Superclusters".

(4) Annual General meeting, Nepal Physical Society, Department of Physics, pulchowk Campus, Pulchowk Lalitpur, T. U., 24th November, 2018, Oral Presentation entitled “ Preferred Alignments of Angular Momentum Vectors of Galaxies in the SDSS S(202-001+0084)".

(5) International Conference on Nanosciences and High Energy Physics, Central Department of Physics, T.U., 4-6 February, 2019, Oral Presentation entitled “Preferred Alignments of Angular Momentum Vectors of Galaxies in the SDSS Superclusters S[230+027+0069]".

(6) National Symposium on Research, Development and Innovation in Physics,

Department of Physics, ST. Xavier's College,Kathmandu, 3-4 September, 2019, Oral Presentation entitled "Spatial Orientation of Galaxies in Superclusters S[173+014+0082]".

Appendix C

SDSS Database of galaxies

Table 19: SDSS DR7 of galaxies in the supercluster S[195+027+0022] that have redshifts range 0.022 to 0.024.The first two columns list the right ascension and declinations.The next two columns shows position and inclination angle.The fifth and sixth columns represent the magnitude in r-band and redshift.

RA(J2000)	$Dec.(J2000)$	$P(deg)$	$i(deg)$	m_r	z	$RA(J2000)$	$Dec.(J2000)$	$P(deg)$	$i(deg)$	m_r	z
171.1601	+22.8754	27.45	73.35	17.40	0.022588	175.6661	+20.1728	80.49	54.04	13.90	0.022670
171.3890	+22.8190	94.78	29.26	13.75	0.022642	175.6745	+20.2997	108.10	50.19	17.09	0.022117
172.1389	+23.5336	83.40	41.69	17.61	0.022568	175.6882	+20.0323	117.21	61.41	17.08	0.022261
172.1644	+23.6709	107.85	45.62	16.78	0.022571	175.6921	+19.9485	70.23	49.99	15.51	0.021768
172.1432	+21.0107	156.12	45.54	13.77	0.021886	175.7124	+20.4421	22.68	43.98	13.91	0.020154
172.1679	+21.0972	53.26	85.91	14.79	0.021467	175.7164	+19.9492	135.74	75.21	15.42	0.020575
172.2150	+20.8083	70.24	65.55	16.99	0.022362	175.7217	+20.1794	134.11	33.04	15.85	0.022137
172.2221	+20.7401	26.95	45.08	16.27	0.022063	175.7218	+20.4007	84.98	46.55	16.60	0.024929
172.2494	+20.7391	121.36	45.24	16.74	0.022200	175.7264	+19.6478	0.59	49.16	15.75	0.023522
172.2680	+20.8532	70.00	21.01	13.83	0.021861	175.7352	+19.9662	156.89	41.45	17.77	0.025411
172.3107	+20.7731	89.52	73.95	17.59	0.022033	175.7461	+20.0869	56.75	30.65	17.08	0.021188
172.3517	+22.4004	12.19	35.07	15.79	0.023032	175.7549	+19.9098	8.52	41.48	15.53	0.022680
172.4244	+22.1154	27.93	33.69	16.14	0.022724	175.7590	+19.6497	114.85	57.52	14.35	0.024337
172.4383	+22.1265	77.49	31.31	17.31	0.022899	175.7763	+19.9390	46.43	45.56	16.85	0.022313
172.6228	+22.3956	54.30	60.45	13.99	0.023243	175.7957	+20.0297	66.24	53.20	14.13	0.024576
172.5537	+24.1696	44.40	59.58	15.67	0.024414	175.8019	+20.3360	134.35	59.56	15.08	0.021382
172.5981	+24.2926	146.32	55.43	13.70	0.024632	175.8045	+19.6130	93.50	53.38	15.70	0.021939
172.6423	+24.2195	135.24	81.23	16.72	0.023743	175.8045	+20.0048	109.90	68.41	16.30	0.024503
172.7789	+22.7681	97.38	36.54	15.88	0.022605	175.8053	+20.1319	4.91	58.82	17.46	0.019418
172.8366	+22.7382	47.42	52.35	13.00	0.022070	175.8159	+20.1951	143.93	44.99	15.57	0.019523
173.0981	+22.7208	59.20	80.78	17.72	0.022256	175.8176	+19.7487	73.91	59.55	16.42	0.026132
173.0176	+24.6697	45.97	76.30	17.21	0.024272	175.8234	+19.3840	166.84	50.36	17.74	0.022296
173.2632	+24.4036	105.99	67.16	17.81	0.024591	175.8235	+19.7827	29.06	40.35	14.12	0.023035
173.2735	+24.6860	28.71	71.91	17.04	0.024486	175.8253	+19.5671	26.76	66.43	14.64	0.023705
173.2821	+24.6526	106.28	70.81	17.18	0.024528	175.8359	+20.1913	12.70	73.43	15.75	0.024456
173.3158	+24.4469	16.82	45.62	15.98	0.024171	175.8415	+19.9516	76.86	34.23	16.57	0.026991
173.3613	+24.0536	144.91	81.24	13.23	0.024585	175.8537	+20.5576	150.03	67.29	17.64	0.020037
173.3934	+24.5343	170.61	33.53	16.15	0.024300	175.8686	+19.2039	157.94	42.17	16.85	0.019930
173.4125	+24.6846	85.01	70.65	15.87	0.023741	175.8918	+20.5106	100.50	65.22	14.77	0.025313
173.4472	+24.3171	134.53	66.80	14.83	0.024584	175.9041	+19.6046	160.27	34.19	16.38	0.023097
173.1376	+20.4171	60.69	73.55	17.09	0.023778	175.9215	+19.8864	148.82	66.48	17.40	0.022238
173.1384	+20.4010	3.53	74.09	15.50	0.024002	175.9231	+20.0270	157.85	72.68	14.54	0.022786
173.4381	+21.3826	151.25	66.36	15.89	0.023177	175.9332	+20.2727	38.83	60.30	16.37	0.024040
173.4580	+21.4222	126.27	74.81	16.45	0.023166	175.9490	+20.3633	114.96	75.78	17.20	0.023570
173.6123	+21.3522	74.52	46.05	16.29	0.022276	175.9537	+20.2483	175.81	49.54	14.02	0.021365
173.7849	+21.2296	118.27	72.66	16.35	0.022073	175.9639	+19.8621	97.86	45.51	15.49	0.024226
173.7231	+20.4881	63.91	69.06	15.12	0.023934	175.9732	+19.7394	118.68	71.56	16.01	0.021621
173.7677	+20.6352	40.90	76.58	14.48	0.024981	175.9851	+19.8946	166.98	23.01	16.74	0.022141
173.7965	+20.5138	102.31	63.76	16.28	0.023476	175.9861	+19.6706	153.15	50.98	15.62	0.023038
173.8404	+20.6446	99.03	18.47	17.55	0.022524	175.9861	+20.0308	72.36	20.11	13.09	0.023813
173.9208	+20.5333	82.67	39.91	16.18	0.022087	175.9868	+19.9558	125.24	40.33	17.51	0.022117
174.0833	+20.5218	62.10	43.25	17.04	0.022515	175.9874	+19.8334	89.90	23.66	16.69	0.020496
174.1183	+19.8114	166.43	34.39	14.29	0.023296	175.9893	+19.9357	98.66	57.48	15.51	0.024512
174.1241	+19.8328	34.08	48.17	13.44	0.022940	175.9894	+20.3006	141.44	60.54	17.79	0.020511
174.1430	+20.3642	−3.38	60.15	17.64	0.022034	175.9904	+20.1900	60.04	44.02	15.30	0.020991
174.2250	+19.9263	174.97	34.69	16.38	0.021901	175.9921	+20.8064	13.77	82.05	14.78	0.022482
174.2250	+19.9695	151.58	60.28	17.61	0.021571	175.9946	+19.9912	98.07	22.72	16.89	0.022291
174.2259	+19.9972	41.26	50.14	15.98	0.023358	175.9957	+20.0770	75.76	47.72	14.98	0.025672
174.2705	+19.9238	154.11	52.04	15.78	0.021889	175.9982	+19.7790	2.92	54.39	17.35	0.019805
174.2898	+19.8980	121.95	39.74	14.20	0.022062	176.0033	+20.0293	30.14	63.46	13.70	0.023783
174.2910	+20.0253	122.54	39.79	15.23	0.021330	176.0042	+19.7160	144.92	30.85	14.50	0.019077
174.2929	+19.9720	17.58	35.58	15.40	0.022308	176.0090	+19.9498	5.41	40.55	13.77	0.021910
174.3168	+19.6195	10.66	82.40	16.81	0.021611	176.0090	+19.9719	111.43	39.55	17.62	0.022198
174.5158	+19.8616	58.17	76.07	16.56	0.021817	176.0126	+19.7402	73.95	66.92	12.13	0.023987
173.9911	+23.0115	15.45	64.43	16.40	0.024850	176.0134	+19.8011	98.33	52.63	13.86	0.027745
174.1540	+22.9157	137.19	75.15	15.86	0.024568	176.0158	+20.0989	33.39	70.59	15.84	0.019658
174.1838	+22.9920	45.89	15.36	14.40	0.024489	176.0198	+19.5335	173.51	69.97	15.06	0.025386
174.1709	+22.6161	112.83	75.40	17.20	0.024032	176.0223	+20.5261	74.47	50.29	15.77	0.025188
174.3767	+22.3997	74.37	62.36	14.00	0.023931	176.0228	+19.9961	112.05	47.89	16.48	0.019954
174.3794	+24.6802	128.09	35.58	17.36	0.023889	176.0240	+20.2482	73.07	60.66	17.59	0.023130
174.6695	+24.5849	55.77	43.32	14.57	0.023937	176.0319	+19.7375	23.21	25.32	14.25	0.026981
174.4926	+20.7786	84.82	62.98	15.83	0.024178	176.0508	+19.9428	79.83	36.00	15.25	0.021757
174.5233	+20.6987	130.41	23.99	16.76	0.023482	176.0579	+19.3365	137.54	72.23	14.45	0.020485
174.6070	+20.6653	68.77	38.71	14.37	0.023606	176.0634	+19.5110	3.91	65.82	16.95	0.023064
174.7468	+20.5603	75.16	27.39	16.47	0.022968	176.0668	+20.2678	166.41	51.98	17.35	0.025146
174.9081	+20.4547	21.75	52.59	16.59	0.024272	176.0687	+20.2169	111.93	53.88	16.56	0.023548
174.9416	+20.5541	77.09	38.57	17.07	0.021743	176.0762	+20.0425	66.45	72.33	16.62	0.019667
174.9622	+20.3949	47.93	52.22	13.41	0.023693	176.0789	+19.8447	124.65	44.09	14.17	0.022352
175.0235	+20.2728	145.48	55.64	15.52	0.022756	176.0791	+20.3036	146.60	39.27	17.36	0.026579
175.1037	+19.9634	150.60	74.80	15.18	0.023595	176.0851	+19.9809	80.31	47.91	13.89	0.022222
175.1527	+20.3137	172.03	40.31	17.61	0.022688	176.0864	+19.8259	20.90	36.29	15.92	0.019588
175.1737	+20.3429	63.55	53.39	15.59	0.022883	176.0926	+19.7745	138.06	41.23	14.16	0.023351
175.2297	+20.3246	148.17	72.07	15.54	0.023112	176.0950	+20.4094	85.44	25.88	14.30	0.025721
175.2940	+20.1885	40.40	35.45	12.38	0.024729	176.1080	+20.1027	103.33	44.66	15.64	0.025776
175.3238	+20.1621	4.70	54.49	15.65	0.020658	176.1095	+19.9975	85.81	43.05	17.62	0.019977
175.3430	+19.9627	75.75	35.87	17.67	0.022970	176.1191	+19.6936	121.99	52.07	15.77	0.021943
175.4501	+20.1037	67.90	48.48	17.36	0.020232	176.1256	+20.3291	34.97	73.29	16.91	0.020677
175.4576	+19.7679	22.88	29.87	13.82	0.027244	176.1273	+20.0767	154.12	64.98	17.17	0.023530
175.4686	+20.2491	28.39	40.30	12.42	0.023880	176.1338	+20.1066	170.94	41.69	15.55	0.025130
175.4763	+20.3431	33.86	84.18	17.64	0.020799	176.1396	+19.6267	154.17	79.04	13.83	0.025103
175.4973	+20.2554	173.95	28.73	15.44	0.023482	176.1523	+19.7516	36.35	59.90	15.34	0.020209
175.5609	+20.0978	141.66	50.02	15.99	0.020899	176.1671	+19.2108	167.35	63.43	16.78	0.020533
175.5616	+19.9765	57.38	62.32	16.12	0.027153	176.1681	+20.4772	132.72	79.92	16.19	0.021353
175.5651	+20.0487	125.87	61.39	14.81	0.021509	176.1715	+19.0529	170.53	57.99	17.07	0.020516
175.5662	+20.2157	82.54	68.21	15.06	0.025201	176.1809	+20.3198	83.88	24.45	16.38	0.025486
175.5755	+19.8378	53.91	53.32	15.46	0.022471	176.1942	+19.7579	61.01	56.38	16.40	0.022505
175.5764	+20.4524	149.80	69.34	15.83	0.020850	176.1977	+19.8764	11.44	59.77	17.25	0.027171
175.5793	+20.0959	103.65	47.62	15.81	0.023672	176.1991	+19.7734	6.95	40.57	14.99	0.029337
175.6020	+20.1193	107.56	63.09	16.56	0.021032	176.1998	+19.6885	91.82	45.61	14.49	0.017426
175.6638	+19.9689	11.80	39.37	16.42	0.025616	176.2006	+19.5809	10.94	12.83	15.39	0.020767

Table 20: SDSS DR7 of galaxies in the supercluster S[195+027+0022] that have redshifts range 0.022 to 0.024.The first two columns list the right ascension and declinations.The next two columns shows position and inclination angle.The fifth and sixth columns represent the magnitude in r-band and redshift.

RA(J2000)	$Dec.(J2000)$	$P(deg)$	$i(deg)$	m_r	z	$RA(J2000)$	$Dec.(J2000)$	$P(deg)$	$i(deg)$	m_r	z
176.2068	+19.9411	40.26	25.09	14.72	0.018870	176.6908	+19.0175	44.34	67.52	17.42	0.021508
176.2089	+19.5328	45.11	45.51	15.34	0.022007	176.6946	+21.2715	6.93	22.58	15.84	0.023234
176.2174	+19.6099	17.49	56.24	16.61	0.022653	176.6966	+20.6754	138.63	31.05	16.46	0.024475
176.2183	+20.1880	57.38	39.62	13.76	0.025341	176.7240	+20.3315	130.40	32.96	14.40	0.022967
176.2210	+19.4566	59.63	57.20	15.01	0.019970	176.7534	+19.4584	5.84	72.53	12.98	0.019062
176.2224	+20.6869	21.12	72.11	17.60	0.021571	176.7733	+19.8372	123.60	48.44	17.79	0.020531
176.2273	+20.0171	100.51	43.94	15.92	0.025399	176.7755	+19.4562	129.24	41.10	16.36	0.019177
176.2285	+19.7765	54.01	35.67	17.78	0.028512	176.7841	+19.7019	40.41	26.65	12.80	0.021777
176.2326	+19.4938	171.95	49.52	16.26	0.022354	176.7932	+20.6019	66.75	45.49	17.44	0.024445
176.2373	+19.7319	61.93	25.05	14.40	0.026950	176.8127	+19.1760	86.53	16.23	17.06	0.021190
176.2570	+20.8519	116.61	68.66	14.95	0.023858	176.8545	+19.3921	96.00	47.02	17.28	0.020658
176.2575	+19.7637	107.81	48.23	14.27	0.028543	176.8791	+19.8724	50.15	53.86	14.45	0.020303
176.2655	+19.8595	166.13	31.59	17.31	0.022216	176.9090	+20.5655	47.73	79.83	16.84	0.023727
176.2662	+19.9737	35.87	48.52	16.64	0.017985	176.9139	+19.9394	134.75	59.16	15.32	0.021615
176.2683	+19.5707	39.06	39.32	16.64	0.022618	176.9457	+19.0819	118.34	84.73	15.88	0.021227
176.2687	+20.6076	117.64	83.52	12.83	0.021257	177.0543	+21.4945	40.47	63.93	14.18	0.025539
176.2698	+19.6821	45.51	28.59	16.89	0.022334	177.0765	+18.9379	168.94	55.28	15.81	0.020860
176.2709	+19.6063	156.72	24.32	16.22	0.022711	177.1040	+21.2280	169.17	72.99	16.22	0.025875
176.2744	+19.6365	2.28	49.99	15.57	0.017401	177.1145	+21.1566	83.93	81.23	17.69	0.023862
176.2746	+20.4379	36.73	49.68	12.51	0.023961	177.1184	+19.7600	162.71	59.69	17.25	0.019779
176.2774	+20.1564	71.55	68.16	17.36	0.021628	177.1392	+20.6825	177.29	64.53	17.23	0.024593
176.2887	+19.5542	109.23	57.77	13.45	0.026169	177.1628	+21.3631	3.03	30.56	17.52	0.027487
176.2945	+19.5332	138.24	53.33	15.24	0.022554	177.1823	+21.0149	89.29	68.14	14.51	0.027054
176.3073	+19.7561	10.23	63.53	15.71	0.028723	177.1829	+21.1900	28.83	43.37	17.45	0.023758
176.3119	+19.8455	93.20	45.56	15.33	0.026877	177.2241	+21.2940	106.38	46.56	17.34	0.025439
176.3146	+21.2042	88.53	61.35	15.60	0.024776	177.2274	+21.4708	6.80	63.46	17.11	0.027510
176.3284	+20.2926	124.72	53.47	13.84	0.024582	177.2278	+21.2558	110.43	43.47	15.74	0.026722
176.3295	+19.3942	104.41	69.77	17.24	0.019664	177.2595	+21.4493	29.42	69.19	15.45	0.027407
176.3351	+19.5495	82.31	77.79	17.02	0.017121	177.2610	+18.8532	92.64	53.37	15.72	0.020535
176.3489	+19.1576	8.69	48.26	17.15	0.020863	177.2777	+19.1684	143.14	60.09	16.08	0.021891
176.3494	+20.3255	77.70	35.76	17.36	0.024452	177.2874	+21.2107	71.90	23.60	17.69	0.025200
176.3555	+19.2981	99.00	22.75	15.10	0.022587	177.2973	+20.9378	144.00	57.21	17.84	0.024747
176.3563	+19.8181	60.34	71.35	13.51	0.029277	177.3112	+19.3616	97.53	37.80	16.52	0.021361
176.3652	+20.8072	88.41	34.30	15.64	0.024256	177.3304	+20.6924	119.64	75.78	15.94	0.024490
176.3672	+20.2943	137.96	72.39	15.50	0.020117	177.3406	+21.3552	78.22	50.23	17.65	0.023492
176.3689	+20.3238	45.09	36.69	13.91	0.022279	177.3503	+21.1112	11.98	33.09	16.78	0.027392
176.3694	+20.0936	67.59	59.16	15.18	0.026072	177.3565	+21.3488	14.77	16.42	17.44	0.028406
176.3734	+19.4002	−1.27	60.71	17.73	0.026068	177.3762	+21.0435	−1.96	64.48	17.12	0.022915
176.3748	+19.4447	80.76	56.50	17.49	0.022373	177.3876	+21.4481	98.60	45.28	16.35	0.029092
176.3877	+20.3321	132.38	71.25	12.96	0.024213	177.3899	+22.1900	157.22	29.76	15.52	0.027397
176.3889	+19.5079	150.13	73.00	13.77	0.016137	177.4379	+21.9544	92.06	72.29	17.51	0.028246
176.3918	+20.0086	148.24	52.47	17.93	0.023958	177.4614	+19.1452	167.75	7.87	14.26	0.021248
176.3961	+19.5917	29.92	40.07	17.18	0.024228	177.4897	+21.6459	1.85	75.08	16.48	0.026940
176.3970	+19.4165	4.85	29.00	17.60	0.025804	177.4919	+20.9538	36.70	61.37	16.86	0.028370
176.3984	+21.3049	−1.66	86.27	16.67	0.024399	177.4963	+21.3045	40.62	23.58	17.50	0.027531
176.4003	+19.2796	173.74	47.14	15.16	0.022525	177.5074	+21.3157	155.17	52.59	17.06	0.027306
176.4010	+20.9896	69.34	44.12	16.28	0.024409	177.5163	+21.7826	29.38	67.97	17.00	0.027881
176.4074	+21.1535	89.41	81.59	17.11	0.023457	177.5166	+20.9616	130.05	67.92	14.93	0.028817
176.4123	+21.3181	54.87	65.34	17.85	0.023696	177.5169	+21.2798	15.75	47.99	16.23	0.026664
176.4179	+19.7174	3.96	29.73	17.44	0.019885	177.5175	+22.1816	128.79	67.48	16.95	0.026468
176.4215	+19.7702	134.52	20.44	15.34	0.019186	177.5476	+21.2369	27.86	59.29	16.80	0.028422
176.4224	+19.2674	48.01	67.85	17.67	0.023030	177.5482	+21.7947	100.26	67.27	17.60	0.027482
176.4319	+19.6485	77.97	57.72	15.09	0.027274	177.5509	+21.0072	59.20	54.91	15.07	0.027122
176.4359	+20.0308	100.87	31.77	16.10	0.018825	177.5525	+21.4150	39.34	17.32	17.43	0.025924
176.4386	+19.6919	61.50	76.07	16.90	0.021654	177.5680	+21.8136	4.66	52.82	16.84	0.027523
176.4403	+19.1638	8.82	57.02	15.54	0.021374	177.5773	+20.7457	106.91	47.10	17.39	0.023452
176.4421	+19.7738	153.36	36.53	17.43	0.019064	177.5795	+20.4803	102.90	38.87	17.58	0.023493
176.4513	+19.4258	61.29	60.73	15.05	0.021879	177.5828	+20.9525	161.81	51.94	17.03	0.026973
176.4523	+19.4670	69.99	63.14	12.68	0.019619	177.5890	+21.3259	159.98	32.04	16.35	0.023807
176.4535	+20.6286	65.36	67.11	17.19	0.024530	177.6083	+21.7648	3.23	75.79	17.68	0.026720
176.4553	+19.7483	170.43	50.02	17.74	0.024887	177.6166	+21.0860	107.25	11.80	15.88	0.026372
176.4710	+19.6115	164.20	71.48	14.43	0.023618	177.6249	+20.0856	132.66	61.34	17.47	0.021185
176.4816	+21.0255	10.71	18.21	17.50	0.023558	177.6469	+20.2132	142.30	72.03	15.97	0.021607
176.4929	+19.6497	40.89	27.43	15.24	0.022478	177.6645	+20.9073	170.61	49.21	17.16	0.022537
176.4942	+19.8030	174.74	57.97	13.46	0.020085	177.6730	+20.0152	134.67	17.43	17.75	0.021474
176.4948	+19.5290	112.16	45.25	16.54	0.019416	177.6762	+21.3923	144.89	72.77	17.01	0.028718
176.4976	+20.4471	145.96	65.21	15.32	0.024709	177.6952	+20.5523	81.51	50.74	16.72	0.022244
176.5036	+19.3844	131.20	57.82	14.29	0.025310	177.7024	+22.0017	122.28	59.19	14.70	0.027743
176.5128	+19.4370	133.42	40.06	14.94	0.018415	177.7041	+22.1267	72.70	57.41	13.00	0.025031
176.5217	+19.5761	42.31	45.23	16.25	0.022575	177.7115	+20.0488	136.27	55.77	17.40	0.022746
176.5229	+19.6618	25.52	39.26	14.70	0.020775	177.7128	+21.3896	51.55	70.67	17.21	0.027554
176.5258	+19.7902	63.14	53.44	16.84	0.019981	177.7144	+20.4969	143.00	62.63	16.01	0.024245
176.5262	+19.6343	65.75	63.73	16.71	0.021920	177.7196	+21.1690	135.21	48.88	15.56	0.026682
176.5375	+20.4475	80.23	71.23	14.47	0.024825	177.7235	+20.9537	106.54	58.68	14.64	0.027641
176.5499	+19.8529	138.55	63.03	15.04	0.019335	177.7273	+22.2905	11.72	49.41	14.06	0.027512
176.5505	+21.2275	175.46	70.45	15.56	0.023212	177.7310	+21.1454	110.65	37.19	13.97	0.022450
176.5508	+20.3917	9.82	44.06	15.28	0.024371	177.7346	+21.9733	168.38	45.88	14.48	0.027091
176.5630	+21.0240	37.20	44.77	15.77	0.023447	177.7401	+21.1888	68.42	51.43	17.55	0.022344
176.5801	+20.6404	162.21	68.82	12.55	0.022984	177.7422	+22.0770	68.65	46.80	15.70	0.025980
176.5906	+19.4843	36.61	69.58	17.62	0.018720	177.7442	+20.7058	87.99	52.29	14.90	0.021522
176.5907	+20.1775	135.47	58.05	16.86	0.021326	177.7443	+20.8868	31.14	68.62	14.69	0.028034
176.5989	+20.0387	16.99	66.50	16.27	0.025855	177.7546	+20.3993	96.23	40.83	15.96	0.022654
176.6095	+19.7199	31.24	74.65	17.52	0.025451	177.7582	+21.9771	32.05	45.02	16.99	0.026868
176.6128	+20.8305	104.98	33.96	16.60	0.023776	177.7672	+20.8826	128.74	73.21	17.51	0.025917
176.6245	+19.7744	168.41	52.58	16.04	0.023677	177.7678	+22.5160	162.72	67.12	17.26	0.027169
176.6296	+19.2503	104.62	40.11	17.70	0.021232	177.7707	+21.2447	137.33	61.63	13.67	0.028138
176.6435	+19.1101	103.10	55.93	15.41	0.021513	177.7726	+20.1467	79.50	45.47	17.73	0.021850
176.6520	+19.8095	67.94	43.09	17.21	0.019172	177.7761	+21.7672	60.07	83.60	17.71	0.026812
176.6593	+21.0888	33.03	76.57	13.91	0.023623	177.7763	+21.1222	154.78	49.73	17.42	0.022659
176.6765	+20.6487	95.10	38.86	17.64	0.023328	177.7882	+20.3080	79.79	63.90	17.59	0.021489
176.6769	+18.8487	123.46	64.62	16.77	0.020453	177.8012	+21.9744	114.27	77.19	15.49	0.027030

Table 21: SDSS DR7 of galaxies in the supercluster S[195+027+0022] that have redshifts range 0.022 to 0.024.The first two columns list the right ascension and declinations.The next two columns shows position and inclination angle.The fifth and sixth columns represent the magnitude in r-band and redshift.

RA(J2000)	$Dec.(J2000)$	$P(deg)$	$i(deg)$	m_r	z	$RA(J2000)$	$Dec.(J2000)$	$P(deg)$	$i(deg)$	m_r	z
177.8062	+22.0389	132.32	16.59	16.88	0.028294	174.8704	+17.0486	121.10	71.96	17.61	0.022164
177.8146	+21.1376	71.29	78.62	15.73	0.024668	174.9041	+17.4391	53.78	72.79	15.50	0.022380
177.8146	+21.7783	168.32	63.92	17.66	0.027221	174.9685	+17.3176	8.23	70.58	17.10	0.023260
177.8204	+21.3136	122.54	62.06	15.76	0.024216	175.1938	+17.2680	124.14	74.85	17.38	0.023415
177.8360	+22.0538	28.68	63.95	17.56	0.028245	175.4110	+17.0774	96.63	71.84	14.90	0.023370
177.8482	+20.8589	104.88	52.08	17.53	0.023966	175.4302	+17.0079	176.02	68.30	13.49	0.023644
177.8500	+21.0682	105.71	13.25	17.43	0.027453	175.5133	+16.7762	3.06	41.66	16.55	0.022725
177.8645	+21.3045	42.80	31.80	15.25	0.026663	175.6772	+16.6064	66.17	61.47	17.67	0.023262
177.8953	+22.0585	16.11	53.89	17.34	0.026785	175.7777	+16.3185	87.24	51.67	16.07	0.023404
177.8997	+20.7326	131.44	42.49	17.17	0.024175	175.8448	+16.4854	52.51	66.34	15.88	0.022952
177.9091	+21.4631	−2.56	56.21	16.64	0.027679	174.8792	+22.4927	118.23	66.48	14.68	0.023820
177.9162	+22.0625	40.26	40.50	15.92	0.028817	174.9369	+22.6852	72.06	21.64	15.28	0.024232
177.9206	+20.9589	42.84	68.62	14.35	0.024659	175.0371	+22.5535	149.67	63.59	17.29	0.024607
177.9259	+20.6612	20.33	39.68	17.39	0.023073	175.0786	+22.4070	45.54	51.76	17.46	0.024017
177.9272	+21.0027	76.23	48.17	14.55	0.024604	175.1853	+22.4464	55.49	80.47	15.72	0.024970
177.9517	+20.4577	25.81	74.12	17.16	0.023175	175.2016	+22.7546	22.77	57.61	13.96	0.024241
177.9563	+21.1541	32.17	74.69	17.16	0.024434	175.0429	+25.3264	163.82	49.70	15.26	0.023463
177.9606	+21.0509	176.03	74.56	17.57	0.026514	175.0434	+25.3096	43.75	40.13	14.16	0.023555
177.9700	+20.4555	45.91	11.00	13.93	0.023950	175.0615	+25.3237	11.27	35.81	17.55	0.023479
177.9887	+20.7982	163.44	46.14	15.16	0.023481	175.0785	+25.3921	36.67	88.84	16.55	0.023723
177.9993	+21.1084	121.98	43.41	17.61	0.023294	175.2488	+21.0098	131.51	37.91	14.65	0.022949
178.0047	+20.6590	80.55	67.11	17.50	0.021275	175.4310	+21.1656	101.36	39.75	17.33	0.022762
178.0830	+21.1023	149.73	40.52	17.58	0.023576	175.6811	+21.0130	74.69	30.92	15.25	0.022040
178.0904	+20.6518	137.99	50.15	16.13	0.024101	175.2782	+20.5085	34.62	68.94	13.90	0.025164
178.1010	+20.3262	61.77	70.37	13.88	0.022787	175.3226	+20.8314	70.41	26.52	17.51	0.024958
178.1130	+20.2174	77.73	60.00	15.25	0.023167	175.4772	+20.6405	129.45	63.46	17.60	0.024136
178.1272	+20.6255	89.95	56.51	14.10	0.023057	175.4411	+21.5083	107.20	41.01	15.72	0.023726
178.1658	+20.7684	110.02	80.17	14.83	0.022545	175.6213	+21.5874	44.36	66.26	15.14	0.023549
178.1776	+20.6313	25.19	37.02	17.13	0.023319	175.6309	+21.8249	113.28	72.15	17.29	0.024645
178.1796	+20.5938	125.28	74.19	17.39	0.024809	175.8050	+22.0064	16.68	67.68	17.53	0.023854
178.1952	+20.9650	169.04	39.22	14.50	0.024150	175.5539	+18.4038	100.81	34.32	15.28	0.024476
178.2006	+20.6191	52.14	22.39	16.14	0.023498	175.6635	+18.3447	24.65	36.72	17.80	0.025424
178.2239	+20.5913	158.31	55.29	12.56	0.023519	175.7635	+18.4619	151.92	54.26	15.47	0.025639
178.2357	+20.4791	151.88	48.30	15.35	0.022840	175.6974	+20.9104	127.45	35.35	14.96	0.024589
178.2370	+20.4429	2.08	51.75	17.08	0.022631	175.9087	+20.8316	87.91	52.58	17.21	0.024070
178.2717	+20.5830	161.18	67.26	17.46	0.023402	175.7461	+22.4570	110.15	71.83	17.74	0.024873
178.2844	+20.7347	171.89	32.55	17.00	0.023823	175.7465	+22.6578	69.13	80.46	14.38	0.024758
178.2863	+20.6477	129.71	59.17	13.23	0.025136	175.8795	+23.0114	85.52	37.78	16.72	0.024140
178.2951	+20.4426	56.52	75.39	16.83	0.024933	175.8810	+22.7254	167.17	39.42	17.16	0.024148
178.3124	+20.7357	118.50	85.71	16.82	0.026297	175.9375	+22.8035	26.53	78.51	17.76	0.023903
178.3165	+20.6313	132.29	37.35	17.01	0.022739	175.7585	+23.9444	149.88	74.83	16.58	0.023821
178.3263	+20.1073	73.84	41.58	16.59	0.021834	175.7856	+24.0045	24.11	61.63	17.51	0.023682
178.3347	+20.7517	96.48	60.89	16.86	0.021723	175.7940	+17.3360	82.62	75.84	16.62	0.023450
178.3359	+21.0215	76.58	27.32	16.09	0.023119	175.8137	+17.3685	68.39	48.15	14.76	0.023593
178.3662	+20.6944	176.99	76.00	16.88	0.023704	175.8773	+21.4125	127.18	45.09	13.02	0.024049
178.3692	+20.4855	71.57	35.59	16.37	0.023363	175.9587	+21.4996	76.66	61.86	16.94	0.024828
178.3794	+20.5906	125.19	53.08	13.07	0.023921	176.1359	+22.1598	130.93	57.42	14.06	0.024782
178.3802	+20.3403	116.59	64.00	14.09	0.021212	176.2019	+22.0988	84.75	85.97	15.41	0.024308
178.4237	+20.8825	15.86	29.53	15.49	0.024287	176.3123	+21.6444	60.03	44.36	16.73	0.023417
178.4579	+21.2192	99.75	41.24	15.69	0.024090	176.5982	+21.7532	30.87	23.56	20.96	0.023310
178.4603	+20.4516	−2.20	28.88	15.99	0.024130	176.4525	+22.6479	122.70	23.23	15.77	0.024143
178.4756	+21.2501	112.64	82.19	17.17	0.024121	176.4763	+22.4556	141.02	85.91	17.08	0.023835
178.4765	+20.7496	171.84	85.49	13.18	0.022366	176.4646	+22.2255	106.00	73.74	16.08	0.022499
178.4826	+20.5516	24.12	68.53	15.10	0.024268	176.7690	+22.2411	139.84	56.09	16.97	0.022578
178.4986	+20.5725	30.74	53.01	17.15	0.023643	176.6516	+23.9546	89.44	30.38	16.14	0.023114
178.5324	+20.6091	168.99	56.48	15.92	0.024653	176.6773	+23.9634	105.82	27.67	15.06	0.022460
178.5430	+20.7468	117.14	68.34	15.06	0.022530	176.8201	+15.3233	52.77	82.90	16.38	0.022566
178.5581	+20.0276	121.74	66.28	15.75	0.021740	176.8321	+15.4750	94.90	24.70	15.59	0.022571
178.6051	+20.7851	130.93	40.71	13.76	0.023327	177.5397	+18.5089	2.60	27.73	15.48	0.022482
178.6821	+20.5362	96.43	30.33	16.94	0.023680	177.5894	+18.5515	146.69	74.65	16.36	0.022617
178.6902	+20.9061	143.53	46.23	15.69	0.023935	177.7397	+23.3092	94.58	88.59	16.66	0.024163
178.9443	+20.8210	41.11	64.85	15.25	0.023422	177.9004	+23.3424	60.27	47.74	16.48	0.024832
179.0581	+20.7355	14.48	45.99	17.88	0.022698	177.9365	+23.4798	27.42	75.61	18.09	0.024554
179.2253	+20.9640	165.56	82.39	15.48	0.023026	177.9843	+23.8115	150.97	37.84	15.88	0.023129
179.2547	+21.1667	139.62	83.03	17.48	0.023190	178.0766	+23.1490	26.88	79.62	17.24	0.024467
174.6173	+19.9806	6.04	35.68	17.79	0.024506	178.1775	+23.7044	106.48	61.61	17.83	0.023027
174.6755	+19.9100	84.26	61.51	16.42	0.023791	178.1851	+23.5722	62.48	79.50	16.12	0.023275
174.6238	+23.0992	70.71	36.51	19.06	0.024336	178.1929	+23.4760	121.06	60.33	16.76	0.023089
174.7477	+22.9673	120.20	57.52	17.31	0.024104	178.2144	+23.5954	135.68	26.01	15.77	0.023848
174.7124	+19.6015	113.68	24.49	16.96	0.023809	178.2290	+23.1105	121.08	45.53	17.23	0.023871
174.8519	+19.5347	77.57	46.49	16.04	0.023660	178.2539	+23.0399	96.24	66.75	14.95	0.023683
174.7208	+21.7721	29.65	56.59	17.37	0.023940	178.4179	+23.1691	72.64	66.38	16.86	0.022153
174.7775	+22.0211	26.49	54.39	16.25	0.022916	178.4219	+23.3822	174.62	62.84	16.12	0.022519
174.7515	+26.6110	158.74	63.27	17.36	0.024362	177.7421	+26.0054	135.13	61.96	16.57	0.023042
174.7657	+26.3617	26.96	41.01	15.07	0.023575	177.8602	+25.8095	57.17	66.93	13.95	0.023168
174.7940	+26.4350	131.90	20.99	14.43	0.024385	177.9818	+19.6459	9.20	68.89	17.06	0.021331
174.8353	+26.3062	9.95	71.47	17.30	0.023898	178.1258	+19.7614	26.98	87.03	16.31	0.022433
174.8673	+26.4898	17.42	67.52	17.77	0.024112	178.0034	+17.7491	138.56	48.63	16.58	0.023345
174.8741	+26.3091	132.80	53.93	17.67	0.024042	178.2197	+17.6012	119.66	75.83	17.06	0.023931
174.8923	+26.3224	124.71	35.42	13.69	0.023904	178.0045	+18.3429	113.88	53.29	13.39	0.022639
175.0642	+26.6477	19.60	50.42	15.30	0.023806	178.1115	+18.3506	130.78	69.16	16.33	0.022858
175.1948	+26.3832	1.99	74.61	15.39	0.024184	178.0948	+25.0831	21.62	69.88	16.11	0.023446
175.2349	+25.7809	0.15	55.99	17.65	0.023944	178.1045	+25.2344	61.00	80.39	16.59	0.022818
175.2677	+26.2716	143.27	82.09	13.95	0.024262	178.1059	+22.7034	72.15	73.91	17.07	0.024989
175.3787	+25.9346	105.20	61.79	16.52	0.023909	178.1345	+22.7571	148.08	72.99	16.76	0.024904
175.3800	+25.8544	76.16	87.15	15.19	0.023967	178.2979	+23.4103	139.70	20.40	16.68	0.025090
175.5309	+26.1220	122.97	37.58	17.71	0.024026	178.4169	+23.6390	23.21	36.55	16.42	0.025346
175.7600	+26.1386	115.73	61.60	13.63	0.024124	178.3022	+15.1140	69.57	58.90	15.38	0.023587
174.7768	+17.1691	166.53	43.26	16.51	0.022751	178.4355	+15.1854	41.53	70.35	16.81	0.023676
174.8073	+17.0509	159.54	53.84	17.66	0.021766	178.4072	+16.0117	99.19	63.44	16.09	0.024292
174.8119	+17.1437	110.37	29.11	17.24	0.022375	178.5836	+16.2417	97.49	56.82	16.67	0.023878

Table 22: SDSS DR7 of galaxies in the supercluster S[195+027+0022] that have redshifts range 0.022 to 0.024.The first two columns list the right ascension and declinations.The next two columns shows position and inclination angle.The fifth and sixth columns represent the magnitude in r-band and redshift.

RA(J2000)	$Dec.(J2000)$	$P(deg)$	$i(deg)$	m_r	z	$RA(J2000)$	$Dec.(J2000)$	$P(deg)$	$i(deg)$	m_r	z
178.4204	+24.4125	36.84	32.97	17.31	0.024393	180.7350	+20.3624	116.76	64.21	13.94	0.022512
178.5596	+24.2626	−2.65	88.98	15.62	0.024384	180.7438	+20.0852	59.61	69.87	15.93	0.024785
178.9917	+22.6390	153.36	49.14	17.73	0.022970	180.7458	+19.9003	108.96	56.11	17.17	0.025047
179.1367	+22.4615	102.52	54.88	15.55	0.023036	180.7596	+20.8940	132.78	44.77	16.82	0.024736
179.1842	+22.1598	132.69	44.27	17.57	0.024008	180.7796	+20.8054	152.92	36.09	17.43	0.024838
179.2669	+22.3126	82.11	75.85	14.86	0.024108	180.7982	+19.7288	110.40	67.60	15.45	0.024996
179.3352	+22.1624	21.27	48.98	17.35	0.023886	180.8069	+19.9654	162.78	68.05	15.17	0.023443
179.0249	+15.1320	21.43	75.43	13.71	0.022398	180.8234	+20.6370	57.02	74.34	15.58	0.021862
179.0265	+15.1367	106.59	27.70	17.52	0.022852	180.8265	+20.9357	132.90	13.40	15.61	0.025537
179.2124	+15.2484	98.61	41.38	17.46	0.023912	180.8481	+19.7744	46.00	55.70	16.07	0.024502
179.0586	+24.2446	13.65	33.27	16.65	0.023166	180.8482	+20.0221	35.08	50.00	17.83	0.022545
179.2415	+24.1295	163.67	66.20	21.48	0.023234	180.8556	+20.2415	55.94	56.74	16.66	0.020613
179.0626	+17.0297	176.93	67.16	21.32	0.023742	180.9079	+20.2534	92.57	53.61	17.11	0.024500
179.0909	+17.0793	28.06	58.27	17.02	0.023303	180.9202	+20.3963	112.33	62.78	17.27	0.024491
179.3236	+26.5172	132.45	74.26	15.81	0.023869	180.9298	+20.3087	129.29	16.52	13.94	0.026971
179.5313	+26.5229	54.62	36.43	14.41	0.023630	180.9376	+20.1062	94.93	47.27	13.17	0.025819
179.5421	+26.4531	47.57	71.85	20.15	0.024093	180.9449	+20.5111	135.04	44.45	17.53	0.025757
179.5586	+26.3095	30.04	88.71	17.00	0.024133	180.9489	+20.3512	1.17	57.14	14.43	0.023972
179.5670	+26.5588	27.22	61.53	17.32	0.023396	180.9510	+20.4163	130.19	35.13	16.26	0.022452
179.7810	+26.6074	125.95	43.79	15.48	0.023474	180.9543	+20.2023	128.24	68.11	16.90	0.023627
179.9173	+26.5465	128.55	30.61	14.01	0.023473	180.9619	+20.4273	147.85	49.91	14.42	0.026619
179.3827	+21.8628	60.09	45.19	17.42	0.023475	180.9638	+20.0528	65.42	43.70	15.57	0.023292
179.5619	+21.8998	27.72	82.75	15.80	0.021718	180.9651	+20.5681	109.00	48.45	16.72	0.025881
179.5790	+21.8597	68.26	29.60	14.98	0.023127	180.9655	+20.3953	153.80	34.76	17.20	0.024256
179.7597	+21.8082	62.55	33.91	15.53	0.022581	180.9685	+20.2081	35.35	56.00	17.78	0.023732
180.0220	+21.6469	40.40	39.85	17.28	0.022442	180.9761	+20.4007	127.55	38.16	16.86	0.023311
180.0230	+21.8142	42.88	70.26	17.73	0.023162	180.9833	+20.4305	105.63	64.07	17.86	0.022926
179.4432	+21.0667	160.34	61.17	16.79	0.026025	180.9845	+20.2179	74.26	50.68	17.20	0.022403
179.5165	+21.2479	79.27	59.31	15.26	0.025858	180.9866	+20.0875	141.09	68.86	15.54	0.021336
179.4719	+23.2251	47.88	27.21	17.56	0.022836	180.9907	+20.3125	113.90	24.50	16.44	0.025729
179.4960	+23.1249	150.91	59.66	16.32	0.022940	180.9983	+20.3217	161.36	28.87	17.76	0.024597
179.6125	+27.0757	164.22	17.71	16.55	0.022643	181.0041	+20.3374	89.01	49.26	15.08	0.023839
179.6891	+26.9006	−2.42	36.42	17.14	0.022763	181.0061	+20.2323	173.10	44.17	17.27	0.025559
179.8787	+22.5308	75.56	67.36	13.33	0.023969	181.0186	+19.9638	94.65	66.23	17.32	0.023004
179.9027	+22.4424	5.58	33.68	15.74	0.023966	181.0206	+20.2468	35.71	43.54	16.61	0.023425
179.9782	+22.7183	80.07	60.99	17.43	0.023310	181.0227	+20.1873	153.88	25.78	17.37	0.026444
179.9853	+22.1907	38.56	75.47	17.24	0.023799	181.0251	+20.3238	39.36	44.59	15.10	0.026596
180.1968	+22.4348	136.28	30.66	13.98	0.023284	181.0257	+20.2351	118.94	35.20	16.47	0.022156
180.3969	+22.5929	153.91	55.48	16.53	0.023903	181.0332	+20.8462	115.39	41.86	16.45	0.025560
180.4696	+22.5314	31.31	81.86	13.20	0.023342	181.0336	+20.0869	11.26	44.91	15.34	0.021381
179.9938	+17.8956	113.33	75.45	17.54	0.024162	181.0348	+20.3911	142.24	23.13	17.05	0.023515
180.1165	+17.7274	11.52	17.42	16.25	0.024346	181.0392	+20.3479	129.57	28.97	14.46	0.025625
180.1476	+18.0203	107.67	17.38	16.79	0.024684	181.0395	+20.1846	36.15	83.32	12.74	0.026498
180.1796	+17.8308	57.33	50.23	16.76	0.025179	181.0429	+20.2064	146.69	60.24	17.19	0.021956
180.2105	+17.6555	59.19	43.85	16.43	0.023996	181.0467	+19.7086	163.93	56.17	13.99	0.023220
180.2250	+17.8945	121.94	77.93	16.33	0.024429	181.0471	+20.4098	53.60	27.75	17.49	0.025021
180.3271	+17.5339	27.69	84.54	15.81	0.024258	181.0506	+20.1736	134.05	58.80	15.36	0.022716
180.3638	+17.8448	11.03	48.94	17.69	0.023192	181.0518	+19.9007	33.64	63.31	12.57	0.022983
180.4347	+17.8989	132.14	33.66	13.88	0.024124	181.0577	+20.2097	33.12	64.55	15.57	0.022901
180.4514	+17.4181	0.57	69.85	17.14	0.022834	181.0903	+20.0713	70.65	57.88	17.85	0.025851
180.5113	+18.1143	90.56	80.35	15.68	0.023056	181.0932	+19.5671	132.33	67.48	15.64	0.023865
180.5199	+17.9132	147.32	59.86	15.26	0.023861	181.0949	+20.2576	9.18	50.63	12.74	0.022164
180.5227	+17.8232	138.82	46.26	16.99	0.024075	181.1055	+20.0801	74.88	57.07	14.86	0.026396
180.5296	+17.7677	117.35	70.33	16.35	0.024471	181.1069	+19.3814	23.17	57.91	17.46	0.023004
180.5348	+17.6902	102.24	30.92	15.60	0.022950	181.1070	+20.2636	88.61	60.58	17.02	0.024909
180.7718	+17.6012	114.39	31.76	14.90	0.024006	181.1123	+20.5919	130.77	80.93	12.63	0.023459
180.2053	+15.4512	3.04	39.19	17.00	0.023671	181.1234	+20.0819	21.41	68.81	15.76	0.023218
180.4984	+15.4175	166.45	67.36	14.08	0.024713	181.1236	+20.3163	100.23	53.01	17.84	0.023691
180.2839	+20.4050	157.75	29.66	15.40	0.023750	181.1355	+20.2049	76.23	31.85	14.49	0.021802
180.3255	+20.1966	13.38	31.07	17.76	0.025313	181.1528	+20.4188	173.14	30.38	17.68	0.025958
180.3659	+20.3105	43.48	60.39	14.77	0.024812	181.1635	+21.2420	3.95	60.41	16.47	0.022796
180.3876	+21.0847	76.15	48.07	13.78	0.023393	181.1660	+20.2281	−0.88	71.78	15.90	0.025016
180.3915	+21.0083	130.00	57.06	17.28	0.023582	181.1685	+20.2328	170.56	85.45	16.29	0.021928
180.3978	+20.7809	158.06	31.27	14.75	0.023222	181.1704	+20.1553	115.69	52.33	16.47	0.026614
180.4137	+21.0569	29.14	75.77	17.80	0.023700	181.1807	+20.3930	164.34	15.76	16.58	0.025208
180.4273	+21.0235	94.12	66.50	15.53	0.024083	181.2005	+20.7544	108.96	38.84	17.10	0.024914
180.4371	+20.3283	34.46	56.67	17.59	0.024487	181.2216	+19.8863	94.74	69.83	17.84	0.025243
180.4485	+21.0857	59.39	65.29	17.04	0.023382	181.2294	+19.9820	84.29	79.29	13.87	0.020672
180.4718	+20.1875	17.55	70.79	16.08	0.024737	181.2344	+21.2405	39.66	17.79	13.14	0.023501
180.4812	+20.7479	123.45	43.18	17.84	0.025187	181.2411	+21.0129	134.16	46.55	17.22	0.026033
180.4870	+20.6247	13.17	44.61	17.38	0.023744	181.2676	+20.6859	157.13	45.98	17.63	0.024776
180.5077	+20.2651	137.15	58.19	16.40	0.023734	181.3062	+20.2981	18.13	46.41	14.78	0.027404
180.5328	+20.4943	11.82	66.86	17.48	0.022819	181.3108	+21.0816	53.72	55.26	17.11	0.024538
180.5394	+20.5776	61.06	81.27	16.96	0.024812	181.3110	+20.2907	125.10	72.99	17.36	0.025315
180.5606	+20.1694	42.42	63.77	16.35	0.024982	181.3135	+20.3107	79.65	69.45	15.38	0.023637
180.5753	+21.0111	50.53	52.54	17.28	0.026708	181.3136	+21.2145	52.87	16.22	16.47	0.023650
180.6203	+20.2236	96.54	71.79	14.03	0.024298	181.3227	+21.2728	45.91	60.39	16.19	0.023998
180.6416	+20.8155	58.25	77.78	15.99	0.023357	181.3591	+20.5407	149.60	59.85	15.56	0.025128
180.6472	+20.4110	119.73	74.28	16.11	0.026005	181.3663	+20.3087	37.87	63.26	14.32	0.025452
180.6500	+20.5451	25.27	59.91	14.21	0.025347	181.3716	+20.5763	69.52	60.60	17.49	0.024402
180.6503	+20.3825	48.92	23.25	14.59	0.025562	181.3724	+20.2467	79.70	40.04	16.80	0.024736
180.6558	+21.1592	80.97	44.48	16.35	0.026022	181.3926	+20.6382	11.09	75.77	17.32	0.025148
180.6575	+20.1027	127.74	32.89	17.40	0.022488	181.3987	+20.2027	135.18	63.29	15.65	0.024568
180.6579	+20.7173	59.25	86.32	15.59	0.023845	181.4031	+20.4774	127.00	56.77	17.78	0.024544
180.6759	+21.0911	122.87	71.14	17.80	0.024068	181.4060	+20.5557	31.40	31.17	15.16	0.025188
180.6935	+21.1598	17.90	68.58	14.74	0.026797	181.4171	+20.5557	41.66	74.61	13.34	0.026633
180.6949	+20.1632	124.08	40.59	16.94	0.024974	181.4327	+20.3926	92.62	74.46	16.23	0.025472
180.7017	+21.1455	26.06	84.03	15.00	0.024444	181.4377	+20.3576	77.29	34.26	16.65	0.026373
180.7019	+20.8146	153.56	43.98	16.98	0.024780	181.4476	+20.3265	170.13	63.18	13.62	0.024351
180.7160	+20.7262	104.19	44.81	15.29	0.024310	181.4614	+20.4077	2.39	64.05	17.71	0.024718
180.7302	+20.2022	60.55	30.86	17.09	0.025429	181.4645	+20.5220	43.86	29.41	13.64	0.024873

Table 23: SDSS DR7 of galaxies in the supercluster S[195+027+0022] that have redshifts range 0.022 to 0.024.The first two columns list the right ascension and declinations.The next two columns shows position and inclination angle.The fifth and sixth columns represent the magnitude in r-band and redshift.

RA(J2000)	$Dec.(J2000)$	$P(deg)$	$i(deg)$	m_r	z	$RA(J2000)$	$Dec.(J2000)$	$P(deg)$	$i(deg)$	m_r	z
181.4657	+20.4352	95.36	74.14	17.28	0.025632	182.0360	+25.7179	87.19	82.81	17.18	0.021542
181.4759	+20.5725	145.42	39.71	16.67	0.024951	182.0379	+25.0789	160.58	39.56	17.65	0.025150
181.4764	+20.6511	128.38	46.27	16.09	0.025812	182.0403	+24.6768	0.83	43.78	17.34	0.024123
181.5013	+20.2626	71.49	66.17	13.43	0.025422	182.0407	+25.6134	120.22	46.20	14.79	0.022782
181.5149	+20.6081	142.12	22.04	13.63	0.025480	182.0498	+25.7571	142.94	52.90	17.66	0.024954
181.5156	+20.6056	160.38	56.57	17.60	0.026778	182.0548	+24.9428	124.43	64.45	17.84	0.023662
181.5168	+20.5369	178.28	52.10	16.66	0.024757	182.0615	+25.4104	41.99	32.90	13.70	0.024087
181.5221	+21.0934	28.76	53.52	15.88	0.025122	182.0639	+25.0357	77.49	63.37	13.10	0.024863
181.5255	+20.3703	124.38	56.56	17.03	0.026678	182.0746	+25.5937	168.54	34.05	16.76	0.023294
181.5273	+20.7850	139.40	34.24	13.80	0.025693	182.0768	+25.1614	100.56	56.27	15.93	0.020467
181.5360	+20.6930	98.41	48.08	16.69	0.024947	182.0853	+25.3349	52.87	63.21	15.98	0.022909
181.5466	+20.5660	33.76	53.55	13.17	0.025787	182.0884	+25.3640	−0.02	47.94	15.25	0.023439
181.5504	+21.2262	161.51	29.60	16.81	0.023622	182.0900	+25.1909	143.73	9.16	16.61	0.021039
181.5758	+20.6121	176.18	60.60	17.66	0.025207	182.0927	+25.3161	16.77	47.73	14.29	0.023713
181.5914	+20.5644	162.19	75.93	13.40	0.025118	182.1231	+25.2656	22.71	64.12	15.94	0.025477
181.6052	+20.1164	160.90	71.30	14.10	0.025631	182.1639	+25.1280	44.42	33.30	15.62	0.022465
181.6184	+20.0200	88.35	75.16	17.11	0.025898	182.1927	+24.9464	152.41	40.50	13.98	0.022373
181.6315	+20.8506	19.65	73.92	17.21	0.026898	182.1993	+25.4709	32.03	52.25	13.88	0.023876
181.6379	+20.6174	82.32	52.60	16.13	0.025451	182.2109	+25.4929	177.87	59.78	16.76	0.023231
181.6399	+20.5516	172.85	40.62	16.76	0.023680	182.2222	+25.5503	123.94	48.66	15.48	0.023410
181.6572	+20.6449	102.59	42.88	16.71	0.024715	182.2305	+25.1917	131.43	45.94	16.91	0.023193
181.6655	+20.4566	28.94	49.29	16.78	0.025278	182.2584	+24.9549	12.89	31.70	15.56	0.023465
181.6701	+21.2932	44.47	54.79	15.16	0.025992	182.2790	+25.2370	94.81	44.65	15.29	0.022670
181.7141	+20.8187	88.39	36.74	15.79	0.025373	182.3247	+24.9675	160.30	40.34	16.02	0.022929
181.7586	+20.6589	163.41	42.60	17.53	0.026081	182.3732	+24.5405	97.49	20.98	16.33	0.024036
181.7742	+21.4623	87.44	78.45	17.48	0.025139	182.4166	+24.7814	71.58	58.93	16.51	0.024094
181.8271	+20.5837	10.29	81.68	15.80	0.025595	182.4758	+25.3112	99.46	65.54	16.05	0.024103
181.8723	+20.6883	99.31	75.54	16.09	0.023493	182.5212	+25.3082	106.94	56.89	16.64	0.022384
181.9540	+20.6449	16.36	27.88	17.09	0.024970	182.5248	+25.6438	137.84	55.74	13.78	0.023542
180.4573	+16.5303	111.41	43.33	17.41	0.022936	182.5611	+25.3089	77.90	57.06	15.52	0.020951
180.4989	+16.7083	98.14	59.38	16.63	0.022831	182.6428	+25.4274	136.15	47.37	17.77	0.022960
180.6654	+16.4024	169.37	44.37	15.06	0.024592	182.6445	+25.9282	172.68	35.60	15.83	0.022456
180.7073	+16.5932	76.27	44.45	16.99	0.023908	182.6881	+25.8442	46.33	84.80	13.89	0.021916
180.7934	+16.4592	172.99	64.49	14.08	0.023826	182.7064	+25.5837	63.81	72.99	14.84	0.021825
180.8354	+16.5101	57.26	44.84	16.44	0.024264	182.7263	+25.2528	169.21	57.46	15.14	0.024018
180.6105	+23.8188	90.61	20.55	16.89	0.023359	182.7628	+25.5163	25.22	66.48	13.73	0.021495
180.6311	+23.8393	56.83	35.56	14.91	0.023326	181.7150	+16.9920	78.31	54.58	17.58	0.023892
180.6513	+23.7831	85.11	28.77	17.82	0.023044	181.7898	+16.9956	151.58	50.11	17.29	0.023489
180.6990	+23.8939	83.58	66.89	16.62	0.023445	181.8274	+16.8414	114.64	40.06	14.28	0.024142
180.8386	+23.2850	113.49	66.90	14.60	0.024019	181.9181	+17.3028	84.64	66.67	17.17	0.023629
180.9952	+23.4606	41.10	45.51	16.53	0.022945	181.9530	+17.1605	64.59	65.15	16.77	0.023714
180.9844	+22.9801	161.37	35.47	15.52	0.023680	182.0960	+17.3303	78.34	42.23	13.32	0.023569
181.0005	+22.8640	143.53	40.11	17.49	0.022750	182.1519	+17.2118	12.34	61.06	13.81	0.024124
181.0355	+22.5994	61.94	70.93	14.64	0.022507	182.2037	+17.1722	37.34	61.54	14.06	0.023652
180.8547	+22.2027	171.04	54.51	14.00	0.022286	182.3871	+17.0143	2.04	45.92	15.93	0.023476
181.0016	+22.1248	134.58	75.70	13.82	0.022714	181.7643	+18.5318	130.38	55.32	16.95	0.025105
181.0686	+21.7982	46.17	68.24	17.26	0.022498	181.8685	+18.4746	120.11	58.50	16.64	0.025574
181.2897	+22.0080	127.19	48.90	17.73	0.023106	181.9607	+19.7675	59.80	71.18	16.30	0.025899
181.2114	+19.2477	142.40	33.95	17.34	0.024455	182.0116	+19.7902	138.89	77.27	15.62	0.025554
181.3114	+18.9835	99.09	66.43	16.32	0.025030	181.9932	+22.7957	20.55	48.87	13.94	0.022747
181.2507	+25.1973	178.38	66.05	17.63	0.023873	182.2531	+22.6881	67.35	44.14	15.06	0.023682
181.3963	+25.0971	28.22	83.54	22.62	0.024581	182.2849	+22.6968	164.96	72.77	15.39	0.023952
181.2588	+15.4222	147.77	71.51	15.86	0.023550	181.9933	+21.9187	88.73	79.91	16.43	0.024651
181.2730	+15.3441	165.87	54.31	16.25	0.024279	182.0294	+22.1011	111.62	16.32	15.33	0.024824
181.3456	+15.4469	118.44	62.14	16.45	0.024244	182.1278	+21.9273	176.25	73.28	14.47	0.023567
181.2833	+23.9270	68.72	37.10	16.77	0.023518	182.1796	+21.7415	163.69	77.19	17.36	0.025163
181.5948	+23.8533	119.00	53.72	17.75	0.023341	182.2312	+21.7775	12.45	41.01	13.53	0.025287
181.7008	+24.0257	5.98	52.86	16.11	0.023409	182.2377	+21.8887	143.11	71.87	13.31	0.025492
181.6586	+25.7502	39.56	45.63	14.46	0.025238	182.3214	+22.2505	146.53	78.08	17.83	0.025301
181.6709	+25.2383	138.76	57.63	14.18	0.024865	182.3359	+22.2368	19.75	85.70	15.99	0.025152
181.6880	+25.4952	32.34	62.55	17.34	0.023714	182.3584	+22.0833	67.19	68.72	17.18	0.025356
181.7061	+25.0032	58.11	39.52	17.79	0.024917	182.3664	+22.1046	84.17	78.55	14.57	0.025358
181.7198	+25.1973	41.93	67.03	13.83	0.022868	182.5714	+22.4894	82.19	40.83	15.72	0.023676
181.7231	+25.5414	104.56	68.33	15.75	0.023490	182.6160	+22.2702	29.81	70.91	16.40	0.024337
181.7271	+25.0342	16.73	36.58	15.01	0.023163	182.0946	+22.4077	167.83	46.17	16.03	0.022927
181.7306	+25.6235	162.38	52.17	17.29	0.024116	182.1075	+22.4166	167.78	45.29	16.10	0.023354
181.7889	+25.9545	71.87	78.43	17.02	0.024420	182.1682	+17.9567	136.15	23.49	15.62	0.026559
181.8153	+25.1160	120.30	28.84	17.04	0.026996	182.3646	+17.9612	18.68	40.07	16.81	0.026258
181.8157	+25.2853	40.52	54.01	17.75	0.022551	182.3979	+17.8113	118.96	57.20	15.17	0.024023
181.8161	+25.0552	153.76	39.69	15.26	0.021675	182.4144	+17.8565	89.39	78.43	16.23	0.022577
181.8221	+25.2636	148.61	38.01	14.66	0.023490	182.6369	+17.8683	160.86	39.50	15.28	0.025142
181.8670	+24.9505	154.64	52.64	17.22	0.023052	182.6580	+17.8702	140.93	43.23	17.30	0.024058
181.8895	+25.3164	16.30	63.18	15.18	0.026550	182.6733	+17.8626	56.03	49.14	15.94	0.023234
181.8943	+25.2805	10.67	70.12	15.42	0.022494	182.6752	+17.8876	162.58	45.39	15.43	0.025077
181.8978	+25.7720	42.85	40.16	16.69	0.024413	182.7389	+17.8015	1.33	36.85	15.81	0.024994
181.9237	+25.2541	45.75	64.79	17.25	0.023403	182.7711	+17.9414	103.07	36.36	15.72	0.024389
181.9425	+25.5201	18.75	19.66	16.78	0.024338	182.8127	+17.8882	83.10	33.62	17.60	0.024536
181.9457	+25.2642	127.07	60.95	16.41	0.022705	183.0398	+17.7570	91.18	40.55	14.73	0.024451
181.9624	+25.7469	166.77	40.60	16.13	0.022509	183.1203	+17.9722	18.02	18.71	15.61	0.023668
181.9671	+25.9855	104.09	66.12	16.83	0.026068	182.5091	+23.8545	171.57	49.61	17.21	0.023613
181.9780	+25.1013	164.30	45.85	15.37	0.024487	182.5611	+23.8880	120.86	74.46	15.00	0.023001
181.9791	+25.0174	138.07	22.10	17.06	0.023224	182.5894	+23.8117	175.61	71.58	15.79	0.023877
181.9927	+25.3212	86.21	62.88	16.03	0.022927	182.6889	+23.7103	111.47	63.50	16.60	0.023392
182.0037	+24.8590	59.94	47.70	15.06	0.025300	182.7079	+23.7144	42.97	46.00	14.61	0.023725
182.0128	+25.1142	68.04	43.32	15.42	0.023346	182.7510	+23.6746	124.48	73.05	17.33	0.025313
182.0211	+25.5903	88.47	31.46	15.94	0.022973	182.9716	+23.6437	100.70	65.29	14.11	0.022972
182.0231	+25.2373	177.37	30.53	15.90	0.023565	183.0462	+23.6765	71.30	83.24	17.88	0.025730
182.0254	+25.2674	59.88	59.58	16.50	0.020347	183.1095	+23.7284	84.40	67.64	16.65	0.026007
182.0299	+24.7903	128.65	61.01	15.82	0.023684	183.1735	+23.4783	135.33	63.65	14.25	0.023404
182.0317	+25.3732	172.05	53.38	17.18	0.021979	183.2857	+23.6728	169.74	27.52	12.68	0.024986
182.0341	+25.0329	145.84	83.86	17.25	0.023687	182.5416	+26.4244	158.87	19.60	15.98	0.022042

Table 24: SDSS DR7 of galaxies in the supercluster S[195+027+0022] that have redshifts range 0.022 to 0.024.The first two columns list the right ascension and declinations.The next two columns shows position and inclination angle.The fifth and sixth columns represent the magnitude in r-band and redshift.

RA(J2000)	$Dec.(J2000)$	$P(deg)$	$i(deg)$	m_r	z	$RA(J2000)$	$Dec.(J2000)$	$P(deg)$	$i(deg)$	m_r	z
182.5761	+26.4307	103.04	49.21	17.23	0.022758	185.2195	+25.4297	106.20	70.49	17.89	0.025009
182.6229	+26.2533	79.87	33.65	14.31	0.023662	185.2942	+25.3252	79.63	72.47	14.96	0.024084
182.7981	+24.9359	42.44	31.68	15.72	0.025644	185.3041	+25.3144	161.35	67.95	16.03	0.024377
183.0157	+25.1190	85.56	49.17	13.92	0.024692	184.7714	+22.3335	64.40	81.49	16.79	0.023882
183.2509	+25.2816	0.51	81.75	16.66	0.025440	184.8061	+22.4315	50.28	31.28	16.09	0.023341
182.8997	+19.8958	29.98	44.43	17.36	0.023190	184.8368	+22.3247	65.04	70.64	15.54	0.023031
182.9086	+19.8454	−0.32	68.35	15.92	0.023496	184.9124	+22.1525	83.98	52.96	16.71	0.024047
182.9669	+21.1128	89.18	76.02	17.10	0.024688	185.2328	+24.6706	99.53	54.76	16.39	0.025177
183.0551	+21.1409	11.35	79.99	17.45	0.024339	185.3261	+24.7127	65.36	31.23	17.24	0.025471
183.2639	+21.0241	169.34	68.18	15.94	0.024981	185.4235	+24.8243	54.71	57.23	14.97	0.025537
183.1241	+21.9114	42.87	50.53	16.36	0.025729	185.3474	+23.9849	146.46	34.25	16.46	0.023190
183.1882	+21.5630	36.13	39.91	17.22	0.024731	185.5224	+23.8852	128.70	81.24	17.63	0.023353
183.2381	+21.4269	90.23	56.52	16.74	0.024783	185.4175	+22.3523	151.74	64.43	13.16	0.024259
183.2598	+21.5511	149.96	45.73	13.05	0.024840	185.5098	+22.2458	153.46	59.82	17.05	0.023653
183.2826	+21.4937	46.58	74.42	17.09	0.024289	185.5645	+22.5077	19.61	78.82	15.67	0.023829
183.3060	+21.7104	81.12	28.42	17.54	0.025970	185.7223	+22.4474	77.10	52.91	13.46	0.023318
183.3082	+21.7904	163.80	33.58	16.91	0.026310	185.4401	+25.8847	148.87	70.24	15.38	0.024055
183.3170	+21.6971	146.40	68.57	14.79	0.026227	185.4851	+25.9568	38.85	71.05	15.56	0.023047
183.3182	+21.6222	29.72	48.23	15.52	0.025560	185.6430	+27.8090	108.85	48.34	16.44	0.023955
183.3242	+21.6544	178.48	49.99	15.39	0.024933	185.6653	+27.7470	85.07	64.26	16.91	0.024943
183.3261	+21.6343	15.85	35.00	17.52	0.025416	185.6839	+27.7371	33.32	45.06	16.89	0.024469
183.3532	+21.6689	71.06	45.81	16.56	0.026480	186.2323	+26.8161	135.75	44.46	14.32	0.025557
183.4788	+21.7561	76.81	34.83	14.79	0.025336	186.4370	+26.7669	172.85	53.89	15.75	0.023880
183.5479	+21.7113	102.84	60.71	17.14	0.026077	186.4548	+26.7399	172.50	13.65	15.30	0.024538
183.5943	+22.1869	40.83	37.27	16.94	0.024831	186.5739	+26.8311	16.78	32.27	20.52	0.024821
183.6541	+21.9891	64.99	53.86	14.85	0.024631	186.7267	+26.6901	134.56	34.40	16.85	0.023225
183.6675	+21.5960	98.54	38.24	17.40	0.025702	186.8978	+26.5399	86.70	45.63	16.94	0.022321
183.7026	+22.1951	23.61	71.34	15.42	0.025390	186.2707	+25.9576	84.42	75.45	17.45	0.023222
183.7257	+22.1418	147.95	78.40	17.67	0.025084	186.2934	+25.8798	76.29	3.14	16.78	0.023257
183.7261	+21.9006	26.35	25.10	14.96	0.025988	186.4424	+26.0825	8.99	66.71	15.63	0.024714
183.7896	+21.9235	10.33	64.00	15.62	0.023112	186.5928	+25.8863	60.37	63.95	16.92	0.022038
183.8304	+21.4915	22.58	55.92	17.13	0.026044	186.6160	+25.8889	124.14	72.95	16.06	0.024007
183.8452	+21.8782	63.76	72.99	15.76	0.025109	186.6637	+29.6330	57.86	76.96	15.36	0.023030
183.8932	+21.8322	82.93	8.30	13.24	0.023723	186.6836	+29.4236	129.71	89.03	14.11	0.023209
183.9038	+21.9093	119.05	81.62	15.25	0.023408	186.7630	+29.5384	118.13	38.82	17.71	0.023061
183.4763	+25.1692	174.79	66.60	14.28	0.023709	186.7478	+22.6396	159.51	58.04	17.43	0.023793
183.6769	+24.9806	176.19	40.34	16.80	0.022975	186.9472	+22.5621	104.39	52.32	15.79	0.023574
183.5209	+24.0674	100.68	17.22	17.63	0.023378	186.8321	+24.9594	45.79	86.65	15.94	0.023859
183.5453	+24.0695	160.04	75.79	17.57	0.025202	186.9665	+24.9422	130.91	64.49	17.28	0.023790
183.6083	+23.7634	42.70	55.33	14.45	0.023213	187.1021	+26.7837	133.85	61.24	16.81	0.022469
183.6096	+24.1821	174.89	33.97	17.31	0.023730	187.2122	+26.7001	145.92	22.74	16.26	0.023109
183.6727	+23.8529	138.90	34.43	17.67	0.023175	187.2609	+27.6405	68.76	48.53	17.00	0.024381
183.7143	+23.9065	117.17	73.14	16.21	0.023250	187.2661	+27.7789	149.42	64.40	14.75	0.024321
183.7368	+23.8685	1.38	53.18	17.30	0.024805	187.3499	+22.3636	7.88	55.42	15.99	0.023697
183.7694	+23.9334	110.72	65.51	17.58	0.023448	187.4558	+22.3721	118.14	48.31	14.09	0.023561
183.7985	+23.9857	161.95	30.32	14.65	0.024632	187.4644	+25.6320	42.18	64.80	16.21	0.023798
183.8162	+23.9582	100.94	41.35	17.34	0.023300	187.6307	+25.3095	77.50	65.41	15.65	0.023289
183.8193	+24.0373	93.35	70.16	16.97	0.024248	187.7478	+25.5619	45.36	32.54	15.84	0.023260
183.8419	+23.9937	102.49	66.09	29.38	0.026031	187.8534	+26.7961	160.55	59.07	15.03	0.024120
183.8552	+23.9482	81.29	53.42	13.97	0.023890	187.9328	+26.8002	105.60	68.99	17.70	0.023654
183.8704	+24.0924	40.29	57.71	15.81	0.024138	188.3071	+27.5841	139.83	48.26	16.69	0.025299
183.8917	+24.0033	131.13	48.68	15.15	0.021925	188.3338	+27.4505	121.88	83.15	17.72	0.024126
183.9065	+23.9819	65.20	36.91	13.98	0.023407	188.5714	+27.4523	65.05	85.37	17.43	0.023869
183.9292	+24.0045	171.91	60.09	17.29	0.023414	188.3707	+26.7380	58.53	72.72	13.35	0.022691
183.9385	+24.0697	65.05	40.29	17.45	0.022665	188.3750	+26.7796	105.29	50.03	17.29	0.024020
183.9634	+24.0066	132.57	34.56	14.95	0.023441	188.4263	+26.6173	3.59	76.53	17.82	0.024793
183.9674	+24.3455	139.65	24.79	15.00	0.023723	188.5289	+26.6708	59.18	53.50	15.15	0.027079
183.9795	+23.5955	45.63	35.45	14.60	0.022502	188.6070	+26.9352	99.45	56.80	17.26	0.024354
183.9883	+23.8681	173.49	76.86	15.12	0.023674	188.6096	+26.8846	68.69	73.09	15.70	0.023750
183.9930	+24.0777	142.88	61.24	17.27	0.021823	188.6407	+26.6578	124.86	67.28	14.78	0.023689
184.0305	+23.8243	56.82	87.78	17.50	0.024929	188.7179	+26.1750	35.78	85.44	13.77	0.022349
184.0305	+23.8243	56.82	87.78	14.18	0.024832	188.7356	+26.6266	129.88	28.24	17.10	0.023834
184.3607	+23.9043	38.08	73.48	16.34	0.025337	188.7494	+26.8841	53.09	59.00	14.38	0.026242
184.0770	+26.7654	38.02	67.18	14.93	0.024301	188.7635	+27.0794	162.00	36.19	17.82	0.025649
184.3421	+26.6242	150.58	55.10	14.78	0.024618	188.7809	+26.9093	120.95	53.27	16.39	0.023665
184.1874	+26.1237	161.47	51.87	14.42	0.023634	188.7838	+26.7397	124.51	49.54	15.49	0.026783
184.5085	+26.0806	46.32	33.53	15.41	0.023653	188.8020	+26.5334	153.75	82.21	15.77	0.022032
184.3709	+24.4860	34.23	72.31	12.94	0.023592	188.8054	+26.4960	90.93	60.96	15.98	0.021654
184.5353	+24.6883	70.89	2.47	16.07	0.023671	188.8090	+26.4723	131.46	29.07	17.47	0.023935
184.5863	+24.5847	47.25	60.45	15.77	0.022590	188.8447	+26.5767	80.12	63.40	16.16	0.023135
184.4882	+25.0765	19.22	30.61	17.31	0.023901	188.8830	+26.4511	19.23	55.83	17.04	0.021620
184.5893	+25.2168	150.48	50.31	15.15	0.024181	188.8996	+26.5667	86.91	41.73	15.33	0.023642
184.7907	+25.2970	32.77	29.62	13.79	0.023700	188.9146	+26.5488	167.25	40.93	15.50	0.024669
184.8479	+25.0507	75.12	55.25	16.29	0.023844	188.9184	+26.9293	51.23	63.32	16.40	0.026670
184.8583	+25.0382	7.71	66.17	17.83	0.023363	188.9188	+26.6429	69.03	27.43	17.00	0.020932
184.8900	+24.9053	140.89	52.55	22.21	0.022994	188.9204	+27.2055	104.04	52.23	14.01	0.025351
185.1950	+24.9156	41.12	53.63	22.21	0.023090	188.9216	+26.5231	115.82	44.03	17.38	0.023193
184.5249	+25.7111	51.97	67.58	23.45	0.024785	188.9222	+26.4824	109.71	57.14	17.14	0.023454
184.5598	+25.6184	103.58	68.29	16.32	0.024024	188.9237	+26.2222	138.39	55.10	16.44	0.022355
184.8021	+25.7150	93.19	32.92	17.10	0.025821	188.9267	+26.9091	81.46	44.66	17.10	0.027288
184.8396	+25.7686	47.09	14.44	17.34	0.024863	188.9326	+27.2806	60.57	52.21	15.73	0.025000
184.8714	+25.8987	173.76	80.39	17.61	0.023990	188.9333	+26.5768	88.72	44.85	16.35	0.023542
184.8752	+25.7426	18.26	54.05	16.80	0.025687	188.9411	+26.9089	85.22	45.33	17.21	0.025736
184.8916	+25.5859	104.68	49.12	17.53	0.024014	188.9482	+26.7555	99.37	58.39	16.54	0.024580
184.9440	+26.0747	49.97	47.91	14.57	0.023426	188.9694	+26.9921	101.66	43.91	17.10	0.026989
184.9527	+26.2856	89.47	55.42	16.79	0.024016	188.9783	+26.8187	148.51	51.56	15.43	0.024873
184.9932	+25.7717	10.21	60.82	15.56	0.023526	188.9822	+26.4221	7.89	61.54	17.18	0.022041
185.0367	+25.5856	38.50	55.64	13.74	0.023477	188.9936	+26.9660	178.56	48.58	16.40	0.025602
185.0891	+25.5995	113.26	45.00	16.07	0.023769	189.0092	+26.7854	28.42	83.80	16.93	0.026091
185.1002	+25.5606	59.00	41.28	17.41	0.023901	189.0163	+27.0782	68.93	57.74	16.50	0.025031
185.1253	+25.5154	150.30	74.36	15.08	0.024296	189.0195	+26.5958	151.29	56.09	15.23	0.022677

Table 25: SDSS DR7 of galaxies in the supercluster S[195+027+0022] that have redshifts range 0.022 to 0.024.The first two columns list the right ascension and declinations.The next two columns shows position and inclination angle.The fifth and sixth columns represent the magnitude in r-band and redshift.

RA(J2000)	$Dec.(J2000)$	$P(deg)$	$i(deg)$	m_r	z	$RA(J2000)$	$Dec.(J2000)$	$P(deg)$	$i(deg)$	m_r	z
189.0200	+26.8996	71.14	51.88	17.09	0.027105	190.4087	+28.5692	73.16	67.02	15.47	0.026177
189.0511	+26.7561	22.49	43.47	16.31	0.025555	190.4246	+28.6500	144.81	48.47	16.54	0.026346
189.0518	+26.4669	178.99	28.62	14.70	0.022911	190.4217	+33.4131	35.32	49.72	16.65	0.023720
189.0536	+26.9414	112.78	51.77	16.58	0.025553	190.6983	+33.2877	61.63	83.62	16.48	0.023789
189.0779	+27.7536	166.46	18.58	12.14	0.025674	190.7034	+33.2906	42.05	42.50	16.42	0.024072
189.0882	+27.0333	59.41	54.32	15.68	0.026006	190.8777	+33.4172	174.17	31.95	18.16	0.023960
189.0941	+26.9366	181.49	71.71	15.63	0.024747	190.5610	+31.6973	63.36	70.66	16.07	0.024348
189.0992	+27.0317	2.58	68.61	14.17	0.025428	190.6217	+31.4553	114.35	28.30	17.14	0.023962
189.1254	+26.2486	19.65	31.24	15.24	0.022806	190.6787	+31.1408	171.10	57.46	17.55	0.023597
189.1351	+28.0287	119.37	40.99	16.82	0.026520	190.7701	+31.1506	77.65	59.83	17.75	0.023927
189.1538	+26.2347	89.29	30.89	15.86	0.023747	190.8043	+31.0556	161.56	79.49	14.67	0.025257
189.1662	+26.8299	114.13	34.17	13.07	0.025323	190.8079	+31.0850	149.51	41.11	17.49	0.024280
189.1690	+27.1475	63.35	45.73	16.24	0.026431	190.6881	+27.1175	119.66	51.63	17.47	0.022844
189.1810	+26.1131	173.43	60.67	13.75	0.021788	190.8141	+27.0856	180.85	73.81	15.42	0.023559
189.1819	+27.0761	43.62	32.95	16.99	0.025614	191.1098	+27.1928	28.36	56.66	17.46	0.022411
189.1907	+27.5668	152.80	81.91	16.87	0.024958	190.7253	+27.7745	154.93	80.96	16.74	0.025741
189.2227	+27.8620	131.57	56.83	14.61	0.025918	190.7723	+27.7141	33.21	43.22	17.89	0.026050
189.2247	+27.7491	6.84	32.29	16.11	0.026755	190.8513	+27.6871	73.32	24.90	16.27	0.025637
189.2531	+27.3603	156.85	50.71	14.74	0.025863	190.8574	+27.3731	48.45	31.52	17.22	0.025418
189.3139	+27.5333	12.55	29.70	15.54	0.026219	190.9255	+27.3730	79.72	64.66	15.88	0.025459
189.3277	+26.5529	115.78	57.44	14.48	0.023201	190.9070	+31.7305	128.75	35.17	17.33	0.024697
189.3338	+28.1472	82.78	56.30	16.11	0.026274	191.1819	+31.6371	168.38	61.59	17.47	0.024462
189.3378	+28.2082	138.94	51.48	17.67	0.026528	191.4001	+31.6427	56.23	60.14	16.32	0.024442
189.3619	+27.2024	156.72	79.75	14.58	0.026604	191.1200	+28.4331	181.62	86.01	17.57	0.024718
189.4294	+27.9150	81.53	49.40	16.45	0.024870	191.2137	+28.5036	95.33	82.94	16.80	0.025511
189.4397	+27.9307	168.39	65.62	17.15	0.024849	191.3027	+29.0125	24.68	51.50	14.35	0.024658
189.4435	+26.2990	90.22	52.80	21.02	0.023034	191.3389	+28.5909	55.62	90.05	19.43	0.024751
189.4620	+28.0000	96.45	78.96	17.24	0.025302	191.3973	+28.7619	18.18	20.12	17.70	0.024076
189.4791	+28.2861	134.36	58.88	16.69	0.026545	191.5380	+28.9585	125.48	48.10	17.39	0.024500
189.4807	+27.6282	98.39	54.76	16.60	0.025030	191.2887	+23.0390	137.56	59.39	17.18	0.023904
189.5528	+26.4921	44.42	59.38	15.77	0.023407	191.3934	+23.0729	112.53	67.53	16.51	0.025116
189.6212	+26.3743	138.14	44.16	13.48	0.024096	191.4010	+28.1196	109.93	67.41	16.24	0.023669
189.7514	+28.3146	30.41	63.25	17.39	0.026076	191.5448	+27.9378	72.72	45.45	17.75	0.024000
189.7891	+28.2698	42.02	56.27	17.10	0.026351	191.7192	+27.7909	93.15	65.19	13.68	0.025207
189.7978	+28.0052	114.57	17.03	16.88	0.025111	191.5400	+27.2470	105.88	61.73	14.34	0.027354
190.0532	+28.3605	32.55	28.02	17.44	0.025829	191.8350	+27.2468	163.12	34.36	15.67	0.026840
188.5843	+24.6001	81.52	53.01	14.93	0.022154	191.9249	+26.9816	61.23	64.01	14.92	0.024801
188.8118	+24.5488	148.36	55.26	14.20	0.022482	191.9683	+27.2668	118.52	50.39	17.77	0.027380
189.1246	+32.0798	34.65	63.68	14.42	0.024420	191.9782	+26.9530	130.77	61.64	14.34	0.024042
189.1915	+32.1158	171.76	64.15	17.51	0.024523	191.9805	+27.2223	88.96	40.20	16.75	0.027520
189.4238	+32.0867	25.59	47.24	16.87	0.024181	192.0113	+27.2785	159.42	76.55	16.88	0.027023
189.6329	+31.9379	53.74	42.45	17.80	0.022689	192.0387	+26.9392	24.88	73.77	16.46	0.024028
189.6847	+32.0179	150.02	50.30	16.89	0.023152	192.1003	+26.8579	117.25	65.97	17.01	0.025646
189.6897	+31.8795	50.00	77.75	13.67	0.023328	192.1540	+27.3664	88.79	47.28	17.39	0.027568
189.7033	+31.9849	98.74	56.15	16.62	0.024070	192.2475	+27.3757	59.30	78.26	16.47	0.021888
189.8264	+31.9899	118.49	39.86	16.48	0.024529	192.2605	+26.8931	155.58	67.66	16.93	0.025529
189.3527	+23.8641	48.63	51.51	17.80	0.023950	192.2868	+27.3688	180.31	64.00	15.26	0.022918
189.4445	+23.6502	126.19	40.56	17.56	0.023931	192.2994	+27.3850	153.30	64.64	17.67	0.021821
189.4033	+33.6152	103.78	41.26	15.84	0.023831	192.3432	+26.7439	148.26	68.64	17.03	0.025040
189.4350	+33.6191	139.31	41.98	17.37	0.024098	192.3655	+27.2676	153.72	41.02	15.19	0.027549
189.4984	+33.5579	56.94	74.09	16.10	0.024056	192.3972	+27.1976	154.30	74.75	16.28	0.021787
189.5189	+33.4588	87.68	41.21	17.54	0.023886	192.4262	+26.8920	147.55	45.13	16.99	0.023798
189.7851	+33.5483	119.77	79.23	17.58	0.023550	192.4362	+27.5918	153.05	65.32	17.63	0.023794
189.8115	+33.3577	133.94	52.18	15.30	0.023332	192.4411	+27.3691	61.60	65.06	14.92	0.023781
189.5075	+27.6140	89.21	50.00	17.64	0.023155	192.4454	+27.6407	180.09	51.84	15.16	0.024588
189.6850	+27.7181	134.36	59.02	15.11	0.023122	192.4911	+27.8224	15.06	39.40	16.90	0.024009
189.7435	+27.5636	2.66	64.49	17.16	0.023394	192.4958	+27.1527	110.62	65.35	17.35	0.027121
189.8251	+27.9086	163.48	78.90	16.79	0.022589	192.5463	+27.3698	77.18	57.85	17.06	0.026665
189.9373	+27.8268	69.55	31.65	17.55	0.023324	192.5561	+26.7761	82.43	44.42	13.51	0.024566
189.9797	+27.8272	140.94	57.09	14.15	0.022636	192.5645	+27.0603	101.10	21.66	17.20	0.023161
190.2021	+27.7761	68.43	72.52	14.72	0.023160	192.5674	+27.3800	153.62	60.48	17.38	0.023249
189.5553	+28.9370	108.82	58.60	14.70	0.025277	192.5830	+27.3240	119.08	78.27	12.65	0.026438
189.5692	+28.8826	29.94	69.46	17.43	0.026447	192.5842	+26.7498	50.69	73.07	15.82	0.024650
189.6985	+28.8417	120.44	26.12	16.79	0.025152	192.5866	+27.9372	110.38	33.06	14.93	0.024252
189.7728	+26.9143	18.46	67.28	15.30	0.024851	192.5942	+27.1754	66.36	77.90	13.74	0.024297
189.8651	+27.1023	55.34	35.21	13.34	0.024487	192.6170	+27.4349	84.62	34.91	17.22	0.022351
189.8214	+26.6778	179.47	28.47	14.34	0.022951	192.6319	+27.3140	39.63	84.42	15.66	0.027631
190.0374	+26.5365	107.12	57.24	16.10	0.024444	192.6330	+26.9101	135.64	40.68	14.81	0.023864
190.0700	+26.4738	58.04	60.48	16.29	0.023040	192.6543	+27.4830	174.55	34.43	14.65	0.023076
190.1078	+26.7321	29.30	21.45	15.19	0.023514	192.7649	+27.3700	19.52	43.81	16.77	0.028640
190.1516	+26.5079	22.17	80.90	15.50	0.023546	192.7815	+27.3204	97.87	61.54	17.02	0.021811
190.1538	+27.0792	174.24	70.95	16.86	0.023164	192.7885	+27.4068	150.13	43.47	15.35	0.023764
190.1604	+26.8936	73.20	68.18	12.96	0.022766	192.8068	+27.5567	34.44	77.72	15.27	0.027363
190.1622	+26.9680	6.78	64.92	17.22	0.023177	192.8571	+28.1208	28.07	77.95	13.36	0.025242
190.1631	+26.5262	87.10	73.29	16.91	0.022926	192.8590	+27.4212	10.77	35.93	17.70	0.025327
190.2029	+27.2710	76.16	50.07	17.01	0.022605	192.8976	+26.6289	181.24	41.04	16.32	0.022228
189.9150	+29.6096	175.84	59.06	16.60	0.024344	192.9082	+27.3106	40.87	64.88	17.51	0.024460
189.9774	+29.6622	95.52	40.54	16.56	0.023764	192.9324	+27.9628	124.01	45.59	13.16	0.024029
190.2065	+29.5002	36.55	47.62	14.77	0.023105	192.9372	+27.0184	119.50	70.29	16.04	0.022252
190.0473	+31.1771	137.59	61.39	16.58	0.024443	192.9600	+27.3608	120.62	48.61	17.38	0.022439
190.1066	+31.1550	60.29	80.48	17.29	0.024554	192.9649	+27.2556	152.94	57.26	14.53	0.023535
190.0930	+27.4509	85.62	58.97	16.04	0.025538	192.9728	+27.9781	8.53	38.93	17.17	0.024076
190.2805	+27.4619	70.73	83.62	14.04	0.024868	192.9814	+26.7829	43.04	67.46	16.03	0.021212
190.3796	+27.2431	46.85	69.61	17.27	0.025488	193.0015	+26.1592	151.48	42.15	14.03	0.021520
190.0948	+25.9798	26.46	37.36	16.73	0.022980	193.0140	+27.1660	182.42	62.54	15.91	0.025984
190.1063	+26.0106	100.31	36.61	21.23	0.022886	193.0286	+27.0263	144.31	49.26	17.37	0.022343
190.1411	+32.5808	55.22	52.11	16.45	0.023804	193.0375	+27.4773	88.84	47.96	16.64	0.020403
190.4556	+32.6264	72.73	25.23	13.87	0.023645	193.0493	+26.8748	111.24	24.33	13.88	0.021696
190.2894	+29.5387	152.99	48.23	14.29	0.024420	193.0726	+27.1582	142.38	84.92	16.09	0.022250
190.5155	+29.6664	12.34	50.71	17.43	0.024813	193.0738	+27.0855	9.82	64.18	17.00	0.021960
190.5454	+29.4475	116.77	45.97	16.75	0.024088	193.1236	+27.8030	48.89	39.53	15.32	0.025229

Table 26: SDSS DR7 of galaxies in the supercluster S[195+027+0022] that have redshifts range 0.022 to 0.024.The first two columns list the right ascension and declinations.The next two columns shows position and inclination angle.The fifth and sixth columns represent the magnitude in r-band and redshift.

RA(J2000)	$Dec.(J2000)$	$P(deg)$	$i(deg)$	m_r	z	$RA(J2000)$	$Dec.(J2000)$	$P(deg)$	$i(deg)$	m_r	z
193.1458	+27.4593	155.47	35.25	14.72	0.025681	193.9845	+27.6098	67.62	73.48	17.09	0.023772
193.1548	+27.3252	52.49	59.54	17.12	0.027322	193.9894	+27.9049	60.11	60.48	14.74	0.022817
193.1712	+26.3658	75.60	30.96	16.27	0.021409	193.9933	+28.4074	97.19	51.05	17.68	0.020936
193.1836	+26.4704	97.26	57.69	22.12	0.022236	193.9990	+27.9551	153.47	60.47	13.89	0.027946
193.1928	+27.9068	63.54	51.89	17.70	0.019858	193.9998	+28.1869	46.43	53.79	16.75	0.019572
193.2037	+27.4018	95.44	40.75	14.08	0.026783	194.0065	+28.0384	149.56	39.45	17.35	0.020709
193.2109	+27.7459	69.93	28.80	16.55	0.020921	194.0073	+26.7566	154.03	27.72	14.01	0.020088
193.2233	+28.3713	33.39	73.84	15.39	0.024540	194.0080	+27.6647	152.74	46.00	16.89	0.021428
193.2347	+26.5947	181.75	33.04	14.44	0.025247	194.0083	+26.9208	14.11	15.92	13.40	0.020022
193.2669	+27.4645	30.09	25.74	15.58	0.023837	194.0114	+28.0480	67.78	39.56	15.35	0.025572
193.2813	+28.2413	178.12	76.69	16.75	0.024409	194.0150	+28.4348	178.86	64.78	15.52	0.023686
193.2815	+27.0382	42.27	66.42	17.09	0.026412	194.0165	+27.1504	116.41	43.26	15.76	0.025441
193.2979	+27.8378	111.62	45.22	17.47	0.023994	194.0175	+27.2855	49.49	40.35	17.64	0.023297
193.3021	+27.3231	165.42	29.43	16.32	0.023062	194.0254	+27.6781	171.91	53.90	16.92	0.017368
193.3025	+28.0040	152.28	71.69	14.67	0.020948	194.0268	+27.6480	115.94	73.48	16.98	0.026285
193.3171	+27.0944	152.69	36.58	15.54	0.021485	194.0398	+28.3109	18.76	36.06	13.79	0.027311
193.3234	+26.3393	53.98	45.63	14.73	0.024028	194.0413	+27.8443	64.66	60.42	16.55	0.026168
193.3275	+28.2114	75.18	39.65	14.16	0.021431	194.0457	+28.1632	14.30	68.73	17.29	0.029906
193.3403	+26.3614	175.83	74.52	14.88	0.020294	194.0594	+27.8156	76.03	73.33	15.37	0.023139
193.3463	+27.0335	97.73	35.29	16.40	0.024615	194.0609	+27.5063	170.62	61.70	15.06	0.025692
193.3478	+27.5131	44.20	43.85	14.80	0.024883	194.0695	+27.4460	18.32	24.67	17.61	0.022260
193.3762	+27.6752	31.46	62.71	17.72	0.020713	194.0775	+26.3589	92.32	52.41	17.48	0.022363
193.3796	+27.4634	168.08	68.16	17.61	0.029209	194.0825	+27.7510	134.90	36.06	16.60	0.023902
193.3982	+27.7588	85.38	49.23	16.72	0.025922	194.0849	+28.0508	175.71	38.99	15.95	0.026271
193.4337	+27.7808	111.12	57.94	14.70	0.023103	194.0854	+26.7040	15.22	35.99	16.45	0.022897
193.4395	+27.2496	181.14	85.32	13.85	0.023924	194.0908	+28.4869	102.56	63.77	15.90	0.022902
193.4443	+27.3858	154.00	85.66	15.58	0.028696	194.0973	+27.5440	77.58	22.54	15.67	0.025450
193.4746	+28.1866	37.98	67.17	15.14	0.026571	194.0990	+27.2340	113.34	34.50	15.18	0.021093
193.4759	+26.9664	81.50	70.84	17.00	0.021545	194.1096	+27.7273	79.97	39.13	15.21	0.023689
193.4807	+28.3938	88.72	69.76	13.53	0.025686	194.1109	+27.8306	177.10	25.00	17.50	0.021809
193.4963	+26.4440	173.09	25.00	17.15	0.024555	194.1161	+26.9874	141.14	40.61	17.27	0.022430
193.5230	+27.0686	181.59	70.48	17.27	0.026159	194.1186	+28.0825	27.56	56.99	16.71	0.024170
193.5249	+27.0189	124.54	63.24	16.99	0.029316	194.1191	+27.2913	66.12	43.49	15.82	0.026009
193.5303	+27.2164	124.20	51.04	15.55	0.028152	194.1205	+26.5434	130.99	39.82	16.45	0.026704
193.5416	+28.0925	110.18	64.98	17.68	0.021944	194.1214	+26.9570	9.42	49.45	17.41	0.024417
193.5668	+27.3037	139.59	63.00	15.14	0.022401	194.1242	+27.9400	58.09	28.62	15.07	0.023054
193.5698	+28.0766	117.08	83.97	17.71	0.023755	194.1335	+27.0556	144.45	56.97	15.46	0.021316
193.5814	+28.0913	73.71	63.87	13.65	0.023402	194.1424	+27.6873	67.26	71.72	15.54	0.023872
193.5929	+27.0842	137.81	36.95	17.64	0.029086	194.1424	+27.5390	128.14	35.42	14.51	0.024569
193.5948	+27.7445	111.22	52.88	15.44	0.024704	194.1443	+27.2276	171.97	34.11	15.56	0.024950
193.5954	+26.7994	75.11	66.41	16.15	0.023523	194.1466	+28.2755	107.93	47.85	17.36	0.025249
193.6031	+27.3640	49.47	47.96	16.06	0.026986	194.1497	+27.7188	131.79	50.12	16.09	0.023309
193.6373	+28.3768	31.66	52.52	17.78	0.024270	194.1501	+26.9048	62.80	46.33	15.12	0.027304
193.6383	+27.6328	101.21	81.27	16.11	0.025319	194.1537	+27.8849	181.19	69.64	13.69	0.021910
193.6534	+26.9349	5.78	71.29	17.59	0.020721	194.1600	+28.1063	41.69	24.48	14.48	0.022465
193.6543	+27.3175	126.09	40.83	15.71	0.025952	194.1602	+27.5709	115.02	76.12	17.16	0.026261
193.6734	+27.0415	155.47	65.42	16.37	0.024583	194.1619	+28.0812	58.36	33.17	16.17	0.028002
193.6744	+28.0460	93.17	39.54	16.28	0.026514	194.1681	+28.2178	164.39	74.77	15.79	0.028640
193.6811	+27.4554	90.17	34.87	16.41	0.027041	194.1705	+27.4478	38.48	71.37	17.65	0.025459
193.6874	+27.4111	44.24	66.03	15.43	0.026745	194.1766	+27.5483	72.73	78.97	16.70	0.026235
193.7088	+26.3249	150.97	67.76	15.20	0.023524	194.1786	+28.0205	162.14	34.41	15.55	0.021769
193.7139	+27.4945	26.69	58.13	16.75	0.024273	194.1800	+26.7420	48.35	62.93	14.37	0.024128
193.7196	+26.5759	35.78	57.06	13.68	0.021025	194.1813	+27.0348	35.05	74.38	12.98	0.019619
193.7237	+28.4170	163.23	50.82	14.23	0.025543	194.1813	+27.1788	45.92	37.03	16.17	0.026233
193.7299	+27.4127	32.81	40.06	16.48	0.027092	194.1911	+28.0516	47.73	33.72	14.92	0.023989
193.7316	+28.0669	134.98	64.65	17.58	0.021954	194.1959	+27.0569	126.81	63.89	16.34	0.022607
193.7365	+28.1263	4.30	63.75	14.35	0.021928	194.1975	+27.2923	170.59	44.83	13.92	0.027086
193.7407	+28.3084	158.88	41.79	13.98	0.021952	194.1990	+27.4210	117.22	73.22	14.40	0.026854
193.7519	+27.1938	168.25	56.73	15.65	0.025713	194.1994	+28.1921	96.46	29.39	14.92	0.020319
193.7535	+27.4834	52.48	48.82	15.31	0.024172	194.2069	+27.0939	148.89	63.95	16.36	0.024062
193.7708	+28.0625	86.20	31.52	15.24	0.021782	194.2109	+28.9298	14.36	70.33	14.60	0.027928
193.7713	+26.7242	43.09	16.51	16.55	0.023078	194.2117	+27.6278	42.90	22.38	15.40	0.027913
193.8078	+27.7089	48.40	61.31	16.77	0.023157	194.2132	+26.8989	11.29	35.28	14.94	0.021631
193.8121	+26.2501	170.65	52.85	16.05	0.022599	194.2178	+26.4877	139.03	22.31	16.59	0.026351
193.8156	+28.2519	152.39	43.16	14.00	0.021943	194.2182	+28.1881	24.20	18.11	16.69	0.022462
193.8296	+27.9251	95.34	40.23	14.75	0.022495	194.2214	+27.9295	119.96	66.22	17.24	0.021319
193.8333	+27.8667	137.66	41.11	14.44	0.024157	194.2330	+27.4624	169.74	60.35	16.70	0.026353
193.8352	+26.7999	125.44	76.86	17.51	0.023721	194.2357	+28.6234	97.61	71.14	17.46	0.022754
193.8366	+27.1497	129.92	41.76	16.78	0.021832	194.2567	+29.0626	27.22	56.49	15.78	0.025937
193.8372	+27.6691	46.86	60.06	16.47	0.024580	194.2571	+27.3721	95.41	59.79	17.04	0.024297
193.8440	+28.4679	139.79	44.61	17.18	0.024346	194.2608	+27.6567	51.85	34.24	17.49	0.023609
193.8519	+27.2805	87.90	56.93	17.35	0.022664	194.2681	+27.5259	37.52	71.57	16.77	0.028606
193.8544	+27.7980	160.13	42.15	16.04	0.025488	194.2689	+27.7730	72.39	67.04	13.90	0.026075
193.8607	+27.6040	105.83	66.08	17.78	0.023562	194.2701	+26.3025	22.74	68.28	16.09	0.022767
193.8623	+27.4225	96.44	21.70	17.07	0.024880	194.2704	+27.6774	57.56	59.20	15.56	0.026974
193.8658	+27.6561	178.07	68.35	14.39	0.024335	194.2773	+28.2966	14.82	63.54	12.98	0.023429
193.8674	+27.9497	93.47	1.40	12.95	0.021676	194.2791	+28.9584	117.06	73.78	15.82	0.028498
193.8712	+27.5214	19.33	35.47	17.52	0.024211	194.2801	+29.0627	33.00	56.23	17.68	0.026353
193.8775	+27.5443	121.54	68.63	16.28	0.024352	194.2819	+27.3406	130.19	36.34	16.40	0.025202
193.8920	+27.8417	164.29	61.77	15.43	0.024259	194.2892	+27.4664	55.75	31.40	15.75	0.025774
193.8988	+27.7671	119.87	65.95	17.75	0.023271	194.2948	+27.4049	134.71	40.41	17.77	0.021619
193.9028	+26.5644	61.44	61.08	15.98	0.022006	194.2975	+29.0451	22.61	68.37	14.59	0.025888
193.9039	+26.9116	54.02	29.22	17.61	0.020721	194.2998	+27.1033	9.64	70.91	14.50	0.025514
193.9060	+26.6421	106.41	52.18	15.60	0.022749	194.3012	+28.0954	7.79	36.91	17.14	0.020719
193.9221	+27.2508	174.64	43.73	16.16	0.024576	194.3029	+28.1337	177.42	66.15	14.39	0.024294
193.9345	+27.7166	130.85	31.09	16.48	0.024791	194.3086	+27.2537	78.00	63.50	14.00	0.018403
193.9391	+27.7963	179.92	41.57	17.71	0.023790	194.3125	+26.4663	7.75	24.52	17.51	0.022478
193.9493	+28.2561	76.72	81.10	17.28	0.027942	194.3138	+27.7298	148.62	74.76	15.20	0.020074
193.9542	+27.9059	148.51	49.85	15.09	0.024057	194.3199	+27.6185	177.91	35.18	17.24	0.025083
193.9553	+27.7519	172.64	22.66	17.26	0.025131	194.3238	+28.4388	49.70	56.89	14.76	0.023937
193.9574	+27.0888	102.71	40.56	17.25	0.023782	194.3242	+27.8109	7.11	60.19	14.30	0.024806

Table 27: SDSS DR7 of galaxies in the supercluster S[195+027+0022] that have redshifts range 0.022 to 0.024.The first two columns list the right ascension and declinations.The next two columns shows position and inclination angle.The fifth and sixth columns represent the magnitude in r-band and redshift.

RA(J2000)	$Dec.(J2000)$	$P(deg)$	$i(deg)$	m_r	z	$RA(J2000)$	$Dec.(J2000)$	$P(deg)$	$i(deg)$	m_r	z
194.3261	+27.7474	69.34	58.14	15.25	0.023822	194.5649	+27.0872	28.74	68.46	14.39	0.026599
194.3273	+26.9796	45.89	53.70	16.82	0.025276	194.5689	+27.8026	48.70	59.62	17.01	0.019844
194.3291	+26.9376	141.07	48.73	16.21	0.026446	194.5725	+28.0401	166.76	25.14	14.62	0.021546
194.3316	+27.6138	6.79	73.17	15.69	0.026811	194.5759	+27.8485	39.94	68.63	14.81	0.026391
194.3332	+26.4323	52.11	59.08	17.46	0.024845	194.5760	+29.1288	23.60	56.31	16.62	0.027267
194.3395	+27.0230	47.61	55.76	17.48	0.027590	194.5776	+27.3108	140.59	57.20	16.35	0.025642
194.3404	+27.4749	18.38	13.60	16.93	0.024125	194.5799	+27.7621	26.86	69.95	13.64	0.019117
194.3406	+27.8804	43.37	45.70	17.33	0.025750	194.5806	+28.6985	89.33	52.97	16.43	0.020187
194.3455	+26.9877	56.80	68.68	17.44	0.028787	194.5822	+28.0948	84.73	49.42	16.05	0.024879
194.3455	+27.4930	60.21	44.23	17.44	0.028371	194.5845	+26.9206	35.84	58.81	16.18	0.024017
194.3482	+27.5499	135.50	62.84	14.19	0.021084	194.5855	+27.4294	20.79	63.43	16.33	0.026079
194.3515	+27.4978	63.57	46.48	14.93	0.025402	194.5904	+28.1488	99.41	45.72	16.45	0.027179
194.3544	+28.4959	5.85	79.45	13.72	0.024935	194.5910	+27.9678	141.40	33.51	16.67	0.020968
194.3552	+27.4046	173.86	33.73	16.17	0.016933	194.5916	+27.8923	156.62	66.08	14.51	0.025237
194.3577	+27.5461	142.38	54.00	17.48	0.019493	194.5923	+28.1521	114.87	54.38	16.34	0.023177
194.3588	+27.6594	141.11	35.97	17.62	0.017839	194.5928	+27.8848	101.20	21.69	16.37	0.015472
194.3616	+26.6939	162.38	36.53	17.06	0.025271	194.5988	+28.3288	23.02	10.53	17.58	0.028180
194.3645	+28.4397	96.79	66.87	16.73	0.026931	194.6054	+27.2000	81.48	43.27	16.21	0.027776
194.3646	+27.6363	14.00	63.23	17.51	0.027761	194.6064	+28.1289	155.98	37.64	17.76	0.028262
194.3673	+27.7008	37.09	50.51	15.44	0.022436	194.6128	+27.7066	99.21	44.31	17.66	0.024371
194.3685	+28.1764	131.84	55.84	17.67	0.028153	194.6129	+27.0235	53.36	59.18	14.13	0.026075
194.3750	+28.1881	157.85	67.59	15.47	0.024066	194.6160	+28.9741	146.82	7.98	14.74	0.024708
194.3775	+27.5430	168.58	48.23	16.79	0.026457	194.6184	+27.5594	31.12	85.15	16.61	0.026248
194.3800	+26.5122	8.09	74.73	17.69	0.025017	194.6230	+28.3011	105.48	62.48	16.55	0.020582
194.3801	+28.0184	166.40	56.98	17.59	0.024495	194.6259	+28.0148	94.64	35.25	17.21	0.024747
194.3831	+28.4769	110.94	39.33	16.91	0.023491	194.6261	+28.8588	15.12	59.87	16.80	0.027549
194.3868	+27.6103	107.26	34.86	16.87	0.021030	194.6285	+26.9949	52.65	49.94	16.96	0.025798
194.3912	+28.4823	25.96	23.77	16.32	0.021776	194.6290	+28.2336	51.75	49.06	14.37	0.025254
194.3945	+27.3103	44.29	38.84	17.59	0.025774	194.6317	+27.6735	59.48	50.42	15.99	0.023993
194.3994	+27.4932	78.04	30.57	15.48	0.025302	194.6330	+28.0496	22.68	34.68	16.10	0.019917
194.4006	+27.4848	47.39	57.10	16.87	0.025044	194.6336	+27.4563	74.19	61.51	16.66	0.024332
194.4011	+28.2334	74.90	48.16	13.86	0.023617	194.6345	+28.3780	65.98	47.41	17.22	0.020752
194.4019	+28.0770	71.23	46.47	17.03	0.023391	194.6381	+27.3644	166.74	59.87	17.21	0.024138
194.4023	+27.0314	117.31	44.74	12.61	0.025456	194.6407	+27.8368	138.67	59.48	16.81	0.015999
194.4050	+28.0404	11.30	33.59	16.72	0.022248	194.6466	+27.5964	80.95	36.03	14.67	0.026613
194.4293	+26.8524	134.22	67.64	15.30	0.022183	194.6472	+27.2647	63.52	28.76	14.21	0.025477
194.4301	+27.5776	156.91	29.83	14.71	0.025019	194.6503	+27.8729	19.48	56.56	16.26	0.024681
194.4338	+29.0204	92.18	52.06	17.23	0.027348	194.6515	+28.1137	57.29	63.86	15.44	0.023606
194.4388	+27.9060	5.75	41.79	16.39	0.028095	194.6515	+27.1041	140.08	58.66	17.19	0.027400
194.4403	+29.1300	174.69	57.54	16.61	0.025943	194.6531	+27.8495	8.62	12.71	16.77	0.021432
194.4406	+27.4293	90.88	83.60	16.92	0.028727	194.6553	+27.1766	16.12	45.22	16.38	0.026495
194.4423	+27.7570	119.43	84.24	16.92	0.021403	194.6576	+27.4640	153.81	82.99	16.07	0.021928
194.4446	+28.1408	60.28	73.29	14.78	0.022345	194.6590	+27.8226	21.70	59.21	17.80	0.018973
194.4460	+29.1495	172.66	39.77	14.12	0.024760	194.6600	+27.5441	166.50	53.41	17.36	0.020803
194.4471	+27.8333	91.35	67.82	16.90	0.021103	194.6612	+27.0132	120.20	78.74	15.25	0.024298
194.4494	+27.7694	93.81	54.47	14.45	0.020204	194.6623	+27.9539	130.29	68.47	15.54	0.020872
194.4503	+27.8831	70.94	46.09	17.29	0.020449	194.6664	+26.7595	118.61	74.55	15.44	0.025785
194.4528	+28.1804	49.26	44.38	12.55	0.025026	194.6697	+27.8269	85.92	64.93	13.87	0.021480
194.4574	+28.6243	148.26	57.05	13.61	0.025924	194.6734	+28.1855	121.99	47.45	15.09	0.027638
194.4593	+28.1704	103.52	52.83	13.36	0.024008	194.6775	+27.7605	87.98	38.00	17.57	0.030069
194.4607	+27.6437	78.69	21.08	16.97	0.023594	194.6801	+28.9100	18.29	33.60	16.34	0.028710
194.4610	+27.8795	21.93	47.63	14.01	0.024090	194.6829	+28.2827	133.11	43.04	15.72	0.026379
194.4615	+27.4909	36.72	44.09	15.16	0.025477	194.6840	+28.0490	160.77	49.46	15.65	0.030465
194.4680	+27.7396	77.59	30.16	16.95	0.023932	194.6894	+27.8800	64.28	41.01	15.15	0.029191
194.4714	+27.7073	40.34	66.38	15.74	0.022358	194.6898	+27.7539	122.60	20.92	17.14	0.022911
194.4747	+28.4998	104.84	50.04	14.86	0.025257	194.6921	+27.8609	78.65	41.68	14.96	0.030206
194.4765	+27.4906	58.82	63.19	16.80	0.017605	194.6975	+27.6747	48.30	43.85	17.28	0.028877
194.4807	+27.2320	94.05	53.62	14.57	0.022506	194.7006	+28.0187	176.39	53.25	13.50	0.024594
194.4843	+27.5813	104.88	49.12	16.32	0.017432	194.7030	+27.8104	73.94	50.09	15.27	0.020665
194.4855	+27.3823	114.92	14.65	17.38	0.018357	194.7039	+28.5400	86.37	48.63	17.37	0.021889
194.4861	+27.0375	160.09	60.53	15.72	0.025685	194.7115	+27.9955	87.11	23.29	14.26	0.023272
194.4863	+27.4426	70.93	53.12	17.53	0.026603	194.7115	+28.0840	163.06	52.28	14.21	0.021153
194.4867	+27.9918	113.11	51.88	17.53	0.016155	194.7118	+28.0070	110.85	31.65	17.15	0.025802
194.4905	+28.0618	71.98	30.17	16.21	0.028047	194.7171	+27.7851	101.97	53.37	15.04	0.019787
194.4942	+26.9393	38.35	70.25	14.80	0.026378	194.7206	+28.2338	46.32	54.40	15.72	0.021174
194.5031	+27.4540	116.96	52.89	15.98	0.026501	194.7211	+27.8134	82.84	64.60	17.34	0.019317
194.5065	+27.4897	84.09	57.02	14.84	0.026348	194.7227	+28.1261	177.20	45.86	15.42	0.024283
194.5071	+27.8536	91.02	43.18	14.96	0.019879	194.7232	+28.2890	39.71	46.24	16.97	0.027047
194.5099	+26.8595	75.73	30.52	16.31	0.025461	194.7269	+28.2230	174.35	30.66	16.49	0.024548
194.5119	+27.9783	12.44	67.49	14.40	0.022850	194.7276	+27.7956	141.39	45.84	16.31	0.022477
194.5132	+26.9160	130.00	52.24	14.70	0.028309	194.7302	+27.9647	180.22	49.08	16.63	0.019792
194.5146	+27.8149	145.08	59.68	17.38	0.024690	194.7338	+28.4636	172.65	49.37	17.01	0.020711
194.5147	+27.6824	101.21	57.36	17.01	0.025078	194.7359	+27.8220	23.38	44.91	16.88	0.030067
194.5201	+26.3706	55.78	28.62	17.03	0.024107	194.7401	+27.7854	56.76	72.98	14.98	0.024089
194.5233	+28.2426	152.85	72.01	15.24	0.024864	194.7421	+27.5947	96.84	56.96	16.35	0.020949
194.5234	+29.0174	122.95	81.04	17.55	0.026581	194.7478	+27.9345	35.61	40.67	17.51	0.020098
194.5243	+28.3710	53.55	60.19	17.75	0.026387	194.7503	+27.9675	149.48	45.72	17.62	0.028655
194.5253	+27.4189	48.32	57.10	16.72	0.020133	194.7568	+27.5369	179.94	43.34	17.11	0.029370
194.5284	+27.5769	105.48	27.76	15.21	0.025896	194.7575	+28.2254	116.67	55.80	17.55	0.027662
194.5285	+29.0345	43.45	52.39	15.19	0.025160	194.7576	+26.8157	93.03	48.50	13.78	0.024791
194.5295	+26.7871	76.74	51.91	17.40	0.024967	194.7663	+28.1237	117.62	36.28	17.31	0.027358
194.5384	+28.7086	87.25	74.22	16.10	0.026374	194.7673	+27.9591	105.47	56.25	14.08	0.024373
194.5386	+26.6641	144.83	70.45	16.69	0.025270	194.7693	+27.9110	38.04	66.68	17.18	0.022249
194.5404	+27.5494	37.10	44.69	15.38	0.024158	194.7693	+26.9582	99.91	73.82	17.50	0.027967
194.5463	+27.8603	67.52	33.28	17.30	0.024232	194.7699	+28.0504	121.78	58.87	15.36	0.027838
194.5476	+27.9399	77.95	0.53	16.98	0.029304	194.7721	+27.6444	24.76	34.09	17.68	0.019008
194.5485	+27.8937	119.40	44.25	15.33	0.020007	194.7751	+27.9967	25.99	45.99	14.65	0.026482
194.5486	+27.5425	132.35	55.76	17.69	0.024607	194.7763	+27.4936	159.80	41.77	17.48	0.028228
194.5555	+28.9481	8.10	75.73	16.54	0.026466	194.7785	+27.7725	64.10	48.38	15.79	0.021767
194.5575	+28.1825	59.57	67.71	14.55	0.024850	194.7812	+27.7678	134.72	29.62	15.29	0.022128
194.5628	+28.5218	92.93	49.67	16.24	0.023965	194.7831	+27.8550	82.65	31.30	17.23	0.022842

Table 28: SDSS DR7 of galaxies in the supercluster S[195+027+0022] that have redshifts range 0.022 to 0.024.The first two columns list the right ascension and declinations.The next two columns shows position and inclination angle.The fifth and sixth columns represent the magnitude in r-band and redshift.

RA(J2000)	$Dec.(J2000)$	$P(deg)$	$i(deg)$	m_r	z	$RA(J2000)$	$Dec.(J2000)$	$P(deg)$	$i(deg)$	m_r	z
194.7842	+27.7841	95.08	34.42	17.57	0.024370	194.9838	+27.7463	37.76	73.62	15.25	0.030807
194.7856	+28.7282	28.43	70.43	16.32	0.024584	194.9860	+27.9300	77.97	55.58	15.32	0.026611
194.7878	+27.8976	53.96	24.46	15.37	0.027061	194.9900	+28.0651	44.92	41.27	15.37	0.020408
194.7894	+28.0409	105.70	68.75	14.02	0.024947	194.9906	+28.2467	178.53	25.16	15.10	0.023273
194.7902	+27.8674	79.80	41.82	15.52	0.023963	194.9978	+27.9406	108.44	20.04	17.25	0.021237
194.7913	+28.1645	180.31	78.98	16.68	0.029565	195.0040	+27.9454	168.51	18.16	15.79	0.023738
194.7925	+26.7204	39.58	80.38	15.74	0.025385	195.0049	+26.9561	30.72	70.70	16.31	0.024804
194.7929	+27.6199	141.74	35.77	15.01	0.020052	195.0062	+27.7313	171.87	58.23	14.29	0.027848
194.7981	+28.0093	162.18	39.05	16.88	0.023930	195.0076	+28.4348	181.85	47.46	17.70	0.027867
194.8062	+27.7746	79.17	50.45	15.73	0.023678	195.0125	+28.2403	30.75	43.99	17.29	0.026602
194.8071	+27.4026	134.70	50.11	15.95	0.019779	195.0156	+27.9647	87.36	49.02	14.98	0.018694
194.8080	+28.0762	58.58	21.85	14.13	0.026942	195.0177	+28.1551	76.80	63.42	17.55	0.022841
194.8109	+27.8956	64.75	41.70	13.48	0.022280	195.0183	+28.6035	8.41	36.82	13.86	0.023646
194.8124	+28.2510	105.28	64.66	13.35	0.025884	195.0185	+27.9876	167.57	22.77	17.70	0.022164
194.8135	+27.9707	23.57	45.59	16.04	0.016998	195.0191	+27.0325	165.12	74.78	16.80	0.024156
194.8184	+27.1581	162.91	50.09	15.35	0.023224	195.0225	+28.0244	157.72	56.60	17.43	0.020590
194.8195	+27.1061	132.39	74.81	16.83	0.028884	195.0229	+27.8076	6.68	73.00	16.77	0.022828
194.8265	+27.7157	67.33	34.86	16.63	0.023215	195.0237	+27.9265	154.11	56.08	16.29	0.027427
194.8269	+27.5135	19.00	70.35	14.44	0.021156	195.0254	+27.9783	128.92	75.38	16.31	0.026360
194.8273	+27.5936	82.12	50.07	14.29	0.018669	195.0261	+27.6853	164.83	40.99	16.69	0.026083
194.8321	+27.9735	70.87	55.54	17.56	0.025045	195.0262	+27.3007	32.83	62.81	15.81	0.027167
194.8328	+28.0843	112.85	59.78	16.51	0.016200	195.0262	+27.7758	147.88	55.95	16.29	0.021512
194.8341	+27.8860	51.96	64.85	14.73	0.022512	195.0266	+28.0041	168.91	16.55	15.19	0.025163
194.8342	+28.0743	81.97	24.47	14.51	0.024787	195.0311	+27.9581	82.99	17.20	14.14	0.021537
194.8346	+27.4352	170.42	24.36	14.09	0.026614	195.0333	+28.0786	127.46	43.75	16.45	0.025035
194.8376	+28.4415	49.44	71.93	16.35	0.022815	195.0336	+27.7733	104.29	70.18	15.29	0.029975
194.8392	+27.9736	84.15	66.53	17.08	0.021108	195.0339	+27.9769	79.18	47.97	16.53	0.022420
194.8443	+27.8969	42.91	31.41	16.50	0.018095	195.0364	+28.1599	131.78	8.75	13.43	0.025799
194.8465	+28.4886	176.08	52.43	16.39	0.024259	195.0380	+28.1704	101.18	50.12	17.18	0.023409
194.8476	+27.9196	111.13	24.82	17.56	0.024050	195.0381	+27.8665	177.00	45.94	17.15	0.018609
194.8525	+27.5173	117.52	38.67	17.34	0.020652	195.0431	+27.9591	44.96	68.80	17.00	0.022036
194.8539	+27.7388	13.34	55.91	15.35	0.021006	195.0434	+27.5950	169.30	47.78	16.36	0.019566
194.8544	+27.9967	72.28	39.94	16.87	0.019261	195.0464	+28.0652	173.62	24.50	16.42	0.025424
194.8555	+27.9679	62.82	45.23	14.52	0.026626	195.0467	+27.4601	92.60	55.37	16.19	0.023713
194.8556	+27.9345	81.69	30.20	14.38	0.026243	195.0526	+27.7818	50.39	19.69	16.49	0.024288
194.8562	+27.9732	41.93	53.50	14.19	0.021217	195.0536	+28.0755	140.51	51.93	17.32	0.025927
194.8576	+28.1870	114.70	15.32	17.51	0.026682	195.0559	+28.0533	80.51	85.64	15.41	0.028237
194.8589	+28.2875	39.33	56.66	16.43	0.027583	195.0568	+27.8672	99.08	43.68	14.16	0.025573
194.8608	+27.9985	139.30	46.48	14.45	0.023128	195.0584	+28.8282	182.21	61.21	16.69	0.025381
194.8638	+27.7851	123.28	75.45	15.36	0.022900	195.0592	+28.4581	88.59	55.18	15.69	0.026921
194.8697	+28.0405	8.88	59.27	16.06	0.019638	195.0614	+28.0413	53.66	28.03	14.86	0.020042
194.8725	+27.8502	152.80	63.99	16.91	0.023567	195.0651	+27.2567	5.50	39.41	17.77	0.024660
194.8748	+27.9564	175.50	53.23	16.50	0.023581	195.0688	+27.9675	34.34	66.59	13.84	0.016370
194.8755	+28.7001	116.67	35.03	16.99	0.024642	195.0709	+28.0639	91.43	46.39	15.48	0.021376
194.8777	+27.7914	121.18	27.24	17.12	0.026822	195.0731	+27.7844	115.28	12.64	15.43	0.024254
194.8784	+27.8842	151.21	39.37	13.58	0.016617	195.0747	+28.2024	153.45	61.25	14.92	0.029351
194.8796	+27.9549	173.47	41.82	15.39	0.024494	195.0754	+27.9566	135.35	36.83	15.87	0.022165
194.8810	+28.0466	122.45	67.99	16.21	0.023990	195.0773	+28.0972	163.09	33.40	17.51	0.026989
194.8817	+28.1005	132.52	10.33	17.59	0.025739	195.0774	+27.8155	80.38	34.38	14.68	0.018810
194.8829	+27.8613	98.30	23.06	16.80	0.016459	195.0782	+27.9370	23.60	57.80	16.82	0.018556
194.8837	+27.7205	140.59	14.73	16.29	0.026364	195.0787	+28.0093	44.88	29.39	11.72	0.021555
194.8866	+27.9836	103.17	41.37	15.30	0.020330	195.0796	+27.5537	81.40	36.87	15.78	0.020534
194.8922	+27.9468	102.06	27.53	15.80	0.024865	195.0797	+28.8781	155.08	39.63	14.85	0.025682
194.8970	+27.8636	62.07	30.26	17.71	0.021888	195.0828	+28.4392	8.21	59.72	15.44	0.024645
194.8986	+28.5514	136.39	56.67	17.11	0.026207	195.0840	+27.8435	183.26	55.09	17.53	0.027178
194.8988	+27.9593	51.67	17.93	15.19	0.024817	195.0903	+27.8985	85.78	44.42	15.84	0.017205
194.9040	+27.8258	60.24	45.71	17.18	0.021750	195.0922	+28.0470	93.98	35.99	16.86	0.028179
194.9056	+27.3360	70.37	52.66	15.57	0.024215	195.0925	+28.2471	34.60	76.13	17.60	0.026032
194.9062	+28.1661	103.09	50.67	17.02	0.019995	195.0932	+27.6236	179.79	68.63	15.64	0.026296
194.9076	+27.7768	98.80	67.07	15.45	0.023652	195.0946	+28.5745	31.60	39.50	15.06	0.022460
194.9080	+27.9073	114.38	39.69	16.54	0.027629	195.0996	+27.2869	166.92	53.45	17.46	0.025166
194.9083	+28.0010	102.85	13.76	16.05	0.017556	195.1034	+27.9266	164.06	68.58	16.50	0.027405
194.9096	+27.9872	46.54	50.35	15.75	0.023628	195.1049	+27.5523	173.84	61.20	14.12	0.025150
194.9152	+27.9539	179.35	67.36	16.76	0.027682	195.1069	+28.8678	175.80	52.13	17.71	0.023494
194.9159	+27.5765	160.03	40.91	15.58	0.017583	195.1119	+27.5156	51.65	39.99	14.76	0.026862
194.9178	+27.9682	53.52	54.47	14.55	0.026171	195.1152	+27.6252	110.25	48.79	17.68	0.020496
194.9197	+28.1446	173.69	32.73	14.02	0.026545	195.1161	+27.2718	9.64	64.01	14.33	0.026806
194.9221	+28.5072	124.14	22.64	17.09	0.028446	195.1165	+27.9560	32.92	41.43	15.36	0.024275
194.9221	+27.6598	90.88	15.91	15.71	0.023385	195.1183	+27.9724	96.56	63.67	17.23	0.026645
194.9263	+27.9247	82.96	34.02	14.30	0.023956	195.1215	+26.6754	49.67	50.09	13.18	0.024875
194.9322	+27.9947	108.41	14.25	20.20	0.023142	195.1218	+27.5148	166.32	57.35	14.84	0.025652
194.9339	+28.1763	137.88	29.96	13.79	0.028646	195.1223	+28.4556	131.37	58.88	17.06	0.025077
194.9342	+27.9584	16.08	66.45	17.59	0.023951	195.1247	+27.7703	57.11	64.82	16.12	0.028694
194.9342	+27.8677	132.72	49.14	17.24	0.021707	195.1258	+28.1600	145.70	52.86	15.72	0.024433
194.9350	+27.9125	22.88	48.56	17.51	0.023270	195.1282	+28.3464	5.67	59.03	17.11	0.020778
194.9357	+28.2565	103.41	58.64	14.21	0.027104	195.1285	+27.3002	154.40	49.61	14.84	0.026598
194.9362	+27.8898	26.76	47.48	14.49	0.023601	195.1290	+28.1084	77.31	57.77	17.30	0.018230
194.9422	+27.8572	152.64	52.82	16.38	0.027898	195.1353	+28.2561	128.54	60.88	17.72	0.021840
194.9456	+27.9919	137.86	27.41	15.05	0.029023	195.1355	+27.7661	105.71	64.09	16.75	0.023151
194.9465	+27.7103	166.69	66.59	12.16	0.028891	195.1390	+27.8242	165.25	65.42	16.94	0.028274
194.9490	+28.0979	171.69	45.81	16.34	0.022226	195.1398	+27.5041	52.03	45.56	14.48	0.019533
194.9552	+26.9743	145.30	53.02	16.35	0.024433	195.1403	+27.6377	61.42	51.65	16.82	0.025879
194.9591	+27.9126	148.93	36.30	16.49	0.025069	195.1434	+27.9347	70.62	9.96	16.19	0.030138
194.9595	+28.1444	162.90	66.31	15.79	0.023534	195.1476	+27.9427	115.21	59.38	16.36	0.024093
194.9625	+27.8330	15.47	70.88	14.67	0.027281	195.1482	+28.1461	169.21	82.83	17.69	0.019138
194.9644	+28.0735	20.59	27.56	17.88	0.025921	195.1486	+27.5742	56.55	81.60	16.90	0.017900
194.9657	+28.0985	38.98	50.40	14.90	0.026427	195.1548	+28.6641	28.88	65.21	16.39	0.024502
194.9764	+26.8200	141.72	33.46	15.08	0.027728	195.1578	+28.0580	152.74	69.93	14.25	0.026342
194.9786	+27.7960	31.41	24.47	15.66	0.028394	195.1615	+28.0145	83.60	52.72	15.19	0.026255
194.9795	+28.1284	48.45	35.78	15.33	0.026144	195.1648	+29.0194	55.28	60.77	16.68	0.025187
194.9834	+28.0347	97.32	40.04	17.60	0.028096	195.1657	+27.9239	31.83	35.41	17.75	0.025914

Table 29: SDSS DR7 of galaxies in the supercluster S[195+027+0022] that have redshifts range 0.022 to 0.024.The first two columns list the right ascension and declinations.The next two columns shows position and inclination angle.The fifth and sixth columns represent the magnitude in r-band and redshift.

RA(J2000)	$Dec.(J2000)$	$P(deg)$	$i(deg)$	m_r	z	$RA(J2000)$	$Dec.(J2000)$	$P(deg)$	$i(deg)$	m_r	z
195.1702	+27.9966	45.90	59.58	15.12	0.024532	195.5897	+28.2308	62.78	68.45	16.36	0.019482
195.1716	+28.0451	168.73	31.35	14.95	0.029664	195.5902	+28.2560	59.20	60.31	14.25	0.023672
195.1781	+27.9713	53.88	35.35	14.26	0.022173	195.6043	+27.9723	50.59	39.94	17.49	0.028451
195.1785	+27.9631	59.40	45.86	15.64	0.028998	195.6069	+28.8581	53.13	66.10	16.94	0.023233
195.1828	+28.4163	33.09	30.43	17.37	0.021849	195.6158	+29.4876	155.22	37.71	17.13	0.024460
195.1843	+28.3373	49.68	63.70	17.61	0.027319	195.6328	+27.9355	42.93	50.26	17.39	0.022972
195.1860	+28.1006	124.05	73.81	17.26	0.022892	195.6332	+28.4393	109.24	41.21	15.40	0.020786
195.1891	+27.8355	107.22	60.33	13.69	0.030163	195.6357	+27.3935	88.03	45.95	16.24	0.019134
195.1975	+27.9222	34.96	60.20	17.66	0.029476	195.6450	+27.9491	184.86	63.73	14.60	0.020189
195.1982	+29.0672	80.68	31.06	17.51	0.025974	195.6466	+27.4394	56.80	59.85	17.71	0.018947
195.2027	+28.0907	107.32	50.45	16.78	0.024161	195.6480	+28.7452	145.45	71.94	12.85	0.021330
195.2033	+28.1583	32.90	56.06	17.15	0.020301	195.6556	+27.1761	156.73	48.76	15.57	0.019190
195.2080	+27.4058	155.69	49.74	15.57	0.022880	195.6590	+28.5019	33.43	67.34	13.48	0.020101
195.2129	+27.7430	134.16	62.72	16.12	0.027971	195.6602	+28.1146	152.17	58.10	17.41	0.025756
195.2132	+28.0471	12.07	45.54	16.04	0.022036	195.6612	+29.0756	140.03	26.76	14.94	0.022993
195.2170	+28.3661	20.12	43.31	15.15	0.026378	195.6700	+28.3713	124.91	82.31	15.19	0.025665
195.2188	+27.8050	28.30	39.74	17.12	0.023678	195.6850	+28.0453	48.67	36.73	13.69	0.021654
195.2197	+27.8256	169.81	52.35	17.07	0.017437	195.7135	+28.4824	75.46	68.19	17.12	0.024421
195.2255	+27.7837	50.94	63.59	14.81	0.028573	195.7198	+27.8666	134.92	67.29	17.29	0.028294
195.2269	+28.0076	105.01	40.13	15.11	0.017512	195.7357	+28.0704	132.73	62.91	14.39	0.026786
195.2282	+27.8420	157.52	63.93	16.93	0.024533	195.7477	+28.2754	99.13	60.40	17.55	0.024799
195.2300	+27.1216	35.06	63.68	14.97	0.022569	195.7536	+28.0325	76.94	68.05	14.19	0.018841
195.2330	+27.8985	139.62	60.41	14.83	0.020909	195.7717	+27.7841	21.26	65.13	17.15	0.026474
195.2336	+27.7909	132.09	39.31	13.74	0.027539	195.7906	+28.5835	36.45	72.84	15.39	0.023736
195.2432	+27.6521	178.41	52.86	14.13	0.018283	195.7910	+28.4896	174.00	70.26	16.87	0.018967
195.2701	+27.8917	179.18	50.29	14.57	0.020177	195.8026	+28.1725	61.02	67.97	15.02	0.025151
195.2736	+28.0621	143.81	67.56	17.26	0.025816	195.8069	+27.3691	98.77	68.97	17.76	0.022169
195.2742	+27.7089	9.79	42.71	13.99	0.030051	195.8177	+28.0304	98.71	84.63	16.00	0.021219
195.2758	+27.3978	47.52	38.79	14.79	0.027951	195.8325	+28.6173	91.07	75.35	14.40	0.020747
195.2783	+26.8095	150.75	46.34	16.33	0.023860	195.8398	+28.3090	96.64	54.96	14.73	0.019298
195.2876	+28.3598	144.58	33.22	14.61	0.023919	195.8441	+28.7965	58.07	28.79	17.72	0.027276
195.2885	+27.8183	43.56	44.03	15.42	0.020622	195.8449	+27.9360	116.23	52.49	16.67	0.020998
195.2893	+28.0331	109.73	23.50	17.50	0.024358	195.8464	+28.8642	49.51	22.62	16.65	0.022790
195.2946	+27.8029	126.98	56.02	16.84	0.023218	195.8477	+27.3070	141.47	64.89	16.09	0.019487
195.2947	+27.2465	134.13	22.61	15.27	0.021585	195.8555	+28.0140	48.25	56.48	15.78	0.027456
195.2968	+27.7425	127.09	41.74	17.15	0.025444	195.8751	+28.2747	99.47	65.99	17.15	0.022320
195.3068	+27.9143	111.09	21.54	13.97	0.020429	195.8801	+28.0923	62.41	68.56	14.98	0.022010
195.3069	+28.0831	20.37	35.23	13.32	0.020280	195.8893	+29.0605	9.92	45.02	15.76	0.026106
195.3133	+27.6692	116.91	72.36	14.06	0.024443	195.8904	+28.2394	37.86	63.49	16.19	0.028344
195.3233	+27.8091	141.55	52.65	16.73	0.025260	195.8998	+28.1670	100.95	73.04	15.09	0.023001
195.3243	+28.0971	158.37	64.17	16.11	0.027740	195.9024	+28.0980	166.85	21.38	16.37	0.021550
195.3294	+28.1281	41.46	64.73	13.70	0.023622	195.9259	+28.9055	159.71	53.05	14.80	0.023200
195.3305	+27.8605	119.59	27.55	17.65	0.028420	195.9368	+28.5459	157.16	61.42	17.66	0.026675
195.3333	+27.9610	132.02	41.58	17.27	0.027204	195.9373	+28.0842	107.38	52.14	14.44	0.019664
195.3449	+28.1960	105.77	47.95	15.08	0.026263	195.9428	+27.9869	80.30	64.22	13.79	0.021516
195.3553	+29.3138	155.10	47.92	13.22	0.024202	195.9581	+28.1857	88.14	68.28	16.79	0.024147
195.3589	+27.8860	112.72	44.42	16.38	0.019155	195.9602	+28.1786	117.31	60.95	14.32	0.022209
195.3612	+28.4359	125.70	57.55	17.57	0.020088	195.9604	+28.0544	172.96	79.03	14.74	0.021873
195.3631	+27.9992	160.02	40.20	16.84	0.026407	195.9617	+27.9884	85.00	21.37	16.66	0.022077
195.3686	+27.9265	132.80	58.38	12.96	0.025967	195.9768	+28.3106	165.39	63.32	13.19	0.027645
195.3700	+27.2657	86.95	72.99	15.12	0.020894	195.9786	+28.1876	130.10	40.87	15.42	0.023819
195.3825	+27.8475	74.17	39.90	16.83	0.019129	196.0198	+27.8505	73.63	82.13	14.25	0.022209
195.3900	+29.1306	134.02	63.52	17.42	0.025444	196.0332	+27.9649	51.06	35.59	17.00	0.020701
195.3910	+27.9111	149.28	66.23	17.69	0.022703	196.0423	+28.2480	24.72	35.81	16.24	0.020705
195.3968	+28.1469	184.33	71.98	15.92	0.018521	196.0469	+27.4904	31.47	39.63	15.43	0.018608
195.4022	+27.7079	4.81	71.89	17.10	0.027302	196.0547	+28.5425	17.57	63.89	14.08	0.027954
195.4055	+28.0158	123.65	45.76	15.09	0.024718	196.0578	+27.5601	124.11	48.56	16.09	0.024162
195.4129	+28.2459	142.81	70.95	15.00	0.026240	196.0657	+28.5454	97.47	73.02	15.72	0.028748
195.4189	+27.5489	81.01	71.09	16.11	0.022678	196.0686	+27.5064	64.07	22.40	17.45	0.024518
195.4303	+28.2978	6.19	60.12	14.92	0.026590	196.0747	+29.0295	101.56	61.34	15.11	0.023645
195.4305	+29.1784	103.65	50.05	16.38	0.024301	196.0768	+28.4681	182.18	60.19	15.66	0.026677
195.4307	+29.0447	87.54	69.73	17.71	0.024472	196.0945	+28.8108	182.26	43.25	17.36	0.027254
195.4333	+28.9995	25.97	74.51	15.42	0.022313	196.1106	+27.3043	69.75	50.02	14.99	0.019287
195.4341	+28.2144	107.17	75.69	15.58	0.027027	196.1221	+28.9875	28.56	31.28	16.56	0.024956
195.4459	+28.0950	89.49	63.38	17.16	0.020245	196.1306	+28.3019	169.34	50.00	15.83	0.027160
195.4461	+29.0766	167.37	44.08	16.34	0.023946	196.1490	+28.6277	88.23	59.93	16.96	0.023247
195.4468	+27.6218	115.50	55.86	16.17	0.026903	196.1538	+28.2505	178.59	77.55	17.01	0.019650
195.4499	+27.3548	4.84	71.04	13.82	0.021144	196.1616	+28.9727	124.85	48.64	17.05	0.026226
195.4512	+27.7284	9.99	69.02	17.41	0.019165	196.1737	+28.2275	25.34	24.43	17.70	0.024915
195.4516	+27.6040	34.30	70.84	16.80	0.028357	196.1806	+28.2516	65.75	74.83	15.29	0.022837
195.4536	+28.1719	142.95	70.59	16.88	0.026318	196.2053	+28.6612	118.46	74.27	16.16	0.027151
195.4593	+27.8935	49.35	31.26	17.49	0.026093	196.2057	+28.2694	132.20	0.87	14.38	0.023617
195.4628	+27.4118	6.56	79.54	14.82	0.021326	196.2638	+27.5371	103.26	66.45	16.81	0.022609
195.4739	+27.6244	56.17	35.35	14.07	0.027135	196.2852	+27.5128	68.57	82.79	12.79	0.024784
195.4826	+29.3228	157.80	39.39	12.56	0.024603	196.2872	+29.8810	58.11	25.76	16.75	0.024013
195.4899	+28.0058	14.85	44.11	16.48	0.026664	196.3016	+27.5698	89.83	44.49	16.14	0.023868
195.4972	+28.7095	163.34	47.82	15.68	0.021148	196.3021	+28.1524	122.16	61.06	14.29	0.022638
195.5006	+27.7827	59.71	75.35	16.92	0.024759	196.3141	+28.6264	87.15	74.50	16.77	0.022807
195.5043	+27.6530	29.08	57.34	17.78	0.024553	196.3186	+29.5876	127.41	76.85	15.31	0.024587
195.5175	+29.2535	155.42	77.15	13.57	0.025212	196.3231	+28.5827	182.78	54.42	16.40	0.026990
195.5181	+27.6995	70.90	54.30	13.41	0.024267	196.3315	+29.1974	155.90	63.47	15.00	0.027902
195.5250	+27.7651	92.90	84.41	16.67	0.025076	196.3455	+27.6787	8.48	55.14	14.31	0.023693
195.5328	+27.6483	75.79	64.88	16.96	0.023838	196.3552	+29.2965	178.25	55.33	15.14	0.024429
195.5340	+28.1510	13.59	23.20	16.64	0.017221	196.4107	+29.3502	172.25	54.91	17.35	0.024800
195.5361	+28.3871	58.89	56.14	17.32	0.026164	196.4382	+27.3154	36.54	74.70	17.66	0.022088
195.5390	+27.5894	178.37	39.58	16.85	0.022422	196.4390	+28.8713	26.51	58.12	17.52	0.027436
195.5429	+28.1918	117.19	34.28	17.51	0.020015	196.4536	+28.1065	180.75	54.23	16.71	0.025284
195.5464	+28.4566	166.89	15.40	17.38	0.021315	196.4625	+29.8100	147.03	12.08	14.51	0.024489
195.5533	+28.2148	166.85	40.86	16.47	0.028212	196.4729	+28.1124	174.70	71.41	15.14	0.025479
195.5589	+28.5071	10.85	68.05	13.74	0.023822	196.4985	+29.2788	178.57	27.94	14.98	0.027303
195.5597	+28.1016	12.41	54.13	14.95	0.020725	196.5217	+28.7874	75.65	58.30	15.13	0.023825

Table 30: SDSS DR7 of galaxies in the supercluster S[195+027+0022] that have redshifts range 0.022 to 0.024.The first two columns list the right ascension and declinations.The next two columns shows position and inclination angle.The fifth and sixth columns represent the magnitude in r-band and redshift.

RA(J2000)	$Dec.(J2000)$	$P(deg)$	$i(deg)$	m_r	z	$RA(J2000)$	$Dec.(J2000)$	$P(deg)$	$i(deg)$	m_r	z
196.5230	+28.5929	38.93	48.10	17.76	0.027317	194.0599	+30.2001	40.23	66.56	17.43	0.025919
196.5397	+28.0644	22.13	46.01	17.52	0.026679	194.1148	+30.4333	57.79	79.45	13.40	0.026212
196.5462	+27.7002	139.05	64.62	15.55	0.023276	194.2279	+30.6764	118.18	52.67	16.81	0.024990
196.5567	+29.1415	14.65	59.59	16.50	0.024047	194.2411	+30.7160	169.07	34.54	16.17	0.025119
196.5630	+29.3662	68.87	59.61	16.57	0.025333	194.2737	+30.6651	77.46	36.18	16.40	0.025419
196.5721	+29.0632	140.93	63.12	17.20	0.024317	194.0771	+29.8078	161.11	41.08	16.13	0.024267
196.5808	+28.0525	178.95	62.68	17.04	0.024976	194.1461	+29.7474	134.26	67.43	16.17	0.025320
196.5894	+29.1701	51.13	28.90	16.34	0.025171	194.2063	+31.4988	129.14	63.64	16.64	0.023788
196.6350	+28.9022	76.99	59.08	15.70	0.024606	194.2620	+31.6255	107.01	74.02	13.16	0.024164
196.6376	+29.3656	168.57	61.63	16.50	0.025182	194.4850	+32.4817	64.76	71.49	17.05	0.024110
196.6663	+28.5175	106.53	30.46	15.68	0.027098	194.5416	+24.3489	145.13	57.51	18.03	0.023598
196.6690	+28.9300	136.56	64.31	17.73	0.026036	194.6448	+24.3935	174.94	53.29	16.83	0.023402
196.6714	+27.8841	47.15	69.94	12.92	0.024437	194.6899	+24.2339	141.44	54.77	15.08	0.023903
196.6746	+28.9068	28.02	33.26	16.12	0.026656	194.8451	+29.8879	124.59	84.95	14.11	0.025659
196.6876	+29.3716	172.89	56.32	16.79	0.027318	195.0047	+29.9041	48.79	30.64	17.11	0.025264
196.6955	+29.1307	42.29	35.84	16.92	0.027310	194.8745	+31.3356	29.73	34.44	17.05	0.026011
196.8050	+28.0469	179.70	19.13	17.16	0.025264	194.9887	+31.5060	165.93	72.31	16.27	0.026610
196.8173	+28.2839	180.81	56.47	16.88	0.025681	194.8771	+26.4353	96.92	56.83	17.10	0.021901
196.9165	+28.8288	172.58	80.14	17.75	0.026912	195.0436	+26.4612	171.25	57.67	16.01	0.022969
196.9912	+28.7106	94.94	44.30	14.23	0.026123	195.0273	+29.4627	10.75	71.07	17.37	0.022660
197.0099	+28.2514	65.80	83.02	17.01	0.025983	195.0447	+29.4665	74.36	70.02	13.97	0.023843
197.1150	+28.3506	144.59	73.95	17.00	0.024703	195.4408	+33.4328	28.61	60.07	15.62	0.024961
197.2148	+28.6293	29.92	75.56	16.66	0.023643	195.5915	+33.2151	179.94	67.78	13.57	0.024876
197.2732	+28.4909	166.10	33.97	15.64	0.026649	195.5230	+27.2973	63.63	82.03	17.26	0.025219
197.3014	+28.4677	166.52	50.23	15.53	0.026443	195.6364	+27.2956	118.30	66.84	15.33	0.026238
197.3267	+28.2126	38.96	45.25	15.34	0.025457	195.5762	+32.8906	98.34	74.05	17.11	0.026145
197.4407	+28.6212	155.20	53.67	14.13	0.023491	195.6640	+25.3836	57.41	52.00	16.76	0.025089
197.4671	+28.3824	74.89	69.87	17.27	0.024644	195.7740	+25.4752	5.54	59.43	15.20	0.025220
197.4870	+28.5581	31.23	19.17	14.31	0.024098	195.6860	+32.0850	118.35	61.63	14.61	0.025234
197.5346	+28.2899	47.10	30.44	16.86	0.024214	195.6866	+31.4782	66.12	35.50	17.80	0.025042
197.7424	+28.5189	82.35	20.14	14.89	0.025292	195.8592	+31.4561	10.46	53.09	15.10	0.024708
191.5423	+30.7319	3.36	65.42	17.22	0.023059	195.9876	+31.6131	24.18	66.12	15.69	0.024437
191.5469	+30.7228	35.64	54.40	17.62	0.022658	196.0911	+31.8829	51.99	37.95	17.57	0.024477
191.5641	+30.6349	14.70	71.71	13.13	0.022750	195.7268	+23.6572	26.69	64.68	15.48	0.025726
191.6131	+30.5158	175.55	56.31	16.55	0.022966	195.8226	+26.0601	33.37	78.66	13.62	0.025809
191.7521	+30.7276	104.63	26.77	15.37	0.023035	196.0618	+26.1162	109.19	44.47	16.23	0.025779
191.5751	+32.1876	159.48	43.78	15.96	0.023773	195.8712	+26.5505	131.93	60.69	14.78	0.022969
191.6060	+32.1819	137.84	63.03	17.76	0.023856	195.9880	+26.7295	97.52	42.15	16.94	0.022960
191.7200	+33.0625	43.18	53.08	16.01	0.023495	196.2182	+26.9191	159.38	45.49	17.68	0.024018
191.7590	+32.8712	18.99	20.14	16.31	0.023688	196.3487	+27.1016	52.07	69.31	15.18	0.025113
191.7964	+29.1885	171.48	87.99	16.88	0.024027	196.3567	+27.0797	18.94	43.45	17.47	0.024599
191.8522	+29.2074	24.97	59.73	16.46	0.024213	196.5759	+27.2550	67.07	60.16	17.29	0.026206
192.0248	+29.4432	23.21	37.16	16.29	0.024020	196.6483	+27.1687	55.17	25.26	15.20	0.026671
192.1259	+29.2602	131.09	63.70	16.20	0.025909	196.0305	+25.7251	39.89	82.42	17.08	0.025146
192.1599	+29.1903	70.89	48.42	16.50	0.024728	196.2127	+25.8393	71.15	57.45	16.28	0.025160
192.1781	+29.2393	69.24	69.05	14.89	0.024212	196.2377	+25.5835	170.50	53.23	16.14	0.022763
192.2062	+29.4243	7.21	72.99	14.79	0.023558	196.4946	+25.4657	104.53	41.01	16.44	0.022658
191.8463	+27.4650	29.28	41.08	16.41	0.023055	196.3168	+25.9576	22.11	26.42	14.83	0.022648
191.8682	+27.4578	24.96	62.85	14.43	0.023026	196.4130	+26.1066	83.60	22.01	16.40	0.021992
192.0129	+26.6332	102.35	7.91	15.75	0.022901	196.5630	+25.4605	148.74	52.89	17.58	0.025083
192.1753	+26.4173	5.24	79.57	17.04	0.023981	196.6082	+25.2381	179.64	75.68	17.16	0.025824
192.1453	+28.8470	154.04	42.78	15.65	0.023362	196.6516	+25.4296	42.40	52.84	15.01	0.024875
192.4220	+28.8448	121.17	56.70	16.30	0.022666	196.6408	+24.9628	67.57	61.15	17.61	0.022012
192.2035	+24.9992	63.59	26.43	17.41	0.023760	196.9284	+24.8106	98.51	60.79	16.76	0.022010
192.5251	+25.0222	136.45	30.12	17.63	0.022561	196.6516	+27.8730	132.82	63.18	15.05	0.021816
192.2435	+27.8358	97.09	64.30	15.84	0.026725	196.8469	+27.8655	36.05	59.85	16.10	0.021368
192.4349	+27.6696	30.19	86.79	15.13	0.026354	197.1256	+27.8793	111.93	0.60	15.86	0.021254
192.3393	+34.2584	68.13	44.29	15.99	0.023186	196.6544	+28.2347	85.97	53.12	17.08	0.022239
192.4166	+34.2551	54.84	43.25	16.18	0.023082	196.6550	+28.3376	10.52	46.12	13.62	0.022538
192.4271	+34.0993	172.19	53.84	17.08	0.023062	196.7290	+28.5480	95.75	53.08	15.59	0.021762
192.5074	+34.4866	36.35	51.85	13.82	0.023740	196.8088	+28.2582	124.21	75.86	16.01	0.022276
192.7206	+34.1569	51.00	48.19	13.61	0.023774	196.8125	+28.3432	117.41	37.02	15.41	0.019561
192.7948	+34.0583	45.74	32.77	15.85	0.024293	196.9079	+28.3258	40.18	71.69	15.46	0.023450
192.8369	+34.1024	150.55	49.50	15.85	0.023798	196.9731	+28.3831	18.63	86.79	16.56	0.022369
192.9411	+34.3437	174.59	39.25	17.43	0.024257	197.0032	+28.0812	118.97	67.75	17.30	0.020058
193.0136	+34.1867	29.84	67.25	17.44	0.024188	197.1105	+28.1354	181.68	49.86	17.32	0.023023
192.4949	+32.3887	19.04	57.61	17.06	0.024109	197.1137	+28.3205	127.63	65.32	17.36	0.022569
192.5782	+32.5474	55.36	49.05	17.18	0.023880	197.2382	+28.2805	19.58	56.28	14.72	0.020358
192.5363	+33.1592	170.87	53.84	16.65	0.024470	197.3396	+28.3116	120.78	67.93	17.13	0.020972
192.8263	+33.1670	164.00	57.45	16.24	0.023950	197.3453	+28.3213	174.39	63.82	16.75	0.020006
192.7333	+31.6877	14.41	61.10	17.79	0.025210	197.3476	+28.2815	180.10	44.65	16.30	0.021723
192.7358	+31.6654	132.94	70.52	15.81	0.025152	197.3598	+28.4159	102.84	73.78	14.14	0.021624
192.8730	+31.8146	93.99	83.37	16.77	0.025426	196.6426	+27.5509	146.68	50.91	17.31	0.025189
192.7572	+28.9280	98.78	63.17	16.50	0.022381	196.9298	+27.5096	138.45	54.09	15.57	0.026175
192.7774	+29.1968	123.62	87.11	16.12	0.022982	197.2450	+27.6140	148.41	70.96	17.30	0.025562
193.0211	+29.2881	30.46	46.52	16.16	0.022642	196.9496	+29.1530	74.97	59.19	17.10	0.024158
193.1532	+30.4168	105.11	29.81	16.40	0.024068	197.0165	+28.9983	180.02	74.94	15.18	0.024991
193.2427	+30.1520	70.88	74.21	17.79	0.025250	197.0902	+29.2284	50.06	36.47	14.62	0.024286
193.2418	+32.4124	176.73	52.06	14.00	0.023663	197.2874	+28.8925	112.34	20.70	17.16	0.025627
193.2480	+32.1367	44.97	75.20	17.55	0.023017	197.4654	+28.9004	8.65	62.33	15.67	0.026621
193.2622	+32.1070	112.39	51.71	14.41	0.023633	197.4998	+28.8152	71.07	36.70	17.50	0.026480
193.2653	+32.3268	21.69	36.60	16.16	0.022705	197.6021	+28.9677	146.72	54.95	15.39	0.024984
193.4688	+32.2417	78.08	44.99	17.78	0.024180	197.6943	+28.6422	80.59	29.69	14.19	0.026918
193.5749	+32.3690	174.66	44.04	17.45	0.023330	197.6980	+28.9952	71.26	65.11	15.51	0.026233
193.6668	+32.3670	181.36	71.31	14.80	0.025142	197.8986	+29.0630	59.87	68.69	16.26	0.025136
193.4335	+32.7043	113.47	56.24	16.33	0.024011	197.0632	+29.0230	112.05	63.05	16.14	0.021424
193.4964	+32.6551	158.02	82.63	17.05	0.024066	197.2977	+28.7765	45.48	39.42	14.33	0.022021
193.6992	+30.5449	157.91	70.55	17.79	0.021671	197.3776	+28.9860	90.42	72.71	17.47	0.021497
193.7808	+30.5127	53.94	40.47	14.72	0.022282	197.2803	+29.8310	72.01	52.51	15.58	0.023956
194.0483	+29.3982	114.93	62.99	16.86	0.024997	197.3434	+24.0924	60.34	33.20	16.00	0.022552
194.2133	+29.3782	67.35	82.89	17.22	0.024778	197.4583	+24.5776	116.91	46.02	13.62	0.024587

Table 31: SDSS DR7 of galaxies in the supercluster S[195+027+0022] that have redshifts range 0.022 to 0.024.The first two columns list the right ascension and declinations.The next two columns shows position and inclination angle.The fifth and sixth columns represent the magnitude in r-band and redshift.

RA(J2000)	$Dec.(J2000)$	$P(deg)$	$i(deg)$	m_r	z	$RA(J2000)$	$Dec.(J2000)$	$P(deg)$	$i(deg)$	m_r	z
197.4690	+24.5605	100.94	15.38	14.82	0.024364	173.5742	+22.9276	114.88	69.91	15.52	0.024155
197.4595	+22.8035	63.20	79.29	16.80	0.022865	173.7661	+22.5152	151.90	55.21	13.98	0.023527
197.7202	+22.6670	85.86	81.24	17.64	0.022966	173.8331	+21.4581	32.61	67.54	17.75	0.024101
197.6958	+25.0790	133.04	76.29	17.77	0.024407	173.9116	+22.3157	154.41	55.80	14.69	0.024882
197.7189	+24.8654	160.85	18.61	15.50	0.025714	174.2779	+18.1939	62.58	70.09	16.82	0.022666
197.8546	+24.8597	91.34	79.52	13.69	0.024627	174.2998	+21.2186	55.64	52.11	16.03	0.024234
197.9878	+24.7012	142.57	60.01	17.37	0.024553	174.3397	+21.8728	113.47	56.03	17.36	0.024075
197.7565	+29.6367	170.15	44.09	16.37	0.024392	174.7177	+23.4465	8.35	51.04	17.64	0.022579
197.7571	+29.5784	171.29	68.00	15.50	0.025116	174.8092	+25.7874	135.65	59.34	17.23	0.024116
197.8257	+29.7941	127.77	76.33	15.89	0.025076	174.8451	+22.1192	142.00	31.15	13.75	0.024129
197.7616	+31.4041	134.27	69.90	15.94	0.024500	174.9855	+20.8372	176.56	77.25	17.29	0.024388
197.9031	+31.5081	20.13	36.23	17.19	0.023973	175.3557	+17.4256	10.26	54.00	16.06	0.022005
197.9050	+22.9933	176.23	74.50	13.72	0.024073	175.4369	+19.4323	131.06	75.80	15.96	0.023261
198.0513	+22.8683	147.81	72.64	15.40	0.024036	175.5646	+19.0699	90.79	63.55	16.81	0.025196
197.9809	+33.3071	48.04	19.90	14.82	0.024288	175.9072	+19.0905	131.66	43.67	17.82	0.023729
198.1125	+33.2209	161.49	57.42	15.79	0.023676	175.9159	+18.7406	20.21	59.49	17.15	0.022984
198.2249	+29.9615	178.62	69.56	15.33	0.022537	176.0836	+15.5943	128.12	17.22	13.17	0.022463
198.2933	+29.9804	81.03	69.37	15.03	0.022644	176.1281	+17.6264	51.75	56.92	14.82	0.023526
198.3007	+30.3622	60.30	54.52	21.54	0.022502	176.1459	+17.0589	110.78	48.02	16.90	0.025195
198.3818	+30.1494	13.38	53.59	15.62	0.022587	176.5339	+22.5395	93.58	85.01	15.18	0.022504
198.6642	+30.2250	50.98	57.27	16.78	0.024382	176.9287	+20.9753	81.56	83.86	15.06	0.025302
198.6688	+29.9972	43.43	79.96	17.45	0.023745	177.0140	+20.0063	51.03	48.77	16.30	0.025231
198.7842	+30.4038	66.09	45.12	16.54	0.024057	177.0556	+19.4479	89.17	34.46	15.15	0.023692
198.3728	+21.8436	36.92	57.98	15.84	0.023706	177.0627	+16.6376	46.79	39.78	14.36	0.023103
198.5060	+29.4070	130.67	68.43	15.30	0.022783	177.2432	+20.3765	101.36	34.69	14.40	0.023695
198.6569	+29.3180	139.63	57.73	15.64	0.022644	177.3760	+22.1396	98.76	38.16	16.66	0.024752
198.6732	+22.4725	142.29	83.63	14.51	0.023033	177.4324	+23.4452	163.10	35.10	16.37	0.022577
198.7657	+22.5896	45.47	42.91	17.73	0.023963	177.6392	+17.8581	83.27	39.63	17.68	0.022432
198.7493	+30.9050	144.78	80.22	16.73	0.023771	177.8466	+26.7844	30.05	68.66	12.78	0.023178
198.7873	+30.7072	105.76	55.63	17.31	0.023221	177.8619	+18.9652	141.67	64.44	17.20	0.021855
198.7682	+24.9388	29.03	68.09	17.17	0.022886	177.8803	+23.8628	148.93	50.99	16.00	0.024526
198.7888	+29.6362	97.32	74.41	17.54	0.023335	177.9520	+19.3581	112.50	81.24	14.84	0.024185
198.8954	+29.6761	126.72	49.67	17.74	0.022853	177.9781	+27.0916	149.68	29.61	17.20	0.023307
198.9077	+29.6586	83.79	50.51	15.05	0.022847	178.2245	+16.8089	149.74	30.17	16.24	0.022661
198.9138	+29.6108	33.86	70.81	17.40	0.022564	178.2577	+24.8304	155.31	45.72	14.91	0.023812
198.9672	+31.6523	10.97	78.48	16.53	0.026713	178.3604	+15.6079	88.84	57.01	19.78	0.023946
199.1390	+31.5467	176.27	45.64	17.58	0.025679	178.5346	+18.5279	32.66	70.80	16.67	0.023832
199.3538	+27.7501	56.01	71.80	16.93	0.024255	178.5487	+25.0354	91.21	22.87	17.34	0.023255
199.4383	+27.5699	103.86	64.75	13.92	0.024220	178.6508	+23.8632	97.58	63.65	17.15	0.022799
199.8292	+31.0518	21.15	42.96	14.87	0.025793	178.6803	+23.1602	117.51	75.73	15.58	0.023841
199.9486	+30.8263	153.32	50.46	16.70	0.025084	178.7066	+22.1029	43.18	45.51	15.83	0.024611
200.0615	+30.9878	42.05	52.60	17.70	0.024777	178.8070	+21.0195	176.33	52.55	15.03	0.021725
200.1772	+31.1850	35.37	58.87	17.38	0.024684	178.8197	+17.4876	99.63	69.65	13.73	0.023732
200.3282	+31.3881	25.75	49.02	15.40	0.024165	178.9365	+17.8881	122.32	72.50	17.10	0.022350
200.3319	+31.5525	56.74	60.32	17.64	0.024690	179.1298	+18.3594	3.29	56.01	16.30	0.022133
200.4394	+31.2372	11.52	57.80	16.30	0.024970	179.3298	+16.2674	168.86	56.72	16.86	0.023950
200.4569	+31.5632	129.09	78.25	12.90	0.023767	179.5010	+18.5687	132.67	48.43	15.72	0.023838
200.5087	+31.2784	24.65	68.48	13.76	0.025717	179.5691	+24.3158	67.08	30.70	17.68	0.023196
200.7026	+31.3244	136.25	46.83	15.14	0.024520	179.6204	+15.2177	139.57	66.20	15.32	0.024025
199.8667	+27.7490	22.49	59.07	17.36	0.024146	179.6510	+18.8631	138.68	62.49	17.56	0.023911
199.9170	+27.7061	28.09	33.60	13.57	0.023989	179.6764	+21.2344	49.03	68.57	16.70	0.024192
199.9848	+30.1190	84.41	24.25	16.29	0.024265	179.8265	+20.1366	9.53	39.00	15.46	0.023173
200.0359	+30.0557	96.51	79.95	15.67	0.023825	179.8441	+24.4973	58.91	83.17	17.80	0.023450
200.2228	+32.1908	85.82	57.50	15.22	0.023851	179.8620	+17.7570	126.15	73.43	15.26	0.022725
200.2905	+31.9463	85.40	72.24	17.62	0.023929	180.0450	+19.2291	60.51	83.90	16.75	0.024325
200.3136	+31.9305	167.40	74.44	17.74	0.024839	180.0905	+24.9162	80.67	48.66	16.78	0.023681
200.6152	+31.8367	89.47	71.89	17.02	0.024858	180.1020	+16.8465	90.27	36.39	15.60	0.023732
200.4857	+24.7290	65.33	74.82	16.10	0.024452	180.1326	+19.7997	2.53	61.18	16.32	0.023982
200.5270	+24.7203	159.46	80.09	17.49	0.024244	180.3946	+16.2123	90.98	74.72	13.70	0.022736
200.4967	+26.7338	182.13	67.05	15.35	0.025146	180.4210	+25.0888	22.53	31.28	15.79	0.023686
200.5026	+26.5200	172.90	59.77	15.12	0.024913	180.4408	+19.3091	25.84	44.95	14.49	0.024877
200.7709	+26.8546	110.03	62.64	14.50	0.024499	180.5686	+24.3749	94.91	42.99	15.62	0.023044
200.5962	+27.1826	178.26	46.07	16.90	0.025334	180.5894	+15.7769	123.08	78.64	16.38	0.024667
200.6803	+27.1982	74.28	57.94	15.27	0.025306	180.7252	+21.6447	43.71	31.50	16.43	0.025617
200.6883	+30.8872	174.28	80.53	16.57	0.023360	180.8129	+24.7961	76.22	45.25	17.33	0.022290
200.9139	+30.9388	115.91	24.17	16.30	0.023288	180.8803	+17.1503	61.62	63.65	13.78	0.023069
200.9872	+30.9880	79.83	52.84	16.06	0.023670	181.0896	+19.5802	171.52	34.28	14.74	0.025779
200.9998	+30.9324	33.06	81.93	15.58	0.023157	181.4361	+19.5990	171.30	47.95	17.51	0.024171
201.0197	+30.9565	175.23	48.39	17.59	0.025410	181.4605	+24.6853	69.75	53.97	16.83	0.022769
201.1705	+31.0265	138.72	59.69	17.57	0.024641	181.4636	+24.3557	98.73	46.28	17.32	0.024444
200.8526	+26.5436	108.87	22.62	16.21	0.025069	181.6251	+19.1702	114.84	36.91	14.55	0.025873
200.8882	+26.5039	183.74	58.66	15.08	0.024072	181.7447	+23.7051	35.71	43.53	14.19	0.024643
201.0933	+26.7816	35.56	71.41	13.14	0.024955	181.7513	+22.3879	115.22	35.73	15.25	0.023321
201.1939	+26.7384	76.17	53.67	16.53	0.024239	182.0314	+18.0088	19.95	59.35	16.72	0.023903
201.2345	+26.4635	92.55	59.30	15.90	0.024857	182.1311	+18.9486	54.85	73.16	13.78	0.025390
201.4095	+31.9941	32.79	74.03	17.27	0.025346	182.1560	+16.1428	5.35	50.16	15.21	0.023741
201.8043	+32.0885	95.90	72.59	16.89	0.025199	182.3093	+18.1494	90.05	64.10	16.63	0.024303
201.8202	+32.0307	121.56	49.91	18.99	0.025201	182.4147	+23.2894	145.40	79.81	17.35	0.024119
201.9444	+32.0602	98.13	68.22	17.59	0.025360	182.4688	+20.9291	81.55	37.79	15.57	0.025464
201.9070	+26.9657	103.97	63.76	13.80	0.024415	182.5786	+20.0890	141.46	61.46	16.34	0.025903
171.7005	+22.5577	151.94	67.07	16.21	0.023696	182.9700	+25.4431	166.22	46.18	17.46	0.023743
171.8060	+23.7696	155.96	45.89	15.35	0.022465	183.0007	+24.5263	140.88	20.43	15.53	0.022296
171.8697	+19.8534	142.14	39.73	13.81	0.022899	183.0585	+28.1556	142.63	64.86	16.42	0.023412
171.9215	+23.2394	45.10	54.77	15.72	0.022616	183.0794	+24.1002	58.26	39.90	16.19	0.023076
171.9663	+21.4092	151.52	65.66	13.82	0.023157	183.1128	+15.9017	108.47	46.81	16.29	0.024825
172.7360	+20.9416	78.15	67.66	14.51	0.024698	183.1427	+22.7831	164.21	27.53	16.62	0.023047
172.9833	+23.9904	109.76	63.26	14.16	0.024327	183.1735	+25.9963	107.59	69.94	14.31	0.023797
173.1384	+22.1158	52.91	68.49	16.78	0.023123	183.4234	+20.8805	69.03	56.70	14.72	0.023588
173.3635	+17.4189	139.60	54.76	14.83	0.022596	183.5058	+23.0103	36.81	63.21	16.98	0.025580
173.4247	+21.8646	143.05	70.98	16.36	0.023765	183.5149	+20.7349	5.84	38.98	17.13	0.025335
173.4251	+23.4127	88.24	61.87	15.76	0.024880	183.8404	+22.6347	149.61	44.36	16.26	0.025287

Table 32: SDSS DR7 of galaxies in the supercluster S[195+027+0022] that have redshifts range 0.022 to 0.024.The first two columns list the right ascension and declinations.The next two columns shows position and inclination angle.The fifth and sixth columns represent the magnitude in r-band and redshift.

RA(J2000)	$Dec.(J2000)$	$P(deg)$	$i(deg)$	m_r	z	$RA(J2000)$	$Dec.(J2000)$	$P(deg)$	$i(deg)$	m_r	z
183.8639	+19.1632	166.64	51.35	15.15	0.025780	193.7309	+29.0124	180.95	34.12	16.70	0.022262
183.8823	+24.7285	84.81	60.98	17.42	0.023842	193.7953	+29.5783	87.44	49.94	17.59	0.025783
183.9953	+17.6296	71.83	34.47	14.23	0.023573	193.8601	+29.5325	68.62	39.46	13.79	0.022225
184.5204	+27.0115	12.40	50.89	16.91	0.024652	193.8938	+32.2060	126.24	49.38	14.66	0.023717
184.7725	+27.2984	148.89	43.39	16.63	0.024276	193.9681	+25.1829	166.18	53.67	14.87	0.023808
184.7785	+27.7857	172.39	39.70	15.56	0.024591	193.9726	+30.9350	106.72	69.82	16.71	0.025628
185.2173	+19.0038	167.95	56.97	14.55	0.024268	194.0825	+32.6550	61.73	53.07	16.41	0.023942
185.4339	+28.4125	154.87	71.07	15.34	0.023533	194.0844	+29.3001	27.67	43.30	17.61	0.023015
185.4638	+26.3636	100.24	54.03	17.74	0.024834	194.2231	+22.3736	143.72	35.49	17.73	0.023184
185.6641	+24.3301	143.96	81.24	17.40	0.023830	194.3465	+33.4560	28.64	53.42	14.59	0.024551
185.6824	+24.8205	15.57	26.78	16.74	0.023545	194.5775	+30.5380	173.30	57.42	16.86	0.026100
185.9275	+26.8490	137.98	70.33	16.79	0.022717	194.5969	+30.1429	128.46	61.14	16.90	0.026718
185.9397	+22.8848	163.75	37.29	22.57	0.023308	194.6814	+33.9354	100.93	83.86	15.03	0.025022
186.4046	+24.1820	79.65	48.89	17.59	0.024140	194.8421	+26.7971	85.10	68.64	17.78	0.022495
186.4846	+30.8436	99.06	67.37	16.75	0.023690	194.9184	+30.2470	45.70	72.50	15.16	0.026323
186.6566	+26.4363	23.74	62.15	16.89	0.025582	194.9389	+32.0450	108.50	39.72	16.26	0.023489
186.8728	+26.1032	85.48	28.54	16.61	0.025544	194.9411	+29.8963	147.89	58.81	17.22	0.022645
186.8937	+27.7399	99.50	67.38	17.21	0.024144	194.9472	+21.8132	116.50	47.37	16.91	0.024764
186.9244	+28.6981	132.40	62.98	15.46	0.024361	195.0017	+30.6651	32.11	77.73	17.21	0.025948
186.9597	+26.9935	102.69	40.12	15.70	0.024789	195.0339	+33.4377	52.83	24.94	16.46	0.024353
187.0623	+25.4326	135.15	51.27	14.25	0.024304	195.2998	+29.6641	149.95	81.24	14.15	0.024770
187.4108	+26.2306	20.58	36.21	17.39	0.023590	195.5741	+26.1426	111.68	41.26	15.91	0.022515
187.4482	+27.2433	10.14	44.88	16.04	0.025637	195.6043	+32.4257	37.52	54.76	16.89	0.025974
187.4678	+28.5259	139.98	63.46	16.68	0.022707	195.6483	+26.6622	118.82	19.74	15.74	0.025555
187.5049	+23.1838	49.33	67.41	14.75	0.024089	195.9230	+29.8183	98.92	88.19	16.70	0.024283
187.5990	+30.9338	31.06	75.18	17.31	0.024203	195.9246	+33.1594	56.25	22.46	14.25	0.024808
187.6533	+22.7602	118.84	64.08	16.54	0.024058	196.0708	+26.4754	113.48	41.20	17.19	0.025955
187.8364	+27.5290	118.49	48.16	16.04	0.024997	196.0885	+24.4304	148.80	85.17	15.95	0.026088
187.8380	+32.3236	59.16	76.35	17.60	0.023453	196.1043	+32.5481	128.28	70.28	15.03	0.023941
187.8456	+25.9140	139.20	71.00	16.87	0.024159	196.1232	+31.2734	57.95	84.86	16.77	0.023984
187.9388	+27.1495	64.77	43.18	13.37	0.024265	196.3704	+33.8488	183.04	68.84	16.29	0.024597
187.9944	+27.8339	55.71	26.48	15.72	0.026181	196.3929	+29.6532	48.34	64.50	16.66	0.022786
188.0370	+30.7153	51.90	33.64	14.34	0.024092	196.4010	+30.7906	155.76	83.01	16.98	0.023082
188.0782	+24.7283	154.31	29.28	17.22	0.024056	196.6025	+31.1367	153.34	77.07	17.98	0.025151
188.2352	+32.1424	81.48	67.82	17.36	0.023117	196.7370	+24.7649	170.43	38.62	20.53	0.023400
188.2852	+26.3494	118.84	31.95	15.68	0.025162	196.7874	+30.3932	140.04	78.02	17.19	0.023811
188.3361	+27.1105	147.47	74.44	15.75	0.026230	196.9067	+27.4991	111.13	63.98	16.96	0.023049
188.5254	+22.8032	167.19	49.49	17.53	0.023798	196.9067	+29.9268	64.72	85.63	15.64	0.026221
188.5483	+28.8740	168.61	54.40	17.74	0.023031	196.9076	+32.7753	103.69	55.17	15.82	0.023489
188.5671	+27.8622	59.59	74.19	17.25	0.024099	197.0379	+27.8266	178.51	48.04	17.29	0.023976
188.7792	+29.9423	21.88	54.39	17.65	0.023514	197.1316	+24.7008	146.80	85.04	17.50	0.024690
188.7869	+28.0564	19.11	40.80	17.34	0.025912	197.1365	+30.7480	58.53	63.51	16.13	0.024355
188.8287	+23.0258	10.89	41.45	15.44	0.024003	197.4063	+26.1591	168.08	66.93	17.63	0.022099
189.1586	+24.4288	45.73	63.50	16.98	0.024113	197.4095	+30.4991	29.08	81.01	13.72	0.025385
189.2113	+27.2781	125.57	70.51	15.73	0.022992	197.5323	+24.1659	105.38	49.70	13.77	0.024202
189.5320	+22.6986	20.93	26.01	15.29	0.024261	197.6985	+29.7099	178.54	40.12	17.60	0.022039
189.5524	+25.4109	122.74	81.68	16.04	0.022541	197.8031	+26.8140	113.49	74.62	16.94	0.022090
189.6137	+28.4801	63.78	85.92	17.29	0.024630	197.8289	+27.9668	61.23	23.00	15.52	0.025304
189.6146	+29.4361	127.86	69.64	17.64	0.024826	197.8772	+32.5265	66.58	79.43	13.53	0.024316
189.7059	+29.9724	24.85	35.24	15.37	0.024177	197.9501	+30.9726	136.71	64.18	17.18	0.025605
189.7833	+30.4065	157.00	71.66	17.52	0.024310	198.0014	+30.3995	129.55	44.03	16.19	0.026134
189.9222	+25.0392	164.57	18.58	16.08	0.022503	198.1077	+28.5377	11.91	56.56	15.77	0.022114
189.9486	+24.1734	147.81	56.06	17.45	0.022720	198.1595	+26.7986	127.94	84.68	14.59	0.023103
190.0956	+25.5515	102.27	55.99	15.03	0.022285	198.2229	+23.6347	139.93	45.88	17.81	0.024210
190.1986	+30.6857	96.74	53.67	16.30	0.023259	198.2922	+30.1914	153.75	68.50	14.70	0.024200
190.2420	+27.9812	22.46	21.86	16.09	0.025257	198.4741	+28.0708	141.09	22.55	16.13	0.024142
190.2464	+24.8713	37.03	38.10	17.12	0.022430	198.6089	+30.2505	169.41	18.63	17.53	0.026195
190.3041	+30.2756	120.78	76.05	15.32	0.024146	198.6352	+30.7058	137.73	34.03	16.57	0.025768
190.3588	+26.3860	10.26	40.47	15.28	0.024785	198.7590	+28.0364	104.66	26.67	15.24	0.022621
190.4864	+26.9694	52.05	41.06	15.58	0.024898	198.8566	+27.3032	60.94	75.29	15.19	0.022507
190.6873	+25.4190	179.44	48.14	16.72	0.024253	199.1713	+30.2484	92.08	55.22	16.06	0.023022
190.7026	+26.6397	18.56	69.00	16.72	0.023202	199.1843	+28.2001	113.96	23.17	16.40	0.024649
190.7059	+22.7728	38.72	49.08	20.34	0.024403	199.2015	+28.3618	85.38	52.76	16.37	0.022579
190.7585	+32.3285	29.33	70.12	13.90	0.024261	199.2058	+26.3463	95.59	80.40	19.91	0.024269
190.7677	+30.3872	146.37	67.79	17.52	0.024841	199.3302	+25.2148	100.87	61.65	16.83	0.024232
190.8388	+26.0927	49.91	72.73	16.38	0.025195	199.4344	+29.6461	112.15	54.07	16.95	0.023532
190.9709	+26.8633	32.38	40.17	17.18	0.026067	199.5249	+30.1410	68.76	81.85	14.09	0.023681
190.9804	+29.3696	94.95	55.29	14.64	0.024511	199.7843	+28.5069	98.80	74.80	17.30	0.022934
191.1775	+27.0139	15.90	48.69	13.30	0.024108	199.8306	+24.9835	32.77	64.66	13.76	0.024377
191.1842	+27.8915	100.94	49.29	15.91	0.022059	199.9417	+29.6925	62.11	60.03	17.50	0.025067
191.2015	+34.3517	162.01	40.63	15.50	0.024250	199.9536	+31.4614	80.77	26.78	17.43	0.023797
191.4216	+24.9556	27.77	53.87	14.85	0.023615	199.9930	+28.2470	156.33	49.59	17.09	0.023526
191.5963	+27.1124	147.59	48.64	13.61	0.024222	200.2494	+28.9695	75.08	67.47	16.55	0.023695
191.7353	+25.6216	164.20	38.97	16.40	0.023596	200.3949	+33.4898	164.03	71.95	19.51	0.024936
191.8590	+29.7877	120.09	28.43	17.16	0.023401	200.5969	+27.5815	147.03	23.58	16.47	0.025382
191.9143	+33.6713	104.31	37.52	17.27	0.023757	200.6517	+30.3171	23.11	49.30	16.62	0.024288
191.9754	+30.3738	129.10	67.96	17.59	0.025513	200.6702	+29.3421	81.72	75.65	17.39	0.024672
192.1036	+28.3069	162.16	56.11	17.70	0.023733	200.7161	+27.3936	54.37	37.56	17.37	0.023906
192.1373	+26.1155	171.35	70.27	17.62	0.022313	200.7587	+33.0598	181.74	55.23	16.80	0.024337
192.2817	+27.7973	171.88	39.94	16.36	0.021882	201.0768	+31.5883	142.12	43.70	16.86	0.025411
192.3155	+28.4975	121.16	43.07	17.41	0.025770	201.1405	+31.5464	74.21	67.71	17.35	0.023992
192.4704	+21.9955	118.54	83.97	19.80	0.023052	201.1432	+32.1960	111.72	33.19	15.14	0.024869
192.5383	+32.0065	112.63	62.36	17.60	0.024620	201.1774	+29.0496	72.27	47.18	17.34	0.024254
192.5413	+29.6762	7.92	62.61	16.56	0.024695	201.1878	+32.5169	86.33	35.26	16.95	0.025125
192.7252	+27.8418	161.15	16.59	15.15	0.026226	201.1957	+33.4629	124.24	30.37	16.84	0.024606
192.8330	+31.0596	166.77	28.95	13.96	0.023674	201.3336	+29.4941	138.49	66.17	18.10	0.023861
192.8569	+28.7203	25.16	38.31	17.31	0.024983	201.4201	+30.7395	175.12	43.67	17.42	0.023186
192.9195	+28.0532	136.56	48.00	22.80	0.021630	201.4883	+31.6183	17.23	60.96	14.37	0.024972
193.2631	+26.4766	114.13	56.87	17.07	0.026632	201.6812	+30.5067	31.47	49.44	17.27	0.024475
193.5103	+29.6036	66.47	85.69	16.90	0.021976	201.7157	+26.5909	7.66	68.22	14.98	0.024479
193.5124	+25.7608	94.94	70.23	14.66	0.025275	201.7334	+28.5609	171.02	15.61	14.88	0.024375
193.5265	+29.2427	14.95	65.29	17.75	0.025554	201.7633	+30.9768	43.77	63.08	13.68	0.023419

Table 33: SDSS DR7 of galaxies in the supercluster S[173+014+0082] that have redshifts range 0.076 to 0.091.The first two columns list the right ascension and declinations.The next two columns shows position and inclination angle.The fifth and sixth columns represent the magnitude in r-band and redshift.

RA(J2000)	$Dec.(J2000)$	$P(deg)$	$i(deg)$	m_r	z	$RA(J2000)$	$Dec.(J2000)$	$P(deg)$	$i(deg)$	m_r	z
171.0650	+15.1340	166.95	45.81	16.96	0.081793	172.7132	+15.5417	36.61	56.60	17.78	0.082140
171.1137	+15.1541	109.80	55.77	16.73	0.081718	172.7166	+15.8323	145.33	65.98	17.64	0.080375
171.1614	+15.5265	46.08	34.17	16.63	0.081983	172.7189	+15.8907	58.03	71.73	17.80	0.082394
171.2458	+15.4568	134.57	73.50	16.03	0.082629	172.7625	+15.8109	122.98	59.01	17.87	0.081734
171.4794	+15.0069	25.97	43.93	15.64	0.081556	172.7774	+15.7668	90.19	33.57	15.57	0.080981
171.5574	+15.0304	121.79	45.52	16.80	0.081801	172.8247	+15.6944	29.52	65.74	16.50	0.080461
171.4878	+15.2288	44.89	44.13	17.48	0.081836	172.8494	+15.7177	135.40	35.05	16.91	0.082070
171.4937	+15.3034	77.91	58.08	17.17	0.080530	172.8886	+15.8134	33.30	53.45	17.28	0.082190
171.5094	+15.2952	25.33	83.12	16.77	0.079668	172.9133	+15.7785	65.33	49.21	16.00	0.082470
171.5278	+14.2684	21.84	71.61	16.93	0.084150	172.9184	+15.7572	139.87	27.91	17.34	0.081578
171.5314	+14.1544	7.02	66.26	16.44	0.083997	172.9991	+15.8262	91.17	67.36	16.35	0.082409
171.6606	+14.9448	58.63	50.25	17.36	0.080523	172.7702	+16.4632	117.46	39.06	17.51	0.083743
171.6910	+14.9174	79.80	22.95	17.74	0.080613	172.8104	+16.4665	40.70	28.00	17.43	0.082680
171.8065	+16.3876	128.12	44.73	17.53	0.081119	172.8111	+16.5227	38.23	36.93	17.11	0.084239
171.8638	+16.3839	45.82	63.21	16.39	0.081508	172.8141	+16.4890	122.06	61.79	15.47	0.085930
171.8299	+12.6663	174.66	75.39	17.06	0.082406	172.8184	+16.6806	70.84	8.48	16.53	0.081365
171.8465	+12.5217	92.08	40.80	17.52	0.081942	172.8388	+16.6413	26.05	61.41	16.92	0.082642
171.9190	+12.5896	102.70	20.95	16.88	0.084103	172.8476	+16.6729	92.62	22.81	16.91	0.083377
171.9346	+12.4879	91.06	56.47	17.01	0.082295	172.8651	+16.5602	166.81	57.04	17.02	0.084811
172.0019	+12.5297	102.87	50.19	15.43	0.083047	172.8695	+16.5227	89.90	65.91	16.83	0.085024
172.0859	+12.5130	109.07	59.90	17.24	0.082314	172.8880	+16.5153	63.98	36.09	16.96	0.081325
172.0863	+12.4487	146.79	57.58	17.36	0.083240	172.9091	+16.5819	23.49	21.39	17.17	0.083079
172.0175	+16.6446	68.63	58.32	15.52	0.081321	172.7777	+14.6318	85.08	59.88	17.89	0.079618
172.0251	+16.6720	154.72	77.37	17.29	0.082039	172.8005	+14.6875	89.46	63.65	16.70	0.081114
172.1018	+16.4767	177.67	21.68	17.62	0.082601	172.7863	+15.4326	61.37	50.27	16.64	0.082370
172.1171	+16.5364	12.63	62.99	16.71	0.083019	172.8157	+15.4024	61.42	59.64	16.17	0.082269
172.1302	+16.5876	109.85	59.78	17.36	0.081273	172.8348	+15.3835	63.11	36.86	17.68	0.083344
172.1331	+15.0116	61.51	46.06	17.43	0.084103	172.8443	+15.2537	113.51	58.09	17.37	0.081992
172.1871	+15.0059	16.81	49.32	16.04	0.083932	172.8564	+15.3542	160.14	55.86	15.36	0.081603
172.2107	+15.0534	4.03	53.64	16.49	0.083920	172.8623	+15.3174	118.25	66.79	16.23	0.081491
172.2207	+16.3873	93.08	29.16	16.87	0.083132	172.9053	+15.3467	62.02	48.52	17.01	0.081748
172.2485	+16.2962	164.47	67.27	16.30	0.083837	172.8317	+15.9915	7.06	41.28	16.83	0.083136
172.2816	+16.5274	115.50	78.28	16.96	0.082580	172.9270	+15.9821	96.37	71.40	17.69	0.082254
172.3084	+16.5577	166.73	50.25	16.80	0.082354	172.8606	+12.7584	35.44	35.56	17.21	0.082006
172.3010	+17.1032	161.71	69.83	17.19	0.083830	172.8762	+12.7218	170.92	86.39	17.85	0.081622
172.3650	+17.1337	35.26	63.54	17.43	0.083652	172.8839	+12.6997	22.61	79.44	15.35	0.082066
172.4280	+17.0983	73.09	39.95	17.13	0.084504	172.9198	+12.6426	75.48	50.26	15.81	0.080637
172.3724	+16.2194	58.49	67.44	16.12	0.083498	173.0139	+12.5934	93.06	37.49	17.38	0.080915
172.4247	+16.1484	167.61	60.58	17.47	0.082332	173.0936	+12.5864	75.29	67.96	16.39	0.082448
172.4380	+16.1932	55.89	45.97	16.86	0.081865	172.8709	+14.5766	133.58	15.14	15.89	0.082310
172.4790	+16.0679	29.79	60.45	17.08	0.081077	172.8959	+14.5826	8.94	49.68	16.93	0.083761
172.5127	+16.1826	128.73	36.57	16.87	0.081529	172.9553	+14.4831	75.25	29.35	17.15	0.083087
172.5409	+16.1158	175.40	60.83	16.42	0.083515	173.0029	+14.4753	173.67	50.68	22.55	0.083100
172.5565	+16.1431	86.26	52.35	17.84	0.083907	173.0210	+14.6745	60.98	81.19	17.08	0.078644
172.5734	+16.2023	134.58	63.86	17.60	0.082935	173.0354	+14.5176	165.95	72.99	17.08	0.076553
172.6072	+16.1002	84.01	39.08	16.44	0.081468	173.0663	+14.5113	26.70	38.91	16.59	0.083488
172.6267	+16.1536	34.87	54.53	16.10	0.081487	173.0792	+14.6076	6.61	46.04	17.28	0.077935
172.6705	+16.2568	24.68	75.86	17.38	0.082562	173.0924	+14.6328	6.48	73.30	16.72	0.082064
172.7025	+16.0726	104.16	33.67	16.37	0.081853	173.0994	+14.7029	47.97	43.78	16.19	0.082872
172.7488	+16.2444	40.11	70.49	17.84	0.083825	173.1052	+14.6202	125.17	59.87	15.94	0.083145
172.8120	+16.2598	98.90	56.69	16.36	0.082982	173.1304	+14.5950	159.18	40.97	17.00	0.078878
172.4362	+14.8441	146.05	70.59	16.51	0.082455	173.1400	+14.4042	107.99	59.00	17.86	0.081480
172.4495	+14.8970	155.96	68.61	15.92	0.083477	173.1443	+14.8081	155.65	34.77	17.52	0.084463
172.4486	+16.3637	81.80	64.76	17.71	0.081132	173.1492	+14.4271	113.40	44.58	17.80	0.084666
172.4589	+16.5185	64.17	83.25	17.87	0.081934	173.1523	+14.4013	23.91	46.38	17.15	0.086445
172.4804	+16.4693	128.63	61.53	17.43	0.081167	173.1560	+14.5844	111.86	58.92	17.27	0.082112
172.4991	+16.5384	52.14	31.49	17.43	0.081836	173.1597	+14.6032	138.88	35.03	17.63	0.080942
172.5935	+16.5796	78.53	17.30	16.13	0.084254	173.1612	+14.5261	129.67	18.76	17.47	0.081447
172.6030	+16.6027	146.35	73.67	16.79	0.081977	173.1757	+14.5073	10.67	33.74	16.67	0.081679
172.6129	+16.5749	38.02	28.50	17.50	0.082375	173.1761	+14.5958	44.14	50.48	16.20	0.080994
172.6938	+16.5692	175.38	38.83	17.61	0.084031	173.1775	+14.4378	146.27	53.87	16.26	0.082976
172.4724	+15.7480	121.75	68.93	17.48	0.082093	173.1793	+14.4647	24.86	61.51	16.67	0.083016
172.4886	+15.7678	24.04	48.84	15.73	0.082071	173.1801	+14.3650	57.24	59.36	17.07	0.081366
172.5208	+15.0840	25.82	35.60	17.68	0.083268	173.1819	+14.2636	165.53	14.72	17.10	0.083635
172.6071	+15.1279	84.40	52.19	17.33	0.081744	173.1880	+14.3362	121.72	36.59	17.07	0.079494
172.7195	+15.1516	151.41	25.62	17.22	0.081556	173.1909	+14.4547	81.01	62.43	17.52	0.082756
172.7278	+15.0841	164.07	34.18	17.49	0.083102	173.1918	+14.4775	24.54	32.22	17.65	0.077598
172.5374	+13.3635	50.44	86.43	16.54	0.083108	173.1941	+14.2431	146.80	61.25	17.15	0.082767
172.5494	+13.3590	96.88	50.61	17.85	0.082393	173.1959	+14.5681	29.05	77.74	17.77	0.080907
172.5632	+16.9671	110.17	38.58	16.09	0.084286	173.1962	+14.3233	156.20	6.08	17.36	0.080039
172.6657	+16.9907	55.90	84.26	16.47	0.084075	173.1979	+14.1955	−3.71	63.63	17.05	0.084852
172.7376	+16.9548	16.64	77.67	17.59	0.084486	173.1989	+14.6152	101.27	25.38	17.74	0.082533
172.7537	+16.9499	2.64	27.19	16.24	0.084214	173.2027	+14.5238	137.86	52.70	17.93	0.082255
172.8052	+17.1454	101.30	55.69	17.73	0.085269	173.2074	+14.4994	162.38	64.95	17.20	0.083224
172.8138	+17.0786	100.00	39.38	16.63	0.084060	173.2095	+14.5192	52.10	76.05	15.18	0.082739
172.8241	+16.8850	7.02	44.57	16.44	0.084213	173.2132	+14.4612	156.67	71.02	14.66	0.082352
172.8279	+16.9506	115.31	80.17	16.91	0.083995	173.2181	+14.4924	133.65	60.12	16.68	0.086288
172.8341	+17.0535	97.39	52.94	16.80	0.082946	173.2191	+14.5182	153.94	31.17	17.63	0.078156
172.9154	+17.0742	111.09	12.43	16.92	0.083321	173.2201	+14.4625	99.92	49.71	17.30	0.081948
172.9209	+17.0350	16.85	65.70	17.22	0.084602	173.2257	+14.4067	70.23	39.42	17.08	0.082983
172.9345	+17.0790	161.24	61.35	17.33	0.084639	173.2275	+14.4176	15.24	67.62	16.69	0.084928
172.9579	+17.1786	107.55	43.80	17.44	0.083830	173.2304	+14.4725	64.41	42.99	16.02	0.087747
173.0071	+17.0599	72.89	43.91	16.18	0.083927	173.2314	+14.3783	99.09	49.21	16.77	0.078216
173.0357	+17.1507	115.56	77.43	16.46	0.084213	173.2414	+14.3071	151.38	32.08	17.67	0.082158
172.6102	+14.5356	78.33	66.58	16.21	0.081301	173.2443	+14.3015	89.05	74.73	17.79	0.084205
172.6221	+14.6491	44.47	69.33	16.52	0.080751	173.2455	+14.6068	15.96	16.98	15.46	0.080750
172.6256	+12.6257	66.75	57.60	17.23	0.082117	173.2560	+14.5345	53.66	41.01	16.40	0.086362
172.7006	+12.6777	37.20	68.00	15.68	0.082552	173.2580	+14.3992	111.51	36.10	16.86	0.086718
172.7382	+14.3128	7.45	63.66	17.38	0.082875	173.2620	+14.3292	80.06	40.03	16.24	0.079417
172.7590	+14.4019	171.72	72.27	22.12	0.082664	173.2687	+14.3982	46.47	49.13	16.64	0.076192
172.6968	+15.5782	15.31	62.41	16.37	0.080717	173.2952	+14.5092	17.65	37.01	17.61	0.084888

Table 34: SDSS DR7 of galaxies in the supercluster S[173+014+0082] that have redshifts range 0.076 to 0.091.The first two columns list the right ascension and declinations.The next two columns shows position and inclination angle.The fifth and sixth columns represent the magnitude in r-band and redshift.

RA(J2000)	$Dec.(J2000)$	$P(deg)$	$i(deg)$	m_r	z	$RA(J2000)$	$Dec.(J2000)$	$P(deg)$	$i(deg)$	m_r	z
173.3147	+14.4560	97.85	33.55	17.00	0.082037	173.9033	+13.8496	158.73	44.24	17.74	0.079081
173.3341	+14.3953	136.53	53.06	17.58	0.082505	173.9053	+13.6302	104.76	40.94	17.38	0.082052
173.3391	+14.3882	22.42	60.26	17.72	0.082418	173.9223	+13.7281	161.30	57.59	16.98	0.078981
173.3407	+14.3706	67.92	22.65	15.97	0.080631	173.9280	+13.6700	123.90	57.49	17.58	0.081284
173.3580	+14.2719	120.11	71.91	16.14	0.080429	173.9302	+13.7625	70.46	54.40	17.35	0.079246
173.3669	+14.5619	69.88	60.70	17.84	0.084209	173.9414	+13.5794	126.82	54.52	16.61	0.078416
173.4284	+14.4273	51.31	53.86	16.45	0.080234	173.9425	+13.4800	76.37	29.60	15.56	0.079633
173.4356	+14.5653	104.74	47.45	16.75	0.081439	173.9487	+13.6073	147.10	78.06	17.53	0.080798
173.4418	+14.4980	63.06	54.23	17.77	0.082602	173.9489	+13.7723	99.94	67.96	17.72	0.083704
173.4642	+14.2087	101.34	59.22	17.22	0.081753	173.9499	+13.6515	11.13	51.94	17.61	0.081012
173.4670	+14.5449	39.01	70.78	17.10	0.080839	173.9728	+13.6421	77.84	69.14	17.56	0.079013
173.4774	+14.3939	31.00	67.95	15.98	0.082547	173.9749	+13.7041	50.42	73.42	15.48	0.080943
173.4782	+14.1571	55.17	89.45	16.50	0.083144	173.9876	+13.6189	109.41	53.09	17.52	0.077546
173.4831	+14.2277	66.14	38.70	16.75	0.083754	173.9885	+13.6406	26.09	39.70	16.84	0.082699
173.4901	+14.3676	136.98	16.51	16.80	0.081354	174.0149	+13.7213	66.33	61.10	15.72	0.082098
173.5111	+14.1772	163.38	68.19	16.94	0.082197	174.0186	+13.4408	31.17	49.62	16.78	0.079437
173.5186	+14.1332	3.10	73.91	16.14	0.082017	174.0281	+13.6883	171.48	43.32	17.77	0.079991
173.5201	+14.3086	64.04	66.82	16.05	0.081742	174.0476	+13.7955	51.06	61.28	17.70	0.084081
173.5339	+14.3752	26.17	31.77	17.64	0.084054	174.0717	+13.6921	95.29	39.92	15.96	0.079823
173.5411	+14.1416	72.58	38.61	17.49	0.081153	174.0767	+13.6749	18.08	67.23	17.48	0.079271
173.5503	+14.4618	107.70	48.09	16.57	0.079745	174.0887	+13.7027	163.95	51.23	17.64	0.079452
173.5822	+14.2479	−2.37	49.05	17.61	0.082764	174.1050	+13.7050	42.75	62.37	17.61	0.081258
173.5879	+14.2922	95.38	68.28	17.50	0.083099	174.1057	+13.6635	32.69	55.34	17.86	0.079164
173.6500	+14.1315	92.75	45.63	16.19	0.082724	173.6624	+12.9836	82.63	27.16	17.01	0.082781
173.6691	+14.0066	39.78	74.32	17.58	0.083257	173.6731	+13.0579	77.15	62.98	17.36	0.081278
173.7112	+14.0933	68.57	47.81	17.37	0.083029	173.8199	+12.7711	171.50	73.84	16.50	0.084432
173.7554	+14.0855	133.06	62.44	17.59	0.083045	173.8527	+12.8694	26.09	49.13	17.77	0.084268
172.8758	+12.4703	112.74	68.87	17.30	0.081694	173.8397	+14.7201	14.36	60.50	17.54	0.081567
172.9340	+12.4743	24.12	74.03	16.52	0.081312	173.8924	+14.7995	105.82	43.34	16.68	0.080406
172.9077	+14.0773	97.79	62.15	15.93	0.081312	173.9197	+14.5949	4.64	61.99	17.82	0.082758
172.9320	+14.0515	36.52	28.34	17.46	0.080877	173.9256	+14.6233	41.91	45.17	16.95	0.083128
173.0212	+15.0314	56.38	74.16	16.36	0.081138	173.9467	+13.9022	69.71	67.25	17.78	0.084305
173.0394	+15.0205	7.41	47.11	16.14	0.080608	173.9483	+13.9584	72.00	28.18	17.31	0.082934
173.0423	+15.0752	80.78	61.27	16.70	0.082866	173.9600	+14.0562	77.97	64.67	16.01	0.081410
173.0869	+14.9286	170.59	36.01	17.51	0.081422	174.0621	+14.0893	61.62	49.59	16.64	0.080548
173.0420	+11.5527	48.33	36.69	17.09	0.083040	174.0944	+14.0158	54.43	53.75	16.76	0.079833
173.1107	+11.5281	122.07	52.48	17.85	0.082753	174.0420	+14.4149	88.19	60.14	16.98	0.083707
173.1267	+11.5885	126.82	44.54	17.75	0.080401	174.1312	+14.4300	72.71	57.48	16.15	0.083072
173.1306	+11.4870	87.08	57.97	17.53	0.082870	174.1410	+14.4038	143.43	52.90	16.53	0.084717
173.1306	+11.5750	85.97	75.43	17.49	0.082703	174.1631	+14.4169	26.64	77.82	16.24	0.083010
173.1310	+11.5642	30.59	37.06	16.55	0.081703	174.2150	+14.4102	56.37	24.05	17.20	0.082676
173.1358	+11.5129	7.92	36.09	17.61	0.083221	174.2335	+14.3554	3.99	68.22	17.55	0.083588
173.0777	+14.0447	153.55	62.49	17.33	0.080375	174.0754	+14.9854	71.16	0.81	17.19	0.084122
173.1106	+14.0011	67.06	31.16	15.18	0.082101	174.0907	+13.4728	153.47	28.62	17.38	0.081773
173.1163	+13.9754	88.59	74.67	16.59	0.084349	174.0670	+13.2611	172.81	45.50	16.43	0.080742
173.1256	+14.0510	35.20	64.34	17.80	0.083259	174.0968	+13.3110	14.29	55.28	15.78	0.079695
173.1893	+14.0045	11.38	48.56	16.43	0.083167	174.1260	+13.2297	115.23	34.77	15.67	0.078637
173.1905	+14.0962	107.88	67.22	16.46	0.080645	174.1768	+13.2932	78.69	51.35	17.24	0.081483
173.1949	+14.0276	83.70	73.34	16.49	0.080767	174.1312	+15.5807	63.22	58.69	15.26	0.083225
173.2948	+14.1534	70.60	67.96	16.77	0.082459	174.2097	+15.5804	68.73	55.50	16.71	0.082951
173.2957	+14.0397	40.84	17.59	16.18	0.081154	174.2728	+12.6851	102.64	20.34	17.31	0.079789
173.2994	+13.9687	95.72	28.03	17.56	0.084080	174.2977	+12.6643	115.63	56.71	16.43	0.081079
173.3270	+14.1107	79.73	13.28	17.12	0.079497	174.3313	+12.6170	40.24	68.33	17.63	0.079112
173.3551	+13.9556	63.13	34.56	17.06	0.082398	174.4487	+12.6541	30.68	60.54	16.65	0.079059
173.4013	+13.9694	148.58	46.19	17.60	0.080967	174.3303	+13.1846	107.54	40.00	16.83	0.080682
173.2389	+16.5744	107.24	31.43	16.16	0.082692	174.3472	+13.0741	53.36	76.38	16.11	0.080676
173.2444	+16.4814	95.00	22.77	16.89	0.081399	174.4146	+13.0611	63.72	44.50	16.74	0.081304
173.2735	+11.5808	129.91	51.69	17.34	0.082059	174.4233	+13.2610	73.68	34.46	17.46	0.083743
173.3124	+11.5976	98.89	34.81	17.80	0.081928	174.4331	+13.2367	25.62	60.61	16.10	0.082981
173.3080	+12.7493	149.40	39.01	17.72	0.080961	174.4488	+13.0007	92.27	34.93	15.96	0.082924
173.3503	+12.8352	48.54	24.44	17.65	0.080652	174.4627	+13.0435	104.27	20.20	17.32	0.082239
173.3234	+14.7870	11.75	56.53	15.40	0.082278	174.4927	+13.2331	154.10	55.94	17.83	0.081661
173.3890	+14.6840	84.88	50.02	16.43	0.080669	174.5008	+13.0986	102.88	45.78	16.50	0.084024
173.3971	+14.7053	115.31	36.46	16.92	0.080609	174.5270	+13.2303	88.28	44.64	15.69	0.083239
173.5031	+14.6933	58.07	32.31	17.01	0.078945	174.5330	+13.2026	28.01	62.59	17.12	0.083414
173.5355	+14.7202	116.18	82.73	16.31	0.078602	174.5580	+13.2758	170.35	41.39	16.81	0.083342
173.3340	+13.7750	58.05	43.96	17.35	0.082367	174.5671	+13.2313	34.47	45.30	16.92	0.082932
173.4261	+13.8025	116.06	58.90	16.16	0.081706	174.5739	+13.0480	138.34	44.20	15.91	0.083476
173.4460	+17.0427	78.87	68.42	16.22	0.084018	174.5797	+13.2828	67.20	50.24	16.92	0.084243
173.5224	+17.1217	105.88	72.23	17.76	0.084077	174.5927	+13.2889	52.50	56.42	16.65	0.085944
173.5398	+17.1122	135.51	29.15	17.62	0.084553	174.5974	+13.1323	61.15	56.21	17.00	0.082015
173.6169	+13.7149	115.75	24.55	16.97	0.083028	174.6519	+13.3715	154.48	55.03	17.71	0.085715
173.6413	+13.7540	18.21	53.70	17.72	0.083008	174.6581	+13.1088	155.03	43.16	17.47	0.082018
173.7067	+13.8692	49.19	45.48	16.24	0.080890	174.6856	+13.3112	119.40	79.29	15.88	0.083833
173.7384	+13.7516	14.84	61.98	16.63	0.082494	174.7001	+13.3202	62.01	68.51	17.40	0.083743
173.7630	+13.9986	23.11	66.36	17.62	0.080675	174.7003	+13.2804	77.74	27.26	17.39	0.083780
173.7670	+13.8505	14.31	37.77	17.38	0.083819	174.7064	+13.2436	145.44	74.54	16.74	0.083341
173.7826	+13.9858	136.19	6.28	15.92	0.081174	174.4355	+13.5583	25.49	44.25	16.92	0.080167
173.7932	+13.7584	0.11	35.48	16.93	0.084137	174.4538	+13.5391	69.64	63.80	16.88	0.079409
173.7950	+13.6526	87.59	59.57	16.88	0.081017	174.4957	+13.7362	24.83	76.64	16.51	0.084973
173.8238	+13.9530	108.71	22.95	15.71	0.082146	174.4966	+13.7905	29.02	72.57	17.58	0.086086
173.8250	+13.8931	94.94	28.32	17.27	0.081968	174.5147	+13.6886	94.42	71.75	17.27	0.083720
173.8339	+13.7058	84.59	27.92	17.01	0.080952	174.5420	+13.7200	122.06	52.96	16.88	0.085138
173.8516	+13.5907	15.48	61.86	17.22	0.081089	174.5900	+13.7918	8.28	85.77	17.69	0.085206
173.8650	+13.7102	−1.64	59.65	17.39	0.078704	174.4974	+14.6261	90.90	77.76	16.55	0.082178
173.8722	+13.8403	20.15	48.01	16.61	0.082417	174.5049	+14.6623	87.11	66.24	17.01	0.081966
173.8737	+13.9245	101.48	17.55	17.70	0.078541	174.5719	+14.6061	41.64	56.60	17.09	0.082549
173.8891	+13.5300	47.24	54.10	16.38	0.077997	174.5046	+12.7978	77.65	35.58	17.58	0.081192
173.8932	+13.8053	86.66	72.87	16.16	0.077127	174.6163	+12.7404	31.72	75.55	16.40	0.081768
173.8973	+13.6814	162.72	46.68	18.07	0.081412	174.6260	+12.7843	12.40	40.70	17.62	0.082303
173.9006	+13.6541	1.47	33.67	16.59	0.081694	174.6639	+12.7836	91.37	23.20	17.18	0.082547

Table 35: SDSS DR7 of galaxies in the supercluster S[247+040+0029] that have redshifts range 0.025 to 0.037.The first two columns list the right ascension and declinations.The next two columns shows position and inclination angle.The fifth and sixth columns represent the magnitude in r-band and redshift.

RA(J2000)	$Dec.(J2000)$	$P(deg)$	$i(deg)$	m_r	z	$RA(J2000)$	$Dec.(J2000)$	$P(deg)$	$i(deg)$	m_r	z
247.5802	+39.8451	57.47	63.41	14.74	0.024637	247.8539	+39.6929	215.51	35.82	16.90	0.028447
247.6387	+39.8307	124.49	71.24	16.55	0.024650	248.0222	+39.9022	82.72	60.89	16.29	0.028455
247.1635	+39.5185	52.76	28.42	14.87	0.025266	247.1502	+39.5338	149.66	49.36	14.91	0.028461
247.7147	+39.9896	54.85	72.50	14.41	0.025452	247.3622	+40.7224	69.23	70.95	15.32	0.028462
247.3878	+39.9030	159.60	54.17	16.80	0.025522	244.9221	+35.1517	109.78	53.67	15.72	0.028465
247.3226	+39.7792	200.65	50.44	13.25	0.025972	252.4070	+40.5796	127.30	28.86	15.48	0.028487
246.7957	+39.3051	56.01	43.62	17.70	0.026003	248.1658	+40.8585	204.29	71.24	15.53	0.028489
247.0593	+39.5456	123.47	66.52	15.37	0.026065	248.5075	+41.3480	125.56	58.98	17.86	0.028505
247.1924	+39.4632	165.63	72.55	16.69	0.026107	247.3942	+39.6302	94.42	79.63	16.09	0.028522
247.3364	+39.8204	226.58	36.83	19.53	0.026175	246.4754	+40.9227	−47.65	73.58	16.78	0.028552
246.9945	+39.6040	189.73	34.75	17.07	0.026223	247.8793	+39.9918	184.78	65.10	15.03	0.028574
247.4043	+40.8483	211.69	44.49	16.24	0.026344	247.4498	+39.7162	185.39	68.42	15.56	0.028580
247.2292	+39.1710	198.69	61.09	17.74	0.026538	244.2502	+34.5237	24.05	36.22	14.17	0.028593
247.0753	+39.1864	78.95	71.76	17.50	0.026644	245.8662	+37.8311	126.31	63.03	15.58	0.028630
247.6585	+40.7085	67.18	70.48	14.59	0.026731	247.5368	+40.5694	162.66	40.04	15.21	0.028630
247.1631	+39.5528	201.62	65.00	17.29	0.026840	245.3673	+40.2036	32.83	48.36	16.03	0.028632
247.0950	+39.2000	227.67	55.70	14.30	0.026970	246.6803	+38.3672	53.67	55.40	17.77	0.028636
247.2851	+39.5333	53.65	64.15	17.41	0.026973	246.7883	+39.5866	128.98	63.82	17.03	0.028639
247.8005	+40.4219	179.41	24.20	14.48	0.026995	247.7107	+40.5948	152.28	48.61	16.60	0.028652
244.2079	+35.7019	−87.24	55.85	17.42	0.027050	246.7494	+41.0989	106.22	73.21	16.69	0.028655
247.2823	+39.1485	168.90	39.57	17.56	0.027072	246.4161	+40.8012	147.54	43.76	16.70	0.028667
244.3200	+35.9205	75.08	55.93	14.34	0.027154	247.7113	+39.5381	194.07	83.57	16.56	0.028671
247.4246	+40.2748	219.20	46.35	15.67	0.027164	244.8392	+37.1340	59.34	56.77	18.13	0.028688
244.4315	+34.9649	133.19	36.02	14.66	0.027191	245.7990	+38.5879	108.52	53.40	15.40	0.028719
247.8444	+40.5507	227.48	21.48	16.52	0.027243	246.2962	+37.9747	58.63	42.50	16.79	0.028724
247.2811	+39.6274	186.00	73.17	16.24	0.027341	244.8310	+35.2677	15.13	76.16	16.39	0.028731
247.8939	+40.5656	124.12	51.95	14.49	0.027378	244.8256	+37.0952	99.05	78.26	17.34	0.028734
246.6446	+40.9138	183.92	73.66	15.49	0.027397	247.1193	+40.7208	192.63	85.75	17.53	0.028778
247.1852	+39.5155	81.62	48.04	17.76	0.027462	246.2598	+40.9466	182.12	44.88	17.07	0.028781
244.1634	+35.8449	39.40	13.42	17.62	0.027518	247.2416	+39.6475	157.22	34.26	15.17	0.028784
247.3491	+40.8750	126.84	59.76	17.62	0.027537	247.4796	+40.0807	218.73	60.48	17.08	0.028784
247.8642	+40.4353	57.18	38.60	14.99	0.027684	245.7015	+36.3374	72.14	23.88	17.26	0.028785
247.4321	+40.0165	201.05	46.00	13.81	0.027711	246.2004	+38.6625	117.85	56.65	13.67	0.028790
244.2873	+34.9360	16.99	70.00	17.74	0.027728	244.2789	+35.1096	96.88	83.11	14.85	0.028794
247.6161	+39.5617	181.22	59.02	14.62	0.027732	244.2249	+34.9545	1.28	90.02	16.51	0.028797
247.6290	+41.0166	77.24	54.81	16.57	0.027760	247.5238	+40.7980	200.53	55.31	15.91	0.028849
247.3197	+40.6505	62.01	52.65	15.81	0.027773	247.1890	+39.6364	60.87	67.88	15.82	0.028855
246.8693	+38.8691	185.06	48.56	17.39	0.027773	246.5073	+40.7431	69.84	79.19	17.67	0.028857
246.8704	+38.9564	64.19	79.72	15.09	0.027824	247.1080	+40.3812	164.41	72.34	17.62	0.028866
247.3333	+39.4290	164.65	60.49	16.76	0.027839	246.7205	+41.2538	99.42	39.74	14.57	0.028875
246.4928	+40.3467	75.27	40.94	17.26	0.027894	247.3244	+39.0300	136.82	62.98	13.07	0.028892
247.6876	+39.7600	165.97	69.91	16.71	0.027895	245.2270	+39.9084	84.88	58.90	15.77	0.028893
247.7914	+41.3132	173.21	69.94	17.26	0.027921	245.2324	+39.8610	227.69	22.41	15.92	0.028893
246.9159	+39.1641	178.65	65.31	13.68	0.027934	245.7791	+38.3413	127.60	30.46	14.60	0.028899
247.3217	+40.4223	176.22	47.92	13.99	0.027954	248.1243	+39.9303	174.38	53.85	15.69	0.028917
247.2566	+40.5349	227.90	63.00	16.50	0.027962	247.4030	+39.7353	205.27	52.22	15.15	0.028927
247.2490	+39.6839	101.68	57.38	15.65	0.027964	247.4919	+40.6285	148.29	64.71	16.61	0.028931
247.6476	+40.6234	219.33	52.48	15.90	0.027977	250.7955	+39.7230	174.86	60.92	16.83	0.028935
247.4865	+39.6608	57.37	68.21	16.75	0.028001	251.6692	+40.7583	215.46	28.32	15.56	0.028939
245.5686	+38.5773	98.54	64.07	14.88	0.028010	251.8534	+41.3788	166.30	70.39	17.24	0.028941
247.6463	+39.7281	161.89	60.67	17.21	0.028029	247.1504	+40.4975	144.11	38.34	16.78	0.028951
248.0825	+40.5751	190.27	54.11	16.54	0.028042	247.3740	+40.8584	208.71	47.84	15.60	0.028959
247.6440	+40.1873	202.04	59.31	17.53	0.028045	245.7445	+40.6977	138.78	20.36	16.50	0.028961
244.3415	+34.8072	−77.52	64.51	14.81	0.028109	245.9385	+38.7930	61.84	59.58	15.94	0.028962
247.5461	+40.6179	149.14	44.84	15.47	0.028125	246.9047	+39.1361	195.88	32.51	17.22	0.028965
247.4487	+40.8720	147.94	90.02	17.13	0.028127	247.7614	+39.7925	232.04	56.27	13.56	0.028965
246.2147	+37.8906	149.35	70.82	17.71	0.028131	246.8243	+39.1431	75.85	64.18	17.46	0.028974
247.5674	+40.6597	171.80	85.52	15.83	0.028146	247.5746	+40.6026	115.89	49.23	16.77	0.028979
247.7118	+40.0248	201.07	60.55	15.55	0.028148	247.4973	+39.5285	81.90	68.37	16.12	0.028986
246.4420	+40.5101	219.91	67.31	16.71	0.028149	247.2800	+39.4957	190.50	24.90	16.91	0.028990
246.8143	+38.9543	150.89	45.10	15.18	0.028157	245.3764	+37.8595	118.05	52.14	15.72	0.028999
246.3915	+38.6762	195.91	66.11	15.38	0.028172	247.0504	+40.7886	204.64	34.22	16.43	0.029003
246.9934	+39.1179	132.33	37.08	17.22	0.028198	247.8315	+39.7905	98.87	48.09	13.86	0.029005
247.6082	+39.3157	109.07	48.61	17.40	0.028200	246.5459	+39.2370	76.66	71.04	14.60	0.029016
245.0047	+37.2170	162.16	73.00	16.46	0.028202	251.9786	+39.2350	142.04	72.45	15.88	0.029036
247.3188	+39.4010	196.11	39.32	14.77	0.028205	246.2693	+38.8857	49.45	62.72	16.05	0.029037
246.3023	+37.9900	64.17	35.58	17.77	0.028250	246.4604	+39.8904	170.11	63.05	15.53	0.029056
246.7666	+39.4334	67.42	28.86	17.23	0.028272	244.8676	+36.2943	−58.46	64.01	17.30	0.029058
247.1684	+39.6713	185.17	50.35	16.38	0.028299	249.4312	+39.9326	113.92	66.04	13.72	0.029066
247.3173	+40.2602	221.20	37.89	17.30	0.028314	247.0115	+41.1418	165.62	37.01	17.03	0.029075
247.5351	+40.8088	87.69	57.20	14.89	0.028316	250.1409	+40.1477	200.82	28.94	15.46	0.029076
248.4271	+39.5978	66.51	42.77	17.12	0.028319	246.4407	+42.7893	162.90	39.97	14.60	0.029079
247.9939	+39.9478	164.01	63.02	13.43	0.028324	246.2743	+40.9288	190.45	27.88	15.88	0.029079
244.0148	+35.5166	70.54	63.73	17.44	0.028334	246.8223	+39.6196	113.87	65.07	17.39	0.029085
245.7217	+38.2459	215.81	83.04	17.69	0.028334	244.8402	+37.0691	113.94	40.63	17.16	0.029090
247.4438	+40.8749	157.68	69.11	16.45	0.028337	247.5226	+40.7662	66.52	42.83	17.45	0.029100
247.2388	+41.1345	230.78	52.11	17.70	0.028354	247.0231	+40.8685	223.49	59.80	17.14	0.029101
248.1423	+39.6146	166.51	52.84	16.92	0.028361	247.8013	+39.9466	154.64	54.76	17.72	0.029102
246.9328	+39.7439	78.09	35.74	17.45	0.028384	245.8474	+40.3014	−58.31	56.99	17.52	0.029103
243.9810	+35.6102	59.14	21.84	17.63	0.028391	246.2958	+38.6482	194.11	58.99	15.20	0.029112
247.3814	+40.4128	97.29	28.79	16.61	0.028394	246.6711	+40.1807	164.81	44.76	14.98	0.029114
248.0160	+39.6089	130.31	56.79	17.81	0.028395	246.9802	+39.2588	177.09	79.66	17.23	0.029116
247.4097	+40.2354	78.91	71.49	15.43	0.028396	245.6109	+38.3864	192.30	86.80	16.39	0.029116
247.1166	+41.2205	81.65	18.61	17.76	0.028401	246.4552	+40.3452	188.32	74.16	16.65	0.029126
247.2663	+39.6696	116.03	65.00	16.93	0.028409	246.1229	+38.7713	66.76	17.79	17.60	0.029133
248.1347	+39.6273	125.51	70.92	16.48	0.028410	246.2572	+40.5261	93.83	60.48	14.51	0.029141
245.9566	+38.0624	183.43	65.41	17.35	0.028413	250.9889	+40.5256	80.97	51.78	17.79	0.029142
246.8458	+39.1274	138.15	73.26	15.92	0.028414	246.8544	+39.8538	197.78	19.52	14.15	0.029146
251.8934	+40.3346	76.79	63.16	15.70	0.028417	247.2158	+40.3515	90.91	23.81	17.80	0.029151
244.4510	+35.0324	161.50	31.41	15.24	0.028422	246.3587	+39.8707	90.43	64.49	14.59	0.029153
246.6771	+39.1452	174.30	56.03	16.87	0.028422	247.0735	+40.9670	191.60	52.48	17.61	0.029159

Table 36: SDSS DR7 of galaxies in the supercluster S[247+040+0029] that have redshifts range 0.025 to 0.037.The first two columns list the right ascension and declinations.The next two columns shows position and inclination angle.The fifth and sixth columns represent the magnitude in r-band and redshift.

RA(J2000)	$Dec.(J2000)$	$P(deg)$	$i(deg)$	m_r	z	$RA(J2000)$	$Dec.(J2000)$	$P(deg)$	$i(deg)$	m_r	z
252.1840	+39.5025	130.74	59.67	17.46	0.029164	247.8301	+39.1508	216.47	74.35	17.24	0.029629
246.4671	+41.0578	−32.55	59.74	15.97	0.029165	246.2309	+39.6194	83.31	18.62	15.10	0.029630
247.6385	+41.4386	101.47	72.02	16.24	0.029168	245.7294	+41.2847	187.36	54.05	15.23	0.029633
248.4651	+40.8295	225.38	74.31	17.08	0.029170	250.4485	+39.6079	233.76	66.20	17.07	0.029648
244.8671	+34.7455	141.01	38.62	14.19	0.029186	246.4492	+40.6217	195.17	62.93	15.51	0.029653
248.1097	+39.5178	174.64	48.68	14.98	0.029190	250.4748	+44.0355	114.44	61.07	17.18	0.029659
246.5335	+39.6850	194.70	34.14	17.50	0.029196	247.9485	+39.8142	157.96	29.23	16.99	0.029664
248.4273	+40.1531	96.29	50.57	14.40	0.029197	246.4963	+39.4201	171.65	36.72	16.00	0.029674
246.3934	+40.7871	85.89	54.51	16.93	0.029198	245.9771	+39.1582	95.42	74.86	16.18	0.029678
246.6459	+39.1800	163.85	60.78	17.27	0.029202	252.8956	+40.0218	63.17	72.06	16.71	0.029688
244.1192	+34.6533	209.06	0.82	17.16	0.029204	246.7091	+40.9998	77.18	47.88	17.62	0.029697
244.0716	+35.7876	169.24	41.67	17.58	0.029207	246.5216	+41.0500	−80.20	76.24	14.72	0.029699
246.6495	+40.9117	136.20	77.07	16.69	0.029220	252.1848	+39.5999	230.87	30.39	14.92	0.029699
251.7532	+39.0613	222.59	45.31	14.47	0.029222	247.3881	+39.8477	205.36	41.33	14.52	0.029700
246.3018	+40.8671	92.15	21.50	19.19	0.029225	247.3041	+41.1509	160.38	24.33	15.36	0.029707
246.6881	+40.6842	125.49	49.27	17.09	0.029229	247.2058	+40.4641	53.40	60.54	16.14	0.029711
247.8236	+39.7940	194.24	52.07	14.08	0.029229	246.7508	+42.6993	164.17	45.34	15.11	0.029715
247.3239	+40.6207	100.94	12.71	14.69	0.029235	247.8821	+39.8976	69.42	33.81	17.59	0.029723
246.9275	+39.3773	211.38	31.50	16.12	0.029235	247.6818	+38.5453	165.50	60.36	15.74	0.029731
247.0225	+40.7546	106.55	64.32	17.74	0.029237	252.2400	+40.1037	69.16	73.05	15.09	0.029733
246.7086	+40.9178	182.39	55.22	15.54	0.029253	245.2828	+35.3732	−51.89	40.57	15.47	0.029741
245.6457	+38.3670	112.08	53.17	17.52	0.029274	247.8033	+40.1345	185.70	45.88	15.97	0.029741
246.7188	+40.9703	69.36	69.41	16.95	0.029297	246.2902	+39.2767	200.38	80.39	16.80	0.029756
247.3373	+40.0640	193.11	31.30	16.19	0.029298	247.4595	+40.6763	144.11	80.77	14.30	0.029758
247.0838	+40.9333	185.50	49.33	16.99	0.029301	246.2574	+40.9210	139.21	35.43	15.48	0.029766
247.5533	+40.9429	139.71	25.66	15.76	0.029303	250.2680	+39.3315	137.20	45.68	17.34	0.029770
245.8682	+37.7232	117.73	38.61	16.11	0.029307	248.4264	+39.1851	201.96	34.38	16.41	0.029770
246.4582	+40.4887	69.35	52.65	16.75	0.029312	247.5724	+39.8894	60.49	22.24	17.10	0.029778
247.6082	+40.6142	201.27	58.67	16.73	0.029313	244.4296	+35.0411	103.42	64.68	17.55	0.029781
247.7835	+40.3881	154.24	64.35	14.43	0.029315	246.7481	+39.0138	75.81	75.08	16.97	0.029786
246.9755	+39.7367	135.56	45.51	14.46	0.029320	246.4803	+40.7791	170.33	59.70	15.50	0.029786
246.0625	+41.1106	81.82	76.36	15.86	0.029350	246.3469	+37.9300	181.50	65.03	14.65	0.029788
245.7733	+41.2319	190.99	75.67	15.16	0.029351	248.3180	+39.2324	216.14	74.92	16.89	0.029796
247.5997	+40.6657	126.89	71.65	17.00	0.029364	250.1231	+39.2351	232.96	50.89	16.61	0.029799
247.4235	+40.3334	160.73	40.79	17.78	0.029367	250.0539	+39.7335	121.23	57.73	15.85	0.029801
246.8460	+40.5659	69.66	72.43	15.83	0.029370	245.7620	+41.0975	−22.96	37.27	15.77	0.029802
245.6667	+37.6098	197.53	53.76	15.20	0.029373	246.2819	+39.4358	125.26	21.05	16.42	0.029802
245.5684	+38.4499	146.97	49.12	16.69	0.029380	245.9249	+39.2398	119.62	49.40	15.07	0.029804
247.1019	+38.9331	131.82	87.66	15.34	0.029386	246.7490	+39.3201	164.50	64.10	14.72	0.029811
247.6036	+39.4647	195.85	60.39	14.75	0.029395	244.7415	+35.3484	−57.08	39.04	16.13	0.029815
247.6843	+39.8999	158.18	32.55	17.48	0.029400	249.9150	+39.5385	91.30	56.50	17.53	0.029827
246.9208	+40.1552	210.83	72.20	15.91	0.029400	247.8180	+39.8760	189.57	78.41	17.53	0.029848
246.5514	+39.1431	165.67	75.60	17.13	0.029409	246.9312	+41.3076	106.38	40.09	16.75	0.029856
245.7555	+38.0780	115.44	64.27	17.26	0.029412	246.2532	+38.9992	174.57	53.24	17.64	0.029872
249.5377	+39.9178	174.31	50.20	17.79	0.029425	248.7796	+39.8254	222.75	41.94	17.57	0.029874
247.5839	+39.8043	109.05	43.12	15.97	0.029432	244.7275	+35.1539	6.27	39.53	17.38	0.029885
247.4372	+40.8116	140.63	39.48	17.32	0.029440	247.0512	+40.8541	189.10	70.60	17.03	0.029885
247.6657	+40.8951	228.61	45.31	17.67	0.029450	244.1797	+35.3055	76.02	34.01	14.42	0.029886
252.4632	+40.4334	80.35	59.19	16.95	0.029454	245.0699	+37.7418	138.51	62.11	16.57	0.029888
248.1419	+39.7778	61.07	42.25	15.94	0.029460	248.6909	+39.4266	123.67	52.92	15.50	0.029896
244.4687	+35.0484	104.49	52.06	13.68	0.029468	246.5810	+39.6036	68.61	50.39	14.89	0.029899
245.7178	+41.0717	−38.68	65.03	17.21	0.029471	250.1606	+44.2037	189.60	76.27	17.27	0.029901
244.5985	+35.1743	115.08	44.18	15.41	0.029486	245.3760	+40.9007	107.22	73.36	16.49	0.029909
247.4790	+38.8749	70.23	48.53	17.80	0.029487	252.7430	+39.7305	91.27	29.53	16.82	0.029913
245.8424	+39.2154	137.89	40.26	14.51	0.029487	249.9996	+44.1334	65.23	54.76	16.01	0.029915
248.4537	+39.6304	123.34	53.24	16.44	0.029496	244.2015	+35.3404	103.31	44.14	17.12	0.029927
247.5577	+40.1897	165.24	32.00	14.75	0.029500	247.6118	+41.4840	173.73	59.94	16.76	0.029932
245.5175	+37.5067	118.99	47.69	16.92	0.029507	244.1921	+35.2849	133.35	45.42	16.87	0.029944
246.0885	+39.3018	62.62	30.84	14.98	0.029513	247.2209	+39.4970	57.77	50.44	15.91	0.029945
251.9468	+39.7339	64.20	75.32	15.84	0.029514	244.6750	+35.2262	−74.45	60.40	14.03	0.029948
244.8379	+34.8297	205.92	57.32	15.51	0.029515	247.6744	+40.5294	140.04	40.28	16.81	0.029957
245.6505	+37.1211	61.77	88.67	17.32	0.029521	244.7825	+34.3575	58.43	28.18	15.24	0.029959
246.1309	+40.6845	64.24	60.30	17.77	0.029521	249.1067	+39.0568	63.21	73.16	15.68	0.029959
247.3624	+40.7714	125.00	27.78	17.75	0.029524	249.3596	+44.4036	174.64	73.45	17.56	0.029959
247.1835	+39.9645	70.57	74.52	17.22	0.029525	246.4243	+39.6001	197.52	35.20	17.56	0.029965
244.2963	+35.5101	−22.13	15.99	14.84	0.029528	252.8776	+40.1078	159.50	30.80	17.15	0.029967
245.2018	+35.5365	−24.21	49.55	17.77	0.029536	247.2046	+39.1490	197.04	47.81	17.66	0.029968
243.9140	+36.8970	213.37	56.47	14.65	0.029538	244.4189	+35.0042	69.14	28.06	15.97	0.029969
246.3928	+38.9333	137.85	54.32	16.89	0.029539	247.1737	+39.8374	131.77	76.30	16.82	0.029969
245.1946	+37.5985	159.77	84.88	16.65	0.029540	252.8841	+39.8880	220.01	50.68	16.35	0.029970
249.1968	+39.3468	203.62	73.43	14.61	0.029541	245.5751	+41.4553	221.67	81.00	16.26	0.029971
252.1899	+39.6344	71.95	59.38	17.34	0.029542	246.0126	+41.3548	50.93	37.80	16.97	0.029990
244.9260	+37.8435	132.17	63.87	16.50	0.029546	245.3420	+40.8105	−76.77	65.35	14.76	0.029996
246.3347	+37.4775	184.09	30.37	15.43	0.029548	250.9469	+36.8956	100.12	69.74	17.01	0.029998
246.6931	+39.4702	61.39	28.76	16.73	0.029552	250.3534	+37.0436	88.95	68.45	14.54	0.030006
246.3658	+39.5520	195.93	17.72	13.27	0.029556	246.8190	+39.3846	194.73	44.51	17.32	0.030016
247.3130	+40.2410	73.84	23.01	16.51	0.029568	241.8926	+36.4840	108.21	59.20	17.64	0.030024
247.8441	+39.1678	187.76	83.78	17.62	0.029572	247.4196	+40.8402	112.42	49.57	17.61	0.030025
252.6384	+40.2245	236.47	45.19	15.46	0.029575	245.6606	+41.4784	51.98	46.40	16.52	0.030032
247.4804	+40.6600	226.43	51.47	14.24	0.029576	246.8494	+40.6778	103.20	62.64	16.32	0.030035
246.2022	+37.5176	51.66	85.67	17.78	0.029589	244.3968	+35.2309	164.62	59.81	15.73	0.030043
246.1321	+40.7656	80.34	24.94	14.85	0.029590	250.9693	+39.9834	125.94	74.90	16.13	0.030048
244.7447	+34.7304	−12.05	60.24	15.53	0.029602	246.6416	+45.0323	91.32	39.67	13.81	0.030055
247.3594	+40.4387	170.58	75.98	16.30	0.029614	247.4897	+40.6307	101.71	27.67	17.63	0.030062
244.4700	+35.2471	204.04	73.83	17.07	0.029614	244.4476	+34.6422	74.66	68.17	17.65	0.030080
246.5913	+40.9119	85.93	55.20	16.40	0.029620	245.7767	+40.8583	164.64	40.88	15.25	0.030081
251.8116	+40.2451	137.46	52.73	17.40	0.029621	248.9092	+38.9728	78.35	70.10	16.74	0.030083
247.5794	+41.1021	202.15	70.02	16.28	0.029621	247.2826	+40.6650	81.88	68.90	16.64	0.030083
243.4611	+35.1469	70.07	68.29	16.97	0.029623	246.2560	+38.6392	109.59	29.77	17.19	0.030084
245.6620	+40.9798	126.31	51.33	17.29	0.029623	244.3848	+35.0839	217.96	72.69	16.66	0.030085
247.0801	+41.1729	54.80	45.74	16.29	0.029625	246.0843	+40.8650	79.28	79.96	16.74	0.030087

Table 37: SDSS DR7 of galaxies in the supercluster S[227+006+0078] that have redshifts range 0.072 to 0.087.The first two columns list the right ascension and declinations.The next two columns shows position and inclination angle.The fifth and sixth columns represent the magnitude in r-band and redshift.

RA(J2000)	$Dec.(J2000)$	$P(deg)$	$i(deg)$	m_r	z	$RA(J2000)$	$Dec.(J2000)$	$P(deg)$	$i(deg)$	m_r	z
225.5733	+8.3725	144.75	61.30	17.69	0.079182	227.1862	+8.3954	53.68	47.66	17.02	0.078225
225.6021	+8.4024	84.27	69.55	16.95	0.079299	227.1922	+8.4343	71.65	22.23	17.47	0.077005
225.6448	+8.3343	148.73	38.18	17.47	0.079748	226.6271	+6.4815	49.81	20.86	17.82	0.080403
225.7301	+6.2241	96.73	58.44	17.68	0.077903	226.7089	+6.4728	182.82	23.47	16.19	0.081017
225.8110	+6.2514	132.93	71.11	16.94	0.080446	226.6583	+6.0821	151.44	54.74	17.26	0.076308
225.8514	+6.3557	150.38	56.29	16.89	0.079602	226.7356	+6.0614	111.74	50.17	17.17	0.076780
225.7409	+7.6531	29.80	18.58	15.82	0.078699	226.6851	+7.1992	95.52	69.06	17.50	0.076671
225.8359	+7.6077	121.78	73.20	15.66	0.078482	226.7288	+7.1890	142.61	72.73	16.95	0.076795
225.8720	+7.5576	30.40	37.54	17.49	0.078397	226.7435	+7.2006	80.90	53.11	17.39	0.076335
225.8020	+7.9002	37.65	46.79	16.58	0.075712	226.8216	+7.1848	71.39	82.05	17.29	0.078544
225.8103	+7.9843	106.70	56.48	16.83	0.075774	226.6994	+7.8647	55.21	44.30	17.47	0.074726
225.8695	+7.9722	162.88	56.53	17.19	0.076063	226.7440	+7.7751	26.67	60.82	16.89	0.077589
225.9201	+8.0274	147.67	69.74	17.55	0.079874	226.7502	+7.8132	116.05	53.33	15.90	0.076117
225.9396	+8.0257	41.07	71.27	16.11	0.081291	226.7936	+7.7796	158.70	52.51	17.44	0.080353
226.0590	+9.0506	126.30	33.96	17.30	0.080744	226.8199	+7.8162	88.40	58.06	17.52	0.077380
226.0843	+9.0062	172.26	68.31	16.90	0.078893	226.8611	+7.8405	88.87	75.28	16.50	0.077209
226.0854	+8.9875	113.58	72.95	17.32	0.079915	226.9044	+7.8049	143.03	33.80	17.73	0.077603
226.1708	+8.9625	67.61	78.84	16.64	0.080583	226.7164	+10.5520	81.50	37.63	17.08	0.078306
226.1562	+5.0378	155.06	39.69	17.03	0.079907	226.7347	+10.4351	148.54	47.94	17.10	0.078828
226.1980	+5.2255	52.32	77.74	17.55	0.077648	226.7363	+10.4508	73.52	52.35	15.37	0.077095
226.2266	+5.0976	138.78	49.69	16.33	0.077894	226.8412	+10.3125	164.25	24.43	15.28	0.076361
226.2560	+5.1317	13.05	48.43	16.07	0.077089	226.8947	+10.3319	101.73	55.51	17.10	0.075580
226.2568	+5.0833	55.72	75.68	16.76	0.077047	226.9503	+10.3173	19.35	56.88	14.80	0.075684
226.2587	+4.9765	65.85	52.20	17.13	0.077219	226.9625	+10.2081	63.31	24.34	16.30	0.077734
226.2683	+5.0676	19.13	35.26	15.35	0.080683	226.9937	+10.3482	166.08	76.38	16.43	0.076515
226.2810	+5.0873	26.52	48.97	15.18	0.077885	227.0008	+10.3671	145.22	50.37	17.27	0.075164
226.2893	+5.1690	161.03	67.47	17.71	0.078309	227.0413	+10.2972	80.43	83.65	17.40	0.080877
226.2934	+4.9988	148.04	70.76	15.76	0.078314	226.8861	+7.7746	88.78	54.02	17.51	0.080791
226.3377	+5.0903	74.17	73.67	15.77	0.077823	226.9516	+7.8072	178.30	86.10	16.63	0.081162
226.3511	+5.0592	14.19	50.91	15.86	0.080639	226.9834	+7.6906	124.56	88.33	17.32	0.077996
226.4497	+4.9367	116.82	37.63	15.84	0.078601	226.8985	+9.9310	75.03	46.52	16.93	0.076137
226.4549	+5.0538	132.24	59.04	17.12	0.078550	226.9503	+9.7834	49.36	70.94	17.18	0.078847
226.4549	+4.9843	27.04	55.18	17.62	0.081093	226.9532	+9.8478	120.11	61.50	17.75	0.078064
226.4694	+5.0380	18.87	84.13	16.43	0.080198	226.9853	+9.7815	105.67	50.67	17.68	0.076283
226.3674	+8.9971	124.06	64.51	17.37	0.080787	226.9181	+4.6433	45.95	65.46	17.20	0.080860
226.4046	+8.9277	155.80	80.03	16.68	0.080002	226.9798	+4.7181	125.42	50.53	17.40	0.080824
226.4362	+8.9571	170.08	33.24	17.29	0.078948	226.9709	+5.3766	42.00	80.67	16.77	0.080761
226.4451	+9.0028	11.44	61.95	16.81	0.079085	226.9764	+5.4896	139.18	38.05	17.46	0.080260
226.4467	+9.0533	58.39	48.15	17.45	0.079562	226.9913	+5.4755	44.61	71.52	16.74	0.080058
226.4572	+10.5307	85.39	26.24	17.57	0.079022	226.9937	+6.2916	77.14	27.58	17.18	0.078264
226.5134	+10.4549	105.60	67.81	16.65	0.079158	227.0137	+6.3426	149.03	81.19	17.88	0.077335
226.5683	+10.4973	178.73	42.45	16.17	0.077154	227.0312	+6.1219	71.86	44.86	17.72	0.077287
226.4899	+4.5201	120.10	66.51	17.21	0.081456	227.0608	+6.2053	26.80	43.45	16.76	0.075884
226.5295	+4.4982	111.90	74.30	16.99	0.081401	227.1401	+6.1885	124.31	59.85	14.35	0.076376
226.5453	+8.9291	81.26	50.61	17.26	0.080464	227.1447	+5.9631	170.73	56.25	17.61	0.079848
226.5622	+8.9017	108.41	36.38	17.86	0.079982	227.1558	+6.1883	185.77	20.18	16.95	0.080139
226.5917	+8.5127	98.89	34.32	17.04	0.075224	227.2033	+5.9864	72.15	60.10	17.54	0.080246
226.6340	+8.4730	146.60	58.00	17.36	0.080588	227.2603	+6.1404	55.42	58.72	16.60	0.081817
226.5952	+5.6576	114.22	77.71	16.25	0.079495	227.2655	+5.9749	63.62	28.96	16.29	0.077112
226.6628	+5.6311	116.77	76.49	16.81	0.080914	227.3076	+5.9125	55.87	56.74	16.93	0.079013
226.6052	+8.7494	98.97	71.71	16.19	0.077257	227.3154	+6.0299	83.06	60.04	17.66	0.080491
226.6804	+8.7128	176.10	63.54	17.49	0.075631	227.3331	+5.9039	169.36	28.00	16.64	0.078950
226.6974	+8.8638	75.39	35.72	17.32	0.075670	227.4117	+5.9412	46.06	53.99	16.87	0.079214
226.7550	+8.7340	117.91	47.31	16.48	0.077812	227.4667	+5.9490	85.55	21.83	17.28	0.079582
226.7693	+8.7518	73.55	35.18	16.17	0.076279	227.4689	+5.6797	63.85	41.70	16.97	0.076808
226.7732	+8.7688	81.74	79.65	16.61	0.081876	227.4720	+6.0921	139.80	61.42	17.78	0.077353
226.7970	+8.4146	75.99	48.15	17.33	0.080602	227.4738	+5.9700	81.23	43.99	17.31	0.075858
226.8052	+8.7596	9.59	39.95	17.58	0.078165	227.4847	+6.0212	72.82	69.82	16.96	0.080364
226.8258	+8.3289	9.94	84.31	17.04	0.078327	227.4856	+6.1994	123.25	31.07	17.53	0.078963
226.8364	+8.7288	89.33	62.12	15.40	0.078007	227.5233	+5.9525	5.21	77.68	16.88	0.080862
226.8500	+8.5059	60.96	42.46	17.16	0.079413	227.5261	+5.8436	106.24	35.42	16.61	0.080084
226.8555	+8.4957	13.61	70.18	14.40	0.077924	227.5392	+5.5724	93.21	34.74	16.51	0.079345
226.8564	+8.6346	36.10	61.09	17.36	0.075738	227.5442	+4.8929	135.04	70.28	17.91	0.079625
226.8606	+8.2799	30.79	54.74	17.78	0.080516	227.5480	+5.4776	157.70	44.75	17.77	0.079767
226.8654	+8.5534	18.12	64.56	16.09	0.079389	227.5492	+6.1612	11.49	28.21	16.65	0.080391
226.8682	+8.0503	37.55	57.65	16.77	0.079424	227.5506	+6.1193	140.60	47.04	16.74	0.080549
226.8773	+8.4240	131.11	55.03	17.75	0.078580	227.5507	+6.0254	84.89	53.85	16.62	0.077281
226.8793	+8.5730	12.57	40.38	17.85	0.078486	227.5508	+6.2143	124.76	56.78	17.01	0.078874
226.8971	+8.6281	121.25	65.85	15.84	0.078877	227.5542	+5.6039	152.34	80.01	15.87	0.078568
226.9072	+8.4498	182.62	68.76	17.19	0.079192	227.5548	+4.7325	79.76	13.66	17.23	0.077199
226.9123	+8.2825	46.32	40.04	15.64	0.078941	227.5636	+5.6348	138.40	54.75	17.50	0.076638
226.9177	+8.1666	187.47	78.12	17.28	0.080923	227.5688	+4.7856	44.91	22.62	17.11	0.076200
226.9225	+8.1974	118.85	51.93	16.42	0.079697	227.5708	+4.7321	168.66	80.30	15.73	0.076162
226.9331	+8.2701	11.54	31.57	15.80	0.078676	227.5723	+5.7012	91.28	75.85	16.62	0.075544
226.9403	+8.2551	156.79	65.71	16.81	0.077387	227.5724	+5.5586	99.39	34.01	16.60	0.077013
226.9863	+8.1292	59.01	88.71	16.79	0.077232	227.5771	+5.9747	169.01	53.93	17.17	0.081882
226.9878	+8.2776	172.36	4.41	16.14	0.078158	227.5775	+4.9333	32.68	39.60	16.63	0.076834
226.9896	+8.6033	127.11	28.20	17.05	0.076814	227.5797	+6.1648	142.93	55.84	17.26	0.081598
226.9932	+8.1903	151.26	75.95	17.11	0.076158	227.5816	+5.7865	102.89	26.17	16.84	0.078212
227.0125	+8.3088	157.49	52.55	17.37	0.074476	227.5858	+5.8550	124.69	81.64	17.77	0.076699
227.0171	+8.2316	41.86	64.96	16.73	0.077069	227.5880	+5.1768	100.09	31.63	17.80	0.079632
227.0215	+8.5242	151.84	71.40	17.35	0.076684	227.5937	+4.6982	108.66	54.30	17.56	0.077327
227.0238	+8.5543	162.01	56.25	17.45	0.075683	227.5960	+6.0797	98.39	24.53	16.99	0.076282
227.0244	+8.3627	43.18	49.43	17.50	0.076724	227.5967	+6.0372	60.32	64.57	16.43	0.080874
227.0286	+8.1157	138.79	58.82	15.92	0.075351	227.5992	+6.2688	129.16	85.31	17.38	0.079244
227.0496	+8.6726	19.35	62.63	15.70	0.077012	227.6010	+4.7757	17.98	51.23	17.80	0.078997
227.0637	+8.2196	64.76	43.77	17.74	0.076060	227.6060	+5.8411	23.14	71.37	15.59	0.078059
227.0796	+8.6112	186.98	46.74	16.92	0.075692	227.6106	+6.0067	69.25	81.18	16.06	0.079613
227.0924	+8.3502	141.79	64.69	17.05	0.075967	227.6196	+5.6382	151.26	42.47	17.36	0.078605
227.0998	+8.5842	73.78	37.76	17.52	0.078846	227.6204	+5.2208	140.55	54.28	17.35	0.079430
227.1369	+8.4824	28.65	25.77	16.31	0.079644	227.6229	+6.1135	75.53	42.94	15.60	0.077613

Table 38: SDSS DR7 of galaxies in the supercluster S[227+006+0078] that have redshifts range 0.072 to 0.087.The first two columns list the right ascension and declinations.The next two columns shows position and inclination angle.The fifth and sixth columns represent the magnitude in r-band and redshift.

RA(J2000)	$Dec.(J2000)$	$P(deg)$	$i(deg)$	m_r	z	$RA(J2000)$	$Dec.(J2000)$	$P(deg)$	$i(deg)$	m_r	z
227.6231	+5.5647	158.16	43.86	17.58	0.079754	227.7732	+5.3138	27.62	89.66	17.02	0.078463
227.6264	+5.5019	134.10	60.81	16.24	0.075980	227.7743	+5.6451	133.84	68.42	17.67	0.079177
227.6319	+5.9992	38.44	23.25	17.36	0.075733	227.7780	+5.7277	162.17	54.50	17.96	0.078887
227.6326	+5.9779	163.53	29.88	17.33	0.075592	227.7801	+5.2117	38.59	21.00	17.24	0.078135
227.6328	+6.2453	145.84	63.14	17.33	0.075439	227.7811	+5.5499	115.65	79.81	16.06	0.078212
227.6332	+5.2560	119.32	72.27	16.87	0.074993	227.7814	+5.2449	175.31	59.42	17.79	0.080443
227.6338	+5.7997	101.78	43.62	17.28	0.075598	227.7823	+5.3271	78.27	37.09	16.43	0.078648
227.6369	+5.8166	171.31	80.96	17.23	0.077483	227.7824	+5.8846	86.73	59.59	16.48	0.078676
227.6378	+4.7997	113.62	46.80	15.14	0.081577	227.7828	+5.3468	132.86	31.95	17.65	0.080152
227.6398	+5.6345	34.28	53.15	17.39	0.077878	227.7853	+5.3913	117.66	56.06	17.74	0.081027
227.6405	+6.2049	30.81	58.48	17.78	0.076268	227.7885	+5.5197	71.67	66.39	17.18	0.080583
227.6449	+5.2119	92.87	32.93	17.05	0.076321	227.7889	+6.5632	57.11	45.20	17.27	0.076146
227.6462	+5.9601	56.24	40.59	17.61	0.080346	227.7894	+5.7960	92.52	55.60	17.43	0.077045
227.6463	+5.6568	147.64	49.47	16.39	0.079847	227.7908	+6.2012	182.61	74.22	16.61	0.076940
227.6517	+5.8344	78.05	49.49	17.66	0.079339	227.7909	+5.2726	73.52	74.73	15.74	0.077343
227.6520	+6.0255	136.89	43.05	15.88	0.079824	227.7910	+5.8137	97.97	43.10	17.92	0.075946
227.6525	+5.5116	32.28	55.43	17.56	0.081266	227.7926	+6.4045	35.00	19.53	17.37	0.076140
227.6566	+5.7913	24.21	35.66	17.54	0.081334	227.7944	+5.8324	150.38	26.44	17.36	0.080347
227.6584	+5.4954	85.73	21.92	17.57	0.077853	227.7963	+5.2574	23.50	75.69	17.79	0.080242
227.6594	+6.2314	184.02	61.98	17.85	0.079828	227.7964	+6.2375	176.31	67.99	17.58	0.077673
227.6604	+5.2388	173.84	27.97	15.73	0.078566	227.7999	+5.6538	48.68	67.12	16.71	0.079492
227.6612	+5.4315	164.73	47.84	17.52	0.079021	227.8013	+6.3298	182.19	78.70	17.19	0.078227
227.6617	+5.6744	61.63	58.78	16.66	0.080093	227.8015	+4.9079	34.19	87.44	15.90	0.078389
227.6621	+5.1826	30.50	44.59	15.38	0.079992	227.8034	+4.6917	150.11	59.51	17.54	0.076612
227.6664	+5.6553	127.22	64.55	16.48	0.079492	227.8038	+6.3050	159.20	52.50	16.71	0.078689
227.6683	+5.9560	45.66	66.66	16.46	0.078316	227.8048	+5.6050	117.17	66.87	17.67	0.079125
227.6706	+5.8208	109.17	62.54	17.87	0.080359	227.8055	+5.3359	120.95	60.34	16.77	0.079316
227.6769	+5.7781	52.79	40.81	17.64	0.077615	227.8117	+5.1849	47.03	15.71	16.00	0.078410
227.6772	+5.7475	84.60	27.92	16.96	0.076184	227.8133	+5.8722	92.74	11.23	16.27	0.078172
227.6799	+6.1981	115.87	47.11	17.49	0.076513	227.8148	+6.2589	129.52	20.39	17.25	0.076621
227.6814	+5.4809	79.20	63.36	17.50	0.075749	227.8166	+5.6966	87.64	72.26	16.63	0.080103
227.6823	+5.9706	38.28	84.79	17.05	0.076810	227.8179	+6.3982	104.51	65.63	15.42	0.077422
227.6824	+5.6715	19.86	67.47	16.97	0.077268	227.8190	+5.5754	71.53	28.02	16.59	0.076279
227.6846	+4.8894	77.83	31.75	16.78	0.075082	227.8194	+6.1217	83.98	53.68	17.41	0.078830
227.6865	+5.8363	66.83	61.55	17.08	0.078243	227.8194	+5.7227	35.81	72.44	17.29	0.077795
227.6937	+5.1147	47.60	84.68	17.19	0.078225	227.8207	+5.8304	18.28	72.85	16.55	0.075059
227.6938	+5.5914	135.06	54.08	17.80	0.080367	227.8219	+6.4396	139.24	70.75	17.31	0.075294
227.6951	+5.7946	108.50	83.50	17.62	0.080911	227.8223	+5.2221	131.94	21.95	15.92	0.076251
227.6981	+5.6491	106.23	45.60	16.96	0.079319	227.8234	+5.2965	166.04	48.76	16.60	0.076801
227.6990	+4.8736	87.75	45.24	17.02	0.080170	227.8235	+6.3704	105.82	73.83	17.12	0.079245
227.6998	+5.7576	145.40	48.37	17.55	0.080507	227.8280	+5.9624	167.17	84.63	17.20	0.080190
227.7055	+5.9476	52.20	52.59	17.23	0.076308	227.8292	+5.2383	24.76	35.85	14.46	0.077407
227.7043	+5.7338	117.01	85.68	17.56	0.077448	227.8310	+5.1985	171.51	67.41	17.46	0.080679
227.7055	+5.9476	52.20	72.73	17.23	0.078402	227.8323	+5.8778	131.06	67.00	16.17	0.079924
227.7113	+5.8408	86.05	44.40	19.10	0.079049	227.8326	+5.7445	125.66	62.17	17.00	0.081763
227.7055	+5.9476	52.20	39.31	17.23	0.077209	227.8348	+6.4202	151.41	57.87	16.59	0.078109
227.7074	+5.8157	174.48	76.81	17.28	0.077194	227.8349	+6.0657	96.41	57.18	15.34	0.077276
227.7104	+5.6248	45.62	75.04	17.87	0.080149	227.8392	+6.3125	102.02	17.34	17.68	0.078344
227.7120	+6.2043	143.62	74.13	17.58	0.079562	227.8397	+5.6890	46.47	60.74	17.32	0.078577
227.7126	+5.8009	108.51	37.76	16.54	0.078040	227.8397	+6.2819	51.19	57.15	17.80	0.080449
227.7172	+5.6575	92.02	42.14	16.50	0.080215	227.8408	+6.0351	115.01	46.46	17.51	0.081366
227.7175	+4.8677	136.93	47.62	15.01	0.078333	227.8424	+6.1700	101.39	27.02	16.38	0.079673
227.7184	+6.1710	46.83	20.17	15.62	0.078814	227.8448	+6.2149	92.96	62.90	17.10	0.080100
227.7190	+5.3237	156.03	60.48	17.57	0.078595	227.8456	+5.5188	24.43	34.26	17.19	0.078600
227.7200	+5.7248	27.21	62.47	16.53	0.076690	227.8487	+5.8822	147.49	80.58	17.86	0.079108
227.7204	+4.8510	27.98	42.66	16.58	0.076975	227.8495	+6.0741	73.29	17.67	17.19	0.080467
227.7225	+5.6996	64.81	76.95	17.74	0.075420	227.8538	+5.2288	137.42	84.57	17.73	0.076171
227.7346	+5.9442	62.97	43.76	21.18	0.081713	227.8554	+5.8099	150.59	36.52	17.09	0.077520
227.7281	+5.7570	6.71	75.82	18.27	0.079313	227.8555	+6.5858	11.14	62.43	17.72	0.077839
227.7346	+5.9442	62.97	46.25	21.18	0.079473	227.8578	+5.3347	101.26	46.06	17.45	0.077814
227.7296	+4.8355	14.71	80.14	17.79	0.078805	227.8579	+5.6308	116.20	55.35	17.05	0.076382
227.7296	+5.5588	74.08	39.07	16.30	0.080108	227.8583	+6.2990	161.32	58.70	17.44	0.078301
227.7359	+5.7758	90.54	66.81	17.28	0.077448	227.8621	+6.5703	138.25	50.10	17.45	0.078082
227.7367	+5.6769	73.44	35.66	17.48	0.080136	227.8729	+6.1931	86.19	69.99	17.25	0.076365
227.7398	+5.9814	115.90	31.73	17.58	0.079499	227.8766	+5.7808	169.90	27.02	17.86	0.077150
227.7422	+5.2475	143.45	65.39	17.08	0.077820	227.8782	+5.2746	46.88	46.43	17.85	0.076568
227.7425	+4.8134	71.69	81.35	15.84	0.078014	227.8802	+6.2630	102.90	65.49	16.63	0.081697
227.7440	+4.7858	24.55	82.73	16.74	0.077783	227.8811	+6.3738	109.19	28.74	17.23	0.078640
227.7442	+5.3181	171.93	56.17	15.73	0.075309	227.8812	+5.8542	128.18	60.04	17.69	0.077789
227.7449	+5.6919	131.09	68.08	16.92	0.074910	227.8854	+6.0898	139.10	67.34	16.99	0.076147
227.7454	+6.1116	82.38	50.83	17.74	0.075092	227.8861	+5.0800	22.24	83.39	17.69	0.076325
227.7467	+6.3358	40.89	50.20	16.60	0.077983	227.8882	+6.4809	156.02	45.98	17.70	0.082285
227.7470	+5.3347	172.53	21.70	17.41	0.076383	227.8888	+4.9909	9.99	45.49	17.88	0.081741
227.7486	+5.7145	74.47	47.12	17.49	0.076113	227.8931	+6.2011	111.28	38.10	15.86	0.078835
227.7497	+4.9458	37.87	61.10	17.08	0.081119	227.8938	+5.4152	152.59	22.15	17.79	0.077504
227.7503	+5.7828	61.98	50.76	15.82	0.078869	227.8947	+6.4327	26.65	63.86	17.73	0.081548
227.7511	+5.4141	77.21	45.00	17.67	0.077550	227.8957	+6.3323	131.26	33.14	16.73	0.076338
227.7536	+5.6613	124.59	28.31	16.31	0.077582	227.8971	+6.3506	79.51	61.71	17.15	0.075887
227.7537	+5.9717	154.50	73.43	17.79	0.077359	227.8973	+6.2527	103.49	58.49	16.99	0.077039
227.7538	+4.8416	48.59	9.25	17.59	0.076307	227.8997	+5.5645	94.32	63.94	16.76	0.079959
227.7547	+5.4493	149.13	48.61	17.42	0.078415	227.9028	+6.1813	37.01	47.00	16.99	0.080601
227.7605	+5.7606	121.31	61.57	17.40	0.079226	227.9058	+6.4618	138.53	38.37	16.23	0.078057
227.7622	+5.2931	112.45	73.02	15.05	0.078010	227.9093	+4.8765	112.42	63.11	17.61	0.078221
227.7628	+6.0404	46.72	51.56	17.55	0.080709	227.9142	+6.2619	33.71	43.81	17.29	0.076896
227.7651	+4.8019	168.08	51.09	17.11	0.078080	227.9172	+5.3376	75.73	74.17	17.04	0.076425
227.7657	+6.3151	65.36	26.28	17.55	0.076279	227.9199	+5.0966	68.15	32.69	17.35	0.076369
227.7690	+5.2725	146.08	53.23	17.74	0.075516	227.9230	+5.9375	135.46	78.40	17.39	0.077364
227.7701	+5.8293	52.46	75.45	17.51	0.077257	227.9237	+6.3441	50.13	52.26	17.88	0.075779
227.7713	+5.3606	97.41	57.72	16.75	0.076768	227.9295	+6.2979	10.69	25.01	16.33	0.077450
227.7721	+4.8358	151.26	69.76	16.70	0.080581	227.9351	+5.6968	160.35	30.60	16.66	0.080642
227.7730	+6.3637	137.76	81.19	16.51	0.078766	227.9351	+6.2621	14.42	35.51	16.36	0.078267

Table 39: SDSS DR7 of galaxies in the supercluster S[231+030+0117] that have redshifts range 0.018 to 0.123.The first two columns list the right ascension and declinations.The next two columns shows position and inclination angle.The fifth and sixth columns represent the magnitude in r-band and redshift.

RA(J2000)	$Dec.(J2000)$	$P(deg)$	$i(deg)$	m_r	z	$RA(J2000)$	$Dec.(J2000)$	$P(deg)$	$i(deg)$	m_r	z
RA(J2000)	$Dec.(J2000)$	$P(deg)$	$i(deg)$	m_r	z	$RA(J2000)$	$Dec.(J2000)$	$P(deg)$	$i(deg)$	m_r	z
228.3178	+30.9716	152.62	65.37	17.77	0.107767	227.2161	+31.2574	110.57	79.90	17.79	0.110495
230.5037	+32.1718	136.58	40.16	17.66	0.107879	229.3014	+33.3605	186.82	34.31	16.61	0.110509
227.2785	+29.8035	202.47	45.59	16.70	0.107911	228.5103	+29.0778	180.99	51.60	16.71	0.110514
231.0973	+29.7178	45.50	43.65	17.05	0.108379	230.4285	+32.1606	129.09	25.72	17.52	0.110536
227.4599	+33.5711	73.73	58.51	17.59	0.108432	228.6854	+30.4847	126.06	40.90	16.76	0.110539
231.1799	+29.7716	158.46	32.77	17.52	0.108498	227.5664	+31.4140	117.38	25.92	16.96	0.110544
230.4334	+32.2795	129.38	43.05	16.80	0.108522	228.3490	+29.7468	104.54	54.60	15.60	0.110561
227.4358	+33.6338	189.74	54.85	16.28	0.108602	228.2370	+30.3045	195.47	34.67	15.79	0.110572
228.1076	+30.5268	105.52	52.05	17.34	0.108647	228.4461	+30.0098	154.27	37.49	17.71	0.110572
227.6446	+30.7459	29.70	60.05	17.65	0.108672	227.8352	+30.2406	161.80	53.03	17.65	0.110576
228.2856	+30.9682	179.82	67.55	16.82	0.108704	229.4270	+30.9020	170.07	50.42	17.47	0.110578
229.2146	+31.2018	100.99	48.03	17.39	0.108769	227.0425	+33.6717	45.50	46.52	17.40	0.110579
228.8058	+31.0421	133.00	55.26	16.84	0.108774	227.0344	+32.7778	53.39	29.03	17.36	0.110587
227.7317	+30.8157	115.17	40.65	17.78	0.108789	230.3331	+32.0449	201.07	75.14	16.87	0.110598
231.1844	+29.8198	172.17	50.89	17.77	0.108854	226.7850	+30.1491	142.41	51.96	16.36	0.110598
229.2022	+31.1842	178.83	58.87	17.20	0.108904	227.0850	+29.5572	89.48	52.14	17.54	0.110611
227.5972	+33.4104	114.53	35.51	17.63	0.108932	231.1678	+29.8302	59.82	45.11	17.54	0.110614
227.5476	+33.4984	75.47	17.17	17.50	0.108976	231.7030	+29.8948	159.91	84.78	16.96	0.110635
227.4941	+33.4736	131.42	23.57	17.76	0.108980	227.4990	+33.4628	57.96	38.38	16.62	0.110651
227.5838	+33.4860	63.03	32.90	15.81	0.109025	228.7367	+30.6949	80.10	55.83	17.01	0.110653
227.7413	+30.8481	185.09	34.53	17.06	0.109086	227.9825	+31.3761	44.32	36.28	17.62	0.110656
227.1503	+31.2372	47.20	34.77	17.48	0.109105	227.2796	+29.8290	202.93	23.54	16.33	0.110663
229.2334	+31.1048	156.80	61.10	17.35	0.109117	227.0330	+31.0094	198.69	44.91	17.03	0.110664
228.8492	+31.0486	176.38	78.52	16.62	0.109119	228.0074	+31.1319	96.13	67.21	16.72	0.110680
227.8281	+30.3489	187.53	69.74	17.19	0.109202	228.8736	+30.5566	187.16	46.32	17.11	0.110711
227.0137	+29.1735	107.52	50.20	16.73	0.109287	227.7702	+31.0965	102.28	78.68	16.75	0.110719
227.7119	+30.0433	44.50	58.38	17.77	0.109292	228.6076	+32.6195	100.10	79.14	16.84	0.110755
228.1918	+30.4040	63.49	68.10	17.45	0.109298	230.7987	+31.7924	178.86	49.56	17.15	0.110765
230.2967	+32.0455	141.94	49.69	17.19	0.109298	227.5847	+33.4903	105.01	51.89	17.14	0.110775
228.8784	+30.8864	203.43	21.44	17.33	0.109321	227.5033	+33.2515	168.18	35.07	15.79	0.110788
227.3559	+29.7391	114.03	64.23	17.79	0.109342	226.7713	+34.5169	94.37	66.62	17.46	0.110794
228.2062	+30.3340	87.26	52.71	17.57	0.109373	227.1334	+29.4344	51.38	78.93	16.92	0.110804
228.7817	+31.1190	158.55	37.78	16.98	0.109399	230.3013	+32.0811	105.31	37.45	17.87	0.110807
227.7888	+30.2260	81.45	47.22	17.83	0.109407	228.2146	+30.1572	158.51	58.49	17.40	0.110829
226.8347	+29.4493	104.03	60.35	17.31	0.109440	228.3576	+30.2597	72.19	75.83	17.86	0.110847
227.5091	+33.5380	180.16	19.20	17.77	0.109466	228.2718	+30.2341	128.57	43.73	16.87	0.110849
228.3026	+30.0709	46.31	54.76	17.78	0.109467	227.2814	+33.3701	200.95	31.90	17.64	0.110853
227.3383	+30.1861	132.35	24.58	17.83	0.109482	229.6878	+32.5451	107.51	49.22	17.49	0.110863
227.5033	+33.5139	104.66	65.21	17.42	0.109496	230.3441	+37.0733	193.02	75.55	17.06	0.110872
230.3439	+29.5048	100.84	44.01	17.33	0.109548	227.1312	+29.4136	180.11	50.89	17.84	0.110880
227.5172	+33.4732	38.26	57.51	17.41	0.109550	231.8135	+29.5626	179.54	82.67	17.77	0.110890
227.0597	+29.2561	186.41	60.91	17.24	0.109569	231.0654	+29.7530	129.76	70.03	16.98	0.110913
228.2021	+30.3197	94.35	44.19	17.31	0.109611	228.2439	+31.6597	100.98	57.91	17.34	0.110930
230.4072	+32.2084	161.95	68.92	17.42	0.109624	230.7595	+30.9979	173.57	37.91	17.51	0.110932
228.1547	+31.1380	77.07	56.86	16.30	0.109636	227.5959	+31.4663	46.96	37.61	17.03	0.110936
228.0706	+30.9313	66.41	56.55	17.55	0.109721	230.4594	+31.3467	208.77	45.79	17.07	0.110940
229.2587	+31.0864	60.05	37.37	17.81	0.109771	227.7189	+31.0737	68.98	60.43	16.69	0.110954
227.2698	+29.2123	128.85	44.32	16.46	0.109815	230.4078	+32.0019	140.01	64.31	17.36	0.110962
227.1211	+29.4543	140.43	58.50	17.62	0.109832	226.9362	+31.2168	40.67	62.39	16.94	0.110977
228.9781	+30.4760	158.29	78.10	17.36	0.109832	230.5837	+29.3197	147.93	30.10	17.46	0.110999
230.3769	+32.1086	116.23	65.09	17.59	0.109837	231.1349	+29.5764	99.20	51.83	16.75	0.111000
230.4994	+32.2972	102.72	36.25	16.50	0.109932	227.7221	+30.8504	32.32	20.81	17.27	0.111015
227.2980	+29.7861	106.39	71.46	17.24	0.109952	229.4392	+33.2526	156.45	55.27	16.58	0.111021
228.3835	+31.0831	158.43	27.61	17.50	0.109963	226.9399	+31.2394	155.96	49.81	17.36	0.111025
227.7632	+33.7524	71.96	45.11	17.33	0.109992	231.3832	+29.8298	166.98	77.58	16.01	0.111033
228.3389	+31.0213	79.11	52.50	16.75	0.110006	230.3603	+31.9650	74.07	68.73	17.80	0.111035
227.6437	+30.1075	38.09	28.63	16.17	0.110074	230.3466	+32.1072	206.89	52.88	16.23	0.111040
227.1203	+29.3779	84.08	61.35	17.06	0.110089	230.3830	+32.2232	166.82	19.92	17.20	0.111041
228.3463	+34.1264	99.93	58.93	17.83	0.110093	227.7668	+33.0740	156.84	41.11	17.44	0.111041
228.0578	+32.9111	90.14	48.13	17.67	0.110102	230.2400	+29.4549	58.44	47.67	16.72	0.111044
228.2037	+30.4168	26.15	30.48	17.57	0.110136	230.9929	+29.9058	116.99	53.71	17.45	0.111050
228.4938	+29.0542	39.29	31.31	17.30	0.110152	230.6409	+31.8448	184.79	53.31	17.56	0.111056
231.1373	+29.8227	77.71	71.96	17.76	0.110170	228.9763	+34.7326	136.03	86.39	16.55	0.111057
230.5198	+32.1560	104.93	53.48	17.80	0.110182	231.1626	+29.8466	114.59	46.61	17.57	0.111058
227.0333	+29.2392	164.90	65.26	17.67	0.110187	226.9133	+34.6078	170.93	59.71	16.89	0.111091
227.2605	+30.3006	83.35	35.38	17.44	0.110191	232.4311	+30.6883	198.26	32.36	17.74	0.111110
230.4674	+32.1250	153.72	26.57	16.83	0.110192	229.2918	+33.3984	130.85	17.35	16.70	0.111113
230.8752	+30.3530	168.71	40.64	17.07	0.110220	227.5797	+31.6438	189.62	49.24	17.54	0.111119
226.4746	+30.0284	124.65	46.85	17.55	0.110259	227.1405	+29.2927	193.37	47.00	16.23	0.111123
227.3121	+34.3322	188.43	36.23	17.61	0.110267	228.1802	+31.0884	133.57	1.19	17.48	0.111125
227.8487	+30.2655	82.28	77.73	17.72	0.110272	227.2426	+30.7837	195.57	56.57	17.22	0.111130
229.0301	+34.8767	68.90	35.46	17.03	0.110272	230.6513	+36.9753	163.52	26.69	16.87	0.111136
227.4195	+29.8685	187.19	81.03	17.35	0.110278	229.8309	+31.6183	114.86	74.13	17.06	0.111149
226.6146	+34.4591	146.81	43.65	16.91	0.110314	230.0847	+36.6762	58.18	57.22	16.73	0.111154
227.1207	+30.1908	202.64	26.88	17.78	0.110315	228.9486	+32.8881	179.38	51.71	17.41	0.111158
229.0732	+30.0652	204.87	35.72	17.96	0.110336	227.3628	+34.3533	52.44	54.11	17.21	0.111165
230.6714	+29.8666	174.23	58.97	17.66	0.110356	230.1896	+32.8007	162.44	28.60	17.77	0.111171
228.1785	+30.8252	58.56	49.81	16.60	0.110358	231.5056	+29.8746	60.46	32.60	17.76	0.111172
227.2615	+31.6318	99.99	14.32	17.80	0.110359	228.7562	+32.1977	39.76	49.39	17.85	0.111194
230.9556	+32.2306	198.98	38.21	17.04	0.110362	230.9334	+30.9520	202.13	65.79	17.53	0.111196
227.3804	+31.5613	53.95	48.56	16.28	0.110380	231.3257	+30.6420	149.89	18.13	17.42	0.111198
228.3469	+29.8257	35.43	52.77	17.40	0.110420	229.9059	+32.7539	45.31	60.85	17.59	0.111199
227.8002	+30.5422	35.60	34.40	17.18	0.110428	230.9650	+29.9154	153.11	19.06	17.14	0.111212
227.4618	+30.1698	97.13	66.87	17.81	0.110439	231.8977	+30.8126	199.90	57.76	17.26	0.111212
227.8765	+31.2013	160.52	57.72	17.08	0.110447	232.0389	+30.9759	194.19	62.43	17.22	0.111217
227.1878	+30.8016	76.40	33.31	16.99	0.110450	227.1887	+29.8172	150.91	61.60	17.70	0.111219
227.6342	+31.4043	190.70	56.21	17.79	0.110458	227.2153	+30.6215	126.94	31.49	17.15	0.111226
227.2895	+32.7483	129.78	74.45	17.31	0.110468	227.5627	+33.3874	112.10	13.79	17.20	0.111227
228.4652	+31.0616	50.64	38.54	17.05	0.110472	231.0335	+32.7349	162.27	72.58	16.33	0.111230
230.3282	+32.0185	111.79	15.78	17.44	0.110486	227.3230	+30.2388	157.91	32.58	17.75	0.111232
228.2092	+29.8343	144.72	21.77	17.55	0.110492	230.8656	+30.0207	111.27	49.67	16.99	0.111239

Table 40: SDSS DR7 of galaxies in the supercluster S[231+030+0117] that have redshifts range 0.018 to 0.123.The first two columns list the right ascension and declinations.The next two columns shows position and inclination angle.The fifth and sixth columns represent the magnitude in r-band and redshift.

RA(J2000)	$Dec.(J2000)$	$P(deg)$	$i(deg)$	m_r	z	$RA(J2000)$	$Dec.(J2000)$	$P(deg)$	$i(deg)$	m_r	z
227.6560	+31.8016	29.75	49.44	17.51	0.111255	227.1005	+35.0391	62.12	64.56	17.38	0.111886
227.0884	+33.4958	53.16	26.43	16.75	0.111258	227.2678	+31.7236	139.65	11.92	17.54	0.111896
230.2956	+29.4458	119.58	45.55	17.53	0.111263	227.7930	+36.0159	182.67	83.40	17.28	0.111907
226.9207	+29.1587	190.34	42.65	17.27	0.111267	230.8434	+30.0554	202.11	66.56	17.53	0.111908
227.3139	+30.2611	160.40	46.38	15.41	0.111270	227.3969	+33.4317	128.85	68.37	17.54	0.111922
228.2182	+30.2266	179.83	31.45	17.02	0.111272	230.8117	+31.0054	30.70	21.71	16.84	0.111922
231.4211	+29.8286	176.86	38.42	17.72	0.111281	226.6813	+34.4720	149.48	59.69	17.55	0.111929
228.9786	+34.7295	146.28	63.24	15.87	0.111289	227.7230	+33.6468	104.98	54.21	17.47	0.111936
230.6434	+29.0188	95.66	15.94	17.36	0.111289	230.8804	+30.6283	193.82	69.94	17.29	0.111943
230.6976	+32.0843	153.38	55.34	17.34	0.111292	231.8140	+29.5500	81.77	30.79	17.22	0.111946
226.9710	+31.2215	120.75	52.33	17.62	0.111296	227.7020	+32.4342	157.84	62.90	17.63	0.111954
227.2517	+31.0329	67.76	77.97	17.18	0.111313	230.6152	+31.0271	106.10	38.70	16.56	0.111981
230.9404	+29.7431	146.63	41.57	17.20	0.111314	228.9977	+34.8053	75.43	61.44	17.18	0.111994
227.4887	+33.1751	144.30	61.13	16.95	0.111330	229.2830	+33.5207	100.40	64.83	17.74	0.111996
229.9456	+31.6847	144.77	48.95	17.31	0.111334	230.9257	+30.0838	90.05	12.40	16.89	0.112000
227.2917	+33.3721	203.15	85.71	17.17	0.111345	227.3714	+33.2428	200.24	46.84	17.31	0.112017
230.6339	+36.8874	105.69	19.82	17.75	0.111354	227.1269	+31.2341	52.49	52.55	17.34	0.112018
230.6386	+29.0365	202.23	43.35	15.86	0.111386	227.8838	+33.6780	73.67	24.14	16.96	0.112018
230.0494	+29.1984	91.49	45.24	16.76	0.111397	227.3605	+31.3884	139.17	67.41	16.47	0.112019
228.7928	+32.7863	196.99	53.73	17.66	0.111415	229.9357	+31.9626	33.70	42.93	17.23	0.112032
227.5064	+33.3998	43.08	54.30	16.80	0.111418	232.1558	+29.0914	42.91	45.30	17.64	0.112041
231.0912	+29.7443	98.27	32.67	17.47	0.111426	228.1497	+30.2595	105.04	34.99	17.43	0.112065
226.9411	+29.1718	171.14	39.55	17.77	0.111427	227.2494	+30.1593	192.27	42.71	17.53	0.112067
231.2477	+29.5664	112.31	64.25	16.84	0.111430	227.4642	+33.1655	197.60	68.09	16.29	0.112075
230.8124	+30.9928	171.00	42.48	16.07	0.111434	230.5218	+29.1466	89.71	62.37	17.78	0.112082
231.0245	+31.2306	53.02	60.83	17.60	0.111438	229.2691	+33.3596	196.70	27.31	17.32	0.112084
229.6389	+33.2077	136.08	53.79	17.06	0.111441	229.3765	+35.5871	57.88	43.50	16.95	0.112099
230.1286	+32.6946	129.30	74.40	16.71	0.111451	230.0807	+31.6545	159.72	31.75	17.52	0.112176
227.0414	+29.2222	199.09	62.12	15.50	0.111455	229.3743	+35.4625	172.51	71.57	17.12	0.112180
229.9604	+31.8951	157.91	60.62	17.74	0.111459	229.5621	+36.1708	179.43	33.48	17.76	0.112183
229.0698	+34.8777	96.05	35.98	17.28	0.111470	230.9305	+29.9269	158.72	57.75	16.51	0.112184
232.0326	+30.9688	52.17	60.03	17.22	0.111474	231.0950	+30.3827	191.71	50.02	16.84	0.112214
228.3600	+29.6996	88.92	53.20	17.42	0.111477	231.9348	+30.6660	90.82	59.67	17.49	0.112219
227.2982	+30.2005	113.64	18.61	16.95	0.111479	230.2441	+29.1288	34.80	31.23	17.52	0.112225
229.2327	+31.2115	134.98	52.47	17.17	0.111479	231.0034	+30.0487	56.36	81.01	17.65	0.112233
230.2565	+36.8294	143.93	74.70	17.55	0.111498	228.1570	+28.3310	122.47	51.55	17.21	0.112236
231.1207	+29.8749	109.31	73.86	16.83	0.111511	231.0158	+29.9357	189.27	43.74	16.63	0.112247
227.6151	+33.2567	203.08	49.32	17.27	0.111517	230.5948	+32.4022	143.29	49.43	17.43	0.112252
228.6424	+32.4324	168.47	20.18	16.17	0.111528	228.7724	+36.0927	103.72	64.17	16.89	0.112255
230.6242	+36.6905	187.22	48.96	15.28	0.111529	229.8947	+36.1413	63.88	57.84	17.57	0.112271
227.1685	+29.3164	66.78	48.76	17.48	0.111537	230.6536	+29.1765	111.06	58.49	17.66	0.112271
230.8859	+30.9034	63.06	64.97	17.06	0.111541	231.4333	+29.8123	73.64	36.13	17.49	0.112275
228.5916	+32.2643	168.58	39.56	17.85	0.111544	230.6724	+30.8345	83.62	82.77	17.81	0.112275
230.2760	+32.0749	107.59	52.09	17.42	0.111565	227.0595	+34.0740	69.55	40.44	17.28	0.112283
230.3886	+29.0448	109.43	64.61	16.96	0.111575	229.0173	+28.0385	33.09	46.71	17.70	0.112294
227.6998	+32.4425	165.86	49.61	17.66	0.111583	228.2787	+29.5370	113.91	27.49	17.83	0.112304
228.2276	+30.1302	46.30	45.97	17.34	0.111603	228.4399	+28.0536	166.80	32.85	17.22	0.112324
227.7941	+31.5677	171.47	61.09	16.81	0.111610	228.0645	+28.3288	163.13	45.32	16.89	0.112327
228.6316	+36.0523	174.83	39.59	17.83	0.111614	228.6303	+28.4074	125.64	15.33	17.52	0.112330
230.3401	+32.2484	146.62	67.07	17.43	0.111615	231.1445	+32.2968	140.59	22.02	17.84	0.112365
230.5604	+28.8147	192.01	24.35	16.75	0.111615	228.2195	+35.7991	151.01	39.10	16.61	0.112370
230.4423	+32.1259	71.12	41.63	17.53	0.111616	227.5842	+28.4442	77.45	29.37	17.16	0.112371
229.2936	+35.4349	67.49	79.03	17.60	0.111627	227.0915	+35.5137	114.86	36.53	17.63	0.112375
228.8664	+29.8393	85.78	45.60	17.32	0.111628	230.0859	+30.6065	146.96	75.65	17.74	0.112378
230.7812	+29.9941	133.22	33.03	17.59	0.111628	228.1978	+35.4249	155.54	32.17	16.82	0.112379
229.3642	+36.5888	31.14	56.01	17.13	0.111647	229.8228	+31.2017	93.96	67.24	17.70	0.112380
230.5749	+37.0933	144.16	57.04	16.32	0.111659	230.4763	+36.2550	138.14	72.06	16.79	0.112397
230.2569	+36.1303	79.09	47.28	17.32	0.111662	231.1546	+29.7465	195.52	65.74	16.99	0.112404
230.1886	+36.6592	78.10	55.50	16.77	0.111671	227.1371	+35.8784	138.79	55.55	17.50	0.112404
231.8956	+29.5499	128.80	68.17	16.92	0.111671	229.4785	+35.2965	134.37	47.73	17.05	0.112406
227.1976	+34.0518	112.67	29.58	17.75	0.111677	228.6283	+32.3907	116.71	39.43	17.69	0.112411
230.2591	+37.0916	127.51	66.84	16.86	0.111678	230.5028	+32.2372	52.31	40.04	17.71	0.112414
226.4105	+33.4654	35.84	54.54	16.83	0.111682	227.3473	+31.7369	88.34	79.21	17.49	0.112442
230.4701	+31.8296	178.05	64.25	17.22	0.111684	228.1288	+32.0974	145.95	71.43	17.12	0.112446
230.8478	+29.9887	89.29	49.58	16.61	0.111687	230.2298	+31.0545	60.87	18.60	17.11	0.112449
227.7515	+33.6721	202.96	58.39	17.37	0.111696	228.3343	+27.7550	88.70	31.02	17.26	0.112451
230.6525	+36.9419	49.60	13.06	16.53	0.111712	227.2651	+33.8300	65.69	34.52	17.00	0.112452
230.8411	+30.9354	90.86	51.40	17.59	0.111730	229.5243	+33.0742	29.53	63.50	16.96	0.112454
227.2719	+33.7864	145.84	37.28	16.87	0.111733	227.2484	+36.1233	71.17	24.05	17.29	0.112460
231.1330	+30.1498	42.10	43.32	17.82	0.111734	231.4369	+29.6976	98.84	52.68	16.47	0.112460
231.4891	+29.8597	204.49	59.34	17.58	0.111736	231.8507	+29.6508	42.80	44.25	17.40	0.112465
231.3154	+29.6488	133.39	22.62	17.28	0.111741	229.3457	+35.1814	109.56	68.84	17.10	0.112472
231.2581	+31.4262	78.61	33.65	16.84	0.111757	230.9187	+30.0595	54.80	48.60	17.05	0.112473
230.5582	+37.0817	102.45	85.62	16.53	0.111764	228.9403	+29.8248	92.30	40.62	17.28	0.112484
230.4285	+32.1827	206.29	44.64	16.78	0.111776	230.7259	+32.1434	201.48	53.72	17.29	0.112485
226.6944	+34.3621	102.05	60.87	17.07	0.111785	231.2008	+29.5826	203.98	59.18	16.33	0.112498
229.6053	+35.5818	147.77	38.10	17.20	0.111791	230.3355	+29.1073	154.78	47.98	17.84	0.112499
228.8845	+33.6557	43.39	68.42	16.20	0.111796	229.3329	+35.8937	77.98	74.52	17.40	0.112499
230.5426	+32.4285	162.04	57.39	17.34	0.111806	227.3622	+30.2668	200.20	63.42	17.58	0.112503
230.6110	+32.0689	205.43	62.61	16.69	0.111807	230.9809	+29.7448	53.78	40.08	17.25	0.112508
230.6827	+29.9690	160.52	49.44	17.74	0.111807	230.6428	+31.7404	36.16	64.33	17.00	0.112517
229.5808	+33.1885	147.49	81.57	17.77	0.111808	227.9760	+35.6750	203.02	59.40	17.44	0.112521
230.3023	+31.8711	121.26	33.94	17.07	0.111811	230.0842	+31.6520	60.14	48.09	17.13	0.112522
230.3902	+32.0950	29.76	17.11	17.26	0.111816	230.0241	+36.7444	130.64	68.40	16.20	0.112524
227.4833	+33.1335	162.98	28.98	17.19	0.111822	227.8669	+36.2992	109.22	56.16	17.36	0.112524
228.8515	+33.6805	127.05	58.48	17.59	0.111824	231.3152	+31.4082	61.95	47.34	17.82	0.112532
227.4592	+33.6915	130.91	40.25	16.84	0.111824	229.5431	+33.2300	50.09	49.76	17.60	0.112536
231.2739	+29.6701	40.38	70.25	15.74	0.111830	227.4514	+34.9955	206.13	65.32	16.70	0.112539
229.0225	+28.0720	138.47	49.53	16.21	0.111863	227.2668	+36.1281	170.23	79.56	16.80	0.112547
229.5847	+35.7652	49.48	60.83	17.82	0.111873	229.1084	+33.8230	51.40	77.46	17.54	0.112551

Table 41: SDSS DR7 of galaxies in the supercluster S[184+003+0077] that have redshifts range 0.070 to 0.085.The first two columns list the right ascension and declinations.The next two columns shows position and inclination angle.The fifth and sixth columns represent the magnitude in r-band and redshift.

RA(J2000)	$Dec.(J2000)$	$P(deg)$	$i(deg)$	m_r	z	$RA(J2000)$	$Dec.(J2000)$	$P(deg)$	$i(deg)$	m_r	z
176.4490	+4.2630	15.76	81.88	17.48	0.075888	177.6343	+4.8048	−54.77	51.65	16.66	0.0770
176.5229	+4.2048	17.64	58.29	16.93	0.075129	177.6404	+4.8102	62.48	79.89	16.72	0.0769
176.5375	+4.2589	124.57	78.50	17.46	0.076310	177.7470	+4.7515	5.64	52.71	17.05	0.0781
176.5426	+4.2377	64.59	76.20	17.24	0.077134	177.6432	+5.3963	105.80	69.46	17.04	0.0754
176.6407	+4.3028	134.23	32.10	15.75	0.077586	177.6527	+5.4670	141.35	77.11	17.25	0.0771
176.5123	+5.6571	90.67	48.70	15.31	0.075292	177.6696	+5.2704	83.76	76.85	15.68	0.0774
176.5178	+5.6785	158.02	73.66	17.57	0.075102	177.6758	+5.3589	53.77	52.92	17.12	0.0774
176.6167	+5.7244	110.59	74.83	16.32	0.075097	177.7472	+5.4038	94.16	73.75	16.81	0.0769
176.5542	+6.3420	71.46	41.04	16.04	0.075862	177.6975	+6.6948	28.21	80.18	16.65	0.0771
176.5959	+6.3273	29.87	84.44	17.24	0.075892	177.7136	+6.6405	113.76	54.64	15.23	0.0775
176.7434	+6.1542	125.22	31.21	17.60	0.074167	177.7541	+6.5438	72.77	31.39	15.66	0.0768
176.7932	+6.2523	16.01	60.27	17.23	0.075140	177.7633	+6.7818	55.92	60.56	17.78	0.0771
176.9031	+6.1867	145.71	60.26	17.72	0.075112	177.7357	+6.5158	17.23	59.62	16.24	0.0743
176.7545	+3.7419	80.86	66.52	17.81	0.076765	177.8246	+6.4172	4.75	87.88	17.82	0.0742
176.7859	+3.8481	119.66	84.29	16.45	0.075946	177.8248	+6.5136	130.53	32.65	17.40	0.0742
176.8489	+3.9068	61.24	62.60	15.46	0.076063	177.8758	+6.3322	161.62	34.97	17.65	0.0753
176.8755	+4.4026	71.09	53.90	17.45	0.077552	177.9014	+6.3075	130.87	32.17	15.79	0.0741
176.9762	+4.3941	4.82	63.01	16.88	0.076053	177.7666	+2.9765	74.78	54.74	17.56	0.0776
176.9687	+5.2491	131.13	52.34	15.91	0.076398	177.7849	+2.9869	33.12	66.66	17.40	0.0773
177.0623	+5.2057	26.32	56.70	17.47	0.076049	177.7963	+2.9682	113.58	54.76	17.87	0.0771
177.0759	+5.2408	171.86	54.59	17.70	0.075712	177.8232	+3.0002	1.75	67.89	16.84	0.0775
177.1193	+5.2838	161.22	41.05	15.84	0.075790	177.7879	+5.0428	101.48	26.44	16.17	0.0775
177.1228	+5.2740	151.02	54.34	16.88	0.074784	177.8025	+5.0622	43.77	1.12	16.52	0.0774
177.1238	+5.2246	15.20	23.35	15.27	0.074099	177.8026	+5.2274	141.76	63.15	17.00	0.0764
177.1266	+5.2392	105.79	47.43	17.61	0.075664	177.8148	+5.0432	27.37	66.16	16.96	0.0753
177.1554	+5.2993	76.11	80.36	17.27	0.075479	177.8231	+5.0317	67.53	65.63	17.34	0.0756
177.0558	+4.0077	147.64	24.04	16.28	0.075987	177.8269	+5.0474	38.39	55.01	15.83	0.0759
177.0770	+4.1202	110.35	77.58	17.66	0.076625	177.8447	+4.9834	60.00	73.34	17.43	0.0759
177.0987	+4.2213	50.97	76.19	16.85	0.076007	177.8541	+5.0385	28.23	39.49	16.19	0.0754
177.1404	+4.2290	105.95	46.30	16.89	0.076328	177.8763	+4.8114	9.66	30.23	15.37	0.0759
177.1494	+4.2337	120.58	28.62	16.85	0.075913	177.8878	+5.1015	−12.96	26.63	14.29	0.0772
177.1530	+4.1184	87.78	67.18	16.05	0.076337	177.8951	+5.0288	57.90	79.75	16.39	0.0763
177.1549	+4.1830	81.03	15.14	16.76	0.076502	177.8959	+5.0187	28.56	79.97	17.38	0.0761
177.1699	+4.1628	175.73	64.71	17.01	0.076393	177.9029	+5.1394	21.98	63.56	15.82	0.0774
177.1760	+4.2284	76.82	55.16	15.43	0.075994	177.9128	+4.8703	152.70	63.82	16.88	0.0766
177.1696	+5.0266	94.08	42.50	17.68	0.076353	177.9140	+4.9797	96.21	53.20	17.61	0.0768
177.2267	+5.0431	21.97	35.06	16.52	0.076405	177.9162	+5.0282	3.27	62.05	17.06	0.0772
177.1800	+4.8228	31.91	77.69	17.55	0.075635	177.9205	+5.1889	25.30	67.28	17.49	0.0771
177.1963	+4.8134	19.71	6.73	17.16	0.075632	177.9232	+4.7606	33.78	60.61	16.47	0.0762
177.1805	+2.8825	24.96	75.37	16.67	0.077873	178.0036	+5.0549	92.63	43.41	16.49	0.0771
177.2583	+2.9565	−40.80	32.99	16.94	0.077539	178.0344	+5.1306	53.40	36.02	17.73	0.0771
177.2912	+2.9472	36.28	48.25	15.93	0.077444	178.0365	+5.0172	20.13	73.96	17.78	0.0758
177.1811	+4.5699	90.10	79.90	17.56	0.076951	178.0688	+5.0202	−3.98	33.75	17.54	0.0787
177.2230	+4.4923	89.38	61.32	17.38	0.077991	178.1109	+5.0278	88.05	81.66	17.80	0.0776
177.2036	+3.9121	47.01	10.97	16.28	0.077278	178.1179	+5.0124	54.66	68.68	16.90	0.0785
177.2724	+4.0086	39.24	39.90	16.85	0.077012	178.1877	+5.0278	−45.11	34.24	15.79	0.0780
177.3331	+4.7047	65.99	68.00	17.52	0.077498	177.8071	+5.9774	165.23	47.33	15.59	0.0752
177.3465	+4.6851	77.47	55.86	16.26	0.078232	177.9025	+5.9186	117.26	66.83	17.77	0.0767
177.3713	+4.6204	146.61	77.18	17.43	0.077873	177.9046	+5.8989	141.63	67.23	16.20	0.0764
177.3410	+5.8815	11.22	66.12	16.99	0.075614	177.9456	+5.8483	166.78	51.08	17.07	0.0760
177.3578	+5.6903	83.38	34.55	17.35	0.076261	177.9520	+3.1758	15.68	33.30	16.11	0.0760
177.3911	+5.7824	165.18	47.89	17.25	0.077018	177.9535	+3.1545	−47.25	21.56	17.13	0.0766
177.4003	+5.6987	105.92	11.27	15.62	0.075999	178.0097	+5.4441	105.60	49.10	17.12	0.0790
177.4294	+5.6893	162.12	89.93	16.61	0.073402	178.0386	+5.5142	−24.51	79.19	17.24	0.0774
177.4652	+5.6611	157.33	62.40	17.06	0.073915	178.0260	+6.6877	19.26	59.43	16.54	0.0759
177.4721	+5.7008	44.36	38.75	15.15	0.075483	178.0564	+6.5589	136.54	80.74	17.58	0.0751
177.4758	+5.6867	137.69	48.03	17.38	0.077598	178.1157	+6.6028	70.35	59.50	17.54	0.0758
177.4797	+5.6795	113.13	79.26	16.75	0.074660	178.1325	+6.6891	18.61	57.03	16.35	0.0765
177.4838	+5.6640	82.02	38.78	17.78	0.077487	178.0682	+5.8067	−0.57	42.03	17.11	0.0766
177.4889	+5.7807	142.14	43.03	17.19	0.076689	178.1806	+5.8189	113.90	49.73	15.50	0.0768
177.4984	+5.6391	119.15	71.02	16.03	0.077234	178.2951	+5.8578	13.01	32.22	17.26	0.0762
177.5001	+5.7140	9.03	46.45	17.34	0.076304	178.1148	+4.0986	37.31	38.62	17.19	0.0774
177.5029	+5.6554	139.41	66.44	16.91	0.076224	178.1523	+4.1014	102.55	9.44	15.99	0.0776
177.5106	+5.6323	10.34	41.76	15.21	0.076487	178.1223	+4.2969	60.84	48.16	16.37	0.0783
177.5106	+5.7081	103.18	36.90	17.17	0.074366	178.1330	+4.3779	128.40	30.12	16.22	0.0766
177.5312	+5.6163	14.34	41.13	16.67	0.074740	178.1354	+4.3255	77.37	27.81	17.57	0.0773
177.5328	+5.6899	19.53	65.38	17.32	0.074243	178.1596	+4.3674	159.57	25.82	16.73	0.0770
177.5503	+5.6419	120.43	55.27	17.76	0.077029	178.2002	+4.2869	−27.38	33.69	16.97	0.0758
177.5573	+5.9371	135.35	44.69	17.66	0.076317	178.2145	+4.2546	−41.65	36.12	17.25	0.0776
177.5627	+5.6394	16.52	45.37	16.30	0.073366	178.2243	+4.3502	10.01	54.76	17.41	0.0778
177.5689	+5.6248	151.09	37.27	15.88	0.073715	178.2256	+4.3113	56.14	32.38	17.18	0.0731
177.5721	+5.9052	127.69	65.74	17.36	0.076386	178.2493	+4.3719	176.19	80.44	17.09	0.0746
177.5724	+5.7016	124.28	24.17	16.87	0.076869	178.2692	+4.3449	83.59	85.69	17.78	0.0755
177.5741	+5.5927	19.36	34.27	17.65	0.074164	178.2692	+4.3175	−38.88	58.22	15.57	0.0764
177.5795	+5.6676	79.83	69.33	17.02	0.077762	178.2792	+4.3650	88.33	51.11	17.58	0.0757
177.5894	+5.6760	134.01	50.88	17.24	0.075642	178.3065	+4.4245	1.75	55.78	17.64	0.0759
177.5981	+6.0228	26.40	47.19	16.74	0.076115	178.3409	+4.3532	51.42	41.82	15.80	0.0775
177.6209	+5.7902	171.41	62.46	17.19	0.076293	178.3538	+4.3261	6.40	81.08	17.62	0.0767
177.6371	+5.6661	91.46	36.77	17.51	0.075593	178.3668	+4.3717	108.95	57.54	17.70	0.0760
177.6490	+6.0822	127.10	22.98	17.07	0.076997	178.3870	+4.4132	−45.48	54.76	15.84	0.0757
177.6730	+5.6603	92.91	79.04	17.61	0.076006	178.1529	+6.4204	143.23	82.08	17.12	0.0743
177.6802	+5.6879	171.34	59.49	16.61	0.076062	178.2049	+6.4630	20.86	17.90	15.90	0.0766
177.6920	+5.6764	152.58	39.47	15.89	0.075097	178.2167	+6.5058	146.31	37.65	17.50	0.0750
177.7413	+6.0873	35.80	74.55	17.73	0.075437	178.1930	+7.0181	103.77	64.67	17.74	0.0768
177.4122	+4.0909	−42.94	83.35	17.06	0.078482	178.1962	+7.0524	18.29	58.99	16.99	0.0767
177.4123	+3.9987	32.92	81.33	16.97	0.076970	178.2001	+5.3156	171.19	49.68	16.63	0.0786
177.5622	+6.9631	60.19	36.41	16.07	0.078710	178.2413	+5.2781	118.66	79.19	17.12	0.0772
177.5662	+6.8421	134.76	36.07	16.86	0.077332	178.2963	+5.4584	59.83	24.75	16.84	0.0780
177.5749	+6.8243	142.61	21.36	16.19	0.078385	178.3408	+5.3647	114.21	56.06	16.20	0.0779
177.6119	+4.1024	81.48	46.16	16.82	0.076529	178.3445	+5.4543	−39.56	61.53	17.16	0.0782
177.6289	+4.1502	96.65	1.44	16.10	0.076585	178.4200	+5.3141	57.33	83.63	17.49	0.0766

Table 42: SDSS DR7 of galaxies in the supercluster S[184+003+0077] that have redshifts range 0.070 to 0.085.The first two columns list the right ascension and declinations.The next two columns shows position and inclination angle.The fifth and sixth columns represent the magnitude in r-band and redshift.

RA(J2000)	$Dec.(J2000)$	$P(deg)$	$i(deg)$	m_r	z	$RA(J2000)$	$Dec.(J2000)$	$P(deg)$	$i(deg)$	m_r	z
178.3071	+4.9251	51.36	73.90	17.49	0.077052	179.4460	+5.2543	7.11	36.89	16.33	0.075308
178.3205	+5.0015	−2.93	69.13	17.38	0.077402	179.4579	+5.1744	83.41	14.19	16.96	0.075674
178.3172	+5.5865	−3.36	57.01	17.68	0.077196	179.4592	+5.2424	52.09	56.95	17.67	0.075726
178.4382	+5.5820	26.00	73.59	17.77	0.076758	179.4643	+5.1153	86.38	52.65	16.98	0.075842
178.3365	+3.8366	22.43	49.95	16.96	0.075185	179.4659	+5.0604	109.18	28.42	15.21	0.076684
178.4019	+3.8291	−15.77	83.12	17.36	0.075319	179.4771	+5.0477	−52.46	43.05	17.37	0.078094
178.4441	+4.7599	78.21	55.47	17.75	0.076368	179.4822	+4.9991	91.45	51.98	17.53	0.077463
178.4929	+4.8594	137.09	12.86	17.08	0.078073	179.4946	+5.0172	38.14	56.63	17.40	0.075710
178.4963	+4.8881	145.58	18.70	16.73	0.077957	179.5131	+5.0177	60.26	75.40	16.91	0.078013
178.5264	+3.9176	109.68	36.87	16.81	0.076219	179.5331	+5.0110	72.27	47.95	17.22	0.076600
178.5271	+3.8711	87.58	68.01	17.72	0.077740	179.5414	+5.2948	5.44	62.11	17.38	0.077108
178.5455	+3.8439	41.78	52.26	17.07	0.075488	179.5487	+4.9972	−16.07	53.49	17.69	0.077038
178.5527	+3.7826	119.00	48.50	17.07	0.076213	178.9081	+5.2316	113.74	52.50	16.48	0.075146
178.5549	+3.8819	99.79	47.72	15.95	0.076133	178.9416	+5.1466	10.27	73.02	17.40	0.074096
178.5961	+4.2739	16.01	39.35	17.67	0.074742	178.9609	+4.4423	114.80	44.87	16.39	0.074348
178.6502	+4.3536	31.97	70.26	17.53	0.076059	178.9977	+4.3483	74.92	70.69	17.33	0.075459
178.7185	+4.2700	40.90	52.83	15.02	0.073536	179.0633	+4.2456	−38.01	61.93	16.52	0.075329
178.7427	+4.2715	79.08	0.51	16.07	0.072745	179.0952	+4.1094	26.04	29.08	17.02	0.074882
178.7907	+4.1710	20.69	57.69	15.48	0.074667	179.1155	+4.1114	13.15	64.65	16.34	0.075664
178.8603	+4.2326	−59.53	45.94	17.60	0.076179	179.1714	+5.5638	59.77	69.53	16.84	0.077519
178.6755	+5.7781	14.29	77.51	17.65	0.076389	179.2013	+5.6457	−26.80	48.52	16.79	0.078209
178.7461	+5.8269	116.49	55.86	16.34	0.075610	179.1881	+0.7423	119.11	72.73	16.21	0.079196
178.8455	+1.5721	121.57	83.75	16.63	0.077961	179.2287	+0.7239	169.74	43.77	16.00	0.079176
178.8786	+1.5508	139.54	70.91	17.62	0.079588	179.2413	+0.7117	111.67	48.08	17.65	0.077773
178.8972	+1.5957	96.47	69.50	17.12	0.079785	179.2458	+3.6606	24.56	45.02	16.44	0.076567
178.8504	+4.9102	−4.22	69.07	17.69	0.074256	179.2891	+3.6491	96.22	74.39	17.34	0.076563
178.8590	+4.8054	55.57	80.84	16.81	0.075254	179.3037	+3.3755	118.25	24.28	17.79	0.076221
178.8800	+4.8539	14.05	41.06	17.13	0.076610	179.3232	+3.3147	−31.26	50.39	16.14	0.076608
178.9126	+4.8582	96.23	74.00	17.74	0.073426	179.4057	+3.4456	−42.39	30.53	17.65	0.077191
178.9769	+4.9574	56.23	87.87	16.95	0.075468	179.4730	+3.3865	−18.57	63.36	17.33	0.076594
179.0044	+4.9137	88.31	52.76	16.53	0.072684	179.4411	+3.6092	106.16	21.71	17.06	0.077238
179.0176	+5.0307	77.93	64.39	15.81	0.080075	179.4949	+3.6806	129.06	66.59	17.69	0.076470
179.0212	+4.9264	57.35	89.78	17.62	0.072519	179.4764	+1.3681	176.69	71.48	17.61	0.080068
179.0401	+4.8817	5.40	49.78	17.06	0.073968	179.4949	+1.3689	134.73	60.18	15.75	0.079480
179.0449	+4.9954	−41.22	36.01	15.47	0.080644	179.5352	+1.3705	159.64	40.96	17.63	0.078721
179.0526	+4.8041	118.93	56.89	17.56	0.074764	179.5602	+1.3556	93.26	68.83	16.29	0.079476
179.0547	+5.0164	−9.77	47.42	15.37	0.072725	179.5719	+0.7673	68.64	46.81	16.12	0.079388
179.0602	+5.0632	−47.99	62.37	17.44	0.078661	179.5898	+0.6655	104.42	56.88	17.04	0.078361
179.0629	+4.9679	9.25	29.70	14.35	0.073770	179.5975	+0.5519	4.56	39.29	15.54	0.077581
179.0706	+4.7722	66.72	70.80	17.72	0.073858	179.6088	+0.7131	151.00	73.64	15.29	0.079713
179.0723	+4.9995	112.70	72.92	15.68	0.073602	179.6344	+0.5982	13.19	57.10	17.15	0.077645
179.0737	+4.9472	133.16	16.46	17.65	0.074186	179.6346	+1.5777	172.00	69.12	17.39	0.079430
179.0808	+4.9603	177.17	58.52	17.00	0.075525	179.6361	+1.6940	168.20	62.15	16.02	0.081088
179.0896	+5.0115	16.95	36.37	17.48	0.077698	179.6928	+1.7125	29.92	69.55	17.56	0.078989
179.1124	+5.1740	101.26	49.52	17.66	0.074783	179.7174	+1.7283	37.37	66.84	16.20	0.079728
179.1208	+5.0216	3.89	45.85	16.31	0.074561	179.7248	+1.7357	41.37	42.25	16.75	0.079683
179.1209	+5.0019	28.27	53.58	17.10	0.079408	179.7829	+1.6435	136.10	79.51	16.88	0.080111
179.1254	+5.1209	59.92	81.24	17.62	0.073532	179.7875	+1.5714	90.57	41.34	17.35	0.079728
179.1273	+4.9664	98.61	85.59	17.65	0.074011	179.7975	+1.7102	79.18	57.25	16.29	0.078531
179.1282	+4.9239	74.70	67.79	17.05	0.074573	179.8376	+1.5185	63.39	77.33	17.35	0.079171
179.1301	+4.9328	178.73	88.26	17.20	0.077416	179.9052	+1.4960	151.82	60.68	17.21	0.079358
179.1425	+5.0531	−6.26	42.49	17.34	0.075629	179.6366	+5.1489	−30.95	41.81	16.35	0.077178
179.1568	+4.9952	64.87	78.42	16.98	0.075113	179.7026	+5.0718	−37.08	73.82	16.88	0.076781
179.1614	+5.0798	74.06	45.74	16.90	0.075883	179.7144	+5.1030	−0.95	36.52	15.51	0.076830
179.1824	+4.9632	−49.33	73.04	17.54	0.077030	179.7146	+5.1770	4.32	60.80	17.35	0.077020
179.1982	+5.0079	59.22	70.70	16.83	0.078530	179.7459	+5.1151	78.36	1.19	17.54	0.076704
179.1997	+5.0073	−49.57	18.33	15.89	0.075330	179.8008	+5.2127	16.97	63.99	17.22	0.078737
179.2053	+5.0378	98.01	68.82	16.14	0.072305	179.8182	+5.0122	11.61	45.46	17.39	0.077924
179.2137	+4.9588	78.92	19.56	15.77	0.076928	179.8757	+5.1224	55.83	70.45	17.47	0.077293
179.2210	+5.2680	84.91	31.16	15.45	0.074266	179.9008	+5.1143	−22.03	54.62	17.17	0.075647
179.2318	+5.0438	105.83	43.58	17.72	0.076202	179.7740	+0.5632	75.35	41.74	16.10	0.079868
179.2374	+4.9581	43.17	55.52	17.41	0.073625	179.7880	+0.4944	58.82	81.31	17.31	0.079672
179.2472	+5.1591	−48.88	68.90	16.06	0.075751	179.7836	+1.9189	154.88	66.31	17.06	0.078804
179.2559	+5.0997	47.53	10.99	16.73	0.076863	179.8755	+1.9051	142.13	75.81	18.03	0.077702
179.2563	+4.9909	105.12	48.49	16.79	0.077321	179.8960	+1.8671	24.72	51.25	16.29	0.078752
179.2690	+5.1038	75.05	46.84	16.56	0.080789	179.9364	+1.8298	115.47	56.63	16.36	0.078415
179.3019	+5.0757	−11.33	54.14	17.01	0.079305	179.9604	+1.7817	28.13	72.00	16.96	0.079410
179.3196	+5.1855	87.59	41.50	16.40	0.077013	179.9909	+1.7980	153.07	88.27	17.70	0.079732
179.3275	+5.0534	91.43	44.98	16.25	0.082291	179.9984	+1.8545	50.02	59.73	16.64	0.078747
179.3297	+5.1036	3.71	60.50	16.54	0.077963	180.0315	+1.8398	171.97	85.15	18.57	0.078686
179.3372	+5.2516	60.86	57.96	17.11	0.082576	179.7886	+5.2833	1.78	48.84	15.89	0.076211
179.3478	+5.2252	108.98	37.15	16.05	0.074438	179.8112	+5.3553	94.36	55.06	17.01	0.074511
179.3489	+5.2834	73.23	16.92	17.70	0.077179	179.8276	+5.2299	−2.91	63.25	16.36	0.073980
179.3495	+5.3086	1.86	69.87	17.44	0.079144	179.8925	+5.3377	−49.23	67.50	17.02	0.074575
179.3594	+5.2826	11.93	58.14	16.72	0.078886	179.8536	+3.0210	117.70	70.26	17.72	0.078582
179.3601	+5.0980	−34.84	44.52	17.23	0.077407	179.8711	+2.9824	12.07	38.59	16.31	0.077972
179.3781	+5.0798	49.84	52.76	16.86	0.076796	179.9165	+2.9172	118.65	28.49	17.23	0.077484
179.3792	+5.1002	−50.17	42.73	17.75	0.074804	179.9356	+1.2965	14.63	73.81	16.28	0.078825
179.3819	+5.1204	3.74	64.28	16.82	0.079173	179.9449	+1.3338	129.28	76.58	16.49	0.078444
179.3859	+5.0476	27.22	35.46	15.98	0.078169	179.9861	+1.3106	12.45	27.19	17.73	0.078052
179.3930	+5.0977	37.47	50.77	15.90	0.081136	179.9530	+5.8558	2.00	74.29	17.46	0.075395
179.3960	+5.1693	−39.55	75.89	16.63	0.078512	180.0082	+5.8693	28.87	46.38	17.64	0.075295
179.3994	+5.0548	91.97	66.62	17.46	0.079926	180.0197	+5.8824	73.09	16.42	17.68	0.075148
179.4128	+5.1115	−47.61	71.43	17.65	0.075758	180.1308	+4.4509	40.64	38.42	15.32	0.077752
179.4189	+5.1874	57.41	60.20	17.05	0.081449	180.1579	+4.3400	−45.25	20.24	17.62	0.077160
179.4237	+5.0409	−27.90	29.35	17.80	0.079771	180.1545	+2.6898	2.89	32.53	17.34	0.077766
179.4269	+5.2008	96.34	37.78	16.87	0.075531	180.2263	+2.6417	112.19	31.49	16.11	0.077687
179.4313	+5.0218	102.90	46.79	17.79	0.080325	180.2341	+2.6659	85.51	50.81	16.23	0.078499
179.4324	+5.1379	72.88	38.40	17.21	0.076544	180.1815	+1.1822	115.58	51.24	16.28	0.080305
179.4373	+5.1934	107.68	33.85	16.05	0.073115	180.2103	+1.1576	97.55	25.08	15.88	0.079736

Appendix D

Program and Input Files

Matlab 7.0.1 is used to write programme and input files for the simulation. As an example, we give program and input file for the galaxies of sample S[195+027+0022] (a sample described in the chapter 4.1.4). The Program and Input Files is as follows

PROGRAM FILE

Polar and Azimuthal angle for the galaxy rotation axes.

name of the program file: polar1

```
clear all;                                  % making the work place free of memory
t=cputime;

input(Type the name of your input file: );

theta1 = asin(-cos(i).*sin(B)+ sin(i).*sin(P).*cos(B));          %polar angle

theta2 = asin(-cos(i).*sin(B)- sin(i).*sin(P).*cos(B));          %polar angle

phi1 = asin ((-cos(i).*cos(B).*sin(L) + sin(i).*(-sin(P).*sin(B).*sin(L)-
cos(P).*cos(L)))./cos(theta1));          %azimuthal angle

phi2 = asin ((-cos(i).*cos(B).*sin(L) + sin(i).*(+sin(P).*sin(B).*sin(L)+
cos(P).*cos(L)))./cos(theta2));          %azimuthal angle

theta1 = theta1.*180/pi;                 %changing to degrees
theta2 = theta2.*180/pi;
phi1 = phi1.*180/pi;
phi2 = phi2.*180/pi;

theta=[theta1; theta2];                  %polar angle
phi=[phi1; phi2];                        %azimuthal angle
```

```
vec=[-87.5:5:87.5];                    %making 36 bins of 5° interval
(theta_n, dx) = hist(theta, vec);      %histogram showing polar angle distribution
(phi_n,dx) = hist(phi, vec);           %histogram showing azimuthal angle dis-
tributiion
theta_n = theta_n'                     %placing theta in column matrix
phi_n = phi_n'                         %placing phi in column matrix
```

INPUT FILE

name of the input file: S[195+027+0022]
10^7 virtual galaxies are generated.
generated parameters

Right Ascension

```
R1=rand(3861,1);
R2=0.59;
R3=R1*R2;
R4=R3+170.75;

        R5=rand(19305,1);
        R2=0.59;
        R6=R5*R2;
        R7=R6+171.34;

                R8=rand(54054,1);
                R2=0.59;
                R9=R8*R2;
                R10=R9+1171.93;

                        R11=rand(38610,1);
                        R2=0.59;
                        R12=R11*R2;
                        R13=R12+172.52;

                                R14=rand(69498,1);
                                R2=0.59;
                                R15=R14*R2;
                                R16=R15+173.11;
```

```
R17=rand(96525,1);
R2=0.59;
R18=R17*R2;
R19=R18+173.7;

        R20=rand(135135,1);
        R2=0.59;
        R21=R20*R2;
        R22=R21+174.29;

                R23=rand(166023,1);
                R2=0.59;
                R24=R23*R2;
                R25=R24+174.88;

                        R26=rand(409266,1);
                        R2=0.59;
                        R27=R26*R2;
                        R28=R27+175.47;

                                R29=rand(482625,1);
                                R2=0.59;
                                R30=R29*R2;
                                R31=R30+176.06;

R32=rand(158301,1);
R2=0.59;
R33=R32*R2;
R34=R33+176.65;

        R35=rand(293436,1);
        R2=0.59;
        R36=R35*R2;
        R37=R36+177.24;

                R38=rand(305019,1);
                R2=0.59;
                R39=R38*R2;
                R40=R39+177.83;
```

```
                                        R41=rand(111969,1);
                                        R2=0.59;
                                        R42=R41*R2;
                                        R43=R42+178.42;

R44=rand(119691,1);
R2=0.59;
R45=R44*R2;
R46=R45+179.01;

          R47=rand(96525,1);
          R2=0.59;
          R48=R47*R2;
          R49=R48+179.6;

                    R50=rand(274131,1);
                    R2=0.59;
                    R51=R50*R2;
                    R52=R51+180.19;

                                        R53=rand(366795,1);
                                        R2=0.59;
                                        R54=R53*R2;
                                        R55=R54+180.78;

R56=rand(301158,1);
R2=0.59;
R57=R56*R2;
R58=R57+181.37;

          R59=rand(289575,1);
          R2=0.59;
          R60=R59*R2;
          R61=R60+181.96;

                    R62=rand(166023,1);
                    R2=0.59;
                    R63=R62*R2;
                    R64=R63+182.55;
```

```
                              R65=rand(146718,1);
                              R2=0.59;
                              R66=R65*R2;
                              R67=R66+183.14;
R68=rand(104247,1);
R2=0.59;
R69=R68*R2;
R70=R69+183.73;
          R71=rand(104247,1);
          R2=0.59;
          R72=R71*R2;
          R73=R72+184.32;
                    R74=rand(84942,1);
                    R2=0.59;
                    R75=R74*R2;
                    R76=R75+184.91;
                              R77=rand(42471,1);
                              R2=0.59;
                              R78=R77*R2;
                              R79=R78+185.5;
R80=rand(54054,1);
R2=0.59;
R81=R80*R2;
R82=R81+186.09;
          R83=rand(69498,1);
          R2=0.59;
          R84=R83*R2;
          R85=R84+186.68;
                    R86=rand(57915,1);
                    R2=0.59;
                    R87=R86*R2;
                    R88=R87+187.27;
```

```
                                                R89=rand(54054,1);
                                                R2=0.59;
                                                R90=R89*R2;
                                                R91=R90+187.86;

R92=rand(177606,1);
R2=0.59;
R93=R92*R2;
R94=R93+188.45;

            R95=rand(189189,1);
            R2=0.59;
            R96=R95*R2;
            R97=R96+189.04;

                        R98=rand(177606,1);
                        R2=0.59;
                        R99=R98*R2;
                        R100=R99+189.63;

                                                R101=rand(115830,1);
                                                R2=0.59;
                                                R102=R101*R2;
                                                R103=R102+190.22;

R104=rand(81081,1);
R2=0.59;
R105=R104*R2;
R106=R105+190.81;

            R107=rand(115830,1);
            R2=0.59;
            R108=R107*R2;
            R109=R108+191.4.24;

                        R110=rand(305019,1);
                        R2=0.59;
                        R111=R110*R2;
                        R112=R111+191.99;
```

```
R113=rand(189189,1);
R2=0.59;
R114=R113*R2;
R115=R114+193.58;

R116=rand(285714,1);
R2=0.59;
R117=R116*R2;
R118=R117+193.17;

R119=rand(594595,1);
R2=0.59;
R120=R119*R2;
R121=R120+193.76;

R122=rand(1019305,1);
R2=0.59;
R123=R122*R2;
R124=R123+194.35;

R125=rand(783784,1);
R2=0.59;
R126=R125*R2;
R127=R126+194.94;

R128=rand(378378,1);
R2=0.59;
R129=R128*R2;
R130=R129+195.53;

R131=rand(270270,1);
R2=0.59;
R132=R131*R2;
R133=R132+196.12;

R134=rand(146718,1);
R2=0.59;
R135=R134*R2;
R136=R135+196.71;
```

```
R137=rand(142857,1);
R2=0.59;
R138=R137*R2;
R139=R138+197.3;

R140=rand(73359,1);
R2=0.59;
R141=R140*R2;
R142=R141+197.89;

R143=rand(81081,1);
R2=0.59;
R144=R143*R2;
R145=R144+198.48;

R146=rand(38610,1);
R2=0.59;
R147=R146*R2;
R148=R147+199.07;

R149=rand(57915,1);
R2=0.59;
R150=R149*R2;
R151=R150+199.66;

R152=rand(88803,1);
R2=0.59;
R153=R152*R2;
R154=R153+200.25;

R155=rand(77220,1);
R2=0.59;
R156=R155*R2;
R157=R156+200.84;

R158=rand(42471,1);
R2=0.59;
R159=R158*R2;
R160=R159+201.43;
```

```
                                                    R161=rand(7722,1);
                                                    R2=0.59;
                                                    R162=R161*R2;
                                                    R163=R162+202.02;
```

```
L = [R4 R7 R10 R13 R16 R19 R22 R25 R28 R31 R34 R37 R40 R43 R46 R49 R52 R55
R58 R61 R64 R67 R70 R73 R76 R79 R82 R85 R88 R91 R94 R97 R100 R103 R106
R109 R112 R115 R118 R121 R124 R127 R130 R133 R136 R139 R142 R145 R148
R151 R154 R157 R160 R163];
L = L* pi/180;
j=randperm(max(size(L)));        % to make above matrix random again
theta2 = theta2.*180/pi;
LL=L(j(:));
L=LL;
```

Declination

```
 D1=rand(3861,1);
 D2=0.63;
 D3=D1*D2;
 D4=D3+14.25;

            D5=rand(50193,1);
            D2=0.63;
            D6=D5*D2;
            D7=D6+14.88;

                        D8=rand(23166,1);
                        D2=0.63;
                        D9=D8*D2;
                        D10=D9+15.51;

                                    D11=rand(54054,1);
                                    D2=0.63;
                                    D12=D11*D2;
                                    D13=D12+16.14;

                                                D14=rand(104247,1);
                                                D2=0.63;
                                                D15=D14*D2;
                                                D16=D15+16.77;
```

```
D17=rand(154440,1);
D2=0.63;
D18=D17*D2;
D19=D18+17.4;
        D20=rand(61776,1);
        D2=0.63;
        D21=D20*D2;
        D22=D21+18.03;
                D23=rand(115830,1);
                D2=0.63;
                D24=D23*D2;
                D25=D24+18.66;
                        D26=rand(474903,1);
                        D2=0.63;
                        D27=D26*D2;
                        D28=D27+19.29;
                                D29=rand(857143,1);
                                D2=0.63;
                                D30=D29*D2;
                                D31=D30+19.92;
D32=rand(648649,1);
D2=0.63;
D33=D32*D2;
D34=D33+20.55;
        D35=rand(320463,1);
        D2=0.63;
        D36=D35*D2;
        D37=D36+21.18;
                D38=rand(320463,1);
                D2=0.63;
                D39=D38*D2;
                D40=D39+21.81;
```

```
D41=rand(247104,1);
D2=0.63;
D42=D41*D2;
D43=D42+22.44;

D44=rand(138996,1);
D2=0.63;
D45=D44*D2;
D46=D45+23.07;

D47=rand(254826,1);
D2=0.63;
D48=D47*D2;
D49=D48+23.7;

D50=rand(239382,1);
D2=0.63;
D51=D50*D2;
D52=D51+24.33;

D53=rand(378378,1);
D2=0.63;
D54=D53*D2;
D55=D54+24.96;

D56=rand(250965,1);
D2=0.63;
D57=D56*D2;
D58=D57+25.59;

D59=rand(544402,1);
D2=0.63;
D60=D59*D2;
D61=D60+26.22;

D62=rand(880309,1);
D2=0.63;
D63=D62*D2;
D64=D63+26.85;
```

```
        D65=rand(1737452,1);
        D2=0.63;
        D66=D65*D2;
        D67=D51+27.48;
            D68=rand(806950,1);
            D2=0.63;
            D69=D68*D2;
            D70=D69+28.11;
                D71=rand(374517,1);
                D2=0.63;
                D72=D71*D2;
                D73=D72+28.74;
                    D74=rand(216216,1);
                    D2=0.63;
                    D75=D74*D2;
                    D76=D75+29.37;
    D77=rand(115830,1);
    D2=0.63;
    D78=D77*D2;
    D79=D78+30;
        D80=rand(158301,1);
        D2=0.63;
        D81=D80*D2;
        D82=D81+30.63;
            D83=rand(131274,1);
            D2=0.63;
            D84=D83*D2;
            D85=D84+31.26;
                D86=rand(142857,1);
                D2=0.63;
                D87=D856*D2;
                D88=D87+31.89;
```

```
D89=rand(57915,1);
D2=0.63;
D90=D89*D2;
D91=D90+32.52;

D92=rand(84942,1);
D2=0.63;
D93=D92*D2;
D94=D93+33.15;

D95=rand(46332,1);
D2=0.63;
D96=D95*D2;
D97=D96+33.78;

D98=rand(3861,1);
D2=0.63;
D99=D98*D2;
D100=D99+34.41;
B=[D4 D7 D10 D13 D16 D19 D22 D25 D28 D31 D34 D37 D40 D43 D46 D49 D52
D55 D58 D61 D64 D67 D70 D73 D76 D79 D82 D85 D88 D91 D94 D97 D100];
B = B* pi/180;
j=randperm(max(size(B)));          % to make above matrix random again
BB=B(j(:));
B=BB;

% Position angle

P1=rand(177606,1);
P2=11.5;
P3=P1*P2;
P4=P3-7.5;

P5=rand(583012,1);
P2=11.5;
P6=P5*P2;
P7=P6+4;

P8=rand(501931,1);
P2=11.5;
P9=P8*P2;
P10=P9+15.5;
```

```
P11=rand(729730,1);
P2=11.5;
P12=P11*P2;
P13=P12+27;

P14=rand(610039,1);
P2=11.5;
P15=P14*P2;
P16=P15+38.5;

P17=rand(648649,1);
P2=11.5;
P18=P17*P2;
P19=P18+50;

P20=rand(610039,1);
P2=11.5;
P21=P20*P2;
P22=P21+61.5;

P23=rand(667954,1);
P2=11.5;
P24=P23*P2;
P25=P24+73;

P26=rand(637066,1);
P2=11.5;
P27=P26*P2;
P28=P27+84.5;

P29=rand(702703,1);
P2=11.5;
P30=P29*P2;
P31=P30+96;

P32=rand(610039,1);
P2=11.5;
P33=P32*P2;
P34=P33+107.5;
```

```
P35=rand(667954,1);
P2=11.5;
P36=P35*P2;
P37=P36+119;

P38=rand(706564,1);
P2=11.5;
P39=P38*P2;
P40=P39+130.5;

P41=rand(602317,1);
P2=11.5;
P42=P41*P2;
P43=P42+142;

P44=rand(633205,1);
P2=11.5;
P45=P44*P2;
P46=P45+153.5;

P47=rand(633205,1);
P2=11.5;
P48=P47*P2;
P49=P48+165;

P50=rand(277992,1);
P2=11.5;
P51=P50*P2;
P52=P51+176.5;
P=[P4 P7 P10 P13 P16 P19 P22 P25 P28 P31 P34 P37 P40 P43 P46 P49 P52];
P = P* pi/180;
j=randperm(max(size(P)));           % to make above matrix random again
PP=P(j(:));
P=PP;

% Inclination angle

I1=rand(19305,1);
I2=5.88;
I3=I1*I2;
I4=I3-1;
```

```
                I5=rand(42471,1);
                I2=5.88;
                I6=I5*I2;
                I7=I6+4.88;
                        I8=rand(123552,1);
                        I2=5.88;
                        I9=I8*I2;
                        I10=I9+10.76;
                                I11=rand(328185,1);
                                I2=5.88;
                                I12=I11*I2;
                                I13=I12+16.64;
                                        I14=rand(386100,1);
                                        I2=5.88;
                                        I15=I14*I2;
                                        I16=I15+22.52;
        I17=rand(679537,1);
        I2=5.88;
        I18=I17*I2;
        I19=I18+28.4;
                I20=rand(837838,1);
                I2=5.88;
                I21=I20*I2;
                I22=I21+34.28;
                        I23=rand(1003861,1);
                        I2=5.88;
                        I24=I23*I2;
                        I25=I24+40.16;
                                I26=rand(1030888,1);
                                I2=5.88;
                                I27=I26*I2;
                                I28=I27+46.04;
```

```
I29=rand(1023166,1);
I2=5.88;
I30=I29*I2;
I31=I30+51.92;

I32=rand(1142857,1);
I2=5.88;
I33=I32*I2;
I34=I33+57.8;

I35=rand(1142857,1);
I2=5.88;
I36=I35*I2;
I37=I36+63.68;

I38=rand(911197,1);
I2=5.88;
I39=I38*I2;
I40=I39+69.56;

I41=rand(806950,1);
I2=5.88;
I42=I41*I2;
I43=I42+75.44;

I44=rand(463320,1);
I2=5.88;
I45=I44*I2;
I46=I45+81.32;

I47=rand(57915,1);
I2=5.88;
I48=I47*I2;
I49=I48+87.2;
i = [I4 I7 I10 I13 I16 I19 I22 I25 I28 I31 I34 I37 I40 I43 I46 I49];
i = i* pi/180;
j=randperm(max(size(i)));          % to make above matrix random again
ii=i(j(:));
i=ii;
```

INPUT FILE

Substructure Analysis of Supercluster

A program file which is used to count number of galaxies within the Superclusters.

Galaxy Counting Code

```
ra=importdata('ra.m');
dec=importdata('dec.m');
sc=[ra,dec];
n=numel(ra)
repeat='y';
while repeat=='y'
radius=input('Enter the radius of circle in degree: ')
for i=1 : n
count=0;
for j=1 : n
r=(ra(i) - ra(j))^2 + (dec(i) - dec(j))^2;
if r <= radius*radius
count=count+1;
end
end
neighgal(i)=count;
end
str=input('enter a _le name to store near galaxy numbers: ','s')
_d=fopen(str,'wt');
fprintf(_d,'fclose(_d);
repeat=input('enter c if you wish to continue for another size or e to
exit: ','s')end
```

Galactic Dynamics in the Era of Large Surveys
Proceedings IAU Symposium No. 353, 2019
M. Valluri & J. A. Sellwood, eds.

doi:10.1017/S1743921319008858

No preferred alignments of angular momentum vectors of galaxies in the SDSS supercluster S[202-001+0084]

Janak R. Malla[1], Walter Saurer[2] and Binil Aryal[3]

[1]Amrit College, Tribhuvan University, Nepal
email: jrmalla@tucdp.edu.np

[2]Institute of Astro-particle Physics, Innsbruck University, Austria
email: walter.saurer@uibk.ac.at

[3]Central Department of Physics, Tribhuvan University, Kirtipur, Nepal
email: baryal@tucdp.edu.np

Abstract. We present spatial orientation of angular momentum vectors of 3038 galaxies in the SDSS supercluster S[202-002+0084] having mean redshift 0.084. The selection effects in the database are removed using random simulation method. The observed distributions of angular momentum vectors of galaxies are compared with expected theoretical distribution using chi-square, auto-correlation and Fourier tests. No preferred alignments of angular momentum vectors of galaxies are noticed in the supercluster S[202-001+0084], supporting hierarchy model.

Keywords. Galaxies: evolution, galaxies: superclusters, galaxies: statistics

1. Introduction

Von Weizsacker and Gamow (1951 & 1952) predicted that the angular momentum of galaxies might reveal the physical conditions under which they formed. The distribution of the angular momentum of galaxies is closely related to the physics of the early universe. There have been handful of studies in the past, predicting various galaxy formation scenarios. The 'pancake model' (Shandarin 1974) predicts that the rotation axes (i.e., angular momentum) of galaxies tend to lie within the cluster plane whereas the 'primordial vorticity model' (Ozernoy 1978) says that the rotation axes of galaxies tend to be oriented perpendicular the cluster plane. The 'hierarchy model' (Peebles 1969) predicts random orientation. In the present study, we analyse preferred alignments of angular momentum vectors of 3038 galaxies in SDSS supercluster S[202-001+0084].

2. Methods

We adopted the method proposed by Flin & Godlowski (1986) to find angular momentum vectors of a galaxy. In their method, this vector is defined by two angles: polar (θ) and the azimuthal (ϕ):

$$\begin{aligned}
\sin\theta &= -\cos i \sin\delta \pm \sin i \sin P \cos\delta \\
\sin\phi &= (\cos\theta)^{-1}[-\cos i \cos\delta \sin\alpha + \sin i \\
&\qquad (\mp \sin P \sin\delta \sin\alpha \mp \cos P \cos\alpha)]
\end{aligned} \tag{2.1}$$

where α, δ, P and i are the right ascension, declination, equatorial position angle, and the inclination angle, respectively. These two angles allowed us to find the orientations of the two possible vectors normal to the galactic plane, one of them assumed to be the galactic rotation axis or spin vector of the galaxy. The position angle of the galaxy

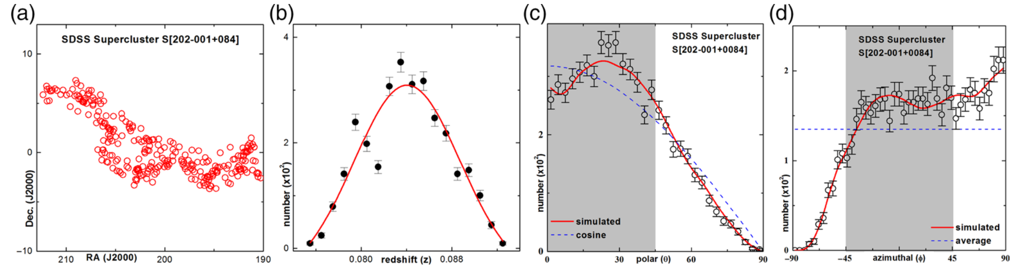

Figure 1. (a) All sky (b) redshift (c) polar and (d) azimuthal angle distributions of galaxies in the supercluster S[202-001+0084]. The solid curves represent Gaussian (b) and expected (c,d) distributions. The dashed curves show cosines (c) and average (d) distributions. The statistical $\pm 1\sigma$ error bars are shown.

(angle between major diameter and north reference direction) with respect to equatorial coordinate system is called equatorial position angle. The inclination angle (i) of galaxies are calculated using Holmberg's (1946) formula: $\cos^2 i = [(b/a)^2 - q^2]/(1-q^2)$ with b/a the measured axial ratio (b/a) and q the intrinsic flatness. We have included only spiral and lenticular galaxies because of their precise intrinsic flatness. Since elliptical galaxies are not supported by rotation, their intrinsic flatness can not be measured precisely. We have not calculated magnitudes of angular momentum because of lack of mass and rotational velocity of galaxy. We run numerical simulation to find the expected isotropic distribution (Aryal & Saurer 2000). We assumed a spatial isotropic distribution of angular momentum vectors of galaxies as a theoretical reference. Our observations are compared with isotropic distribution curves in both θ and ϕ. For this we use three statistical tests: chi-square, Fourier, and auto correlation, as suggested by Aryal *et al.* (2007).

3. Result & Discussion

Fig. 1a shows all sky distribution of 3038 galaxies in the supercluster S[202-001+0084]. Four substructures are seen when making number density map. These substructures are found to be connected from eastern to western part. Fig. 1b shows redshift distribution of galaxies in the supercluster. This distribution is found to be Gaussian with Gaussian center 0.0841 and width 0.0094. The distribution of angular momentum vectors (polar angle) of galaxies and their projections are shown in Fig. 1c,d. A very good agreement between the solid curve and the observed distributions can be seen. Any hump in the grey shaded region in Fig. 1c represents that the supercluster galaxies preferred to lie in the reference plane, supporting pancake model. Similarly, any hump in the non grey shaded region suggest primordial vorticity theory. In the polar angle distribution, chi-square probability ($P(>\chi^2)$) is found to be 0.226, suggesting no preferred alignments. Similar trend is shown by auto-correlation test ($C/C(\sigma) = 0.95$). The first order Fourier coefficient ($P(>\Delta_1)$) and probability ($P(>\Delta_1)$) are found to be 0.001 and 0.222, advocating isotropy. In the azimuthal angle distribution, the statistical parameters are found as follows: $P(>\chi^2) = 0.630$, $C/C(\sigma) = 0.36$, $P(>\Delta_1) = -0.001$ and $P(>\Delta_1) = 0.983$. These values suggest that the angular momentum vectors of galaxies in the supercluster S[202-001+0084] do not show any preferred trend, however their projections tend to be oriented towards the center of the chosen co-ordinate system. The reason of this will be studied in the future.

References

Aryal, B., Paudel, S., & Saurer, W. 2007, *MNRAS*, 379, 1011
Aryal, B. & Saurer, W. 2000, *A&A lett.*, 364, L97

Flin, P. & Godlowski, W. 1986, *MNRAS*, 222, 525
Gamow, G. 1952, *Phys. Rev.*, 86, 251
Holmberg, E. 1946, *Medd. Lund. Astron. Obs.*, Ser VI, No. 117
Ozernoy, L. M. 1978, in: Longair M.S., Einasto J., eds, Proc. IAU Symp. 79, *The Large Scale Structure of the Universe.* Reidel, Dordrecht, p. 427
Peebles, P. J. E. 1969, *Astrophys. J.*, 155, 393
Shandarin, S. F. 1974, *Soviet Astron.*, 18, 392
Weizsäcker, C. F. 1951, *ApJ*, 114, 165

Spatial Orientation of Galaxies in the Substructures of SDSS Supercluster S[184+003+0077]

Janak Ratna Malla[1], Walter Saurer[2], Binil Aryal[3]
[1] Central Department of Physics, Tribhuvan University, Kirtipur, Nepal
[2] Institute of Astroparticle Physics, Innsbruck University, Innsbruck, Austria
[3] Institute of Science & Technology, Tribhuvan University, Kirtipur, Nepal
binil.aryal@cdp.tu.edu.np
(Submitted on 18.10.2021. Accepted on 22.02.2022)

Abstract. We present substructures and preferred alignments of 1 365 galaxies in the supercluster S[184+003+0077]. A study of the magnitude, color, redshift and number density of the nearest neighbor galaxies was carried out. The 'galaxy counting code' is used to count nearest neighbors of each galaxy by varying the radius. We found 4 substructures in the supercluster region. An empirical relation between the number of galaxies and mean redshift of substructures is observed. The spatial distribution of the angular momentum vectors of galaxies in the supercluster and its substructures are studied. The selection effects in the database are removed using the random simulation method. The observed distributions of the angular momentum vectors of galaxies are compared with the expected theoretical distribution using chi-square, auto-correlation and Fourier tests. No preferred alignments of the angular momentum vectors of galaxies are noticed in the supercluster S[184+003+0077], supporting the hierarchy model. In the substructures, local groupings are observed.
Key words: Galaxies: evolution galaxies: superclusters galaxies: statistics

1 Introduction

Superclusters are the largest observed structures in the Universe. A supercluster constitutes several clusters and groups of galaxies which are a gravitationally bound system. A large database of superclusters is available in the Sloan Digital Sky Survey Data Release 7 (SDSS DR7 hereafter) and the pioneer work by Einasto et al. (2003, 2011, 2014, 2016). Einasto et al. (2003) investigated superclusters of galaxies in the SDSS and found that the clusters located at high-density environment showed luminosity a factor of 5-10 times higher than in low-density environment of the field. Further Einasto et al. (2011) classified the morphology of a set of superclusters using the SDSS DR7 database and calculated their luminosity to determine superclusters from a flux-limited sample of galaxies and finally selected superclusters with 300 and more galaxies. A widely different morphology of superclusters is found. In the next paper, Einasto et al. (2014) compared the galaxy populations in SDSS superclusters of different morphology in the nearby Universe (180 h^{-1}Mpc < d < 270 h^{-1}Mpc) and concluded that both the local (group) and global (supercluster) environments play an important role in the formation and evolution of galaxies. In the same year, Einasto et al. (2016) studied the dynamical state of galaxy superclusters from the Sloan Great Wall (SGW) which is the richest galaxy system in the nearby Universe. They concluded that the rich SGW superclusters with their high-density cores represent dynamically evolving environments, which are well suited for studies of the properties of galaxies and galaxy systems.

Von Weizsäcker and Gamow (1951 & 1952) predicted that the angular momentum of galaxies can explore the initial conditions under which these systems formed. The distribution of the angular momentum of galaxies in the supercluster might reveal the origin of the early universe. There have been a handful of studies in the past, predicting three galaxy formation scenarios: the 'pancake model' (Shandarin 1974) predicts that the rotation axes (i.e., angular momentum vectors) of galaxies tend to lie within the cluster plane whereas the 'primordial vorticity model' (Ozernoy 1978) claims that the rotation axes of galaxies tend to be oriented perpendicular the cluster plane. The 'hierarchy model' (Peebles 1969) predicts a random orientation.

In order to understand the formation and evolution of a supercluster, its substructures and their spatial orientation should be well understood. In the present work, we aim to study as follows: (a) the color-magnitude diagram, (b) the number density maps, (c) identify individual substructures in the supertructures, (d) study the preferred alignments of angular momentum vectors of galaxies in the substructures in the superclusters, and finally (e) compare subclustering and the preferred alignments with the galaxy evolution models.

2 SDSS Supercluster S[184+003+0077]

We have compiled a database (positions, redshifts, r- and u-magnitudes) of 1 365 galaxies in the supercluster S[184+003+0077] using the SDSS database. The all sky distribution of galaxies in the superclusters is shown in Fig. 1a. A marker galaxy in the supercluster is the brightest galaxy near the highest density peak in the supercluster volume (Liivamägi et al., 2012). The aim of this is to tie a supercluster to an already observed cross identifier.

Fig. 1b shows the redshift contour map of the supercluster region. Redshift is found to be distributed in such a way that the marker galaxy lies in the low redshift region, whereas it is surrounded by a high redshift region. We have analyzed the magnitude (m_r), color (m_u-m_r) and redshift (z) distributions of galaxies in the supercluster. The color ($\log(m_u$-$m_r)$) – magnitude (m_r) diagram (Fig. 1c) is fitted by

$$\log(m_u - m_r) = -0.04 m_r + 1.08 \tag{1}$$

Here the slope is found to be slightly negative, suggesting that the color is mostly independent of magnitude.

3 Methods

We have determined the number density around each galaxy using an algorithm named 'galaxy counting code' (Appendix A). The variable is the radius (r) from each and every galaxy. We set the values of r from 0.1° to 2.0° in steps of 0.05°. We determined the standard deviation in each step. Then selected the steps where the standard error of the deviation is found to be maximum. In addition, the least number of galaxies in the substructures has been set as the cutoff values of that particular standard deviation.

We have used the method developed by Flin & Godlowski (1986) to find the angular momentum vectors of a galaxy. In their method, the angular momentum vector is defined by two angles: polar (θ) and azimuthal (ϕ):

$$\begin{aligned} \sin\theta &= -\cos i \sin\delta \pm \sin i \sin P \cos\delta \\ \sin\phi &= (\cos\theta)^{-1}[-\cos i \cos\delta \sin\alpha + \sin i \\ &\quad (\mp \sin P \sin\delta \sin\alpha \mp \cos P \cos\alpha)] \end{aligned} \tag{2}$$

where α, δ, P and i are the right ascension (R.A.), declination (Dec.), equatorial position angle, and the inclination angle, respectively. The inclination angle (i) of galaxies is calculated using Holmberg's (1946) formula: $\cos^2 i = [(b/a)^2 - q^2]/(1-q^2)$ with b/a the measured axial ratio (b/a) and q the intrinsic flatness. We run a numerical simulation to find the expected isotropic distribution (Aryal & Saurer 2000). Our observations are compared with isotropic distribution curves in both θ and ϕ. For this we use three statistical tests: chi-square, Fourier, and auto correlation, as suggested by Aryal et al. (2007).

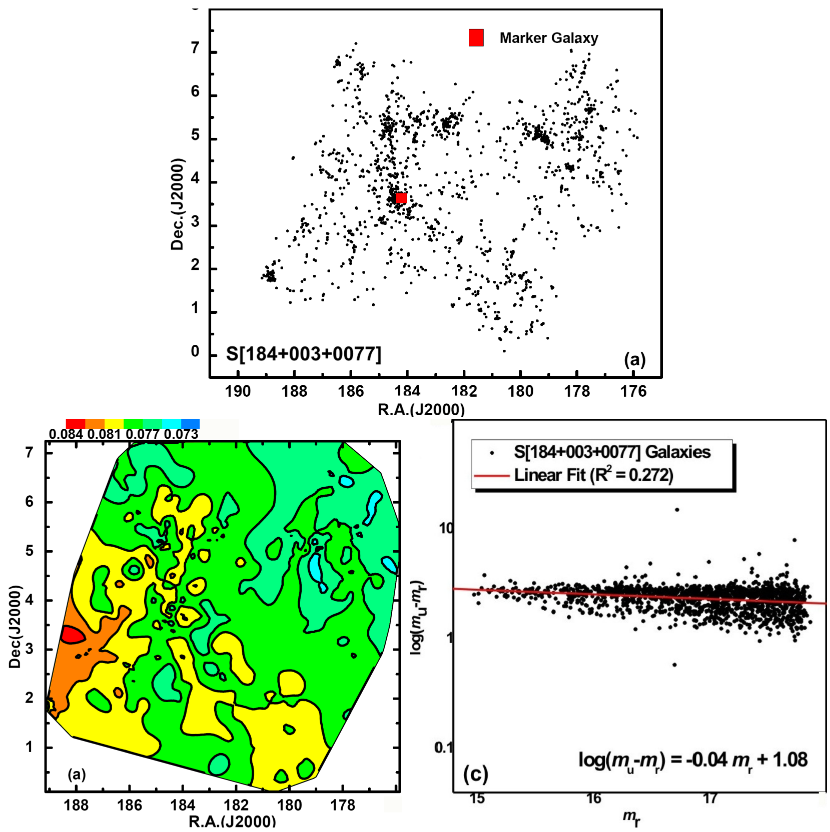

Fig. 1. (a) Sky distribution of the galaxies in the supercluster S[184+003+0077]. Each open circle represents a galaxy. The marker galaxy is denoted by a filled square. (b) The redshift map of the supercluster region. The redshift color bar is shown as well. (c) Color (log(m_u-m_r)-magnitude (m_r) diagram of galaxies in the supercluster S[184+003+0077]. Each black dots represents a galaxy. The best fit lines and equation are shown.

For the plotting and statistics, we use the software ORIGIN 8.0. To count the nearest neighbor galaxies within a radius r, a code was written using MATLAB 6.1.

4 Results & Discussion

Fig. 2a,b shows the number density map of the galaxies in the supercluster S[184+003+0077]. The contour levels and the color bars are shown. We consider the region of high density as a substructure of the supercluster. In the supercluster S[184+003+0077], we noticed 4 such regions in which the number density of galaxies exceeds the limits of the standard deviation. The respective number of galaxies in these substructures is found as 170, 91, 68 and 70. The names of substructures are given as S1[185+0035+0077], S2[180+0050+0079], S3[185+0050+0079] and S4[183+0050+0080]. The mean values of the magnitude (m_r) of these substructures are listed in the third column of Table 1.

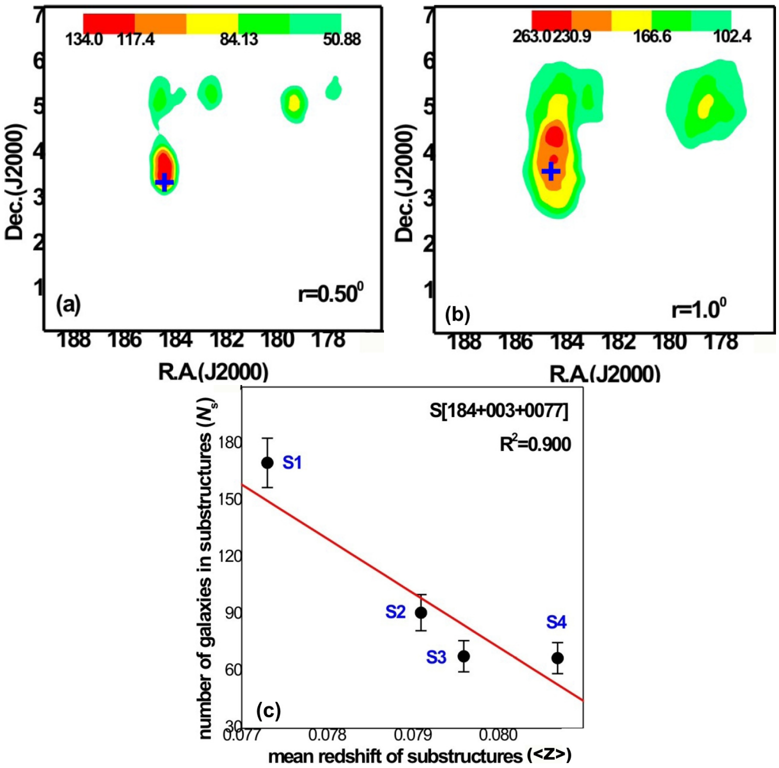

Fig. 2. Number density map of galaxies in the supercluster S[184+003+0077]. Nearest neighbor distance of each galaxies at $r = 0.5°$ (a) and $1.0°$ (b). The color bars are shown. (c) Number of galaxies in substructures versus mean redshift plot in the supercluster S[184+003+0077]. The statistical $\pm 1\sigma$ error bars are shown. Here S1, S2, S3, S4 represent substructures in the supercluster. The coefficient of regression is shown.

Fig. 2c shows a plot of the number of galaxies in the substructures versus the mean redshift ($< z >$) of that substructure.

The best fit line is,

$$N = -2.8 \times 10^4 < z > +2353.2 \tag{3}$$

Substructures S2 and S3 showed similar values of the mean redshift ($< z >$) and magnitude (m_r) (Fig. 2a,c & Table 1), suggesting a close association between them. They are either in the process of aggregation or separation. Therefore, the angular momentum vectors of these two groups are expected to show peculiarities.

We study the spatial orientation of the angular momentum vectors of galaxies with respect to the equatorial coordinate system. Any deviation from the expected isotropic distribution will be tested using four statistical parameters, namely the chi-square probability (P$> \chi^2$), auto-correlation coefficient (C/C(σ)), first order Fourier coefficient $\Delta_{11}\sigma(\Delta_{11})$, and first order Fourier probability (P$> \Delta_1$). The conditions for anisotropy are the following: P($> \chi^2$) < 0.050, C/C(σ) and $\Delta_{11}/\sigma(\Delta_{11}) > 1$, and P($> \Delta_1$) < 0.150. These statistical limits were proposed by Godlowski (1994). The polar (θ) and azimuthal (ϕ) angle distributions of galaxies in S[184+003+0077] are shown in Fig. 3. The statistical values are listed in Table 1. In the supercluster S[184+003+0077], the value of the chi-square probability [P($>\chi^2$)] is found to be 0.084, suggesting no preferred alignments. A similar trend is shown by the auto-correlation test [C/C(σ)=1.0]. The first order Fourier coefficient [$\Delta_{11}/\sigma(\Delta_{11})$] and Fourier probability [P($>\Delta_1$)] are found to be 0.6 and 0.790, suggesting isotropy.

A very good agreement between the observed (solid circle with error bars) and expected (solid line) distributions can be seen in Fig. 3a. At $\theta = 27.5°$, a hump can be seen. There is a larger number of observed galaxies (285) than the expected (250). Thirty five galaxies showed a preferred alignment at this angle. This preference might be because of a sub-clustering phenomena due to the tidal or gravitational shearing effect. In the azimuthal angle distribution (Fig. 3b), the observed and expected distributions are in closer agreement. All four statistical parameters [(P($>\chi^2$), C/C(σ), $\Delta_{11}/\sigma(\Delta_{11})$] and P($>\Delta_1$) suggest isotropy (Table 1). This means that, the projections of the angular momentum vectors of galaxies in S[184+003+0077] showed no preference. In the shaded region, at $\phi = -5°$, a hump can be seen at the 2σ level. But this hump is cancelled by two dips at $-45°$ and $5°$. Therefore, vanishing angular momentum is noticed in the supercluster.

The polar and azimuthal angle distributions of galaxies in four substructures of the supercluster S[184+003+0077] are shown in Fig. 4. The largest substructure S1[185+0035+0077] consists of 170 galaxies. This means that, redshift ($< z >$) is similar to that of the supercluster. In the polar angle (θ hereafter) distribution, the value of the chi-square probability [P($> \chi^2$)] and first order Fourier probability [P($> \Delta_1$)] are found to be 0.648 and 0.623. Both these probabilities are more than 60%, suggesting no preferred alignments. Similarly, the auto-correlation [C/C(σ)] and first order Fourier coefficients [$\Delta_{11}/\sigma(\Delta_{11})$] are found to be less than one, suggesting isotropic distribution. In the azimuthal angle (ϕ hereafter) distribution of substructure S1, three statistical parameters namely P($> \chi^2$), P($> \Delta_1$) and $\Delta_{11}/\sigma(\Delta_{11})$ showed isotropy (Table 1). Only the auto correlation coefficient [C/C(σ)] showed a

Table 1. Statistics of the polar (θ) and azimuthal angle (ϕ) distributions of galaxies in the supercluster S[184+003+0077] and its four substructures S1[185+0035+0077], S2[180+0050+0079], S3[185+0050+0079] and S4[183+0050+0080]. The first column lists the name of the supercluster and its substructures. The second and third columns give R.A.(J2000), number of galaxies (N), Dec.(J2000) and mean values of (m_r) magnitude. The fourth and fifth columns list the values of the chi-square probability (P(> χ^2)) and auto-correlation coefficient [C/C(σ)]. The last two columns give the first order Fourier coefficient [$\Delta_{11}/\sigma(\Delta_{11})$] and the first order Fourier probability [P(> Δ_1))], respectively.

subsample			P(> χ^2)	C/C(σ)	$\Delta_{11}/\sigma(\Delta_{11})$	P(> Δ_1)
polar angle	RA(J2000)	N				
S[184+003+0077]	183.815°	1365	0.084	+1.0	+0.6	0.790
S1[185+0035+0077]	179.205°	170	0.648	+0.9	+0.9	0.623
S2[180+0050+0079]	182.579°	91	0.888	+0.2	−0.2	0.973
S3[185+0050+0079]	184.378°	68	0.912	+0.1	+0.3	0.904
S4[183+0050+0080]	177.450°	67	0.815	−0.4	-0.5	0.846
azimuthal angle	Dec.(J2000)	m_r				
S[184+003+0077]	+3.358°	17.9	0.580	+0.3	+0.8	0.490
S1[185+0035+0077]	+3.601°	17.8	0.129	−1.1	+0.5	0.860
S2[180+0050+0079]	+5.038°	17.9	0.960	−0.1	−0.3	0.909
S3[185+0050+0079]	+5.350°	17.8	0.339	−1.1	−0.7	0.712
S4[183+0050+0080]	+5.639°	18.0	0.822	−0.1	+0.5	0.885

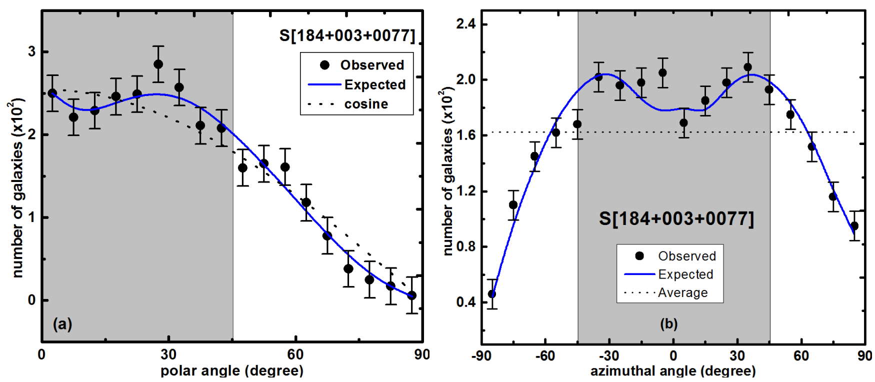

Fig. 3. Polar (a) and azimuthal angle (b) distributions of galaxies in the supercluster S[184+003+0077]. The solid curves represent the expected distributions. The dotted curves show the cosines (a) and average (b) distributions. The statistical $\pm1\sigma$ error bars are shown.

weak deviation (1.1σ) from isotropy. In Fig. 4a, a number of humps (12.5°, 27.5°, 32.5°) and dips (2.5°, 42.5°) at small angles suggest a local effect, supporting the formation of subgroups within the substructure S1. These effects are possibly enhanced by the tidal effect, due to which the angular momentum vectors of neighboring galaxies get affected (Godlowski, 2012). However, these humps and dips cancel each other to show isotropy. Four alternative humps (−25°, −5°, 15°, 45°) and dips (−45°, −15°, 5°, 35°) can be seen in the ϕ distribution (Fig. 4b). A hump followed by a dip suggests either a binning effect in the histogram or a successive deviation of the angular momentum vectors and their projections due to subclustering. In the substructure S2, there are 91 galaxies with mean redshift ($< z >$) 0.079 which is slightly larger than that of the supercluster as a whole. Therefore, substructure S2 is moving away with a relatively larger speed than that of substructure S1. Thus, the effect of gravitational shearing can not be denied here. Let us discuss its effect in the alignments. The distributions of the angular momentum vectors (polar angle, θ) and their projections (azimuthal angle, ϕ) of galaxies in the substructures S2 are shown in Figs. 4c,d. All eight statistical values in both θ and ϕ distributions suggest isotropy (Table 1). Similar to the substructure S1, this substructure showed several systematic humps and dips in both the θ and ϕ distributions. Instead of alternate humps and dips, here we noticed successive groups of deviations (for example, 12.5° to 32.5°, 37.5° to 57.5° in Fig. 4c and −75 to −55°, −15 to 5° in Fig. 4d) from the expected. In the statistical tests, these deviations cancel each other to show isotropy in both the θ and ϕ distributions.

Substructure S3 has exactly the same values of the mean redshift as S2. This means that, both substructures are moving with identical radial velocities. Fig. 4e,f show the θ and ϕ distributions of galaxies in the substructures S3. If we look at the observed distribution of galaxies in the polar angle, humps (2.5°, 22.5°, 37.5°, 47.5°, 57.5°, 67.5°) and dips (7.5°, 12.5°, 42.5°, 77.5°, 77.5°) at both smaller and larger angles are seen. In the statistical tests, these humps and dips cancel each other to show isotropy in the θ distribution. In the ϕ distribution, the statistical parameters $P(> \chi^2)$, $P(> \Delta_1)$ and $\Delta_{11}/\sigma(\Delta_{11})$ show isotropy (Table 1) whereas the auto correlation coefficient ($C/C(\sigma)$) shows a small deviation (1.1σ) from isotropy. Similar to Fig. 4e, a large number of humps and dips are seen in the ϕ distribution (Fig. 4f). The successive deviation in the alignments might be a clue regarding the substructure formation in the supercluster. So, the distribution of such a local effect should be studied in the future.

The fourth substructure S4[183+0050+0080] has 67 galaxies with mean redshift 0.080, which is larger than that of substructures S1, S2 and S3. In other words, this substructure is leading in terms of mean radial velocity. If we look at the distributions (θ and ϕ, Fig. 4g,h), a poor agreement between the observed and expected values is seen. A large number of humps (at 2.5°, 12.5°, 32.5°, 47.5°, 57.5° in θ; at −85°, −45°, −35°, −15°, 15°, 25°, 45°, 65° in ϕ) and dips (at 7.5°, 17.5°, 22.5°, 42.5°, 77.5° in θ; at −75°, −65°, −15°, 5°, 15°, 55°, 75°, 85° in ϕ) can be seen. All these humps and dips are at $>1\sigma$ level. In contrast to these successive and alternative humps and dips, in the statistical tests, all four statistical parameters suggest strong isotropy. There-

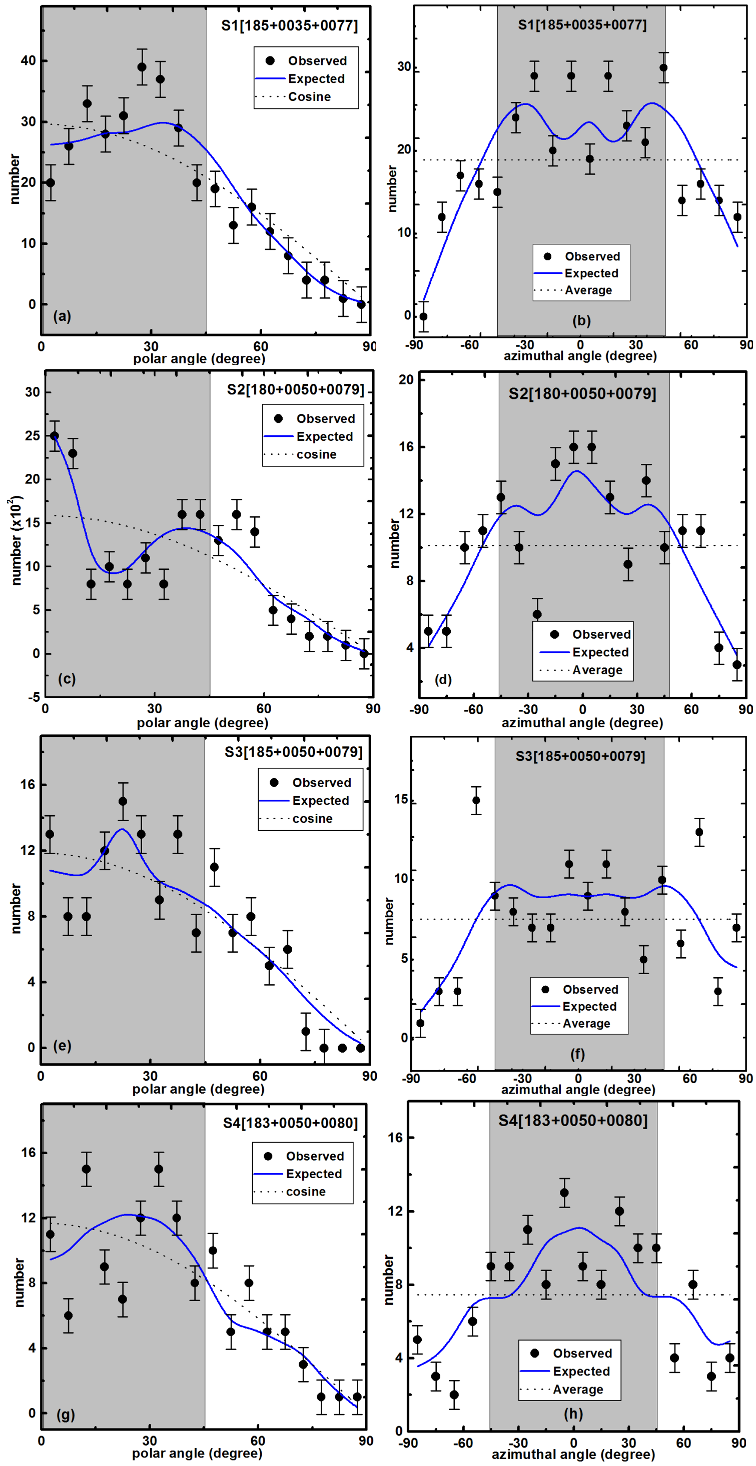

Fig. 4. Polar (a,c,e,g) and azimuthal angle (b,d,f,h) distributions of galaxies in the substructures of supercluster S[184+003+0077]. The solid curves represent the expected distributions. The dashed curves show the cosines (a,c,e.g) and average (b,d,f,h) distributions. The statistical $\pm 1\sigma$ error bars are shown. The names of the substructures are given.

fore, the substructure S4 shows 'vanishing angular momentum' as suggested by Godlowski et al. (2010).

Melkonian & Nikogosian (1998) studied a substructure of the core of the Perseus Supercluster of galaxies. They noticed hierarchical substructures in which a radial segregation of galaxies is found. However, the position angle distribution of galaxies is found to be uniform. Godlowski et al. (1998) studied the rich cluster of galaxies Abell 754 and found evidence for non-random alignment of the galaxies and confirmed the presence of subclustering.

Baier et al. (2003) studied the galaxy cluster Abell 14 and confirmed the presence of subclustering. They noticed a preferred alignment of the angular momentum vectors of galaxies in the cluster Abell 14. Norena et al. (2018) proposed an idea that substructures could be formed due to the tidal stream produced in galactic mergers. Panko et al. (2018) investigated the 2D distribution of galaxies in 254 rich open galaxy clusters. They noticed that about 25% of clusters showed four kinds of regular substructures namely crossing and divaricating filaments (or X and Y-type peculiarities) and curved strips with short dense chains. Malla et al. (2020) studied the preferred alignments of galaxies in the SDSS supercluster S[202-001+0084]. They noticed a random orientation of the angular momentum of galaxies in this supercluster. We also noticed a similar result in the supercluster S[184+003+0077].

To sum up, we noticed a random orientation of the angular momentum vectors and their projections in the supercluster S[184+003+0077], as well as in all four substructures S1[185+0035+0077], S2[180+0050+0079], S3[185+0050+0079] and S4[183+0050+0080] with a signature of local groupings. We intend to study the alignment of galaxies in these small groups in the substructure to reveal the reason behind it.

5 Conclusion

We have studied the distribution of the nearest neighbor galaxies to find substructures in the supercluster S[184+003+0077] region. The spatial orientation of 1 365 galaxies in the supercluster S[184+003+0077] having a redshift of 0.077 and its substructures are studied. We summarize our results as follows:

1. Four substructures are found in the supercluster S[184+003+0077]. These are S1[185+0035+0077], S2[180+0050+0079], S3[185+0050+0079] and S4[183+0050+0080] with a mean redshift of 0.077, 0.079, 0.079 and 0.080, respectively. An empirical relation between the mean redshift ($< z >$) and the number of galaxies (N) in the substructures is found.
2. The distribution of the angular momentum vectors of galaxies in the supercluster S[184+003+0077] showed isotropy, suggesting no preferred alignments. In the substructures, despite having alternate and successive deviations from the expected distributions, the overall effect is found to be that of a vanishing angular momentum. Thus, no preferred alignments of the angular momentum vectors of galaxies are found in the supercluster and its all four substructures, supporting the hierarchy model (Peebles, 1969).
3. The projections of the angular momentum vectors of galaxies in the supercluster S[184+003+0077] is found to be random. In the substructures, these projections are found to be alternately deviated from the expected distribution. However, isotropy is found to be maintained.

4. The substructures showed higher values of the mean redshift than that of the supercluster S[184+003+0077]. This corresponds to the fact that the subclusters are moving with higher radial velocities than that of the supercluster. Thus, the gravitational shearing effect can not be ruled out in the large scale structure formation (Li, 1998)

Acknowledgement

We are thankful to anonymous reviewer for critical and constructive comments and suggestions. One of the authors (JRM) acknowledges Nepal Academy of Science & Technology, Central Department of Physics, Amrit Campus, Tribhuvan University, Nepal for various kinds of support during Ph.D. work. We are thankful to Dr. Shiv Narayan Yadav, Mr. Ek Narayan Poudel, Mr. Mohan Gaire and Mr. Balendra Bhatt for their help during data compilation. We have used SDSS database (https://classic.sdss.org/dr7/), SIMBAD (http://simbad.u-strasbg.fr/simbad/) for providing database and software ALADIN 2.5 (https://aladin.u-strasbg.fr/).

References

Aryal B., Paudel S., Saurer, W., 2007, *MNRAS* 379, 1011
Aryal B., Saurer W., 2000, *A&A* 364, L97
Baier F. W., Godlowski W., MacGillivray H. T., 2003, *A&A* 403, 847
Einasto J., Hütsi G., Einasto M., Saar E., Tucker D. L. et al. 2003, *A&A* 405, 425
Einasto M., Liivamägi L. J., Tago E., Saar E., Tempel E. et al., 2011, *A&A* 532, 20
Einasto M., Lietzen H., Tempel E. Gramann M. Liivamägi L. J. et al., 2014, *A&A*, 562, 14
Einasto M., Lietzen H., Gramann M., Tempel E., Saar E. et al., 2016, *A&A* 595, 12
Flin P., Godlowski W., 1986, *MNRAS* 222, 525
Gamow G., 1952, *Phys. Rev.* 86(2), 251
Godlowski W., 2012, *ApJ* 747, 1, 7
Godlowski W., 1994, *MNRAS* 271, 19
Godlowski W., Baier F. W., MacGillivray H. T., 1998, *A&A* 339, 709
Godlowski, W., Piwowarska, P., Panko, E., Flin, P., 2010, *ApJ* 723, 2, 985
Holmberg, E., 1946, *Medd. Lund. Astron. Obs.*, Ser. VI, No. 117
Li, L. X. 1998, *General Relativity and Gravitation* 30, 497
Liivamägi L. J., Tempel E., Saar E., 2012, *A&A* 539, 14
Malla, J. R., Saurer, W., Aryal, B., 2020, *Galactic Dynamics in the Era of Large Surveys*, Proceedings of the International Astronomical Union, Vol. 353, 259.
Melkonian A. A., Nikogosian E. G., *Astrophysics* 41, 1, 41
Norena D. A., Muñoz-Cuartas J. C., Quiroga L. F., Libeskind N., 2019, *Revista Mexicana de Astronomía y Astrofísica* 55, 273
Ozernoy L. M., 1978, in Longair M. S., Einasto J., eds, Proc. IAU Symp. 79, The Large Scale Structure of the Universe. Reidel, Dordrecht, p.427
Panko E. A., Andrievsky S. M., Yemelianov S. I., Stepaniuk A. M., 2018, *Astron. Reports* 62(12), 911
Peebles P. J. E., 1969, *ApJ* 155, 393
Shandarin S. F., 1974, *Astr. Zh* 51, 667 (in Russian), Soviet Astron 18, 392 (in English)
Von Weizsäcker C., 1951, *ApJ* 114, 165

Appendix A

Galaxy Counting Code (MATLAB 6.1)

```
ra = importdata('ra.m');
dec = importdata('dec.m');
```

```
sc = [ra,dec];
n = numel(ra) repeat = 'y';
while repeat =='y' radius = input('Enter the radius of circle in degree: ') for
i=1 : n count=0;
for j=1 : n r = (ra(i) - ra(j))^2 + (dec(i) - dec(j))^2;
if r <= radius*radius count=count+1;
end
end
neighgal(i)=count;
end str = input('enter a −le name to store near galaxy numbers: ','s') −d=fopen(str,'wt');
fprintf(−d,'fclose(−d);
repeat=input('enter c if you wish to continue for another size or e to exit:
'end')
```

INTERNATIONAL
ISSN 2321-2993
MPHIN/2011/37381

Identification of substructures in the Supercluster S [195+027+0022] having redshift 0.022

Janak Ratna Malla* Walter Saurer Binil Aryal*****

Abstract

We present the substructure classification of galaxies in supercluster S [195+027+0022]. Using the SDSS DR 12 galaxies, we studied number density maps in the region of substructure. Our main goal is to find out the substructures within the large scale structure using the contour maps of number densities of galaxies by varying radius. We found three substructures in the supercluster region having slightly different redshifts ranging from 0.022 to 0.024. A discussion on redshift maps of these substructures is presented..

Keywords : Galaxy: Evolution, Supercluster, Substructure, Orientation.

Introduction

The whole universe, before the Big Bang, was compressed into a singularity (Smith, 1988). The creation process began with expansion. According to standard model the large-scale structure in the universe is the region where most of the density is dominated by cold matters, however it has had difficulty in matching the relatively quiet velocity field of galaxy and observed structure on very large scales. The growth of primordial fluctuations by gravitational instability is the main cause in the formation and evolution of large scale structure (Smith, 1988). The Big Bang happened everywhere so space itself began to expansion, eventually expansion stopped: self-gravity, finally the expansion turned around collapsing into bound structures. The fact: smaller structures collapse first and are later incorporated in larger collapsing structure.

As we know galaxy can be defined as a huge assembly of stars, dust, & gases mutually held together by gravitational force (dekel et.al., 2009). Galaxies are the most visible matters that concentrated at any point in universe having self-gravitational mass. They are made up of mainly three different entities stars, an interstellar medium (gas with dust) & dark matter. There is an inter-play between the stars & gas with star forming out of the gas & with gas being ejected back into the interstellar medium from evolved star. The dark matter affects the other matter through its strong gravitational potential but very little is known about it directly. The interaction between distributions of matter that is interaction between stars, cloud of gases or dust particles even between two near neighbor galaxies is very important over the life of galaxy (Kravtsov & Borgani, 2012).

It is slightly difficult topic in astronomy at present, although a great research concerning with galaxies formation, their motion and structure characters knows galaxies are much less well understood than say that of stars. Group of galaxies forms a large structure in the cosmos called superclusters. Multiple of galaxies together form a cluster instead of being dispersed randomly

* *Central Department of Physics, Kirtipur, Kathmandu, Nepal*
** *Institute of Astro-Particle Physics, Innsbruck University, Austria*
*** *Central Department of Physics, Kirtipur, Kathmandu, Nepal*

because of gravitational force. So, in superclusters multiple of galaxies are bounded by gravitational (Pontzen & Governato, 2014). To understand the physical condition, structure and formation of galaxies and clusters different research has been carried out. The evolutions of these systems are determined by time and manner of formation & the process of how their structure and constituent have been changing with time. The rotation of galaxies and spatial orientation of spin vectors of galaxies are also key point to study the physical condition of galaxies as well superclusters.

Data Compilation

The database of supercluster S [195+027+0022] used in our current work comprises galaxies located within the survey region of Sloan Digital Sky Survey (SDSS) (York et al., 2000) and those were obtained from SDSS data release seven (Percival J., Will et al., 2010) through our collaboration with Prof. Walter Saurer's group at the institute of Astroparticle Physics, Innsbruck University, Austria. There were 2,603 galaxies in our region of interest. We have excluded number of galaxies in our database based on the value of intrinsic factors q = 0.2 and q = 0.13. First of all we used intrinsic factor q = 0.2 to find the inclination angle of galaxies and again used the intrinsic factor q = 0.13 to those galaxies which did not give inclination angle for q = 0.2 (Heidmann et.al., 1972). Among 2,603 galaxies, 13 were excluded due to b/a 0.13 i.e. their inclination angle cannot be determined. Finally, we have 2,590 in our sample with known value of Right Ascension, Declination, Position angle and Inclination angle. After shorting 2,590 galaxies by numbers of density within the circle and neglected 1,202 galaxies to make statistical tests more significant. And then all sky view of 1,388 galaxies was observed to identify substructure. Finally we identified substructures as S1 [195+028+0022], S2 [176+020+0023] and S3 [181+020+0024] with galaxy numbers 810, 347 and 152 respectively.

Method of Analysis

From all sky distribution of galaxies in a large-scale structure, the distribution of galaxy is not uniform (takami et.al, 2009). We found some region with high density contrast, so we must study about the density contrast to understand how overall structure and contrast region affect the evolution and formation of galaxies in that region (Einasto et.al., 1984). We have classified our database-total sample into substructure on the basis of number density of galaxies. First, we try to find the number of galaxies around the each galaxy within the different radius values such as 0.2°, 0.3°, 0.35°, 0.4°, 0.5°, 0.75°, 1.0°, 1.25° and 1.5°. Since a common radial velocity for a group of galaxies permits us to identify the group as a cluster of genetically related galaxies, which may be a great importance for study the structure evolution in large scale (Harris, 1986). By analyzing the distribution of galaxy in the contour map in various radius values, we choose particular value of radius for which clear substructure is seen. Finally, we have chosen 0.5°, 0.75°, 1.0°, 1.25°and 1.5° as two values of radius for our work.

Results & Discussion

We have to search substructures in the supercluster S [195+027+0022]. For that the process of figuring out the different structures within the given large structure. Here we observed the given large structure S [195+027+0022] by varying the radius value of the circle and viewed on contour map as shown in the figure 1 below.

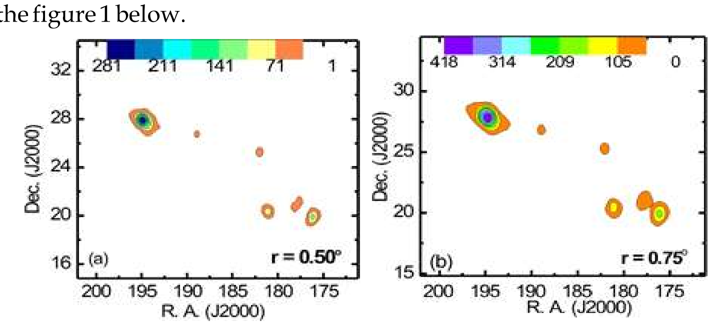

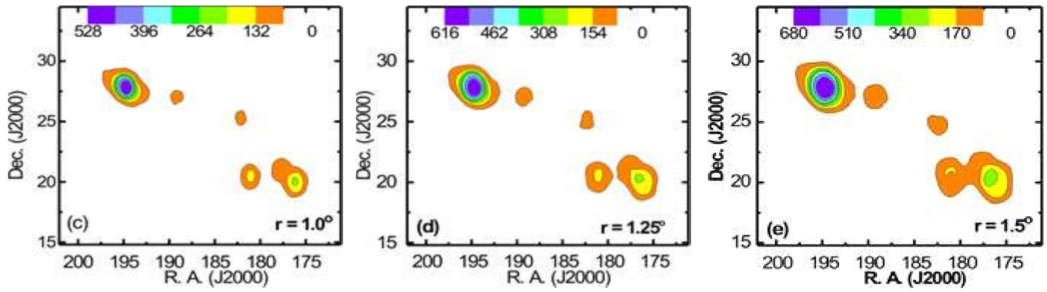

Figure 1: A contour view of given supercluster S [195+027+0022]. In above figure, a, b, c, d and e represent the contour map with radius values 0.5º,0.75º, 1.0º, 1.25º and 1.50º respectively. The contour levels are shown; X-axis and Y-axis represent right ascension and declination.

From the above figure, we can see the substructures of different shapes and size within the given large structure. On changing the size of the circle, the pattern of the substructure seems somehow similar. By our analysis of above five patterns, we decided to proceed the pattern with size having 1º and found three substructures (i.e. substructure S1 [195+028+0022], S2 [176+020+0023] and S3 [181+020+0024]). Here we have proceeded the statistical tests (i.e. chi-square, auto-correlation and Fourier) on these three substructures by neglecting those galaxies that does not include at least 70 galaxies taking them as a reference centre of circle having radius 1º to make the tests more significant and found galaxy numbers 810, 347, and 152 for S1 [195+028+0022], S2 [176+020+0023] and S3 [181+020+0024] respectively.

The all sky distribution of 2,590 galaxies of our database in the supercluster S [195+027+0022] is shown in Fig 2. We expect homogeneous distribution of galaxies according to cosmological principle. But the inhomogeneous distributions can be observed in the figure. A spider like structure is seen. In some region more galaxies are found to be concentrated forming substructure region.

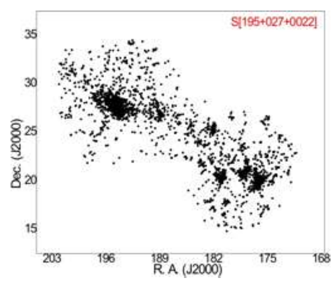

Figure 2: All sky distribution of galaxies in the equatorial co-ordinate system for supercluster S [195+027+0022]. Similarly all sky view of substructures S1 [195+028+0022], S2 [176+020+0023] and S3 [181+020+0024] with respective galaxy number 810, 347 and 152 is shown in the figure below.

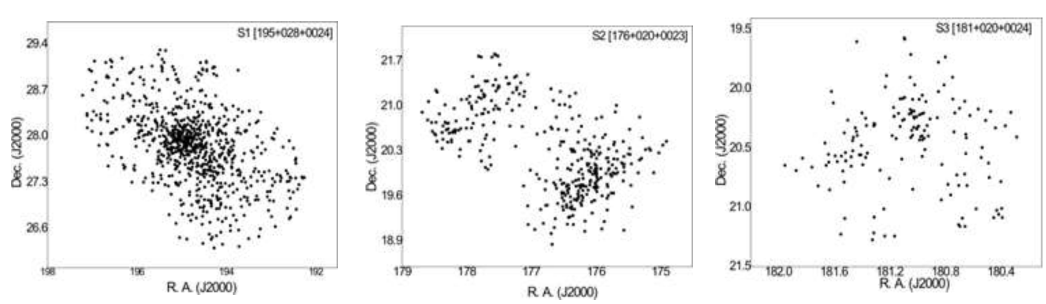

Figure 3: All sky view of substructures S1 [195+028+0022], S2 [176+020+0023] and S3 [181+020+0024]. The X-axis and Y-axis represent right ascension and declination respectively.

As we know that many celestial objects are receding from us (i.e. redshifted) and few are approaching to us (i.e. blueshifted) with different speed. Since a common radial velocity for a group of galaxies permits us to identify the group as a cluster of genetically related galaxies, which may be a great importance for study the structure evolution in large scale. Here we have presented the velocity contour map of our database on the basis of redshift values as shown in the Fig. 4.

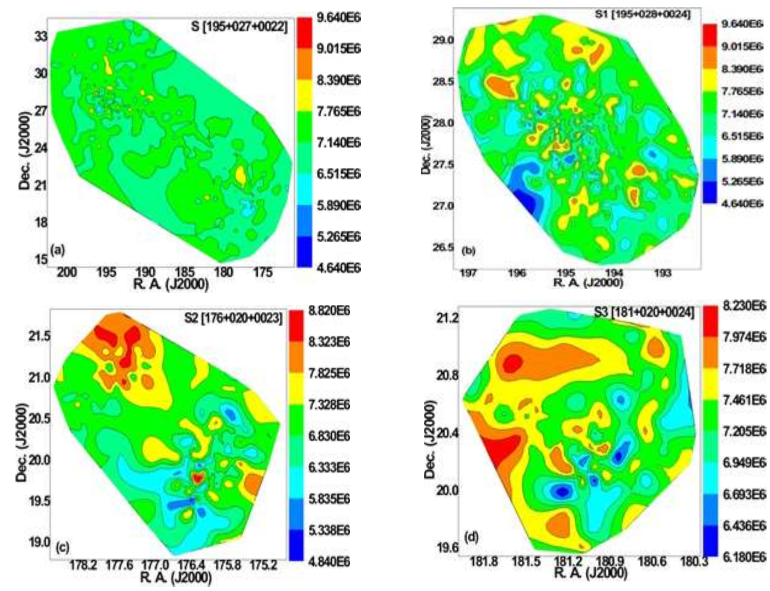

Figure 4: Radial velocity contour maps of galaxies in the supercluster (a) and subclusters (b-d). X-axis and Y-axis represent right ascension and declination respectively and vertical line on right side represent velocity in kilometer per second.

According to Hierarchy model (Peebles, 1969), the radial velocity distribution should not be unipolar. Also from here, we can easily predict that our database is nearer of isotropy because higher number of contour formation with different velocity profile can be observed within all four structures S[195+027+0022], S1 [195+028+0022], S2 [176+020+0023] and S3 [181+020+0024]. Out of these four contour maps S3 [181+020+0024] have higher degree of isotropy.

Acknowledgements

One of the authors (J.R.Malla) wish to express his sincere thanks to the Department of Astro-Particle Physics, Innsbruck University, Austria, for providing data access . One of them (J.R.Malla) also records his gratitude to the authorities of the SDSS for providing the database.

Conclusion

In this paper, studied substructure classification of the 2,590 galaxies surveyed by SDSS (York et al., 2000) in the supercluster S [195+027+0022].These data (7th data release) were taken by SDSS Telescope located at Apache Point Observatory, New Mexico, USA and made available to us by collaboration with Institute of Astroparticle Physics, Innsbruck University, Austria (Percival J., Will et al., 2010). From these data, we plotted all sky diagrams and observed the nature of that plot. Using the galaxies density map to identify substructure, three eminent substructures, namely S1 [195+028+0022], S2 [176+020+0023] and S3 [181+020+0024] for radius value 1^{o} three substructures, namely S1[195+028+0022], S2 [176+020+0023]and S3 [181+020+0024]has been found.

Therefore, in both supercluster and in substructure, the distribution of galactic plane is isotropic supporting "Hierarchy model" of galaxies formation.

References

1. Dekel, A., Sari, R., and Cereino,D.(2009). Formation of Massive Galaxies at the high redshift: cold streams, clumpy disks, and compact Spheroids, The Astrophysical Journal, 703, 1,785.
2. Einasto, J., Klypin, A.A., Saar,E.and Shandarin,S.F.(1984). Structure of Superclusters and Supercluster formation-III.Quantative study of the local Supercluster. Monthly Notices of the Royal Astronomical Society, 206, 03,529-588.
3. Harris,W.E.(1986). Globular clusters in galaxies beyond the local group V-The giant elliptical reconsidered. The Astrophysical Journal, 91,822-841.
4. Heidmann,J., Heidmann, N.,& De vaucouleurs,G(1972).Inclination and absorption effects on the apparent diameters, optical luminosities and neutral hydrogen radiation of galaxies-I. Optical and 21-cm line data. Memories of the Royal Astronomical Society, 175, 85-104.
5. Kravtsov, A.V.and Borgani, S. (2012). Formation of galaxy clusters, Annual review of Astronomy and Astrophysics, 50,353-409.
6. Peebles, P. J. E. (1969). Origin of the angular momentum of Galaxies. The Astrophysical Journal, 155, 393-402.
7. Percival J., Will, ReidA. Beth, EisensteinJ. , Daniel, Bahcall A., Neta , Budavari, Tamas , & 23more (2010),Baryon acoustic oscillations in the sloan digital sky survey data release 7 galaxy sample , Monthly Notices of the Royal Astronomical Society, 401(4), 2148–2168.
8. Pontzen,A. & Governato, F. (2014).Cold dark matter heats up. Nature, 506, 171-178.
9. Smith, Q. (1988). The uncaused beginning of the Universe. Philosophy of Science, 55, 1, 39-57.
10. takami, H., Nishimichi, T., Yahata, K. and Sato, K. (2009). Cross-Correlation between UHECR arrival distribution and large-scale structure. Journal of Cosmology and astroparticle physics. 9(06), 31.
11. York, D. G., Adelman, J., Anderson, J. E., Anderson, S.F., Annis,J., Bahcall, N.A., Bakken, J.A., & 137 more. The sloan digital sky survey:Technical summary. The Astronomical Journal, 120, 1579-1587(2000)

C/o Mr. D.K. Singh, Pragati Gas Service
Steelganj Talab, Bahraich, 271-801
janak_malla@yahoo.com

BIBECHANA

ISSN 2091-0762 (Print), 2382-5340 (Online)

Journal homepage: http://nepjol.info/index.php/BIBECHANA

Publisher: Department of Physics, Mahendra Morang A.M. Campus, TU, Biratnagar, Nepal

Spatial orientation of galaxies in supercluster S[227+006+0078]

Janak Ratna Malla[1*], Walter Saurer[2], Binil Aryal[3]**

[1]Amrit Campus, T.U., Kathmandu

[2]Institute of Astro-particle Physics, Innsbruck university, Austria[2]

[3]Central Department of Physics, kirtipur ,Kathmandu

Email: *Janak_malla@yahoo.com, **aryalbinil@gmail.com

Article Information:

Received: August 21, 2019

Accepted: December 07, 2019

Keywords:

SDSS

Supercluser

Redshift

Galaxy

ABSTRACT

We present a study of spin vector orientation of 1218 SDSS (Sloan Digital Sky Survey) galaxies in Supercluster S [227+006+0078] having redshift 0.07 to 0.09. The database of these galaxies is taken from SDSS (Sloan Digital Sky Survey) 7th and 9th data release. We have converted two dimensional data to three dimensional by Godlowskian Transformation using position angle-inclination angle method. We intend to find non-random effects in the spatial orientation of galaxies in the Supercluster. No preferred alignment of angular momentum vectors is noticed, supporting Hierarchy model of galaxy formation.

DOI: https://doi.org/10.3126/bibechana.v17i0.26582

1. Introduction

Modern cosmology is based on two fundamental assumptions: First, the dominant interaction on cosmological scales is gravity, and second, the cosmological principle is a good approximation to the Universe. The cosmological principle states that the universe, smoothed over large enough scales, is essentially homogeneous and isotropic. 'Homogeneity' has the intuitive meaning that at a given time the universe looks the same everywhere, and 'isotropy' refers to the fact that for any observer moving with the local matter the universe looks (locally) the same in all directions. Von Weizsacker and Gamow (1951 & 1952) verified that the observed rotation of the galaxies is important for cosmology: the fact that the galaxies rotate may be clue to the physical conditions under which these systems formed. In the instability picture, one imagines that large irregularity like galaxies grew under the in influence of gravity from small imperfections in the early Universe [1, 2]. In this picture one must abandon the idea that the angular momentum of the galaxies was given as the initial value, or developed in some sort of primeval turbulence (as was proposed by von Weizsaker [3] and Gamow [4] , for otherwise the galaxies would have formed too soon [2]. On the other hand, huge low red shift galaxy surveys such as the 2-degree field galaxy red shift survey and the Sloan Digital Sky Survey (SDSS) [5] have convinced most cosmologists that not only isotropy but also homogeneity is in fact a reasonable assumption for the universe. The Universe is homogeneous and isotropic on scales larger than

100 Mpc, but on smaller scales we observe huge deviations from the mean density in the form of galaxies, galaxy clusters, and the cosmic web being made of sheets and filaments of galaxies. How do structures grow in the universe and how can we describe them? The most accepted view on the formation and evolution of large scale structure is that it was formed as a consequence of the growth of primordial fluctuations by gravitational instability [6]. In the current favored model, smaller structures collapse first and are later incorporated in larger collapsing structures in a bottom-up scenario that provides a natural explanation for the formation of galaxies, clusters, filaments and Superclusters [7] .

There are three predictions about the spatial orientation of spin vectors of galaxies. These are the `*pancake model*', the `*hierarchy model*,' and the `*primordial vorticity theory*.' The `pancake *model*' [8, 9] predicts that the angular momentum vectors of galaxies tend to lie within the cluster plane. According to the `hierarchy model' [2], the directions of the angular momentum vectors should be distributed randomly. The `Primordial Vorticity Theory' [10,11] predicts that the spin vectors of galaxies are distributed primarily perpendicular to the cluster plane.

In this paper, we analyze spatial orientation of angular momentum vectors of 1218 galaxies in the SDSS supercluster S [227+006+0078]. The methods and results are described in the following chapters.

Godlowskian Transformation

The three dimensional orientation of the angular momentum vectors of a galaxy is characterized by two angles: the polar angle (θ) between the galactic SV and a reference plane (here equatorial plane), and the azimuthal angle (ϕ) between the projection of a galactic SV on to this reference plane and the X-axis within this plane. The detail derivations of the expressions of the angles θ and ϕ are given in Flin & Godłowski [12] . When using equatorial coordinate system as reference, then θ and ϕ can be obtained from measurable quantities as follows:

$$\sin\theta = -\cos i \sin\alpha \pm \sin i \sin p \cos\delta \qquad (1)$$

$$\sin\phi = (\cos\theta)^{-1}\left[-\cos i \cos\delta \sin\alpha + \sin i\left(\mp \sin p \sin\delta \sin\alpha \mp \cos p \cos\alpha\right)\right] \qquad (2)$$

where , i is the inclination angle, the angle between the normal to the galaxy plane and the observer's line-of-sight, α- is right ascension, δ is declination and p is position angle. The inclination angle can be computed from the formula

$$\cos^2 i = \frac{(q^2 - q^{*2})}{(1 - q^{*2})} \qquad (3)$$

This expression is valid for oblate spheroids [13]. Here, q and q^* represent the measured axial ratio (*b/a)* and the intrinsic flatness of the galaxy, respectively. Hiedmann *et al*.[14] showed that the values of q^* range from 0.083 for Sd spirals to 0.33 for ellipticals. For the galaxies with unknown morphology q^*= 0.20 is assumed Holmberg [13].

2. Method of analysis

Here we describe the procedure for the removal the selection effects to obtain the isotropic distributions for both θ and ϕ as given by Aryal & Saurer [15]. Theoretically, the isotropic distribution curve for polar angle is cosine and that for azimuthal angle is the average distribution curve, with the restriction that the database is free from selection effect. Aryal & Saurer [15] concluded that any selections imposed on the database may cause severe changes in the shapes of the expected isotropic distribution curves. In their method, a true spatial distribution of the galaxy rotation axis is assumed to be isotropic. Then, due to the projection effects, i can be distributed as sin i, B can be distributed cos$B$, the variables α and p can be distributed randomly, and the equation (1,2) can be used to calculate the corresponding values of polar (θ) and azimuthal (ϕ). We run simulations in order to define expected isotropic distribution curves for both the θ and ϕ distributions. The isotropic distribution curves are based on simulations including 10^7 virtual galaxies. At first we observed the distributions of α, δ, p and i for the galaxies in our samples and distributed by creating 10^7 virtual galaxies for respective parameters. We use these numbers to make input file and the expected distribution by running simulation in MATLAB 15.0.

Our observations (real observed data set) are compared with the isotropic distribution curves (obtained from simulation) in both θ and ϕ distributions. For this comparison we use four different statistical tests: chi-square probability, First order Fourier Coefficient ($\Delta_{11}/\sigma(\Delta_{11})$), Fourier Probability ($P > \Delta_1$) and auto correlation-test ($C/C(\sigma)$).

3. Results and Discussion

Figure 1(a) shows all sky distribution of galaxies in the Superclusters S [227+006+0078] several groups of galaxies can be seen. These groups can form a substructure, ultimately a cluster of galaxies. Figure 1(b) shows redshift distribution of galaxy in this supercluster where we can see low redshifted galaxies in the substructure region. High redshifted galaxies are found to be distributed randomly.

Any deviation from expected isotropic distribution will be tested using four statistical parameters, namely chi-square probability ($P>\chi^2$), autocorrelation coefficient ($C/C(\sigma)$), first order Fourier coefficient ($\Delta_{11}/\sigma(\Delta_{11})$) and first order Fourier probability ($P > \Delta_1$). For anisotropy, the limit of chi-square probability $P(>\chi^2)$ is <0.050, auto correlation coefficient ($C/C(\sigma)$) is >1.0, first order Fourier coefficient ($\Delta_{11}/\sigma(\Delta_{11})$) is >1.5 and Fourier probability $P(>\Delta_1)$ is <0.150 respectively. Any `hump' (more solutions than the expected) or `dip' (less solutions than the expected) in the histogram will be discussed as a local effect in the samples. The statistics for the polar and azimuthal angle distributions is given in Table 1 . In the statistics of θ, a negative value of first order Fourier coefficient suggests that the spin vectors of galaxies tend to be oriented perpendicular with respect to the equatorial coordinate system. Similarly, a positive value of first order Fourier coefficient suggests that the spin vectors of galaxies tend to be oriented parallel with respect to the

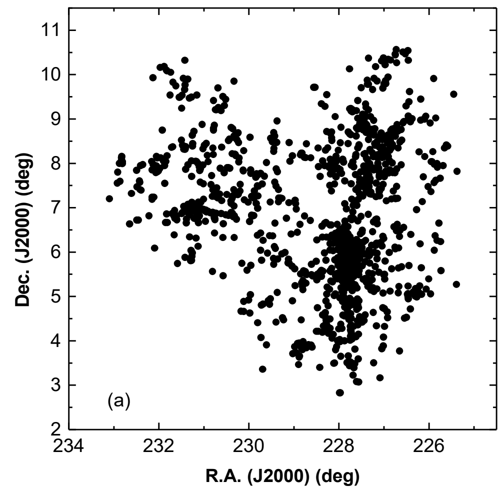

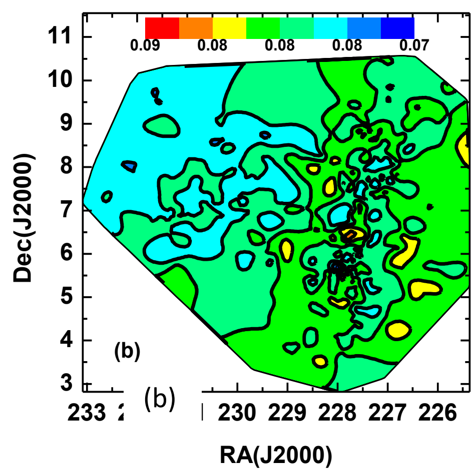

Fig. 1 : (a) All Sky distribution of galaxies and (b) red shift distribution map.

equatorial coordinate system. Whereas, in the statistics of ϕ, a positive ($\Delta_{11}/\sigma(\Delta_{11})$) with significant value suggests that the spin vector projections of galaxies tend to point radially with respect to the center of the equatorial coordinate system. Similarly, a significant negative value of ($\Delta_{11}/\sigma(\Delta_{11})$) implies that the spin vector projection of galaxies tend to orient tangentially with respect to the equatorial coordinate system.

In addition to the statistical tests, we also study the `humps' and `dips' in the polar and azimuthal angle distributions. The solid curve, in the histogram of the θ-distribution, represents the expected isotropic distribution whereas dashed curve is the cosine distribution. The solid circles with ±1σ error bars represent the observed distribution. The shaded portion represents the range 0°<θ<45°. A hump (or dip) in the smaller θ ($\theta< 45^0$) suggests that the spin vectors of galaxies tend to orient parallel (or perpendicular) with respect to the equatorial coordinate system. Similarly, a hump (or dip) in the larger θ (θ >45°) suggests that the spin vectors of galaxies tend to orient perpendicular with respect to the equatorial coordinate system. In figure 2, there is a hump on polar angle distribution at θ = 46.This hump is due to 13 more expected solution than observed solutions in the range $\theta > 45°$.

Similarly, a hump (or dip) in the larger ϕ indicates that the spin vectors of galaxies tend to be oriented perpendicular with respect to the equatorial coordinate system .In the histogram of the ϕ-distribution, solid curve represents the expected isotropic distribution whereas dashed curve is the average distribution. The solid circles with ±±1σ error bars represent the observed distribution. The shaded portion represents the range --45°<ϕ<+45°. The humps and dips in the histograms of ϕ-distribution are not so easy to interpret as compared to ϕ-distributions. It is because the range of ϕ is -90° to +90°. In the histogram of the ϕ-distribution, ϕ = 0° means spin vector projections tend to point radially towards the center of the equatorial coordinate system. A hump in the middle (central eight bins) of the histogram suggests that the spin vector projections of galaxies tend to point towards the center of the chosen co-ordinate system. Similarly, a hump at first four and last four bins indicates that the spin vectors projections of galaxies tend to be oriented tangentially with respect to the chosen reference co-ordinate system. A hump in the middle (central eight bins) of the plot suggests that the spin vector projections of galaxies tend to point towards the center of the chosen co-ordinate system.

Table 1: Statistics of the polar and azimuthal angle distributions of galaxies in the Supercluster S(227+006+0078). The first column represents the statistics used, P(>χ^2) represents the chi-square probability (second row). Similarly, C/C(σ) represents the auto-correlation coefficient(third row). The last two rows give the first order Fourier coefficient (Δ_{11}/σ(Δ_{11}) and first order Fourier probability P(>Δ_1).

Statistics	Polar angle(θ)	Azimuthal angle (ϕ)
P(>χ^2)	0.045	0.000
C/C(σ)	0.688	5.681
$\Delta_{11}/\sigma(\Delta_{11})$	0.823	-1.894
P(>Δ_1)	0	0.000

The statistics for the θ-distribution of galaxies of Supercluster S [227+006+0078] is shown in the Table 1. The statistics for the polar angle distribution in this sample shows that the value of chi-square probability (P(>χ^2) to be 0.045 (Smaller than the significant level 0.050 i.e., 5.0%). The auto-correlation coefficient (C/C(σ))is found to be 0.688 (Smaller than 1σ limit). The first order Fourier coefficient (Δ_{11}/σ(Δ_{11})) is found to be 0.0823 (smaller than 1.5σ the limit). The first order Fourier probability (P>(Δ_1)) is found to be 0 (Smaller than 0.15 i.e.,15%). Except first order Fourier coefficient and chi-square probability, other statistical tests suggest anisotropy. Isotropy in the first order Fourier coefficient test suggests that the direction of departure from isotropy.

The statistics of the φ-distribution of galaxies of Supercluster S [227+006+0078] is shown in the Table 1. The statistics for the azimuthal angle distribution in this sample shows that the value of chi-square probability (P(>χ^2)) to be 0.0 i.e., 0(Smaller than the significant level 0.050 i.e., 5.0%). The auto-correlation coefficient (C/C(σ)) is found to be 5.681 (greater than 1σ limit). The first order Fourier coefficient ($\Delta_{11}/\sigma(\Delta_{11})$)is found to be -1.894 (smaller than 1.5σ the limit). The first order Fourier probability (P>(Δ_1)) is found to be 0.0 (Smaller than 0.15 i.e., 15%). Except first order Fourier coefficient, other statistical tests suggest anisotropy. Isotropy in the first order Fourier coefficient test suggests that the direction of departure from isotropy.

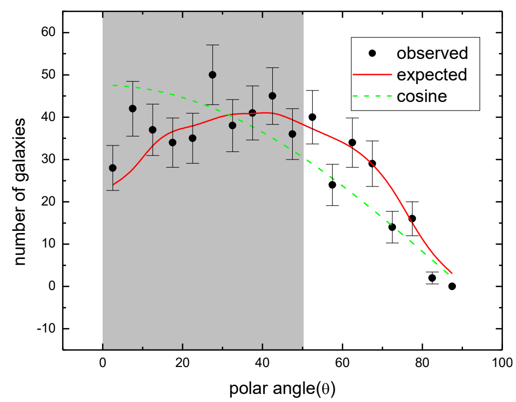

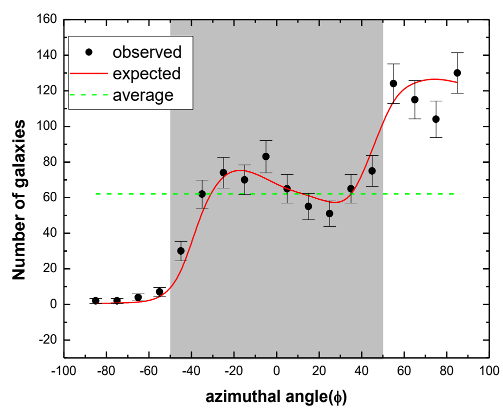

Fig. 2: The polar (θ) and azimuthal (ϕ) angle distributions of galaxies in the Supercluster S[227+006+0078]. The solid line represents the expected isotropic distributions. The dash lines represent the cosine and average distributions respectively. The solid circles with ±1σ error bars are represent the observed distribution.

4. Conclusion

We have studied the preferred alignment of spin vector orientation of 1218 SDSS galaxies of Supercluster S [227+006+0078] that have redshift in the range 0.07 to 0.09. We used the method proposed by Flin & Godlowski [12] in order to compute two-dimensional data to three dimensional galaxy rotation axis (polar & azimuthal angles). We have carried out random simulation by creating 10^7 virtual galaxies and adopting the method proposed by Aryal & Saurer [15] in order to find theoretical distribution of galaxy rotation axes. We have compared the differences between theoretical distributions and observed distributions using three statistics, namely chi-square, auto-correlation and the Fourier. The distribution of spin vector and spin vector projections of total SDSS galaxies that have redshift in the range 0.07 to 0.09 are found to be random in all samples, our results support Hierarchy model [2].

However, a local effect that causes the humps and dips in the angular momentum distribution is observed in different samples. In the deep field, density fluctuation is expected and observed in the local scale. Existence of Superclusters in the region of interest cannot be ruled out. We have used equatorial system as a physical reference in order to study non-random effects concerning galaxy orientation. Hierarchy model predicts that the choice of co-ordinate system do not alter preferred alignments.

References

[1] G. Gamow, E. Teller, On the origin of great Nebulae, Phys. Rev. 55 (1939) 654. https://doi.org/10.1103/phys Rev.88.654.

[2] P. J. E. Peebles, Origin of the angular momentum of Galaxies, The Astrophysical Journal 155(1969)393. http://adsabs.harvard.edu/full/1969ApJ...155..393P

[3] V. Weizsaker, The evolution of Galaxies and stars, The Astrophysical Journal 114 (1951) 165. https://adsabs.harvard.edu/full/1951 Apj..114..165V.

[4] G. Gamow, The role of Turbulence in the Evolution of the Universe, Phys. Rev. 86 (1952) 251. https://doi.org/10.1103/phys Rev.88.251.

[5] D. G. York, J. Adelman, J. E. Anderson, The Sloan Digital Sky Survey: Technical Summary, The Astronomical journal 120 (2000) 1579-1587. https://iopscience.iop.org/article/10.1086/301513.

[6] S. Codis, A. Jindal, N. E. Chisari, D. Vibert, Y. Dubois, C. Pichon, J. devriendt, Galaxy orientation with the cosmic web across cosmic time, Monthly Notices Royal Astron. Soc. Monthly 481 (2018) 4753-4774. https://academic.oup.com/mnras/articleabstract/481/4/4753/5104417redirected

[7] P. Pajowska, W. Godłowski, Z. H. Zhu, J. Popiela, E. Panko, P. Flin, Investigation of the orientation of galaxies in clusters: the importance, methods and results of research, Journal of Cosmology and Astroparticle Physics 02 (2019) 005. https://doi.org/10.1088/1475-7516/2019/02/005

[8] A. G. Doroshkevich, The orientation of rotation of galaxies, Astrophysical Letters 14 (1973) 1113.

[9] A. G. Doroshkevich, S. F. Shandarin, Spatial structure of protoclusters and the formation of Galaxies, Monthly Notices Royal Astron. Soc. 184(1978)643–660. https://doi/10.1093/mnras/184.3.643.

[10] L. M. Ozernoy, M. S. Longair, J. Einasto, Large scale structure of the Universe, IAU Symp. 79 (1978) 409.

[11] R. Stein, Galaxy formation from Primordial Turbulence, Astron. & Astrophys. 35 (1974) 17 - 29. https://adsabs.harvard.edu/full/1974.26 A..35..175.

[12] P. Flin, W. Godlowski, The Orientation of Galaxy Groups and formation of the local Supercluster, Monthly Notices Royal Astron. Soc. 222 (1986) 525. https://doi.org/10.1093/mnras/222.3.525

[13] E. Holmberg, On the apparent diameters and the orientation in space of extragalactic Nebulae, Medd. Lund. Astron. Obs. 117 (1946) 3-82.

[14] J. Heidmann , N. Heidmann , G. de Vaucouleurs, Inclination and absorption effects on the apparent diameters, optical luminosities and neutral hydrogen radiation of galaxies-III. Theory and applications, Memories of the Royal Astron. Soc.75 (1972) 121.

[15] B. Aryal, W. Saurer, Comments on the expected isotropic distribution curves in the galaxy orientation studies, Astronom. Astrophys. lett. 364 (2000)L97-L100. http://articles.adsabs.harvard.edu/pdf/2000A%26A..364L..97A.

BIBECHANA
ISSN 2091-0762 (Print), 2382-5340 (Online)
Journal homepage: http://nepjol.info/index.php/BIBECHANA
Publisher: Department of Physics, Mahendra Morang A.M. Campus, TU, Biratnagar, Nepal

Spatial orientations of angular momentum vectors of galaxies in Supercluster S [173+014+0082]

Janak Ratna Malla[1*], Walter Saurer[2], Binil Aryal[1]
[1]Central Department of Physics, Kirtipur, Kathmandu
[2]Institute of Astro-particle Physics, Innsbruck University, Austria
[*]Email: janak_malla@yahoo.com

Article Information:
Received: May 28, 2020
Accepted: June 16, 2020

Keywords:
SDSS
Supercluser
Galaxy
Redshift
Intrinsic flatness

ABSTRACT

The spin vector orientation of 1302 SDSS (Sloan Digital Sky Survey) galaxies in Supercluster S[173+014+0082] having redshift 0.076 to 0.091 has been analysed. The positions, position angles and inclination angles of galaxies are used to convert two-dimensional observed parameters into three-dimensional angular momentum vectors of the galaxy using the `position angle-inclination' method. The expected isotropic distribution curves are determined performing numerical simulation by generating 107 virtual galaxies. The observed distribution is compared with the expected isotropic distribution curves using three statistical tools namely Chi-square test, auto-correlation test and Fourier test. Redshift map is studied and found that the distributions fit with the Gaussian. No preferred alignment of angular momentum vectors is noticed, supporting Hierarchy model of galaxy formation.

DOI: https://doi.org/10.3126/bibechana.v18i1.29165

1. Introduction

During the path of history different ideas had been recommended describing the starting place of the universe. The most persuasive model is the standard Big Bang model, which remains valid. This model shows the creation technique of the universe began with an enlargement 20 billion years ago. Nowadays, the big Bang model is believed to be the beginning of space and time. The tiny, hot (10^{12}K) universe started out to cool and fundamental symmetry damaged down. The breaking of this symmetry results in the inflation of the universe exponentially. Within a fraction of second, after the Big Bang, the procedure of Nucleosynthesis, baryongenesis & leptogenesis took place. After this procedure the universe entered into the matter dominated era. During dark epoch, the stars and galaxies are assumed to be formed. Today, how matter is distributed in the universe is the crucial field of study in cosmology and astronomy.

The mutual attraction between the galaxies due to the gravitational force leads to the formation of clusters. Depending upon the number of galaxies inside the cluster, they're labeled as poor and rich clusters. In case of poor clusters the force of gravity is weak to keep them tightly due to lower mass of the galaxy. Thus they seem irregular in shape. Our Milky Way is part of a poor cluster referred to as a local group which includes 54 galaxies [1]. The Virgo cluster is an example of a moderately rich cluster that is closest to us and the coma cluster is a rich cluster, has thousands of spiral and elliptical galaxies. The clustering technique of galaxy clusters lead to the formation of large scale structures known as superclusters. Thus they're collections of galaxy clusters, with 20-100h^{-1}Mpc [2]. The scientist assumed that the variety of superclusters in the universe is set 10 million and it occupies the 10% area of the universe. As it contains organizations and clusters of galaxies, it provides the strong proof that galaxies inside the universe are not distributed uniformly. Abell catalogue is the pioneer work in the study of superclusters. It was proposed by George Abell in 1958 and he called them second order cluster or clusters of clusters [3]. The study of superclusters highly benefited from the 2dF Galaxy Redshift Survey (2dFGRS) and the Sloan Digital Sky Survey (SDSS) [4]. Currently Sloan Digital Sky Survey (SDSS) is taking data from the deep sky. Our work is based totally on the data provided by SDSS-DR7.

As suggested by Weizscker & Gamow [5, 6], the observe of origin of angular momentum of galaxies might be the clue for the physical properties of the initial situations of galaxies. Thus, the observed rotation of galaxy is critical to the cosmology and subsequently it is essential to recognize how they obtained their angular momentum. Pebbles [7] put forward detail calculations of the acquisition of angular momentum in early stage of proto-galactic evolution. He argued that, the gravitational interplay of quadrapole moment of the system with tidal field of the matter causes transformation of angular momentum to the developing proto-galaxy. The transformation of angular momentum between rotation and orbital motion is a outcome of the gravitational instability [8]. Peebles assumed that, as soon as the primeval plasma has recombined and decoupled from the primeval fireball radiation, gravitation appears to be the dominant force transferring the angular momentum to a developing proto-galaxy.

On the basis of orientation of angular momentum vectors of galaxies one can determine the evolution of large scale structure, i.e., Supercluster. The alignment of rotational axes of galaxies in the Supercluster provides us information about the formation process of galaxies in early epoch [9]. There had been contradictory theoretical models predicting various galaxy cluster formation. The Hierarchy model [7] predicts random orientation of angular momentum vectors. The Pancake model [10] predicts the parallel orientation whereas the primordial vorticity model [11] says angular momentum vector distributed perpendicular to the cluster plane. We are interested to study the evolution of galaxies in the Supercluster by analyzing their preferred alignments.

2. Materials and Method

Database

The analyzed data set has been recorded by Sloan Digital Sky Survey (SDSS). With the collaboration of Prof. Walter Saurer's group at the Institute of Astro-particle Physics, Innsbruck University, Austria, we obtained the set of SDSS (7th Data release) data. This Supercluster S [173 + 014 + 0082] contains a total number of 1302 galaxies having redshift ranges from 0.076 to 0.091. In this work, r-filter is used to study the spin vector orientation of the galaxies. In order to calculate inclination angle first of all we used intrinsic flatness (q*) = 0.2 (Holmberg, [12]) and, then 0.13 for those galaxies whose inclination angle was undetermined from the previous value of q*. In this process nine galaxies were excluded whose intrinsic flatness is less than 0.13. Hence, finally there are 1293 galaxies in the data set whose position (right ascension and declination), position angle and inclination are known.

Godlowskian transformation

The two dimensional parameters such as position, position angle and diameter can be transformed into 3 dimensional parameters using the method proposed by Flin and Godlowski [13] and polar (θ) and azimuthal (ϕ) angle can be calculated for each galaxy. The polar angle (θ) is the angle between galactic spin vector (SV) and reference plane, and azimuthal angle (ϕ) is the angle between projection of a galactic spin vector to the reference plane and X-axis. These angles are given below.

$$\sin\theta = -\cos i \sin\alpha \pm \sin i \sin p \cos\delta \quad (1)$$

$$\sin\phi = (\cos\theta)^{-1}[-\cos i \cos\delta \sin\alpha + \sin i(\mp\sin p \sin\delta \sin\alpha \mp \cos p \cos\alpha)] \quad (2)$$

Here, i, δ, α, and ρ represent the inclination angle, declination, right ascension and position angles respectively and $\mp$ and $\pm$ indicate the two possible solution.

The inclination angle (i) defined the angle between normal to the galaxy plane and line of sight of the observer. This is given by following relation:

$$cos^2 i = \frac{\left(\frac{b}{a}\right)^2 - q^{*2}}{1-q^{*2}} \quad (3)$$

Here b/a is axial ratio and q^*represents the intrinsic flatness factor of the galaxy. For the disk galaxies its value depends upon the morphological type. Holmberg [12] showed that the values of q^*varies from 0.083 for Sd spirals to 0.3 for elliptical. At first, $q^*= 0.20$ for morphologically unidentified galaxies which leads to the removal of a certain number of galaxies that have axial ratio (b/a) is less than 0.20. Then, we used $q^*= 0.13$ for those galaxies that have b/a < 0.20.

Method of analysis

Aryal & Saurer [14], proposed a method for the removal the selection effects and the expected isotropic distribution curves (θ and ϕ) are determined using the numerical simulation. For this, a true spatial distribution of the galaxy rotation axis is assumed to be isotropic. Then, due to the projection effects, i can be distributed $\propto \sin i$, latitude can be distributed $\propto \cos B$, the variables longitude (α) and position angle (p) can be distributed randomly and formulae (1) and (2) can be used to simulate (numerically) the corresponding distribution of θ and ϕ. At first, the isotropic distribution curves are based on simulations including 10^7 virtual galaxies Aryal & Saurer [14]. We use these numbers to make an input file and the predicted distribution by using a running simulation in MATLAB 15.0.

Finally, the observed and expected distributions are compared with the help of appropriate statistical tests. In order to use ORIGIN 5.0 to determine the all sky distribution of galaxies where as ORIGIN 8.0 used for the redshift distribution of galaxy.

3. Results and Discussion

All sky distribution is the pictorial representation of distribution of galaxies within a certain range of right ascension and declination in the sky. The all sky distribution plot for our Supercluster S [173++014+0082] is shown in Fig. 1. The diagram shows that galaxies are distributed within the range of right ascension from 170^0 to 181^0 and declination from 6^0 to 18^0.

Figure 1 shows that galaxies are distributed inhomogenously. To study the preferred alignment of each galaxy, we plotted the various parameters of galaxies. For each parameter the proper bin size is calculated using ORIGIN 5.0. These plots are presented in following Fig. 2. From these histogram plots of galaxies it is seen that the distribution of observed numbers of galaxies are clearly inhomogeneous.

Figure 3 shows redshift distribution of the galaxy in the supercluster S [173 + 014 + 0082] [15]. In the map, low redshift galaxies are found in the substructure region. High redshifted galaxies are found to be distributed randomly [16]. The color map shows that the velocity dispersion is minimum in the region where the number density of the galaxy is minimum. In the substructure region, at 8^0 declination, the redshift dispersion is found to be $\Delta z = 0.084$, whereas the lower substructure shows $\Delta z = 0.076$ and 0.080, respectively. It seems that there is Gaussian distribution between redshift dispersion and number density of galaxies in the substructures. It shows that the Superclusters evolve naturally.

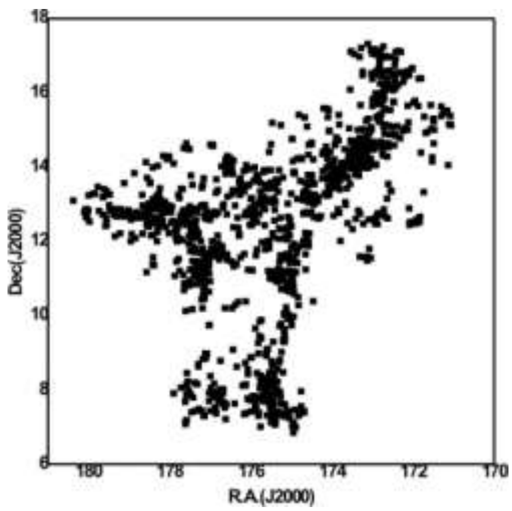

Fig. 1: All sky distribution of galaxies in the SDSS Supercluster S[173 + 014 + 0082] in equatorial coordinate system. Right ascension (R.A.) and Declination (Dec.) are given in degree.

In order to identify the preferred alignment of the spin vector of galaxies we have performed three different statistical tests [17]. For anisotropy, the limit of chi-square probability P ($> \chi^2$) is < 0.050, auto correlation coefficient (C/C (σ)) is > 1.0, first order Fourier coefficient ($\Delta_{11}/\sigma(\Delta_{11})$) is >1.5 and Fourier probability P($>\Delta_{11}$) is < 0.150 respectively.

For θ distribution (Table 1), the result of these tests is found as: the chi square probability P ($> \chi^2$) is 0.653 which is greater than critical value (0.05) for anisotropy. In addition to this, the auto-correlation coefficient C/C (σ)) is 0.410 which is less than critical value; this result is in favor of isotropic distribution. Similarly, the first order Fourier coefficient ($\Delta_{11}/\sigma(\Delta_{11})$) and Fourier probability (P $>\Delta_1$) found to be 0.860 and 0.643 respectively. These two results also support the isotropic distribution of θ. Hence, all three statistical tests show isotropic distribution of Supercluster S[173 + 014 + 0082] indicating random orientation of spin vectors of galaxies. From this result we can conclude that the galaxy formation model of Supercluster S [173 + 014 + 0082] follows the Hierarchy model. According to this model galaxies are believed to be formed from the clustering.

Fig. 4(a) shows the polar (θ) distribution of galaxies of the Supercluster S[173 + 014 + 0082]. In the figure, solid and dotted curves represent expected isotropic and cosine distribution. In the small angle ($\theta < 45^0$) angle region i.e. shaded region no significant hump and dip are observed. While, in a larger angle ($\theta > 45^0$) a significant dip is observed at an angle 75^0 with 1σ error limit. In the shaded region the observed number of solutions is 1674 and expected number of solutions is 1652. Thus the observed number of solutions exceeds the expected solution by 22. This means that there are 11 more galaxies observed. On the other hand, in a larger angle region the observed solution is less than expected solution by 24. This causes deficiency of 12 galaxies in that region. Furthermore, at the bimodal region one extra galaxy is observed. Thus these humps at small angle regions are totally nullified by the dip at the larger angle. The excess number of galaxies in the smaller angle can be regarded as transfer of the galaxies from the larger angle region. This may happen due to the gravitational tidal effect.

In ϕ distribution, the statistics (Table 1) support the isotropic distribution. The chi square probability (P $> \chi^2$) and auto-correlation coefficient (C/C(σ) found to be 0.610 (greater than 0.05) and -0.481 (less than 1σ). Similarly, the value of first order Fourier coefficient (Δ_{11}/σ (Δ_{11})) and first order Fourier probability (P > Δ_1) is -0.358 (less than 1.5σ) and 0.883 (greater than 0.15). These results are strong evidence to advocate the Hierarchy model of galaxy evolution in the Supercluster S[173 + 014 + 0082].

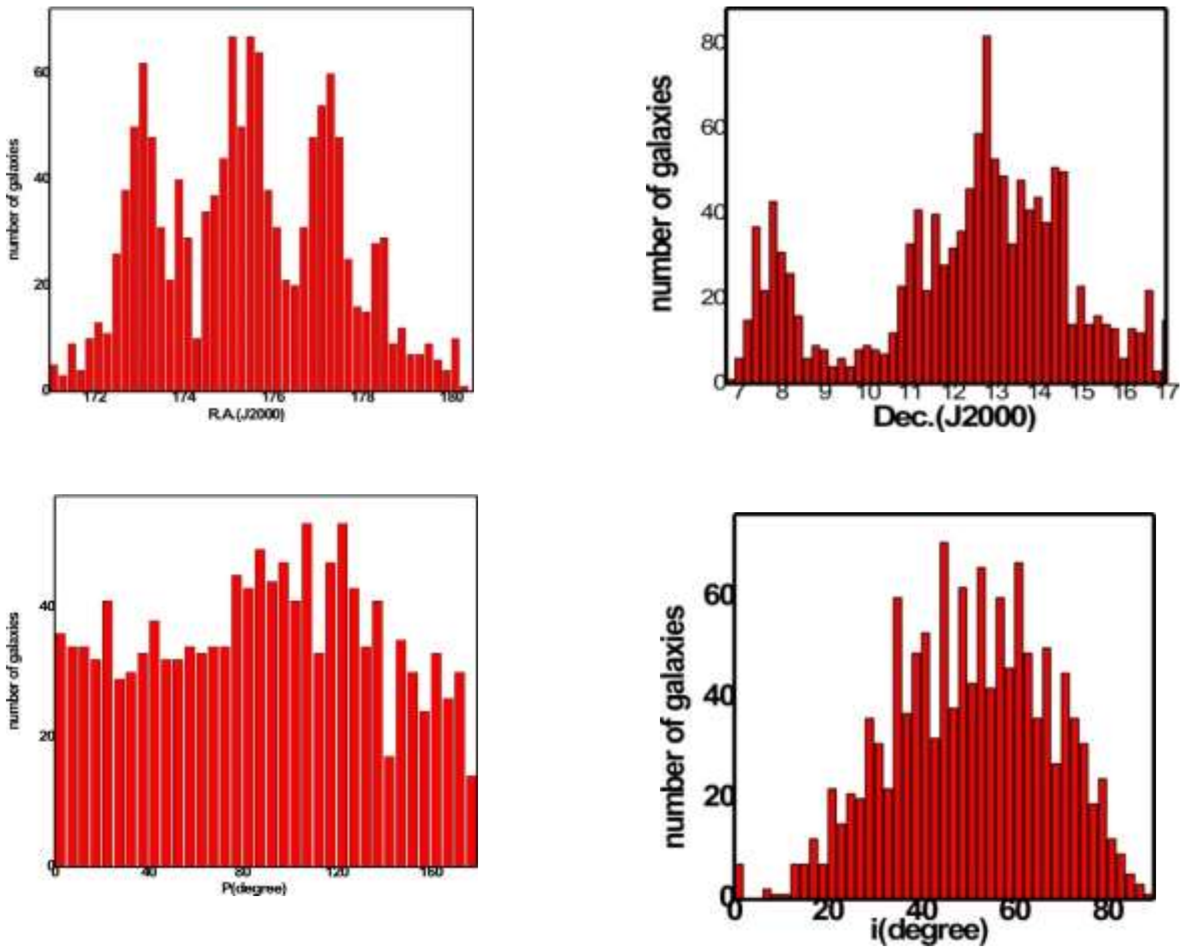

Fig. 2: The distribution of right ascension (α), declination (δ), position angle (P) and inclination angle (i) of galaxies in the Supercluster S [173 + 014 + 0082]. The Y-axis represents the number of observed galaxies. The inhomogeneous distribution of galaxies can be seen.

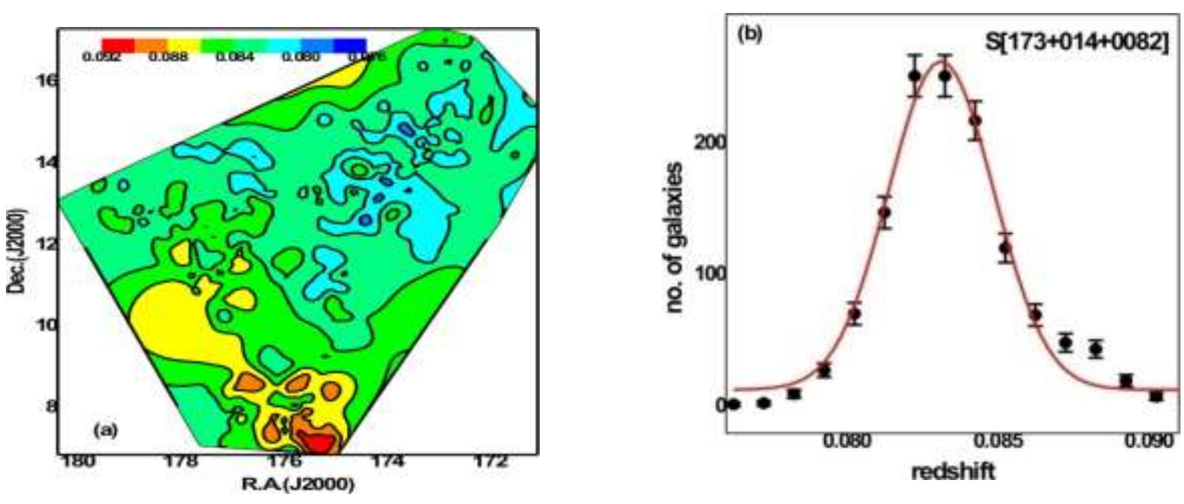

Fig. 3: (a) red shift map and (b) the distribution of galaxies in the Supercluster region. Solid curves represent Gaussian fit. The statistical error bars are shown.

Fig. 4(b) represents the distribution of azimuthal angle of Supercluster S[173 + 014 + 0082]. The solid and dotted line indicate the expected and average distribution. The observed number of solutions in the small angle region ($-90^0 < \phi < -45^0$) is 19 more than expected solution; however, no significant humps are observed in the distribution curve. Similar result is obtained at a larger angle region ($45^0 < \phi < 90^0$) also. The shaded region represents the bimodal region ($-45^0 < \phi < 45^0$). In this region the expected and observed numbers of solutions are 1405 and 1396 respectively. From the figure, two crystal clear humps are observed at -5^0 and $5^0$and dip is observed at -15^0within error limit 1σ.

Table 1: Statistics of the polar and azimuthal angle distributions of galaxies in the Supercluster S[173+014+0082]. The first column represents the statistics used, P ($> \chi^2$) represents the chi-square probability (second row). Similarly, C/C(σ) represents the auto-correlation coefficient(third row). The last two rows give the first order Fourier coefficient (Δ_{11}/σ (Δ_{11})) and first order Fourier probability P (>Δ_1).

Statistics	Polar angle (θ)	Azimuthal angle (ϕ)
P ($> \chi^2$)	0.653	0.610
C/C(σ)	0.410	-0.481
(Δ_{11}/σ (Δ_{11}))	0.860	-0.358
P (>Δ_1).	0.643	0.883

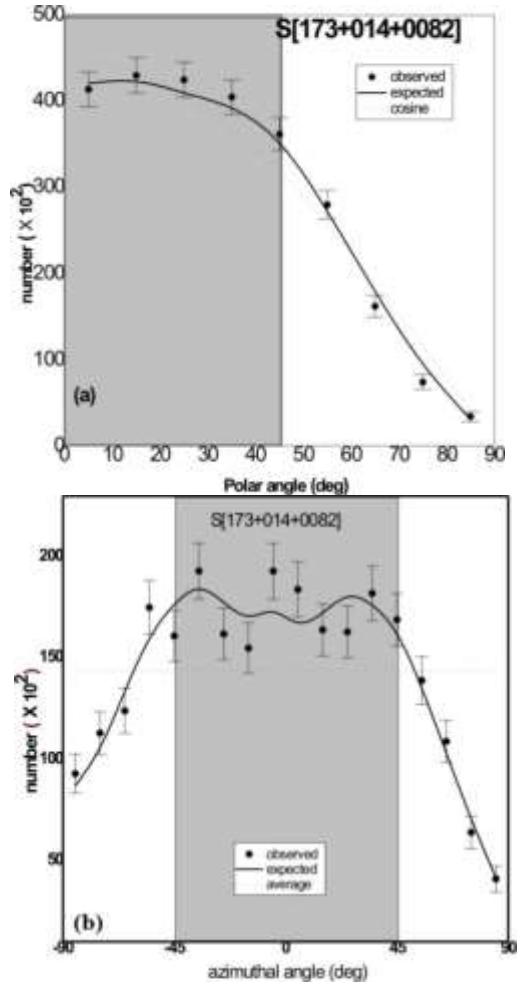

Fig. 4: (a) The polar (θ) and (b) azimuthal (φ) angle distributions of galaxies in the Supercluster S[173+014+0082]. The solid line represents the expected isotropic distributions. The dash lines represent the cosine and average distributions respectively. The solid circles with ±1□ error bars are represent the observed distribution.

4. Conclusions

The Supercluster S[173+014+0082] consists of 1302galaxies of which position angles, right ascension, declination, and axial ratio are known. These are obtained from two dimensional projections on the celestial sphere by SDSS DR 12 Survey. The conversion of two dimensional observed parameters into three dimensional is carried out by using `position angle-inclination' method. In order to find out the theoretical distribution of galaxy rotation axes we ran random simulation by generating 10^7 virtual galaxies as proposed by Aryal & Saurer. Here we assumed cosmological principle: distribution of galaxies in the large scale structure is homogeneous and isotropic. The simulated results were compared with the observed distribution using the statistical tools namely chi-square test, auto-correlation test and Fourier test. The distribution of spin vector and spin vector projections of total SDSS galaxies that have redshift in the range 0.076 to 0.091 are found to be random in all samples. We conclude our results as follows:

(a) The polar and azimuthal angles of supercluster galaxies shows isotropic isotropic distribution suggesting no preferred alignment of angular momentum vectors as well as its projection. In other words we observed vanishing angular momentum in the Supercluster. This result advocates the Hierarchy model of galaxy evolution as suggested by Peebles.

(b) The redshift distribution of galaxies in Supercluster showed Gaussian-like nature, suggesting the distribution of galaxies' Hubble recessional velocity is isotropic, satisfying cosmological principle.

Acknowledgements

One of the authors (J.R.Malla) is thankful to the Department of Astro-Particle Physics, Innsbruck University, Austria, for providing data access . One of them (J.R.Malla) is grateful to the authorities of the SDSS for providing the database.

References

[1] S. Colids, Jindal A Jindal., N. E. chisari, D. Vibert, Y. Dubois, C. Pichon, J. Devriendt. Galaxy Orientation with the cosmic web across cosmic time, Monthly Notice of the Royal Astronomical Society 481(2018) 4753-4774. https://doi.org/10.1093/mnras/sty2567.

[2] L. J. Liivamagi, E.Tempel and E.Saar, SDSS DR7 superclusters, Astronomy and Astrophysics 539 (2012) 1-14. https://doi.org/10.1051/0004-6361/201016288

[3] G. Abell, The distribution of rich clusters of galaxies, Astrophysical Journal Supplement 3 (1958) 211.

[4] D. G York, J. Adelman, J. E Anderson, Scott F. Anderson, James Annis, Neta A. Bahcallet.al. The sloan digital sky survey: Technical Summary. The Astronomical journal 120 (2000) 1579-1587.

[5] C. F. Weizscker, The new picture of the universe, Astrophysical Journal 114 (1951) 165.

[6] G. Gamow, The role of turbulence in the evolution of the Universe, Phys. Rev. 86 (1952) 251. https://doi.org/10.1103/phys Rev.88.251.

[7] P. J. E. Peebles, Origin of the angular momentum of Galaxies, The Astrophysical J.155 (1969) 393.

[8] B. Aryal, S.N. Yadav & W. Saurer , Spatial orientation of galaxies in the Zone of Avoidance. Bulletin of the Astronomical Society of India 40 (2012) 65.

[9] S. Djorgovski, Nearly normal galaxies, edited by S. M .Faber, Springer (1987)

[10] A. G. Doroshkevich, S. F. Shandarin, E. Saar, Spatial structure of protoclusters and the formation of Galaxies, Monthly Notices Royal Astron. Soc. 184 (1978) 643 – 660. https://doi.org/10.1093/mnras/184.3.

[11] L. M .Ozernoy, Sov.Astron, Whirl theory of the Origin and clusters of galaxiex, 15 (1972) 923.

[12] E. Holmberg, On the apparent diameters and the orientation in space of extragalactic Nebulae, Medd. Lund. Astron. Obs. 117 (1946) 3-82.

[13] P. Flin, W. Godlowski, The orientation of galaxy groups and formation of the local Supercluster, Monthly Notices Royal Astron. Soc. 222 (1986) 525.

[14] B. Aryal, W. Saurer, Comments on the expected isotropic distribution curves in the galaxyorientation studies, Astronom. Astrophys. lett. 364 (2000) L97-L100. http://articles.adsabs.harvard.edu/pdf/2000A%26A..364L..97A.

[15] C. M. casey ,D.Narayanan, A.Cooray, Dusty star-forming galaxies at high redshift, Physics Reports Elsevier science Direct. 541 (2014) 45-161.

[16] S. N Yadav, B. Aryal, A study of r-and u-Magnitude Dependence in the spatial Orientation of spin vectors of SDSS Galaxies having redshift 0.10 < z < 0.11. Himalayan Physics 5 (2015) 1-11. https://doi.org/10.3126/hj.v5io.12814.

[17] S. N Yadav, B. Aryal, W. Saurer, Preferred alignments of angular momentum vectors of six galaxies in six dynamically unstable Abell clusters. Research in Astronomy and Astrophysics, 17 (2017) 7. https://doi.org/10.1088/1674–4527/17/7/64

Journal of Institute of Science and Technology, 25(2), 72-79 (2020)
ISSN: 2469-9062 (print), 2467-9240 (e)
Doi: https://doi.org/10.3126/jist.v25i2.33743

Research Article

PREFERRED ALIGNMENTS OF ANGULAR MOMENTUM VECTOR OF GALAXIES IN THE SDSS SUPERCLUSTER S[231+030+0117]

Janak Ratna Malla[1*], **Walter Saurer**[2], **Binil Aryal**[1]

[1]*Central Department of Physics, Tribhuvan University, Kirtipur, Kathmandu, Nepal*
[2]*Institute of Astro-particle Physics, Innsbruck University, Austria*
[*]*Corresponding author: janak_malla@yahoo.com*

*(**Received:** May 27, 2019; **Revised**: October 03, 2020; **Accepted:** October 05, 2020)*

ABSTRACT

The distribution of angular momentum vectors of 1,172 galaxies in the Supercluster S[231+030+0117] with redshift in the range 0.107 to 0.123 was studied. Present work aimed to check any deviation from isotropic distribution in the galaxy orientation study and interpret those deviations with the existing theoretical models that describe galaxy evolution in the Superclusters. For this purpose, two-dimensional observed parameters received from the SDSS telescope was transformed into the three-dimensional. Random simulation technique was applied to remove the selection effects in our database and obtain the expected isotropic curves using numerical simulation. Then the observed and expected distribution curves were compared using the three statistical tests namely: Chi-square, Auto-correlation, and the Fourier test. From statistical analysis, the study confirm that the evolution of galaxies in the Supercluster supports the `Hierarchy model' suggesting the angular momentum vectors of galaxies tends to be oriented randomly to the equatorial coordinate system. Besides, the magnitude of galaxies was found to be independent of angular momentum vectors and its projections in the Supercluster.

Keywords: Evolution, Galaxies, Orientation, Substructure, Supercluster

INTRODUCTION

The Universe is built up by various large scale structures. Stars are collected together into galaxies, galaxies aggregated into galaxy groups, and galaxy groups are gathered together into galaxy clusters. These are held together by gravity. Hence, galaxy clusters are gravitationally bound large scale structures in the universe. To understand the evolution of galaxy and galaxy clusters, it is essential to know when and how they were formed and how their structures and constituents have been changing with time. The galaxy evolution processes are not well understood to date. One reason behind it is that the galaxies are made of three very different entities: stars, an interstellar medium (gas, dust, etc.), and dark matter. We have more information about the star, only a few about the interstellar medium and almost nothing about the dark matter. The orientation of angular momentum vectors of galaxies can reveal its kinematics.

Weizsaker (1951) and Gamow (1952) postulated that the observed rotations of galaxies are important for cosmology. According to them, the fact that galaxies rotate should provide a clue for the physical conditions under which these systems were formed. Thus, the angular momentum vectors of galaxies are important, which help reveal the directional preference of the galaxy. To explain the origin of the angular momentum of galaxies and their evolution, there are mainly three theoretical models namely: `Primordial vorticity model', `Pancake model' and `Hierarchy model'. According to the `Primordial Vorticity Theory' (Ozernoy, 1978; Stein 1974), the spin vectors of galaxies are distributed primarily perpendicular to the cluster plane. The `pancake model' (Doroshkevich, 1973; Doroshkevich & Shandarin, 1978) predicts that the angular momentum vectors of galaxies tend to lie within the cluster plane. The `Hierarchy model' (Peebles, 1969) predicts that the directions of the angular momentum vectors should be distributed randomly. According to this scenario, galaxies were first formed and then their angular momentum was obtained by tidal forces while they were gathering gravitationally to form a cluster with no dissipation.

The redshift of any astronomical object is the displacement of its spectral features to longer wavelengths due to a combination of the gravitational redshift, Doppler motions, and the general expansion of the Universe. Using Hubble's law, the redshift can be used to calculate the distance of an object from the Earth. By combining redshift with an angular position data, a redshift survey maps the 3D distribution of matter within a field of the sky. These observations are used to measure the properties of the large-scale structure of the universe. By systematically and sensitively observing a large fraction of the sky, the Sloan Digital Sky Survey (SDSS) (York *et al.*, 2000) will have a significant impact on astronomical studies as diverse as the large-scale structure of the Universe, the origin and evolution of galaxies, the relation between dark and luminous matter, the structure of Milky Way, and the properties and distribution of the dust from which stars like the sun were created. The SDSS has made enormous contributions across a wide span of astronomical fields, including contributions to many of the discoveries. It has exemplified a new mode of astronomical discovery, with teams of scientists cooperating in organized, systematic surveys to produce large data sets that are made publicly available and support a rich variety of investigations. The SDSS will be a new reference point, a field guide to the Universe that will be used by scientists for decades to come.

An investigation to study the spatial orientation of angular momentum vectors of 1,172 galaxies in the SDSS Supercluster S[231+030+0117], intended to answer following questions: (1) Do the orientation of galaxies in the Supercluster show a directional preference? (b) If yes, which theoretical model supports this preference? (3) Does inhomogeneity in the magnitude (or brightness) of galaxies play any roles in the preferred alignments of the angular momentum of galaxies in the Superclusters? The novelty of this work is to test the cosmological principle (isotropy and inhomogeneity) in the ground of galaxy evolution in large scale structure.

MATERIALS AND METHODS

Data compilation

In this paper, a Supercluster S[231+030+0117] was chosen with all photometric data obtained from Sloan Digital Sky Survey (SDSS) data release 7 (Percival *et al.*, 2010). The SDSS database was compiled in collaboration with the Institute of Astrophysics, Innsbruck University, Austria. At first, the values of the intrinsic flatness of galaxies were used to find the values of the inclination angle of galaxies (Heidmann *et al.*, 1972). The inclination angle of 15 galaxies could not be determined due to their unknown morphology. Finally, we have 1,172 galaxies in this Supercluster S[231+030+0117] of which the positions (right ascension and declination), position angle, and inclinations were known.

Godlowskian transformation

Transformation to the Supergalactic co-ordinate systems is essential to calculate angular momentum vectors using position angle (PA hereafter) and inclination angle of a galaxy to a given coordinate system. Based on the PA to the equatorial system (P), the PA concerning the Supergalactic co-ordinate system (p) can be calculated, which was first observed by Jaaniste and Saar (1978) and explained by Flin and Godlowski (1986). The `Godlowskian transformation' is the method to obtain three-dimensional information of the angular momentum vectors of galaxies. The method was epitomized as follows. At first, position of the galaxy, its magnitude, diameters, and the position angles were compiled using SDSS database. The inclination angle i was calculated by using Holmberg formula (1946).

$$\cos^2 i = \frac{(\frac{b}{a})^2 - q^{*2}}{1 - q^{*2}} \quad (1)$$

Where, b/a is the axial ratio and q^* is a true axial ratio that represents the intrinsic flatness of the galaxy. The intrinsic flatness factor of the disk galaxy depends upon the morphological type. Heidmann *et al.* (1972) suggested a value of $q^*= 0.33$ for elliptical and $q^*= 0.20$ for oblate spheroid.

The spatial (three dimensional) orientation of the angular momentum vector of a galaxy can be expressed by two angles namely, the polar angle (θ), the angle between the normal to the galaxy and the equatorial plane, and azimuthal angle (ϕ), the angle between the projection of this normal on the equatorial plane and directed towards the equatorial center. These angles were given by Flin and Godlowski (1986) in the 'Godlowskian transformation' equations as follows:

$$\sin\theta = -\cos i \sin\alpha \pm \sin i \sin p \cos\delta \quad (2)$$

$$\sin\varphi = (\cos\theta)^{-1}[-\cos i \cos\delta \sin\alpha + \sin i(\mp \sin p \sin\delta \sin\alpha \mp \cos p \cos\alpha)] \quad (3)$$

Where, $\mp$ & $\pm$ signs indicate two possible solutions.

Here, i, δ, α and p represent the inclination angle, declination, right ascension, and position angles respectively.

Considering the ambiguity of the rotation direction of the galactic disk, there is more than one solution of the spatial distribution for a galaxy. All the possibilities were counted independently in the analysis. As a theoretical reference, a spatial isotropic distribution of spin vectors of galaxies was assumed. In the next step, the observations (the distribution of two angles) were compared with these isotropic distribution curves and analyzed by statistical methods to detect any non-random trends.

According to the Hierarchy model, galaxies grow by subsequent merging of proto-galactic condensations or even by merging of already fully formed galaxies. Peeble (1969) assumed that the torque experienced by a young galaxy is the product of its quadrupole moment and the tidal field due to other galaxies.

To find quadrupole moment of a young galaxy, a homogeneous ellipsoid of revolution model was taken into consideration. The quadrupole moment is given by (Peeble, 1969),

$$Q = \int \rho(3z^2 - r^2) d^3r \quad (4)$$

Where, ρ represent volume charge density, z and r position of field point, and position of source point, respectively.

Considering another neighbor galaxy having mass *M*, is at a distance *r* away in a direction *Θ* relative to the z-axis,the magnitude of the torque exerted by the tidal field of this galaxy was given by,

$$\tau = \frac{3}{4}\frac{GMQ}{r^3}\sin 2\theta \tag{5}$$

Now ensemble average value was determined by considering point masses and two-point distribution function. The expression for the mean square torque takes this form,

$$\tau^2 >= (\frac{3}{4}GMQ)^2 \int p(r) d^3r \frac{\sin^2 2\theta}{r^6} \tag{6}$$

Here, *p(r)* is the two-point distribution function which gives the probability that a galaxy is at $r_0 + r$, given that a galaxy is at r_0 is the position of reference point. The radius of the volume belonging to each galaxy was found to be,

$$D \sim (\frac{3M}{4\pi\rho})^{\frac{1}{3}} \tag{7}$$

Therefore, the ensemble average of torque was given by,

$$\tau^2 >^{\frac{1}{2}} (\frac{2\pi}{5})^{\frac{1}{2}} \frac{GMQ}{D^{\frac{3}{2}}} (\frac{\rho}{M})^{\frac{1}{2}} = \frac{1}{3}(\frac{2}{15})^{\frac{1}{2}} \frac{Q}{t^2} \tag{8}$$

Where, $t^2 = \frac{2R^3}{(9GM)}$

A few globular clusters can be disrupted because of tidal interactions between merging fragments. In the hierarchical merger model, the disrupted systems would have led to the present distribution of halo stars throughout the spheroid. It can be expected that there is no net rotation of objects in the halo because of many random mergers. Besides, this model predicts that a few proto-galactic fragments should still be out there. A significant number of small galaxies orbiting the Milky Way and nearby Andromeda are possible examples.

Method of analysis

To remove selection effects from the database and determine expected isotropic distribution curves (Θ and ϕ) we adopted the numerical simulation method as proposed by Aryal and Saurer (2000). For this, a true spatial distribution of the galaxy rotation axis was assumed to be isotropic. Theoretically, the isotropic distribution curve for the polar angle is *cosine* and that for azimuthal angle is the *average*, with the restriction that the database is free from selection effects. Numerical simulation was performed by generating 107 virtual galaxies to find the expected distribution of angular momentum vectors of galaxies (Malla *et al.*, 2020).

Figure 1 shows the observed distribution of positions (right ascension or longitude and declination or latitude), position angle and inclination angle of galaxies in the Supercluster S[231+030+0117]. In each histogram, fluctuations were noticed either throughout the range or at the middle. These fluctuations suggest applying simulation by creating a large number of virtual galaxies in each bin, to satisfy the cosmological principle (isotropy and homogeneity). For this, we adopt the method suggested by Aryal and Saurer (2000) which satisfied the cosmological principles by removing selection effects in the SDSS database (observed fluctuations in Fig. 1). They concluded that any selections imposed on the database may propose severe changes in the shapes of the predicted isotropic distribution curves.

In their method, a true spatial distribution of the galaxy rotation axis was assumed to be isotropic. Because of the projection outcomes, the inclination angle (i) and latitude (B) were distributed as ∝ sini, and ∝ cosB, respectively, and the variables longitude (α) and position angle (p) are distributed randomly (Aryal & Saurer, 2000). Now the equations (2) and (3) can be used to calculate the corresponding values of polar (Θ) and azimuthal (ϕ) angle. Also, we ran simulations to define predicted isotropic distribution curves for each of the Θ and ϕ distributions creating virtual galaxies. The isotropic distribution curves for both polar and azimuthal angles were based totally on simulations including 10^7 virtual galaxies. At first, the distribution α, δ, p, and *i* were found for the galaxies in the samples and distributed with the aid of growing 10^7virtual galaxies for respective parameters. Those numbers were used to make an input file and the predicted distribution by simulating in MATLAB 15.0.

These observations (observed data set) were compared with the isotropic distribution curves (obtained from simulation) in both Θ and ϕ distributions. For this comparison, four different statistical tests were used i.e.: chi-square probability, First-order Fourier coefficient (Δ11/σ (Δ 11)), Fourier probability (P > Δ 1) and autocorrelation test (C/C (σ)). For the all sky distribution of galaxies, the ORIGIN 5.0 was used whereas for the redshift distribution of galaxy (the contour plot of Supercluster was done), in the ORIGIN 8.0.

The number of galaxies was found to increase with right ascension (RA) and declination (Dec.) in the beginning and decrease finally (Fig. 1). The number of galaxies was found to be fluctuating with the position angle (P). Interestingly, the inclination angle (i) distribution seems to show normal distribution in Fig. 1.

RESULTS AND DISCUSSION

The all sky distribution of the total number of galaxies in the Supercluster S[231+030+0117], as shown in Fig. 2(a).

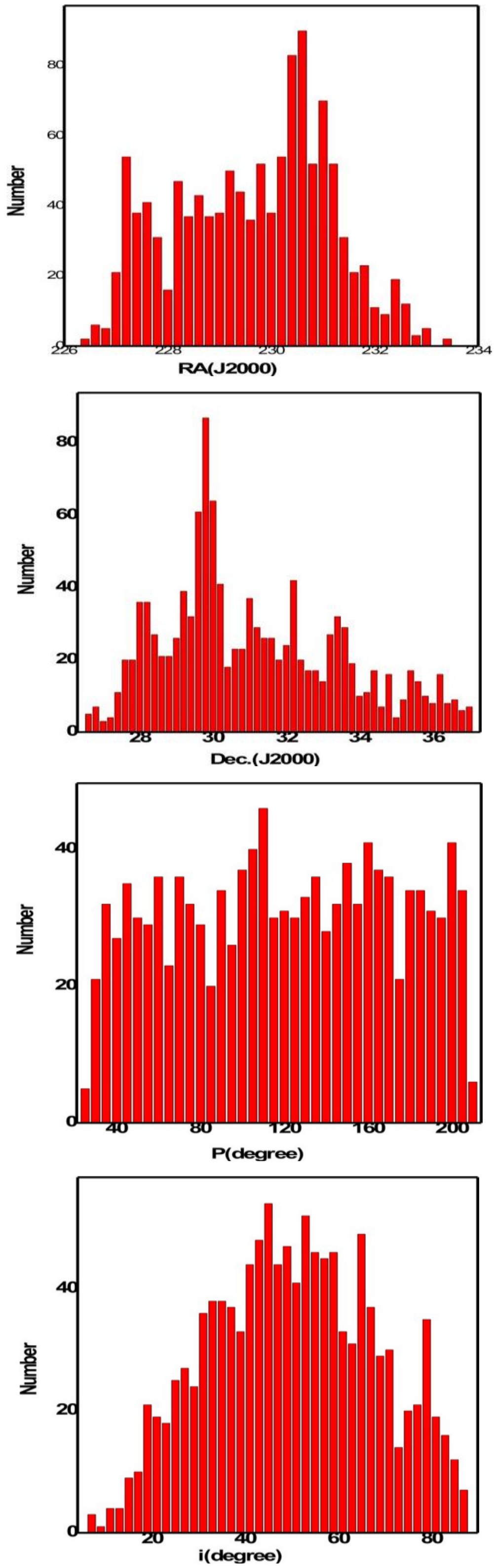

Fig. 1. The observed distributions of right ascension (α), declination (δ), position angle (P), and inclination angle (i) of the galaxies in the Supercluster S[231+030+0117]

The homogeneous distribution of galaxies according to cosmological principles was expected. But the figure shows that the galaxies are not equally distributed throughout the whole region i.e. a heterogeneous distribution. The galaxies are distributed homogeneously within the range of right ascension 226.4° to 233.5° and declination 26.5° to 37°. Morphologically, this Supercluster can be classified as filament type. Figure 2(b) shows the redshift distribution of galaxies in this Supercluster where low red-shifted galaxies in the substructure region can be seen. High red-shifted galaxies were found to be distributed randomly. The mean redshift of Supercluster is 0.114. The contour levels are at the redshift 0.108, 0.112, 0.115, 0.119, 0.123. In the substructure region, galaxies hardly have identical redshifts.

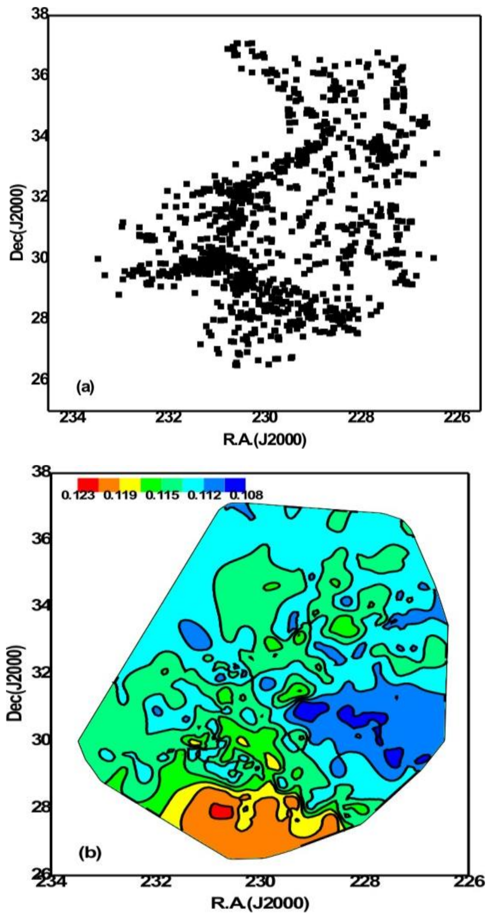

Fig. 2. (a) All sky distribution of galaxies in the supercluster S[231+030+0117] and (b) redshift map of the same region. The levels of the contours are shown

The color map shows that the velocity dispersion is minimum in the region where the number density of the galaxy is minimum, as shown in Fig. 2(b). In the substructure region at 28° declination, the redshift is found to be maximum (Δ z = 0.114).

Figure 3 shows the magnitude map of galaxies in the Supercluster S [231+030+0117]. The SDSS r-magnitude (m_r) refers to the peak wavelength 6165.0 Å with the bandwidth 702.8 Å. This wavelength range covers Hα, ionized Oxygen, and ionized Nitrogen lines as well as respective continuum. In the substructure region, the mean magnitude was identical in both filters. In the u-filter (m_u), the substructure located in the northern region has a higher magnitude. As it is known, the higher the magnitude, the lower is the brightness. Therefore, substructure regions are UV inactive regions, suggesting a lower abundance of newly formed stellar objects.

Gaussian fits in both magnitudes of the Supercluster S [195+027+0022] can be seen in Figs. 3 (c) and (d). The solid curve represents a Gaussian fits. The Gaussian center was found to be at 17.364 for r- and 19.769 for u-magnitudes. Here, in both cases, distribution deviated from standard Gaussian distribution. This indicates that the magnitude distributions of galaxies in the Supercluster might be different from that of the field galaxies.

The main purpose of this study was to find the non-random effects in the galaxy alignments. Any deviation from the expected isotropic distribution will be tested using four statistical parameters, namely chi-square probability ($P > \chi^2$), autocorrelation coefficient ($C/C(\sigma)$), first-order Fourier coefficient ($\Delta_{11}/\sigma(\Delta_{11})$), and first-order Fourier probability ($P > \Delta_1$). For anisotropy, the limit of chi-square probability $P(>\chi^2)$ was <0.050, autocorrelation coefficient ($C/C(\sigma)$) was>1.0, first-order Fourier coefficient ($\Delta_{11}/\sigma(\Delta_{11})$) was>1.5 and Fourier probability $P(>\Delta_1)$ was <0.150 respectively. These statistical limits were proposed by Godlowski (1993, 1994) in galaxy orientation studies.

In the statistics of Θ, if the value of the first-order Fourier coefficient is negative then it suggests that the spin vectors of galaxies tend to be oriented parallel to the equatorial coordinate system. Similarly, if the value of the first-order Fourier coefficient is positive then it suggests that the spin vectors of galaxies tend to be oriented perpendicular to the equatorial coordinate system. Whereas, in the statistics of ϕ, a positive ($\Delta_{11}/\sigma(\Delta_{11})$) with significant value suggests that the spin vector projections of galaxies tend to point radially towards the center of the equatorial coordinate system. Similarly, a significant negative value of ($\Delta_{11}/\sigma(\Delta_{11})$) implies that the spin vector projection of galaxies tends to orient tangentially to the equatorial coordinate system. In addition to the statistical tests, this paper also studies the `humps' (bins with more solutions than the expected) and `dips' (bins with fewer solutions than the expected) in the polar and azimuthal angle distributions.

In the plot of the Θ –distribution, as shown in Fig. 4(a), a dip (or hump) at Θ< 45° suggests that the spin vectors of galaxies tend to orient perpendicular (or parallel) to the

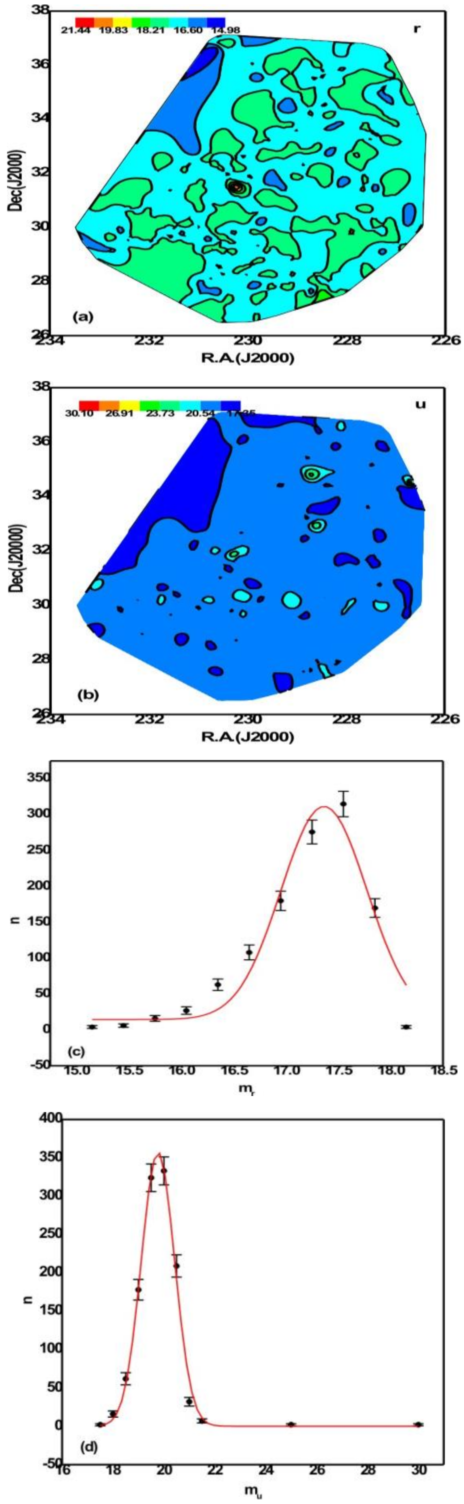

Fig. 3. Magnitude maps of the galaxies in the Supercluster S[231+030+0117]: (a) r-magnitude (m_r), (b) u-magnitude (m_u). The color bars are shown. The contour levels are at 14.98, 16.00, 18.21, 19.83, 21.44 for r magnitude and 17.35, 20.54, 23.73, 26.91, 30.10 for u-magnitude, respectively. (c) r-magnitude (m_r) and u-magnitude (m_u) distributions

equatorial coordinate system. Similarly, a hump (or dip) in the larger Θ (> 45°) indicates that the spin vectors of galaxies tend to be oriented perpendicular to the equatorial coordinate system. In the plot of the ϕ -distribution [Fig. 2(b)], the humps and dips were not easy to interpret as compared to Θ -distributions. It is because the range of ϕ is -90° to +90°. In plot, ϕ = 0° means spin vector projections tend to point radially towards the center of the equatorial coordinate system. A hump in the middle (central eight bins) of the histogram suggests that the spin vector projections of galaxies tend to point towards the center of the chosen coordinate system. Similarly, a hump at the first four and last four bins indicates that the spin vector projections of galaxies tend to be oriented tangentially to the chosen reference coordinate system. The statistics of polar angle (Θ) and azimuthal (ϕ) angle distribution of galaxies in this Supercluster S [231+030+0117] are given in Table 1.

Table 1. Statistical parameters of the polar (Θ) and azimuthal (ϕ) angle distributions of galaxies in the Supercluster S [231+030+0117]

Parameters	Polar angle (θ)	Azimuthal angle (ϕ)
$P(>\chi^2)$	0.884	0.779
C/C(σ)	-0.601	-0.077
$\Delta_{11}/\sigma(\Delta_{11})$	0.012	0.181
$P(>\Delta_1)$	0.999	0.905

The statistics for the polar angle distribution in Supercluster S [231+030+0117] showed that the value of chi-square probability (P $(>\chi^2)$ was 0.884 i.e., 88.4 % (Greater than the significant level 0.050 i.e., 5.0 %). The auto-correlation coefficient (C/C (σ)) was found to be -0.601 (Smaller than 1σlimit). The first order Fourier coefficient (Δ_{11}/σ (Δ_{11})) was 0.012 (less than 1.5σthe limit). The first order Fourier probability (P> (Δ_1)) was 0.999 i.e., 99.4 % (more than 0.15 i.e., 15 %). All the statistical tests suggest very strong isotropy.

The number of observed solutions for Θ< 45° was found to be 1559, whereas the expected solutions was 1554, as shown in Fig. 4(a). Thus, the number of observed solutions or galaxies was greater by 5 than that of the expected. There was one dip at an angle 22.5° and one hump at an angle 32.5° with 1.5σ and 1σ error limit. At the bimodal region i.e., (Θ ~45°), the number of observed and expected solutions was 228 and 240 respectively. This indicates that the number of observed galaxies is less by 12 than that of expected galaxies. For large angles (Θ> 45°), the observed number of solutions (557) exceeded the expected solutions (550) by 7. There was one significant hump at an angle 52.5° with a 1.5 σ error limit. The hump and dip observed in this distribution was due to the local effect. Thus, in the conclusion, no preferred alignment of spin vectors of galaxies is found was polar angle distribution.

The statistics for the azimuthal angle distribution in Supercluster S [231+030+0117] showed the value of chi-square probability (P $(>\chi^2)$) to be 0.779 i.e., 77.9 % i.e., (more than the significant level 0.050 i.e., 5.0 %). The auto-correlation coefficient (C/C (σ)) was found to be -0.077 (Smaller than 1σlimit). The value of first-order Fourier coefficient (Δ_{11}/σ (Δ_{11})) was 0.181 (less than 1.5σ the limit) and the first-order Fourier probability (P> (Δ_1)) was 0.905 i.e., 90.5 % (Greater than 0.15 i.e., 15 %). All these statistical tests suggest that there was a strong isotropy.

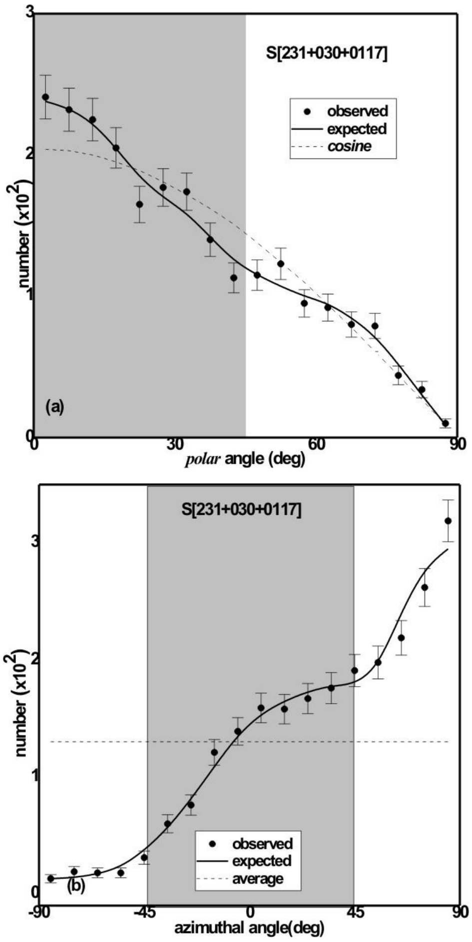

Fig. 4. (a) The polar (Θ) and (b) azimuthal (ϕ) angle distributions of galaxies in the Supercluster S[231+030+0117]

In Fig. 4(b), the observed solutions in eight central bins ϕ ~ (+45°,-45°) was found to be 1056 and that of expected solutions is 1052. This shows that the observed solution exceeds the expected by 4, but no humps and dips were observed in this region. In the bimodal region (ϕ ~ ±45°), the observed solutions (222) was 6 greater than expected (216).

The first four bins (ϕ<-45°), the observed solution (68) exceeded the expected (67) by only 1. Moreover, for the last four bins (ϕ> 45°), the observed and expected solutions were 998 and 1009 respectively. This indicates that the observed solution is less than the expected by 11. One hump was observed at an angle of 85° within 2 σ error limit, which was due to the local effect. Thus, no preferred alignment was noticed in azimuthal angle distribution. Thus, after a careful study of both statistics and graphs of polar and azimuthal angles, it was concluded isotropy in spin-vector orientation of galaxies in the Supercluster and lack of preferred alignment. This supports the hierarchy model of galaxy evolution.

Yadav *et al.* (2017) studied preferred alignments of angular momentum vectors of galaxies in six clusters having multiple number-density peaks with a spatial segregation of high- and low-velocity galaxies. The position angle - inclination method was used to convert two-dimensional parameters into three-dimensional parameters (e.g., positions, diameters, PA). The observed and expected isotropic distributions were compared using five statistical tests, namely chi-square, autocorrelation, Fourier, K-S, and Kuiper-V. Thus, no preferred alignment was noticed for all six clusters, supporting the hierarchy model as predicted by Peebles (1969).

Aryal *et al.* (2012), studied the spatial orientation of spin vector orientation of 410 zone of avoidance (ZOA) galaxies found in the region 20° <ℓ<80°, -10°<b<-5° on the first Palomar Observatory Sky Survey. To find the three-dimensional rotation axis of galaxies from two-dimensional, the position angle-inclination method was used (Flin & Godlowski, 1986). Moreover, this paper used the preferred alignments of spin vectors of galaxies to equatorial, galactic, and supergalactic coordinate systems and obtained all three possible scenarios (Pancake, Primordial vorticity, and Hierarchy model).

CONCLUSION

We studied orientation of 1172 galaxies in the Supercluster S[231+030+0117] with redshift in the range 0.107-0.123. We used the method proposed by Flin & Godlowski (1986) and Aryal & Saurer (2000) to find angular momentum vectors (polar and azimuthal angles) of galaxies for observed and expected distributions, respectively. Then, three statistical methods were used to check whether the distribution of angular momentum vectors throughout the Supercluster is isotropic or not. We conclude our results as follows:

1. No preferred alignment of angular momentum vectors of galaxies was noticed in the supercluster S [231+030 + 0117].
2. The redshift distribution of galaxies in supercluster showed Gaussian like nature, suggesting the distribution of galaxies within the supercluster is random.
3. The magnitude distribution of galaxies in the supercluster was found to be independent of the distribution of angular momentum vectors and its projections, supporting Hierarchy model of galaxy formation.
4. In the future, the substructure analysis should be carried out within the supercluster region.

ACKNOWLEDGEMENT

One of the authors (JRM) expresses his sincere thanks to the Department of Astro-Particle Physics, Innsbruck University, Austria, for providing data access and SDSS for providing the database.

REFERENCES

Aryal, B., & Saurer, W. (2000). Comments on the expected isotropic distribution curves in the galaxy orientation studies. *Astronomy and Astrophysics Letter*, *364*, L97-L100.

Aryal, B., Yadav S. N., & Saurer , W. (2012). Spatial orientation of galaxies in the zone of avoidance. *Bulletin of the Astronomical Society of India, 40*, 65-76.

Doroshkevich, A. G. (1973). Spatial structure of perturbations and origin of galactic rotation in fluctuation theory. *Astrophysics, 6*(4), 320-330.

Doroshkevich, A. G., & Shandarin, S. F. (1978). Spatial structure of protoclusters and the formation of Galaxies. *Monthly Notices Royal Astronomy Society*, *184*(3), 643-660.

Flin, P., & Godlowski, W. (1986). The orientation of galaxy groups and formation of the local supercluster. *Monthly Notices Royal Astronomy Society*, *222*(3), 525-541.

Gamow, G. (1952). The role of turbulence in the evolution of the universe. *Physics Review*, *86*, 251.

Godlowski, W. (1993). Galactic orientation within the local supercluster. *Monthly Notices of Royal Astronomical Soiety, 265*(4), 874-880.

Godlowski, W. (1994). Some aspects of the galactic orientation within the local supercluster. *Monthly Notices Royal Astronomy Society*, *271*(1), 19-30.

Heidmann, J., Heidmann, N., & De Vaucouleurs, G. (1972). Inclination and absorption effects on the apparent diameters, optical luminosities and neutral hydrogen radiation of galaxies-I. Optical and 21-cm line data. *Memories of the Royal Astronomical Society, 175*, 85-104.

Holmberg, E. (1946). On the apparent diameters and the orientation in space of extragalactic Nebulae. *Meddelanden Fran Lunds Astronomiska Observatorium Series II*, *117*, 3-82.

Jaaniste, J., & Saar, E. (1978). Orientation of spiral galaxies as a test of theories of galaxy formation. *International astronomical union-Symposium*, *79*, 448-449.

Malla, J. R., Saurer, W., & Aryal, B.(2020*)*. Spatial orientation of galaxies in the supercluster S[227+006+0078]. *Bibechana*, *17*, 117-122.

Ozernoy, L. M. (1978). The whirl theory of the origin of structure in the Universe. *International astronomical union-Symposium*, *79*, 427-438.

Peebles, P. J. E. (1969). Origin of the angular momentum of Galaxies. *The Astrophysical Journal*, *155*, 393-402.

Percival, W. J., Reid, B. A., Eisenstein, D.J., Bahcall, N. A.,……., & Budavari, T. (2010). Baryon acoustic oscillations in the Sloan digital sky survey data release 7 galaxy sample. *Monthly Notices of the Royal Astronomical Society*, *401(4)*, 2148–2168.

Stein, R. (1974). Galaxy formation from primordial turbulence. *Astronomy & Astrophysics*, *35*(1), 17-29.

Weizsacker, C.F.V. (1951). The evolution of galaxies and stars. *The Astrophysical Journal*, *114*(2), 165-186.

Yadav S. N., Aryal, B., & Saurer , W.(2017). Preferred alignments of angular momentum vectors of six galaxies in six dynamically unstable Abell clusters. *Research in Astronomy and Astrophysics*, *17*(7), 64 (pp. 10).

York, D. G., Adelman, J., Anderson, J. E., Anderson, S.F., Annis, J., Bahcall, N.A., Bakken, J.A., …, & Yasuda, N. (2000). The Sloan digital sky survey: Technical summary. *The Astronomical Journal*, *120*(3), 1579-1587.

JNPS **7** (1): 39-48 (2021)
ISSN: 2392-473X (Print), 2738-9537 (Online)
Research Article © Nepal Physical Society
DOI: http://doi.org/10.3126/jnphyssoc.v7i1.36974

Spatial Orientations of Angular Momentum Vectors of Galaxies in Supercluster S [247+040+0029] and Substructures

J. R. Malla[1,*], W. Saurer[2], B. Aryal[1]
[1]Central department of Physics, Kirtipur, Kathmandu, Nepal
[2]Institute of Astro-particle Physics, Innsbruck University, Austria
[*]Corresponding Email: janak.745711@cdp.tu.edu.np

Received: *10 August, 2020;* ***Revised:*** *15 February, 2021;* ***Accepted:*** *19 February, 2021*

ABSTRACT

We present an analysis of spatial orientations of 1331 galaxies in the supercluster S [247+040+0029]. The main goal of this work is to search for a new substructure candidate and examine the orientation of angular momentum in the framework of three different scenarios (hierarchy, pancake, and primordial vorticity models) using "position angle-inclination method", and to test the dependence on magnitude with the angular momentum orientations and their projections. We identified five substructures studying number density contour map with considerably high concentration of galaxies. Using random simulation method to remove the selection effect on database, we carried out expected isotropic distribution using cosmological principle. We then used three statistical tests: Chi-square, Auto-correlation, and Fourier to identify isotropy between observed and expected isotropic distributions. We varied radius in the range $0.3^o$to 1.0^o to find substructures in supercluster. From this we found five sub-structures when taking radius 0.3^o and two substructures for 1.0^o radius in the number density counter maps of galaxies. By analyzing the result obtained through statistical tests, we are able to conform that evolution of galaxy in the supercluster and substructures supports "Hierarchy model" giving the angular momentum of galaxies in the large scale structure tends to be oriented random with respect to the reference coordinate system.

Keywords: Galaxies: evolution, Supercluser, Substructure, Orientation.

1. INTRODUCTION

The galaxy clusters are gravitationally bound large-scale structures of multiple galaxies. The evolution of these galaxy clusters is determined by time and scenario of formation of nature of change of their structures and constituents. Weizacker [1951] and Gamow [1939] postulated the rotation of galaxies might be a clue of physical conditions under which these systems formed. Thus, understanding the distribution of spatial orientation of the spin vectors of galaxies is crucial to understanding the origin of the angular momenta of galaxies.

There are number of contradictory theoretical models predicting the various galaxy cluster formation scenarios. The `hierarchy model' (Peebles, 1969) predicts that the direction of angular momentum is entirely random. According to this scenario, galaxies were first formed and then obtained their angular momentum by tidal forces while they were gathering gravitationally to form a cluster with no dissipation. The `pancake model'(Doroshkevich, 1973; Doroshkevich & Shandarin, 1978) predicts that the angular momentum of galaxies tend to lie within the cluster plane whereas the `primordial vorticity model'(Ozernoy, 1978; Stein 1974) says that the angular momentum of galaxies tend to be oriented perpendicular to the cluster plane. Lee and Pen (2002) found the observational evidence for the alignment of galaxy spin axes with the local tidal share field. Their result is consistent with the linear tidal-torque model based on gravitational instability. In an analytical study, in order to concluded a large-scale coherence in the orientation of galaxies in the two-dimension sheet like structures in the frame of the tidal-torque theory.

According to some scenarios of cosmological structure evolution, the orientation of galactic axes in clusters should favor a certain direction while in other scenarios galaxies are expected to be randomly oriented. Attempts to reveal any deviation from isotropy have been performed over the past years with different and sometimes contradictory results. The work done before 1985 is described by MacGillivray and Dodd (1985), they pointed out that, most studies agree on a random galactic distribution within the local super cluster (LSC) plane, however they suggested that the galactic planes can be oriented preferentially parallel to the LSC plane at some distance from it. In a paper Kapranidis and Sullivan (1983) analyzed samples of bright spirals belonging to the LSC and found no strong evidence for alignment of these galaxies.

However, Jaaniste and Saar (1977) claimed the existence of mean perpendicularity of galactic planes with respect to the LSC plane. Since the earlier approaches were based mostly on analysis of highly inclined and edge-on galaxies, Jaaniste and Saar took all galaxies into consideration, including the face on ones. This approach was critically discussed and modified by Flin and Godlowski (1986). These authors and later Godlowski (1993 - 1994) analyzed large samples within the LSC and come to the conclusion that there exists a preferential orientation of galactic planes perpendicular to the LSC plane and that there is evidence for aligning the galactic rotation axes along the direction toward the Virgo cluster centre.

In the present study, we are interested to find our angular momentum vectors of all galaxies in a supercluster S [247+040+0029] and look at the number density map to find the possibilities of substructures there. Finally, we intend to correlate the orientation of galaxies in those substructures with the whole supercluster.

2. DATABASE

In this work, we have chosen a supercluster S[247+040+0029]whose all photometric data came from SDSS survey (York *et. al.,* 2000). We received the SDSS database through our collaboration with Prof. Walter Saurer's group at the institute of Astroparticle physics, Innsbruck University, Austria. This supercluster includes 1331 galaxies out of which we excluded number of galaxies in our database based. Holmberg (1946) suggested a value of $q^{*}= 0.2$ for oblate spheroid and $q^{*}= 0.13$ for elliptals. At first, we used $q^{*}= 0.2$ to find inclination angle, we used $q^{*}= 0.13$ for those galaxies which did not give inclination angle for $q^{*}= 0.2$. Finally we have excluded those galaxies (5 galaxies) which do not give inclination angle for $q^{*}= 0.13$. Thus, we have 1326 galaxies in our sample of which position (Right Ascension and Declination), ratio of minor and major diameter, position angles in r-filter of all SDSS passbands are available.

3. GODLOWSKIAN TRANSFORMATION

The Polar angle (ρ) between the galactic spin vectors and a reference plane, and the Azimuthal angle (ϕ) between the projection of a galactic spin vectors onto the reference plane and x-axis within this plane are used to view the three dimensional (spatial) orientation of the spin vector SV of a galaxy (Flin, & Godlowski, 1986). These angles are given by the equations

$$\sin\theta = -\cos i \sin\alpha \pm \sin i \sin p \cos\delta \qquad 1$$

$$\sin\varphi = (\cos\theta)^{-1}[-\cos i \cos\delta \sin\alpha + \sin i(\mp \sin p \sin\delta \sin\alpha \mp \cos p \cos\alpha)] \qquad 2$$

Here i, α, δ and P represent the inclination angle, declination, right ascension and position angles respectively.

The inclination angle (i) is the angle between the normal to the galaxy plane and the observers line-of-sight and can be calculated by using the formula Holmberg (1946),

$$\cos^2 i = (b/a)^2 - \frac{q_*^2}{1-q_*^2} \qquad 3$$

Here q* represents the intrinsic flatness factor of the galaxy. The intrinsic flatness of a disk galaxy depends on the morphological type and is taken from Heidmann *et. al.* (1972). Any selection effect on the parameters (e.g. positions, position angles, inclination angle etc) in the right hand side of equation (1, 2) plays a major role in determining the expected isotropic distributions of polar angle (∇) and azimuthal angle (ϕ). This effect can be observed in the inclination angle distribution also.

Thus in our database different kinds of selection effects can be noticed. To remove such selection effects, we use the method proposed by Aryal and Saurer (2000).

4. METHOD OF ANALYSIS

To reduce selection effects, we use the method proposed by Aryal & Saurer (2000) the spatial distribution of the galaxy rotation axis is assumed to be isotropic. Theoretically, the isotropic distribution of polar angle is cosine and that of azimuthal angle is the average distribution curve with the restriction that the database is free from selection effect. We run simulations in order to define expected isotropic distribution curves for both the theta and phi distributions. The isotropic distribution curves are based on simulations generating 10^7virtual galaxies.

Here we describe the procedure for the removal the selection effects to obtain the isotropic distributions for both ∇ and ϕ as given by the Aryal & Saurer (2000). We present the process of numerical simulation for the galaxies in the sample S [247+040+0029]. At first we observed the distributions of α, δ, P and i for the galaxies in the sample S[247+040+0029]. Fig. 1 shows the distributions of α,δ, P and i for the galaxies in the sample S [247+040+0029]. The histograms represent the number of observed galaxies. We see that in the fig. 1 the right ascension (α) is randomly distributed from 240.09º ≡to 252.97º in 24 bins of bin size 0.56º. The declination δis randomly distributed in the range 32.85 ≡ to 45.15º in 42 bins of bin size 0.3º (Fig. 1). The distribution of the position angle P (Fig. 1) is little homogeneous and distributed in the range -90º to 240º in 34 bins of bin size 10º. And there is again an inhomogeneous distribution of the inclination angle i in the range 1º to 89º in 23 bins of bin size 4º (Fig. 1).

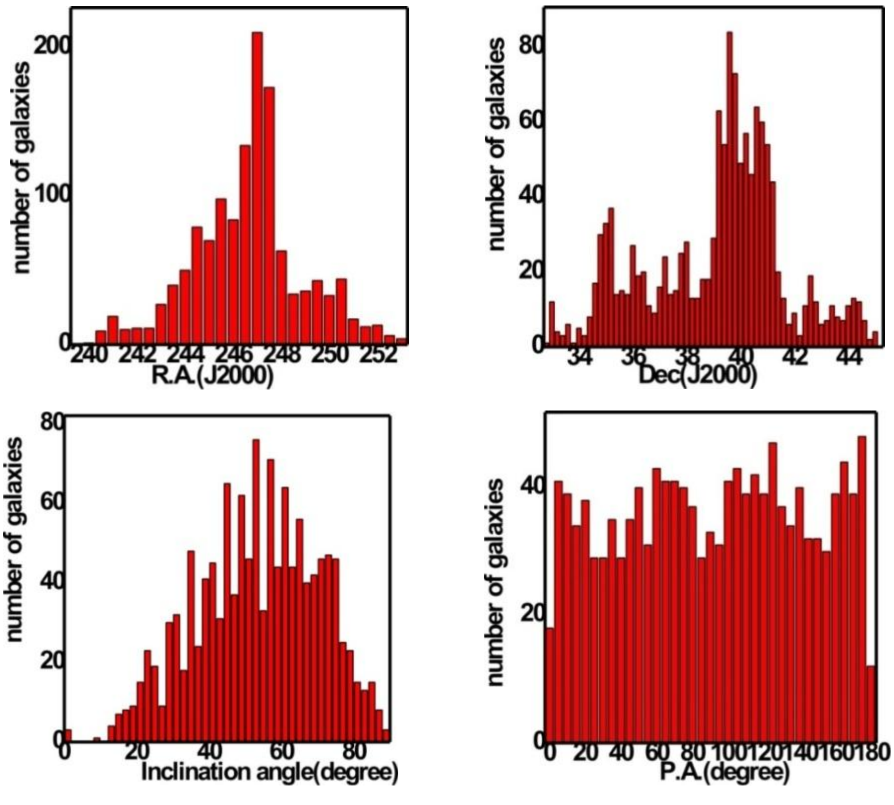

Figure 1: The distributions of right ascension (α), declination (δ), position angle (P) and inclination angle (i) of the galaxies in the sample S [247+040+0029]. The y-axes of histograms represent the number of observed galaxies.

5. RESULTS & DISCUSSION

The all sky distribution of galaxies of our database in supercluster S [247+040+0029] is shown in Fig 2, which indicates the inhomogeneous distribution of galaxies. We can see that, almost all the galaxies were found to be grouped in the different region of space of supercluster.

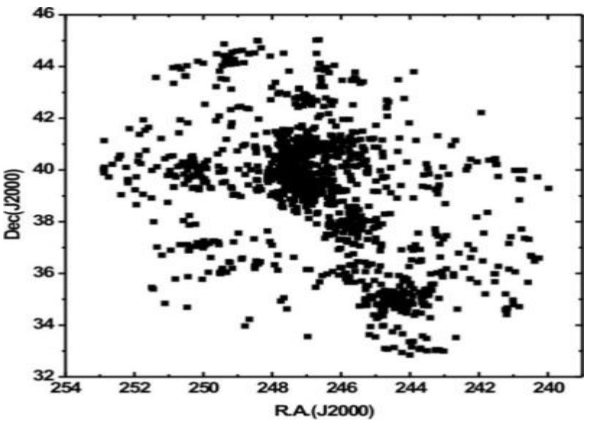

Fig. 2: All sky distribution of total galaxies of superclusters S[247+040+0029] in the equatorial co-ordinate system. The apparent distribution of the galaxies is because of the nature of the survey (7th data release).

At first, we discuss the distribution of polar (∇) and azimuthal (ϕ) angles of galaxy rotation axes in r-filter in de Vaucouleurs system of supercluster S [247+040+0029]. Any deviation from expected isotropic distribution will be tested using four statistical parameters, namely chi-square probability ($P>\chi^2$), auto-correlation coefficient (C/C (σ)), first order Fourier coefficient ($\Delta_{11}/\ \sigma\ (\Delta_{11})$) and first order Fourier probability ($P > \Delta_1$). For anisotropy, the limit of chi-square probability P ($>\chi^2$) is <0.050, auto-correlation coefficient (C/C (σ)) is >1.0, first order Fourier coefficient ($\Delta_{11}/\ \sigma\ (\Delta_{11})$) is >1.5 and Fourier probability P ($>\Delta_1$) is <0.150 respectively. These statistical limits were proposed by the Godlowski (1993-1994) in galaxy orientation studies.

Table 1: Statistical parameters in the polar and azimuthal angles of galaxies in the Supercluster S[247 +040 + 0029] and its sub- structures (first column). The chi-square probability $P>\chi^2$) is given in the second column. The third and fourth columns show first order Fourier coefficient ($\Delta_{11}/\ \sigma\ (\Delta_{11})$) and Fourier probability P ($>\Delta_1$) the last column tests the auto co-relation coefficient (C/C (σ)).

Sample	(P ($>\chi^2$)	($\Delta_{11}/\ \sigma\ (\Delta_{11})$)	P ($>\Delta_1$)	(C/C (σ)).
Polar Angle				
S [247 +040+0029]	0.511	-0.180	0.954	-0.747
S1[247 +040+0029]	0.943	-0.316	0.952	-1.186
S2[247 +040+0029]	0.909	-0.123	0.987	-0.886
S3[247+040+0029]	0.893	0.179	0.982	-0.584
S4[247+041+0029]	0.996	-0.327	0.871	-0.139
S5[244 +035+0029]	0.822	-0.003	0.983	-1.098
Azimuthal angle				
S [1247 +040+0029]	0.954	0.401	0.633	-2.206
S1[247 +040+0029]	0.570	-0.260	0.855	-1.041
S2[247 +040+0029]	0.911	0.166	0.964	-0.059
S3[247 +040+0029]	0.969	-0.102	0.966	-0.028
S4[247 +041+0029]	0.838	-0.469	0.804	-0.906
S5[244 +035+0029]	0.081	1.383	0.303	-0.405

The supercluster S [247+040+0029] from SDSS catalogue consists of 1331 galaxies out of which five galaxies have been omitted because of unclear position angles. As shown in table1, The values of chi-square probability ($P(>\chi^2)$, first order Fourier coefficient ($\Delta_{11}/\ \sigma\ (\Delta_{11})$), first order Fourier probability P ($>\Delta_1$) and auto-correlation coefficient (C/C (σ)) obtained for the polar angle (∇) are 0.511,-0.180 , 0.954 & -0.747 respectively. Here, all statistics shows the isotropic distribution of spin vectors in the supercluster.

We also study the `humps' (bins with more solutions than the expected) and `dips' (bins with less solutions than the expected) in the polar and azimuthal angle distributions in addition to the statistical tests. In the plot of the ∇-distribution (see Fig.3a as an example), solid curve represents the expected isotropic distribution where as dashed curve is the cosine distribution. The solid circles with ±1 σ error bars represent the observed distribution. A dip (or hump) at ∇ <45° suggests that the spin vectors of galaxies tend to orient perpendicular (or parallel) with respect to the equatorial coordinate system. Similarly, a hump (or dip) in the larger ∇ (∇ >45°) indicates that the spin vectors of galaxies tend to be oriented perpendicular with respect to the equatorial coordinate system. In Fig.3a there is a hump on polar angle distribution at ∇ = 55°. This hump is due to 13 more observed solutions than expected solutions in the range ∇ >45°.

For the plot of azimuthal ϕ -distribution, the statistics value obtained for the chi-square probability (P> χ^2), first order Fourier coefficient (Δ_{11}/ σ (Δ_{11})), first order Fourier probability (P > Δ_1) and auto-correlation coefficient (C/C (σ)) are 0.950, 0.401, 0.633 and -2.206 respectively. Here, all statistical tests show strong isotropic distribution of spin vectors.

In the figure 3b, solid curve represents the expected isotropic distribution whereas dashed curve is the average distribution. The solid circles with ±1 σ error bars represent the observed distribution. The humps and dips in the plots of ϕ -distribution are not so easy to interpret as compared to ∇ -distribution. It is because the range of ϕ is -90° to +90°. In the plot of the ϕ -distribution, ϕ = 0° means spin vector projections tend to point radially towards the center of the equatorial coordinate system. A hump in the middle (central eight bins) of the plot suggests that the spin vector projections of galaxies tend to point towards the center of the chosen co-ordinate system. Similarly, a hump at first four and last four bins indicates that the spin vectors projections of galaxies tend to be oriented tangentially with respect to the chosen reference co-ordinate system.

There are two small dip in the plot of azimuthal angle at ϕ = -75° and at ϕ = 55°, but they are insignificant and they are due to difference in number of observed solutions than that of expected. So, we can conclude that there is no preferred alignment of spin-vectors of galaxies.

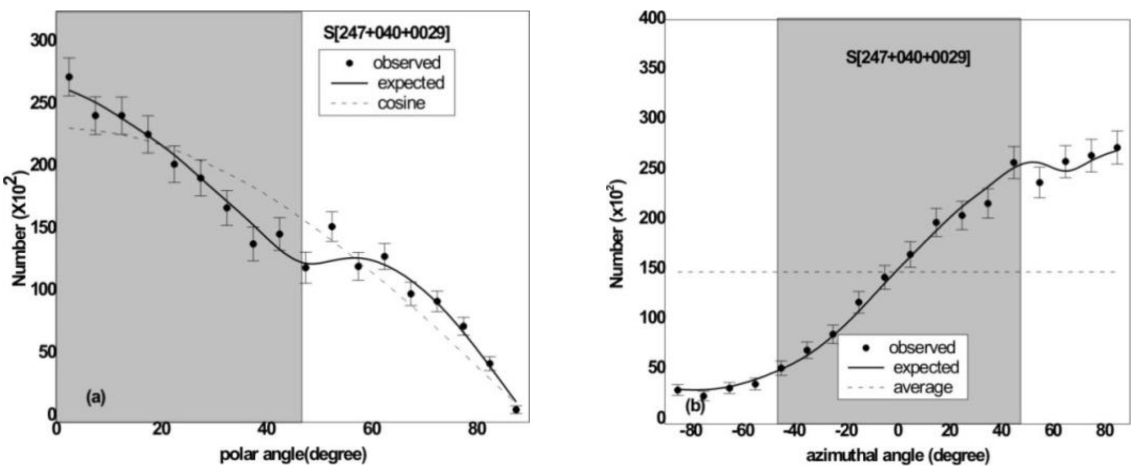

Fig. 3: (a) Polar and (b) azimuthal angle distribution of galaxies in supercluster S [247+040+0029]. The dashed line represents theoretical cosine distribution for polar angle and average distribution for azimuthal angle, B-spline represents expected isotropic distribution obtained through simulation and solid circles with ±1σ error bars represents observed distribution of polar and azimuthal angle.

The substructure S1 [247 +040+0029] that we have chosen from the contour map of number density of galaxies of total supercluster (SDSS catalogue consists of 1365 galaxies) consist of 500 galaxies. By statistics, the values of chi-square probability (P> χ^2), first order Fourier coefficient (Δ_{11}/ σ (Δ_{11})), first order Fourier probability (P > Δ_1) and auto-correlation coefficient (C/C (σ)) obtained for the polar angle (ρ) are found to be 0.943, -0.316,0.952 &-1.186, respectively. Here, all statistics shows the distribution of spin vectors is strong isotropic distribution. For the plot of azimuthal ϕ -distribution, the statistics value obtained for chi-square probability (P> χ^2), first order Fourier coefficient (Δ_{11}/ σ (Δ_{11})), first order Fourier probability (P > Δ_1) and auto-correlation coefficient (C/C (σ)) are 0.570, -0.260, 0.855 and -1.041, respectively.

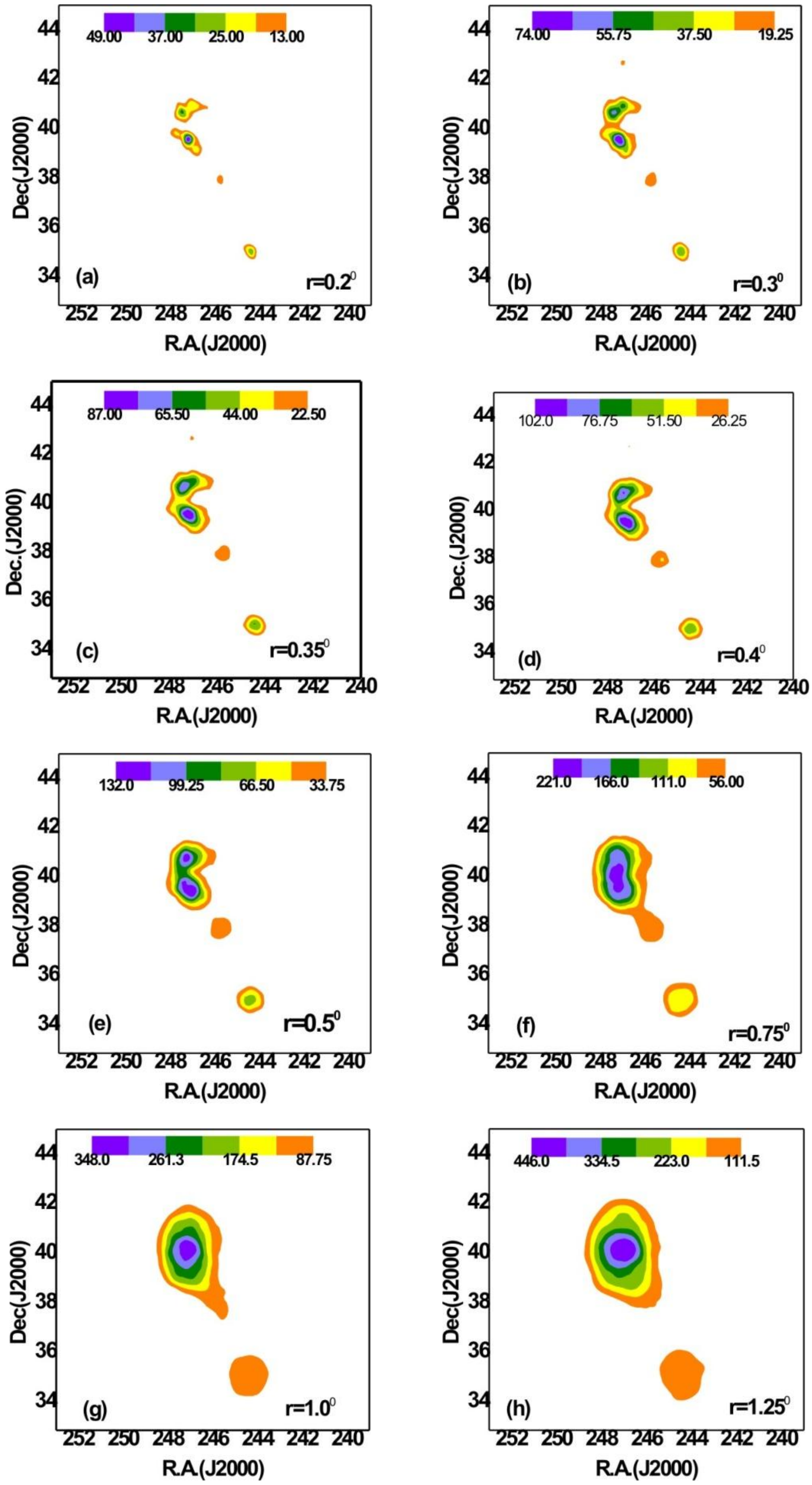

Figure 4: Number density map of galaxies in the Supercluster S[247+040+0029] having nearest neighbor distance of each galaxies at (a) r=0.2°, (b) r=0.3°,(c) r=0.35°, (d) r=0.4° (a) r=0.5°, (b) r=0.75°,(c)r=1.0°, (d) r=1.25° and The color bar is shown. As the radius increases, the subclustering becomes prominent.

In the Fig 5a, the number of observed solution that have P < 45º is found to be 699 and that for expected solutions are 670. The difference between observed and expected solution in that range is 1. At this region, there is one dip at 22º. For the large angles (P > 45º), the number of expected solutions are less by 1 than that of observed. Again there is one dip at 47º in that range. These dips are due to local effect. Thus, we conclude no preferred alignment of spin vectors of galaxies.

In the azimuthal angle distribution as shown in Fig 5b, the observed solutions for range -45º < ϕ <+45º are found to be 556, whereas the expected solutions are 549. This shows that observed solutions are more than the expected solution by 7. There is a significant dip at 38º. For ϕ < -45º, observed solution are 49 and that for expected are 52 that is observed solutions are 3 less than expected. Due to difference in observed and expected solutions, there is a dip at -55ºin this range. For the large angles (ϕ > 45º), the observed 395 solutions are 4 less than what was expected. There are no hump and dip in this range. So we can conclude that there is no preferred alignment among spin-vectors of galaxies.

The substructure S2[247 +040+0029] that we have chosen from the contour map of number density of galaxies of total supercluster (SDSS catalogue consists of 1331 galaxies) consist of 188 galaxies. From statistics, the values of chi-square probability ($P > \chi^2$), first order Fourier coefficient ($\Delta_{11}/\sigma(\Delta_{11})$), first order Fourier probability ($P > \Delta_1$) and auto-correlation coefficient (C/C (σ)) obtained for the polar angle (ρ) are found to be 0.909, -0.123, 0.984&-0.886 respectively. Here, all statistics shows the strong isotropic distribution of spin vectors of galaxies. For the plot of azimuthal ϕ - distribution, the statistics value obtained for the chi-square probability ($P > \chi^2$), first order Fourier coefficient ($\Delta_{11}/\sigma(\Delta_{11})$), first order Fourier probability ($P > \Delta_1$) and auto-correlation coefficient (C/C (σ)) are 0.911, 0.166, 0.964 &-0.059 respectively. In the Fig 5c, the numbers of observed solution are equal to that of expected solutions. At this region, there is one dip at 18º. For the large angles (P >45º), there is again one significant dip at 67º. These dips are may due to local effects. Thus, we conclude that there is no preferred alignment of spin vectors of galaxies.

In the azimuthal angle distribution as shown in Fig 5d, there is no significant hump and dip. We again conclude that there is no preferred alignment among spin-vectors of galaxies.

The substructure S3[244+0035+0029] that we have chosen from the contour map of number density of galaxies of total supercluster (SDSS catalogue consists of 1365 galaxies) consist of 149 galaxies. By statistics, the values of chi-square probability ($P> \chi^2$), first order Fourier coefficient ($\Delta_{11}/\sigma(\Delta_{11})$), first order Fourier probability ($P > \Delta_1$) and auto-correlation coefficient (C/C (σ)) obtained for the polar angle (ρ) are found to be 0.893, 0.179, 0.982 &-0.584 respectively. Here, all statistics shows the distribution of spin vectors in large supercluster is strong isotropic. For the plot of azimuthal ϕ - distribution, the statistics value obtained for the chi-square probability ($P> \chi^2$), first order Fourier coefficient ($\Delta_{11}/\sigma(\Delta_{11})$), first order Fourier probability ($P > \Delta_1$) and auto-correlation coefficient (C/C (σ)) are 0.969, -0.102, 0.966&-0.028 respectively. In the Fig 5e, the number of observed solution that have P < 45º is found to be 206 and that for expected solutions are 208.

The difference between observed and expected solution in that range is 2. At this region, there is one dip at 13º. For the large angles(P >45º), the number of expected solutions are less by 2 than that of observed and there is one significant hump at 48º in that range which cancel the dip observed at lower angles . Thus, we conclude no preferred alignment of spin vectors of galaxies.

In the azimuthal angle distribution as shown in Fig 5f, the observed solutions for range -45º < ϕ <+45º are found to be 161, whereas the expected solutions are 165. This shows that observed solutions are less than the expected solution by 4. For ϕ <-45º, observed solution are 12 and that for expected are 11 that is observed solutions are more than expected by 1. For the large angles (ϕ >45º), the observed 125 solutions are 3 more than what was expected. There is one significant dip at -75º which cancels the significant hump at -65º.But there is no more hump and dip in other range so we can conclude that there is no preferred alignment among spin-vectors of galaxies.

The substructure S4 [247+0041+0029] that we have chosen from the contour map of number density of galaxies of total supercluster (SDSS catalogue consists of 1331 galaxies) consist of 134 galaxies. By statistics, the values of chi-square probability ($P> \chi^2$), first order Fourier coefficient ($\Delta_{11}/\sigma(\Delta_{11})$), first order Fourier probability ($P > \Delta_1$) and auto-correlation coefficient (C/C (σ)) obtained for the polar angle (ρ) are found to be 0.996, -0.327, 0.871&-0.139 respectively. Here, all statistics shows the isotropic distribution of spin vectors. For

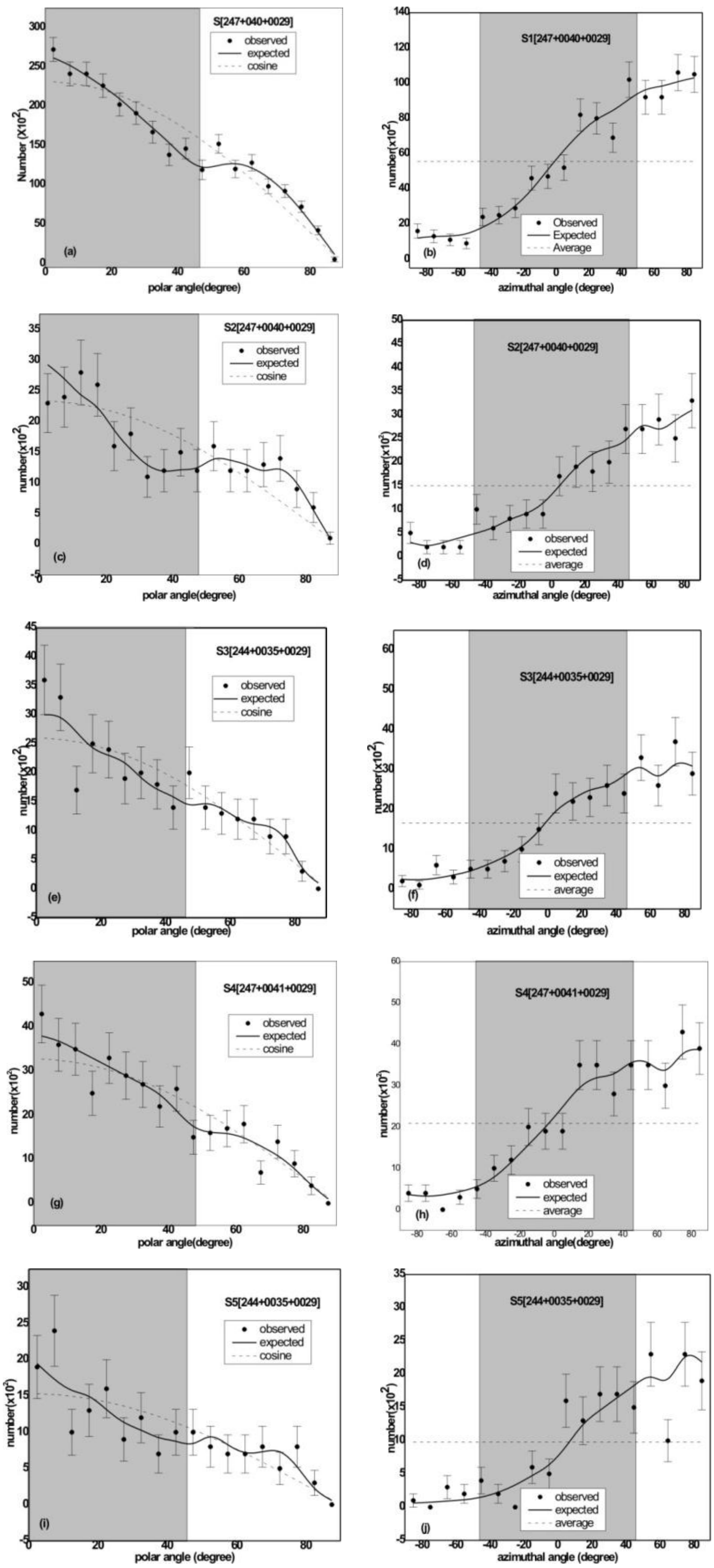

Fig. 5: (a, c, e, g, i) The polar (P) and (b, d, f, h, j) azimuthal angle (ϕ) distributions of galaxies in the substructure of supercluster S [247+040+0029]. The solid line represents the expected isotropic distributions. The cosine and average distributions (dashed) are shown for the comparison. The solid circles with ±1 σ error bars represent the observed distribution.

the plot of azimuthal ϕ -distribution, the statistics value obtained for the chi-square probability ($P>\chi^2$), first order Fourier coefficient ($\Delta_{11}/\sigma(\Delta_{11})$), first order Fourier probability ($P>\Delta_1$) and auto-correlation coefficient (C/C (σ)) are 0.838, -0.469,0.804 &-0.906respectively. In the Fig 5g, the number of observed solution that have P <45º is found to be 173 and that for expected solutions are 174. There is no significant difference between observed and expected solution in that range. At this region, there is one dip at 3º. For the large angles P >45º, the number of expected solutions are less by 1 than that of observed. So there is no preferred alignment of spin vectors of galaxies.

In the azimuthal angle distribution as shown in Fig 5h, the observed solutions for range -45º < ϕ <+45º are found to be 143, whereas the expected solutions are 142. This shows that observed solutions exceeded the expected solution by 1. For ϕ <-45º, observed and expected solutions both are 11. For the large angles (ϕ >45º), the observed 114 solutions are 1 less than what was expected. There is a significant hump at -45º. It is due to local effect but there are no other significant humps and dips. We again conclude that there is no preferred alignment among spin-vectors of galaxies.

The substructure S5[244 +0035+0029] that we have chosen from the contour map of number density of galaxies of total supercluster (SDSS catalogue consists of 1365 galaxies) consist of 88 galaxies. By statistics, the values of chi-square probability ($P>\chi^2$), first order Fourier coefficient ($\Delta_{11}/\sigma(\Delta_{11})$), first order Fourier probability ($P>\Delta_1$) and auto-correlation coefficient (C/C (σ)) obtained for the polar angle (θ) are found to be 0.822, -0.003,0.983&-1.098 respectively. Here, all statistics shows the distribution of spin vectors in large supercluster is strong isotropic distribution. For the plot of azimuthal ϕ -distribution, the statistics value obtained for the chi-square probability ($P>\chi^2$), first order Fourier coefficient ($\Delta_{11}/\sigma(\Delta_{11})$), first order Fourier probability ($P>\Delta_1$) and auto-correlation coefficient (C/C (σ)) are 0.081, 1.383, 0.303 &-0.405 respectively.

In the Fig 5i, the number of observed solution that have θ<45º is found to be 120 and that for expected solutions are also 120. At this region, there is a hump at 9º and a dip at 13º due to local effects. For the large angles (∇ >45º), there is no significant hump and dip in that range. Thus, we conclude no preferred alignment of spin vectors of galaxies.

In the azimuthal angle distribution as shown in Fig 5j, the observed solutions for range -45º < ϕ <+45º are found to be 95, whereas the expected solutions are 88. This shows that observed solutions are more than the expected solution by 7. For ϕ <-45º, observed solution are 6 and that for expected are 3 that is observed solutions are 3 more than expected. For the large angles (ϕ >45º), the observed 75 solutions are 9 less than what was expected. There is one significant hump at 5º and a dip at 65º. It is due to local effect. We again conclude that there is no preferred alignment among spin-vectors of galaxies.

6. CONCLUSION

We have studied the spatial orientation of spin vectors of SDSS galaxies in supercluster S [247+040+0029] containing 1331 galaxies. The method involved for this study is proposed by Flin and Godlowski (1986). To remove selection effect and obtain theoretically expected isotropic distribution, we randomly generated 10^7 virtual galaxies through numerical simulation using the method suggested by Aryal & Saurer (2000). Furthermore, using the galaxies density map to identify substructure, three eminent substructures, namely S1 [247+040+0029], S2[247+040+0029], S3[244+0035+0029] , for radius value 0.3 degree and two substructures, namely S4 [247+0041+0029] and S5[244 +0035+0029] for radius value 1degree has been found. Three statistical tools are used to check whether the distribution of galactic plane throughout the supercluster and in identified sub-structure is isotropic or not.

The main conclusions of our work are numbered as below:

- In this work, no preferred alignment of spin vectors of galaxies is obtained in the supercluster S[247+040+0029], so there is no anisotropic distribution. This suggests that galactic rotation axes favor the “hierarchy model" as suggested by Peebles (1969) of galactic evolution within the supercluster. Same trend are found in the substructure evolution. However, local effect can be seen in some sub-structure suggesting gravitational shearing effect.
- We also found no preferred alignment of angular momentum vectors of galaxies in any of the sub-structures S1 [247+040+0029], S2 [247+040+0029], S3 [244+0035+0029], S4 [247+0041+0029] and S5[244 +0035+0029]. This suggests hierarchical evolution of galaxies in those substructures too.

The lack of preferred alignment of galaxies in superclusters as well as in its substructures suggests the substructures are yet to evolve by merging and collisions through gravitation to obtain anisotropy in galactic orientation.

ACKNOWLEDGEMENT

One of the authors (J.R.Malla) wishes to express his sincere thanks to Astro-Particle Physics, Innsbruck University, Austria, for providing data access and the authorities of the SDSS for providing the database.

Editor's Note: This manuscript was submitted to Association of Nepali Physicists in America (ANPA) Conference 2020 for publication in special issue of Journal of Nepal Physical Society.

REFERENCES

[1] Aryal, B., & Saurer, W. Comments on the expected isotropic distribution curves in the galaxy orientation studies. *Astronomy and Astrophysics letter*, **364**: 97-100 (2000).

[2] Doroshkevich, A. G. The orientation of rotation of galaxies. *Astrophysical Letters*, **14**: 11-13 (1973).

[3] Doroshkevich, A. G. & Shandarin, S. F. Spatial structure of protoclusters and the formation of Galaxies. *Monthly Notices Royal Astronomy Society*, **184**: 643-660 (1978).

[4] Flin, P. & Godlowski, W. The Orientation of Galaxy Groups and formation of the local Supercluster. *Monthly Notices Royal Astronomy Society*, 222, 525 (1986).

[5] Gamow, G. & Teller, E. On the origin of great Nebulae. *Physics Review*, **55**: 654-657 (1939).

[6] Godlowski, W. Galactic orientation within the local Supercluster. *Monthly Notices Royal Astron. Soc.*, **265**: 874-880 (1993).

[7] Godlowski, W. Some aspects of the galactic orientation within the local Supercluster. *Monthly Notices Royal Astronomy Society*, **271**: 19-30 (1994).

[8] Heidmann, J.; Heidmann, N. & De vaucouleurs, G. Inclination and absorption effects on the apparent diameters,optical luminosities and neutral hydrogen radiation of galaxies-I.Optical and 21-cm line data. *Memories of the Royal Astronomical Society*, **175**: 85-104 (1972).

[9] Holmberg, E. On the apparent diameters and the orientation in space of extragalactic Nebulae. *Meddelanden fran Lunds Astronomiska Observatorium Series II*, **117**: 3-82 (1946).

[10] Jaaniste, J. A.; Saar, E. M. An accretion theory of the spiral structure of galaxies. *Pis'ma Astron.Zh*. **3**: 9-12 (1977).

[11] Kapranidis, S. & Sulivan, W. T. The orientation in space of spiral galaxies in the local Supercluster. *Astronomy and Astrophysics*, **118**: 33-38 (1983).

[12] Lee, J.; Pen, U. L. Detection of galaxy spin alignments in the point source catalog redshift survey shear field. *The Astrophysical Journal Letters*, **567**(2): L111-L114 (2002).

[13] MacGillivray, H. T.; Dodd, R. J.The distribution of faint galaxies in a field of 15 square degrees near the south galactic pole. *Monthly Notices of the Royal Astronomical Society*,**193**: 1-6 (1985).

[14] Ozernoy, L. M. The whirl theory of the origin of structure in the universe. *IAU Symposium*, **79**: 427-438 (1978).

[15] Peebles, P. J. E. Origin of the angular momentum of Galaxies. *The Astrophysical Journal*, 155, 393 (1969).

[16] Stein, R. Galaxy formation from Primordial Turbulence. *Astronomy & Astrophysics*, **35**: 17-29 (1974).

[17] Weizsaker, V. The evolution of Galaxies and stars. *The Astrophysical Journal*, **114**: 165-186 (1951).

[18] York, D. G.; Adelman, J.; Anderson, J. E.; Anderson, S. F.; Annis, J.; Bahcall, N. A.; Bakken, J. A. & 137 more. The sloan digital sky survey: Technical summary. *The Astronomical Journal*, **120**: 1579-1587 (2000).

JNPS **7** (2): 81-88 (2021)
ISSN: 2392-473X (Print), 2738-9537 (Online)

Research Article © Nepal Physical Society
DOI: https://doi.org/10.3126/jnphyssoc.v7i2.38627

Spatial Orientations of Angular Momentum Vectors of Galaxies in Supercluster S [195+027+0022] and Substructure

J. R. Malla[1, *], W. Saurer[2] and B. Aryal[1]
[1]Central Department of Physics, Tribhuvan University, Kirtipur, Kathmandu, Nepal
[2]Institute of Astro-particle Physics, Innsbruck University, Austria
[*]Corresponding Email: janak_malla@yahoo.com

Received: *15 April, 2021;* ***Revised:*** *05 May, 2021;* ***Accepted:*** *27 June, 2021*

ABSTRACT

This paper presents an analysis of the spin vector orientations of SDSS (Sloan Digital Sky Survey) galaxies in the Supercluster S [195+027+0022] using the seventh data release (2008 October). By using the spectroscopic database of galaxies, identified number density map in the region of Superclusters. Several density enhancements are observed, suggesting the possibility of substructure in the Supercluster. Two-dimensional observed parameters that we received from the database are used to compute three-dimensional galaxy rotation axes by applying `position angle-inclination' method. Apply the selection effects by performing the random simulation method. The expected distribution curves are obtained from the simulation. Chi-square, auto-correlation, and Fourier tests are used to examine non-random effects in the polar and azimuthal angle distributions of the galaxy rotation axes. To check these results with the different galaxy evolution models namely Hierarchy, Primordial, and Pancake model. The result supports the Hierarchy model.

Keywords: Galaxy: Evolution, Supercluser, Substructure, Galaxies: cluster

1. INTRODUCTION

Galaxy formation is a core theme of cosmology. Galaxies are a slightly laborious topic in astronomy, with many problems relating to their formation and evolution and even with aspects of their structure. Study deeply about the origin and evolution of these large-scale structures. It is necessary to understand how and when galaxies formed and how their constituents have changed with time.

According to Gamow (1952) [1] and Weizsacker (1951) [2]; the observed rotation of the galaxies is very important to understand the origin of the angular momentum of galaxies regarding the beginning of the large scale structures like galaxies and help to get right insight into the initial condition that triggered the formation of these structure Peebles, 1969 [3].

This paper analyzes the spatial orientation of the angular momentum vector of galaxies and their densities in various regions in a Supercluster. In a previous study, a method of searching for sub-clustering in galaxy clusters, based on the analysis of the alignment of the galaxy plane [4]. This work, studied substructure within Supercluster morphologically.

Three main theories advocate predictions concerning the spatial orientation of angular momentum vectors of galaxies. According to the hierarchy model (Peebles, 1969) [3], the angular momentum vector of galaxies is distributed randomly to the plane of the Supercluster. In the turbulence model (Ozernoy, 1978) [5], the angular momentum vectors of galaxies tend to perpendicular to the plane of the Supercluster. The pancake model (Doroshkevich & Shandarin, 1978) [6] angular momentum vector of galaxy parallel to the cluster plane [7].

2. MATERIALS AND METHODS

Data base

The database used in the current work comprises galaxies located within the survey region of Sloan Digital Sky Survey (SDSS) [8] that have redshift in the range of 0.022 to 0.024. These databases have been obtaining from the SDSS database through our collaborator. There were 2,603 galaxies in the region of interest. Among them, 13 galaxies excluded due to the axial ratio (b/a) is 0.2, so their inclination angle cannot be determined shown in Fig. 1b. Thus, 2,590 galaxies are in the final sample. The value of right ascension, declination, position angle, and axial ratio (b/a) provided on the database.

Godlowskian Transformation

The two-dimensional (2-D) information obtained from primary data contains right ascension(α), declination (δ), position angle (p), and axial ratio (b/a) of galaxies in our Supercluster. Adopted position angle inclination method proposed by Flin and Godlowski to convert two-dimensional given parameters into three-dimensional parameters [5].

The inclination angle (i) of a galaxy is the angle between the normal to the galaxy plane and the observer's line-of-sight. It can be calculated from the Holmberg formula [9],

$$\cos^2 i = \frac{(\frac{b}{a})^2 - q^{*2}}{1 - q^{*2}} \quad \text{... (1)}$$

Here q^* represents the intrinsic flatness factor of the galaxy. The flatness of a disk galaxy depends on the morphological type. Holmberg [9] suggested a value of $q^*= 0.20$ for oblate spheroid.

The distribution of the galactic plane and its PA are considered in the equatorial coordinate system. For each galaxy, two angles are determined: the polar angle (θ), the angle between the normal to the galaxy and the equatorial plane, and azimuthal angle (ф), the angle between the projection of this normal on the equatorial plane and directed towards the equatorial center. These angles are given by the equation Flin and Godlowski [10].

$$\sin\theta = -\cos i \sin\alpha \pm \sin i \sin p \cos\delta \text{ ... (2)}$$

$$\sin\varphi = (\cos\theta)^{-1}[-\cos i \cos\delta \sin\alpha + \sin i(\mp \sin p \sin\delta \sin\alpha \mp \cos p \cos\alpha)] \text{ ... (3)}$$

$$cos\phi = (\cos\theta)^{-1}[-\cos i \cos\delta \cos\alpha + \sin i(\mp \sin p \sin\delta \cos\alpha \mp \cos p \sin\alpha)] \text{ ... (4)}$$

Here, i, δ, α, and P represent the inclination angle, declination, right ascension, and position angles respectively and $\mp$ and $\pm$ indicates the two possible solutions.

3. METHOD OF ANALYSIS

The selection effect on the parameters (e.g., position, position angles, inclination angles, etc.) in the right-hand side of equation (2, 3, and 4) affects the distributions of θ and ф. In the database, three kinds of selection effects can be noticed:

1. Inhomogeneity in the distribution of the position of galaxies
2. Lack of knowledge of position angles (PAs) of face-on galaxies and
3. Lack of edge-on galaxies.

In the selection of position and inclination angle make by the SDSS survey, there may cause various errors in the results. To remove these selection effects, we have to use the numerical simulation method proposed by Aryal and Saurer [11]. For the simulation, the correct spatial distribution of the galaxy rotation axis is supposed to be isotropic. Then, latitude (δ), longitude (α), inclination angle (i), and position angle (p) can be distributed randomly, and equation (2, 3, and 4) used to simulate the corresponding distribution of θ and ф.

4. RESULTS AND DISCUSSION

From the all-sky distribution of galaxies in a large-scale structure, the distribution of galaxies is not uniform (As shown in Fig. 1a). There seen some regions are high-density contrast, so must study such density contrast to understand how the overall structure and contrast region affect the evolution and formation of galaxies in that region. In order to identify substructure within the Supercluster S [184+003+00077], try to find the number of galaxies around each galaxy within the different radius values such as 0.5º, 0.75º, 1.0º, 1.25º, and 1.5º. By analyzing the distribution of galaxy in the contour map in various radius values, we choose the particular value of radius for which a clear substructure is seen. In Fig. 2a, we can see four clear high-density contrast regions at 28º declination. Now, the nearest neighbour distance is increased to 0.75º, 1.0º and 1.25º from each galaxy. The number density contour map is shown in Figs. 2b, c. The size of the largest substructure at 28º declination continuously increased. But other different substructure, there is no prominent structure because the density contrast region begins to overlap. Due to this region, it is very difficult to separate different substructure to study precisely. Similarly, in Fig. 2d and e, two additional substructures appeared at 20º declination. When the radius is increased to 1.5º, the lower substructure gets merged. It is, therefore, we set the nearest neighbour radius r = 1.25º for the substructure classification.

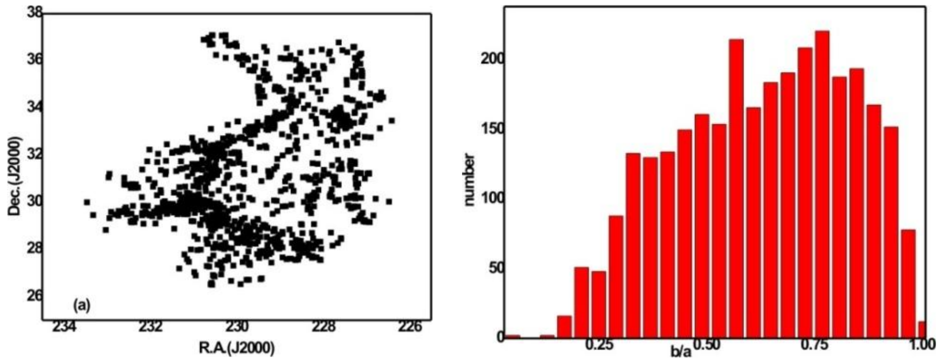

Fig. 1: (a) All-sky distribution of total galaxies of Supercluster S [195+027+0022] in the equatorial coordinate system. R.A. and Dec. represent the right ascension and declination in degree. Each solid circle represents a galaxy. There are 2590 galaxies in this Supercluster. Inhomogeneous distribution of galaxies can be seen. (b) Axial ratio (b/a) distribution of galaxies. The Y-axis represents the number of observed galaxies in the Supercluster S[195+027+0022].

For the substructure identification, "Origin 8.0" and "Matlab 7.0.1" software are used. The contour plot is the process of figuring out the different structures within the given large structure of Supercluster. The contour plot of Supercluster S [195+027+0022] within the different radii of the circle is shown in figure 2 below.

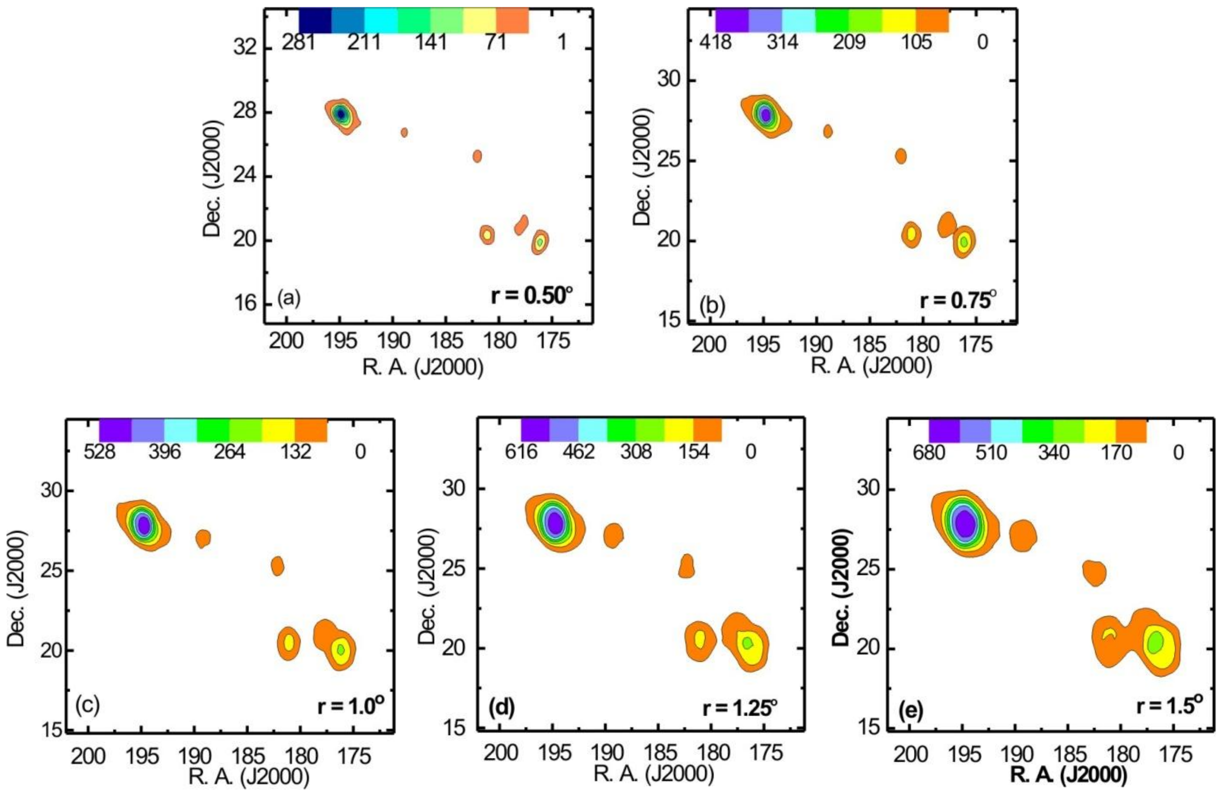

Fig. 2: Number density map of Supercluster S [195+027+0022]. The above diagram, a, b, c, d, and e represent the contour map along the different radii of the circle namely, 0.5º, 0.75º, 1.0º, 1.25º, and 1.50º respectively. The X-axis and Y-axis represent right ascension (R. A.) and declination (Dec.), respectively.

This work explained the spatial orientation of the spin vectors of galaxies to the equatorial coordinate system based on the distribution of polar (θ) and azimuthal (ϕ) angle of galaxy rotation axes in Supercluster S [195+027+0022]. By using statistical tools chi-square probability P ($>\chi^2$), auto-correlation coefficient (C/C (σ)), first- order Fourier coefficient (Δ_{11}/σ (Δ_{11})), and Fourier probability P ($>\Delta_1$) to test any deviation from expected isotropic distribution. For anisotropy, the limit of chi-square probability P ($>\chi^2$) is < 0.050, auto correlation coefficient (C/C (σ)) is >1.0, first order Fourier coefficient (Δ_{11}/σ (Δ_{11})) is >1.5 and Fourier probability P ($>\Delta_1$) is < 0.150 respectively. These statistical limits were proposed by Godlowski [12, 13] in a galaxy orientation study.

The statistics for the polar angle (θ) and azimuthal angle (ϕ) distribution is given in Table 1. In this study of polar angle (θ), a positive value of first order Fourier coefficient suggests that the spin vectors of galaxies tend to be oriented parallel with respect to the equatorial co-ordinate system. While negative value suggests that perpendicular orientation with respect to equatorial co-ordinate system.

Similarly in the statistics of azimuthal angle (ϕ), a positive value of first order Fourier coefficient suggests that the spin vector projections of galaxies tend to point radially outwards the center of the equatorial co-ordinate system while negative value implies spin vectors projection of galaxies tend to orient tangentially with respect to the equatorial co-ordinate system. In addition to the statistical tests, we also studied the `humps' (bins with more solutions than expected) and `dips' (bins with less solutions than expected) in the polar (θ) and azimuthal angle (ϕ) distributions.

In the following Table 1, the first column lists the sample, the second column represents chi-square probability (P ($>\chi^2$), the third column represents first order Fourier coefficient ($\Delta_{11}/\ \sigma$ (Δ_{11})), and the last two columns give first order Fourier probability P ($>\Delta_1$) and auto-correlation coefficient (C/C (σ)).

Sample	**(P ($>\chi^2$)**	**($\Delta_{11}/\ \sigma$ (Δ_{11}))**	**P ($>\Delta_1$)**	**(C/C (σ)).**
Polar Angle				
S [195+027+0022]	0.932	0.24	0.942	0.06
S1[195 +028+0022]	0.924	0.57	0.848	-0.29
S2[176 +020+0023]	0.534	0.07	0.917	-0.35
S3[181+020+0024]	0.976	-0.37	0.923	-0.08
Azimuthal angle				
S [195+027+0022]	0.661	-0.15	-0.943	-0.81
S1[195 +028+0022]	0.416	-0.27	0.999	-1.08
S2[176 +020+0023]	0.274	-0.49	0.999	-0.17
S3[181+020+0024]	0.980	-2.60	0.021	-0.35

Fig. 2 shows polar (θ) and azimuthal (ϕ) angle distributions of galaxies in the Spercluster S [195+027+0022]. Table 1 shows the statistics for the polar angle (θ-distribution in the Supercluster S [195+027+0022]. In the polar angle distribution, chi-square probability (P ($>\chi^2$) is found to be 0.932 i.e., 93.2% (greater than the significant level 0.050 i.e. 5.0 %). The first order Fourier coefficient ($\Delta_{11}/\ \sigma$ (Δ_{11})) is 0.24 (less than significant level i.e., 1.5σ), first order Fourier probability (P ($>\Delta_1$)) to be 0.942 i.e., 94.2% (greater than 0.15 i.e., 15%), and auto-correlation coefficient (C/C (σ)) is 0.06 which is less than 1σ. Thus, all statistical tests suggest isotropic distributions.

Here, the positive value of first order Fourier coefficient suggests that the spin vectors of galaxies tend to be oriented parallel with respect to the equatorial co-ordinate system.

The polar angle (θ) distribution in the Supercluster S [195+027+0022] as shown in Fig. 2a, there are no significant hump and dip observed. This is due to binning effect.

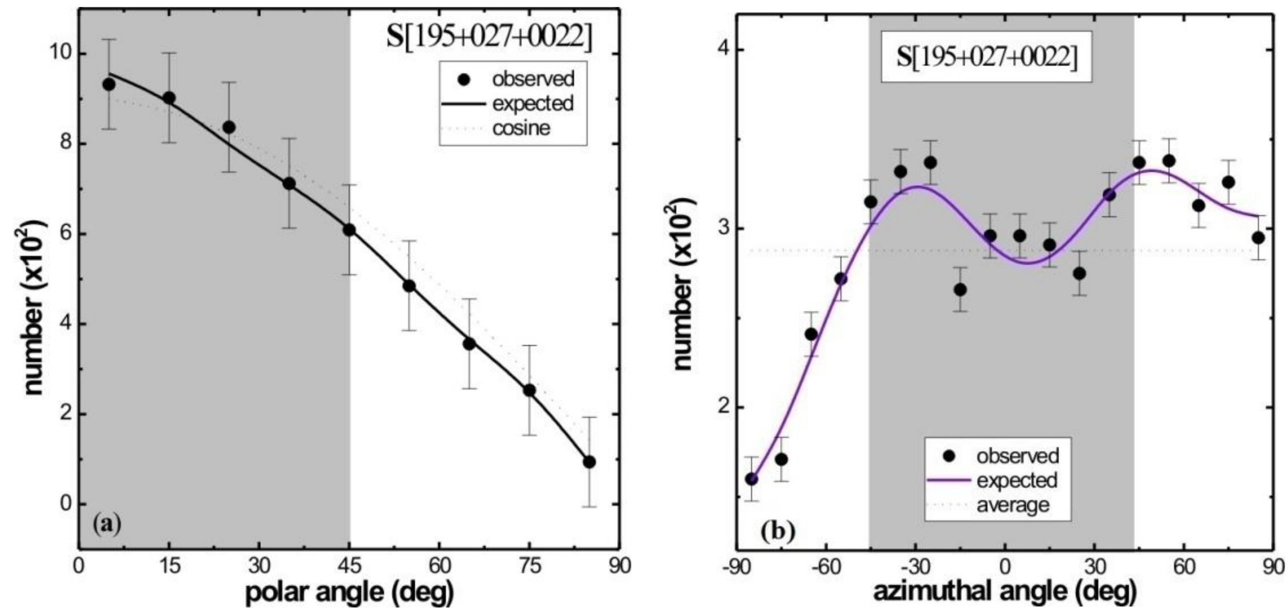

Fig. 2: Polar (a) and azimuthal (b) angle distributions of galaxies in the Supercluster S [195+027+0022]. The solid circles with statistical error bars (±1σ) represent the observed distribution. The solid curves are obtained from random simulation assuming isotropic distributions. The grey shaded region shows a predominance of the Pancake model (Doroshkevich et al., 1978) [6] if observed solution is found to be more than that of expected.

Fig 2(b) shows the azimuthal angle (ϕ distribution. Table 1 shows the statistics for the azimuthal angle (ϕ-distribution in the Supercluster S [195+027+0022]. In the azimuthal angle distribution, chi-square probability (P ($>\chi^2$) to be 0.661 i.e., 66.1% which is greater than 0.050 i.e. 5%, first order Fourier coefficient ($\Delta_{11}/\ \sigma\ (\Delta_{11})$) found to be -0.15 less than 1.5σ, first order Fourier probability (P ($>\Delta_1$)) to be 0.943 i.e., 94.3% more than 0.150 i.e. 15% and auto correlation coefficient (C/C (σ)) is -0.81 less than 1σ. Thus, all statistics tests supporting isotropy.

Here, the negative value of first order Fourier coefficient implies spin vectors projection of galaxies tends to orient tangentially with respect to the equatorial co-ordinate system.

Fig 2b shows the azimuthal angle (ϕ) distribution, there are no significant hump and dip are seen in the region except, for the region bimodal region (-45º<ϕ<+45º), two dips at -25º and +25º are observed. This is due to local effect. This suggests that the projection of spin vectors of galaxies tends to orient parallel with respect to the equatorial co-ordinate system.

Thus, these `humps' and `dips' suggest the possibility of grouping or substructuring because of the tidal or gravitational shearing effects between the co-moving galaxies. Thus, the random orientations of the angular momentum vectors of galaxies are found, suggesting the Hierarchical model of the structure formation as suggested by Peebles [3].

Table 1 shows statistics for the polar angle distribution in the substructures S1 [195+028+0022]. In the polar angle (θ) distribution, chi-square probability (P ($>\chi^2$) is 0.924 i.e., 92.4% much more than 0.05 i.e., 5% significance level, First order Fourier coefficient ($\Delta_{11}/\ \sigma\ (\Delta_{11})$) is found to be 0.57 which is less than 1.5 σ. The First order Fourier probability (P($>\Delta_1$)) to be 0.848 i.e., 84.8%% greater than 0.15 i.e., 15% significance level and auto-correlation (C/C (σ)) to be found -0.29 less than 1σ. However, all these statistical tests suggest isotropy. Thus, there is no preferred alignment of galaxies in the Supercluster S1 [195 + 027 + 0022].

The polar angle (θ) distribution is shown in Fig. 3a below. There are no significant `humps' and `dips' are observed, due to binning effect. No preferred alignment i.e. the random orientation is observed supporting the Hierarchical model (strong isotropy) as suggested by Peebles [3].

Table 1 shows statistics for the azimuthal angle distribution in the substructures S1 [195+028+0022]. In the azimuthal angle (ϕ) distribution, chi-square probability (P ($>\chi^2$) is 0.416 i.e., 41.6% is greater than 0.005 i.e., 5%.

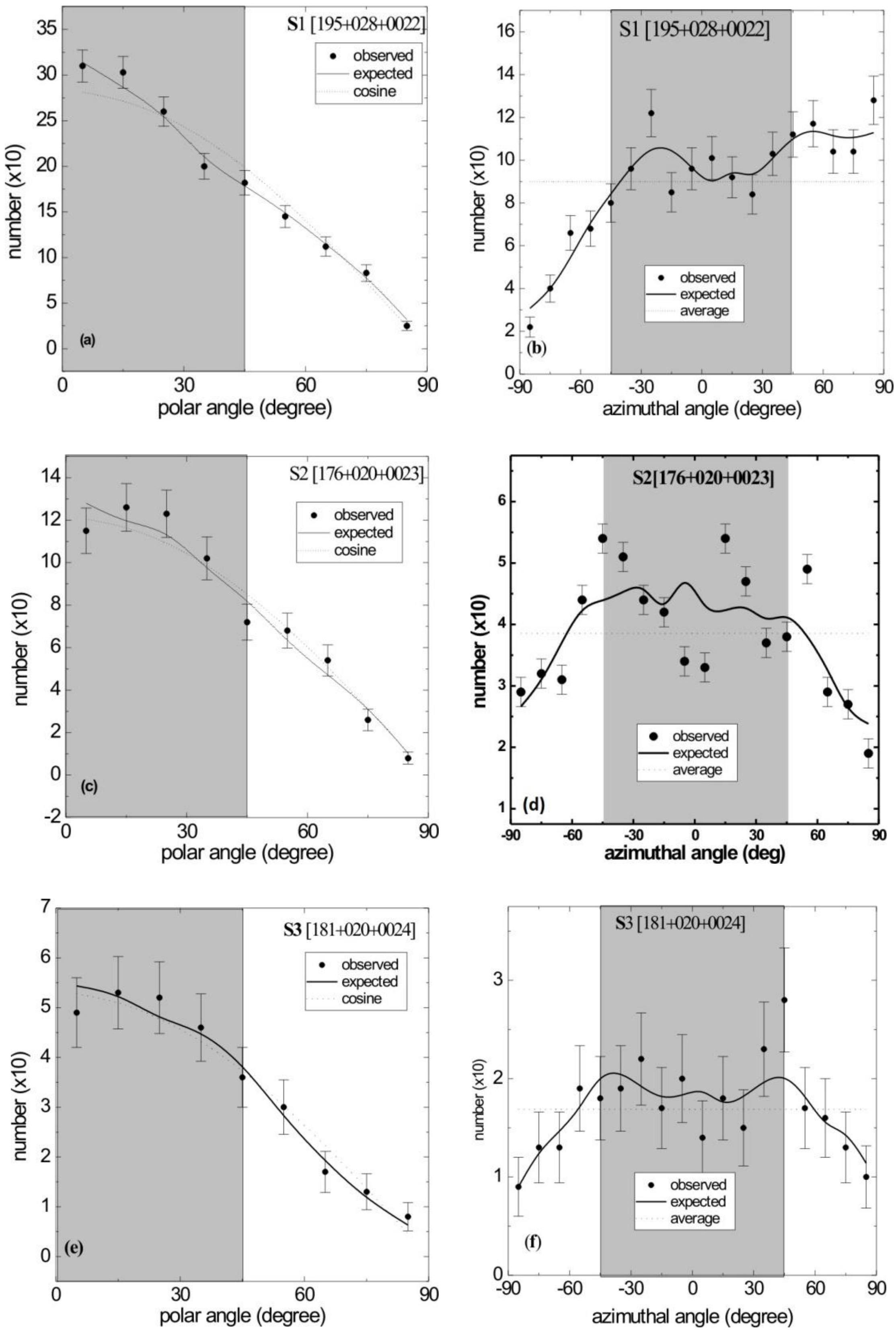

Fig. 3: Polar (a, c, e) and azimuthal angle (b, d, f) distributions of galaxies in the substructures of Supercluster S[195+027+0022]. Solid circles with statistical error bars (±1σ) represent observed distributions. The expected distributions are represented by solid curves. These solid curves are obtained by performing random simulations. The grey-shaded region supports the pancake model if there is excess solution than expected.

First order Fourier coefficient ($\Delta_{11}/ \sigma (\Delta_{11})$) is -0.27 which is less than 1.5σlevel, Fourier probability (P ($>\Delta_1$)) is 0.999 i.e., 99.9% greater than 0.15 i.e., 15% significant limit whereas value of auto-correlation coefficient (C/C (σ)) is -1.08 less than 1.5σ. All these statistics support the strong isotropy in ϕdistributions of this sample.

The azimuthal angle (ϕ) distribution is shown in Fig. 3b below. There are three `humps' at -65º, -25º,-85º and three `dips' at -85º, -15º, and 25º are seen due to the expected and observed values. Like polar angle, no preferred alignment is seen in the azimuthal angle distribution.

Table 1 shows statistics for the polar angle distribution in the substructures S2 [176+020+0023]. In the polar angle (θ) distribution, chi-square probability (P ($>\chi^2$) is found to be 0.533 i.e., 53.3% greater than 0.05 i.e., 5% significance level, First order Fourier coefficient ($\Delta_{11}/ \sigma (\Delta_{11})$) is 0.074 less than 1.5 σ. The First order Fourier probability (P($>\Delta_1$)) to be 0.916 i.e., 91.6%% greater than 0.15 i.e., 15% significance level and auto-correlation (C/C (σ)) to be -0.347 less than 1σ. Thus, all these statistical tests advocate isotropy.

The polar angle (θ) distribution is shown in Fig. 3c below. The observed solution for the region θ<45º, two `dips' can be observed within the shaded region at 5º and bimodal regions (at 45º). Then a number of observed (538) and the expected (542) solutions for small angle (up to 45º), which indicates 4 less solutions are observed than expected. Also, one hump is seen at 25º within a limit of 1 σ. There are no humps and dips observed in regions 45º <θ>90º. This is due to binning effects.

The statistics for the azimuthal angle (ϕ) distribution in the substructures S2[176+020+0023] as shown in Table 1. In the azimuthal angle (ϕ) distribution, chi-square probability (P ($>\chi^2$) is 0.273 i.e., 27.3% more than 0.05 i.e., 5% significance level, First order Fourier coefficient ($\Delta_{11}/ \sigma (\Delta_{11})$) to be -0.490 which less than 1.5 σ. The First order Fourier probability (P ($>\Delta_1$)) is found to be 0.878 i.e., 87.8% greater than 0.15 i.e., 15% significance level, and auto-correlation (C/C (σ)) to be -0.169 less than 1σ. Here, all these statistical tests supporting isotropy.

In Fig 3d, the azimuthal angle (ϕ)) distribution is shown. In the azimuthal angle (ϕ)) distribution, at (ϕ<45º), small `dip' is seen at -65º and in the bimodal region (-45º <ϕ<45º) two `humps' at -45º and 15º are seen and two strong `dips' at -5º and 5º are seen. The `humps' and `dips' in ϕ-distribution are not so easy to interpret as compared to the θ-distribution. It is because the range of ϕ is -90º to 90º. At (ϕ>45º), one `hump' at 55º and a small `dip' in 85º can be observed.

Table 1 shows statistics for the polar angle distribution in the substructures S3 [181+020+0024]. In the polar angle (θ) distribution, chi-square probability (P ($>\chi^2$) is 0.976 greater than 0.05 significance level, First order Fourier coefficient ($\Delta_{11}/ \sigma (\Delta_{11})$) is -0.370 less than 1.5 σ. The First order Fourier probability (P($>\Delta_1$)) to be 0.923 greater than the 0.15 significance level, and auto-correlation (C/C (σ)) to be -0.082 less than 1σ. All these statistical tests suggest the isotropic distribution of polar angle, suggesting random orientation of angular momentum of galaxies as suggested by Peebles [3].

The polar angle θ- distribution is shown in Fig. 3e below. In polar angle (θdistribution, there are no significant `humps' and `dips' are seen. This is due to binning effect. Thus, the random orientation of the angular momentum of the galaxies is found, suggesting the hierarchical model of structure formation as suggested by Peebles [3].

The statistics for the azimuthal angle (ϕ) distribution in the substructures S3[181+020+0024] as shown in Table 1. In the azimuthal angle (ϕ) distribution, chi-square probability (P ($>\chi^2$) is 0.980 more than 0.05 i.e., 5% significance level, First order Fourier coefficient ($\Delta_{11}/ \sigma (\Delta_{11})$) to be -2.602 which less than 1.5 σ. The First order Fourier probability (P ($>\Delta_1$)) is found to be 0.021 i.e., 2.1% less than 0.15 i.e., 15% significance level, and auto-correlation (C/C (σ)) to be -0.349 less than 1σ. Here, all these statistical tests supporting isotropy except First order Fourier probability.

The azimuthal angle (ϕ- distribution is shown in Fig. 3f, there are several humps at (-25º, 35º, 45º) and dips at (-45º, 5º, 25º) are observed. These effects may be due to binning.

5. CONCLUSION

This paper studied the spatial orientation of 2,590 galaxies surveyed by SDSS in the Supercluster S [195+027+0022]. These data (7th data release) were taken by SDSS Telescope located at Apache Point Observatory, New Mexico, USA, and made available to us by collaboration with the Institute of Astroparticle Physics, Innsbruck University, Austria. From these data, we plotted all-sky diagrams and observed the nature of that plot. We have used the `PA-inclination method' proposed by

Flin and Godlowski [10] to convert two-dimensional observed parameters to three-dimensional galaxy rotation axes (polar and azimuthal angles) and carried out random simulation by generating 10^7 virtual galaxies in order to remove selection effects from the database [11]. To check for isotropy and anisotropy, we have carried out three statistical tests: chi-square, auto-correlation, and the Fourier. There are `humps' and `dips' in the polar angle distributions, these `humps' and `dips' do not alter the statistics of the sample. Thus we suppose these as binning effects. Similarly in azimuthal distributions, all samples show isotropic distributions as explained above.

Since observed distributions do not vary significantly from the expected distributions for total sample and substructures S1 [195+028+0022], S2 [176+020+0023], and S3 [181+020+0024]. In general, observed that there is no preferred alignment of spin vectors of galaxies. The result of θ-distributions supports the hierarchical clustering scenario (Peebles1969) [3], which predict that the random orientation of the directions of the spin vectors of galaxies. Similarly for the ϕ-distribution, for total sample and substructures S1 [195+028+0022], S2 [176+020+0023], and S3 [181+020+0024], we found the negative value of first order Fourier coefficient. Therefore in general the spin vector projection of the galaxies tends to oriented perpendicular to the equatorial plane.

ACKNOWLEDGMENTS

One of the authors (J. R. Malla) wishes to express his gratefulness to the Department of Astro-Particle Physics, Innsbruck University, Austria, for providing data access and also thanks to the authorities of the SDSS for providing the database.

REFERENCES

[1] Gamow, G. The role of turbulence in the evolution of the universe. *Physical Review*, **86** (2): 251 (1952).

[2] Von Weizsäcker, C. The evolution of galaxies and stars. *The Astrophysical Journal*, **114**: 165 (1951).

[3] Peebles, P. J. E. Origin of the angular momentum of Galaxies. *The Astrophysical Journal*, **155**: 393-402 (1969).

[4] Baier, F. W.; Godlowski, W.; MacGillivray, H. T. Substructures and galaxy orientations in clusters II. Cluster Abell 14. *Astronomy and Astrophysics Journal*, **403**: 847-856 (2003).

[5] Ozernoy, L. The whirl theory of the origin of structure in the universe. *In Symposium-international astronomical union*, **79**: 427–438 (1978).

[6] Doroshkevich, A. G. and Shandarin, S. F. A statistical approach to the theory of galaxy formation. *Soviet Astronomy*, **22**: 653-660 (1978).

[7] Aryal, B. & Saurer, W. Spin vector orientations of galaxies in seven Abell clusters of BM type III. *Astronomy and Astrophysics Journal*, **432**: 841-849 (2005).

[8] York, D. G.; Adelman, J.; Anderson, J. E.; Anderson, S. F.; Annis, J.; Bahcall, N. A.; Bakken, J. A. & 137 more. The sloan digital sky survey: Technical summary. *The Astronomical Journal*, **120** (3): 1579-1587 (2000).

[9] Holmberg, E. On the apparent diameters and the orientation in space of extragalactic Nebulae. *Meddelanden fran Lunds Astronomiska Observatorium Series II*, **117**: 3-82 (1946).

[10] Flin, P.; Godlowski, W. The Orientation of Galaxy Groups and formation of the local Supercluster, *Monthly Notices Royal Astron. Soc.* **222** (3): 525-541 (1986).

[11] Aryal, B. & Saurer, W. Comments on the expected isotropic distribution curves in the galaxy orientation studies. *Astronomy and Astrophysics letter*, **364**: L97-L100 (2000).

[12] Godlowski, W. Galactic orientation within the local Supercluster. *Monthly Notices Royal Astron. Soc.*, **265**: 874-880 (1993).

[13] Godlowski, W. Some aspects of the galactic orientation within the local Supercluster. *Monthly Notices Royal Astronomy Society*, **271**: 19-30 (1994).

Study of substructure analysis of supercluster S [227+006+0078] radial velocity range of 21300 km/s to 23400 km/s

Janak Ratna Malla*, **Walter Saurer**** **and Binil Aryal*****

* Department of Physics, Amrit Campus, Tribhuvan University, Kathmandu, Nepal.

** Institute of Astro-particle Physics, Innsbruck University, Austria.

*** Central Department of Physics, Tribhuvan University, Kathmandu, Nepal.

Abstract: This paper presents the search for substructures within the Supercluster S [227+006+0078]. To use the spectroscopic database (7th data release) of galaxies, studied the number density, all-sky distribution, and redshift maps to identify substructures based on their richness and compactness. And also to find out the substructures within the Supercluster, using the contour plot of number densities of galaxies within the appropriate radius values and number of nearby galaxies.

Keywords: Large- scale structure of the universe- galaxies; Substructures; Supercluster; Orientation.

Introduction

The formation of the Universe is still an unsolved problem of astrophysical research. The Universe is based on observational evidence and a few theoretical concepts. The discovery of the Expansion of the Universe provided the most important established feature of the modern cosmological picture. In addition, the observation of the Cosmic Microwave Background Radiation (CMBR) provided a strong connection of the present cosmological picture to fundamental Particle Physics. Observational data support the picture of a Universe that is to a very good approximation homogeneous (all places are alike) and isotropic (all directions are alike). The hypotheses of homogeneity and isotropy are referred to as the Cosmological Principle. Such a Universe is called uniform. The most remarkable feature of the mega parsec-scale matter distribution in the Universe is the presence of a cosmic web the network of galaxies, groups, and clusters[1]. We have to understand the role of small-scale (group) and large-scale (Supercluster) environments in galaxy formation and evolution. We need to study the properties of Superclusters and their galaxy and group populations together. The large-scale structure of the Universe is formed by a hierarchy of galaxy systems from isolated galaxies to groups, substructures, and Superclusters of galaxies[2]. The clustering phenomenon does not stop with galaxies. Galaxy clusters attract each other to produce Superclusters. Superclusters are largest structures of the cosmos. Superclusters are important tracers of dark and baryonic matter in the Universe; they also provide information regarding the different orientations of angular momentum vectors of galaxies and their distribution which is beneficial to know about the initial condition of the formation of these

Author for correspondence: Janak Ratna Malla, Department of Physics, Amrit Campus, Tribhuvan University, Kathmandu, Nepal.
Email: janak_malla@yahoo.com

Received: 09 Oct 2021; First Review: 31 Oct 2021; Second Review: 20 Mar 2022; Accepted: 22 Mar 2022.
Doi: https://doi.org/10.3126/sw.v15i15.45667

large scale structures. We have to search substructures within Supercluster and to understand their properties. We need to know how to identify them and how to quantify their properties. Supercluster varies in its shape, extension, galaxy content, etc. Morphology of a Supercluster studied with the help of Minkowski functional. The determination of cosmic structure using the density field, to study their morphology with Minkowski functionals and shape finders is quite an interesting approach. These Minkowski functional used to differentiate Superclusters into various morphological types Spider, multi spider, filaments, and multi-branching filaments[2]. The study of the distribution of galaxies in the Supercluster can lead to the identification of substructure: visualized substructure cluster; galaxies group connected by filament etc.

Einasto et al. analyzed the structure of rich galaxy clusters in Superclusters of different morphologies and showed that clusters in Superclusters of spider morphology have higher probabilities of having substructure and their main galaxies have higher peculiar velocities than clusters in Superclusters of filament morphology[2, 3].

Data compilation

The database used in this work consists of galaxies within Supercluster S [227+006+0078] located within the survey regions of Sloan Digital Sky Survey (SDSS)[4] (7th data release). The Supercluster has a redshift limit in the range of 0.071 (or radial velocity 21300 km/s**)** to 0.078 (or radial velocity 23400 km/s**)**. There were 1213 galaxies of Supercluster S [227+006+0078] after removing the galaxies having axial ratio, $q = b/a < 0.13$. Where a and b are semi-major and semi-minor axes. All-sky distributions of 1,213 galaxies were observed to identify substructures. Finally, we identified two substructures as S1 [228+006+0079], S2 [227+008+0078] with galaxy numbers 287, and 188, respectively.

Method of analysis

According to cosmological principles, the expected distribution of galaxies in the equatorial coordinate system should be homogeneous5. In contrast, the all-sky distribution of galaxies shows the inhomogeneous distribution. Thus, for a detailed study of the Supercluster, the substructure within the Supercluster needs to be identified. Density analysis of galaxy distribution could reveal the presence of substructures as a region of high galaxy aggregation, and their properties and distribution within a Supercluster6. The galaxies are not uniformly distributed within the Supercluster: they can consist of isolated individual galaxies, smaller galaxy groups, or rich clusters of galaxies. These substructures can be in the process of evolution through collision, merger, and fragmentation.

Thus, In order to identified substructure within the Supercluster S [227+006+0078], to classified database (total sample) into substructure based on the number density of galaxies. By analyzing the distribution of galaxy in the contour map in various radius values (0.25º, 0.5º, 0.75º, 1.0º), we choose the particular value of radius for which a clear substructure is seen. So, we choose the suitable counting bin size of (0.25º, 0.5º, 0.75º, 1.0º one by one) square degree in the RA-Dec all sky map of Supercluster to count number of galaxies within the neighborhood of each galaxies in the Supercluster.

The MATLAB7.0.1 code used for this purpose is as follows:

Galaxy Counting Code

```
ra = importdata('ra.m'); dec = importdata('dec.m');

sc = [ra,dec];  n = numel(ra)

repeat = 'y';

while repeat =='y'

radius =input('Enter the radius of circle in degree: ')

for i=1 : n count=0;

for j=1 : n

r = (ra (i) - ra (j)) ^2 + (dec (i) - dec (j)) ^2;

if r <= radius*radius
```

```
count =count+1;

end

neighgal (i)=count;

str = input('enter a _le name to store near galaxy numbers: ','s')_d=fopen (str,'wt');

fprintf (_d,'fclose(_d);

repeat =input('enter c if you wish to continue another size or to exit: 'end')
```

We have used ORIGIN8.0 for the calculation and plotting.

Results and discussion

The contour plot for different radius (0.25º, 0.5º, 0.75º, and 1.0º) values of Supercluster S [227+006+0078] is shown in Figure 1 below. To identify, substructure within the Supercluster S [227+006+0078] through looking at the contour plot of different radius values, we can be distinguished, in which radius value of the clear substructure.

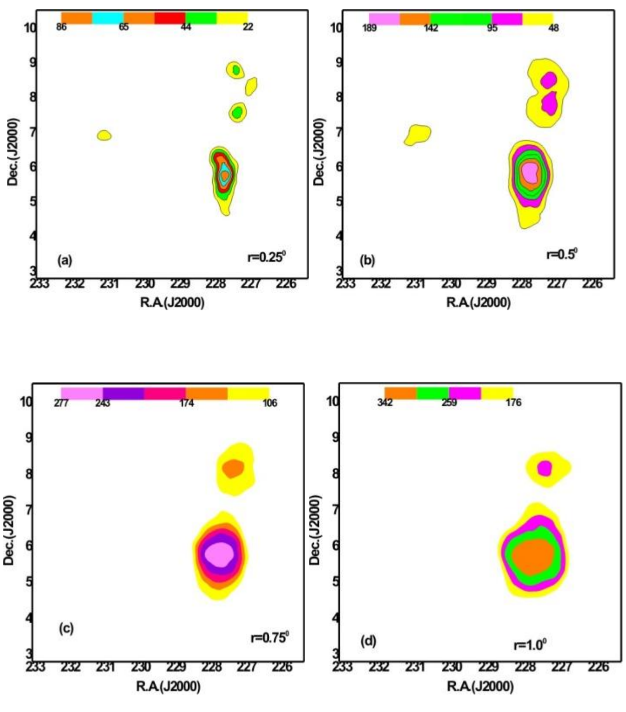

Figure 1: Number density map of Supercluster S [227+006+0078]. In the above diagram, a, b, c, d and represent the contour map along the different radius of circle namely, 0.25º, 0.5º,0.75º, and 1.0º respectively. The X-axis and Y-axis represent right ascension (R.A.) and declination (Dec.), respectively.

In Figure 1(a), here r = 0.25º, we can see five high-density contrast regions at the different regions in the equatorial coordinate system. If we increase the radius value (r = 0.5º) in Figure 1(b), even though we can visualize different substructures, there is no prominent structure because the density contrast region begins to overlap. Due to this region, it is very difficult to separate substructures to study precisely. Similarly, in Figure 1(c) r = 0.75º and (d) r = 0.1º, there only seen two different substructures, however, we are searching for as many as different strong density regions. For radius values, 0.75º and 0.1º, found two substructures, namely S1 [228+006+0079] and S2 [227+008+0078], and found galaxy numbers 287 and 188, respectively.

The all-sky distribution of the total number (1213) of galaxies in the Supercluster S [227+006+0078] is shown in Figure 2. This distribution reveals that the galaxies are not equally distributed throughout the whole region: a heterogeneous distribution. The inhomogeneous nature of the distribution of galaxies in this Supercluster shows that a large number of galaxies are concentrated in the region of right ascension between 227º to 228º. The morphology of this Supercluster can be defined as a spider-type as shown in Figure 2.

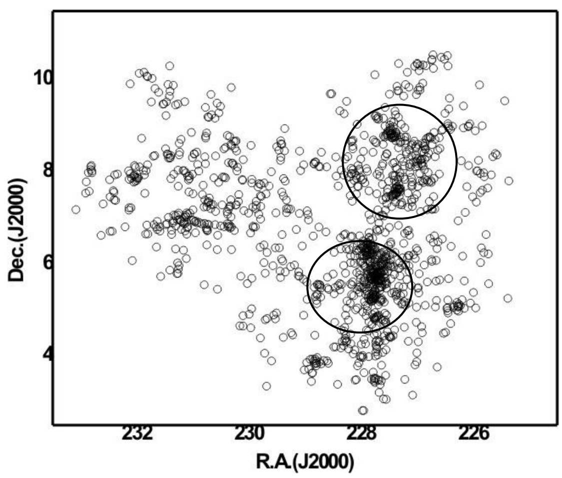

Figure 2: All sky distribution of galaxies in the equatorial co-ordinate system for Supercluster S [227+0067+0078]. Each circle represents a galaxy. The X-axis and Y-axis represent right ascension and declination respectively.

Similarly, as shown in Fig. 3, all-sky view of the galaxy of substructures S1 [228+006+0079] and S2 [227+008+0078] with numbers of galaxy 287 and 188, respectively.

Figure 4a shows a redshift map of galaxies in the Supercluster that have a mean redshift of 0.077. The color map shows that the velocity dispersion is minimum in the region where the number density of galaxy is minimum. The color bars for redshift are shown. The yellow region is the region of high redshift galaxies sky blue region consists of low redshift galaxies in this Supercluster. It seems that there is a linear relationship between redshift dispersion and the number density of galaxies in the substructures and found to be a good correlation coefficient as shown in Figure 4b.

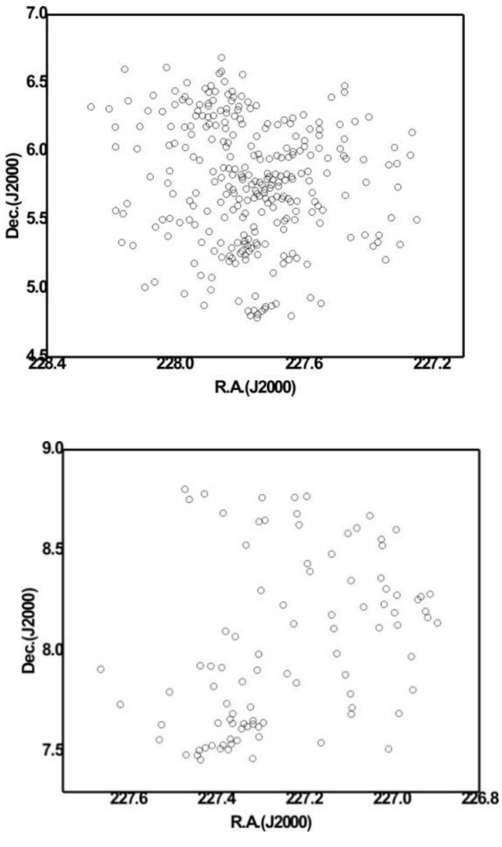

Figure 3: All sky view of substructures S1 [228+006+0079] and S2 [227+008+0078].

The redshift or radial velocity of galaxies in the Supercluster and substructures are found to be independent of the distribution of angular momentum vectors and its projection, supporting the hierarchy model of galaxy formation as suggested by Peebles (Figure 4).

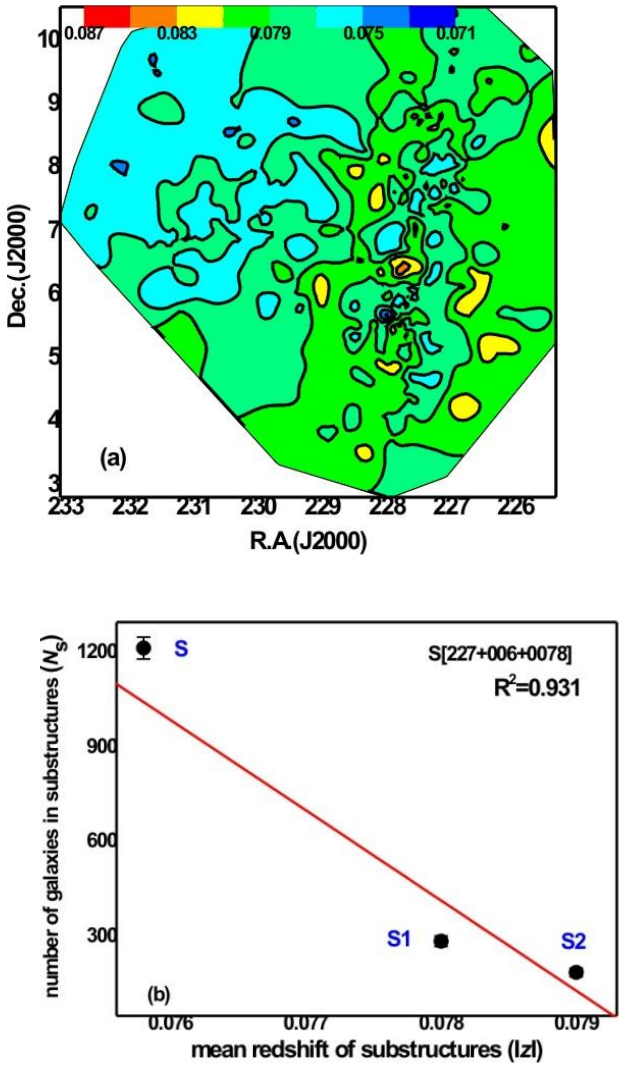

Figure 4: (a) Redshift map is shown for galaxies in the Supercluster S [227+006+0078]. (b) The Number of galaxies in two substructures and Supercluster itself versus redshift dispersion plot. The statistical ±1σ error is shown.

Conclusion

This paper identified two substructures S1 [228+006+0079] and S2 [227+008+0078], to the study of the number density map of galaxies, all-sky distribution of galaxies, and redshift map of galaxies in the Supercluster S [227+006+0078]. This Supercluster consists of 1213 galaxies, and two substructures have 287 and 188 galaxies, respectively.

Acknowledgements

Authors are thankful to the Department of Astro-Particle Physics, Innsbruck University, Austria, for providing data access and also grateful to the authorities of the SDSS for providing the database.

References

1. Einasto, M., Liivamägi, L., Saar, E., Einasto, J., Tempel, E., Tago, E. and Martínez, V. 2011. SDSS DR7 superclusters-principal component analysis. *Astronomy &Astrophysics*. **535 (A36).** https://doi.org/10.1051/0004-6361/201117529
2. Einasto, M., Lietzen, H., Tempel, E., Gramann, M., Liivamägi, L. and Einasto, J. 2014. SDSS superclusters: morphology and galaxy content. *Astronomy & Astrophysics*. **562(A87).** https://doi.org/10.1051/0004-6361/201323111
3. Einasto, M., Liivamägi, L., Tempel, E., Saar, E., Vennik, J., Nurmi, P., Gramann, M., Einasto, J., Tago, E., Heinämäki, P., A. Ahvensalmi, A. and Martínez, V. J. 2012. Multimodality of rich clusters from the SDSS DR8 within the supercluster-void network. *Astronomy & Astrophysics*. **542 (A36)**: 1-19.
4. York, D. G., Adelman, J., Anderson, J. E., Anderson, S. F., Annis, J., Bahcall, N. A., Bakken, J. A. and 137 more. The sloan digital sky survey: technical summary. *The Astronomical Journal*. **120**: 1579-1587.
5. Takami, H., Takahiro, N., Kazuhiro, Y. and Katsuhiko, S. 2009. Cross-correlation between UHECR arrival distribution and large-scale structure. *Journal of Cosmology and Astrophysics.* **06**: 1-21.
6. Einasto, J., Klypin, A. A., Saar, E. and Shandarin, S. F. 1984. Structure of superclusters and supercluster formation-III. Quantative study of the local supercluster. *Monthly Notices of the Royal Astronomical Society*. **206(03):** 529-588.
7. Peebles, P. J. E. 1969. Origin of the angular momentum of galaxies. *The Astrophysical Journal*. **155**: 393-402.